Invasive Imaging of Coronary Atherosclerosis

Hector M. Garcia-Garcia

Cover image: *Yolosóchitl* o *yoloxóchitl* (del náhuatl, literalmente "flor de corazón"; *yolotl* = corazón + *xochtil* = flor)

ISBN: 978-90-8559-541-0

Printed by Optima Grafische Communicatie, Rotterdam, The Netherlands

Invasive Imaging of Coronary Atherosclerosis

Invasieve Beeldvorming van Coronaire Atherosclerose

Thesis

to obtain the degree of Doctor from the
Erasmus University Rotterdam
by command of the
Rector Magnificus

Prof.dr. S.W.J. Lamberts

and in accordance with the decision of the Doctorate Board.
The public defense shall be held on
Wednesday, May 27, 2009 at 9.45 hours

by

Hector Manuel Garcia Garcia
born at Jerez (Zacatecas), Mexico

DOCTORAL COMMITTEE

Promotor: Prof.dr. P.W.J.C. Serruys

Other members: Prof.dr. P.J. de Feyter
Prof.dr. W.J. van der Giessen
Prof.dr.ir. E. Boersma

This thesis book is dedicated to my wife Lulú.

Table of contents

Introduction

Unheralded acute coronary syndromes are a common initial manifestation of coronary atherosclerosis, and most of these events arise from coronary lesions which are not flow limiting. Pathological studies have retrospectively proposed that plaque composition is a crucial determinant of the propensity of an atherosclerotic lesion to rupture. A large study of victims of sudden cardiac death showed that 60% of acute coronary thrombi had as a substrate, a ruptured thin-cap fibroatheromatous (TCFA) lesion. Furthermore, 70% of those patients had additional TCFAs in their coronary tree that had not ruptured. A large necrotic core (avascular, hypocellular, lipid-rich area), a thin fibrous cap with inflammatory infiltration and paucity of smooth muscle cells, and the presence of expansive (positive) remodelling have been identified as the major criteria to define TCFA lesions. In vivo early detection of these non-obstructive, lipid necrotic-rich, high-risk plaques may have an important impact on the prevention of acute myocardial infarction and sudden death.

For many years coronary angiography has been the gold standard to assess the morphology, and severity of atherosclerotic lesions in the coronary tree. Nevertheless, quantitative angiographic measurements can be deceptive because this technique only allows the assessment of the luminal silhouette. In contrast, atherosclerosis is a disease of the vessel wall, and due to the compensatory expansive remodelling effect, the lumen remains unaffected until final stage of the disease. Intravascular ultrasound (IVUS) is a safe catheter-based diagnostic tool that provides a real-time, high resolution, tomographic view of coronary arteries. Thereby it enables evaluation of the morphology, severity and extension of coronary plaque. In vivo plaque characterization through visual interpretation of grey-scale IVUS is suboptimal especially when assessing heterogeneous, lipid-rich plaques. The accuracy of grey-scale IVUS for discriminating lipid from fibrous tissue is limited, because in addition to the large amounts of extracellular lipid which have low echo-reflectance, the lipid core contains cholesterol crystals, necrotic debris and microcalcifications which are highly echo-reflective. On the contrary, spectral analysis of IVUS radiofrequency (RF) data [IVUS-Virtual Histology (VH)] has emerged as a tool able to provide an objective and accurate assessment of coronary plaque composition. Four tissue components [calcified (white), fibrous (green), fibro-fatty (greenish-yellow) and necrotic core (red)] are identified using autoregressive classification systems. IVUS-RF data analysis may follow the progression of the disease not only with regards to its volume, but also to its composition. In addition, this novel IVUS application may potentially expand towards natural history studies.

In this thesis, it has been explored the in vivo accuracy and precision of IVUS-RF data analysis for the assessment of plaque composition. To achieve this,

we have investigated both the classification accuracy of the technique (chapter 2.1) and its reproducibility (chapter 2.2). In addition, we have carried out an extensive program to define its potential clinical value. With this in mind we have compared our results to previous histo-pathological, and clinical studies as an indirect validation of the technique. IVUS-RF was therefore used to describe the extent, distribution, morphology and composition of coronary atherosclerosis in non-intervened coronary arteries. The association between flow dynamics and plaque composition is explored in chapter 3, whilst the correlation between plaque composition and demographical data is evaluated in chapter 4.

This thesis would not be complete without exploring IVUS-VH as a tool to detect the two major components of plaque vulnerability (i.e. necrotic core and remodelling). In chapter 5 we discuss the global characteristics of plaque rupture; the relationship between coronary remodelling and plaque composition; and the prevalence and distribution of an in vivo histological surrogate of TCFA.

We also discuss the treatment of coronary atherosclerosis, in two modalities, applied locally (chapter 6) or systemically (chapter 7).

Complementary to greyscale IVUS, tissue characterization by IVUS-RF analysis has the potential to add valuable information on the pathogenesis of stent thrombosis by providing information on plaque composition, specifically on the amount of necrotic core and its location (superficial or deep). Chapter 8.1. We also explore the potential usefulness of IVUS-RF to assess edge-stent restenosis (chapter 8.2) and its capabilities to evaluate serial changes in plaque type and composition in patients treated with bioabsorbable stents (chapter 8.3).

A very important piece of the thesis is part II, where the effects of medication such as statins, ACE inhibitors and anti-diabetic drugs on coronary atherosclerosis are explored.

Part III focuses on optical coherence tomography. This imaging technique has helped to improve our understanding of high-risk plaque, and also the delicate relationship between focal treatment (i.e. stenting) and vessel wall.

To conclude, the aim of this thesis was fourfold: (1) to explore in vivo the size, morphology, distribution and composition of coronary atherosclerosis, and its relationship with established cardiovascular risk factors; (2) to explore potential IVUS RF and optical coherence tomography surrogates of plaque vulnerability as well as to help find a role for these techniques in the clinical setting; (3) to asses in vivo the effect of conventional medical interventions on plaque size and composition and (4) to evaluate the interaction of stents and the vessel wall.

CHAPTER 1.1

Novel intravascular imaging technologies.

Garcia-Garcia HM, Gonzalo N, Barlis P, Serruys PW.

In: Imaging in Clinical Management. Co-Editors: Dr Stephen Nicholls and Professor Stephen Worthley. Jones and Bartlett Publishers, Inc. 2009

ABSTRACT

Recently, several novel imaging coronary techniques have emerged aimed at describing mainly vulnerable plaques. Thin capped fibroatheroma has been postulated as the precursor of plaque rupture. Detection of these vulnerable plaques *in vivo* is essential to assess their natural history and to evaluate potential treatment modalities which may ultimately impact on the prevention of acute coronary syndromes and death. Currently, conventional grayscale intravascular ultrasound (IVUS), IVUS virtual histology (VH) and palpography are all acquired using the same catheter and pullback. Combining this catheter with either thermography or additional imaging capabilities with optical coherence tomography (OCT) or spectroscopy would herald an exciting era of invasive diagnostic imaging. Other modalities like intravascular magnetic resonance imaging also have tremendous potential in the detection of atherosclerotic plaque components. To date however, none of the techniques described above have been sufficiently validated and, more importantly, they have not demonstrated a sound ability to predict future adverse cardiac events. Very rigorous and well-designed studies are compelling to help define the role of each diagnostic modality.

Key words: Atherosclerosis, plaque rupture, thin-capped fibroatheroma, acute coronary syndromes.

INTRODUCTION

The ability to detect vulnerable plaques *in vivo* is essential to study their natural history and to evaluate potential therapeutic interventions that may ultimately favorably impact on acute coronary syndrome (ACS) and death. Coronary angiography offers valuable information on the long-term behavior of complex coronary lesions but does have several limitations. Goldstein et al(1) reported that patients with ST-segment elevation myocardial infarction (STEMI) and multiple complex lesions had an increased incidence of recurrent ACS during the year following STEMI compared to patients with a single complex lesion (19.0% vs. 2.6%, p <0.001, respectively). Taking this into consideration however, angiography only permits a 2-dimensional view of the arteries and is unable to give precise detail about the vessel wall. As a result, a number of invasive imaging modalities are being tested or used, specifically geared toward the evaluation of vulnerable plaque (2). These techniques are capable of providing unique detail on the vessel wall, lumen, plaque tissue composition and the status of inflammation and therefore circumvent many of the limitations of coronary angiography. This chapter will provide a contemporary review of these technologies with particular reference to their use in the assessment of vulnerable plaque and coronary stents.

1. HISTOPATHOLOGICAL VULNERABLE PLAQUE DEFINITIONS

The "classical", most described phenotype of vulnerable plaque is a thin capped fibroatheroma (TCFA) (3), characterized by a large necrotic core with an overlying thin cap infiltrated by macrophages. Smooth muscle cells within the cap are absent or few. The thickness of the fibrous cap near the rupture site measures 23 ± 19 μm, with 95% of caps measuring <65 μm(4,5). Rupture of a TCFA with exposure of the thrombogenic necrotic core to circulating platelets is thought to be responsible for 60% of all acute coronary syndromes (5). Macrophage infiltration of the thin cap with release of matrix metalloproteinases and local inflammation can cause extracellular matrix degradation and subsequent plaque rupture (6,7). Excessive mechanical strain, particularly at the junction of the TCFA and the normal vessel wall is another factor predisposing to rupture (8,9).

Chevuru et al. (10) reported new pathological evidence on TCFA characterization. The prevalence of TCFA and rupture is *low* (0.46±0.95 and 0.38±0.70 per heart, respectively), *focal* in nature and located in the *proximal segments* of coronary arteries. In earlier studies, up to 3 TCFA were found per heart(11). Necrotic core size was relatively *small* for both, TCFA (1.6±1.8mm$^{2;}$ length 2.7±2.0mm)

and ruptured plaques (2.2±1.9mm^2; length 1.9±3.6mm). In previous studies, the size of necrotic core in TCFAs was 1.7±1.1mm^2 with a length of 8mm (range 2-17mm), and in ruptured plaques 3.8±5.5mm^2, with a length of 9mm (range 2.5-22mm) (12).

The second recognized phenotype of vulnerable plaque, accounting for approximately 40% of coronary thromboses in pathology series is plaque erosion in lesions consisting of either pathological intimal thickening or thick-capped fibroatheroma (13). These lesions typically have a high smooth muscle cell content and are rich in proteoglycans and are more common in young women and smokers, but are not associated with other conventional risk factors such as hypercholesterolemia (14,15).

Thirdly, there are calcified nodules, which may protrude into the vessel lumen and comprise up to 5% of lesions in pathological series. These lesions are characterized by an absence of endothelial and inflammatory cells (15). In addition, intra-plaque hemorrhage secondary to leakage from the vasa vasorum may also a pathological role (16).

2. IMAGING OF VULNERABLE PLAQUES

Angioscopy

Coronary angioscopy (CAS) is a well-established technique that allows direct visualization of the plaque surface and intra-luminal structures. It enables assessment of the plaque color (white, red, yellow), and can illuminate plaque complications such as rupture, intimal tears and thrombosis with a higher sensitivity compared to angiography (17-20). On angioscopy, normal artery segments appear as glistening white, whereas atherosclerotic plaques can be categorized based on their angioscopic color as yellow. Platelet-rich thrombus at the site of plaque rupture is characterized as white granular material, and fibrin/erythrocyte-rich thrombus as an irregular, red structure protruding into the lumen. Yellow plaques are associated with ACS (21) and thrombosis (22). They have also been correlated with other features of vulnerability such as positive remodeling and increased distensibility (23). Quantitative colorimetric angioscopic analysis provides objective and highly reproducible measurements of angioscopic color. This technique can correct for important chromatic distortions present in modern angioscopic systems. It can also help overcome current limitations in angioscopy research and clinical use imposed by the reliance on visual perception of color (24).

The major limitation of angioscopy is that it is a rather specialized technique that requires a blood-free field during image acquisition, which can be obtained either by complete vessel occlusion or by continuous saline flushing distal to the angioscope. Presently, coronary angioscopy (Vecmova®, Clinical Supply Co., Gifu, Japan) can be performed while blood is cleared from the field of view by injection of 5-10 ml normal saline. Nevertheless, angioscope only allows limited assessment of the coronary tree (i.e. vessels > 2 mm diameter) and assessment of stenotic lesions may prove technically difficult. Furthermore, imaging is only of the luminal surface and, although changes in the vessel wall are reflected on the surface, this might not be sufficiently sensitive to detect subtle alterations in plaque composition or plaque burden in the presence of positive remodeling (25).

Kubo et al (20) recently used CAS, optical coherence tomography (OCT) and IVUS to assess culprit lesion morphology in acute myocardial infarction (AMI). The incidence of plaque rupture observed by OCT was 73%, 47% by CAS (p=0.035) and by IVUS 40%, (p=0.009). Furthermore, OCT (23%) was superior to CAS (3%, p=0.022) and IVUS (0%, p=0.005) in the detection of fibrous cap erosion. The intra-coronary thrombus was observed in all cases by OCT and CAS, but was identified in 33% by IVUS (vs. OCT, p<0.001).

Intravascular ultrasound radiofrequency analysis: Virtual histology

Description of the technique

Greyscale IVUS imaging is formed by the envelope (amplitude) of the radiofrequency signal, discarding a considerable amount of information lying beneath and between the peaks of the signal. The frequency and power of the signal commonly differ between tissues, regardless of similarities in the amplitude. IVUS-Virtual Histology (IVUS-VH, Volcano Corp., Rancho Cordoba, USA) involves spectral analysis of the data and evaluates different spectral parameters (Y-intercept, minimum power, maximum power, mid-band power, frequency at minimum power, frequency at maximum power, slope, etc.) to construct tissue maps that classify plaque into four major components (fibrous, fibrolipidic, necrotic core and calcium). Different plaque components are assigned different color codes: calcified (white), fibrous (green), fibrolipidic (greenish-yellow) and necrotic core (red) (26). Although this classification was initially evaluated *in vitro*, more recently IVUS-VH pre- and post-procedure have also been correlated with pathological atherectomy specimens showing good correlation for all 4 tissue types (27). As assessed by IVUS-VH, the sensitivity and specificity for fibrous tissue was 86% and 90.5%, fibro-fatty 79.3% and 100%, necrotic core 67.3% and 92.9% and dense calcium 50% and 98.9% respectively. More recently, these tissue-maps

have been validated using ex-vivo by comparison with histology via 899 selected regions (n=94 plaques) that comprised 471 fibrous tissue, 130 fibro-fatty, 132 necrotic core and 156 dense calcium regions. The overall predictive accuracies were 93.5% for fibrous, 94.1% for fibro-fatty, 95.8% for necrotic core and 96.7% for dense calcium with sensitivities and specificities ranging from 72 to 99%. The kappa statistic was calculated to be 0.845 indicating very high agreement with histology(28).

IVUS-VH data is currently acquired using a commercially available 64-element phased-array catheter (Eagle Eye™ 20 MHz catheter, Volcano Corporation, Rancho Cordova, USA). Using an automated pullback device, the transducer is withdrawn at a continuous speed of 0.5 mm/s up to the ostium. IVUS-VH acquisition is ECG-gated at the R-wave peaks using a dedicated console.

IVUS B-mode images are reconstructed by customized software and contour detection is performed using cross-sectional views with semi-automatic contour detection software to provide quantitative geometrical and compositional measurements. Due to the limitations of manual calibration (29), the radiofrequency data is normalized using a technique known as "Blind Deconvolution", an iterative algorithm that deconvolves the catheter transfer function from the backscatter, thus accounting for catheter-to-catheter variability (30,31).

It has been our observation that in the near field, an excessive amount of necrotic core is present. The developers have accounted for this with a corrected version introduced in the latest release of the classification tree.

Virtual histology and plaque characterization

Lesion classification is based on static images obtained from autopsy specimens. In brief, some believe that atherosclerotic lesion progression starts with pathologic intimal thickening in which lipid accumulates in areas rich in proteoglycans (lipid pools), but no trace of necrotic core. Others believe that the earliest change of atherosclerosis is the fatty streak, also called as intimal xanthoma. The earliest lesion with a necrotic core is the fibroatheroma (FA), and this is the precursor lesion that may give rise to symptomatic heart disease. Thin-capped fibroatheroma (TCFA) is a lesion characterized by a large necrotic core containing numerous cholesterol clefts. The overlying cap is thin and rich in inflammatory cells, macrophages and T lymphocytes with few smooth muscle cells. Plaques prone to rupture are those with decrease cap thickness, large lipid-necrotic core and severe inflammatory infiltrate A study done by Burke et al(4). identified a cut-off value for cap thickness of <65 microns for vulnerable coronary plaque definition.

Virtual Histology can potentially identify detect thin-capped fibroatheromas (TCFAs). In addition, the progression of the disease can also be followed-up.

Table 1: VH-IVUS Proposed Lesion Types

Lesion Type	Brief Description
Adaptative Intimal Thickening (AIT)	<600 µm of intima thickness
Pathological Intimal Thickening (PIT)	≥600 µm thickness for >20% of the circumference with FF >15%, and no confluent NC or DC
Fibrotic Plaque (FT)	Dominant FT and no confluent NC or DC
Fibrocalcific Plaque (FC)	Confluent DC with no confluent NC
Fibroatheroma (FA)	Confluent NC not at the lumen on three consecutive frames
Thin Cap Fibroatheroma (TCFA)	Confluent NC at the lumen on three consecutive frames

FT – fibrous tissue; FF – fibro-fatty tissue; NC – necrotic core; and DC – dense calcium.

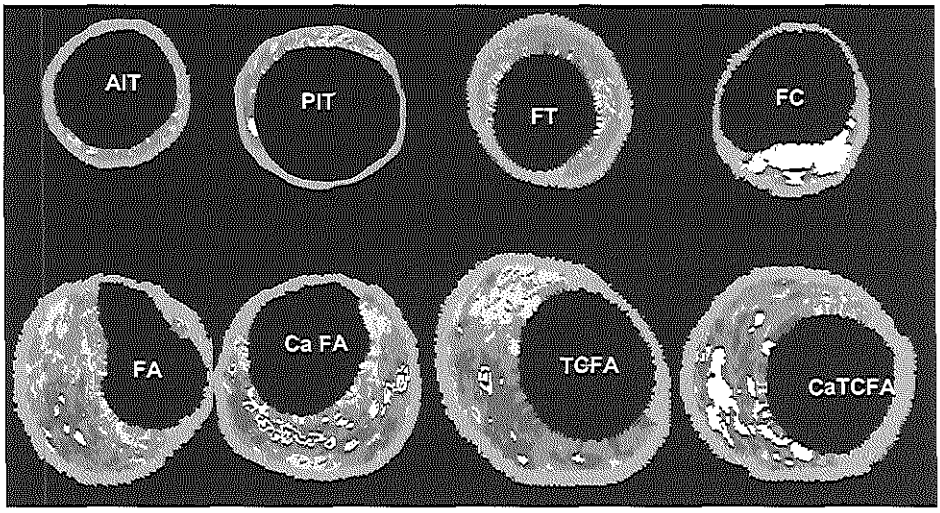

Figure 1. IVUS-Virtual histology proposed lesion types. AIT, adaptative intimal thickening; PIT, pathological intimal thickening; FT, fibrotic plaque; FC, fibrocalcific; FA, fibroatheroma;CaFA, calcified fibroatheroma; TCFA, thin-capped fibroatheroma.

Table 1 outlines the virtual histology plaque and lesion types that are proposed based on the above pathologic data. **(figure 1).**

Our group recently evaluated the incidence of IVUS-derived thin-cap fibroatheroma (IDTCFA) using IVUS-VH (32). Two independent IVUS analysts defined IDTCFA as a lesion fulfilling the following criteria in at least 3 consecutive cross-sectional areas: 1) necrotic core ≥10% without evident overlying fibrous tissue, 2) lumen obstruction ≥40 %. In this study, 62% of patients had at least one IDTCFA in the interrogated vessels. ACS patients had a significantly higher incidence of IDTCFA than stable patients [3.0 (interquartile range 0.0, 5.0) IDTCFA/coronary vs. 1.0 (interquartile range 0.0, 2.8) IDTCFA/coronary, p= 0.018]. Finally, a clear clustering pattern was seen along the coronaries, with 66.7 % of all IDTCFAs located in the first 20 mm whereas further along the vessels the incidence was significantly lower (33.3%, p=0.008). This distribution

of IDTCFAs is consistent with previous *ex vivo* and clinical studies, with a clear clustering pattern from the ostium demonstrating a non-uniform distribution of vulnerable plaques along the coronary tree (33). Patients presenting with ACS had a significantly higher prevalence of IDTCFA even in non-culprit vessels, supporting the concept of a multi-focal process (34). Of note, the lesion percent area stenosis and the mean necrotic core areas of the IDTCFAs detected by IVUS-VH were also similar to previously reported histopathological data (55.9 % vs. 59.6 % and 19 % vs. 23 % respectively) (12).

It is worth mentioning that, although the most accepted threshold to define a cap as "thin" has previously been set at <65 μm, this was based on post mortem studies that studied ruptured plaques (35). Extrapolation of such criteria to *in vivo* studies therefore requires caution. It is well established that tissue shrinkage occurs during tissue fixation (36). Shrinkage (particularly of collagen, the main component of fibrous caps) of up to 60 %, 15 % and 80% can occur during critical-point-drying, free-drying, and air-drying respectively (37). Furthermore, post-mortem contraction of arteries is an additional confounding factor (38,39). Since the axial resolution of IVUS-VH is 246 μm, we assumed that the absence of visible fibrous tissue overlying a necrotic core suggested a cap thickness of below 246 μm and used the absence of such tissue to define a thin fibrous cap (40).

We have recently developed software to quantify the amount of necrotic core in contact with the lumen, enabling refinement of our analysis. Our current definition of an IVUS-derived TCFA (IDTCFA) is a lesion fulfilling the following criteria in at least 3 consecutive cross-sectional areas (CSAs): 1) plaque burden ≥ 40%; 2) confluent necrotic core ≥ 10% in direct contact with the lumen (i.e. no visible overlying tissue) in the investigated CSA; all consecutive CSAs having the same morphologic characteristics are considered as part of the same IDTCFA lesion (41). In a recent study, using this refined definition of TCFA as assessed by IVUS-VH, in patients with ACS underwent IVUS of all three epicardial coronaries, on average, there were 2 IVUS-derived thin cap fibroatheroma (IDTCFA) per patient with half of them showing outward remodeling(41).

The potential value of IVUS-VH in the prediction of adverse coronary events is currently under evaluation in two international multicentre prospective studies (PROSPECT and IBIS 2 trials).

Virtual histology and coronary embolization

Identification of subclinical high-risk plaques is potentially important because they may have greater likelihood of rupture and subsequent thrombosis. In 55 patients, a nonculprit vessel with < 50% diameter stenosis was studied with IVUS-VH. Mean necrotic core percentage was significantly larger in patients with

acute coronary syndrome when compared with stable patients (12.26% +/- 7.0% vs 7.40% +/- 5.5%, P = .006). In addition, stable patients showed more fibrotic vessels (70.97% +/- 9.3% vs 63.96% +/- 9.1%, P = .007)(42). However, not only the amount of necrotic is larger in patients with ACS, but it appears that NC is also unevenly distributed. In 51 consecutive patients, a non-culprit vessel was investigated through IVUS-Virtual Histology. The overall length of the region of interest, subsequently divided into 10 mm segments, was 41.5+/-13 mm long. No significant change was observed in terms of relative plaque composition along the vessel with respect to fibrous, fibro-fatty, and calcified tissue, whereas the percentage of necrotic core resulted to be increased in the first (median: 8.75%; IQR: 5.7-18) vs. the third (median: 6.1%; IQR: 3.2-12) (P=0.036) and fourth (median: 4.5%; IQR: 2.4-7.9) (P=0.006) segment. At multivariable regression analysis, distance from the ostium resulted to be an independent predictor of relative necrotic content [beta=-0.28 (95%CI: -0.15, -0.41)], together with older age, unstable presentation, no use of statin, and presence of diabetes mellitus(43).

Recently, two studies evaluated the usefulness of IVUS-VH plaque composition to predict the risk of embolization during stenting (44,45). In one of them, 71 patients with STEMI that underwent primary PCI within 12 hours of the beginning of the symptoms were included. After crossing the lesion with a guidewire and performing thrombectomy with an aspiration catheter, VH-IVUS of the infarct-related vessel was performed. The stent was then deployed without embolic protection. ST segment re-elevation was used as a marker of distal embolization during stenting. Eleven patients presented with ST segment re-elevation after stenting. Total plaque volume was similar in both groups, but the NC volume was significantly higher in the group of patients with ST segment re-elevation (32.9 ± 14.1 mm^3 vs. 20.4 ± 19.1 mm^3, $p < 0.05$). On receiver-operating characteristic curves, NC volume was the best predictor of ST re-elevation after stent deployment as compared with fibrous, fibro-lipid, dense calcium, and total plaque volumes. The cut-off point for NC volume that was best predictive for ST re-elevation was 33.4 mm^3, with a sensitivity of 81.7% and a specificity of 63.6%. The second study included 44 patients who underwent elective coronary stenting. Plaque composition was assessed with VH-IVUS, and small embolic particles liberated during stenting were detected as high-intensity transient signals (HITS) with a Doppler guidewire. Patients were divided into the tertiles according to the HITS counts. Dense calcium and NC area were significantly larger in the highest tertile. In the multivariate logistic regression analysis, only necrotic core area was an independent predictor of high HITS counts (odds ratio 4.41, p = 0.045).

Intravascular Ultrasound Radiofrequency analysis: Palpography

This technique allows the assessment of local mechanical tissue properties. For a defined pressure difference, soft tissue (e.g. lipid-rich) components will deform more than hard tissue components (e.g. fibrous, calcified) (46,47). Radiofrequency data obtained at different pressure levels are compared to determine the local tissue deformation.

Each palpogram represents the strain information for a certain cross section over the full cardiac cycle. The longitudinal resolution of the acquisitions depend on heart rate and pullback speed. With a heart rate of 60 bpm and a pullback speed

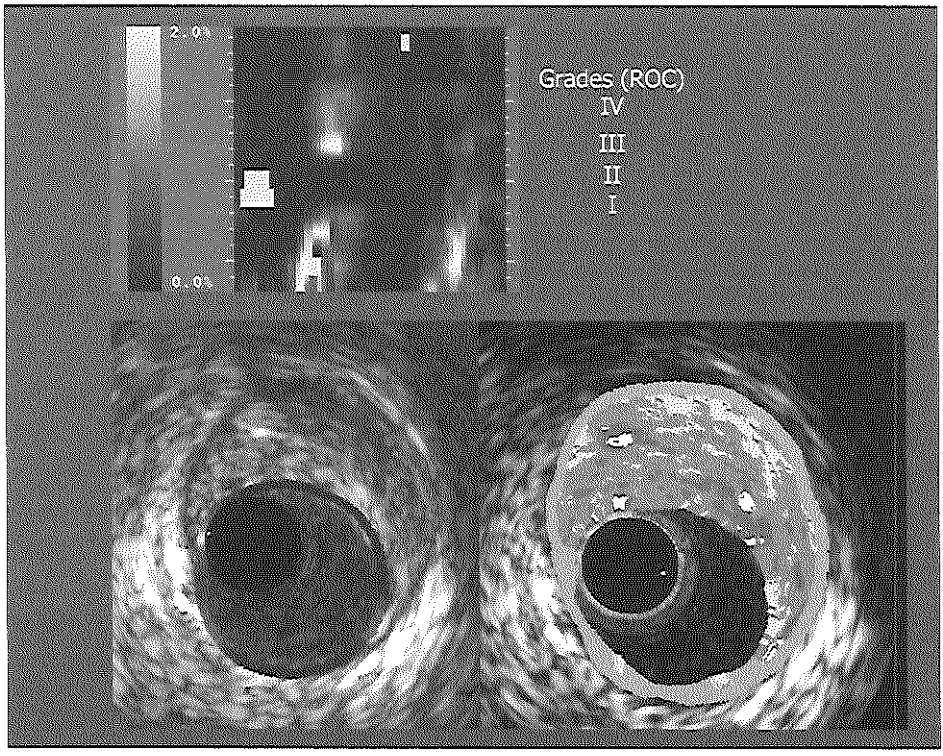

Figure 2. IVUS-palpography. In the upper left side the palpography strain map is opened up. The local strain is calculated from the gated radiofrequency traces using cross-correlation analysis and displayed, color-coded, from blue (for 0% strain) to red to yellow (for 2% strain). Plaque strain values are assigned a Rotterdam Classification (ROC) score ranging from I to IV (ROC I= 0-<0.6 %; ROC II= 0.6- <0.9 %; ROC III= 0.9-<1.2 %; ROC IV= >1.2 %). At the bottom, in the same cross-sectional area a high-strain spot (ROC III) is shown (left); in the virtual histology (VH) image (right) a confluent necrotic core area in contact with the lumen is seen, suggesting an IVUS-derived thin capped fibroatheroma. The IVUS-VH color-code is fibrous tissue (green), fibro-fatty tissue (light green), necrotic core (red) and dense calcium (white).

of 1.0 mm/s, the longitudinal resolution is 1.0 mm. Palpograms are acquired using a 20-MHz phased array IVUS catheter (Eagle Eye™ 20 MHz catheter, Volcano Therapeutics, Rancho Cordova, USA). Digital radiofrequency data are acquired using a custom-designed workstation.

The local strain is calculated from the gated radiofrequency traces using cross-correlation analysis and displayed, color-coded, from blue (for 0% strain) to red to yellow (for 2% strain) (48). Plaque strain values are assigned a Rotterdam Classification (ROC) score ranging from I to IV (ROC I= 0-<0.6 %; ROC II= 0.6- <0.9 %; ROC III= 0.9-<1.2 %; ROC IV= >1.2 %) (49) **(figure 2).** Our group has demonstrated that palpography has a high sensitivity (88%) and specificity (89%) to detect vulnerable plaques *in vitro* (46). Postmortem coronary arteries were investigated with intravascular elastography and subsequently processed for histology. There was a positive correlation between the presence of high strain and the degree of macrophage infiltration ($P<0.006$) and an inverse relation between the amount of smooth muscle cells and strain ($P<0.0001$). Vulnerable plaques identified by palpography had a thinner cap than non-vulnerable plaques ($P<0.0001$). In a subsequent study, 55 patients with either stable or unstable angina, or acute MI were analyzed. Among patients with stable angina, the prevalence of deformable plaques was significantly lower per vessel (0.6+/-0.6) than in patients presenting with unstable angina (1.6+/-0.7, p=0.0019) or with acute MI (2.0+/-0.7, p<0.0001). In the IBIS I study, on palpography, both the absolute number of high-strain spots (grade III/IV) in the ROI (p=0.009) and their density per cm (p=0.012) decreased significantly between baseline and follow-up. This decrease in the overall population was largely driven by changes in the subgroup of patients with STEMI; this group had both the highest number of high-strain spots at baseline and the most marked relative decrease during follow-up compared to patients with other clinical presentations. At 6-month follow-up, the density of high-strain spots (1.2±1.4/cm) was comparable among clinical subgroups (50).

The potential value of IVUS-palpography is currently under evaluation in two international multicentre prospective studies, PROSPECT and IBIS 2 trials. These two studies have also obtained IVUS-virtual histology during the same IVUS pullback, allowing for the assessment of both morphological and biomechanical properties of a particular plaque. Assessing several characteristics of a given plaque could potentially enhance invasive risk stratification by identifying very high-risk plaques, thereby lowering the number of vulnerable plaques that deserve to be serially followed and ultimately treated (**figure 2**).

Optical coherence tomography

Optical coherence tomography (OCT) is an optical analogue of ultrasound, however it uses light instead of sound to create an image (51,52). For OCT imaging, low coherence, near infrared light with a wavelength around 1300 nm is used since it minimizes the energy absorption in the light beam caused by protein, water, hemoglobin, and lipid. The light waves are reflected by the internal microstructures within biological tissues as a result of their differing optical indices.

This technique provides a resolution of 10-20μm *in vivo* (53); this level of detail is well beyond the level of resolution of IVUS (100-150μm) (54). OCT has been demonstrated to be highly sensitive and specific for characterizing atherosclerotic plaques *in vitro* when compared with histological analysis (55-57) with a sensitivity and specificity of 71-79% and 97-98% for fibrous plaques, 95-96% and 97% for fibrocalcific plaques, and 90-94% and 90%-92% for lipid-rich plaques, respectively. In addition, the inter- and intra-observer reliabilities of OCT assessment were high (kappa values of 0.88 and 0.91, respectively) (57). *In vitro* comparison of OCT with IVUS have demonstrated superior delineation by OCT of structural details such as thin caps, lipid pools or tissue proliferation (58). An *in vitro* comparison of OCT, integrated backscatter IVUS (similar methodology to IVUS-VH) and conventional IVUS found that OCT had the best potential for tissue characterization of coronary plaques, with higher sensitivity and specificity compared to the other imaging modalities (59). However, a recent study comparing OCT to histopathology reported a lower sensitivity for plaque components. Misclassification occurred in 41% of lesions, predominantly due to a combination of incomplete penetration depth into the vessel wall and the inability to distinguish calcium deposits from lipid pools (60).

In a pilot clinical study, our group performed *in vivo* OCT analysis of the coronary arterial wall in patients who were undergoing percutaneous coronary intervention. Imaging was possible in all patients and the entire vessel circumference was visualized at all times. A wide spectrum of different plaque morphologies was observed. OCT allowed for differentiation of the normal artery wall and inhomogeneous, mixed plaques, as well as thin cap fibroatheromas with inhomogeneous, low-reflecting necrotic cores, covered by highly-reflecting thin fibrous caps (54).

As a result of its high axial resolution, there is no doubt that OCT is the *in vivo* gold standard for identifying and measuring the thickness of the fibrous cap (**figure 3**); an *in vivo* study found a significant difference in minimal cap thickness between acute MI and stable angina patients, with median (interquartile range) values of 47.0 (25.3-184.3) μm and 102.6 (22.0-291.1) μm respectively (p= 0.02) (61). On top of its reliability as a tool to measure the thickness of the cap *in*

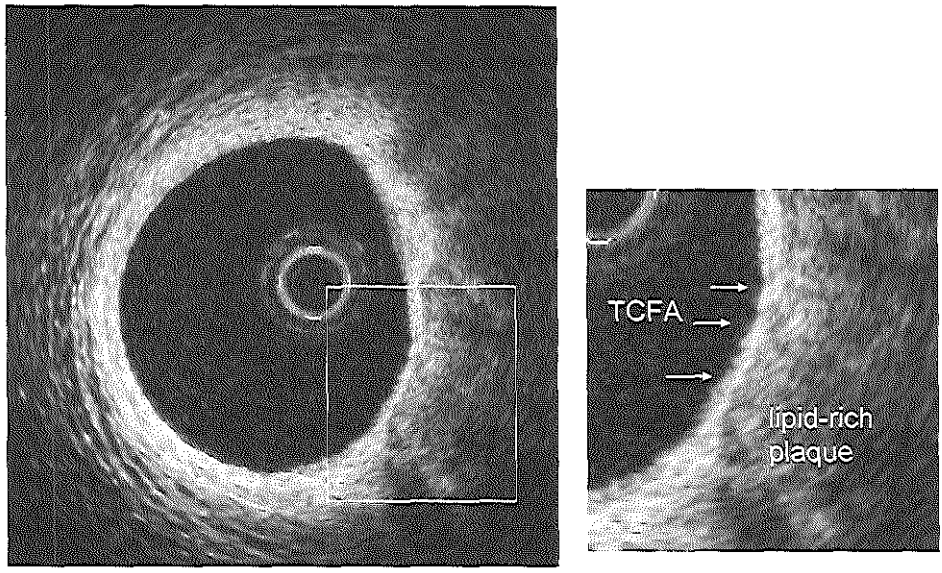

Figure 3. The optical coherence tomography image shows thin cap fibrous atheroma (TCFA). The cross-section demonstrates a region of low reflectivity with diffuse borders between the 3 and 5 o'clock position consistent with a lipid-rich plaque. This is covered by a thin, highly reflective fibrous cap (TCFA) which measured between 10-30 microns in thickness

vivo, recent post-mortem and *in vivo* studies have shown that OCT is capable of evaluating the macrophage content of infiltrated fibrous caps (62,63).

Kubo et al. (20) evaluated the ability of intracoronary OCT to assess culprit lesions during primary PCI in patients with acute MI. The thickness of the remnants of the fibrous cap after symptomatic rupture measured was 49±21μm. The main limitation of OCT is the shallow tissue penetration depth (1.5-2mm) which hampers imaging of the entire vessel wall in large vessels and light absorbance by blood that currently needs to be overcome by saline infusion and balloon occlusion, thereby precluding interrogation of long and proximal segments of the coronary tree. This has recently been partly overcome with the use of non-occlusive techniques whereby contrast is flushed through the guiding catheter during simultaneous image acquisition at 3.0mm/seconds (M3, LightLab Imaging Inc., Westford, MA, USA). Furthermore, even more encouraging is the use of optical frequency domain imaging (OFDI) that enables even faster pullback speeds without compromise of image quality and resolution.

Thermography

Atherosclerosis is accompanied by inflammation, and vulnerable plaques have been associated with increased macrophage activity, metabolism and inflammation (64). Activated macrophages produce thermal energy, which might be detected on the surface of these atherosclerotic lesions using specially-designed catheters equipped with thermistor sensors at the distal tip (65). A rise in temperature can be found in atherosclerotic plaques as compared to disease-free coronary segments. Temperature differences between an atherosclerotic plaque and normal vessel wall increase progressively from patients with stable angina to patients with acute MI with a maximum temperature difference to the background temperature of 1.5±0.7°C (66). In a prospective study, Stefanadis et al reported an association between temperature heterogeneity and the incidence of adverse events at follow-up in patients with coronary artery disease undergoing successful PCI (67). In addition, treatment with statins seemed to affect the thermographic results: in non-culprit lesions the temperature difference was lower in the group treated with statins compared with the untreated group (0.06 ± 0.05°C vs. 0.11 ± 0.10°C; p = 0.05) (68).

More recently, a correlation between morphologic and functional characteristics of culprit lesions (CL) in patients with acute coronary syndromes and chronic stable angina (CSA) has been reported(69). In 81 consecutive patients (48 with ACS and 33 with CSA), remodeling index (Ri) by IVUS and temperature difference (DeltaT) by angioscopy between the CL and the proximal vessel wall were measured. Patients with ACS had greater remodeling index than patients with CSA (1.15±0.18 vs. 0.90±0.12; $p < 0.01$), as well as increased DeltaT (0.08±0.03 degrees C vs. 0.04±0.02 degrees C; $p < 0.01$). Patients with positive Ri had higher DeltaT than patients with negative Ri (0.07±0.03 degrees C vs. 0.04±0.02 degrees C; $p < 0.001$). Patients with rupture plaque had increased DeltaT compared with patients without rupture plaques (0.09±0.03 degrees C vs. 0.05± 0.02 degrees C; $p < 0.01$). Multivariate analysis showed that DeltaT was independently correlated with the presence of rupture plaque, positive Ri, and ACS.

However, there are several different aspects that deserve further investigation. The prevalence and distribution of inflammatory cells in stable and unstable atherosclerotic plaque is unclear, and the predictive value of 'warm' lesions remains elusive. Furthermore, the impact of different coronary flow conditions on plaque temperature ('cooling effect') is still not completely understood (70,71). Simulations have revealed that the correct interpretation of intravascular thermographic measurements requires data on the flow and on the morphologic characteristics of the atherosclerotic plaque (72).

There are a few limitations to the routine use of thermography in the catheterization laboratory: (i) most of the catheters used still comprise over-the-wire systems; (ii) accurate temperature assessment requires direct contact of the thermistors with the vessel wall, with the associated potential risk of endothelial damage (73) and (iii) as the temperature within the vessel changes rapidly with fluid application, any intracoronary injection of contrast, flush or medication has to be avoided before and during measurements(74).

Intravascular Magnetic Resonance

Magnetic resonance (MR) is a non-ionizing diagnostic tool exploiting the spins of the nuclear protons in a strong magnetic field. For intravascular diagnosis, two different approaches have been introduced.

The first, conventional approach visualizes the anatomical structure by using a coil placed in a catheter or wire in combination with an external magnet (MR imaging). While this approach has previously been shown to be able to provide detailed information on structure and composition of the arterial wall and plaque, (75) the procedure has to be performed in a MR room, not in a cardiac catheterization laboratory. The accuracy for MRI differentiation of plaque components has been validated in vitro and feasibility demonstrated in vivo (76). The 0.030-inch IVMRI coil had a sensitivity and specificity of 73% and 85% respectively for lipid, 83% and 81% respectively for fibrous tissue and 100% and 97% respectively for calcification. Subsequently, the same system was applied in human iliac arteries *in vivo* using a 1.5T magnet with a resolution of 312µm. Complete vessel wall analysis was possible in all 25 patients and required 20 minutes for an arterial segment of 20mm length. Compared to IVUS, mean lumen diameters were similar, but the outer wall area was overestimated by IVMRI (mean 116.4±4.7mm^2 vs. 86.6±5.8mm^2, p=0.0001). However, inter-observer agreements for IVMRI were much higher (kappa 0.68-0.79) than for IVUS (kappa 0.21).

The other, novel approach analyses the chemical composition by placing both, the coils and miniaturized magnets on the tip of a catheter, without the need of external magnets (MR spectroscopy) and can be performed in the cardiac catheterization laboratory (77).

MR spectroscopy can identify fibrous and lipid-rich tissue by measuring differential water diffusion in a field of view. Acquired data is displayed as color-code sectors based on the lipid fraction index (LFI) for each zone of the FOV. Blue indicates no lipid, gray correspond to intermediate lipid content and yellow indicates high-lipid content (**figure 4**). Clinical feasibility of catheter-based, self-contained

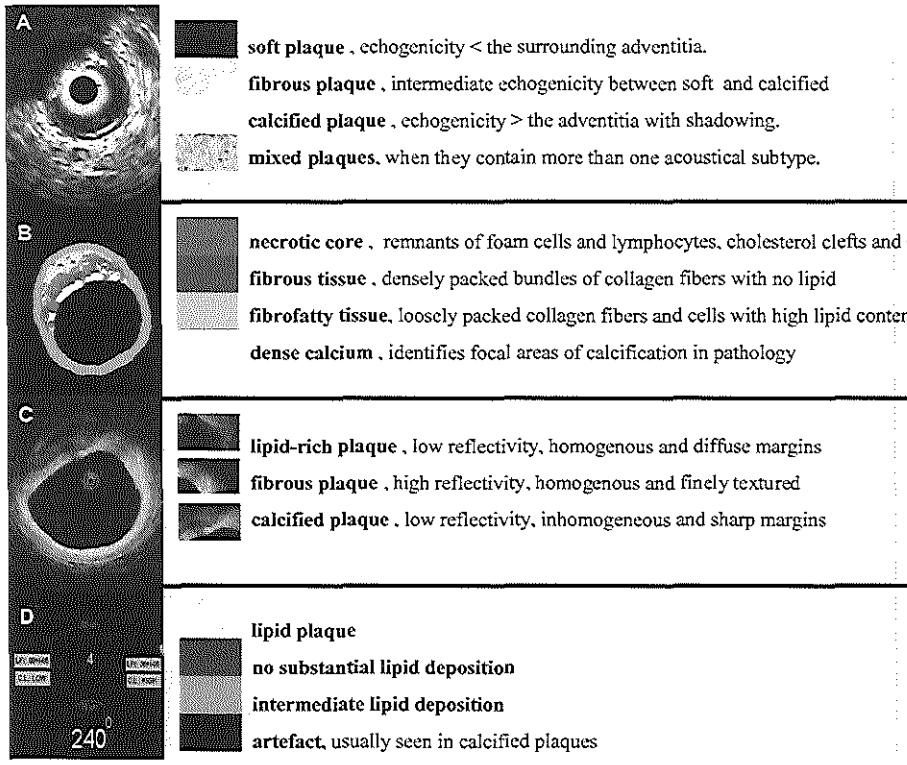

Figure 4. Multi-imaging in the coronary arteries. The same coronary segment (represented by one frame) has been imaged by 4 different imaging techniques. In the greyscale IVUS (panel A), IVUS-virtual histology (panel B), optical coherence tomography (panel C) and intravascular magnetic resonance spectroscopy (IVMR) the results of the same frame across different techniques are shown. Of note, in the upper left quadrant of the plaque a calcified area is seen in three imaging modalities, but in IVMR where an artifact is observed. On the right hand side, the different plaque and tissues types across the coronary imaging techniques is shown.

IV MR spectroscopy has been recently demonstrated in patients scheduled for coronary catheterization(78).

Preclinical trials employing this technology demonstrated its capacity to differentiate plaque components of human aortas, coronary and carotid arteries in vitro: IVMR spectroscopy was able to accurately detect different components (fibrous cap, smooth muscle cells, organizing thrombus, fresh thrombus, edema, lipid and calcium) with sensitivities and specificities ranging from 84-100%. Agreement with histology for grading the extent of intra-plaque lipid accumulation was 74% and 80% for grading intimal thickness. Further analysis revealed high correlation to histological analysis of a wide spectrum of plaque types in 15 of 16 (94%) aortic lesions and 16 of 18 (89%) coronary lesions (sensitivity 100%, specificity 89%), including one plaque rupture, three TFCAs, seven thick-cap fibrous

atheroma, four fibrocalcific plaques, two intimal xanthomas, and one adaptive intimal thickening (79).

Current limitations include the limited field of view, the size of the catheter, the need for direct vessel wall contact and the time required for acquisition. In the past, the use of an auto-perfusion balloon during data acquisition has been proposed to limit ischemia(80).

Clearly IVMR diagnostics remain an exciting area still under development. Catheter-based system will further increase the user friendliness, their sample volume and allow for scanning of longer arterial segments. Upcoming developments include the improvement MR plaque differentiation by the use of contrast agents, such as paramagnetic gadolinium-based contrast(81) or supraparamagnetic contrast agents (iron oxide nanoparticles), that can accumulate in macrophages (82). There are still a few unanswered questions, including the effect of the thermal energy generated on small arteries and on coronary artery stents, although conventional MRI appears safe in this setting(83).

Recently in our center, a study has been started to explore a multi-modality imaging approach of atherosclerotic plaque in-vivo. The same coronary segment is assessed by greyscale IVUS, IVUS-VH and OCT and IVMR (**figure 4**). This has been a challenging process, since we are dealing with the different imaging resolutions and the lack of common nomenclature and classification across these imaging techniques.

Raman and near infrared spectroscopy

A number of spectroscopic intravascular imaging techniques have been developed recently and are still under investigation (84). Spectroscopy can provide qualitative and quantitative information about chemical plaque composition. The Raman effect is created when incident laser light (typically 750-850nm wavelength) excites molecules in a tissue sample, which scatter light at a different wavelength. This change in wavelength, called the "Raman effect" is dependent on the chemical components of the tissue sample (85,86) and can therefore provide quantitative information about molecular composition (87-89). Raman spectroscopy has shown acceptable correlation compared with histology ($r = 0.68$ for cholesterol and $r = 0.71$ calcification) (89) and with IVUS *in vitro* (88).

Raman spectroscopy technology collect scattered light with optical fibers and route the collected signal to spectrometer systems for analysis. Previously optical fiber probes utilized a region of the Raman spectrum called the "fingerprint" (FP) region ($< \sim 1800$ cm^{-1} shifted light) to conduct remote assays, but due to technical problems with this approach, it has been recently replaced by using another region

of the Raman spectrum, called high wavenumber (HW) Raman shifted light (> ~2500 cm^{-1} shifted light). This allows us to collect Raman spectra via a single optical fiber, simplifying the size and complexity of the catheter and making it clinically feasible (Eurointervention 2008, in press). Thus, the optical catheter system (OCS) (vPredict™) has been introduced as a tool for measuring the chemical composition of coronary vessels *in-vivo* using Raman spectroscopy and the subsequent mapping and quantification of the vessel and plaque components for evaluating plaque progression. In a xenograft model, lipid-laden plaque were identified with the collected Raman spectra by utilizing the overall cholesterol content, i.e. the sum of the free cholesterol and cholesterol esters contents, and setting a decision threshold at 12 %, as determined in previous studies. As expected, the lipid laden plaques exhibit an increased content of free cholesterol and cholesterol esters, while the non-atherosclerotic samples are mainly protein and triglycerides. **Table 2.**

The vPredict OCS delivers infrared light to the vessel wall through optical fibers contained within a small flexible catheter and captures a portion of the reflected light for spectral analysis. This analysis provides information about the composition of the underlying tissue. **Figure 5.**

Alternatively, near infrared (NIR) molecular vibrational transitions can be measured in the NIR region (750–2500 nm) (90) and laser spectroscopy using wavelengths of 360-510 nm has been evaluated *in vitro* (91).

Near-infrared spectroscopy observes how different substances *absorb* and *scatter* NIR light to different degrees at various wavelengths. A NIR spectrometer emits light into a sample and measures the proportion of light that is returned over a wide range of optical wavelengths. The return signal is then plotted as a graph of absorbance (y-axis) at different wavelengths (x-axis) called a spectrum.

Table 2. Plaque/vessel components detectable by Raman spectroscopy.

Demonstrated:	Collagen, Elastin, Myosin, Triglycerides, Beta-carotene, Foam cells, Cholesterol/esters, Hemoglobin, Fibrin
Possible:	Metalloproteinases, Low density lipoprotein (LDL), Oxidized LDL, Proteoglycans, Glycosaminoglycans, Plasmin, Nucleic acids, Nitrotyrosine

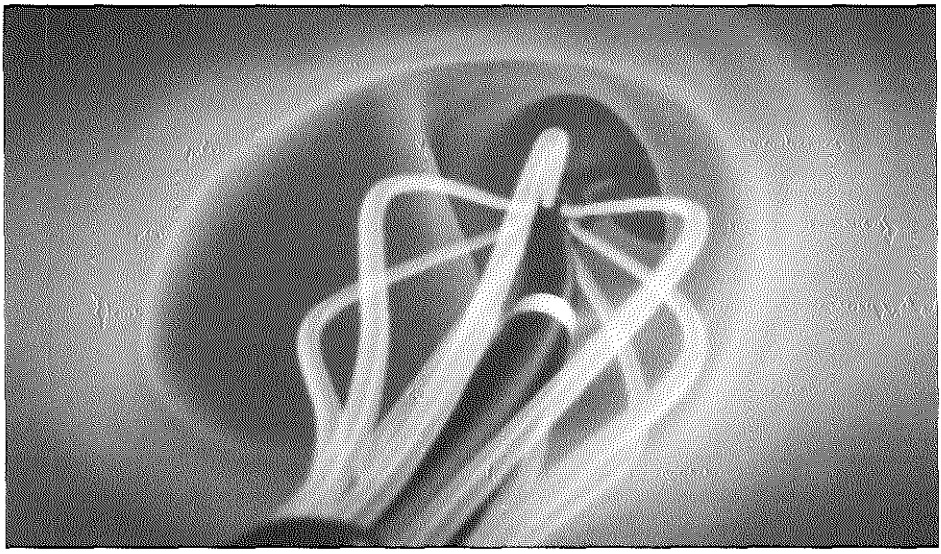

Figure 5. vPredict™ optical catheter system (OCS). This catheter has 8 optical fibers that deliver infrared light to the vessel wall and captures a portion of the reflected light for spectral analysis. Image courtesy of Prescient Medical, Inc

In aortic and coronary artery autopsy specimens, the ability of the technique to identify lipid-rich TCFA through blood has been confirmed (92). A catheter-based system has been developed to address the challenges— of access to the coronary artery, blood, motion, and the need to scan—that must be overcome for use in patients. Initial clinical experience in six patients with stable angina demonstrates that high-quality NIR spectra can be safely obtained (93). Additional studies are planned to validate the ability of the technique to identify lipid-rich coronary artery plaques and ultimately link chemical characterization with subsequent occurrence of an ACS (94,95).

3. IMAGING OF CORONARY STENTS

Intravascular Ultrasound radiofrequency analysis: Virtual Histology

Intravascular ultrasound– virtual histology classifies stent struts as "dense calcium" (DC) and "necrotic core" (NC). We applied this property to follow-up the degradation of a bioabsorbable stent by measuring the temporal changes in IVUS-VH characteristics. 27 consecutive patients treated with a single bioabsorbable everolimus-eluting stent (BVS, Abbott Laboratories, IL USA) in simple lesions were imaged with IVUS-VH after predilation (pre-stenting cohort of 13

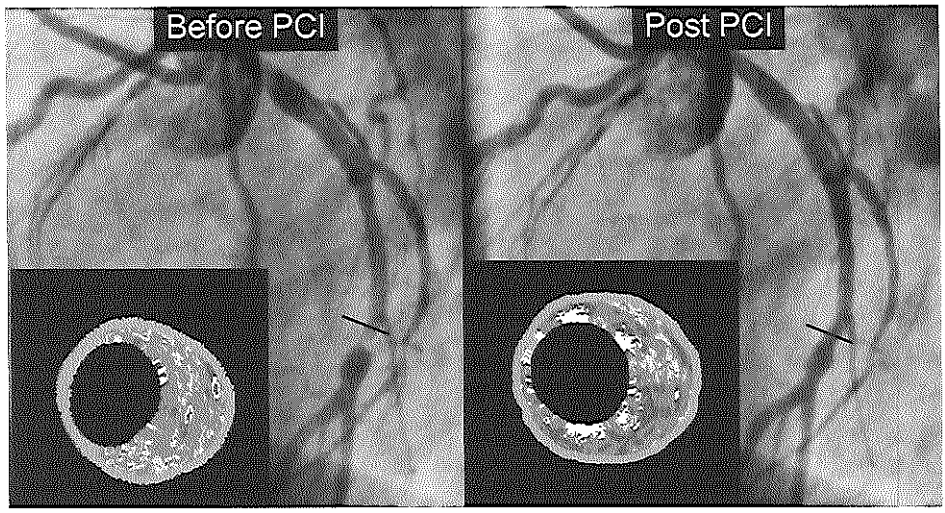

Figure 6. IVUS-virtual histology in stented segments. In the left hand side, a coronary angiogram of the left coronary system shows on the distal segment of the left circumflex artery an eccentric lesion. A pre-stenting virtual histology (VH) frame showed a fibrotic type of plaque (location of VH frame is indicated by a black line). On the right hand side, the post-stenting VH frame is depicted. Of note, at the lumen and surrounding areas an increase in the amount of "dense calcium" and "necrotic core" is observed. This is due to the presence of stent struts that are misclassified by VH. PCI, percutaneous coronary intervention.

pts), post-stenting and again following 6 months. There was an increase in absolute "dense calcium" and "necrotic core" by 297% and 256% respectively from pre- to post-stenting. Overall, patients (n=27) with post-stenting and follow-up VH showed a significant decrease in "dense calcium" (28.3% vs. 20.9, p<0.001). Individually, in 21 out of 27 patients, there was a regression in the "calcified" pattern. Although not significantly, "necrotic core" content also decreased (22.4% vs. 20.3, p=0.227). In turn, both fibro-fatty and fibrous tissue increased (5.0% vs. 7.4, p=0.024 and 44.3% vs. 51.4%, p=0.006 respectively). In conclusion, the quantitative assessment of the IVUS-VH changes at 6 months suggests a reduction of the DC compatible with early struts alteration of the BVS. (**figure 6**).

Optical coherence tomography

OCT permits the detailed assessment of stents and their relation to the vessel wall, both immediately following implantation and, at follow-up. Furthermore, OCT also allows the quantification of neointimal tissue surrounding each individual stent strut. Unlike bare metal stents (BMS), which develop circumferential coverage with an average thickness of 500μm or more, well visualized with IVUS and angiography, (96) drug-eluting stents (DES) delay and prevent this hyperplastic

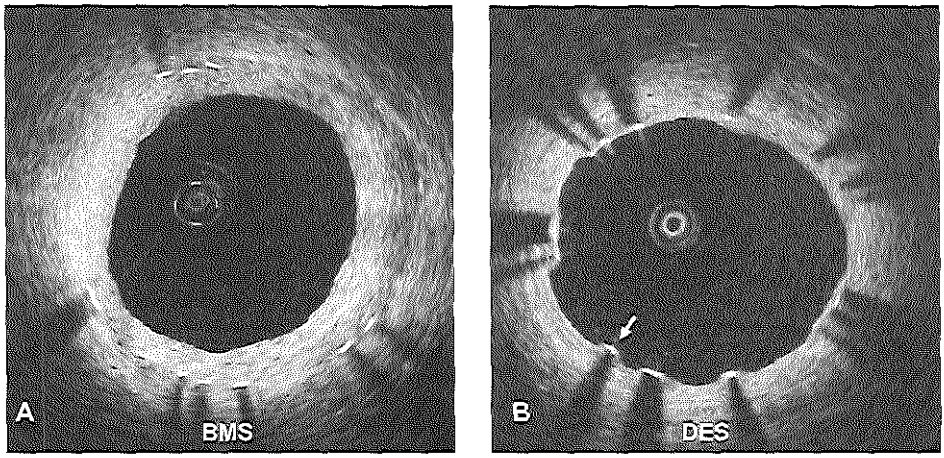

Figure 7. OCT and stent. Panel A: Demonstrates the optical coherence tomography (OCT) imaging of a bare metal stent 4 months following implantation. The circumferential tissue struts are visible with shadowing induced by the metal. The neointimal tissue measured between 140 and 220 microns in thickness. Panel B: OCT imaging of a drug-eluting stent (DES) at 4 months follow-up showing the circumferential struts with a very thin neointimal layer (10-40 microns thick). The arrow indicates a strut with no visible tissue coverage

response so that the average late lumen loss can be as low as 0.1 or 0.2mm, (97,98) which means the amount of intimal tissue will not be detectable with IVUS. (96)

Several small studies have recently been published highlighting the application of OCT in the detection of stent tissue coverage at follow-up. Matsumoto et al (99) studied 34 patients following sirolimus-eluting stent (SES) implantation. The mean neointima thickness was 52.5 microns, and the prevalence of struts covered by thin neointima undetectable by IVUS was 64%. The average rate of neointima-covered struts in an individual SES was 89%. Nine SES (16%) showed full coverage by neointima, whereas the remaining stents had partially uncovered struts.(99) Similarly, Takano et al (100) studied 21 patients (4,516 struts) 3 months following SES implantation. Rates of exposed struts and exposed struts with malapposition were 15% and 6%, respectively. These were more frequent in patients with ACS than in those with non-ACS (18% vs 13%, $p < 0.0001$; 8% vs 5%, $p < 0.005$, respectively). The ability of OCT to image at high resolution is the major advantage over IVUS and it also affords the potential to quantify the amount of neointimal tissue formed over struts, an application which remains elusive for a technique like angioscopy. OCT is now also being incorporated in more and more clinical stent trials with the goal of assessing neointimal tissue coverage, an important potential surrogate marker for late thrombosis. (101,102) (**figure 7**)

CONCLUSION

Several invasive imaging techniques are currently under development to detect vulnerable coronary plaques in human coronary arteries *in vivo*. To date however, none of the techniques described above have been sufficiently validated and, more importantly, they have not demonstrated a sound and reproducible ability to predict future adverse cardiac events. Intravascular palpography and virtual histology, based on conventional IVUS catheters, appear to be very promising and their predictive role is presently under investigation in a large international trial.

Very rigorous and well-designed studies are compelling for defining the role of each imaging modality. Non-invasive techniques and the assessment of humoral and genetic factors comprise complementary and important tools in this direction.

At present, the main purpose of all these evolving techniques is to improve our understanding of atherosclerotic disease and to define its natural history. Ultimately, the aim is to identify patients at high risk for future cardiovascular events and to evaluate the benefits from either local or systemic therapeutic interventions.

REFERENCES

1. Goldstein JA, Demetriou D, Grines CL, Pica M, Shoukfeh M, O'Neill WW. Multiple complex coronary plaques in patients with acute myocardial infarction. N Engl J Med 2000;343:915-22.
2. Waxman S, Ishibashi F, Muller JE. Detection and treatment of vulnerable plaques and vulnerable patients: novel approaches to prevention of coronary events. Circulation 2006;114:2390-411.
3. Kolodgie FD, Burke AP, Farb A, et al. The thin-cap fibroatheroma: a type of vulnerable plaque: the major precursor lesion to acute coronary syndromes. Curr Opin Cardiol. 2001;16:285-92.
4. Burke AP, Farb A, Malcom GT, Liang YH, Smialek J, Virmani R. Coronary risk factors and plaque morphology in men with coronary disease who died suddenly. N Engl J Med 1997;336:1276-82.
5. Virmani R, Kolodgie FD, Burke AP, Farb A, Schwartz SM. Lessons from sudden coronary death: a comprehensive morphological classification scheme for atherosclerotic lesions. Arterioscler Thromb Vasc Biol 2000;20:1262-75.
6. Moreno PR, Falk E, Palacios IF, Newell JB, Fuster V, JT. F. Macrophage infiltration in acute coronary syndromes. Implications for plaque rupture. Circulation 1994; 90:775-8.
7. Ross R. Atherosclerosis -- An Inflammatory Disease. N Engl J Med 1999;340:115-126.
8. Loree HM, Kamm RD, Stringfellow RG, RT. L. Effects of fibrous cap thickness on peak circumferential stress in model atherosclerotic vessels. Circ Res 1992;71: 850-8.
9. Richardson PD, Davies MJ, GV. B. Influence of plaque configuration and stress distribution on fissuring of coronary atherosclerotic plaques. Lancet 1989;2:941-4.
10. Cheruvu PK, Finn AV, Gardner C, et al. Frequency and distribution of thin-cap fibroatheroma and ruptured plaques in human coronary arteries: a pathologic study. J Am Coll Cardiol 2007;50:940-9.
11. Kolodgie FD, Virmani R, Burke AP, et al. Pathologic assessment of the vulnerable human coronary plaque. Heart 2004;90:1385-91.
12. Virmani R, Burke AP, Kolodgie FD, Farb A. Vulnerable plaque: the pathology of unstable coronary lesions. J Interv Cardiol 2002;15:439-46.
13. Farb A, Burke AP, Tang AL, et al. Coronary Plaque Erosion Without Rupture Into a Lipid Core : A Frequent Cause of Coronary Thrombosis in Sudden Coronary Death. Circulation 1996;93:1354-1363.
14. Arbustini E, Dal Bello B, Morbini P, et al. Plaque erosion is a major substrate for coronary thrombosis in acute myocardial infarction. Heart 1999;82:269-272.
15. Virmani R, Kolodgie FD, Burke AP, Farb A, Schwartz SM. Lessons From Sudden Coronary Death : A Comprehensive Morphological Classification Scheme for Atherosclerotic Lesions. Arterioscler Thromb Vasc Biol 2000;20:1262-1275.
16. Kolodgie FD, Gold HK, Burke AP, et al. Intraplaque Hemorrhage and Progression of Coronary Atheroma. N Engl J Med 2003;349:2316-2325.

17. Mizuno K, Satomura K, Miyamoto A, et al. Angioscopic evaluation of coronary-artery thrombi in acute coronary syndromes. N Engl J Med 1992;326:287-291.
18. Sherman CT, Litvack F, Grundfest W, et al. Coronary angioscopy in patients with unstable angina pectoris. N Engl J Med 1986;315:913-919.
19. de Feyter PJ, Ozaki Y, Baptista J, et al. Ischemia-Related Lesion Characteristics in Patients With Stable or Unstable Angina : A Study With Intracoronary Angioscopy and Ultrasound. Circulation 1995;92:1408-1413.
20. Kubo T, Imanishi T, Takarada S, et al. Assessment of culprit lesion morphology in acute myocardial infarction: ability of optical coherence tomography compared with intravascular ultrasound and coronary angioscopy. J Am Coll Cardiol 2007; 50:933-9.
21. Thieme T, Wernecke KD, Meyer R, et al. Angioscopic evaluation of atherosclerotic plaques: validation by histomorphologic analysis and association with stable and unstable coronary syndromes. J Am Coll Cardiol 1996;28:1-6.
22. Ueda Y, Ohtani T, Shimizu M, Hirayama A, Kodama K. Assessment of plaque vulnerability by angioscopic classification of plaque color. Am Heart J 2004;148:333-5.
23. Takano M, Mizuno K, Okamatsu K, Yokoyama S, Ohba T, Sakai S. Mechanical and structural characteristics of vulnerable plaques: analysis by coronary angioscopy and intravascular ultrasound. J Am Coll Cardiol 2001;38:99-104.
24. Lehmann KG, Oomen JA, Slager CJ, deFeyter PJ, Serruys PW. Chromatic distortion during angioscopy: assessment and correction by quantitative colorimetric angioscopic analysis. Cathet Cardiovasc Diagn 1998;45:191-201.
25. Smits PC, Pasterkamp G, de Jaegere PP, de Feyter PJ, Borst C. Angioscopic complex lesions are predominantly compensatory enlarged: an angioscopy and intracoronary ultrasound study. Cardiovasc Res 1999;41:458-64.
26. Nair A, Kuban BD, Tuzcu EM, Schoenhagen P, Nissen SE, Vince DG. Coronary Plaque Classification With Intravascular Ultrasound Radiofrequency Data Analysis. Circulation 2002;106:2200-2206.
27. Nasu K, Tsuchikane E, Katoh O, et al. Accuracy of In Vivo Coronary Plaque Morphology Assessment: A Validation Study of In Vivo Virtual Histology Compared With In Vitro Histopathology. Journal of the American College of Cardiology 2006;47: 2405-2412.
28. Nair A MP, Kuban BD, Vince DG. Automated coronary plaque characterization with intravascular ultrasound backscatter: ex vivo validation. Eurointervention 2007;3: 113-130.
29. Rodriguez-Granillo GA, Aoki J, Ong AT, et al. Methodological considerations and approach to cross-technique comparisons using in vivo coronary plaque characterization based on intravascular ultrasound radiofrequency data analysis: insights from the Integrated Biomarker and Imaging Study (IBIS). Int J Cardiovasc Intervent 2005;7:52-8.
30. Kaaresen K. Deconvolution of sparse spike trains by iterated window maximization. IEEE Trans Signal Process 1997;45:1173-1183.
31. Kaaresen K, Bolviken E. Blind deconvolution of ultrasonic traces accounting for pulse variance. IEEE Trans Ultrason Ferroelectr Freq Control 1999;46:564-573.
32. Rodriguez-Granillo GA, Garcia-Garcia HM, Mc Fadden EP, et al. In Vivo Intravascular Ultrasound-Derived Thin-Cap Fibroatheroma Detection Using Ultrasound

Radiofrequency Data Analysis. Journal of the American College of Cardiology 2005;46:2038-2042.
33. Wang JC, Normand SL, Mauri L, Kuntz RE. Coronary artery spatial distribution of acute myocardial infarction occlusions. Circulation 2004;110:278-84.
34. Rioufol G, Finet G, Ginon I, et al. Multiple Atherosclerotic Plaque Rupture in Acute Coronary Syndrome: A Three-Vessel Intravascular Ultrasound Study 10.1161/01.CIR.0000025609.13806.31. Circulation 2002;106:804-808.
35. Burke AP, Farb A, Malcom GT, Liang Y, Smialek J, R V. Coronary Risk Factors and Plaque Morphology in Men with Coronary Disease Who Died Suddenly. N Engl J Med 1997;336:1276-1282.
36. Lowder ML, Li S, Carnell PH, RP. V. Correction of distortion of histologic sections of arteries. Journal of Biomechanics;In Press, Corrected Proof.
37. Boyde A, Jones SJ, Tamarin A. Dimensional changes during specimen preparation for scanning electron microscopy. Scanning Electron Microsc 1977;1:507-18.
38. Fishbein MC, Siegel RJ. How big are coronary atherosclerotic plaques that rupture? Circulation 1996;94:2662-6.
39. Siegel RJ, Swan K, Edwalds G, Fishbein MC. Limitations of postmortem assessment of human coronary artery size and luminal narrowing: differential effects of tissue fixation and processing on vessels with different degrees of atherosclerosis. J Am Coll Cardiol 1985;5:342-6.
40. Nair A, Calvetti D, DG V. Regularized Autoregressive Analysis of Intravascular Ultrasound Data: Improvement in Spatial Accuracy of Plaque Tissue Maps. IEEE Trans Ultrason Ferroelectr Freq Control 2004;51:420-431.
41. Garcia-Garcia HM, Goedhart D, Schuurbiers JC, et al. Virtual histology and remodeling index allow in vivo identification of allegedly high risk coronary plaques in patients with acute coronary syndromes: a three vessel intravascular ultrasound radiofrequency data analysis. Eurointervention 2006;2:338-344.
42. Rodriguez-Granillo GA, McFadden EP, Valgimigli M, et al. Coronary plaque composition of nonculprit lesions, assessed by in vivo intracoronary ultrasound radio frequency data analysis, is related to clinical presentation. Am Heart J 2006;151: 1020-24.
43. Valgimigli M, Rodriguez-Granillo GA, Garcia-Garcia HM, et al. Distance from the ostium as an independent determinant of coronary plaque composition in vivo: an intravascular ultrasound study based radiofrequency data analysis in humans. Eur Heart J 2006;27:655-63.
44. Kawaguchi R, Oshima S, Jingu M, et al. Usefulness of virtual histology intravascular ultrasound to predict distal embolization for ST-segment elevation myocardial infarction. J Am Coll Cardiol 2007;50:1641-6.
45. Kawamoto T, Okura H, Koyama Y, et al. The relationship between coronary plaque characteristics and small embolic particles during coronary stent implantation. J Am Coll Cardiol 2007;50:1635-40.
46. Schaar JA, de Korte CL, Mastik F, et al. Characterizing Vulnerable Plaque Features With Intravascular Elastography. Circulation 2003;108:2636-2641.
47. Schaar JA, Regar E, Mastik F, et al. Incidence of High-Strain Patterns in Human Coronary Arteries: Assessment With Three-Dimensional Intravascular Palpography and Correlation With Clinical Presentation. Circulation 2004;109:2716-2719.

48. de Korte CL, Carlier SG, Mastik F, et al. Morphological and mechanical information of coronary arteries obtained with intravascular elastography; feasibility study in vivo. Eur Heart J 2002;23:405-13.
49. van Mieghem CAG, Bruining N, Schaar JA, et al. Rationale and methods of the integrated biomarker and imaging study (IBIS): combining invasive and non-invasive imaging with biomarkers to detect subclinical atherosclerosis and assess coronary lesion biology. The International Journal of Cardiovascular Imaging (formerly Cardiac Imaging) 2005;21:425-441.
50. Van Mieghem CA, McFadden EP, de Feyter PJ, et al. Noninvasive detection of subclinical coronary atherosclerosis coupled with assessment of changes in plaque characteristics using novel invasive imaging modalities: the Integrated Biomarker and Imaging Study (IBIS). J Am Coll Cardiol 2006;47:1134-42.
51. Regar E vLA, Serruys PW. Optical coherence tomography in cardiovascular research. London: Informa Healthcare 2007;ISBN 1841846112.
52. Huang D, Swanson EA, Lin CP, et al. Optical coherence tomography. Science 1991; 254:1178-81.
53. Brezinski ME, Tearney GJ, Bouma BE, et al. Imaging of coronary artery microstructure (in vitro) with optical coherence tomography. Am J Cardiol 1996;77:92-3.
54. Regar E, Schaar JA, Mont E, Virmani R, Serruys PW. Optical coherence tomography. Cardiovascular Radiation Medicine 2003;4:198-204.
55. Jang IK, Bouma BE, Kang DH, et al. Visualization of coronary atherosclerotic plaques in patients using optical coherence tomography: comparison with intravascular ultrasound. J Am Coll Cardiol 2002;39:604-9.
56. Patwari P, Weissman NJ, Boppart SA, et al. Assessment of coronary plaque with optical coherence tomography and high-frequency ultrasound. Am J Cardiol 2000;85: 641-4.
57. Yabushita H, Bouma BE, Houser SL, et al. Characterization of Human Atherosclerosis by Optical Coherence Tomography. Circulation 2002;106:1640-1645.
58. Brezinski ME, Tearney GJ, Weissman NJ, et al. Assessing atherosclerotic plaque morphology: comparison of optical coherence tomography and high frequency intravascular ultrasound. Heart 1997;77:397-403.
59. Kawasaki M, Bouma BE, Bressner J, et al. Diagnostic Accuracy of Optical Coherence Tomography and Integrated Backscatter Intravascular Ultrasound Images for Tissue Characterization of Human Coronary Plaques. Journal of the American College of Cardiology 2006;48:81-88.
60. Manfrini O, Mont E, Leone O, et al. Sources of Error and Interpretation of Plaque Morphology by Optical Coherence Tomography. The American Journal of Cardiology 2006;98:156-159.
61. Jang IK, Tearney GJ, MacNeill B, et al. In Vivo Characterization of Coronary Atherosclerotic Plaque by Use of Optical Coherence Tomography. Circulation 2005;111: 1551-1555.
62. Tearney GJ, Yabushita H, Houser SL, et al. Quantification of Macrophage Content in Atherosclerotic Plaques by Optical Coherence Tomography. Circulation 2003; 107:113-119.

63. MacNeill BD, Jang IK, Bouma BE, et al. Focal and multi-focal plaque macrophage distributions in patients with acute and stable presentations of coronary artery disease. Journal of the American College of Cardiology 2004;44:972-979.
64. Fuster V. Human lesion studies. Ann N Y Acad Sci 1997;811:207-24; discussion 224-5.
65. Casscells W, Hathorn B, David M, et al. Thermal detection of cellular infiltrates in living atherosclerotic plaques: possible implications for plaque rupture and thrombosis. Lancet 1996;347:1447-51.
66. Stefanadis C, Diamantopoulos L, Vlachopoulos C, et al. Thermal heterogeneity within human atherosclerotic coronary arteries detected in vivo: A new method of detection by application of a special thermography catheter. Circulation 1999;99: 1965-71.
67. Stefanadis C, Toutouzas K, Tsiamis E, et al. Increased local temperature in human coronary atherosclerotic plaques: an independent predictor of clinical outcome in patients undergoing a percutaneous coronary intervention. J Am Coll Cardiol 2001;37:1277-83.
68. Toutouzas K, Drakopoulou M, Mitropoulos J, et al. Elevated plaque temperature in non-culprit de novo atheromatous lesions of patients with acute coronary syndromes. J Am Coll Cardiol 2006;47:301-6.
69. Toutouzas K, Synetos A, Stefanadi E, et al. Correlation between morphologic characteristics and local temperature differences in culprit lesions of patients with symptomatic coronary artery disease. J Am Coll Cardiol 2007;49:2264-71.
70. Stefanadis C, Toutouzas K, Tsiamis E, et al. Thermal heterogeneity in stable human coronary atherosclerotic plaques is underestimated in vivo: the "cooling effect" of blood flow. J Am Coll Cardiol 2003;41:403-8.
71. Diamantopoulos L, Liu X, De Scheerder I, et al. The effect of reduced blood-flow on the coronary wall temperature: Are significant lesions suitable for intravascular thermography? 10.1016/S0195-668X(03)00440-8. Eur Heart J 2003;24:1788-1795.
72. ten Have AG, Gijsen FJ, Wentzel JJ, Slager CJ, van der Steen AF. Temperature distribution in atherosclerotic coronary arteries: influence of plaque geometry and flow (a numerical study). Phys Med Biol 2004;49:4447-62.
73. Verheye S, De Meyer GRY, Krams R, et al. Intravascular thermography: Immediate functional and morphological vascular findings. Eur Heart J 2004;25:158-165.
74. ten Have AG GF, Wentzel JJ, Slager CJ, Serruys PW, van der Steen AFW. Intracoronary thermography: heat generation, transfer and detection. Eurointervention 2005;1: 105-114.
75. Correia LC, Atalar E, Kelemen MD, et al. Intravascular magnetic resonance imaging of aortic atherosclerotic plaque composition. Arterioscler Thromb Vasc Biol 1997; 17:3626-32.
76. Larose E, Yeghiazarians Y, Libby P, et al. Characterization of human atherosclerotic plaques by intravascular magnetic resonance imaging. Circulation 2005;112:2324-31.
77. Blank A, Alexandrowicz G, Muchnik L, et al. Miniature self-contained intravascular magnetic resonance (IVMI) probe for clinical applications. Magn Reson Med 2005; 54:105-12.

78. Regar E HB, Grube E, Halon D, Wilensky R.L, Virmani R, Schneiderman J, Sax S, Friedmann H, Serruys PW, Wijns W. First-In-Man application of a miniature self-contained intracoronary magnetic resonance probe. A multi-centre safety and feasibility trial. Eurointervention 2006;2:77-83.
79. Schneiderman J, Wilensky RL, Weiss A, et al. Diagnosis of thin-cap fibroatheromas by a self-contained intravascular magnetic resonance imaging probe in ex vivo human aortas and in situ coronary arteries. J Am Coll Cardiol 2005;45:1961-9.
80. Quick HH, Ladd ME, Hilfiker PR, Paul GG, Ha SW, Debatin JF. Autoperfused balloon catheter for intravascular MR imaging. J Magn Reson Imaging 1999;9: 428-34.
81. Barkhausen J, Ebert W, Heyer C, Debatin JF, Weinmann HJ. Detection of atherosclerotic plaque with Gadofluorine-enhanced magnetic resonance imaging. Circulation 2003;108:605-9.
82. Kooi ME, Cappendijk VC, Cleutjens KB, et al. Accumulation of ultrasmall superparamagnetic particles of iron oxide in human atherosclerotic plaques can be detected by in vivo magnetic resonance imaging. Circulation 2003;107:2453-8.
83. Porto I, Selvanayagam J, Ashar V, Neubauer S, Banning AP. Safety of magnetic resonance imaging one to three days after bare metal and drug-eluting stent implantation. Am J Cardiol 2005;96:366-8.
84. Moreno PR, Muller JE. Identification of high-risk atherosclerotic plaques: a survey of spectroscopic methods. Current Opinion in Cardiology 2002;17:638-647.
85. Brennan JF, 3rd, Romer TJ, Lees RS, Tercyak AM, Kramer JR, Jr., Feld MS. Determination of human coronary artery composition by Raman spectroscopy. Circulation 1997;96:99-105.
86. Baraga JJ, Feld MS, Rava RP. In situ Optical Histochemistry of Human Artery Using Near Infrared Fourier Transform Raman Spectroscopy. PNAS 1992;89:3473-3477.
87. Romer TJ, Brennan JF, Fitzmaurice M, et al. Histopathology of Human Coronary Atherosclerosis by Quantifying Its Chemical Composition With Raman Spectroscopy. Circulation 1998;97:878-885.
88. Romer TJ, Brennan JF, Puppels GJ, et al. Intravascular Ultrasound Combined With Raman Spectroscopy to Localize and Quantify Cholesterol and Calcium Salts in Atherosclerotic Coronary Arteries. Arterioscler Thromb Vasc Biol 2000;20:478-483.
89. van de Poll SWE, Kastelijn K, Schut TCB, et al. On-line detection of cholesterol and calcification by catheter based Raman spectroscopy in human atherosclerotic plaque ex vivo. Heart 2003;89:1078-1082.
90. Wang J, Geng YJ, Guo B, et al. Near-infrared spectroscopic characterization of human advanced atherosclerotic plaques. J Am Coll Cardiol 2002;39:1305-13.
91. Marcu L, Fishbein MC, Maarek JM, Grundfest WS. Discrimination of Human Coronary Artery Atherosclerotic Lipid-Rich Lesions by Time-Resolved Laser-Induced Fluorescence Spectroscopy. Arterioscler Thromb Vasc Biol 2001;21:1244-1250.
92. Moreno PR, Lodder RA, Purushothaman KR, Charash WE, O'Connor WN, Muller JE. Detection of lipid pool, thin fibrous cap, and inflammatory cells in human aortic atherosclerotic plaques by near-infrared spectroscopy. Circulation 2002;105: 923-7.

93. Moreno PR, Muller JE. Identification of high-risk atherosclerotic plaques: a survey of spectroscopic methods. Curr Opin Cardiol 2002;17:638-47.
94. Caplan JD, Waxman S, Nesto RW, Muller JE. Near-infrared spectroscopy for the detection of vulnerable coronary artery plaques. J Am Coll Cardiol 2006;47:C92-6.
95. Waxman S, Ishibashi F, Caplan JD. Rationale and use of near-infrared spectroscopy for detection of lipid-rich and vulnerable plaques. J Nucl Cardiol 2007;14:719-28.
96. Tanigawa J, Barlis P, Di Mario C. Intravascular Optical Coherence Tomography: Optimisation of image acquisition and quantitative assessment of stent strut apposition. EuroIntervention 2007;3:128-136.
97. Morice MC, Serruys PW, Sousa JE, et al. A randomized comparison of a sirolimus-eluting stent with a standard stent for coronary revascularization. N Engl J Med 2002;346:1773-80.
98. Fujii K, Mintz GS, Kobayashi Y, et al. Contribution of stent underexpansion to recurrence after sirolimus-eluting stent implantation for in-stent restenosis. Circulation 2004;109:1085-8.
99. Matsumoto D, Shite J, Shinke T, et al. Neointimal coverage of sirolimus-eluting stents at 6-month follow-up: evaluated by optical coherence tomography. Eur Heart J 2006.
100. Takano M, Inami S, Jang IK, et al. Evaluation by optical coherence tomography of neointimal coverage of sirolimus-eluting stent three months after implantation. Am J Cardiol 2007;99:1033-8.
101. Finn AV, Joner M, Nakazawa G, et al. Pathological correlates of late drug-eluting stent thrombosis: strut coverage as a marker of endothelialization. Circulation 2007;115:2435-41.
102. Finn AV, Nakazawa G, Joner M, et al. Vascular responses to drug eluting stents: importance of delayed healing. Arterioscler Thromb Vasc Biol 2007;27:1500-10.

CHAPTER 1.2

Tissue Characterization Using Intravascular Radiofrequency Data Analysis: Consensus Recommendations for Acquisition, Analysis, Interpretation and Reporting.

Garcia-Garcia HM, Mintz G, Lerman A, Vince DG, Margolis MP, van Es GA, Morel MA, Nair A, Virmani R, Burke AP, Stone GW, Serruys PW.

EuroInterv.2009;4-online publish-ahead-of-print March 2009

EuroIntervention

Tissue characterisation using intravascular radiofrequency data analysis: recommendations for acquisition, analysis, interpretation and reporting

Héctor M. García-García[1], MD, MSc; Gary S. Mintz[2], MD, FACC; Amir Lerman[3], MD, FACC; D. Geoffrey Vince[4], PhD; M. Pauliina Margolis[4], MD, PhD; Gerrit-Anne van ES[5], PhD; Marie-Angèle M. Morel[5], BSc; Anuja Nair[4], PhD; Renu Virmani[6], MD, FACC; Allen P. Burke[6], MD, FACC; Gregg W. Stone[2], MD, FACC; Patrick W. Serruys[1]*, MD, PhD, FACC, FESC

1. Thoraxcenter, Erasmus MC, Rotterdam, The Netherlands; 2. Cardiovascular Research Foundation, New York, USA; 3. Mayo Clinic, Rochester, Minnesota, USA; 4. Volcano Corporation, Rancho Cordova, California, USA; 5. Cardialysis, BV, Rotterdam, The Netherlands; 6. CVPath Institute, Inc., Gaithersburg, Maryland, USA

Pauliina Margolis is vice president of scientific affairs and medical director of Volcano Corporation. She and her husband declare ownership interest. D. Geoffrey Vince and Anuja Nair are also Volcano Corporation employees. Gary Mintz declares ownership interest and is also a consultant of the company. Renu Virmani is consultant to Volcano Corporation and she has received research support from Volcano Corporation. Gregg Stone is consultant to Volcano Corporation. He has received research support from Boston Scientific and Abbott Vascular.

KEYWORDS
Imaging, patients, plaque, radiofrequency data analysis, ultrasonics

Abstract

This document suggests standards for the acquisition, measurement, and reporting of radiofrequency data analysis (virtual histology – VH) intravascular ultrasound (IVUS) studies. Readers should view this document as the authors' best attempt in an area of rapidly evolving investigation, an area where rigorous evidence is not yet available or widely accepted. Nevertheless, this document is based on known pathologic data as well as previously reported imaging data; where practical, this data is summarised in the current document, a document which will also include recommendations for future evolution of the technology.

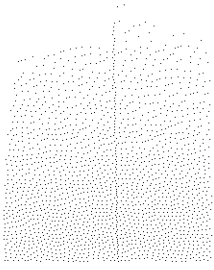

* *Corresponding author: Department of Cardiology, Erasmus Medical Center, Thoraxcenter, Ba583a, Erasmus MC, 's-Gravendijkwal 230, 3015 CE Rotterdam, The Netherlands*
E-mail: p.w.j.c.serruys@erasmusmc.nl

Introduction

There is increasing attention in the possibility that recognition and treatment of high-risk plaques would improve the progress made against coronary artery disease. To address the former issue, innovations in invasive imaging techniques – i.e. intravascular radiofrequency data analysis for tissue composition (Virtual Histology™) – may help to better understand coronary atherosclerosis. Indeed, Virtual Histology (VH) can potentially detect thin-capped fibroatheromas (TCFAs). In addition, the progression of the disease can also be followed-up. The technique has been validated *in vivo* and *ex vivo* and its reproducibility tested in patients with encouraging results. Therefore, several studies in different contexts have been already reported in the literature. Furthermore, large natural history studies and randomised controlled trials are ongoing in which the technique is being used. Thus, there is a need to establish standards on acquisition guidelines, analysis, definitions and reporting.

Description of the technique

VH-IVUS is a technique that allows tissue characterisation of vascular lesions. It is based upon the spectral analysis of the raw backscattered ultrasound data that has been correlated with vascular tissue types determined from histology. Once the spectral signature of four tissue types (fibrous tissue, fibro-fatty tissue, necrotic core [NC], and dense calcium) are determined, these signatures are programmed into software, either on the IVUS console or stand-alone software packages, for the analysis of patient data. Independent studies have demonstrated *in vivo* a relatively high level of accuracy and reproducibility of IVUS-VH in human arteries. The technique has been validated *in vivo*, utilising directional coronary atherectomy specimens[1], yielding predictive accuracies of up to 95% in non-ACS patients. Recent *ex vivo* studies[2] that validated VH images directly with the histopathology sections gave accuracies of up to 97%.

The reproducibility of the technology using same and different catheters has been studied using *ex vivo* IVUS pullbacks through excised human coronary arteries and *in vivo* from randomly selected patients undergoing elective percutaneous coronary intervention (PCI). No statistical differences were found between the pullbacks from the *ex vivo* or *in vivo* studies irrespective of whether the same or a different catheter was used[3]. VH is an IVUS based technology and as such is subject to the limitations of IVUS. The axial resolution of IVUS is approx 100µm and the lateral resolution is 250 µm. In addition, VH analyses data in blocks of 250 µm. Therefore, for example, detection of thin fibrous caps <65 µm in thickness, is below the resolution of the technology.

Screening and image acquisition

VH-IVUS is a technique that is specific to equipment and (as of this writing) solid-state IVUS catheters manufactured by Volcano (Rancho Cordova, CA, USA). VH-IVUS image acquisition requires ECG gating, and although the ECG is not recorded along with the VH-IVUS data, it is important to ensure that the ECG signal is generating only one frame per cardiac cycle ("R tops"). If there is no ECG recording (at this moment only detectable when acquired together with palpography), then the study should not be analysed.

Step by step procedure

In the past, Virtual Histology was acquired using the In-Vision Gold console and a 20 MHz Eagle Eye™ Gold catheter. Currently, the Volcano s5 Imaging System is used for the qualitative and quantitative evaluation of vascular morphology in the coronary arteries and vessels of the peripheral vasculature. One of its components, the Virtual Histology System, is intended to perform spectral analysis of RF ultrasound signals of vascular features during routine diagnostic ultrasound imaging examinations. Although two types of catheters can be used with this system, a 20 MHz electronic catheter or a 45 MHz mechanical catheter, the VH-IVUS for the 45 MHz is under development.

System description

The Volcano s5 system offers two options for IVUS acquisition: the s5 tower and the s5i (integrated) system.

The s5 tower – The hardware system consists of the system console that includes monitor a keyboard, and the patient interface module (PIM). The cabling connector at the PIM end allows for the PIM to be disconnected and replaced.

The s5i system – This system can be integrated into any of the available angiographic systems. The CPU is the heart of the s5i platform. The CPU can be located in different locations, such as in the control room, the patient exam room or in an equipment closet. The s5i control panel with a slide out keyboard can be mounted on a support bracket from a patient table DIN rail. It can also be placed on a table in the control room. A separate joystick option or a touch panel is available for the physician at the bedside if desired which will provide basic systems functions from the bedside.

Guidelines for acquisition

It is worth mentioning that before IVUS is performed, administration of between 100 and 300 µg of intracoronary nitroglycerin is highly desirable in order to avoid spasm of the vessel and minimise ischaemia. Consider patient's blood pressure before nitroglycerin is administered.

The detailed acquisition process is described in Table 1.

Because image acquisition is ECG-gated, while the pullback speed is constant, the number of frames/mm will vary with the heart rate. The higher the heart rate, the more data (number of frames per mm) is collected: the pullback speed should, ideally, be 0.5 mm/sec. At this pullback speed and depending on the heart rate, three to six image slices will be acquired per 1.5 mm segment. Studies must be acquired using motorised catheter pullback. Manual pullback is unacceptable and should not be done when acquiring VH-IVUS data. Volcano manufactures two motorised pullback devices: TrackBack II and R-100. The TrackBack II device is not the most recommended for VH-IVUS image acquisition because of the absence of steady grasp of the catheter (related, in part, to the lubricious nature of the catheter shaft itself) and the weakness of roller movement causing the catheter to be withdrawn unevenly. The R-100 device is the best pullback device currently available for the solid-state IVUS catheter. When imaging single stents of known length, 80-85% of stents measured using the R-100 device were within 20% of known length compared to only 65-70% of stent measured using the TrackBack II device[4]. Third party

Table 1. Step-by-step acquisition procedure

You must perform the following before you begin using the s5 system for imaging:

– Ensure that the Patient Interface Module (PIM) is attached

– Prepare the catheter in the same manner as for standard IVUS acquisition

– Have a DVD-R ready

VERY IMPORTANT: The ECG cable must be connected and capturing the R wave. The amplitude of the R wave must be at least 2X the amplitude of the T wave in order to ensure appropriate capture of data (the larger the "R" wave, the better).

– A red heart is visible on the upper right of the screen. It must be flushing at the speed of the patient's heart rate indicating the trigger to acquire the RF data. It is important to confirm this function in order to ensure the acquisition.

– The IVUS pullback can be performed viewing the grey scale IVUS modus. After the pullback, it is useful to switch to the virtual histology (VH) modus to confirm the quality of the data. VH is generated in real time and therefore it is immediately visible using preliminary automatic borders.

Step by step

1. Check the *settings*: Date, time, language, archive (what information you want included with save frames and recorded loops, e.g. measurements, annotations, graticules). VH-IVUS, click VH ON by default. ***Adjust the default opacity levels for each VH parameter.*** This allows you to customise the type of tissue colour to be displayed. For example, you may be most interested in necrotic (red) tissue. ***This last option is especially useful for clinical decision-makers who are colour blinded.*** Gain refers to the intensity of the ultrasound echoes. As Gain is increased, the echoes become more intense and the image becomes brighter. To change the Gain: 1. Open the **Adjust Image** dialog box. For IVUS Eagle Eye Gold catheter the range is 1-68 and the default gain is 50. ***Changes in the default gain settings will not affect tissue characterisation in VH.***

2. Enter patient information, press the **Patient** tab on the menu bar. The patient information dialogue box displays.

3. Select the **IVUS** tab on the interface user.

4. Plug the catheter into the PIM at the patient's bedside.

5. Place the catheter in the ostium of the vessel is going to be imaged.

6. Press the **Ringdown** button to eliminate ringdown artefact when used with an Eagle Eye catheter. Manual ringdown from the s5i Controller can be done for peripheral catheters. It is often desirable to perform Ring Down because phase array IVUS transducers produce an area of noise around the catheter. This noise is caused by transducer resonance after an ultrasound pulse. The Ring Down process normalises the transducer noise.

5. Position the catheter distal to the lesion of interest and implement the pullback device if desired. This last is recommended when volumetric measurements are required.

6. Press the **Record** button on user interface unit to begin recording.

The default mode for the Eagle Eye Gold catheter is "VH On" if the ECG trigger is available. VH will be visible in real time once the VH mode is selected. During the pullback the borders are defined on the longitudinal view and, depending on the configure uration of the settings, the VH analysis appears automatically.

The collection of VH data is interrupted/terminated once the ECG trigger stops and a message is displayed indicating the recording stopped due to a loss of the ECG trigger

7. During the pullback and at any time after, the **Bookmark** button can be used to mark locations of interest if desired.

8. Press the **Stop** button on user interface to end Recording.

9. Choose a pullback speed (1.0mm/sec, 0.5mm/sec or Manual).

10. Press **Play** to review the current Recording, or select from the Playback list button.

11. Longitudinal view for the s5 system displays a sagittal view of the blood vessel that offers additional information for lesion diagnosis, longitudinal measurements, and other diagnostic and treatment options.

motorised pullback devices require validation before being used for VH-IVUS acquisition. Currently, the Global VH Registry includes a combination of TrackBack II and R-100 acquired cases; IBIS-2 and PROSPECT studies used only the R-100 device. In general, pullbacks of the solid-state IVUS catheter appear to be less uniform in tortuous vessels, the left circumflex coronary artery, and in stented and calcified segments; therefore, consideration should be given to excluding tortuous or heavily calcified vessels.

Non-continuous image acquisition

During pullback, the catheter can stall or "stick" during image acquisition. In addition, typically when imaging very long lengths of the coronary artery, VH-IVUS data must be acquired in two overlapping segments because the length of the artery is greater than the capacity of the pullback device. Non-continuous or overlapping pullback sections should be deleted from the file, and the two residual ends stitched together electronically during image analysis. However, the cut-and-paste technique should be used only if there is one long segment of the pullback that is continuous (i.e. >10 mm) that contains clearly identifiable landmarks; no more than two segments can be joined together, and the cut-and-paste technique should not be used to extend the length of the analysis segment if there is a good, continuously imaged, 40 mm long segment that can be analysed. If the cut-and-paste technique is used, it is very important that the same (identical) landmarks (fiduciary points) at both ends of the reconstructed analysis segment be identified and used in the baseline and follow-up studies. It is equally important that the segment that is to be removed have its own identifiable proximal and distal fiduciary points. It is possible that the distribution of atherosclerosis will be skewed by the use of the cut-and-paste technique; therefore, this technique should not be used if the number of patients in the study is small. If cutting and pasting has taken placed during the process, this should be described in the methodology.

ECG or zoom setting problems

Because VH-IVUS requires ECG-gating with one image slice per cardiac cycle, it is recommended that the software be modified so that at the time of recording and analysis, the ECG signal is clearly visible. It is essential that the ECG leads be connected to the patient

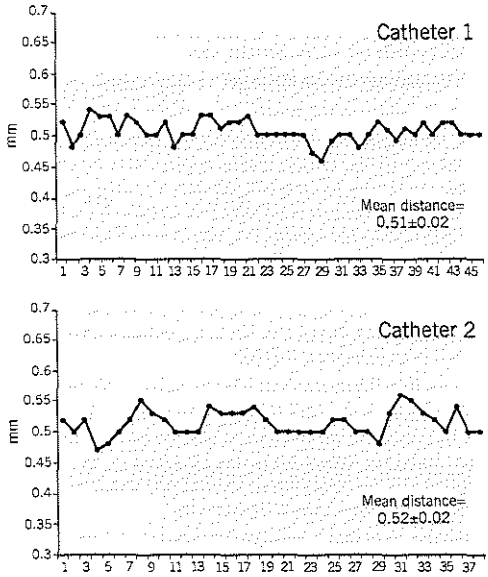

Figure 1. This patient was imaged in the same region with two different catheters during the same procedure. The graphs show all the frames acquired (x axis) and in the y axis the distance between them is given. Small variations in the intervals were observed.

such that a good ECG tracing is obtained and output to the IVUS system (Figure 2). The R wave must be at least 2X the amplitude of the T wave in order to ensure appropriate capture of data (the larger the "R" wave, the better).

The zoom factor should NOT be changed during pullback. To ensure that the entire circumference of the artery is imaged

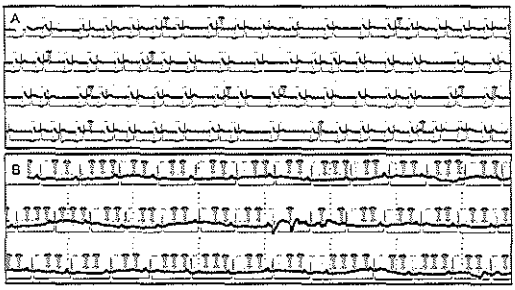

Figure 2. This figure shows the heart beats recorded during VH-IVUS acquisition (in this case palpography was also recorded simultaneously). In black, the ECG signal; in purple the "R" top marker; in green and red the acquired VH-IVUS frames. The blue line indicates the segmentation per heart beats based on the blood pressure signal (blood pressure curve not shown). In panel A, a quasi-normal ECG-gating acquisition is seen, the VH-IVUS frames (green markers) were constantly acquired throughout the pullback. Only few extra VH-IVUS non-"R"-top related were acquired (red markers). In panel B, due to a bad ECG signal the ECG gating was poor. This graph has been created by Frits Mastik at Erasmus Medical Center.

throughout its length, the proximal part of the vessel should be imaged while inserting the catheter in order to set the zoom factor. Gain settings do not influence VH-IVUS data and analysis and can be adjusted during pullback. Eventually, segments with an inadequate ECG, incorrect triggering, or with the media "out of the image" are unreliable and should not be analysed.

Segment lengths

There is no upper limit to the length of artery that can be assessed using VH-IVUS. It is limited only by the memory (or hard disk space) of the instrument and the capacity of the pullback device.

Scrambling of image slices

Scrambling of the image slices occurs because of antegrade / retrograde motion of the transducer during systole and diastole. In sheath-based, mechanical IVUS catheters, this averages 1.5 mm (range 0.5 to 5.5 mm)[4]. For this reason (as well as because of pullback issues), the following is recommended.

Up to three consecutive scramble slices should be deleted from the file ("ignored frame"), and the two residual ends stitched together electronically during image analysis. To this end, clear anatomical landmarks, such as side-branches, must be taken into account to recognise the scramble frames.

Vessel-specific limitations

It is often difficult to image the very proximal segment of the RCA because the guiding catheter is in the ostium. Even the conus branch is frequently covered by the guiding catheter. One option is to disengage the guiding catheter, taking care not to introduce too much tension into the coaxial system. Another option is to use a distal side-branch as the primary, fiduciary landmark. The priority for the fiduciary point when imaging the RCA should be the aorto-ostial junction, then the conus branch or a proximal atrial branch, and finally a distal side branch.

A similar problem exists when imaging the left main (LM). However, it is easier to disengage the guiding catheter from the LM while maintaining catheter stability. It is recommended that the LAD or LCX be imaged first and then the guiding catheter disengaged to image the LM. The carina is the most recommended fiduciary point.

Contours

There are only two reproducible borders (contours) in non-stented arteries: the external elastic membrane (EEM) and the lumen. Once the borders are traced, there will be a VH-IVUS classification of all structures within this region of interest. Therefore, accurate contour detection is critical. While there is a "flare" (ring down artefact) around the catheter, the lumen contour must be drawn away from this flare (Figure 3).

On the current VH-IVUS display, the grey contour representing the media can occupy up to 40% of the plaque area, although this area can be subtracted to obtain only the VH-IVUS plaque and its four tissue types; it was built into the display as a landmark denoted the outer edge of the vessel. Histologically, the "normal" media is 250 microns thick, but it is frequently destroyed during various pathologic processes including atherosclerosis. Media thickness

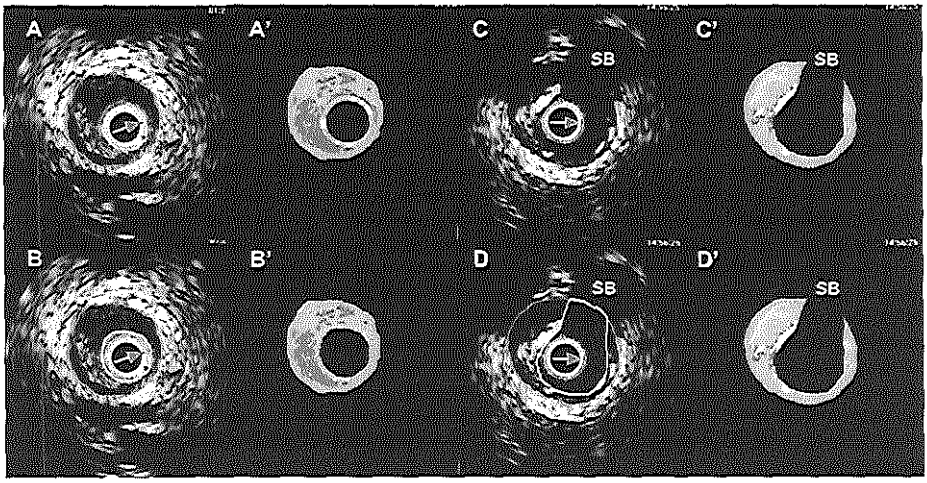

Figure 3. Panels A and A' show that the lumen border was drawn halfway into the flare (ring down artefact) of the catheter (yellow circle), in the VH frame this was misclassified as dense calcium. Panels B and B' show the recommended approach to draw the lumen border, away from the flare of the catheter. Panels C and D show the proposed method to draw the contours at side-branches. Luminal contour (yellow line) should be drawn just beyond the vessel contour, so that in the VH-IVUS this appears as an empty space. SB, side-branch.

cannot be measured using either greyscale or VH-IVUS imaging. Because 1) media thickness is variable, 2) the contours for greyscale IVUS, VH-IVUS, and other derived techniques such as palpography should be the same, and 3) the plaque cross-sectional area measured by greyscale IVUS, VH-IVUS, and other derived technologies should also be the same. New software modifications will allow the display with or without the grey contour for media.

Side branches

Cross-sectional image slices containing a side-branch should not be ignored or deleted from the VH-IVUS analysis (unless the side-branch opening is > 90 degrees). Nevertheless, because side-branch containing cross-sections do not display the artery as a "circle," some rules are necessary for defining the contours of the EEM and lumen 1) The EEM contour should be interpolated as to follow the pre- and post-side branch frames EEM morphology. 2) The lumen contour should be drawn just beyond the EEM contour to avoid computation of tissue types and to create in the VH-IVUS images an empty area indicating the position of the side-branch (Figure 3).

Thrombus

Currently, there is no VH-IVUS classification for thrombus. It is not clear when or if such a classification will emerge because thrombi evolve and develop over time so that a single classification for thrombus may never be possible. Work is ongoing for identification of fresh thrombus; however, identification of late thrombus appears to be more difficult. With higher frequency greyscale IVUS, the real-time, continuously changing appearance of a clot during imaging is a useful criterion for the presence of a thrombus. However, even with 40/45 MHz transducers, the sensitivity/specificity of detecting thrombus is low[6]; and with 20 MHz and ECG gating used for VH-IVUS, temporal resolution is lost along with many of the subjective criteria of thrombus. Thrombus is misclassified as fibrous or fibrofatty by VH-IVUS[7]. However, it is advisable that the luminal border should be drawn to include the thrombus as part of the plaque for the following reasons (Figure 4): 1) there is no consistent border between thrombus and plaque that would clearly separate

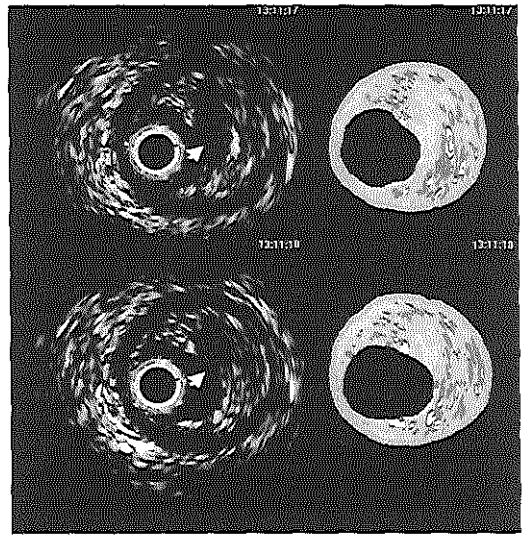

Figure 4. Two consecutive frames showing a ruptured plaque in a patient with an acute coronary syndrome. The luminal contour (not shown to allow visualisation of the discontinuity area of plaque surface) should be drawn including the cavity (white arrow) in the analysis.

thrombus from plaque and allow quantification of just the plaque. 2) Thrombus is a moving target, changing with age. 3) Mural and intramural thrombus is even more difficult to detect than intraluminal thrombus and impossible to quantify. 4) Lumen dimensions (and, therefore, stenosis severity) are affected by the presence of thrombus. 5) When/if a classification for thrombus is developed, it will only be necessary to reprocess the images, not to redraw the lumen contours. However, it is recommended that lesions suspected of containing thrombus be flagged for future study and reanalysis.

Pathological plaque characteristics

Plaque rupture

Based on post-mortem studies, there are three main causes of thrombosis in atherosclerotic coronaries. The most frequent cause of thrombosis is plaque rupture, which in the coronary arteries accounts for 65 to 70% of cases dying suddenly, plaque erosion accounts for 30 to 35% of cases and calcified nodule for another 2 to 5%.
The rupture of a thin fibrous cap over a necrotic core is the most common underlying mechanism of atherothrombosis[8]. Although pathologic features that predict plaque rupture are elusive, increasing size of the necrotic core, decreasing thickness of the cap, intraplaque haemorrhage, and concentration of macrophages within the cap are associated with plaque instability. As the plaque ruptures, the exposure of the tissue factor to flowing blood results in activation of the coagulation cascade with formation of a platelet-rich thrombus (Figure 5).

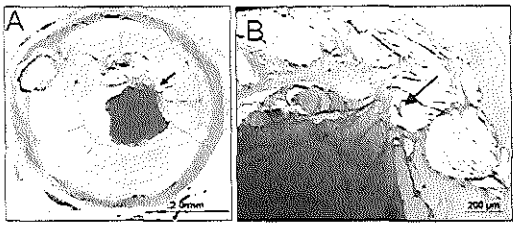

Figure 5. Coronary plaque rupture with overlying luminal thrombus. A shows the area of the thrombus and rupture site (arrow) and B shows the site of rupture (arrow) with the overlying thrombus at higher magnification.

In smaller calibre arteries such as the coronaries, the plaque rupture results in luminal thrombus but the necrotic core contents tend not to embolize distally; the core contents (free cholesterol crystals, cellular debris) intermingle with red cells, fibrin and platelets. The platelet thrombus is seen to embolize downstream in 40% of cases dying suddenly. However, post-mortem data implies that in large arteries, such as the aorta and carotid, excavation of the necrotic core underlying the rupture site is frequent, with creation of a deep filling defect or ulcer crater with superficial organization of thrombus (Figure 6). Because of high flow conditions in the carotid, the contents of the necrotic core along with platelet rich thrombus embolize. Using grey scale IVUS, the

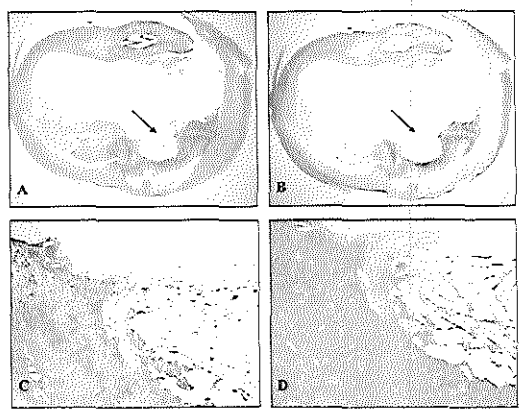

Figure 6. Ulcerated plaque, carotid artery. A. Haematoxylin eosin stain. B. Movat pentachrome stain showing the ulcerated plaque (arrow) and the various plaque components. C. Macrophage staining (CD68) showing macrophages (brown) close to the area of the ulceration and the underlying core. D. There is abundant fibrin within the ulcerated necrotic core.

site of the plaque rupture with disrupted fibrotic cap may appear as an empty cavity due to the space left from the embolised necrotic core and flow within the crater or the deep ulcer (Figure 6).
The greyscale IVUS definition of a plaque rupture is a cavity within the plaque that communicates with the lumen with or without an overlying fibrous cap fragment[9,10]. However, not all plaque ruptures are detected by greyscale IVUS because the cavity is often filled with thrombus and blood. Information from greyscale IVUS should be used to define the residual plaque and exclude the cavity from VH-IVUS analysis, when/if this is empty. When a plaque rupture is present on greyscale IVUS, this should be noted to imply previous presence of a thin capped fibroatheroma (TCFA) even though the NC may no longer be in contact with the lumen on VH-IVUS because of overlying thrombus.

Calcification

Focal calcification of atherosclerotic plaques is a nearly universal finding in advanced plaques and in elderly patients. Because several components of the plaque can calcify, there is significant heterogeneity of the morphology of calcium deposits within atherosclerotic lesions. This heterogeneity precludes general statements associated with plaque calcification and plaque stability/instability
It is believed that calcification is an active cellular process. Intimal smooth muscle cells calcify by the formation of membrane vesicles (so-called "matrix vesicles") which pinch off from the cell, calcify, and form a nidus for surrounding collagen calcification. This mechanism of calcification has been studied *in vitro* using cultures of vascular smooth muscle cells that have the propensity for calcification under certain conditions of the growth medium and in conditions of cell death (apoptosis). Other patterns of plaque calcification have not been studied in detail due to a lack of *in vitro* models. Matrix calcification, especially in lipid-rich pools (pathologic

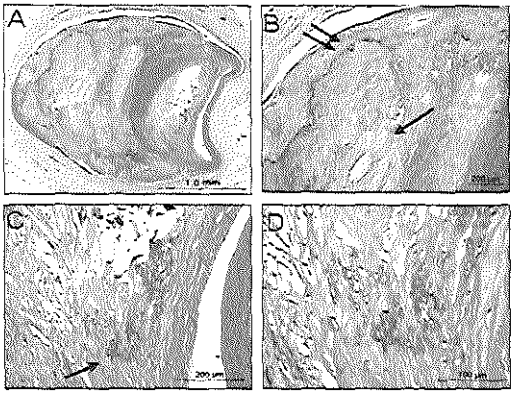

Figure 7. Stable plaque, coronary artery. A shows focal calcification (dark purple areas). B shows an area of sheet calcification (double arrow) of a collagen rich plaque where as the single arrow points to an area of necrotic core calcification. C illustrates as area of speckled calcification along a necrotic core. D is the area from C underneath the arrow at higher magnification showing single cell calcification.

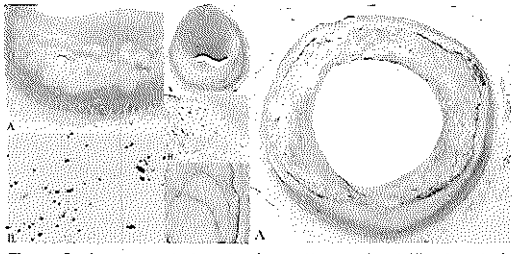

Figure 8. Coronary arteries showing patterns of calcification. Left: A. Pathologic intimal thickening. B. Calcium stain demonstrating microscopic calcifications (von Kossa). Middle: A. Fibrocalcific plaque, non-occlusive. B. Speckled calcification within an early necrotic core (Movat stain). C. Shows fibrous plaque calcification. Right: A. "Pipestem" calcification circumferentially around the vessel, with apparent stabilisation of the plaque.

Figure 9. Unstable calcification. A. Macrophage marker (CD 68) demonstrating macrophage infiltration of an early necrotic core. B. Higher magnification of spicule of calcification (arrow) within an area of necrotic core.

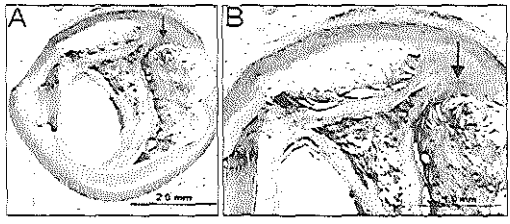

Figure 10. Coronary plaque showing healing plaque rupture. A and B at higher magnification show the site of previous plaque rupture where the fibrous cap is disturbed (arrow) and overlying healing thrombus. The rupture is almost fully healed towards the lumen.

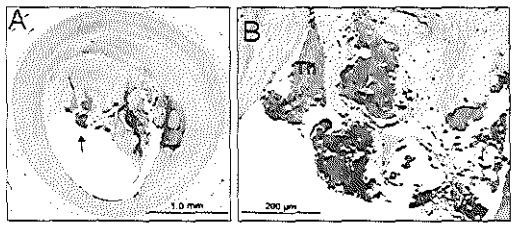

Figure 11. Nodular calcification in a coronary plaque. Note the calcification (A) some of which is nodular in nature in the area close to lumen. B is area underneath arrow in A at higher power showing nodular calcification with fibrin (dull red) in between nodules (bright red).

Intimal thickening) has been observed morphologically. Proteoglycans, especially decorin, may play a role in binding of phospholipids initiating extracellular calcification. In the absence of significant inflammation, calcification may have a "stabilising" effect as dense collagenous calcified plates radiographically seen as "blocks" of calcium. However, macrophages may also form a nidus for calcification, resulting in "speckled" calcium that is associated with plaque instability and plaque rupture. Calcification of necrotic cores is often partial and "speckled" radiographically. Necrotic cores, along with surrounding collagen and block of calcium, are more often seen in stable plaques (so-called fibrocalcific plaques, which are considered stable) (Figure 7 to 10). In plaque rupture calcification is most often seen as speckled or fragments of calcification which involve either necrotic core or fibrous tissue and calcification is observed in 80% of plaques that rupture. Finally, there is a form of calcification associated with calcified nodules with overlying platelet thrombus which has been termed "nodular calcification" (Figure 11). This form of calcification is most often associated with deposition of fibrin and even bone formation. Nodular calcification is an uncommon cause of luminal thrombosis in the coronary arteries. However, in the carotid arteries, nodular calcification is more common occurring in 5-10% of cases of thrombosis by histology.

There is an ongoing controversy whether VH-IVUS can see behind calcium. If there is a solid "rock" of calcium, then VH-IVUS cannot see behind the calcium. Solid "rocks" of calcium can be superficial (near the lumen) or deep (near the adventitia). Conversely, if the calcium is non-confluent with gaps of approximately 100 microns (typical with speckled calcium that is present in a necrotic core), then some signal is present even if it is attenuated. On VH-IVUS imaging large confluent calcium deposits can be solid "rocks" of calcium or represent multiple, nearby, calcium deposits. It is also

unclear how often there is a definable signal and how often there is mostly noise; the current hardware and software do not make this distinction. Therefore, in some cases, the signal behind calcium is mostly noise while in other cases it contains useful data. Studies are currently underway to determine when there is enough signal to accurately assess plaque composition behind calcium and when there is mostly noise and the signal ambiguous.

Nevertheless, in the case of both solid and speckled (or multifocal) calcium, shadowing caused by the presence of calcifications necessitates extrapolation of the EEM contours. Extrapolation can be assisted by longitudinal reconstruction of the cross-sectional images. The following are suggested guidelines. Extrapolation can be performed 1) if the arc of calcium is ≤90 degrees or 2) if the arc of calcium is 90-180 degrees, <5mm in length, and the "continuation" of the EEM evident using longitudinal views. Extrapolation should not be performed if the arc of calcium is >180 degrees and/or >5 mm in length. However, these are just guidelines, and the location of the transducer relative to the calcium also influence the validity of extrapolation. The presence and qualitative assessment of calcification may be prognostically important, even though quantification of its thickness and of the tissue behind the calcium are difficult.

Pathologic plaque progression

Pathology of lesion classification is based on autopsy observations which are based on static images. Although the natural history of coronary atherosclerosis is unknown, some believe that atherosclerotic lesion progression starts with pathologic intimal thickening in which lipid accumulates in areas rich in proteoglycans (lipid pools), but in absence of necrotic core. Others believe that the earliest change of atherosclerosis is the fatty streak, also called as intimal xanthoma.

The earliest lesion with a necrotic core is the fibroatheroma (FA), and this is the precursor lesion that may give rise to symptomatic heart disease. It is believed that rupture of an atherosclerotic plaque is the underlying cause of 70% of symptomatic disease. It has been shown in patients dying suddenly without prior symptomatic heart disease that at least 60% of cases will show prior rupture site or "healed plaque rupture" (Figure 10) suggesting that rupture of an atherosclerotic plaque may occur in the absence of symptoms. On the other hand, only 11% of ruptured plaques in patients dying sudden have a virgin rupture i.e., the first time that a plaque had ruptured. In the majority of cases, plaque rupture is silent, heals and leads to plaque progression through repetition of this cycle.

Pathological intimal thickening (PIT)

The pathological intimal thickening (Figure 12 and 13) is a poorly defined entity sometimes referred in the literature as "intermediate lesion". This type of plaque does not encroach the lumen and consists of intimal thickening composed of fibrous plaque with extracellular lipid and proteoglycans. True necrosis is not evident. The area overlying the lipid is rich in smooth muscle cells and may contain a variable number of macrophages and T lymphocytes. It has been demonstrated that in the coronaries the majority of erosions occur over areas of pathological intimal thickening giving rise to a clinically significant role for these lesion types.

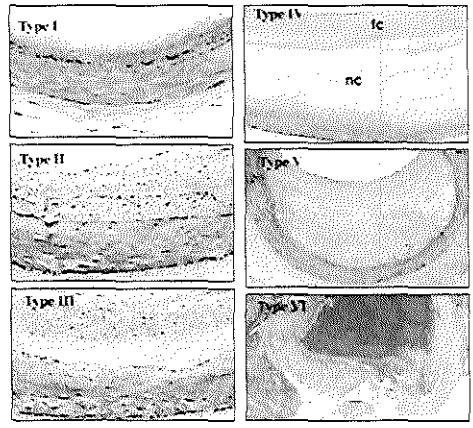

Figure 12. AHA plaque classification. (Stary HC. The histological classification of atherosclerotic lesions in human coronary arteries. In: Fuster V, Ross R, Topol E, eds. Atherosclerosis and Coronary Artery Disease.). fc: fibrous cap; nc: necrotic core

Fibrous cap atheroma (fibroatheroma)

This type of lesion is constituted by a large lipid-necrotic core (Figure 12 and 13) comprising large amounts of extra cellular lipid, cholesterol crystals, and necrotic debris, surrounded by a fibrous cap consisting principally of smooth muscle cells in a collagenous-proteoglycan matrix, with varying degrees of infiltration by macrophages and T lymphocytes, and a variable number of surrounding inflammatory cells surrounded also the lipid-necrotic core. This lesion, according to the AHA classification which distinguishes between lesion types IV and V on the basis of the development of complicating features, may progress and became highly calcified or develop complications such as mural haemorrhage.

Thin capped fibroatheroma (TCFA)

This lesion is characterised by a large necrotic core containing numerous cholesterol clefts (Figure 12 and 13). The overlying cap is thin and rich in inflammatory cells, macrophages and T lymphocytes with few smooth muscle cells. Plaques prone to rupture are those with decrease cap thickness, large lipid-necrotic core and severe inflammatory infiltrate A study done by Burke et al[21] has identified a cut-off value for cap thickness of <65 microns for vulnerable coronary plaque definition.

Healed lesions

Healed ruptures are characterised by a disrupted fibrous cap filled in by smooth muscle cells, proteoglycans, and collagen (Figure 12 and 13). Healed ruptures are best identified by picrosirius red staining, whereby newly synthesised type III collagen is seen overlying a ruptured fibrous cap consisting primarily of type I collagen. The matrix within the healed fibrous cap defect may consist of a proteoglycan-rich mass or a collagen-rich scar depending on the phase of healing. Lesions with healed ruptures may exhibit multi-layering of lipid and necrotic core, suggestive of previous episodes of thrombosis.

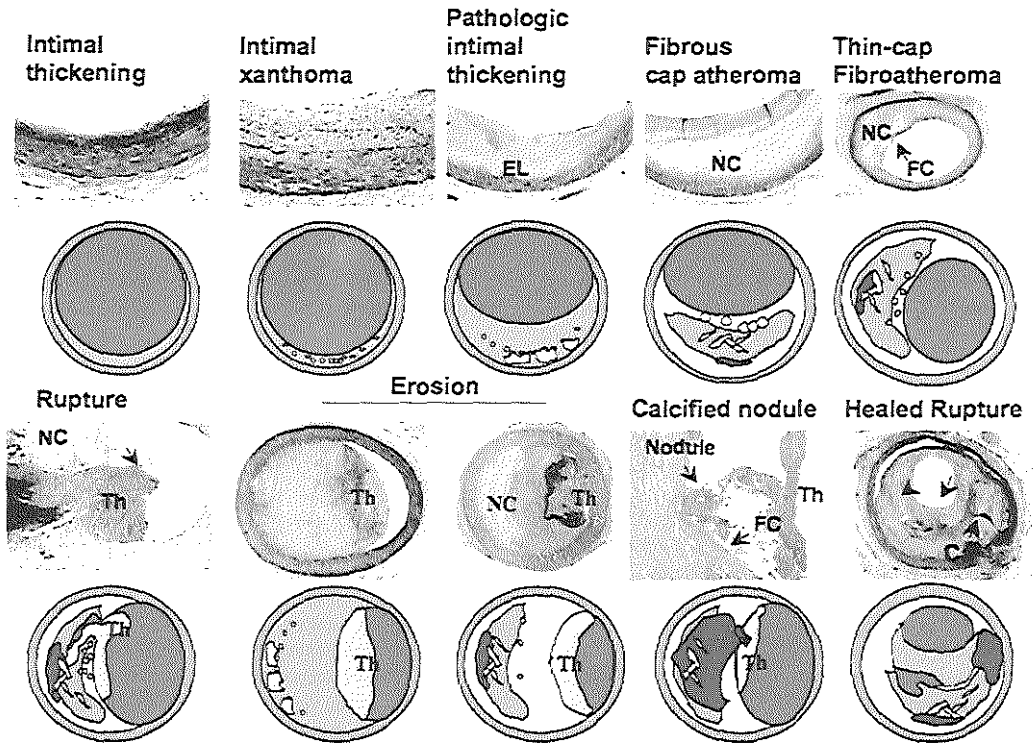

Figure 13. Modified AHA classification, Virmani et al, ATVB 2000; 20:1262-75. EL: extracellular lipid; nc: necrotic core; fc: fibrous cap; th: thrombus

Fibrocalcific lesions

Fibrotic plaques with extensive accumulations of calcium are called fibrocalcific plaques (Figure 12 and 13).

VH-IVUS lesion type or classification

Table 2 outlines the plaque and lesion types that are proposed based on the above pathologic data.

Confluence is important to minimise over reporting isolated islets or individual pixels of VH-IVUS detected necrotic core which can be artefacts. The term confluent is defined as a substantial area of necrotic core or dense calcium that is present in the VH-IVUS image as an aggregate indicative of the plaque type not just image 'noise.' This was determined based on observations from numerous VH-IVUS images and corresponding histology images, such that a 'confluent area' is equivalent to an area of approximately 10% of necrotic core. Two other important concepts are 1) the size of the major confluent necrotic core (area, volume, length, and arc) and 2) size of the major necrotic core in contact with the lumen (length and arc). IVUS derived TCFAs (VH-TCFA) or fibroatheromas can also be subclassified according to 1) the number of necrotic cores or the presence of multiple layers of necrotic core; 2) presence or absence of calcification and number of focal or layered calcific deposits (presumed evidence of previous rupture); and 3) plaque burden (or lumen compromise). Given any two-dimensional (2D) VH-IVUS image, the following text outlines a possible algorithm for lesion analysis.

Table 2. VH-IVUS proposed lesion types.

Lesion type	Brief description
Intimal Medial Thickening (IMT)	<600 μm of intima thickness
Pathological Intimal Thickening (PIT)	≥600 μm thickness for >20% of the circumference with FF >15%, and no confluent NC or DC
Fibrotic Plaque	Dominant FT and no confluent NC or DC
Fibrocalcific Plaque	>10% Confluent DC with no confluent NC
Fibroatheroma (FA)	>10% Confluent NC on three consecutive frames
Virtual Histology Thin Cap Fibroatheroma (VH-TCFA)	>10% Confluent NC on three consecutive frames and arc of NC in contact with the lumen for 36 degrees along lumen circumference

FT: fibrous tissue; FF: fibro-fatty tissue; ND: necrotic core; DC: dense calcium

The plaque thickness is first checked to determine if the VH-IVUS image represents intima-medial thickening (IMT) or a lesion. For this criterion to be satisfied, the plaque has to be greater than 360 µm thick for over 20% of the circumference covered by the plaque. For VH-IVUS images, this distance is calculated beyond the grey-coloured media area that is considered to be 250-350 µm, representing healthy media. Hence, the total cut-off distance is approximately 600 µm. Next, an area of confluent necrotic core or dense calcium is searched for in the image. Confluent necrotic core or confluent dense calcium can also be present together with their co-existence resulting in the formation of calcified fibroatheroma and calcified thin cap fibroatheroma categories. If a confluent necrotic core is found, its proximity to the lumen is determined to define whether the lesion is a FA or a VH-TCFA. The term confluent at the lumen is defined as a confluent necrotic core that is consistently present for at least 36 degrees along the circumference of the lumen. If the confluent necrotic core is not at the lumen, the plaque is simply a fibroatheroma. The addition of attached confluent-dense-calcium lends to the presence of either Ca fibroatheroma or Ca VH-TCFA dependent on the lumen confluency condition. If confluent necrotic core is absent but confluent dense calcium is present, the plaque is fibrocalcific. In absence of both confluent necrotic core and confluent dense calcium, the remaining categories are either PIT or fibrous plaque. Presence of >15% fibro-fatty component indicates PIT and <15% fibro-fatty component indicates fibrous plaque.

A plaque becomes a lesion when the plaque burden (plaque/EEM) exceeds 40% over three consecutive frames. Lesions separated by 5mm lengths of artery with a plaque burden <40% should be considered separate lesions. Lesions should be classified according to the worst-case scenario or highest risk lesion. We hypothesise that an "evolutionary" lesion classification will be, in order, IMT, PIT, Fibrotic plaque, Fibroatheroma, VH-TCFA, and (finally) Fibrocalcific (Figure 14). We also hypothesise that a classification in term of vulnerability will be different with VH-TCFA being highest risk plaque: IMT, PIT, Fibrotic, Fibroatheroma, and VH-TCFA. Thus, there should be different approaches for pharmacological versus prognostic versus interventional studies. The interventional cardiologist may be more concerned with plaque morphology that influences the procedure (ie. calcification, necrotic core-rich plaque), lesion preparation pre-intervention, acute complications post-intervention (plaque shifting, stent thrombosis), and final results. Pharmacologic or other natural history studies may be more interested in serial changes in plaque composition, lesion classification, and lesion vulnerability.

Stents

Currently, VH-IVUS has not been validated for metal stents, for intimal hyperplasia, for tissue surrounding and behind stent struts in general, and for the chronic effect of drug-eluting stent polymers. Metallic stent struts appear white surrounded by a red halo; thus, stent metal is artefactually included in the calculation of both calcium and necrotic core. However, from a quantitative point it would be interesting to develop a third (stent) contour with validation of stent metal and peri-stent tissue. This should be feasible because stent struts are small and the gaps between stent struts are large. For example, in the TAXUS-II study[12], there was a chronic increase in EEM dimensions; it would be interesting to know what type of tissue contributed to this process. It is recommended that frames containing stents being marked as containing a stent and that these frames be assessed visually, but not included in the VH-IVUS calculations similar to the approach recommended for heavy calcification (above).

However, a distinction should be made for bioabsorbable stents. Recently, the feasibility and safety of a bioabsorbable everolimus-

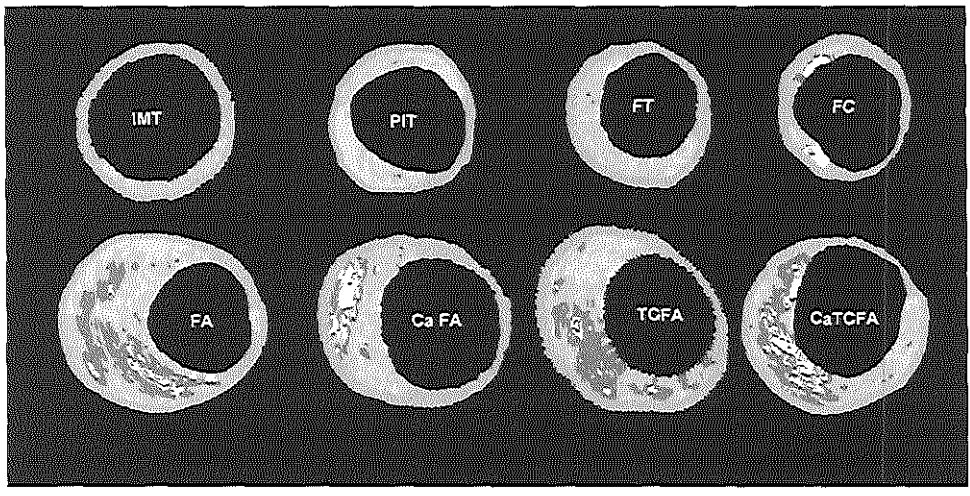

Figure 14. Examples of VH-IVUS images classified by a two-dimensional lesion analysis. (IMT) intimal medial thickening; (PIT) pathological intimal thickening; (FT) fibrotic plaque; (FC) fibrocalcific plaque; (FA) fibroatheroma and (caFA) calcified fibroatheroma; (VH-TCFA) Virtual Histology-thin cap fibroatheroma and (VH-caTCFA) Virtual Histology-calcified thin cap fibroatheroma.

eluting stent (BVS) was assessed. In a prospective, open-label study, 30 patients with a single de novo lesion that was suitable for treatment with a single BVS, were enrolled. Stent struts are classified as "dense calcium" (DC) and "necrotic core" (NC) by IVUS-VH. From pre- to post-stenting, in 13 patients imaged with VH (n=13), there was an increase in mean "DC" (9.8 vs. 25.4%, p=0.0002) and "NC" (15.5 vs. 30.5%, p=0.0002). Comparing post-stenting with six months follow-up (n=27), VH showed a decrease in "DC" (29.7% vs. 21.1%, p=0.0001). "NC" also decreased (26.9 vs. 21.5%, p=0.0027).

The quantitative assessment of the IVUS-VH changes at six months suggests early strut alteration of the BVS stent with reduction of radiofrequency backscattering. Thus, virtual histology helps in assessing the bioabsorption rate of such stents[13].

Core labs, analysis software, and their validation

Based on current experience with programs developed by individual laboratories, the following should be incorporated into an ideal software package.

1. Optimised automatic contour detection
2. Quantitative output of data along the longitudinal axis of the segment to include "Greyscale" parameters such as EEM, lumen, and plaque+media areas and remodeling
3. Absolute and relative VH-IVUS plaque components (in which the total of the four components equals the absolute "greyscale" plaque area)
4. Presence of "normal" or non-diseased cross-sections
5. Volumetric analyses
6. Automated targeted lesion classification software
7. Manual annotation – for example, lesion classification, evidence of plaque rupture on greyscale imaging, presence of a stent, presence of multiple necrotic cores, artefacts, presence of a non-diseased cross-section, etc.
8. Manual selection of reference segments for calculation of remodelling

Only one analysis software package should be used in a given study; unfortunately, this may result in not being able to switch to the latest, most efficient software when it becomes available.

Either phantoms or a standard set of cases be developed for validation of new software and new core laboratories. Inter and intra-observer reproducibility should include all sources of variation from image acquisition to core lab analysis: general precision/accuracy of the technique, 1st vs 2nd pullback, 1st vs 2nd catheter, one type of catheter vs another, 1st vs 2nd observer, and 1st vs 2nd core lab, 1st vs 2nd set of contours, and lesion classification.

Study-design related recommendations

Single point-in-time studies (transversal or observational studies)

Each artery should be divided into segments defined by proximal and distal fiduciary branches, most often side-branches. The shortest segment that should be analysed at one point in time is 1.5 mm within a >10 mm continuously imaged vessel segment and near to one or more definable fiduciary points that can be used for interpolation. The rationale for this recommendation is 1) a 1.5 mm segment will contain at least three consecutive frames at a pullback speed of 0.5 mm/sec (when heart rate is 60 bpm); 2) this is the average antegrade/retrograde catheter motion during systole / diastole; and 3) the Medis quantitative angiographic analysis system reports coronary artery lengths as short as 1.5 mm. Therefore, VH-IVUS can be referenced to the coronary angiogram using nearby sidebranches that can be identified on both studies. It is highly recommended that a picture of the angiogram be provided for comparative purposes. PROSPECT is analysing the three major epicardial arteries in 1.5 mm segments.

Serial studies (longitudinal or natural history studies)

The shortest segment that should be analysed on serial studies is 10 mm. It is also recommended that the zoom setting be the same for each of the serial studies. Because the number of frames/mm will vary with heart rate and because the heart rate may differ between two VH-IVUS studies, serial studies should use both a proximal and distal landmark to define the analysis segment; and the VH-IVUS data should be averaged on a per segment basis or reported as a normalised volume. (This is similar to what has been done for greyscale IVUS analysis of progression/regression.)

Vulnerable plaque studies

Because of angiographic studies documenting the distribution of acute coronary occlusions and because of greyscale IVUS studies documenting the location of ruptured plaques, it is recommended that long-term prognostic studies include VH-IVUS analysis of the proximal 40 mm of the LAD and LCX and the RCA down to the crux[14-18]. However, this may not always be possible or practical. Therefore, at the very least, the most proximal 30 mm of each of the three major epicardial arteries should be imaged. The US FDA recommends imaging 1) at least a 30 mm long non-stented segment of an untreated artery or 2) a 30 mm long non-stented segment of a treated artery that is at least 10mm removed from the stent edge. The minimum length of LM that should be imaged is 5mm or 50% of LM length. However, natural history studies in which the origin and morphology of vulnerable plaques were prospectively identified have not been completed. In the PROSPECT study the left main coronary artery and the proximal 6-8 cm of the three major epicardial coronary arteries have been imaged in >600 patients, with follow-up ongoing.

Reporting

VH-IVUS data can be reported per lesion, per segment, per vessel, and per patient (Table 3). On one hand, a study geared to providing prognostic information should aim at the most complete assessment of the coronary tree possible. The minimal segment to be analysed should be 1.5 mm. It is unclear whether such short segments of coronary tree are independent of each other in terms of VH classification. However, we assume that there is some degree of interdependence. Thus, there maybe a value in analysing the entire length of the coronary tree for statistical power. On the other hand, a study geared to assessing coronary intervention should focus in the lesion, itself.

Whenever possible, all VH-IVUS continuous data should be reported as continuous variables.

Table 3. VH-IVUS variables for reporting.

VH-IVUS
Lesion level
1. Lesion length
2. Lesion location
3. CASS segment (because a lesion can cover more than one CASS segment, the lesion should always be assigned to the more proximal CASS segment where the lesion is initiated)
4. Conventional greyscale IVUS parameters [external elastic membrane (EEM), lumen, plaque&media, plaque burden, eccentricity, and remodelling] at specified locations (i.e. the site of the minimum lumen area) as well as averaged over the entire lesion
5. Absolute and relative Virtual Histology (VH)-IVUS parameters [fibro-fatty (FF), fibrotic, necrotic core (NC), and dense calcium) at specified locations, averaged over the entire lesion, and reported as mean areas and/or as volumes
6. Lesion type and full description of necrotic core and calcification
7. Presence of bifurcation
8. Presence of stent
Segment level
1. Proximal and distal fiduciary branches
2. Segment length
3. Segment location
4. Absolute and relative VH-IVUS parameters (FF, fibrotic, NC, and dense calcium) averaged over the entire segment and reported as mean areas and/or as volumes
5. The 10 mm long worst section within this segment can also be reported separately
6. Lesions and their classification
7. Plaque free length
Vessel level
1. Proximal and distal fiduciary branch
2. Vessel length
3. Vessel location
4. Absolute and relative VH-IVUS parameters (FF, fibrotic, NC, and calcium) averaged over the entire vessel and reported as mean areas and/or as volumes
5. Lesions and their classification
6. Plaque free length
Patient level
1. Absolute and relative VH-IVUS parameters (FF, fibrotic, NC, and calcium) averaged over the entire vessel and reported as mean areas and/or as volumes
2. Lesions and their classification
3. Plaque free length

Greyscale IVUS

Greyscale and VH-IVUS data should be integrated. In addition to VH-IVUS, a complete report should also include full greyscale quantification: EEM, lumen, and plaque&media area; plaque burden (plaque&media divided by EEM); remodelling (lesion EEM compared to a pre-determined reference EEM); eccentricity (based on maximum and minimum plaque&media thickness); and calcium (arc, length, and location).

When assessing remodelling, the EEM CSA of a single, pre-specified lesion site cross-section should be compared to a pre-defined reference. For non-bifurcation lesions, it is recommended that the reference segment be the single frame (or three consecutive frames) with least plaque burden within the same segment as the lesion. If the lesion extends over more than one segment, then the single, pre-specified lesion site cross-section should be compared to the pre-defined reference within the same segment.

In the case of a bifurcation lesion, if the image slice with the minimum lumen area is proximal to the carina, then a proximal reference should be used to calculate remodelling. If the image slice with the minimum lumen area is distal to the carina, then a distal reference should be used to calculate remodelling.

Remodelling should be reported as a continuous plot over the length of the coronary segment based on the reference segments that are selected.

References

1. Nasu K, Tsuchikane E, Katoh O, Vince DG, Virmani R, Surmely JF, Murata A, Takeda Y, Ito T, Ehara M, Matsubara T, Terashima M, Suzuki T. Accuracy of in vivo coronary plaque morphology assessment: a validation study of in vivo virtual histology compared with in vitro histopathology. *J Am Coll Cardiol* 2006;47:2405-12.

2. Nair A MP, Kuban BD, Vince DG. Automated coronary plaque characterization with intravascular ultrasound backscatter: ex vivo validation. *Eurointerv* 2007;3:113-130.

3. Rodriguez-Granillo GA, Vaina S, García-García HM, Valgimigli M, Duckers E, van Geuns RJ, Regar E, van der Giessen WJ, Bressers M, Goedhart D, Morel MA, de Feyter PJ, Serruys PW. Reproducibility of intravascular ultrasound radiofrequency data analysis: implications for the design of longitudinal studies. *Int J Cardiovasc Imaging* 2006 Oct;22(5):621-31.

4. Tanaka K, Carlier SG, Mintz GS, Sano K, Liu X, Fujii K, de Ribamar Costa J Jr, Lui J, Moses JW, Stone GW, Leon MB. The accuracy of length measurements using different intravascular ultrasound motorized transducer pullback systems. *Int J Cardiovasc Imaging* 2007;23:733-8.

5. Arbab-Zadeh A, DeMaria AN, Penny WF, Russo RJ, Kimura BJ, Bhargava V. Axial movement of the intravascular ultrasound probe during the cardiac cycle: implications for three-dimensional reconstruction and measurements of coronary dimensions. *Am Heart J* 1999;138:865-72.

6. Kubo T, Imanishi T, Takarada S, Kuroi A, Ueno S, Yamano T, Tanimoto T, Matsuo Y, Masho T, Kitabata H, Tsuda K, Tomobuchi Y, Akasaka T. Assessment of culprit lesion morphology in acute myocardial infarction: ability of optical coherence tomography compared with intravascular ultrasound and coronary angioscopy. *J Am Coll Cardiol* 2007;50:933-9.

7. Nasu K, Tsuchikane E, Katoh O, Vince DG, Margolis PM, Virmani R, Surmely JF, Ehara M, Kinoshita Y, Fujita H, Kimura M, Asakura K, Asakura Y, Matsubara T, Terashima M, Suzuki T. Impact of intramural thrombus in coronary arteries on the accuracy of tissue characterization by in vivo intravascular ultrasound radiofrequency data analysis. *Am J Cardiol* 2008;101:1079-83.

8. Virmani R, Kolodgie FD, Burke AP, Farb A, Schwartz SM. Lessons from sudden coronary death: a comprehensive morphological classification scheme for atherosclerotic lesions. *Arterioscler Thromb Vasc Biol* 2000;20:1262-75.

9. Mintz GS, Nissen SE, Anderson WD, Bailey SR, Erbel R, Fitzgerald PJ, Pinto FJ, Rosenfield K, Siegel RJ, Tuzcu EM, Yock PG. American College of Cardiology Clinical Expert Consensus Document on Standards for Acquisition, Measurement and Reporting of Intravascular Ultrasound Studies (IVUS). A report of the American College of Cardiology Task Force on Clinical Expert Consensus Documents. *J Am Coll Cardiol* 2001;37:1478-92.

10. Mintz GS, Maehara A, Bui AB, Weissman NJ. Multiple versus single coronary plaque ruptures detected by intravascular ultrasound in stable and unstable angina pectoris and in acute myocardial infarction. *Am J Cardiol* 2003;91:1333-5.

11. Burke AP, Farb A, Malcom GT, Liang YH, Smialek J, Virmani R. Coronary risk factors and plaque morphology in men with coronary disease who died suddenly. *N Engl J Med* 1997;336:1276-82.

12. Serruys PW, Degertekin M, Tanabe K, Russell ME, Guagliumi G, Webb J, Hamburger J, Rutsch W, Kaiser C, Whitbourn R, Camenzind E, Meredith I, Reeves F, Nienaber C, Benit E, Disco C, Koglin J, Colombo A; TAXUS II Study Group. Vascular responses at proximal and distal edges of paclitaxel-eluting stents: serial intravascular ultrasound analysis from the TAXUS II trial. *Circulation* 2004;109:627-33.

13. Garcia-García HM, Gonzalo N, Pawar R, Kukreja N, Dudek D, Thuesen L, Ormiston J, Regar E, Serruys PW. Assessment of the Absorption Process Following Bioabsorbable Everolimus-Eluting Stent Implantation: Temporal Changes in Strain Values and Tissue Composition Using Intravascular Ultrasound Radiofrequency Data Analysis. A substudy of the ABSORB clinical trial. *Eurointerv* 2009;4:443-448.

14. Wang JC, Normand SL, Mauri L, Kuntz RE. Coronary artery spatial distribution of acute myocardial infarction occlusions. *Circulation* 2004;110:278-84.

15. Gibson CM, Kirtane AJ, Murphy SA, Karha J, Cannon CP, Giugliano RP, Roe MT, Harrington RA, Ohman EM, Antman EM. Distance from the coronary ostium to the culprit lesion in acute ST-elevation myocardial infarction and its implications regarding the potential prevention of proximal plaque rupture. *J Thromb Thrombolysis* 2003;15:189-96.

16. Rodriguez-Granillo GA, García-García HM, Mc Fadden EP, Valgimigli M, Aoki J, de Feyter P, Serruys PW. In vivo intravascular ultrasound-derived thin-cap fibroatheroma detection using ultrasound radiofrequency data analysis. *J Am Coll Cardiol* 2005;46:2038-42.

17. Rodriguez-Granillo GA, García-García HM, Valgimigli M, Vaina S, van Mieghem C, van Geuns RJ, van der Ent M, Regar E, de Jaegere P, van der Giessen W, de Feyter P, Serruys PW.Global characterization of coronary plaque rupture phenotype using three-vessel intravascular ultrasound radiofrequency data analysis. *Eur Heart J.* 2006, 27(16):1921-7.

18. García-García H, Goedhart D, Schuurbiers JCH, Kukreja N, Tanimoto S, Daemen J, Morel M-A, Bressers M, van Es GA, Wentzel J, Gijsen F, van der Steen A, Serruys PW. Virtual histology and remodeling index allow in vivo identification of allegedly high risk coronary plaques in patients with acute coronary syndromes: a three vessel intravascular ultrasound radiofrequency data analysis. *EuroInterv* 2006;2:338-344.

CHAPTER 2.1

Combined optical coherence tomography and intravascular ultrasound radio frequency data analysis for plaque characterization: Classification accuracy of human coronary plaques in vitro related to image artifacts.

Goderie TPM, van Soest G, **Garcia-Garcia HM**, Gonzalo-Lopez N, Koljenovic S, van Leenders A, Regar E, Serruys PW, van der Steen AFW.

Submitted

ABSTRACT

Aims: The purpose of this study was to characterize coronary plaque types, with special interest in misclassification in both optical coherence tomography (OCT) and in intravascular ultrasound (IVUS) radiofrequency (RF) data analysis, and to investigate the possibility of error reduction by combining both techniques.
Methods and results: Regions of interest were selected and imaged with OCT in 50 cross-sections and IVUS in 36 cross-sections, from 14 human coronary arteries, sectioned from 14 hearts at autopsy. Plaques were classified based on IVUS RF data analysis (VH-IVUS™), OCT and the combination of those. Histology was the benchmark. OCT was able to correctly classified 32 out of 50 cross-sections; VH-IVUS correctly classified 26 out of 36 cross-sections. VH-IVUS and OCT combined were able to correctly classify 28 out of 36 cross-sections. Systematic misclassifications in OCT were intimal thickening (IT) classified as fibro-atheroma (FA) in 7 cross-sections and IT classified as thin-cap fibro-atheroma (TCFA) in 3 cross-sections. Misclassifications in VH-IVUS were IT as FA in 3 cross-sections and IT as calcified fibro-atheroma in 3 cross-sections.
Conclusions: Typical image artifacts, both new ones and previously identified, were found to affect the interpretation of OCT data. Adding VH-IVUS to OCT reduced the error rate.

BACKGROUND

Pathology studies have demonstrated that most of acute coronary syndromes originate from vulnerable plaques.[1-5] These plaques have a mechanically weak cap, consisting of a thin fibrotic layer that is infiltrated by macrophages, overlying a lipid-rich necrotic core.[2,6-9] The current challenge is to specifically identify *in vivo* plaques that exhibit these characteristics and thus are likely to cause acute coronary syndrome[10]. Clinical diagnosis may benefit from complementary information gathered by different imaging technologies, as they may be sensitive to specific aspects of the anatomy.[6,11-16]

Grayscale Intravascular Ultrasound (IVUS) has since long been a standard diagnostic tool in cath labs worldwide, and intravascular Optical Coherence Tomography (OCT) looks set to rapidly become one as well.[14,17-20] Radio frequency (RF) data analysis adds plaque composition information to grayscale IVUS, which may help to distinguish high-risk lipid-rich necrotic plaques from other types of plaques.[21-23] IVUS RF data analysis (commercially available as VH-IVUS™; Volcano, Rancho Cordova, CA) aims to provide quantitative information on plaque composition classifying plaque as fibrotic, fibro-fatty, necrotic core or dense calcium, based on spectral analysis of the RF signal.[12] Although criteria have been formulated for VH-IVUS to detect TCFA, as a standalone technique it is not able to recognize this type of lesion because of its limited resolution (> 250 μm).[16,24-26] In this article, we will refer to IVUS RF data analysis as VH-IVUS, since we used that technology specifically.

Optical coherence tomography (OCT) generates real time tomographic images from backscattered infrared light with a high resolution (10-15 μm axial).[14,27] Its resolution allows direct imaging of a thin fibrotic cap, in principle. Main disadvantages are the limited depth of penetration (approximately 1.5 mm) and the need to flush blood from the imaged artery.[14] This latter issue is relieved by the advent of high-speed intracoronary imaging systems that allow full imaging of a coronary artery with only short flush.[17]

The relatively small penetration depth of OCT limits the reliability of differentiation of heterogeneous plaques.[28] Misinterpretations of calcified tissue as lipid in OCT have been reported, leading to misclassified OCT-derived TCFA.[16]

The cause of misclassification of a lesion may be an interpretation error by the image reader, or image artifacts inherent to the technique. As confounders are likely to be specific to a certain technique, studies using the combined strengths of multiple modalities, for instance OCT and VH-IVUS, could lead to a better classification of plaques than interpretation of the techniques' imagery separately.

The aim of this study was to compare the ability of OCT and VH-IVUS to classify plaque and to assess the performance of a combination of the two modalities to identify different plaque types. While a few *in-vivo* studies have been published,[16,29] in this work we present the first comparison between VH-IVUS and OCT, using histology as a benchmark.

METHODS

Study population

Between June 2007 and January 2008, 14 coronary arteries have been collected from 14 human hearts acquired during autopsy (57% men, 12 left anterior descending arteries, 2 right coronary arteries, mean age 64) at the Department of Pathology of the Erasmus MC. All patients died of non-coronary causes. Permission to use autopsy material for scientific study was obtained from the relatives. This study was approved by the local institutional review board.

Tissue preparation and data acquisition

Atherosclerotic human coronary artery segments were excised from the heart and imaged within 36 hours postmortem. During the excision all side branches were closed with sutures. The arteries were mounted between 2 sheaths in a water tank filled with physiological saline. A water column system, also containing physiological saline solution, was connected to the proximal sheath, to pressure-load the vessel. The vessels were pressurized to 100 mmHg to close up remaining leakages.

The vessels were imaged with OCT (M2-CV and ImageWire 2 catheters; Lightlab Imaging, Westford, MA) and IVUS (In-vision Gold; Eagle-Eye™ 20 MHz catheters; Volcano, Rancho Cordova, CA). Regions of interest (ROIs) were selected based on the presence of plaque and plaque size. ROIs were marked with a needle.[12] After imaging the needle was replaced by a suture.

ROIs were first imaged with the IVUS-system, followed by OCT. The vessels were pressurized to 100 mmHg for imaging. For IVUS, the vessels were kept at room temperature 20 ± 2°C; OCT was performed at 37°C.[30,31]

After imaging, the artery sections were pressure fixed at 100 mmHg in formaldehyde for 24h at room temperature, and subsequently stored in formaldehyde at 4°C for further processing. Vessels were partially decalcified for 24 hours in formic acid.[32] After fixation and decalcification, sutures marking the imaged

cross-sections were replaced by ink dots. The tissue was embedded in paraffin and serially sectioned for histological staining. Each imaged cross-section was stained with Hematoxylin-Eosin (H&E), Picrosirius red, Elastic van Gieson (EvG) and immunohistochemical stain CD68.

DATA CLASSIFICATION

Plaques were characterized in the images acquired with the two modalities, as well as in histology. As histological tissue slices are much thinner (5 μm) than the thickness sampled by OCT (25 μm) or IVUS (~200 μm) [33,34] there is an unavoidable sampling error. Imaged cross-sections that were obviously mismatched with histology, based on anatomical features, were removed from the data set before analysis.

VH-IVUS

VH-IVUS constructs tissue maps that classify plaque into four major components (fibrous – green, fibrofatty – light green, NC – red, and dense calcium – white).[35] Data were acquired, and B-mode images were reconstructed from the RF data by customized software (pcVH 2.2, Volcano Corporation), which allows a semiautomatic detection of the lumen and the media-adventitia borders and provides the compositional parameters. VH cross-sections were quantitatively measured and were classified as one of the categories described in table 1 by an experienced analyst that was blind for pathological and OCT findings.[36-38]

OCT

Classification of OCT was based on characteristics as mentioned in table 1 by an experienced OCT reader.[14,36,37,39] Because of the limited depth of imaging and the limited penetration in OCT, tissue types could not be expressed as percentages of the intima like in VH-IVUS, but had to be based on the visible part of the OCT image. In cross-sections with no visible cap, defined by a transition of signal from homogeneous signal rich to otherwise, the cross-section was classified as intimal thickening. In presence of a cap the dominant tissue type behind the cap was used to assess lesion type.

Combined OCT and VH

After independent analysis of each technique, side-by-side visual assessment of VH-IVUS and OCT cross-sections allowed us to evaluate the plaque types in a combined fashion. The criteria in Table 1 were applied for both techniques. If the classifications diverged between VH-IVUS and OCT, signal rich regions in OCT overruled VH-IVUS tissue characterization. In signal poor regions in OCT, VH-IVUS overruled OCT. This choice was made because a loss of OCT signal can occur due to artifacts, whereas artifacts are unlikely to cause a gain in image intensity.

Table 1. Criteria for plaque characterization; NC = necrotic core, DC = dense calcium, FA = fibro-atheroma, CaFA = calcified fibro-atheroma, TCFA = thin-cap fibro-atheroma, CaTCFA = calcified TCFA.

Lesion type	Brief description in VH [36-38]	Brief description in OCT [14,26,37,39]
Intimal thickening	Plaque with <10% of NC and <10% of calcified tissue	Homogeneous signal-rich region
Fibrocalcific plaque	>10% of confluent DC with <10% of confluent NC	Homogeneous sharply delineated signal poor regions
Fibro-atheroma	plaque with >10% of confluent NC	Heterogeneous signal poor regions poorly delineated
Calcified FA	FA containing >10% of confluent DC	Areas of heterogeneous signal poor regions mixed with sharply defined signal poor regions
TCFA	>10% Confluent NC in contact with the lumen	FA with a cap <65 µm measured at the thinnest point
CaTCFA	TCFA containing >10% of confluent DC	Same as CaFA but the NC is covered by a cap <65 µm

Histology

Histological cross-sections were characterized by two observers blinded for the VH-IVUS and OCT results. Characterization was done by making a map of all the cross-sections, with color coding for different types of tissue, separating fibrotic tissue, lipid pool, necrotic core and dense calcium. In case of disagreement between the two pathologists, pathologist 1 and pathologist 2 re-evaluated the slides and reached a consensus diagnosis. Classification of cross-sections was done using the modified American Heart Association (AHA) classification.[37]

RESULTS

Comparison of histology and optical coherence tomography

OCT imaging, with positively matched histology, succeeded in 50 cross-sections of 14 vessels. By histology, 33 cross-sections were classified as intimal thickening of which OCT correctly classified 21. There were two cross-sections misclassified as IT by OCT. There were four fibrocalcific plaques in histology, two were correctly classified by OCT. Further, OCT misclassified three cross-sections as fibrocalcific plaque. Out of the six fibroatheromas by histology, OCT correctly classified three. Of note, OCT misclassified another seven. In histology, there were seven calcified fibroatheromas, six correctly classified by OCT. In addition, OCT misclassified six more plaques, two as calcified fibroatheroma, three as thin capped fibroatheroma and one as calcified thin capped fibroatheroma. These results are summarized in Table 2.

Table 2. Classification and misclassification by OCT in 50 cross-sections. IT = intimal thickening, FC = fibrocalcific, FA = fibro-atheroma, CaFA = calcified fibroatheroma, TCFA = thin-cap fibro=atheroma, CaTCFA = calcified thin-cap fibro-atheroma, OCT = optical coherence tomography.

	OCT+	OCT-	Histology
IT+	21	12	33
IT-	2	15	17
FC+	2	2	4
FC-	3	43	46
FA+	3	3	6
FA-	7	37	44
CaFA+	6	1	7
CaFA-	2	41	43
TCFA+	0	0	0
TCFA-	3	47	50
CaTCFA+	0	0	0
CaTCFA-	1	49	50

Virtual histology findings

Out of 50 cross-sections, 36 cross-sections in 9 vessels also had VH-IVUS data. By histology, 29 cross-sections were classified as intimal thickening of which VH-IVUS correctly classified 25. There were six cross-sections misclassified as IT by VH-IVUS. There was only one fibrocalcific plaque in histology, which was not correctly classified by VH-IVUS. Further, VH-IVUS misclassified one cross-section as fibrocalcific plaque. Out of the six necrotic core-rich plaques

Table 3. Classification and misclassification by OCT, VH-IVUS and OCT/VH-IVUS combined, using histology as a benchmark, in 36 cross-sections. IT = intimal thickening, FC = fibrocalcific, FA = fibro-atheroma, CaFA = calcified fibroatheroma, TCFA = thin-cap fibro=atheroma, CaTCFA = calcified thin-cap fibro-atheroma, OCT = optical coherence tomography, VH = VH-IVUS.

	OCT+	OCT-	VH+	VH-	OCT/VH+	OCT/VH-	Histology
IT+	19	10	25	4	26	3	29
IT-	2	5	6	1	5	2	7
FC+	1	0	0	1	0	1	1
FC-	1	34	1	34	1	34	35
FA+	1	1	0	2	0	2	2
FA-	5	29	3	31	1	33	34
CaFA+	3	1	1	3	2	2	4
CaFA-	1	31	0	32	0	32	32
TCFA+	0	0	0	0	0	0	0
TCFA-	3	33	0	36	1	35	36
CaTCFA+	0	0	0	0	0	0	0
CaTCFA-	0	36	0	36	0	36	36

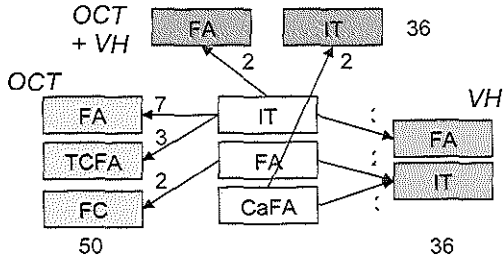

Figure 1. Chart of misclassifications. Only misclassifications occurring ≥2 are included in the figure. Misclassifications are derived from 36 cross-sections in VH-IVUS and OCT and VH-IVUS combined, misclassifications in OCT are derived from 50 cross-sections. Yellow = histology, green = VH-IVUS, orange = OCT, OCT/VH-IVUS = red. IT = intimal thickening, FC = fibrocalcific, FA = fibro-atheroma, CaFA = calcified fibroatheroma, TCFA = thin-cap fibro-atheroma. For example: of the lesions that were identified as IT in histology, 7 were classified as FA in OCT, 3 as FA in VH-IVUS, and 2 as FA in OCT and VH-IVUS combined.

classifed by histology, VH-IVUS classified only one correctly, that was a calcified fibroatheroma. Unlike OCT, VH-IVUS did not misclassify any plaque as thin capped fibroatheroma.

Table 3 lists the results of the comparison between histology and OCT for 50 cross-sections. Figure 1 shows misclassifications and directions of misclassifications. Only repetitive misclassifications are included.

DISCUSSION

The results in Tables 2 and 3 demonstrate that the classifications by both OCT and VH-IVUS agree with histology in most cases. Figure 2 illustrates a representative example, where both OCT and VH detect a calcified fibro-atheroma, which is in accordance with the histological classification.

Manfrini et al. were the first to apply the American Heart Association criteria to lesion classification with OCT.[28] Classification was done in four groups using the AHA criteria of 1995.[36] In this study we used a modified version of the AHA criteria, including the extra categories, calcified fibro-atheroma, TCFA and calcified TCFA.[37] The study of Manfrini showed a sensitivity of 45% for FA, 68% for calcified lesions and 86% for fibrotic lesions. Similar results in our study were seen in the detection of FA (3/6 correctly classified). Our study used three categories for calcified plaque FC, CaFA, and CaTCFA, having the following results; 2/4, 6/7 and 0/0 classified correctly, respectively. Subclassification of calcified plaque did not affect the results, compared to the Manfrini study. Fibrotic plaque, categorised in our study as intimal thickening, showed slightly different results compared to the Manfrini study (21/33 correctly classified).

The sample size in our study was sufficient to detect repetitive misclassifications and provide an explanation of those misclassifications based on the image data. These systematic misinterpretations of the data also suggest future possibilities how combining intravascular imaging techniques could help reduce errors in classification. The limited size of our study did not permit reliable calculation of sensitivities and specificities, however.

Recent studies in OCT showed difficulties detecting TCFA in OCT and in characterizing plaques with OCT.[16,28] Misclassifications were reported as a result of limited penetration depth, problems in distinguishing lipid pool from calcifica-

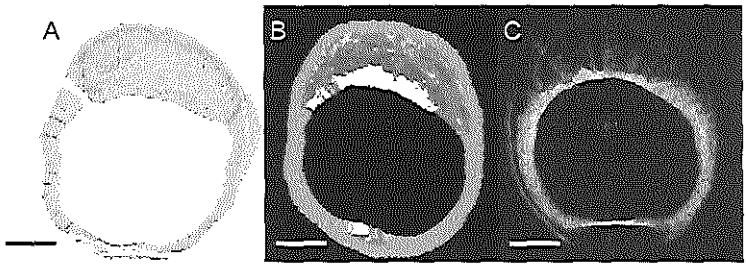

Figure 2. (A) Histology of a calcified fibroatheroma (hematoxylin-eosin stain). (B) Corresponding VH-IVUS classified as calcified fibroatheroma. (C) Corresponding OCT classified as calcified fibroatheroma. The needle used to mark the site can be seen in the bright feature at 6 o'clock in OCT, as well as in the appearance of dense calcium in that location in VH-IVUS.

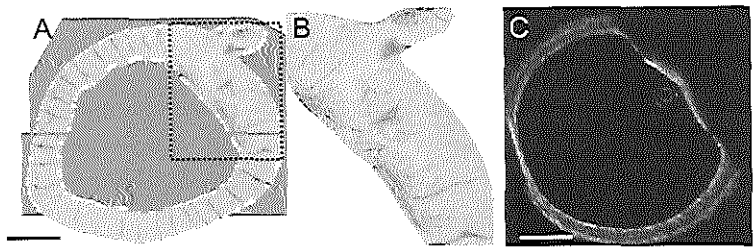

Figure 3 (A) CD68 stained cross-section. The intima consisting of a collagen/glycoprotein matrix is densely infiltrated by macrophages. (B) Magnification of selected region in A. (C) Corresponding OCT image. The region infiltrated by macrophages appears as a thin-cap fibro-atheroma. The bar indicates 1 mm.

tions and vice versa, or heterogeneity of necrotic cores, consisting of necrotic debris and calcifications.[14-16,28,29]

In our data we have encountered the same confounders. In addition, we observed the following features, compromising the classification of lesions based on OCT. Dense infiltration of macrophages in the intima or the outer layers of a fibrotic plaque led to high scattering of OCT signal, causing the underlying collagen/glycoprotein matrix to appear as a (thin-cap) FA. Figure 3 shows an example. In such sections, signal-poor regions were seen, with poorly delineated borders, which is the exact definition of lipid pool.[14,39] The possibility of detecting macrophages with OCT has been reported earlier, but their potential to confound lesion classification was not noted at that time.[40,41] In four cross-sections, scattering caused by dense macrophage infiltration led to misclassification in which two times an IT in pathology was called a FA in OCT and in two times an IT in pathology was called a TCFA in OCT.

Catheter position may also interfere with image features and definition. The published image classification schemes are based on features that are routinely observed with a catheter that is well centered in the lumen. Light from an eccentric catheter, or one that is even touching the vessel wall, may be incident on the tissue under a glancing angle. The light path through tissue to a certain radial depth in the vessel wall is longer in such an imaging geometry than in one where the imaging beam strikes the interface perpendicularly. The limited penetration depth or large attenuation occurring over a limited radial distance, leads to fibrotic areas misinterpreted as FA or TCFA. This situation is illustrated in Figure 4.

Finally, we observed that the efficiency of the optical catheter to emit or receive the imaging light beam may vary with rotation scan angle in some catheter specimens. This leads to darker sectors in the image, and these regions can appear as signal poor regions like FAs, see Figure 5. A possible cause for this observation is optical impurities sticking to the outside of the catheter. These can be picked up

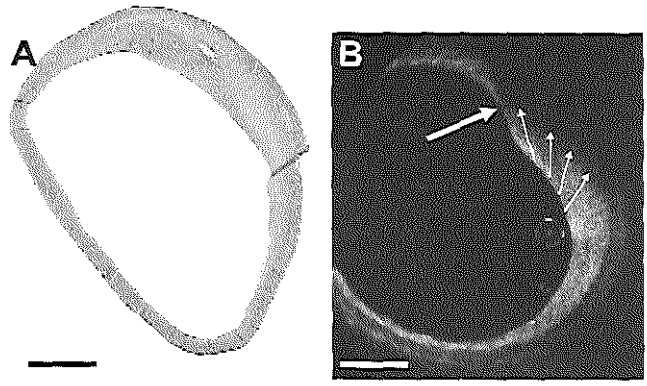

Figure 4. (A) H&E stained cross-section. (B) Intimal thickening is misinterpreted as thin-cap fibro-atheroma (TCFA) in optical coherence tomtography (OCT). The large arrow points at the spot interpreted as a thin-cap. The four small arrows indicate the OCT beams and are all of the same length. The loss of signal due to tissue penetration is similar for each arrow. Because of eccentric catheter position this cross-section, classified as intimal thickening in histology, appears as a thin-cap fibro-atheroma (TCFA) in OCT. The bar indicates 1 mm.

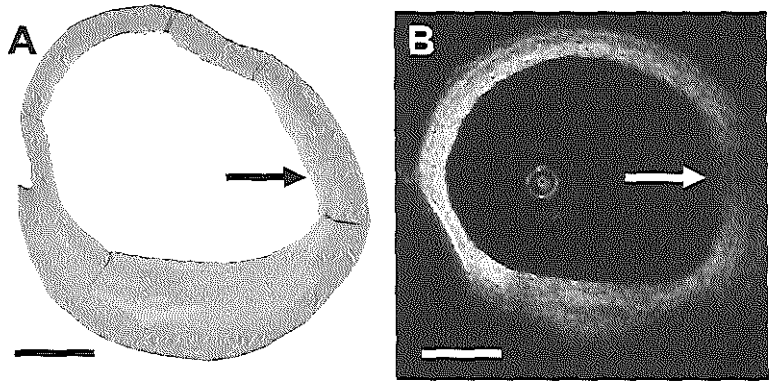

Figure 5. (A) H&E stained cross-section with (B) the corresponding optical coherence tomography (OCT). The arrow indicates a collagenous region in histology mistaken for a lipid region in OCT. Reduced optical efficiency of the catheter in this image section creates a dark sector, making mild intimal thickening appear as a fibro-atheroma. The bar indicates 1 mm.

on insertion of the catheter, for example. While the in vitro setting, in absence of flow, may aggravate this problem compared to clinical use, it is difficult to ascertain intra-procedurally that the image quality is constant across the rotation.

In VH-IVUS incorrect drawing of lumen and media borders may have led to misclassification in 3 cross-sections. Incorrect drawing of borders was seen in two typical situations: lumen borders at sites where the catheter was against the lumen wall, and media borders at sites where the adventitia was invisible due to

acoustic shadowing. Drawing borders with knowledge of histology retrospectively corrected the misclassifications in 2 out of 3 cross-sections.

Cross-sections were imaged in a static situation, not performing a pullback. In this situation a plaque can not be seen in the context of its surrounding which complicates identification of correct borders. Also, excised specimens do not always have sufficient adventitia to help differentiate the media border from its surroundings.

Qualification of plaques in VH-IVUS is straight-forward and the lesion type could often easily be assessed by the bare eye. Plaques with confluent NC or Ca around 10% might fall in one or the other classification group, and hence may be sensitive to misclassification.

In VH-IVUS, classification is an automatic process, giving less inter-observer variability, but also giving no explanation of errors in VH-IVUS compared to histology. Misclassification that could not be explained was seen in five cross-sections. In three cross-sections it involved classification as FA while there was in histology little NC (2x) or no NC (1x) at all. In two cross-sections it involved histological FA classified as IT in VH-IVUS.

Overall, VH-IVUS classified plaque correctly 26 out of 36 cross-sections. Detection of IT (25/29 correctly identified) corresponds to the sensitivity as reported by Dietrich et al (89%).[38] However, detection of FA (sensitivity = 54,1% by Diethrich et al) did not correspond to our data (0/2 correctly identified).[38] Our sample size is to small to draw definitive conclusions out of these numbers however our results are in line with previous findings of Granada who reported lower sensitivities and specificities.[12,35,42,43] Misclassification in VH-IVUS alone typically also led to misclassification in OCT and VH-IVUS combined. VH-IVUS could positively influence OCT in cases where OCT misclassified plaques as FA, that were IT according to histology. The artifacts mentioned above led to a high false-positive number of FAs in OCT. FA or TCFA in OCT, which was classified as IT in VH-IVUS, meant in 6 out of 7 times it was indeed an IT in histology. In three out of six it involved plaques classified as TCFAs by OCT.

A recent study describes the low incidence of histology-derived TCFA and FA (1.5% and 10.5% of advanced lesions, respectively).[44] Our data show a relatively high false-positive rate for TCFA or FA: IT in histology was classified in OCT as TCFA or FA in 10 cross-sections.[37] Given the incidence of FA and especially of TCFA, the positive predictive value of OCT, an important parameter in rare incidence, could be small for these clinically significant plaque types. Since the group of non-TCFAs appears to be 98.5% in advanced lesions, the finding of a TCFA in OCT must be regarded with caution, and corroborated with other evidence if possible. An in vivo study by Sawada et al. combined VH-IVUS and

OCT for detection of TCFA. Only lesions classified as TCFA both in OCT and in VH-IVUS were considered real TCFAs.[16] This definition is indeed a sensible one, as the resolution of VH-IVUS is insufficient per se to identify thin caps, and OCT is seen to suffer from many false positives.

In conclusion, adding VH-IVUS to OCT could help reduce misclassification by OCT of FAs and TCFAs. In vitro studies with larger sample sizes are needed to assess the full potential of the added value of OCT and VH-IVUS combined. Criteria for classifying VH-IVUS combined with OCT have not been optimally validated and could possibly be improved using larger datasets.

REFERENCES

[1] F. D. Kolodgie, R. Virmani, A. P. Burke, A. Farb, D. K. Weber, R. Kutys, A. V. Finn, and H. K. Gold, *Pathologic assessment of the vulnerable human coronary plaque.* Heart, 2004. **90**(12): p. 1385-1391.

[2] J. A. Schaar, J. E. Muller, E. Falk, R. Virmani, V. Fuster, P. W. Serruys, A. Colombo, C. Stefanadis, S. W. Casscells, P. R. Moreno, A. Maseri, and A. F. W. van der Steen, *Terminology for high-risk and vulnerable coronary artery plaques. Report of a meeting on the vulnerable plaque, June 17 and 18, 2003, Santorini, Greece.* Eur Heart J, 2004. **25**(12): p. 1077-1082.

[3] J. F. Granada, G. L. Kaluza, A. E. Raizner, and P. R. Moreno, *Vulnerable plaque paradigm: Prediction of future clinical events based on a morphological definition.* Catheter Cardiovasc Interv, 2004. **62**(3): p. 364-374.

[4] J. E. Muller, G. S. Abela, R. W. Nesto, and G. H. Tofler, *Triggers, acute risk factors and vulnerable plaques: the lexicon of a new frontier.* J Am Coll Cardiol, 1994. **23**(3): p. 809-813.

[5] M. J. Davies and A. C. Thomas, *Plaque Fissuring - the Cause of Acute Myocardial-Infarction, Sudden Ischemic Death, and Crescendo Angina.* Br Heart J, 1985. **53**(4): p. 363-373.

[6] J. A. Schaar, C. L. de Korte, F. Mastik, C. Strijder, G. Pasterkamp, E. Boersma, P. W. Serruys, and A. F. W. van der Steen, *Characterizing vulnerable plaque features with intravascular elastography.* Circulation, 2003. **108**(21): p. 2636-2641.

[7] R. Virmani, A. P. Burke, A. Farb, and F. D. Kolodgie, *Pathology of the vulnerable plaque.* J Am Coll Cardiol, 2006. **47**(8): p. C13-C18.

[8] E. Falk, P. K. Shah, and V. Fuster, *Coronary plaque disruption.* Circulation, 1995. **92**(3): p. 657-671.

[9] P. D. Richardson, M. J. Davies, and G. V. Born, *Influence of plaque configuration and stress distribution on fissuring of coronary atherosclerotic plaques.* Lancet, 1989. **2**(8669): p. 941-944.

[10] S. Waxman, F. Ishibashi, and J. E. Muller, *Detection and treatment of vulnerable plaques and vulnerable patients - Novel approaches to prevention of coronary events.* Circulation, 2006. **114**(22): p. 2390-2411.

[11] R. A. Baldewsing, M. G. Danilouchkine, F. Mastik, J. A. Schaar, P. W. Serruys, and A. F. W. van der Steen, *An Inverse Method for Imaging the Local Elasticity of Atherosclerotic Coronary Plaques.* IEEE Trans Inf Technol Biomed, 2008. **12**(3): p. 277-289.

[12] A. Nair, B. D. Kuban, E. M. Tuzcu, P. Schoenhagen, S. E. Nissen, and D. G. Vince, *Coronary plaque classification with intravascular ultrasound radiofrequency data analysis.* Circulation, 2002. **106**(17): p. 2200-2206.

[13] M. Naghavi, P. Libby, E. Falk, S. W. Casscells, S. Litovsky, J. Rumberger, J. J. Badimon, C. Stefanadis, P. Moreno, G. Pasterkamp, Z. Fayad, P. H. Stone, S. Waxman, P. Raggi, M. Madjid, A. Zarrabi, A. Burke, C. Yuan, P. J. Fitzgerald, D. S. Siscovick, C. L. de Korte, M. Aikawa, K. E. J. Airaksinen, G. Assmann, C. R. Becker, J. H. Chesebro, A. Farb, Z. S. Galis, C. Jackson, I. K. Jang, W. Koenig, R. A. Lodder, K. March, J. Demirovic, M. Navab, S. G. Priori, M. D. Rekhter, R. Bahr, S. M. Grundy, R. Mehran, A. Colombo, E. Boerwinkle, C. Ballantyne, W. Insull, R. S.

Schwartz, R. Vogel, P. W. Serruys, G. K. Hansson, D. P. Faxon, S. Kaul, H. Drexler, P. Greenland, J. E. Muller, R. Virmani, P. M. Ridker, D. P. Zipes, P. K. Shah, and J. T. Willerson, *From vulnerable plaque to vulnerable patient - A call for new definitions and risk assessment strategies: Part I.* Circulation, 2003. **108**(14): p. 1664-1672.

[14] I. K. Jang, B. E. Bouma, D. H. Kang, S. J. Park, S. W. Park, K. B. Seung, K. B. Choi, M. Shishkov, K. Schlendorf, E. Pomerantsev, S. L. Houser, H. T. Aretz, and G. J. Tearney, *Visualization of coronary atherosclerotic plaques in patients using optical coherence tomography: Comparison with intravascular ultrasound.* J Am Coll Cardiol, 2002. **39**(4): p. 604-609.

[15] M. Kawasaki, B. E. Bouma, J. Bressner, S. L. Houser, S. K. Nadkarni, B. D. MacNeill, I. K. Jang, H. Fujiwara, and G. J. Tearney, *Diagnostic accuracy of optical coherence tomography and integrated backscatter intravascular ultrasound images for tissue characterization of human coronary plaques.* J Am Coll Cardiol, 2006. **48**(1): p. 81-88.

[16] T. Sawada, J. Shite, H. M. Garcia-Garcia, T. Shinke, S. Watanabe, H. Otake, D. Matsumoto, Y. Tanino, D. Ogasawara, H. Kawamori, H. Kato, N. Miyoshi, M. Yokoyama, P. W. Serruys, and K. Hirata, *Feasibility of combined use of intravascular ultrasound radiofrequency data analysis and optical coherence tomography for detecting thin-cap fibroatheroma.* Eur Heart J, 2008. **29**(9): p. 1136-1146.

[17] S. H. Yun, G. J. Tearney, B. J. Vakoc, M. Shishkov, W. Y. Oh, A. E. Desjardins, M. J. Suter, R. C. Chan, J. A. Evans, I. K. Jang, N. S. Nishioka, J. F. de Boer, and B. E. Bouma, *Comprehensive volumetric optical microscopy in vivo.* Nat Med, 2006. **12**(12): p. 1429-1433.

[18] S. E. Nissen and P. Yock, *Intravascular ultrasound: novel pathophysiological insights and current clinical applications.* Circulation, 2001. **103**(4): p. 604-616.

[19] T. Kubo, T. Imanishi, S. Takarada, A. Kuroi, S. Ueno, T. Yamano, T. Tanimoto, Y. Matsuo, T. Masho, H. Kitabata, K. Tsuda, Y. Tomobuchi, and T. Akasaka, *Assessment of culprit lesion morphology in acute myocardial infarction - Ability of optical coherence tomography compared with intravascular ultrasound and coronary angioscopy.* J Am Coll Cardiol, 2007. **50**(10): p. 933-939.

[20] P. W. Serruys, H. M. Garcia-Garcia, and E. Regar, *From Postmortem Characterization to the In Vivo Detection of Thin-Capped Fibroatheromas: The Missing Link Toward Percutaneous Treatment: What If Diogenes Would Have Found What He Was Looking For?* J Am Coll Cardiol, 2007. **50**(10): p. 950-952.

[21] M. P. Moore, T. Spencer, D. M. Salter, P. P. Kearney, T. R. Shaw, I. R. Starkey, P. J. Fitzgerald, R. Erbel, A. Lange, N. W. McDicken, G. R. Sutherland, and K. A. Fox, *Characterisation of coronary atherosclerotic morphology by spectral analysis of radiofrequency signal: in vitro intravascular ultrasound study with histological and radiological validation.* Heart, 1998. **79**(5): p. 459-467.

[22] N. Komiyama, G. J. Berry, M. L. Kolz, A. Oshima, J. A. Metz, P. Preuss, A. F. Brisken, M. P. Moore, P. G. Yock, and P. J. Fitzgerald, *Tissue characterization of atherosclerotic plaques by intravascular ultrasound radiofrequency signal analysis: an in vitro study of human coronary arteries.* Am Heart J, 2000. **140**(4): p. 565-574.

[23] A. Murashige, T. Hiro, T. Fujii, K. Imoto, T. Murata, Y. Fukumoto, and M. Matsuzaki, *Detection of lipid-laden atherosclerotic plaque by wavelet analysis of radiofre-*

quency intravascular ultrasound signals: in vitro validation and preliminary in vivo application. J Am Coll Cardiol, 2005. **45**(12): p. 1954-1960.

[24] A. Nair, D. Calvetti, and D. G. Vince, *Regularized autoregressive analysis of intravascular ultrasound backscatter: improvement in spatial accuracy of tissue maps.* IEEE Trans Ultrason Ferroelectr Freq Control, 2004. **51**(4): p. 420-431.

[25] G. A. Rodriguez-Granillo, H. M. Garcia-Garcia, E. P. Mc Fadden, M. Valgimigli, J. Aoki, P. de Feyter, and P. W. Serruys, *In vivo intravascular ultrasound-derived thin-cap fibroatheroma detection using ultrasound radiofrequency data analysis.* J Am Coll Cardiol, 2005. **46**(11): p. 2038-2042.

[26] H. M. Garcia-Garcia, D. Goedhart, J. C. H. Schuurbiers, N. Kukreja, S. Tanimoto, J. Daemen, M. A. M. Morel, M. Bressers, G. A. van Es, J. J. Wentzel, F. Gijsen, A. F. W. van der Steen, and P. W. Serruys, *Virtual histology and remodelling index allow in vivo identification of allegedly high-risk coronary plaques in patients with acute coronary syndromes: a three vessel intravascular ultrasound radiofrequency data analysis.* EuroIntervention, 2006. **2**(3): p. 338-344.

[27] D. Huang, E. A. Swanson, C. P. Lin, J. S. Schuman, W. G. Stinson, W. Chang, M. R. Hee, T. Flotte, K. Gregory, C. A. Puliafito, and J. G. Fujimoto, *Optical coherence tomography.* Science, 1991. **254**(5035): p. 1178-1181.

[28] O. Manfrini, E. Mont, O. Leone, E. Arbustini, V. Eusebi, R. Virmani, and R. Bugiardini, *Sources of Error and Interpretation of Plaque Morphology by Optical Coherence Tomography.* Am J Cardiol, 2006. **98**(2): p. 156.

[29] N. Gonzalo, P. W. Serruys, P. Barlis, J. Ligthart, H. M. Garcia-Garcia, and E. Regar, *Multi-modality intra-coronary plaque characterization: A pilot study.* Int J Cardiol, 2008.

[30] J. A. Schaar, C. L. de Korte, F. Mastik, and A. F. van der Steen, *Effect of temperature increase and freezing on intravascular elastography.* Ultrasonics, 2002. **40**(1-8): p. 879-881.

[31] F. J. van der Meer, D. J. Faber, I. Cilesiz, M. J. van Gemert, and T. G. van Leeuwen, *Temperature-dependent optical properties of individual vascular wall components measured by optical coherence tomography.* J Biomed Opt, 2006. **11**(4): p. 041120.

[32] G. J. Friedrich, N. Y. Moes, V. A. Muhlberger, C. Gabl, G. Mikuz, D. Hausmann, P. J. Fitzgerald, and P. G. Yock, *Detection of intralesional calcium by intracoronary ultrasound depends on the histologic pattern.* Am Heart J, 1994. **128**(3): p. 435-441.

[33] N. Bruining, S. Verheye, M. Knaapen, P. Somers, J. Roelandt, E. Regar, I. Heller, S. de Winter, J. Ligthart, G. van Langenhove, P. J. de Feijter, P. W. Serruys, and R. Hamers, *Three-dimensional and quantitative analysis of atherosclerotic plaque composition by automated differential echogenicty.* Catheter Cardiovasc Interv, 2007. **70**(7): p. 968-978.

[34] J. Rieber, O. Meissner, G. Babaryka, S. Reim, M. Oswald, A. Koenig, T. M. Schiele, M. Shapiro, K. Theisen, M. F. Reiser, V. Klauss, and U. Hoffmann, *Diagnostic accuracy of optical coherence tomography and intravascular ultrasound for the detection and characterization of atherosclerotic plaque composition in ex-vivo coronary specimens: a comparison with histology.* Coron Artery Dis, 2006. **17**(5): p. 425-430.

[35] A. Nair, M. P. Margolis, B. D. Kuban, and D. G. Vince, *Automated coronary plaque characterization with intravascular ultrasound backscatter: ex vivo validation.* EuroIntervention, 2007. **3**(9): p. 113-120.

[36] H. C. Stary, A. B. Chandler, R. E. Dinsmore, V. Fuster, S. Glagov, W. Insull, Jr., M. E. Rosenfeld, C. J. Schwartz, W. D. Wagner, and R. W. Wissler, *A definition of advanced types of atherosclerotic lesions and a histological classification of atherosclerosis. A report from the Committee on Vascular Lesions of the Council on Arteriosclerosis, American Heart Association.* Circulation, 1995. **92**(5): p. 1355-1374.

[37] R. Virmani, F. D. Kolodgie, A. P. Burke, A. Farb, and S. M. Schwartz, *Lessons from sudden coronary death - A comprehensive morphological classification scheme for atherosclerotic lesions.* J Am Coll Cardiol, 2000. **20**(5): p. 1262-1275.

[38] E. B. Diethrich, M. P. Margolis, D. B. Reid, A. Burke, V. Ramaiah, J. A. Rodriguez-Lopez, G. Wheatley, D. Olsen, and R. Virmani, *Virtual histology intravascular ultrasound assessment of carotid artery disease: the Carotid Artery Plaque Virtual Histology Evaluation (CAPITAL) study.* J Endovasc Ther, 2007. **14**(5): p. 676-686.

[39] H. Yabushita, B. E. Bourna, S. L. Houser, T. Aretz, I. K. Jang, K. H. Schlendorf, C. R. Kauffman, M. Shishkov, D. H. Kang, E. F. Halpern, and G. J. Tearney, *Characterization of human atherosclerosis by optical coherence tomography.* Circulation, 2002. **106**(13): p. 1640-1645.

[40] G. J. Tearney, H. Yabushita, S. L. Houser, H. T. Aretz, I. K. Jang, K. H. Schlendorf, C. R. Kauffman, M. Shishkov, E. F. Halpern, and B. E. Bouma, *Quantification of macrophage content in atherosclerotic plaques by optical coherence tomography.* Circulation, 2003. **107**(1): p. 113-119.

[41] B. D. MacNeill, I. K. Jang, B. E. Bouma, N. Iftimia, M. Takano, H. Yabushita, M. Shishkov, C. R. Kauffman, S. L. Houser, H. T. Aretz, D. DeJoseph, E. F. Halpern, and G. J. Tearney, *Focal and multi-focal plaque macrophage distributions in patients with acute and stable presentations of coronary artery disease.* J Am Coll Cardiol, 2004. **44**(5): p. 972-979.

[42] K. Nasu, E. Tsuchikane, O. Katoh, D. G. Vince, R. Virmani, J. F. Surmely, A. Murata, Y. Takeda, T. Ito, M. Ehara, T. Matsubara, M. Terashima, and T. Suzuki, *Accuracy of in vivo coronary plaque morphology assessment: a validation study of in vivo virtual histology compared with in vitro histopathology.* J Am Coll Cardiol, 2006. **47**(12): p. 2405-2412.

[43] J. F. Granada, D. Wallace-Bradley, H. K. Win, C. L. Alviar, A. Builes, E. I. Lev, R. Barrios, D. G. Schulz, A. E. Raizner, and G. L. Kaluza, *In vivo plaque characterization using intravascular ultrasound-virtual histology in a porcine model of complex coronary lesions.* Arterioscler Thromb Vasc Biol, 2007. **27**(2): p. 387-393.

[44] P. K. Cheruvu, A. V. Finn, C. Gardner, J. Caplan, J. Goldstein, G. W. Stone, R. Virmani, and J. E. Muller, *Frequency and distribution of thin-cap fibroatheroma and ruptured plaques in human coronary arteries: A pathologic study.* J Am Coll Cardiol, 2007. **50**(10): p. 940-949.

CHAPTER 2.2

Reproducibility of intravascular ultrasound radiofrequency data analysis: implications for the design of longitudinal studies.

Rodriguez-Granillo GA, Vaina S, **Garcia-Garcia HM**, Valgimigli M, Duckers E, van Geuns RJ, Regar E, van der Giessen WJ, Bressers M, Goedhart D, Morel MA, de Feyter PJ, Serruys PW.

Int J Cardiovasc Imaging. 2006; Oct;22(5):621-31

The International Journal of Cardiovascular Imaging (2006)
DOI 10.1007/s10554-006-9080-0

Reproducibility of intravascular ultrasound radiofrequency data analysis: implications for the design of longitudinal studies

Gastón A. Rodriguez-Granillo[1], Sophia Vaina[1], Héctor M. García-García[1], Marco Valgimigli[1], Eric Duckers[1], Robert J. van Geuns[1], Evelyn Regar[1], William J. van der Giessen[1], Marco Bressers[2], Dick Goedhart[2], Marie-Angele Morel[2], Pim J. de Feyter[1] & Patrick W. Serruys[1]

[1]*Department of Interventional Cardiology of the Erasmus Medical Center, Rotterdam, The Netherlands;* [2]*Cardialysis BV, Rotterdam, The Netherlands*

Received 24 November 2005; accepted in revised form 19 January 2006

Key words: agreement, atherosclerosis, plaque characterization, reproducibility, ultrasonography

Abstract

Objectives: The purpose of this study was to assess in vivo the reproducibility of tissue characterization using spectral analysis of intravascular ultrasound (IVUS) radiofrequency data (IVUS-VH). *Background*: Despite the need for reproducibility data to design longitudinal studies, such information remains unexplored. *Methods and results*: IVUS-VH (Volcano Corp., Rancho Cordova, USA) was performed in patients referred for elective percutaneous intervention and in whom a non-intervened vessel was judged suitable for a safe IVUS interrogation. The IVUS catheters used were commercially available catheters (20 MHz, Volcano Corp., Rancho Cordova, USA). Following IVUS-VH acquisition, and after the disengagement and re-engagement of the guiding catheter, an additional acquisition was performed using a new IVUS catheter. Fifteen patients with 16 non-significant lesions were assessed by 2 independent observers. The relative inter-catheter differences regarding geometrical measurements were negligible for both observers. The inter-catheter relative difference in plaque cross-sectional area (CSA) was 3.2% for observer 1 and 0.5% for observer 2. The limits of agreement for (observer 1 measurements) lumen, vessel, plaque and plaque burden measurements were 0.82, −1.10 mm^2; 0.80, −0.66 mm^2; 1.08, −0.66 mm^2; and 5.83, −3.89%; respectively. Limits of agreement for calcium, fibrous, fibrolipidic and necrotic core CSA measurements were 0.22, −0.25 mm^2; 1.02, −0.71 mm^2; 0.61, −0.65 mm^2; and 0.43, −0.38 mm^2 respectively. Regarding the inter-observer agreement, the limits of agreement for lumen, vessel, plaque and plaque burden measurements were 2.61, −2.09 mm^2; 2.20–3.03 mm^2; 1.70, −3.04 mm^2; and 9.16, −16.41%; respectively, and for calcium, fibrous, fibrolipidic and necrotic core measurements of 0.08, −0.09 mm^2; 0.89, −1.28 mm^2; 0.74, −1.06 mm^2; and 0.16, −0.20 mm^2; respectively. *Conclusions*: The present study demonstrates that the geometrical and compositional output of IVUS-VH is acceptably reproducible.

Introduction

Intravascular ultrasound (IVUS) imaging has been shown to provide safe, accurate, real-time, tomographic measurements of coronary vessels in vivo [1–4]. Over the past decade, IVUS has been used to describe the extent, severity, distribution, and morphology of coronary atherosclerosis [5–7]. Furthermore, several studies have evaluated the temporal effect of conventional and novel medical

therapies on plaque progression by means of IVUS [8–10].

Since the fate of coronary atherosclerotic plaques has been related to their histological composition [11], precise in-vivo tissue characterization could provide important additional information and become a target for future drug therapy studies.

In-vitro studies have shown that visual interpretation of IVUS gray-scale images for plaque characterization is imprecise, in particular when assessing heterogeneous, lipid-rich plaques [12]. This has lead investigators to explore the radiofrequency data analysis, a potential source for in-vivo tissue characterization. Indeed, a recent ex-vivo study on explanted coronary segments showed that plaque characterization using spectral analysis of IVUS radiofrequency data (IVUS-VH) was feasible and provided a high predictive accuracy to estimate the composition of atherosclerotic plaques [13]. Several in-vivo studies have been conducted thereafter using this approach [14–17]. Nevertheless, although prior knowledge about the reproducibility of measurements are essential for the internal validity of any study using this technique, to date, only indirect evidence on the reproducibility of the technique is available [18]. Accordingly, we sought to study the inter-observer and inter-catheter agreement of IVUS-VH measurements at a single time-point.

Methods

Patient population

This was a single-center prospective, investigators-driven study that sought to explore in vivo the reproducibility of spectral analysis of IVUS radiofrequency data (IVUS-VH, Volcano Corp., Rancho Cordova, USA). The study population consisted of consecutive patients that were referred for elective percutaneous intervention and in whom a non-intervened vessel was judged suitable for a safe IVUS interrogation of a vessel segment of at least 30 mm.

Exclusion criteria included the presence of severe calcification, vessel tortuosity, and haemodynamic instability. The study protocol was approved by the institutional ethics committee and a written informed consent was obtained from all patients.

IVUS-VH

IVUS-VH evaluates different spectral parameters of the radiofrequency data (Y-intercept, minimum power, maximum power, mid-band power, frequency at minimum power, frequency at maximum power, slope, etc.) to construct tissue maps that classify plaque into four major components. In preliminary in vitro studies, four histological plaque components (fibrous, fibrolipidic, necrotic core and calcium) were correlated with a specific spectrum of the radiofrequency signal [13]. These different plaque components were assigned color codes. Calcified, fibrous, fibrolipidic and necrotic core regions were labeled white, green, greenish-yellow and red respectively.

IVUS-VH acquisition

The IVUS catheters used were commercially available phased array catheters (Eagle Eye Gold™ 2.9 F 20 MHz, Volcano Corp., Rancho Cordova, USA). The catheter probe was advanced at least 10 mm distal to a clearly visible side-branch and angiographic cine runs, before and during contrast injection, were performed to define the position of the IVUS catheter before the pullback was started. Using an automated pullback device, the transducer was withdrawn at a continuous speed of 0.5 mm/s. IVUS-VH acquisition was ECG-gated and acquired using a dedicated console (Volcano Corporation, Rancho Cordova, USA). IVUS-VH data was acquired after intra-coronary administration of isosorbide dinitrate and data was stored on DVD. Subsequently, and after the disengagement and re-engagement of the guiding catheter, the same procedure was performed using a new catheter (Eagle Eye Gold™ 2.9 F 20 MHz, Volcano Corp., Rancho Cordova, USA) and with the same side-branches as landmarks.

IVUS-VH analysis

IVUS-VH analysis was performed by an independent core laboratory (Cardialysis BV, Rotterdam,

The Netherlands) using a semi-automatic contour detection software (IVUSLab 4.4, Volcano Corp., Rancho Cordova, USA). A region of interest (ROI) was identified using the inner side of two clear side-branches as reference and avoiding the presence of large side-branches within the ROI. Subsequently, the same ROI was identified in the other catheter's acquisition using side-by-side longitudinal and cross-sectional, contour-free views.

Contour detection of the lumen and the media-adventitia interface was performed by 2 independent experienced IVUS analysts. The same 2 IVUS analysts re-analyzed the same cases, leading to the possibility of multiple comparisons: 2 sets (observers 1 and 2) of intra-catheter agreement, and 1 set of inter-observer agreement [observer 1 (catheters 1 and 2) vs. observer 2 (catheters 1 and 2)].

The contours of the external elastic membrane (EEM) and the lumen–intima interface enclosed an area that was defined as the coronary plaque plus media area. Geometrical and compositional data were obtained for each cross-sectional area (CSA) and an average was calculated for each ROI. Plaque burden was calculated as $[(EEM_{area} - Lumen_{area}/EEM_{area}) \times 100]$. The lumen and vessel eccentricity indexes were calculated dividing the minimum (lumen and vessel, respectively) diameter by the maximum diameter, whereas the plaque eccentricity index was calculated dividing the minimum plaque thickness by the maximum plaque thickness.

Statistical analysis

Discrete variables are presented as counts and percentages. Continuous variables are presented as means ± SD. The inter-observer and inter-catheter agreement were assessed using Bland–Altman plots [19]. This method plots the mean against the difference in measurements. Limits of agreement were determined by adding two standard deviations to the mean difference for the upper limit and by substracting two standard deviations from the mean difference for the lower limit. A two-sided p value of less than 0.05 indicated statistical significance.

Results

Fifteen consecutive patients with 16 non-significant lesions were included in the study. Baseline characteristics of the patients included are depicted in Table 1. The study vessel was the left anterior descending in 9 patients (60.0%), the left circumflex in 5 (33.3%), and the right coronary artery in 1 patient (6.7%). There were no peri-procedural complications.

Inter-catheter agreement

The studied length determined by landmarks was 19.71 ± 10.5 mm for catheter 1 and 21.01 ± 11.1 mm for catheter 2 ($p = 0.32$). Geometrical and compositional data of matched ROIs interrogated with IVUS-VH using 2 subsequent 20 MHz catheters are extensively depicted in Tables 2 and 3. The relative inter-catheter differences regarding geometrical measurements were negligible for both observers. Of note, the inter-catheter relative difference in plaque CSA was 3.2% for observer 1 and 0.5% for observer 2. Only other less common indirect measurements such as plaque eccentricity and plaque minimal thickness showed relative differences >5%. Compositional measurements showed higher relative differences, although not

Table 1. Study population ($n = 15$).

	n (%)
Age (years ± SD)	63.1 ± 8.6
Male sex	8 (53.3)
Diabetes	2 (13.3)
Hypertension	11 (73.3)
Current smoking	1 (6.7)
Previous smoking	5 (33.3)
Hypercholesterolemia	8 (53.3)
Family history of coronary disease	9 (60.0)
Lipid lowering agents	11 (73.3)
Clinical presentation	
Stable angina	14 (93.3)
Unstable angina	1 (6.7)
Study vessel	
Left anterior descending	9 (60.0)
Left circumflex	5 (33.3)
Right coronary artery	1 (6.7)

Table 2. Mean CSA geometrical measurements of matched ROI with two subsequent 20 MHz IVUS imaging catheters (*n*:16).

	Catheter 1	Catheter 2	Absolute Δ	Relative Δ (%)
Observer 1				
Lumen CSA (mm^2)	11.08 ± 3.5	10.94 ± 3.5	0.14 ± 0.5	1.3
Lumen max. diameter (mm)	4.03 ± 0.7	4.01 ± 0.6	0.02 ± 0.1	0.4
Lumen min. diameter (mm)	3.37 ± 0.6	3.34 ± 0.6	0.03 ± 0.1	0.9
Lumen mean diameter (mm)	3.69 ± 0.6	3.67 ± 0.6	0.02 ± 0.1	0.6
Lumen eccentricity	0.84 ± 0.0	0.83 ± 0.0	0.00 ± 0.0	0.5
Vessel CSA (mm^2)	17.40 ± 4.0	17.46 ± 4.0	0.07 ± 0.4	0.4
Vessel max. diameter (mm)	4.92 ± 0.6	4.93 ± 0.6	0.01 ± 0.1	0.3
Vessel min. diameter (mm)	4.36 ± 0.6	4.37 ± 0.6	0.01 ± 0.1	0.2
Vessel mean diameter (mm)	4.63 ± 0.6	4.64 ± 0.6	0.01 ± 0.0	0.2
Vessel eccentricity	0.89 ± 0.0	0.89 ± 0.0	0.00 ± 0.0	0.1
Plaque CSA (mm^2)	6.32 ± 2.0	6.53 ± 2.1	0.21 ± 0.4	3.2
Plaque max. thickness (mm)	1.01 ± 0.2	1.02 ± 0.2	0.01 ± 0.1	0.7
Plaque min. thickness (mm)	0.09 ± 0.1	0.09 ± 0.1	0.01 ± 0.0	8.2
Plaque eccentricity (mm)	0.09 ± 0.1	0.10 ± 0.1	0.01 ± 0.0	10.0
Plaque burden (%)	36.80 ± 9.9	37.77 ± 9.9	0.97 ± 2.4	2.6
Observer 2				
Lumen CSA (mm^2)	10.66 ± 3.8	10.67 ± 3.8	0.01 ± 0.4	0.1
Lumen max. diameter (mm)	3.90 ± 0.7	3.91 ± 0.7	0.01 ± 0.1	0.2
Lumen min. diameter (mm)	3.34 ± 0.6	3.33 ± 0.6	0.01 ± 0.1	0.3
Lumen mean diameter (mm)	3.61 ± 0.6	3.61 ± 0.7	0.00 ± 0.1	0.0
Lumen eccentricity	0.86 ± 0.0	0.85 ± 0.0	0.01 ± 0.0	0.6
Vessel CSA (mm^2)	17.76 ± 4.0	17.80 ± 4.0	0.05 ± 0.4	0.3
Vessel max. diameter (mm)	4.95 ± 0.6	4.96 ± 0.6	0.01 ± 0.1	0.3
Vessel min. diameter (mm)	4.41 ± 0.6	4.42 ± 0.6	0.01 ± 0.1	0.1
Vessel mean diameter (mm)	4.68 ± 0.6	4.69 ± 0.6	0.01 ± 0.0	0.1
Vessel eccentricity	0.89 ± 0.0	0.89 ± 0.0	0.00 ± 0.0	0.1
Plaque CSA (mm^2)	7.10 ± 2.1	7.13 ± 2.2	0.03 ± 0.4	0.5
Plaque max. thickness (mm)	1.05 ± 0.2	1.04 ± 0.3	0.00 ± 0.1	0.2
Plaque min. thickness (mm)	0.16 ± 0.1	0.16 ± 0.1	0.01 ± 0.0	4.7
Plaque eccentricity (mm)	0.16 ± 0.1	0.17 ± 0.1	0.01 ± 0.0	6.7
Plaque burden (%)	40.75 ± 10.7	40.93 ± 11.2	0.19 ± 1.8	0.5

LCSA, VCSA and PCSA refer to lumen, vessel and plaque CSAs. Plaque burden was calculated as $[(EEM_{area} - Lumen_{area}/EEM_{area}) \times 100]$.

exceeding 10%, except from calcium (11%) for observer 1 and fibrolipidic tissue (13%) for observer 2 (Table 3). Indeed, Bland–Altman plots showed a good inter-catheter agreement for geometrical (Figure 1) and compositional (Figure 2) measurements. The limits of agreement for (observer 1 measurements) lumen, vessel, plaque and plaque burden measurements were 0.82, −1.10 mm^2; 0.80, −0.66 mm^2; 1.08, −0.66 mm^2; and 5.83, −3.89%; respectively. Limits of agreement for calcium, fibrous, fibrolipidic and necrotic core CSA measurements were 0.22, −0.25 mm^2; 1.02, −0.71 mm^2; 0.61, −0.65 mm^2; and 0.43, −0.38 mm^2 respectively.

Inter-observer agreement

For the assessment of the inter-observer agreement, a comparison between the same matched cross-sections (653 frames for catheter 1 and 663 frames for catheter 2) were analyzed by 2 independent observers. These 2 datasets were merged resulting in a paired inter-observer agreement evaluation of 1316 frames.

Inter-observer differences were larger than the inter-catheter measurements (performed by the same observer). This was particularly noticed in indirect measurements such as plaque CSA (10%), plaque minimal thickness (53%) and plaque

Table 3. Mean CSA compositional measurements of matched ROI with two subsequent 20 MHz IVUS imaging catheters (n:16).

	Catheter 1	Catheter 2	Absolute Δ	Relative Δ (%)
Observer 1				
Calcium CSA (mm^2)	0.17 ± 0.3	0.16 ± 0.2	0.01 ± 0.1	8.0
Calcium (%)	4.27 ± 5.2	3.82 ± 3.8	0.45 ± 2.6	11.1
Fibrous CSA (mm^2)	1.96 ± 1.0	2.11 ± 1.1	0.16 ± 0.4	7.7
Fibrous (%)	60.37 ± 9.2	62.15 ± 8.7	1.78 ± 10.0	2.9
Fibrolipidic CSA (mm^2)	0.66 ± 0.4	0.63 ± 0.3	0.02 ± 0.3	3.5
Fibrolipidic (%)	21.10 ± 9.8	19.58 ± 7.0	1.53 ± 8.3	7.5
Necrotic core CSA (mm^2)	0.40 ± 0.4	0.43 ± 0.4	0.02 ± 0.2	5.7
Necrotic core (%)	11.27 ± 6.8	10.87 ± 6.6	0.40 ± 5.4	3.6
Observer 2				
Calcium CSA (mm^2)	0.17 ± 0.3	0.16 ± 0.2	0.01 ± 0.1	8.7
Calcium (%)	4.08 ± 5.0	3.74 ± 3.4	0.34 ± 2.4	8.7
Fibrous CSA (mm^2)	2.21 ± 1.1	2.28 ± 1.2	0.07 ± 0.4	3.1
Fibrous (%)	58.12 ± 10.5	60.63 ± 7.9	2.51 ± 10.1	4.2
Fibrolipidic CSA (mm^2)	0.88 ± 0.6	0.77 ± 0.4	0.11 ± 0.4	13.1
Fibrolipidic (%)	22.97 ± 11.7	20.95 ± 10.8	2.01 ± 9.6	9.2
Necrotic core CSA (mm^2)	0.42 ± 0.4	0.45 ± 0.5	0.03 ± 0.2	6.1
Necrotic core (%)	10.75 ± 6.9	11.02 ± 6.5	0.26 ± 5.5	2.4

LCSA, VCSA and PCSA refer to lumen, vessel and plaque CSAs. Plaque burden was calculated as $[(EEM_{area} - Lumen_{area}/EEM_{area}) \times 100]$.

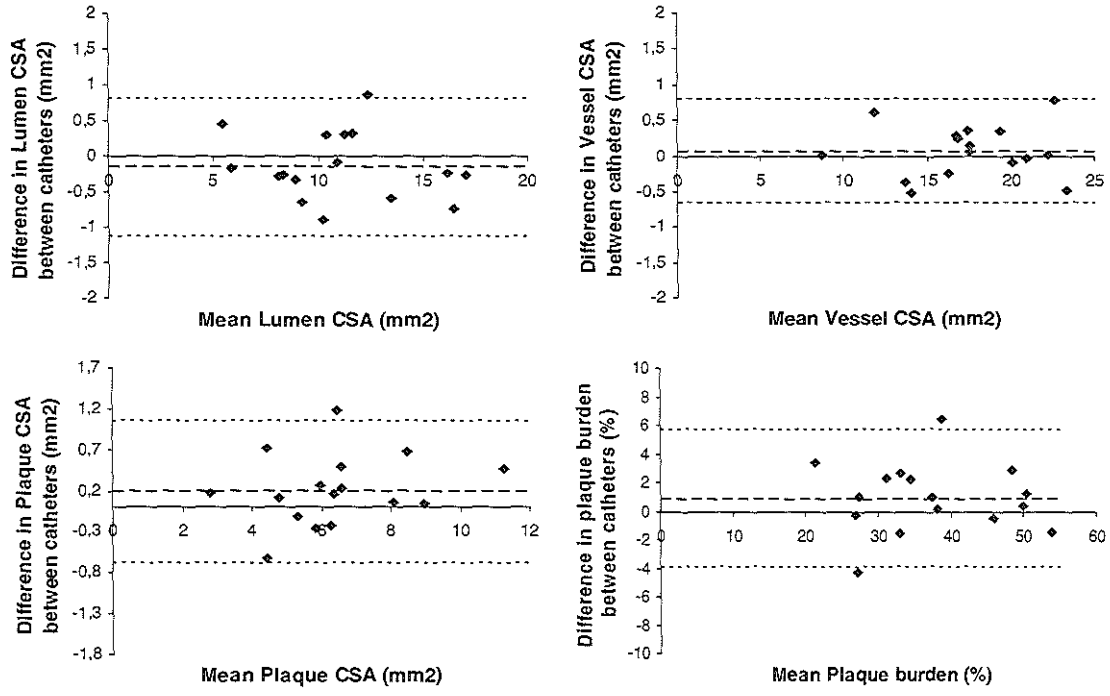

Figure 1. Bland–Altman plots depicting the (observer 1) agreement between catheters for geometrical measurements ($n = 16$).

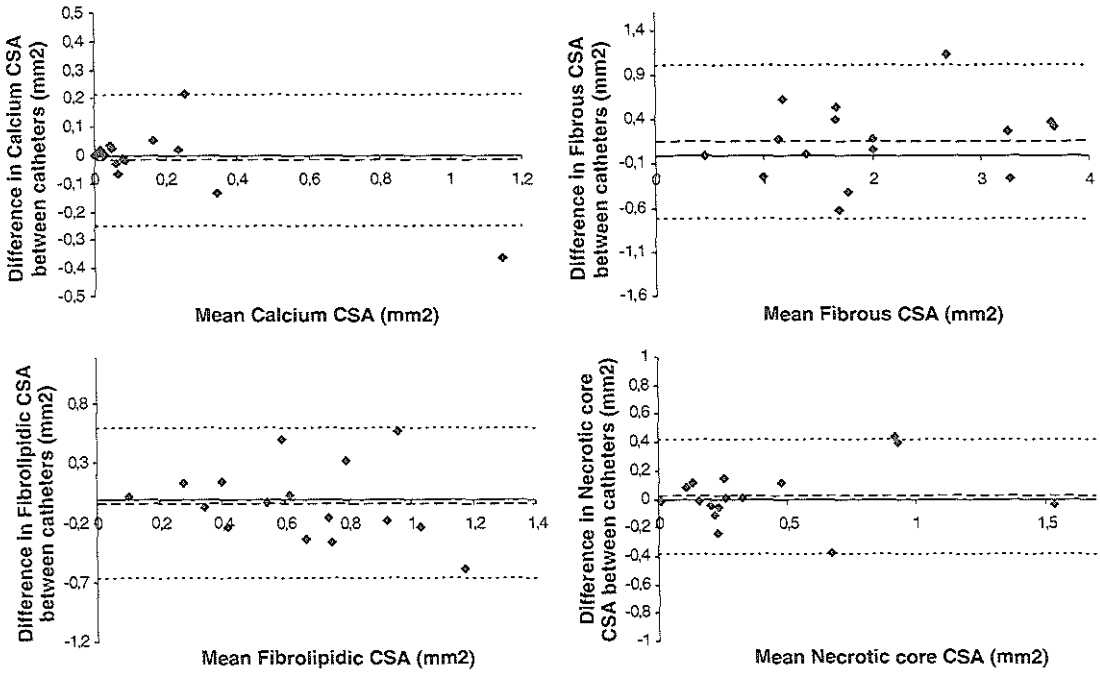

Figure 2. Bland–Altman plots depicting the (observer 1) agreement between catheters for compositional measurements ($n = 16$).

eccentricity (54%). The largest relative difference was found in fibrolipidic measurements (Table 4).

Narrow limits of agreement and few outliers (Figures 3 and 4) were found between observers both for geometrical (limits of agreement for lumen, vessel, plaque and plaque burden measurements of 2.61, −2.09 mm^2; 2.20–3.03 mm^2; 1.70, −3.04 mm^2; and 9.16, −16.41%; respectively) and compositional (limits of agreement for calcium, fibrous, fibrolipidic and necrotic core measurements of 0.08, −0.09 mm^2; 0.89, −1.28 mm^2; 0.74, −1.06 mm^2; and 0.16, −0.20 mm^2; respectively) measurements. It is noteworthy that the fibrous and fibrolipidic CSA measurements were highly accurate when assessing cross-sections with small fibrous or fibrolipidic content (Figure 4).

Discussion

Over the past few years, IVUS has been employed as a tool to assess the temporal effect of conventional and novel drug therapies on coronary plaque size in longitudinal studies [8, 20]. More recently, the discordance between the beneficial clinical effects of secondary prevention strategies and their effect on plaque volume had lead investigators to explore a potential significant effect on plaque composition [21].

Tissue characterization by means of IVUS radiofrequency (RF) data analysis is a potential tool to enable an accurate evaluation of the composition of coronary plaques [13]. Several investigators have explored the potential of RF data analysis in vivo and reported promising findings [15–17, 22, 23]. This technique has the potential to detect temporal changes in plaque composition and therefore studies have been conducted to assess the effect of conventional drug therapies on the phenotype of coronary atherosclerosis [18, 22, 23]. In addition, there are currently several large trials being conducted with the aim to assess the natural history of high-risk plaques by means of this technique.

Table 4. Geometrical and compositional measurements of matched CSAs between different observers (n:1316).

	Observer 1	Observer 2	Absolute Δ	Relative Δ (%)
Geometrical data				
Lumen CSA (mm^2)	10.83 ± 3.8	10.51 ± 4.0	0.26 ± 1.2	2.5
Lumen max. diameter (mm)	3.96 ± 0.7	3.86 ± 0.8	0.08 ± 0.4	2.1
Lumen min. diameter (mm)	3.34 ± 0.6	3.31 ± 0.7	0.01 ± 0.3	0.2
Lumen mean diameter (mm)	3.65 ± 0.7	3.58 ± 0.7	0.04 ± 0.3	1.1
Lumen eccentricity	0.84 ± 0.1	0.86 ± 0.1	0.02 ± 0.1	2.3
Vessel CSA (mm^2)	16.90 ± 4.2	17.22 ± 4.3	0.41 ± 1.3	2.4
Vessel max. diameter (mm)	4.84 ± 0.6	4.87 ± 0.6	0.06 ± 0.4	1.1
Vessel min. diameter (mm)	4.30 ± 0.6	4.35 ± 0.6	0.08 ± 0.3	1.7
Vessel mean diameter (mm)	4.56 ± 0.6	4.61 ± 0.6	0.07 ± 0.3	1.5
Vessel eccentricity	0.89 ± 0.1	0.89 ± 0.1	0.01 ± 0.1	1.1
Plaque CSA (mm^2)	6.07 ± 2.3	6.72 ± 2.3	0.67 ± 1.2	10.3
Plaque max. thickness (mm)	0.96 ± 0.3	1.01 ± 0.3	0.03 ± 0.2	3.4
Plaque min. thickness (mm)	0.09 ± 0.1	0.16 ± 0.1	0.07 ± 0.1	53.3
Plaque eccentricity (mm)	0.09 ± 0.1	0.16 ± 0.1	0.07 ± 0.1	53.6
Plaque burden (%)	36.62 ± 12.2	40.07 ± 12.5	3.63 ± 6.4	9.5
Compositional data				
Calcium CSA (mm^2)	0.12 ± 0.2	0.12 ± 0.2	0.00 ± 0.0	2.9
Calcium (%)	3.66 ± 6.4	3.51 ± 6.0	0.13 ± 2.4	3.7
Fibrous CSA (mm^2)	1.86 ± 1.3	2.05 ± 1.3	0.20 ± 0.5	10.2
Fibrous (%)	61.48 ± 18.2	60.05 ± 18.2	1.10 ± 14.3	1.8
Fibrolipidic CSA (mm^2)	0.60 ± 0.5	0.75 ± 0.7	0.16 ± 0.5	23.5
Fibrolipidic (%)	22.34 ± 14.0	22.09 ± 15.3	1.86 ± 11.8	8.8
Necrotic core CSA (mm^2)	0.35 ± 0.4	0.37 ± 0.4	0.02 ± 0.1	6.3
Necrotic core (%)	10.45 ± 10.1	10.22 ± 9.8	0.17 ± 5.7	1.6

LCSA, VCSA and PCSA refer to lumen, vessel and plaque CSAs. Plaque burden was calculated as $[(EEM_{area} - Lumen_{area}/EEM_{area}) \times 100]$.

As the impact of drug therapies on the atherosclerotic plaque burden and composition over time is relatively small, highly reproducible IVUS-VH measurements are essential. Despite such pivotal need for reproducibility data to address the stability of the technique, such studies are lacking. Only indirect evidence of reproducibility has been reported such as a study conducted by our group to assess the 6-month change in plaque composition with no controlled therapeutic intervention [18], and the study conducted by Kawasaki et al. who reported the intra and inter-observer variability of measurements performed using the same pullback [22].

The present study has a unique characteristic since we used two catheters of the same kind at the same time-point, thus simulating the scenario of a longitudinal study.

The main finding of the present study was that IVUS-VH measurements had an acceptable reproducibility. As expected, compositional measurements were more variable than geometrical measurements. Nevertheless, it is noteworthy that inter-catheter differences were predominantly lower than 10%, highly correlated and showed a good agreement. Of note, necrotic core measurements, probably the most relevant component of coronary plaques and currently subject of intense research, showed an excellent inter-catheter and inter-observer agreement. This has a major importance since the temporal change of such component could potentially become an imaging endpoint of longitudinal studies. Similarly, calcium measurements, another important component of atherosclerotic plaques, showed good inter-catheter and inter-observer agreement. The relatively high inter-observer variability of some IVUS-VH variables raises some caution and should be taken into consideration when performing longitudinal studies analyzed by

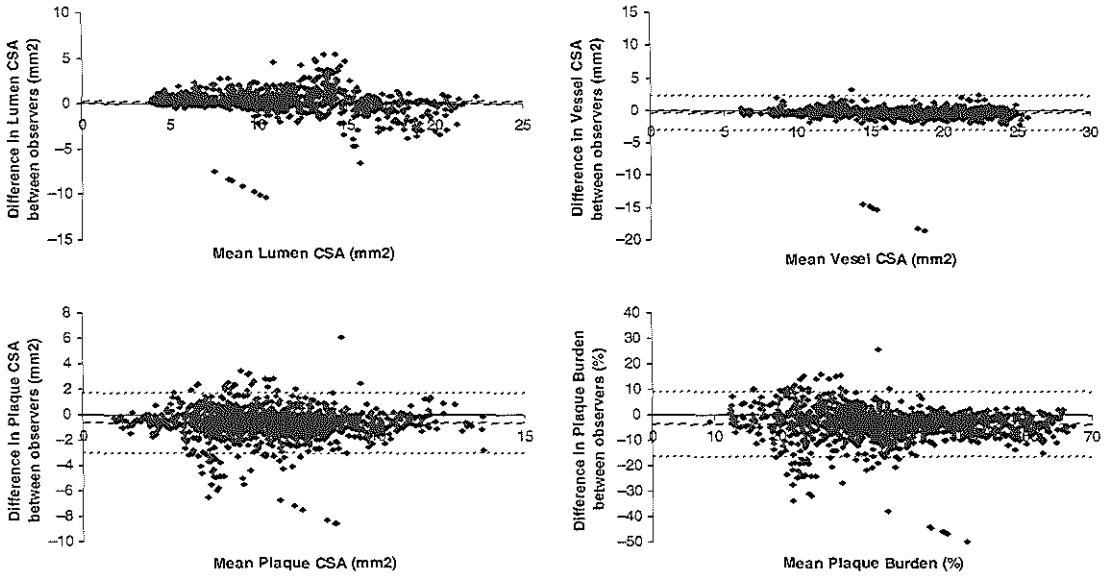

Figure 3. Bland–Altman plots showing the inter-observer agreement for geometrical measurements ($n = 1316$).

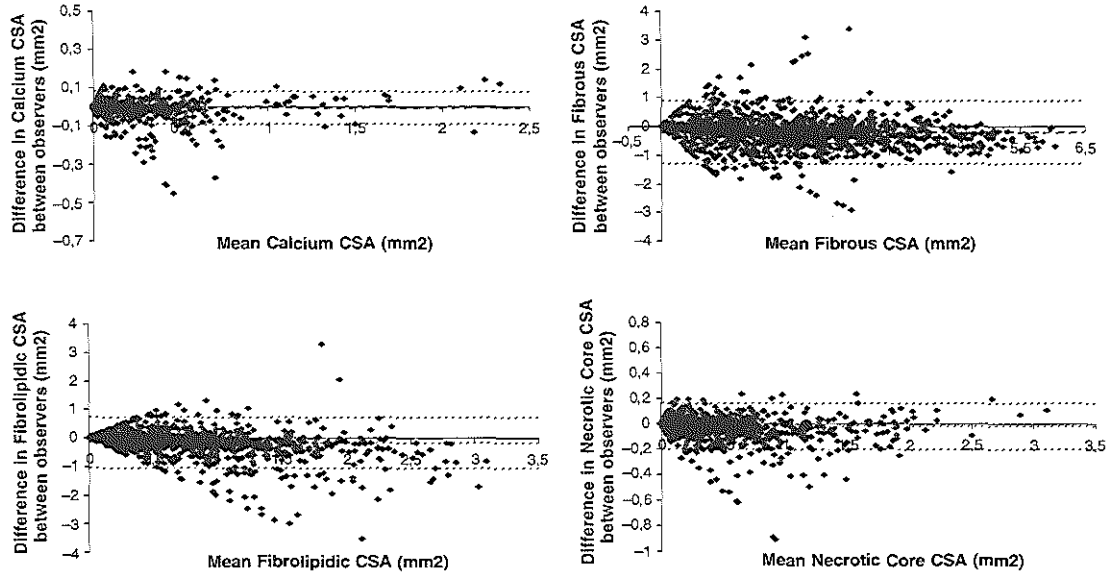

Figure 4. Bland–Altman plots showing the inter-observer agreement for compositional measurements ($n = 1316$).

core laboratories. Overall, the inter-catheter and inter-observer differences shown might provide boundaries over which changes are statistically significant.

It is evident yet worth mentioning that precise contour detection probably has an essential role in the reproducibility of IVUS-VH measurements. The inter-observer relative difference in plaque CSA measurements was 10%, the commonly accepted threshold. This gives an additive value to our study, since it provides a "real-world" scenario that can aid investigators to perform precise power calculations for longitudinal studies.

Finally, although we aimed at studying non-tortuous and non-severely calcified vessels, phased-array IVUS imaging catheters are devoid from a covering sheath and pullbacks are therefore occasionally prone to be non-uniform. This clearly has an impact on determination of the size and composition of atherosclerotic plaques and needs to be taken into consideration for the design of longitudinal studies (Figure 5).

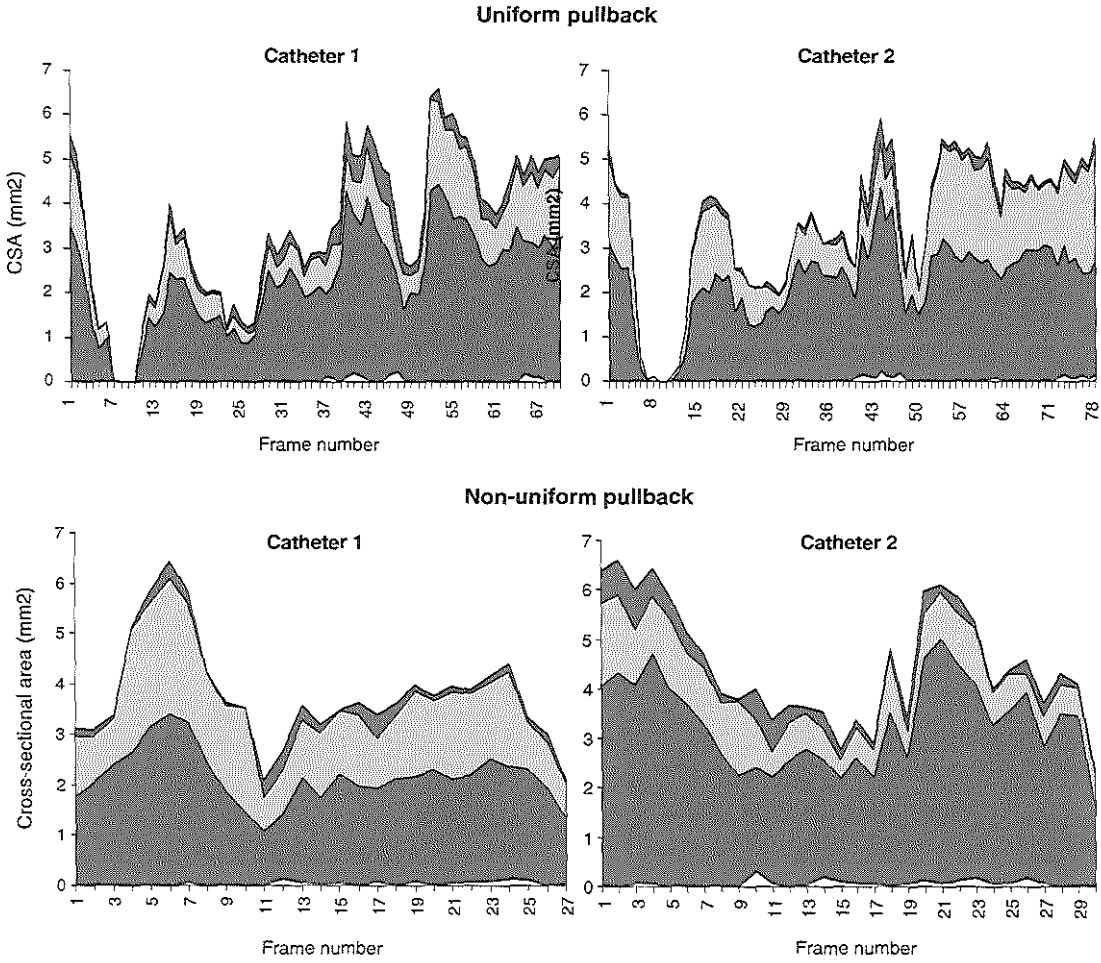

Figure 5. Sequential plotting of a matched ROI interrogated with two catheters. The mean CSA (*y* axis) of each plaque component is colour-coded (calcium: white, fibrous: green, fibrolipidic: greenish-yellow and necrotic core: red). This figure shows an example of the impact of non-uniform pullbacks on geometrical and compositional measurements.

Limitations

The studied population was relatively small. Nevertheless, the conductance of large in vivo studies of this nature is complicated due to obvious ethical issues. The selection of a population of patients with non-tortuous and non-severely calcified vessels was driven by the aim to study the reproducibility of the technique itself, not of the pullback device. Nevertheless, as shown in Figure 5, the impact of non-uniform pullback speed was not negligible potentially influencing the results.

Conclusions

The present study demonstrates that the geometrical and compositional output of IVUS-VH is acceptably reproducible. In addition, by providing a "real-world" scenario, this study can aid investigators to perform precise power calculations for longitudinal studies.

References

1. Guedes A, Keller PF, L'Allier PL, Lesperance J, Gregoire J, Tardif JC. Long-term safety of intravascular ultrasound in nontransplant, nonintervened, atherosclerotic coronary arteries. J Am Coll Cardiol 2005; 45: 559–564.
2. Wenguang L, Gussenhoven WJ, Zhong Y, et al. Validation of quantitative analysis of intravascular ultrasound images. Int J Card Imaging 1991; 6(3–4): 247–253.
3. de Jaegere P, Mudra H, Figulla H, et al. Intravascular ultrasound-guided optimized stent deployment. Immediate and 6 months clinical and angiographic results from the Multicenter Ultrasound Stenting in Coronaries Study (MUSIC Study). Eur Heart J 1998; 19: 1214–1223.
4. Fitzgerald PJ, Oshima A, Hayase M, et al. Final results of the Can Routine Ultrasound Influence Stent Expansion CRUISE study. Circulation 2000; 102: 523–530.
5. Jeremias A, Huegel H, Lee DP, et al. Spatial orientation of atherosclerotic plaque in non-branching coronary artery segments. Atherosclerosis 2000; 152: 209–215.
6. Kimura BJ, Russo RJ, Bhargava V, McDaniel MB, Peterson KL, DeMaria AN. Atheroma morphology and distribution in proximal left anterior descending coronary artery: in vivo observations. J Am Coll Cardiol 1996; 27: 825–831.
7. Smits PC, Pasterkamp G, Quarles van Ufford MA, et al. Coronary artery disease: arterial remodelling and clinical presentation. Heart 1999; 82: 461–464.
8. Nissen SE, Tsunoda T, Tuzcu EM, et al. Effect of recombinant ApoA-I Milano on coronary atherosclerosis in patients with acute coronary syndromes: a randomized controlled trial. JAMA 2003; 290: 2292–2300.
9. Fang JC, Kinlay S, Beltrame J, et al. Effect of vitamins C and E on progression of transplant-associated arteriosclerosis: a randomised trial. Lancet 2002; 359: 1108–1113.
10. Nissen SE, Tuzcu EM, Schoenhagen P, et al. Effect of intensive compared with moderate lipid-lowering therapy on progression of coronary atherosclerosis: a randomized controlled trial. JAMA 2004; 291: 1071–1080.
11. Davies MJ, Richardson PD, Woolf N, Katz DR, Mann J. Risk of thrombosis in human atherosclerotic plaques: role of extracellular lipid, macrophage, and smooth muscle cell content. Br Heart J 1993; 69: 377–381.
12. Peters RJ, Kok WE, Havenith MG, Rijsterborgh H, van der Wal AC , Visser CA. Histopathologic validation of intracoronary ultrasound imaging. J Am Soc Echocardiogr 1994; 7: 230–241.
13. Nair A, Kuban BD, Tuzcu EM, Schoenhagen P, Nissen SE, Vince DG. Coronary plaque classification with intravascular ultrasound radiofrequency data analysis. Circulation 2002; 106: 2200–2206.
14. Rodriguez-Granillo GA, Aoki J, Ong AT, et al. Methodological considerations and approach to cross-technique comparisons using in vivo coronary plaque characterization based on intravascular ultrasound radiofrequency data analysis: insights from the Integrated Biomarker and Imaging Study (IBIS). Int J Cardiovasc Intervent 2005; 7: 52–58.
15. Rodriguez-Granillo GA, Serruys PW, Garcia-Garcia HM, et al. Coronary artery remodelling is related to plaque composition. Heart 2005 Jun 17; (Epub ahead of print).
16. Rodriguez-Granillo GA, Garcia-Garcia H, Mc Fadden E, et al. In vivo intravascular ultrasound-derived thin-cap fibroatheroma detection using ultrasound radiofrequency data analysis. J Am Coll Cardiol 2005; 46(11): 2038–2042.
17. Rodriguez-Granillo GA, McFadden E, Valgimigli M, et al. Coronary plaque composition of non-culprit lesions assessed by in vivo intracoronary ultrasound radio frequency data analysis, is related to clinical presentation. Am Heart J 2006; In press.
18. Rodriguez-Granillo GA, Serruys PW, Mc Fadden E, et al. First-in-man prospective evaluation of temporal changes in coronary plaque composition by in vivo ultrasound radio frequency data analysis: an integrated biomarker and imaging study (IBIS) substudy. Eurointervention 2005; 3: 282–288.
19. Bland JM, Altman DG. Statistical methods for assessing agreement between two methods of clinical measurement. Lancet 1986; 1: 307–310.
20. Takagi T, Yoshida K, Akasaka T, Hozumi T, Morioka S, Yoshikawa J. Intravascular ultrasound analysis of reduction in progression of coronary narrowing by treatment with pravastatin. Am J Cardiol 1997; 79: 1673–1676.
21. Schartl M, Bocksch W, Koschyk DH, et al. Use of intravascular ultrasound to compare effects of different strategies

of lipid-lowering therapy on plaque volume and composition in patients with coronary artery disease. Circulation 2001; 104: 387–392.
22. Kawasaki M, Sano K, Okubo M, et al. Volumetric quantitative analysis of tissue characteristics of coronary plaques after statin therapy using three-dimensional integrated backscatter intravascular ultrasound. J Am Coll Cardiol 2005; 45: 1946–1953.
23. Yokoyama M, Komiyama N, Courtney BK, et al. Plasma low-density lipoprotein reduction and structural effects on coronary atherosclerotic plaques by atorvastatin as clinically assessed with intravascular ultrasound radio-frequency signal analysis: a randomized prospective study. Am Heart J 2005; 150: 287.

Address for correspondence: Patrick W. Serruys, Thoraxcenter, Bd 406, Dr Molewaterplein 40, 3015 GD, Rotterdam, The Netherlands
Tel.: +31-10-4635260; Fax: +31-10-4369154
E-mail: p.w.j.c.serruys@erasmusmc.nl

CHAPTER 3.1

Relation of plaque size to necrotic core in the three major coronary arteries in patients with acute coronary syndrome as determined by intravascular ultrasonic imaging radiofrequency.

Garcia-Garcia HM, Goedhart D, Serruys PW.

Am J Cardiol. 2007;99:790-2.

Relation of Plaque Size to Necrotic Core in the Three Major Coronary Arteries in Patients With Acute Coronary Syndrome as Determined by Intravascular Ultrasonic Imaging Radiofrequency

Héctor M. García-García, MD[a], Dick Goedhart, PhD[b], and Patrick W. Serruys, MD, PhD[a,*]

According to pathologic studies, the content of a necrotic core increases in a "linear fashion" as plaque enlarges. In addition, these 2 plaque characteristics have been associated with plaque vulnerability. This study assessed the relation between plaque cross-sectional area (CSA) and content of necrotic core (NC). Twenty-five patients (75 arteries) with acute coronary syndrome were studied. In total, 7,834 CSAs were analyzed. An analysis of plaque CSA in percentiles was performed (median 5.5 mm^2, interquartile range 3.7 to 7.8); subsequently, plaque CSA values were categorized as small (≤3.7 mm^2), medium (>3.7 to ≤7.8 mm^2), and large (>7.8 mm^2). There was a difference in content of the NC between arteries within each plaque CSA category. This observation was confirmed in a multivariate analysis in which only 2 variables remained statistically significant, plaque CSA (estimate 1.34, SE 0.05, $p < 0.0001$) and studied artery (left anterior descending coronary artery, estimate 0.29, SE 0.08, $p = 0.0003$; left circumflex coronary artery, estimate 0.23, SE 0.07, $p = 0.0014$; and these vs the right coronary artery). In conclusion, the NC and plaque increase in patients with acute coronary syndromes. (Am J Cardiol 2007;99:790–792)

The mechanisms of how atherosclerotic plaques grow are not fully understood. Two main mechanisms of plaque progression have been postulated; the first describes a continuous and progressive lipid accumulation and collagen synthesis,[1] whereas current evidence favors a stepwise process resulting from progressive accumulation of a necrotic core (NC), thinning of the fibrous cap and its rupture with consequent healing leading to an increase in luminal narrowing,[1,2] or intraplaque hemorrhage that abruptly increases the plaque.[3] In any case, according to pathologic studies, it seems that the content of a NC increases in a "linear fashion" as plaque enlarges.[4,5] In addition, these 2 plaque characteristics have been associated with plaque vulnerability.[6] Pathology offers detailed and accurate information on these atherosclerotic plaques. However, pathologists can only analyze retrospectively and somewhat incompletely because they study the coronary vessel every 3 to 5 mm.[5,7] Conversely, the sampling rate of in vivo imaging techniques such as intravascular ultrasound (IVUS) can be set up every 0.25, 0.5, or 1 mm,[8] although the resolution is lower. IVUS allows tomographic assessment of the vessel wall that has been recently complemented with backscatter radiofrequency data analysis, also called IVUS virtual histology (IVUS-VH; Volcano Therapeutics, Rancho Cordova, California). To date, no in vivo study has assessed the relation between plaque cross-sectional area (CSA) and content of the NC.

Methods and Results

This prospective investigator-driven study included patients with an acute coronary syndrome (ACS), namely, unstable angina pectoris according to the Braunwald classification, non–ST-segment elevation myocardial infarction, and ST-segment elevation myocardial infarction, in which all 3 coronary arteries were interrogated using IVUS radiofrequency data analysis. IVUS-VH was performed with 20-MHz catheters (Eagle Eye, Volcano Therapeutics), and contour detection was determined using a previously reported methodology.[9] This radiofrequency data analysis allows tissue characterization.[10,11] Specifically, it can identify 4 different tissues (NC, red; dense calcium, white; fibrofatty tissue, greenish; and fibrotic tissue, green). Informed consent was obtained from all patients. Data acquisition was electrocardiographically gated and recorded during automated withdrawal of the catheter using a mechanical pull-back device (Volcano Therapeutics) at a pull-back speed of 0.5 mm/s. Cine runs before and during contrast injection were performed to define the position of the IVUS catheter before pullback was started.

The IVUS-VH sampling rate during pullback is gated to the peak R wave and is therefore dependent on heart rate. For instance, during a constant heart rate of 60 beats/min, data will be collected every 0.5 mm.

Discrete variables are presented as counts and percentages. Continuous variables are presented as means ± SDs. A 2-sided p value <0.05 indicated statistical significance. Assumptions for normality were checked after transformation based on a p value >0.20 when using the Kolmogorov-Smirnov test and on visual assessment of Q-Q plots of residuals. Accordingly, log transformation was performed on variables with skewed distribution.

All CSAs were assessed as a function of the distance from the ostium of the artery. Coronary artery length was divided into 3 segments; the proximal segment comprised the first 3 cm, the midsegment the second 3 cm, and the distal segment the following 3 cm. Using a general mixed model and allowing an autoregressive correlation structure with content of the NC (square millimeters) as a dependent

[a]Thoraxcenter, Erasmus MC; and [b]Cardialysis BV, Rotterdam, The Netherlands. Manuscript received August 11, 2006; revised manuscript received and accepted October 9, 2006.

*Corresponding author: Tel: 31-10-463-5260; fax: 31-10-436-9154.
E-mail address: p.w.j.c.serruys@erasmusmc.nl (P.W. Serruys).

0002-9149/07/$ – see front matter © 2007 Elsevier Inc. All rights reserved.
doi:10.1016/j.amjcard.2006.10.037

Table 1
Compositional and geometric analysis (n = 25 patients, 75 arteries)

Calcified (mm^2)	0.17 ± 0.36
Calcified (%)	3.6 ± 5.7
Fibrous (mm^2)	2.1 ± 1.8
Fibrous (%)	64.6 ± 13.2
Fibrolipid (mm^2)	0.65 ± 0.76
Fibrolipid (%)	19.6 ± 13.4
NC (mm^2)	0.48 ± 0.69
NC (%)	12.2 ± 10.8
Vessel CSA (mm^2)	17.2 ± 7.5
Lumen CSA (mm^2)	10.5 ± 5.3
Plaque CSA (mm^2)	6.7 ± 3.6
Plaque eccentricity (min/max)	0.14 ± 0.15
Plaque burden (%)*	39.0 ± 12.6

Values are means ± SDs.
* Defined as $EEM_{area} - lumen_{area}/EEM_{area} \times 100$, where EEM is external elastic membrane, max = maximum; min = minimum.

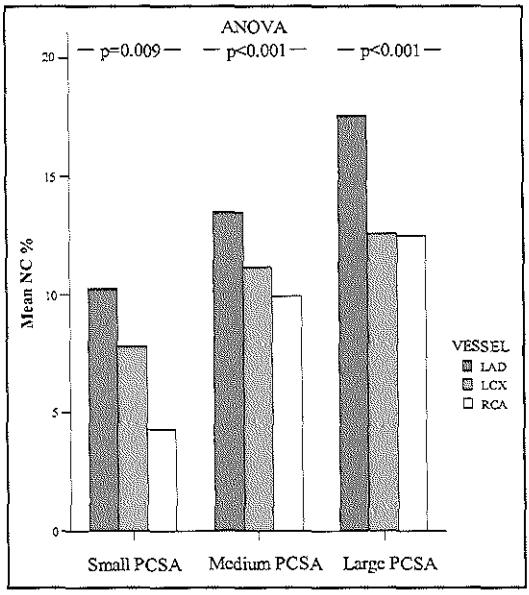

Figure 1. Bar graph shows plaque CSA (PCSA) categorized into 3 groups according to plaque size (x axis) and relative amount of the NC (y axis) in the left anterior descending coronary artery *(blue bars)*, left circumflex coronary artery *(green bars)*, and right coronary artery *(yellow bars)*. ANOVA = analysis of variance.

variable and the artery, the culprit vessel, location of CSAs (i.e., proximal, mid, and distal), plaque CSA, lumen CSA, and interaction between plaque CSA and location and between artery and location as independent covariates, the hypothesis was tested.

Twenty-five patients (75 arteries) were studied. Patients' mean age was 53 ± 11 years. Most were men (84%), and 12% were diabetic. Forty-eight percent presented with ST-segment elevation myocardial infarction. In total, 7,834 CSAs were studied. The overall compositional and geometric analysis is presented in Table 1. Analysis of plaque CSA in percentiles was performed (median 5.5 mm^2, interquartile range 3.7 to 7.8); subsequently plaque CSA values were categorized as small (≤3.7 mm^2), medium (>3.7 to ≤7.8 mm^2), and large (>7.8 mm^2). Figure 1 shows percent differences in content of NC between vessels within each plaque CSA category. This observation was confirmed in multivariate analysis, where only 2 variables remained statistically significant, namely, plaque CSA (estimate 1.34, SE 0.05, $p < 0.0001$) and studied vessel (left anterior descending coronary artery, estimate 0.29, SE 0.08, $p = 0.0003$; left circumflex coronary artery, estimate 0.23, SE 0.07, $p = 0.0014$; these vs right coronary artery).

Overall, the Pearson correlation coefficient was 0.62 ($p < 0.001$) between plaque CSA and NC. In particular, the Pearson correlation coefficient was 0.68 ($p < 0.001$) in the left anterior descending coronary artery compared with 0.50 ($p < 0.001$) and 0.64 ($p < 0.001$) in the left circumflex and right coronary arteries (Figure 2).

Plaque CSA in patients with unstable angina/non–ST-segment elevation myocardial infarction was 5.4 ± 2.8 versus 7.1 ± 4.2 mm^2 in patients with ST-segment elevation myocardial infarction ($p < 0.001$); content of the NC in patients with unstable angina/non–ST-segment elevation myocardial infarction/ST-segment elevation myocardial infarction was 0.30 ± 0.43 mm^2; in patients with ST-segment elevation myocardial infarction, the content of NC was 0.58 ± 0.82 mm^2 ($p < 0.001$). Pearson's correlation coefficients between plaque CSA and NC were 0.54 ($p < 0.001$) and 0.65 ($p < 0.001$) in patients with unstable angina/non–ST-segment elevation myocardial infarction and in patients with ST-segment elevation myocardial infarction, respectively.

Discussion

Regarding instability of plaque, the size of the NC is of critical importance. In thin cap fibroatheromas, there are different degrees of disease. Not all of these plaques will actually rupture. Those that do rupture are significantly more obstructive and contain a larger NC, macrophage infiltration, calcium, fewer smooth muscles cells, and more positive remodeling than nonruptured thin cap fibroatheromas.[6]

Although the increment in plaque size is followed by an increase in the NC, it seems that this occurs to a slightly different degree in each vessel. In this study, the CSAs with the same plaque size in the left anterior descending artery compared with the left circumflex and right coronary arteries had a significantly larger NC. This finding is in line with what has been reported in many clinical studies in which the left anterior descending coronary artery is the most common culprit vessel. Further, although in this CSA-based analysis, simple correlations do not properly assess the relation of plaque CSA and the NC mainly due to a lack of independency, the slope of the regression line is steeper in the left anterior descending than in the left circumflex coronary artery and similar to the right coronary artery. Subsequently, multivariate analysis was performed to take into account the serial correlation (consecutiveness of CSAs along the vessel) and dependency of the variables, and plaque CSA and vessel were found to be the only predictors of NC.

Interestingly, in patients with ST-segment elevation myocardial infarction, plaque CSA was larger than in pa-

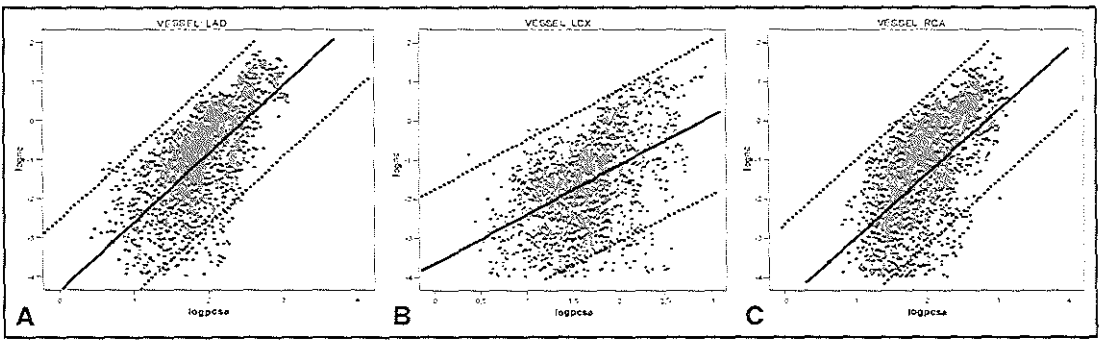

Figure 2. Scatterplots show simple correlation between plaque CSA and the NC in the *(A)* left anterior descending coronary artery (LAD), *(B)* left circumflex coronary artery (LCX), and *(C)* right coronary artery (RCA). Abbreviation as in Figure 1.

tients with unstable angina/non–ST-segment elevation myocardial infarction, as was the content of the NC. This finding is in line with previous studies in which different markers of vulnerability were found to be different between these 2 populations.[12]

Thus, plaque size could be a surrogate of NC size in the coronary tree of patients presenting with ACS. This observation extends the concept of "act local, act global" by Libby,[13] which incorporates the need to further assess the coronary tree beyond the culprit lesion; apart from the culprit lesion, in the same vessel or in the other 2 main coronary vessels, other NC-rich atherosclerotic plaques might be encountered, more likely those with a large plaque burden. This concept, from a clinical point of view, seems logical and simple but has a tremendous effect on midterm follow-up in this specific population. Goldstein et al[14] reported that patients with ST-segment elevation myocardial infarction and multiple complex lesions during the year after ST-segment elevation myocardial infarction had an increased incidence of recurrent ACS compared with patients with single complex lesions (19.0% vs 2.6%, $p < 0.001$, respectively) and repeated angioplasty, particularly of noninfarct-related lesions (32.0% vs 12.4%, $p < 0.001$).

Caution should be used with these results, because this is a highly selective population in terms of clinical presentation, i.e., all patients had an ACS. A previous report by our group[15] found that patients with ACS had a significantly larger percent mean NC compared with stable patients ($12.26 \pm 7.0\%$ vs $7.40 \pm 5.50\%$, $p = 0.006$). Therefore, the relation between plaque CSA and the NC might differ in patients with stable angina.

Acknowledgement: The authors thank Neville Kukreja, MRCP, for his critical review of this report.

1. Mann J, Davies MJ. Mechanisms of progression in native coronary artery disease: role of healed plaque disruption. *Heart* 1999;82:265–268.
2. Burke AP, Kolodgie FD, Farb A, Weber DK, Malcom GT, Smialek J, Virmani R. Healed plaque ruptures and sudden coronary death: evidence that subclinical rupture has a role in plaque progression. *Circulation* 2001;103:934–940.
3. Virmani R, Kolodgie FD, Burke AP, Finn AV, Gold HK, Tulenko TN, Wrenn SP, Narula J. Atherosclerotic plaque progression and vulnerability to rupture: angiogenesis as a source of intraplaque hemorrhage. *Arterioscler Thromb Vasc Biol* 2005;25:2054–2061.
4. Stary HC, Chandler AB, Glagov S, Guyton JR, Insull WJ, Rosenfeld ME, Schaffer SA, Schwartz CJ, Wagner WD, Wissler RW. A definition of initial, fatty streak, and intermediate lesions of atherosclerosis. A report from the Committee on Vascular Lesions of the Council on Arteriosclerosis, American Heart Association. *Circulation* 1994;89:2462–2478.
5. Mann JM, Davies MJ. Vulnerable plaque. Relation of characteristics to degree of stenosis in human coronary arteries. *Circulation* 1996;94:928–931.
6. Kolodgie FD, Virmani R, Burke AP, Farb A, Weber DK, Kutys R, Finn AV, Gold HK. Pathologic assessment of the vulnerable human coronary plaque. *Heart* 2004;90:1385–1391.
7. Burke AP, Farb A, Malcom GT, Liang YH, Smialek J, Virmani R. Coronary risk factors and plaque morphology in men with coronary disease who died suddenly. *N Engl J Med* 1997;336:1276–1282.
8. Di Mario C, Gorge G, Peters R, Kearney P, Pinto F, Hausmann D, von Birgelen C, Colombo A, Mudra H, Roelandt J, Erbel R. Clinical application and image interpretation in intracoronary ultrasound. Study Group on Intracoronary Imaging of the Working Group of Coronary Circulation and of the Subgroup on Intravascular Ultrasound of the Working Group of Echocardiography of the European Society of Cardiology. *Eur Heart J* 1998;19:207–229.
9. Rodriguez-Granillo GA, Serruys PW, Garcia-Garcia HM, Aoki J, Valgimigli M, van Mieghem CA, McFadden E, de Jaegere PP, de Feyter P. Coronary artery remodelling is related to plaque composition. *Heart* 2006;92:388–391.
10. Kawasaki M, Takatsu H, Noda T, Sano K, Ito Y, Hayakawa K, Tsuchiya K, Arai M, Nishigaki K, Takemura G, et al. In vivo quantitative tissue characterization of human coronary arterial plaques by use of integrated backscatter intravascular ultrasound and comparison with angioscopic findings. *Circulation* 2002;105:2487–2492.
11. Nair A, Kuban BD, Tuzcu EM, Schoenhagen P, Nissen SE, Vince DG. Coronary plaque classification with intravascular ultrasound radiofrequency data analysis. *Circulation* 2002;106:2200–2206.
12. Van Mieghem CA, McFadden EP, de Feyter PJ, Bruining N, Schaar JA, Mollet NR, Cademartiri F, Goedhart D, de Winter S, Granillo GR, et al. Noninvasive detection of subclinical coronary atherosclerosis coupled with assessment of changes in plaque characteristics using novel invasive imaging modalities: the Integrated Biomarker and Imaging Study (IBIS). *J Am Coll Cardiol* 2006;47:1134–1142.
13. Libby P. Act local, act global: inflammation and the multiplicity of "vulnerable" coronary plaques. *J Am Coll Cardiol* 2005;45:1600–1602.
14. Goldstein JA, Demetriou D, Grines CL, Pica M, Shoukfeh M, O'Neill WW. Multiple complex coronary plaques in patients with acute myocardial infarction. *N Engl J Med* 2000;343:915–922.
15. Rodriguez-Granillo GA, McFadden EP, Valgimigli M, van Mieghem CA, Regar E, de Feyter PJ, Serruys PW. Coronary plaque composition of nonculprit lesions, assessed by in vivo intracoronary ultrasound radio frequency data analysis, is related to clinical presentation. *Am Heart J* 2006;151:1020–1024.

CHAPTER 3.2

Plaque composition in the left main stem mimics the distal but not the proximal tract of the left coronary artery: influence of clinical presentation, length of the left main trunk, lipid profile, and systemic levels of C-reactive protein.

Valgimigli M, Rodriguez-Granillo GA, **Garcia-Garcia HM**, Vaina S, De Jaegere P, De Feyter P, Serruys PW.

J Am Coll Cardiol. 2007;49(1):23-31.

Plaque Composition in the Left Main Stem Mimics the Distal But Not the Proximal Tract of the Left Coronary Artery

Influence of Clinical Presentation, Length of the Left Main Trunk, Lipid Profile, and Systemic Levels of C-Reactive Protein

Marco Valgimigli, MD, PhD, Gastón A. Rodriguez-Granillo, MD, PhD, Héctor M. Garcia-Garcia, MD, Sophia Vaina, MD, PhD, Peter De Jaegere, MD, PhD, Pim De Feyter, MD, PhD, Patrick W. Serruys, MD, PhD

Rotterdam, the Netherlands

Objectives We sought to investigate whether plaques located in the left main stem (LMS) differ in terms of necrotic core content from those sited in the proximal tract of the left coronary artery.

Background Plaque composition, favoring propensity to vulnerability, might be nonuniformly distributed along the vessel, which might explain the greater likelihood for plaque erosion or rupture to occur in the proximal but not in the distal tracts of the coronary artery or in LMS.

Methods A total of 72 patients were included prospectively; 48 (32 men; mean age 57 ± 11 years; 25 with stable angina and 23 affected by acute coronary syndromes) underwent a satisfactory nonculprit vessel investigation through spectral analysis of intravascular ultrasound radiofrequency data (IVUS-Virtual Histology, Volcano Corp., Rancho Cordova, California). The region of interest was subsequently divided into LMS and LMS carina, followed by 6 consecutive nonoverlapping 6-mm segments in left anterior descending artery in 34 patients or in circumflex artery in 14 patients.

Results Necrotic core content (%): 1) was minimal in LMS (median [interquartile range]: 4.6 [2 to 7]), peaked in the first 6-mm coronary segment (11.8 [8 to 16]; $p < 0.01$), and then progressively decreased distally; 2) was overall greater in patients with acute coronary syndromes (11.4 [5.5 to 19.8]) than stable angina (7.3 [3.2 to 12.9]; $p < 0.001$); 3) was largely independent from plaque size; and 4) did not correlate to systemic levels of C-reactive protein or lipid profile.

Conclusions Plaques located in the LMS carry minimal necrotic content. Thus, they mimic the distal but not the proximal tract of the left coronary artery, where plaque rupture or vessel occlusion occurs more frequently.
(J Am Coll Cardiol 2007;49:23–31)

The distribution of ruptured or prone-to-rupture plaques is known to be nonuniform throughout the coronary tree (1–5). Pathological studies have suggested the so called "thin-cap atheromas"—necrotic-rich core plaques at high risk for rupture—are infrequent in the left main stem (LMS) and in the distal tracts of the coronary vessels, whereas they group together with ruptured and healed plaques in the proximal segments of the 3 main coronary arteries (1).

Similarly, 1) angiographic studies in patients with ST-segment elevation myocardial infarction recently have shown that sites of occlusion are clustered within the proximal third of each of the vessels (2,3), and 2) intravascular ultrasound (IVUS) analyses have observed that plaque rupture rarely occurs in the LMS or the distal part of the coronary arteries, whereas it is far more common in the proximal part of the coronary vessels (4), especially in the left anterior descending (LAD) artery (5).

The reasons why vulnerable or ruptured plaques tend to spare the LMS and distal segments of the left coronary vessels remain poorly understood. Plaque composition, favoring propensity to vulnerability (6–8), might also be nonuniformly distributed along the coronary arteries.

From the Erasmus Medical Center, Thoraxcenter, Rotterdam, the Netherlands. Dr. Rodriguez-Granillo has received a research grant from Volcano Corp.

Manuscript received December 1, 2005; revised manuscript received February 28, 2006, accepted March 7, 2006.

Abbreviations and Acronyms

ACS = acute coronary syndrome
CFX = circumflex artery
CRP = C-reactive protein
CSA = cross-sectional area
EEM = external elastic membrane
HDL = high-density lipoprotein
IQR = interquartile range
IVUS = intravascular ultrasound
LAD = left anterior descending artery
LDL = low-density lipoprotein
LMS = left main stem
VH = virtual histology

We sought to investigate whether the plaques located in the LMS, which are known to be at low probability of rupture, differ in terms of composition from those sited in the proximal tract of LAD or circumflex artery (CFX), where rupture or occlusion occurs more frequently. This may contribute establishing in vivo the role of plaque composition as key determinant of vulnerability in humans. In this context, the role of clinical presentation, length of LMS, lipid profile, and systemic level of C-reactive protein (CRP) also were investigated.

Methods

Study protocol and patient enrollment. This was a single-center, investigator-driven, observational study aimed at evaluating the distribution of plaque composition along the left coronary artery in consecutive patients referred to our institution for elective or urgent percutaneous coronary intervention in whom the nonculprit, nontreated vessel was judged suitable for a safe IVUS 35-mm pullback or more, based on angiographic (absence of the following: >50% stenotic disease, extensive calcification, severe vessel tortuosity) and clinical (hemodynamic stability) findings.

According to the protocol, not more than one vessel per patient could be evaluated, and the region of interest was subsequently divided into the following coronary segments: LMS and LMS carina, based on anatomical landmarks, followed by 6 consecutive nonoverlapping 6-mm segments, with the first one to be started at the coronary ostium of either the LAD or CFX arteries. The length chosen for those coronary segments located distally to the LMS carina was based on the median length of LMS in the study population.

To ensure that the ostial-proximal part of the LMS was included in the IVUS pullback and to rule out the occurrence of deep intubation by the guiding catheter, the last part of the pullback was filmed and each angiogram carefully inspected before patient inclusion. An analyzable interrogated vessel length of at least 35 mm beyond LMS carina, starting from coronary ostium, was the main selection criterion, once the patient was included in the study. This protocol was approved by the hospital ethics committee and is in accordance with the Declaration of Helsinki. Written informed consent was obtained from every patient.

Intravascular ultrasound-virtual histology (VH) acquisition and analysis. Details regarding the validation of the technique, on explanted human coronary segments, have previously been reported (9). Briefly, IVUS radiofrequency data (IVUS-Virtual Histology, Volcano Corp., Rancho Cordova, California) uses spectral analysis of IVUS radiofrequency data to construct tissue maps that classify plaque into 4 major components. In preliminary in vitro studies, 4 histological plaque components (fibrous, fibro-lipid, necrotic core, and calcium) were correlated with a specific spectrum of the radiofrequency signal (9). These different plaque components were assigned color codes. Calcified, fibrous, fibrolipidic, and necrotic core regions were labeled white, green, greenish-yellow, and red, respectively (10).

IVUS-VH data were acquired after intracoronary administration of nitrates using a continuous pullback (0.5 mm/s) with commercially available mechanical sector scanners (Ultracross 30-MHz catheter, Boston Scientific, Santa Clara, California or Eagle Eye 20-MHz catheter, Volcano Corp.), by a dedicated IVUS-VH console (Volcano Corp.). The IVUS-VH data were stored on a CD-ROM/DVD and sent to the imaging core lab for offline analysis (Cardialysis). IVUS B-mode images were reconstructed from the RF data by customized software and contour detection was performed using cross-sectional views with a semi-automatic contour detection software to provide geometrical and compositional output (IvusLab 3.0 for 30 MHz acquisitions and IvusLab 4.4 for 20-MHz acquisitions, respectively; Volcano Corp.) (10).

The contours of the external elastic membrane (EEM) and the lumen-intima interface enclosed an area that was defined as the coronary plaque plus media area. Plaque burden was calculated as $([EEM_{area} - Lumen_{area}/EEM_{area}] \times 100)$. Plaque eccentricity was defined as minimum plaque thickness divided by maximum plaque thickness. Geometrical and compositional data were obtained for each cross-sectional area (CSA), and an average was calculated for each coronary and for the total coronary tree. RF data were normalized using a technique known as "blind deconvolution," an iterative algorithm that deconvolves the catheter transfer function from the backscatter, thus accounting for catheter-to-catheter variability (11,12).

Biochemical measures. Antecubital venous blood was collected from all patients at entry, left in ice for 45 min, centrifuged at 1,700 *g* at 4°C for 15 min and serum obtained finally stored at −80°C. High-sensitivity CRP was measured in serum using a commercially available kit (N High Sensitivity CRP, Dade Behring, Marburg, Germany). Plasma concentrations of total cholesterol, high-density lipoprotein (HDL) cholesterol, and triglycerides were measured in the local laboratory. The Friedewald formula was used to derive low-density lipoprotein (LDL) cholesterol levels.

Statistical analysis. The sample size was calculated on the assumption that plaques located in the most proximal 6-mm segment of the LAD or CFX would display a mean necrotic core content of approximately 10% and a standard deviation of 10%, based on previous findings (13), with a relative necrotic core content of around 5% in plaques located in the

LMS. To detect this effect size with 80% power and a type I error (alpha) of 0.05, at least 46 patients were required (model 1). Model 2 also was created to explore whether in patients with LMS length beyond median value (long LMS cohort) plaque composition differs in the proximal compared to the distal tract of the LMS. No formal sample size was calculated for model 2 as it was meant to be a hypothesis generating analysis.

Values are expressed as mean ± SD and median and interquartile range (IQR) whenever appropriate. Because all cross-sectional areas, provided by IVUS analysis, were shown to have a non-normal distribution at Kolmogorov-Smirnov goodness-of-fit test, they were log-transformed before analysis. Similarly, to all percentages relative to stenosis rate and plaque composition an arcsin transformation was applied (14). Assumptions for normality were checked after transformation based on a p value >0.20 at Kolmogorov-Smirnov test and on visual assessment of Q-Q plots of residuals.

Comparisons between the 2 groups were performed with the Student *t* test. The Fisher exact test was used for categorical variables. Comparisons among coronary segments were accomplished through a general linear mixed model and post-hoc comparisons by Tukey honest significance difference test (15). Spearman's correlation coefficients were used to detect any association between variables. Probability was significant at a level of <0.05. Statistical analysis was performed using Statistica 6.1 Software (Statsoft Inc., Tulsa, Oklahoma) and R-language (R Foundation, Free Software Foundation, Boston, Massachusetts).

Results

From December 11, 2003, to July 27, 2005, 72 patients were prospectively included in the protocol. Twenty-four patients were subsequently excluded from the final analysis because of short (<36 mm) IVUS pullback in 16, uncertainty regarding the true interface lumen-vessel wall based on IVUS grey-scale in 4 and occurrence of angiographically confirmed deep intubation of the guiding catheter during the pullback in 4 patients. Thus, 48 patients (32 men), ages 30 to 75 years (mean age, 57 ± 11 years) constituted the final patient population. Their baseline characteristics are provided in Table 1.

The study vessel was the LMS and the LAD artery in 34 (71%) patients and LMS and CFX in 14 (29%). The overall LMS length was 7.49 ± 4 mm (median [IQR], 6 [4.8 to 9.3]; range, 3.4 to 20) in the SA group versus 7.8 ± 5 mm in the acute coronary syndromes (ACS) group (p = 0.64). Lumen and vessel CSAs decreased significantly, starting from the first 6-mm segment of the coronary artery as compared with LMS (Table 2). Plaque CSA in the LMS

Table 1 Study Population

Variable	Patients: All (n = 48)	SA Group (n = 25)	ACS Group (n = 23)	p Value
Age (yrs)	57 ± 11	58 ± 11	57 ± 12	0.81
Males, n (%)	32 (67)	16 (64)	16 (65)	>0.99
Weight (kg)	82 ± 12	81 ± 12	84 ± 12	0.36
Height (cm)	174 ± 9	173 ± 8	176 ± 10	0.28
BMI (kg/m^2)	27 ± 3	27 ± 4	27 ± 2	0.81
Diabetes, n (%)	11 (23)	5 (20)	6 (26)	0.75
Hypertension, n (%)	37 (77)	20 (80)	17 (74)	>0.99
Current smokers, n (%)	19 (40)	8 (32)	11 (48)	0.32
Previous smoker, n (%)	16 (33)	9 (36)	7 (30)	0.50
C-reactive protein (mg/l)	29 ± 48	12.7 ± 15	38 ± 58	0.19
Low-density lipoprotein (mmol/l)	3.09 ± 1.22	3.26 ± 1.3	2.9 ± 1.3	0.44
HDL (mmol/l)	1.22 ± 0.5	1.30 ± 0.6	1.14 ± 0.4	0.39
Cholesterol/HDL ratio	4.26 ± 1.49	4.26 ± 1.5	4.25 ± 1.2	0.99
Medical history, n (%)				
CABG	2 (4)	2 (6)	0 (0)	0.29
PCI	11 (23)	8 (32)	3 (13)	0.32
Acute coronary syndrome	18 (37)	10 (40)	8 (35)	>0.99
Medical treatment, n (%)				
Aspirin	48 (100)	25 (100)	23 (100)	>0.99
Clopidogrel	48 (100)	25 (100)	23 (100)	>0.99
Statin	42 (88)	23 (92)	19 (83)	0.84
ACE inhibitor	40 (83)	25 (100)	15 (65)	0.39
Beta-blocker	42 (88)	23 (92)	19 (83)	0.84

Plus-minus values are mean ± SD.

ACE = angiotensin-converting enzyme; ACS = acute coronary syndrome; BMI = body mass index; CABG = coronary artery bypass grafting; HDL = high-density lipoprotein; PCI = percutaneous coronary intervention; SA = stable angina.

Table 2 Quantitative Vessel Analysis at IVUS Stratified into Coronary Segments

	Cross Sectional Areas (mm^2)			Plaque Eccentricity Index	Plaque Burden (%)
	Lumen	Vessel	Plaque		
Model 1 (n = 48)					
Coronary segments					
LMS	15.2 (12–17)	24.5 (19–26)	8 (6–9)	0.11 (0.05–0.18)	34.3 (29–38)
LMS carina	12.2 (11–15)	20.4 (16–24)	6.7 (6–8)	0.03 (0.01–0.06)*	33.8 (31–39)
1° (0–6 mm)	9.9 (7–11)*	16.2 (14–18)*	6.4 (5–7)	0.09 (0.07–0.14)	38.6 (36–46)
2° (6–12 mm)	9.1 (7–10)*	16 (14–18)*	6.8 (5–8)	0.11 (0.06–0.16)	40 (39–45)
3° (12–18 mm)	8.6 (7–10)*	15 (13–17)*	6.9 (5–8)	0.10 (0.08–0.15)	41 (40–46)
4° (18–24 mm)	8.2 (7–10)*	14 (13–16)*	6.3 (5–7)	0.13 (0.06–0.17)	41 (37–51)
5° (24–30 mm)	7.5 (6–9)*	13.2 (12–15)*	5.6 (5–6)	0.16 (0.10–0.20)	40 (38–54)
6° (30–36 mm)	7.2 (6–8)*	12.3 (11–14)*	4.9 (4–6)*	0.12 (0.08–0.21)	42 (36–47)
p value	<0.0001	<0.0001	0.0006	0.0001	0.16
Model 2 (n = 24)					
Coronary segments					
Proximal LMS	16.1 (13–19)	23.4 (21–27)	7.5 (5–9)	0.11 (0.07–0.15)	32 (29–39)
Distal LMS	14.6 (12–17)	25.8 (20–27)*	8.9 (7–10)	0.11 (0.07–0.25)	38 (33–43)
LMS carina	13.1 (11–15)*	21.2 (18–25)*	7.7 (7–8)	0.05 (0.02–0.08)	37 (31–43)
1° (0–6 mm)	9.9 (8–11)*	16.3 (15–19)*	7.1 (6–8)	0.13 (0.09–0.14)	43 (37–48)
2° (6–12 mm)	9.1 (7–11)*	16.6 (14–19)*	7.7 (6–9)	0.15 (0.08–0.17)	47 (45–50)†
3° (12–18 mm)	8.6 (7–10)*	15.7 (14–18)*	7.4 (6–8)	0.11 (0.09–0.21)	50 (45–53)†
4° (18–24 mm)	8.2 (7–10)*	14.5 (13–16)*	7.0 (5–8)	0.14 (0.09–0.17)	48 (38–51)†
5° (24–30 mm)	8.2 (6–10)*	14.0 (12–17)*	5.7 (5–7)	0.19 (13–24)	45 (34–54)
6° (30–36 mm)	7.0 (6–8)*	12.0 (11–14)*	5.1 (4–7)†	0.19 (0.11–0.30)	45 (39–51)
p value	<0.001	<0.0001	0.002	0.019	0.0093

p values refer to results for the whole model at general linear analysis. *p < 0.01; †p < 0.05 at adjusted post-hoc comparison as compared with left main stem (LMS) in model 1 and to proximal LMS in model 2. Results are given as median (interquartile range).

IVUS = intravascular ultrasound.

was significantly increased only compared with the most distal 6-mm segment. The degree of plaque eccentricity was relatively constant throughout the vessel except in the LMS carina, where it resulted to be higher compared with both the LMS and the coronary segments distal to the first one. Plaque burden did not change along the vessel in model 1, despite a trend being progressively increased from proximal to distal.

Model 2 (Table 2), in which LMS has been stratified into the proximal and distal segment after selection of those patients (n = 24) with long LMS (length >6 mm), mainly confirmed the trends observed along the vessels in model 1.

Change in plaque composition along the study vessel. Fibrous tissue was the most prevalent component of plaque composition in each analyzed segment throughout the 2 models, followed by fibrolipidic tissue, necrotic core and calcium (Table 3). No significant change was observed in terms of relative plaque composition throughout the study vessel with respect to fibrous and calcified tissue content. The percentage of fibrolipidic tissue decreased in the second and third 6-mm segment when contrasted to the LMS. When compared to the sixth coronary segment, however, no difference emerged among the vessel tracts in terms of fibrolipidic content at post-hoc analysis.

The necrotic core increased significantly in the first, second, and third 6-mm segment compared with the LMS. When the most distal segment of the study vessel was taken as reference, the necrotic core remained greater in both the first and second 6-mm segment at post-hoc analysis. As shown in Figure 1, the necrotic core was the plaque component with the highest relative change along the vessel. Changes in terms of plaque composition in model 2 are shown in Table 3.

Change in plaque composition according to clinical presentation. No significant change in calcium, fibrous, and fibrolipidic content with respect to clinical presentation (stable vs. unstable) was observed when all 384 coronary segments were pooled together (Fig. 2). Necrotic core (%) was significantly increased in patients with (median [IQR]: 11.4 [5.5 to 19.8]) as compared with those (median [IQR]: 7.3 [3.2 to 12.9]) without ACS ($p < 0.001$) (Fig. 2). After introducing anatomical location stratified into 8 coronary segments in the model, the increase in necrotic core in patients with ACS was mainly confined to the LMS (6.9 [2.6 to 9.4] vs. 3.5 [1.4 to 6.2] in stable patients; $p = 0.02$), in the first (14.9 [7.7 to 19.6] vs. 11.5 [4.9 to 17.3] in stable patients; $p = 0.03$), second (12.2 [5.5 to 16.1] vs. 9.4 [5.1 to 20.6] in stable patients; $p = 0.03$), and third 6-mm coronary segment (11.4 [5.4 to 15] vs. 8 [3.6 to 14.4] in stable patients; $p = 0.04$). However, the statistical interaction between necrotic core and the anatomical location of the segments did not reach the significance ($p = 0.12$).

Table 3 Plaque Composition Along the Left Coronary Artery Stratified Into Coronary Segments

	Plaque Composition (%)			
	Calcium Core	Fibrous Core	Fibrolipidic Core	Necrotic Core
Model 1 (n = 48)				
Coronary segments				
LMS	0.65 (0.2–1.7)	63.5 (57–68)	24.9 (20–29)	4.6 (2–7)
LMS carina	1.1 (0.3–1.6)	63.6 (62–71)	23.0 (15–28)	7.2 (4–9)
1° (0–6 mm)	2.1 (0.8–3.8)	61.6 (59–70)	19.8 (8–24)	11.8 (7.8–16)†
2° (6–12 mm)	2.2 (1.1–3.3)	62.4 (59–68)	15 (10–24)*	10.8 (7–16)*
3° (12–18 mm)	1.9 (1.0–3)	64.4 (60–70)	17.4 (10–21)*	9.5 (6.5–13.3)*
4° (18–24 mm)	1.6 (1–3)	61.7 (57–70)	17.6 (11–23)	8.7 (6–10)
5° (24–30 mm)	1.2 (1–3)	63.4 (58–66)	18.7 (13–26)	7 (4–11)
6° (30–36 mm)	1.4 (0.6–2.4)	61.5 (57–67)	18.4 (11–25)	6.1 (3–9)
p value	0.32	0.88	0.01	0.0001
Model 2 (n = 24)				
Coronary segments				
Proximal LMS	0.85 (0.08–1.5)	62.8 (55–69)	24.6 (20–30)	3.8 (2.3–6.8)
Distal LMS	1.0 (0.3–2.1)	64.1 (59–69)	25 (22–28)	6.5 (4.5–8.8)
LMS carina	1.3 (0.3–1.6)	64 (61–71)	28.8 (20–29)	7.3 (4.2–8)
1° (0–6 mm)	2.3 (1–3.4)	62.9 (60–71)	20.9 (13.1–25)	11.3 (8–16)†
2° (6–12 mm)	2.3 (1.2–5.0)	62.6 (55–69)	18.8 (13–27)	9.1 (7–13)*
3° (12–18 mm)	2.2 (0.98–4.3)	64.2 (60–70)	20 (16–23)	8.7 (6.7–13.3)*
4° (18–24 mm)	1.2 (0.9–4.5)	64.4 (57–71)	19.5 (11–26)	8.9 (8–10)*
5° (24–30 mm)	1.3 (0.3–4.8)	63.4 (58–68)	22.5 (13–27)	4.9 (4–8)
6° (30–36 mm)	1.2 (0.6–4)	59.9 (52–66)	22.2 (13–29)	3.5 (1.8–6)
p value	0.36	0.89	0.19	<0.0001

p values refer to results for the whole model at general linear analysis. *p < 0.05; †p < 0.01 at adjusted post-hoc comparison as compared with left main stem (LMS) in model 1 and to proximal LMS in model 2. Results are given as median (interquartile range).

Length of LMS as a predictor of plaque composition along the study vessel. Patients were stratified into 2 groups based on median LMS length (short LMS ≤6 mm and long LMS >6 mm). These 2 groups did not differ in terms of baseline and procedural characteristics. When each coronary segment was separately analyzed, no difference emerged between the 2 groups for IVUS-derived quantitative vessel analysis. The same held true if all 384 coronary segments were cumulatively considered independently from their anatomical location. Calcium, fibrous, and fibrolipid content did not differ between the 2 groups (data not shown). The pattern of necrotic distribution in relation to LMS length is shown in Figure 3.

Correlations. In a segment-based analysis, necrotic core was largely independent from plaque area ($r = 0.17$; $p = 0.06$; $R^2 = 0.09$) (Fig. 4). Similarly, we failed to find an association between necrotic core content and CRP levels ($r = 0.09$, $p = 0.8$), level of LDL cholesterol ($p = 0.11$, $p = 0.23$), or HDL cholesterol ($r = -0.2$, $p = 0.4$) at entry. However, there was a significant, although weak, direct correlation between necrotic core and cholesterol/HDL ratio ($r = 0.18$, $p = 0.01$; $R^2 = 0.1$).

Discussion

There is increasing evidence that the distribution of ruptured or prone-to-rupture plaques is not uniform along the coronary vessel: they cluster in the proximal tract of the 3 major coronary vessels whereas they tend to spare both the LMS and distal segments of coronary arteries (4,16).

These findings have been recently confirmed by mapping the distribution of angiographic sites of occlusive or non-occlusive culprit lesions along the coronary arteries in patients with ST-segment elevation ACS (2,3).

The reason why vulnerable plaques show a tendency to cluster in partially predictable hot spots located within the proximal tracts of coronary vessel is largely unknown. Atherosclerotic plaques also cluster within the proximal portions of the 3 major coronaries (17–20). Thus, the risk to undergo rupture may be identical for each coronary plaque independently from its anatomical location, being rupture simply more likely to occur where atherosclerotic plaques are more frequently clustered (21). This may easily explain the nonuniform distribution of ruptured or prone-to-rupture plaques without calling into question the idea that plaque rupture is partially a site-specific phenomenon.

Alternatively, plaques located within the proximal third of each coronary may harbor some specific hallmark of vulnerability which makes them individually more likely to undergo rupture. To gain some insights into this topic of debate, we hypothesized that plaque necrotic core content, which is a well-known determinant of vulnerability (7,8,22), may differ along the coronary

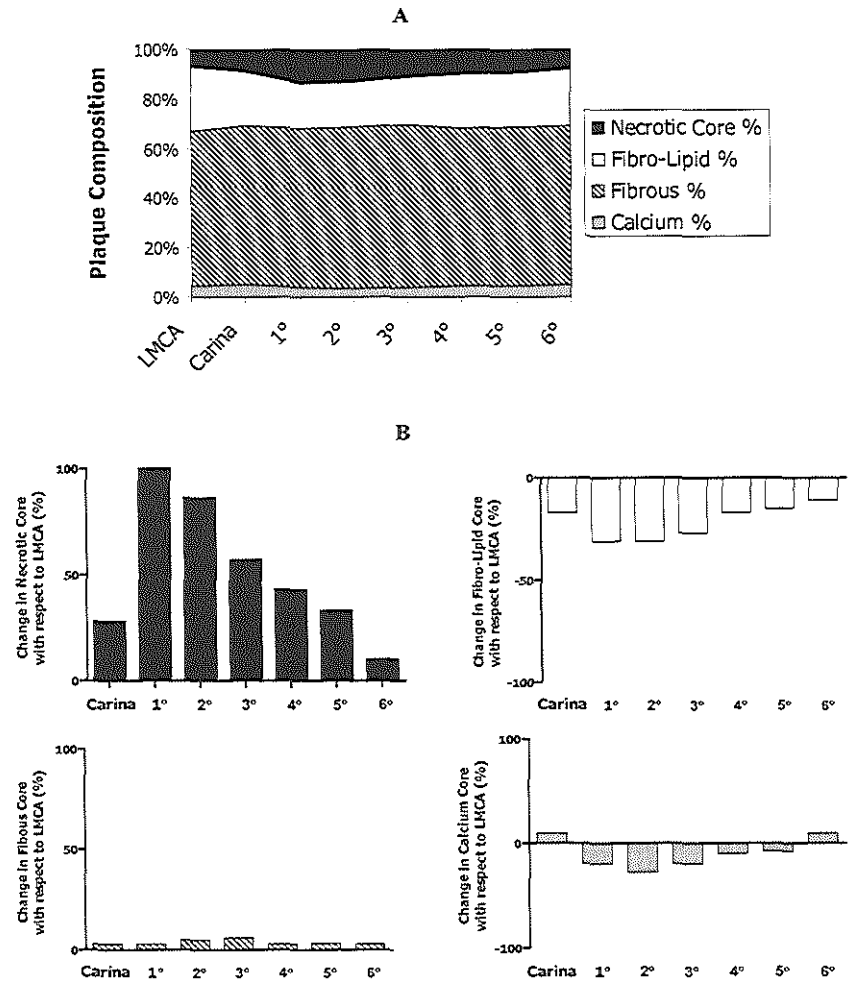

Figure 1 **Change in Plaque Composition Along the Left Coronary Artery**

Plaque composition in terms of median necrotic, fibrolipid, fibrous, and calcium core content along the left coronary vessel **(A)**. In **panel B**, the percentage of each plaque component is reported with respect to left main coronary artery (LMCA) taken as reference. All analyses are based on model 1.

vessel, being greater at the spots where plaque rupture is known to be more frequent.

Our main findings can be summarized as follows:

1. The plaque necrotic content was minimal in the LMS, particularly in the most proximal tract, whereas it peaked in the first 6-mm segments after the ostium of the 2 major left coronaries, progressively decreasing toward the more distal segments.
2. The plaque CSA was largely unrelated to necrotic core content throughout the left coronary vessel. This statement is supported by the absence of correlation between necrotic content in plaques and plaque CSA at the segment-based analysis and by the observation that plaque CSA showed a progressive increase in the distal-proximal direction along the vessel whereas plaque necrotic content did not.
3. The necrotic core was greater in patients with clinical instability presenting with ACS compared to those affected by stable atherosclerotic disease.
4. The necrotic core content was not related to systemic inflammatory status, as measured by a well-recognized prognostic marker of inflammation such as CRP nor

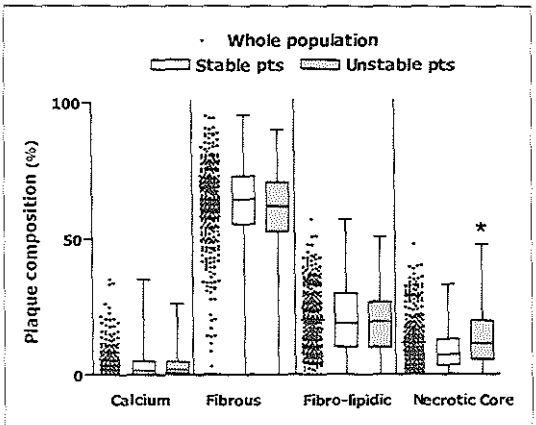

Figure 2 **Plaque Composition in Relation to Clinical Presentation**

Plaque composition on a per-segment based analysis in patients with stable angina (stable patients) or with acute coronary syndromes (unstable patients). The necrotic core (%) was significantly increased in patients with (median [interquartile range] 11.4 [5.5 to 19.8]) as compared to those without (7.3 [3.2 to 12.9]) an acute coronary syndrome. *$p < 0.001$ versus stable patients.

LDL or HDL alone, whereas it showed a significant although weak correlation to cholesterol/HDL ratio.

5. The length of left main trunk was shown to affect the distribution of necrotic core along the vessel. In patients with long LMS, necrotic core content peaked immediately in the first coronary segment after LMS and rapidly decreased distally. Conversely, the necrotic core content peaked in the second 6-mm segment in patients with short LMS and it resulted to be increased in the 2 most distally analyzed segments compared to the long LMS group.

It is tempting to speculate that the observed clustering of ruptured or prone-to rupture plaques in the proximal segment of each coronary artery is not just a simple reflection of the nonuniform distribution of atherosclerosis along the coronary vessel. The necrotic content of those plaques located in these proximal segments, independent of their size, was greater, both compared with the LMS and with those segments that are more distally located. The plaques located within the proximal segments of the left coronary artery, being relatively richer in necrotic content, may undergo rupture more easily than those located in the LMS or in the distal tracts of the vessel.

Some preliminary unpublished findings by our group suggest that plaque necrotic core content, as assessed through IVUS-VH, may be the only independent predictor for mechanically deformable regions (high-strain spots) (23) throughout the coronary arteries in humans. Thus, when our findings are put in perspective of current evidence, they support the idea that vulnerability may cluster in necrolipid-rich regions throughout the vessel.

Necrotic core content in the present study was greater in patients with ACS, suggesting again that plaque composition in itself may play a pivotal role in determining vulnerability. Interestingly, it was recently reported that when rupture of coronary plaques occurs in the LMS, the distal half of LMS is more likely to be involved (24). Our findings that the distal LMS tends to harbor a greater necrotic core content compared with proximal half, together with the well-established role of shear stress in bifurcated lesions (25), may contribute to explain the nonuniform distribution of plaque rupture even within the LMS.

The reasons why the plaque necrotic core seems to exceed in the proximal as compared with the distal tracts of the coronary vessel or the LMS remain speculative at the present time. Low-oscillatory shear stress is known to induce a loss of the physiological flow-oriented alignment of the endothelial cells, an enhancement of the expression of adhesion molecules, and a weakening of cell junctions, ultimately leading to an increase in permeability to lipids and macrophages (25). The segments located in the first few centimeters of the coronary arteries, because of flow turbulence generated by high-velocity blood impacting against anatomical flow dividers (26), may be more exposed to low-oscillatory shear stress compared with the most proximal (i.e., LMS) or more distal coronary segments, thus possibly explaining our present findings (27). Concomitant quantitative measurement of shear stress and plaque composition along coronary vessels in vivo would be pivotal in corroborating this working hypothesis.

Study limitations. On the basis of previous findings and the well-known role of necrotic core content in determining vulnerability (6–8,22), our investigation was primarily fo-

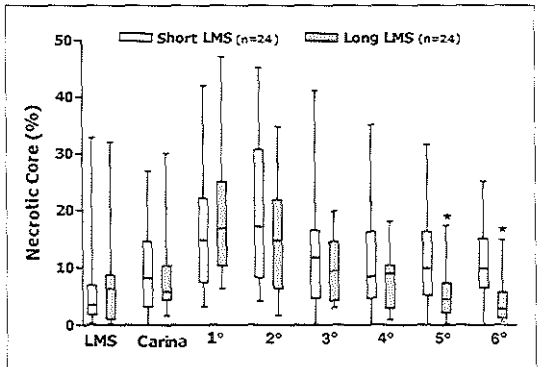

Figure 3 **Necrotic Core Distribution Along the Left Coronary Artery According to the Length of LMS**

The necrotic core peaked in the first and in the second 6-mm segment in patients with long (above median value) and short left main coronary artery (LMS), respectively. After the peak, the necrotic core decrease was more pronounced in the long than in the short LMS group. As a consequence, the necrotic core content resulted to be significantly increased in the fifth and sixth 6-mm segments in the short as compared with the long LMS group. *$p < 0.05$ versus short LMS.

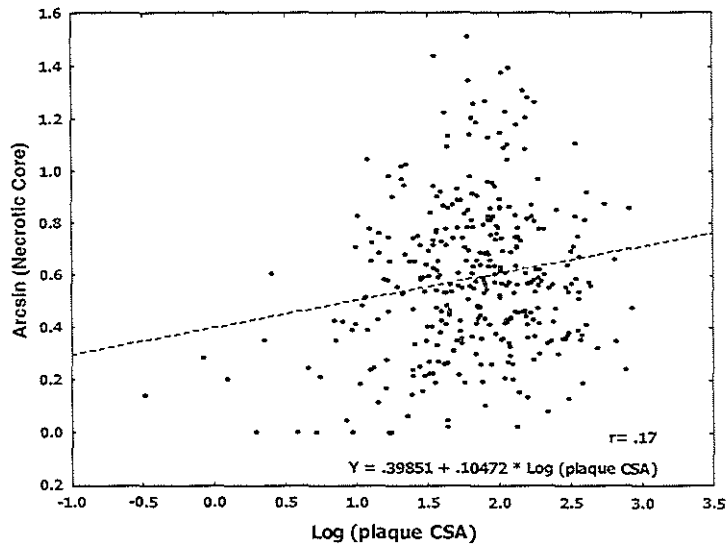

Figure 4 **Correlation Between Necrotic Core and Plaque Size**

No correlation was found between arcsin-transformed necrotic core content and plaque size evaluated through log-transformed plaque cross-sectional area (CSA). Arcsin is the inverse of sine and is the inverse trigonometric function.

cused on the distribution of necrotic core content along the left coronary artery. To assess relatively minor changes in plaque composition along the longitudinal artery axis, such as that observed for fibrous tissue, a larger, properly powered sample size is clearly needed. In keeping with previous considerations, all other analyses and comparisons performed in the current report should be regarded as exploratory and hypothesis-generating because we cannot rule out the possibility that inflation of type I error due to multiple comparisons may have confounded our results.

In our study, the operators were left free to wire the most suitable vessel for the IVUS pullback, provided it was supplying a major left ventricle territory, which resulted in the predominance of LAD as a region of interest, whereas the CFX artery was mainly investigated in those patients presenting with small or tortuous LAD. The distribution of necrotic core along the vessel did not differ in LAD as compared with CFX. The same held true for other studied plaque components. However, the applied selection process may have biased this comparison. Thus, whether the distribution of plaque composition may differ in relation to the studied vessel remains to be tested. Similarly, to maximize patients' safety and avoid potential IVUS-related complications, individuals with severe angiographic calcification were excluded. Despite the fact this decision may have clearly contributed to generate some selection bias, the distribution of calcium along the coronary vessel intriguingly mirrored the one observed for the necrotic core. Further studies are needed to investigate the specific role of calcium content in determining plaque vulnerability.

Patients with proximal occlusions have bigger myocardial ischemia and, thus, they are more likely to present to hospital and be referred for angioplasty. Similarly, myocardial infarction with LMS as culprit artery often may result in immediate death. Thus, it may be argued that a selection bias might have artificially increased the prevalence of patients with culprit lesions located in the proximal compared to distal tracts of coronaries or LMS. This is obviously theoretical possible. However, for the following reasons, we believe that this possibility is relatively unlikely:

1. The necrotic core in our series clustered in the same coronary spots in which previous studies, based on postmortem examination, found a greater prevalence of ruptured or healed plaques.
2. Our results are based on the investigation of the nonculprit vessel. Thus, they are potentially less prone to suffer from clinical selection due to the location of the culprit lesion in the culprit vessel.
3. Although it seems to be exacerbated in patients presenting with clinical instability, the nonuniform distribution of plaque composition along the vessel also has been observed in patients with stable coronary disease, in whom the selection bias due to the importance of the culprit lesion is less obvious, at least for the comparison LMS versus proximal tracts of LAD or CFX.

Thus, based on these considerations, we think that our findings, especially when put in the context of previous evidence (1–5), may help reinforcing the notion that there may be some hot spots along the coronary vessel which are per se more prone to develop vulnerable plaque and as such undergo plaque rupture.

Summary and conclusions. Plaque composition was found to be not uniformly distributed along the left coronary artery with a progressive increase in necrotic core starting from the proximal half of the LMS to the most proximal segments of the LAD or CFX, followed by a steady decline toward those segments which are more distally located along the vessel. The necrotic core appeared to be increased in patients with ACS, especially in the LMS and in the 3 proximal coronary segments of LAD or CFX, whereas it did not correlate with the CRP or lipid profile. The relatively site-specificity of necrotic core content toward the proximal segment of the left coronary artery is in keeping with the increasing evidence that a clear clustering of ruptured or prone to rupture plaques occurs in humans within this region (2,3,5). Our findings 1) reinforce the notion the plaque composition may be a major determinant for and subsequently a potential target of plaque vulnerability in humans and 2) call for prospective evaluation of the independent role of plaque composition on long-term outcome in patients with established coronary artery disease.

Reprint requests and correspondence: Prof. Patrick W. Serruys, Thoraxcenter, Bd-406, Dr Molewaterplein 40, 3015-GD Rotterdam, the Netherlands. E-mail: p.w.j.c.serruys@erasmusmc.nl.

REFERENCES

1. Kolodgie FD, Burke AP, Farb A, et al. The thin-cap fibroatheroma: a type of vulnerable plaque: the major precursor lesion to acute coronary syndromes. Curr Opin Cardiol 2001;16:285–92.
2. Gibson CM, Kirtane AJ, Murphy SA, et al. Distance from the coronary ostium to the culprit lesion in acute ST-elevation myocardial infarction and its implications regarding the potential prevention of proximal plaque rupture. J Thromb Thrombolysis 2003;15:189–96.
3. Wang JC, Normand SL, Mauri L, Kuntz RE. Coronary artery spatial distribution of acute myocardial infarction occlusions. Circulation 2004;110:278–84.
4. von Birgelen C, Klinkhart W, Mintz GS, et al. Plaque distribution and vascular remodeling of ruptured and nonruptured coronary plaques in the same vessel: an intravascular ultrasound study in vivo. J Am Coll Cardiol 2001;37:1864–70.
5. Hong MK, Mintz GS, Lee CW, et al. The site of plaque rupture in native coronary arteries: a three-vessel intravascular ultrasound analysis. J Am Coll Cardiol 2005;46:261–5.
6. Shah PK. Mechanisms of plaque vulnerability and rupture. J Am Coll Cardiol 2003;41 Suppl S:15S–22S.
7. Naghavi M, Libby P, Falk E, et al. From vulnerable plaque to vulnerable patient: a call for new definitions and risk assessment strategies: part II. Circulation 2003;108:1772–8.
8. Naghavi M, Libby P, Falk E, et al. From vulnerable plaque to vulnerable patient: a call for new definitions and risk assessment strategies: part I. Circulation 2003;108:1664–72.
9. Nair A, Kuban BD, Tuzcu EM, Schoenhagen P, Nissen SE, Vince DG. Coronary plaque classification with intravascular ultrasound radiofrequency data analysis. Circulation 2002;106:2200–6.
10. Rodriguez-Granillo GA, Aoki J, Ong ATL, et al. Methodological considerations and approach to cross-technique comparisons using in vivo coronary plaque characterization based on intravascular radiofrequency data anlaysis: insights from the integrated Biomarker and Imaging Study (IBIS). Int J Cardiovasc Intervent. 2005;7:52–8.
11. Käresen K. Deconvolution of sparse spike trains by iterated window maximization. IEEE Trans Signal Proc 1997;45:1173–83.
12. Kaaresen KF, Bolviken E. Blind deconvolution of ultrasonic traces accounting for pulse variance. IEEE Trans Ultrason Ferroelectr Freq Control 1999;46:564–73.
13. Mann JM, Davies MJ. Vulnerable plaque. Relation of characteristics to degree of stenosis in human coronary arteries. Circulation 1996;94: 928–31.
14. Draper NR, Smith H. Applied Regression Analysis. 2nd edition. New York, NY: Wiley, 1981.
15. Diggle PJ, Heagerty PJ, Liang KY, Zeger SL. Analysis of Longitudinal Data. 2nd edition. New York, NY: Oxford University Press, 2002.
16. Virmani R, Burke AP, Kolodgie FD, Farb A. Pathology of the thin-cap fibroatheroma: a type of vulnerable plaque. J Interv Cardiol 2003;16:267–72.
17. Vieweg WV, Warren SE, Alpert JS, Hagan AD. The distribution and severity of coronary artery disease and left ventricular dysfunction among patients with single coronary artery disease and angina pectoris. Clin Cardiol 1980;3:241–5.
18. Vieweg WV, Alpert JS, Johnson AD, et al. Distribution and severity of coronary artery disease in 500 patients with angina pectoris. Cathet Cardiovasc Diagn 1979;5:319–30.
19. Hochman JS, Phillips WJ, Ruggieri D, Ryan SF. The distribution of atherosclerotic lesions in the coronary arterial tree: relation to cardiac risk factors. Am Heart J 1988;116:1217–22.
20. Fox B, James K, Morgan B, Seed A. Distribution of fatty and fibrous plaques in young human coronary arteries. Atherosclerosis 1982;41: 337–47.
21. Abaci A. Letter regarding article by Wang et al. "Coronary artery spatial distribution of acute myocardial infarction occlusions." Circulation 2005;111:e369.
22. Shah PK. Pathophysiology of plaque rupture and the concept of plaque stabilization. Cardiol Clin 2003;21:303–14, v.
23. Schaar JA, Regar E, Mastik F, et al. Incidence of high-strain patterns in human coronary arteries: assessment with three-dimensional intravascular palpography and correlation with clinical presentation. Circulation 2004;109:2716–9.
24. Tyczynski P, Pregowski J, Mintz GS, et al. Intravascular ultrasound assessment of ruptured atherosclerotic plaques in left main coronary arteries. Am J Cardiol 2005;96:794–8.
25. McLenachan JM, Vita J, Fish DR, et al. Early evidence of endothelial vasodilator dysfunction at coronary branch points. Circulation 1990; 82:1169–73.
26. Kimura BJ, Russo RJ, Bhargava V, McDaniel MB, Peterson KL, DeMaria AN. Atheroma morphology and distribution in proximal left anterior descending coronary artery: in vivo observations. J Am Coll Cardiol 1996;27:825–31.
27. Rodriguez-Granillo GA, Garcia-Garcia HM, Wentzel J, et al. Plaque composition and its relationship with acknowledged shear stress patterns in coronary arteries. J Am Coll Cardiol 2006;47:884–5.

CHAPTER 3.3

Distance from the ostium as an independent determinant of coronary plaque composition in vivo: an intravascular ultrasound study based radiofrequency data analysis in humans.

Valgimigli M, Rodriguez-Granillo GA, **Garcia-Garcia HM**, Malagutti P, Regar E, de Jaegere P, de Feyter P, Serruys PW.

Eur Heart J. 2006;27(6):655-663.

European Heart Journal
doi:10.1093/eurheartj/ehi716

Clinical research

Distance from the ostium as an independent determinant of coronary plaque composition *in vivo*: an intravascular ultrasound study based radiofrequency data analysis in humans

Marco Valgimigli, Gastón A. Rodriguez-Granillo, Héctor M. Garcia-Garcia, Patrizia Malagutti, Evelyn Regar, Peter De Jaegere, Pim De Feyter, and Patrick W. Serruys*

Erasmus Medical Center, Thoraxcenter Bd-406, Dr Molewaterplein 40, 3015-GD Rotterdam, The Netherlands

Received 15 June 2005; revised 3 November 2005; accepted 15 December 2005

KEYWORDS
Plaque;
Lipid core;
Imaging;
Vulnerable plaque;
Virtual histology

Aims Relative plaque composition, more than its morphology alone, is thought to play a pivotal role in determining propensity to vulnerability. Thus, we investigated *in vivo* whether the distance from coronary ostium to plaque location independently affects plaque composition in humans. This may help explaining the recently reported non-uniform distribution of culprit lesions along the vessel in acute coronary syndromes.

Methods and results In 51 consecutive patients (45 men), aged 38–76 years (mean age: 58 ± 10), a non-culprit vessel was investigated through spectral analysis of IVUS radiofrequency data (IVUS-Virtual Histology™). The study vessel was the left anterior descending artery in 23 (45%) patients; the circumflex artery in nine (18%), and right coronary artery in 19 (37%). The overall length of the region of interest, subsequently divided into 10 mm segments, was 41.5 ± 13 mm long (range: 30.2–78.4). No significant change was observed in terms of relative plaque composition along the vessel with respect to fibrous, fibrolipidic, and calcified tissue, whereas the percentage of lipid core resulted to be increased in the first (median: 8.75%; IQR: 5.7–18) vs. the third (median: 6.1%; IQR: 3.2–12) ($P = 0.036$) and fourth (median: 4.5%; IQR: 2.4–7.9) ($P = 0.006$) segment. At multivariable regression analysis, distance from the ostium resulted to be an independent predictor of relative lipid content [$\beta = -0.28$ (95%CI: −0.15, −0.41)], together with older age, unstable presentation, no use of statin, and presence of diabetes mellitus.

Conclusion Plaque distance from the coronary ostium, as an independent determinant of relative lipid content, is potentially associated to plaque vulnerability in humans.

Coronary plaque rupture or erosion, by triggering local thrombosis is thought to play a pivotal role in the genesis of acute coronary syndromes (ACS) and sudden death.[1,2]

A series of landmark angiographic studies in the mid-1980s demonstrated that nearly two-thirds of all myocardial infarction originate from non-flow limiting atherosclerotic lesions and prior angiographic studies focusing on plaque morphology alone failed to identify quiescent plaques prone to rapidly progress or rupture.[3–7]

Consequently, the mechanical and biological properties of coronary plaques, which overall reflect plaque composition, along with systemic inflammation has mainly been targeted for the diagnosis and treatment of plaque instability.[8]

Epidemiological studies in patients with ST-segment elevation myocardial infarction (STEMI) report that sites of occlusion are not uniformly distributed throughout each of the major epicardial coronary arteries but tended to cluster within the proximal third of each of the vessels.[9,10] Accordingly, despite the recognition that several factors involved in the pathogenesis of plaque vulnerability are widespread,[11–14] local trigger(s) should be also targeted to explain the presence of high-risk coronary spots.[15]

Plaque composition, favouring propensity to vulnerability, might also be non-uniformly distributed along each coronary vessel. This might explain the higher likelihood for plaque erosion or rupture to occur proximally in the coronary tree.

To investigate this hypothesis, the non-culprit, non-treated vessel containing angiographically non-obstructive (<50%) lesions was systematically investigated to assess plaque composition through spectral analysis of IVUS radiofrequency data [IVUS-Virtual Histology™ (IVUS-VH)] in consecutive patients referred to our institution for percutaneous coronary intervention (PCI).

Our findings support for the first time to the best of our knowledge *in vivo* the hypothesis that plaque composition

* Corresponding author. Tel: +31 10 4635260; fax: +31 10 4369154.
E-mail address: p.w.j.c.serruys@erasmusmc.nl

in humans may differ in relation to plaque localization along the coronary tree.

Methods

Study protocol and patients enrolment

This was a single-center, investigators-driven, observational prospective study aimed to evaluate the distribution of plaque composition along the coronary vessel in consecutive patients referred to our institution for elective or urgent PCI, in whom the non-culprit, non-treated vessel was judged suitable for a safe IVUS 30 mm-pullback or more, based on angiographic (absence of the following: >50% stenotic disease, extensive calcification, severe vessel tortuosity) and clinical (haemodynamic stability) findings. According to the protocol, not more than one vessel-per patient could be evaluated and the region of interest (ROI), subsequently divided into 10 mm segments, had to start from the coronary ostium. Thus, an analysable interrogated vessel length of at least 30 mm, starting from coronary ostium, was the main selection criterion, once the patient was included in the study.

In the group of patients presenting with an ACS, the culprit lesion has been categorized as complex or non-complex, based on angiographic findings as previously described.[12]

This protocol was approved by the Hospital Ethics Committee and is in accordance with the declaration of Helsinki. Written informed consent was obtained from every patient.

IVUS-VH acquisition and analysis

Details regarding the validation of the technique, on explanted human coronary segments, have previously been reported.[16] Briefly, IVUS-VH uses spectral analysis of IVUS radiofrequency data to construct tissue maps that classify plaque into four major components. In preliminary *in vitro* studies, four histological plaque components (fibrous, fibro-lipid, lipid core, and calcium) were correlated with a specific spectrum of the radiofrequency signal.[16] These different plaque components were assigned colour codes. Calcified, fibrous, fibrolipidic, and lipid-necrotic regions were labelled white, green, greenish-yellow, and red, respectively.[17]

IVUS-VH data was acquired after intracoronary administration of nitrates using a continuous pullback (0.5 mm/s) with a commercially available mechanical sector scanner (Ultracross™ 2.9F 30 MHz catheter, Boston Scientific, Santa Clara, CA), by a dedicated IVUS-VH console (Volcano Therapeutics, Rancho Cordova, CA). The IVUS-VH data were stored on a CD-ROM and sent to the imaging core lab for offline analysis. IVUS B-mode images were reconstructed from the RF data by customized software (IVUSLab, Volcano Therapeutics, Rancho Cordova, CA).[17] Manual contour detection of both the lumen and the media-adventitia interface was performed and the RF data was normalized using a technique known as 'Blind Deconvolution', an iterative algorithm that deconvolves the catheter transfer function from the backscatter, thus accounting for catheter-to-catheter variability.[18,19]

Statistical analysis

The sample size was calculated on the assumption that plaques located in the proximal segment of the coronary artery, defined as the first 10 mm coronary segment, would display a mean lipid content of around 40%, with a sigma of around 35% based on previous findings,[20] with a lipid content of 10% in the distal plaques, defined as those located beyond the first 20 mm from the coronary ostium. To detect this effect size with 80% power and a type-I error (alpha) of 0.05, 48 patients were required. Four main models were constructed based on the number of 10 mm segments that were included.

Model 1 comprised three 10 mm segments available in all patients included.
Model 2 comprised four 10 mm segments available in 43 patients.
Models 3 and 4, composed of five and six 10 mm segments in 20 and 11 patients, respectively, were considered as exploratory analysis because of limited sample size.

Values are expressed as mean ± SD and median and inter-quartile range (IQR) as appropriate.

As all cross-sectional areas (CSA) provided by IVUS analysis, were shown to have a non-normal distribution at Kolmogorov–Smirnov goodness-of-fit test, they were log-transformed before analysis. Similarly, to all percentages relative to stenosis rate and plaque composition were applied an arcsin transformation.[21] Comparisons between the two groups were performed with the Student's *t*-test. Fisher's exact test was used for categorical variables. Comparisons among 10 mm segments were accomplished through a general linear mixed model with a compound symmetry correlation structure and the intercept as only random effect. Maximum likelihood method was adopted to estimate parameters in the models. Linear contrasts were applied to evaluate effects of distance, analysed as dummy variable, on the studied parameters. *Post hoc* comparisons were systematically performed by Turkey honest significance difference test.[22]

Because of limited statistical power in models 3 and 4, the multivariable analysis regarding both clinical presentation and plaque location along the vessel, along with the interaction between the two was restricted to models 1 and 2.

In order to establish the determinants of lipid relative content in the plaques in our model and confirm distance from the coronary ostium as an independent predictor of relative lipid content, a univariate (including age, sex, history of hypertension, hypercholesterolaemia, cardiovascular disorders in the family, diabetes mellitus, levels of LDL, HDL, and triglycerides, use of statin, coronary vessel analysed, clinical presentation, and distance for the ostium stratified into 10 mm segments) and multivariable (with all variables showing a *P*-value of ≤0.1 at univariate analysis) linear mixed model using percentage of lipid content in all 10 mm segments, analysed as outcome variable, was also applied.

All statistical tests were two-tailed. Probability was significant at a level of <0.05. Statistical analysis was performed using Statistica 6.1 Software (Statsoft Inc.) and R-language (R Foundation).

Results

From 16 April 2003 to 10 September 2004, 67 patients were prospectively included in the protocol. Sixteen patients were subsequently excluded from the final analysis because of short (<30 mm) IVUS pullback in 10, poor IVUS quality in two and lack of coronary plaque at IVUS investigation in four patients. Thus, 51 patients (45 men), aged 38–76 years (mean age: 58 ± 10) constituted the final patient population. Their baseline characteristics are provided in *Table 1*. Overall, 33 patients were affected by stable angina (SA), whereas the remaining 18 patients were admitted to hospital because of a non-ST-elevation ACS. In the SA group, the mean Cardiovascular Canadian Score was 2 ± 1, whereas the TIMI risk score, the percentage of patients with troponin T above upper limit of normal (0.02 μg/L) and the delay from symptoms onset to PCI were 4 ± 2, 56% and 4±3 days in the ACS group, respectively. In the ACS group, the culprit lesion was located in the proximal coronary segments in 13 (72%) patients, including 6 (33%) in the left anterior descending artery (LAD), four (22%) in the circumflex artery (CFX), and three (17%) in the right coronary artery (RCA), while in the remaining five (28%) patients the culprit lesion was located in the mid or distal segment of the coronary vessels. Overall, 11 out of 18 identified culprit lesions in the ACS group satisfied the criteria for complex lesions

Table 1 Study population

Variables	Patients		
	All ($n = 51$)	SA Group ($n = 33$)	ACS Group ($n = 18$)
Age (years)	58 ± 10	56 ± 12	59 ± 9
Males, no. (%)	45 (88)	28 (85)	16 (94)
Weight (kg)	80 ± 9	80 ± 8	81 ± 9
Height (cm)	174 ± 7	174 ± 7	175 ± 8
BMI (kg/m^2)	27 ± 4	27 ± 3	28 ± 5
Diabetes, no. (%)	12 (23)	8 (24)	4 (22)
Hypertension, no. (%)	20 (39)	14 (42)	6 (33)
Current smokers, no. (%)	19 (37)	13 (39)	6 (33)
Previous smoker, no. (%)	16 (31)	9 (27)	7 (39)
Medical history, no. (%)			
CABG	3 (6)	2 (6)	1 (6)
PCI	11 (22)	8 (24)	3 (17)
ACS	23 (45)	18 (54)	5 (28)
Medical treatment at entry, no. (%)[a]			
Aspirin	51 (100)	33 (100)	18 (100)
Clopidogrel	51 (100)	51 (100)	18 (100)
Statin	38 (75)	25 (76)	13 (72)
ACE-inhibitor	40 (78)	30 (91)	10 (56)
β-Blocker	48 (94)	32 (97)	16 (89)

Plus-minus values are means ± SD. BMI, Body mass index; CABG, coronary artery bypass grafting; ACE, angiotensin converting enzyme.

The SA group was well matched (P-value >0.3) with the ACS group with respect to all variables reported earlier.

[a]For this analysis we considered all medications administered in the previous 4 or more days. At discharge all patients except one were taking statins.

based on angiographic findings. The study vessel was the LAD artery in 23 (45%) patients, the CFX in nine (18%), and RCA in 19 (37%). The overall length of the ROI was 41.5 ± 13 mm long [(range: 30.2–78.4) (41 ± 13 in SA group vs. 42 ± 13 in ACS group, $P = 0.6$)]. The results regarding quantitative coronary IVUS analysis in the whole population, stratified into 10 mm vessel length (paired-segment analysis), are reported in *Table 2*. Lumen CSA significantly decreased every 10 mm in model 1, whereas this happened starting from the third segment, as compared with first coronary tract, in model 2.

As compared with ostial 10 mm segment, vessel CSA resulted to be decreased in the third and fourth segment in models 1 and 2, respectively, whereas plaque CSA reduction reached statistical significance only in the fourth segment of model 2. Distance from the coronary ostium did not affect the percentage of stenosis. The third and fourth models, restricted to a progressively lower number of patients but based on a longer vessel length, mainly confirmed the trends observed in the first two models.

Change in plaque composition along the study vessel

The results regarding quantitative coronary plaque composition analysis are reported in *Table 3*.

Fibrous tissue was the most prevalent component of plaque composition in each 10 mm segment throughout the four models considered, followed by fibrolipidic tissue, lipidic core, and calcium.

No significant change was observed in terms of relative plaque composition passing from the most proximal to those progressively more distally located segments along the vessel with respect to fibrous, fibrolipidic, and calcified tissue. Conversely, the percentage of lipid core resulted to be increased in the first [(mean: 13%; 95%CI: 10, 16), (median: 8.75%; IQR: 5.7, 18)] with respect to the third segment [(mean: 8.7%; 95%CI: 6.5, 11), (median: 6.2%; IQR: 2.6, 12.1)] in model 1 ($P < 0.05$; primary endpoint) and to third [(mean: 8.4%; 95%CI: 6, 11), (median: 6.1%; IQR: 3.2–12)] ($P < 0.05$) and fourth [(mean: 6.8%; 95%CI: 4, 9.6), (median: 4.5%; IQR: 2.4–7.9)] ($P < 0.01$) segment in model 2 (*Figure 3*). A similar shift in relative plaque composition along the vessel was observed in models 3 and 4. Interestingly, ACS patients presenting with the culprit lesion located in the proximal segment of the coronary artery did not differ in terms of relative plaque distribution along the vessel with respect to those with culprit lesion sited in the mid of distal tract.

Clinical presentation and change in plaque composition along the study vessel

No significant change in calcium content with respect to clinical presentation (stable vs. unstable) was observed (data not shown). In model 1, fibrous plaque content was overall significantly increased in stable (68%) [95%CI: 65%, 71%] vs. unstable (63%) [95%CI: 59%, 64.7%] group, whereas a decrease in stable (17%) [95%CI: 16%, 19%] vs. unstable (22%) [95%CI: 20%, 24%] patients was observed for

Table 2 Quantitative vessel analysis at IVUS

Coronary segments	Mean cross-sectional areas (mm^2)			Stenosis (%)
	Lumen	Vessel	Plaque	
Model 1; $n = 51$				
1 (0–10 mm)	9.4 ± 3.6	17.1 ± 8.1	7.3 ± 3.7	41.4 ± 10.5
2 (10–20 mm)	7.8 ± 2.9†	15.7 ± 7.8	7.2 ± 3.4	46 ± 12
3 (20–30 mm)	7.1 ± 2.8‡	14.2 ± 8‡	6.2 ± 2.7	45 ± 11
P-value	0.002	0.01	0.12	0.08
Model 2; $n = 43$				
1 (0–10 mm)	9.3 ± 3.6	17.4 ± 8.6	7.6 ± 3.9	42 ± 11
2 (10–20 mm)	7.7 ± 2.7	15.9 ± 8.2	7.3 ± 3.5	46 ± 12
3 (20–30 mm)	7 ± 2.6*	14.5 ± 8.7	6.3 ± 2.8	45 ± 11.2
4 (30–40 mm)	6.4 ± 2.7†	13.5 ± 9.7†	6 ± 3.4†	45.3 ± 12.4
P-value	0.0002	0.001	0.02	0.4
Model 3; $n = 20$				
1 (0–10 mm)	10.4 ± 4.3	20.5 ± 11.5	9 ± 5.2	39.8 ± 10.5
2 (10–20 mm)	8.8 ± 2.8	19 ± 11	8.2 ± 4.7	41.7 ± 12
3 (20–30 mm)	8 ± 2.9	17.4 ± 12	6.9 ± 3	42 ± 10
4 (30–40 mm)	7.3 ± 3.2	16.5 ± 13.3	6.8 ± 4.2	42 ± 12
5 (40–50 mm)	7 ± 2.9	16.2 ± 15	5.7 ± 2.3	41 ± 11.4
P-value	0.07	0.12	0.054	0.98
Model 4; $n = 11$				
1 (0–10 mm)	10.7 ± 2.8	19.3 ± 2.7	8.6 ± 2.1	45 ± 7.8
2 (10–20 mm)	9.3 ± 3.7	18 ± 4	8.6 ± 2.4	49 ± 10
3 (20–30 mm)	8.6 ± 2.3	16.8 ± 4.6	8.2 ± 2.4	48 ± 8.3
4 (30–40 mm)	8.3 ± 2.2	17.1 ± 5	8.8 ± 2.8	51 ± 5.7
5 (40–50 mm)	7.5 ± 2.5	15.3 ± 4.9	7.8 ± 2.6	51.3 ± 4.8
6 (50–60 mm)	6.7 ± 2.6†	13 ± 4	6.2 ± 2	48.2 ± 9.7
P-value	0.023	0.06	0.063	0.4

*$P < 0.01$; †$P < 0.05$; ‡$P < 0.001$ as compared with segment 1 at *post hoc* analysis.
Results are given as mean ± SD.

fibrolipid content when all 227 segments were pooled together ($P = 0.03$ and $P = 0.006$, respectively). However, when distance from the ostium, stratified into 10 mm segments, was also inserted into the model, only trends towards increase in fibrous and decrease in fibrolipidic content in stable vs. unstable patients were observed, which did not reach statistical significance. This was confirmed in model 2. In contrary, even when analysed simultaneously, both plaque location along the vessel ($P = 0.044$ and $P = 0.002$ for models 1 and 2, respectively) and clinical presentation (stable vs. unstable) ($P = 0.01$ and $P = 0.004$ for models 1 and 2, respectively) resulted to be independent predictors of lipid content (*Figures 1B* and *2B*) after adjustment for age, sex, diabetic status, type of coronary artery analysed, and use of statin. Finally, in order to evaluate whether the shift in lipid content along the vessel was influenced by clinical presentation, the interplay between these two main determinants of lipid content was investigated, but no statistical interaction emerged between plaque location and lipid core content ($P = 0.8$ and $P = 0.49$ for models 1 and 2, respectively).

Distance from the ostium as an independent predictor of lipid content

In *Table 4* the variables found to be associated to the relative lipid content along the vessel are shown. The lipid core in the most distally located coronary segment (segment 3) in model 1 was significantly lower compared with segment 1, taken as a reference, independently from all other identified predictors. When all 227 segments were included in the model, distance from the ostium, stratified into 10 mm segments, resulted to be an independent predictor of relative lipid content along vessel wall, together with older age, unstable presentation, no use of statin, and the presence of diabetes mellitus. In keeping with the results obtained at the *post hoc* analysis, after adjusting for clinical presentation, relative lipid content in segment 1 did not differ from segment 2 [β −0.08 (95%CI: −0.28, 0.116)], while it did so starting from segment 3 [β −0.22 (95%CI: β 0.39, β 0.05)], with a progressively lower β-value for segment 4 [β −0.34 (95%CI: −0.39, −0.05)] and 5 [β −0.38 (95%CI: −0.55, −0.21)].

Discussion

Several lines of research in the last decades have clearly pointed out how factors involved in pathogenesis and progression of atherosclerotic lesions are widespread throughout the circulatory bed.[8,11,12,14,23,24]

As a corollary to this, evidence that a single pharmacological or mechanical treatment, when applied locally, is able to affect progression of coronary atherosclerosis is weak and not conclusive.[25] On the other hand, systemic

Table 3 Plaque composition stratified into 10 mm segments

Coronary segments	Plaque composition (%)			
	Calcium	Fibrous	Fibrolipidic	Lipid core
Model 1; $n = 51$				
1° (0–10 mm)	0.69 (0.26–1.98)	67.1 (60–74.4)	16.86 (11.2–24)	8.8 (5.7–18)
2° (10–20 mm)	0.67 (0.3–1.58)	68.3 (60–77)	18.1 (12.7–23.1)	9.6 (4.3–15.1)
3° (20–30 mm)	0.79 (0.37–1.82)	69 (64–78)	18.7 (13.4–25.3)	6.2 (2.6–12.1)*
P-value	0.67	0.40	0.84	0.039
Model 2; $n = 43$				
1° (0–10 mm)	0.76 (0.28–2.3)	64.7 (59.3–74)	17.7 (13.4–24.5)	8.01 (5.7–18)
2° (10–20 mm)	0.70 (0.4–1.58)	66.9 (57.9–77)	18.6 (14–24.4)	10 (4.2–16.7)
3° (20–30 mm)	0.75 (0.37–1.82)	69 (63.9–77.8)	19.8 (14.3–25.4)	6.1 (3.5–12)*
4° (30–40 mm)	0.48 (0.09–1.5)	68.7 (60.8–75)	21.1 (17–28.2)	4.5 (2.4–8)†
P-value	0.36	0.55	0.63	0.0058
Model 3; $n = 20$				
1° (0–10 mm)	0.77 (0.5–2.6)	71.4 (49.7–76.4)	17.3 (13.4–23.7)	8 (6–25)
2° (10–20 mm)	0.49 (0.18–1.15)	72.3 (57.9–79.59)	17.2 (100–22.7)	9.3 (4.1–14.6)
3° (20–30 mm)	0.87 (0.1–2.4)	69.3 (61.1–79.6)	17.4 (13.1–25.3)	6.8 (4.1–12)
4° (30–40 mm)	0.9 (0.2–2.6)	67.8 (57.1–77.6)	19.1 (17.4–30)	6.1 (3–8.3)
5° (40–50 mm)	0.65 (0–1)	75.3 (60.6–81.4)	16.4 (14.5–32.6)	3.5 (0.7–5.8)*
P-value	0.14	0.8	0.71	0.039
Model 4; $n = 11$				
1° (0–10 mm)	0.3(0.2–1.6)	74.1 (61–79)	20.8 (16–28)	5.97 (2.25–12)
2° (10–20 mm)	0.8 (0.4–1)	74 (64–79)	20.5 (18–22)	5.7 (3–13)
3° (20–30 mm)	0.54 (0.13–1.6)	75.1 (70–80)	18.5 (16.8–22)	5 (2.8–6.5)
4° (30–40 mm)	0.63 (0.1–1.8)	75.7 (66–77)	21 (20–27)	3.4 (92.4–5.7)
5° (40–50 mm)	0.38 (0.1–1.3)	73.1 (67–81)	21.2 (15–27)	3.2 (2.7–5.3)
6° (50–60 mm)	0.37 (0–0.8)	77.3 (66–79)	24 (19–28)	2.7 (1–4.3)*
P-value	0.65	0.78	0.98	0.036

* $P < 0.05$; † $P < 0.01$ as compared with segment 1 at *post hoc* analysis.
Results are given as median (IQR).

therapy, such as an intensive lipid-lowering treatment, has been convincingly shown to be able to stop atherosclerotic disease progression and even induce coronary lesions regression in some studies.[26–30] The same paradigm is thought to be true for factors involved in atherosclerotic lesions vulnerability, albeit probably in a more elusive way.[25]

These findings should be combined, however, with the evidence provided by recent epidemiological studies, which corroborate the hypothesis according to which sites of occlusions are not uniformly distributed throughout the coronary tree, rather they show a tendency to cluster in partially predictable hot spots located within the proximal third of each coronary vessels.[9,10]

Thus, the interplay among systemic and local factors able to promote progression and vulnerability of atherosclerotic coronary lesions should be probably both targeted in the attempt to control the chronic and acute consequences of coronary atherosclerosis.[15]

Among local factors known to affect genesis and progression of coronary atherosclerotic lesions, shear stress (SS) has been extensively investigated.

Fluid SS, acting on genes 'sensitive' to local haemodynamic forces, is known to elicit a large number of humoural, metabolic, and structural responses in endothelial cells (EC).[31] Low SS on ECs partially explains the local arterial susceptibility to atherosclerosis, as low SS enhances the oxidation of lipids and their accumulation in the intima.[31,32]

Moreover, fluid turbulence in itself is able to directly activate platelets, thus possibly playing a pivotal role in thrombogenesis as well.[33]

It is tempting to speculate that other local factors could play additional roles in modulating progression and instability of atherosclerotic lesions in coronary arteries. Among them, pathological studies have suggested that the distribution of thin-cap atheromas, which are lipid rich core plaques known to be at particularly high-risk for rupture, are not uniformly distributed along the coronary vessels in post-mortem examinations.[34] Rather, they cluster in the proximal segments of the three main coronary arteries, which is in keeping with the longitudinal distribution of both ruptured and healed plaques.[34]

This non-uniform distribution of vulnerable plaques in humans could partially explain the clustering of occlusive culprit lesion in the proximal or middle tract of coronary arteries. In this regard, we hypothesized that plaque composition was also not uniformly distributed *in vivo* in humans in patients with symptomatic coronary disease. Thanks to a recently developed technology based on spectral analysis of IVUS radiofrequency data (IVUS-VH),[16,17] we prospectively evaluated whether plaque composition is independently affected by the distance from coronary ostium in a

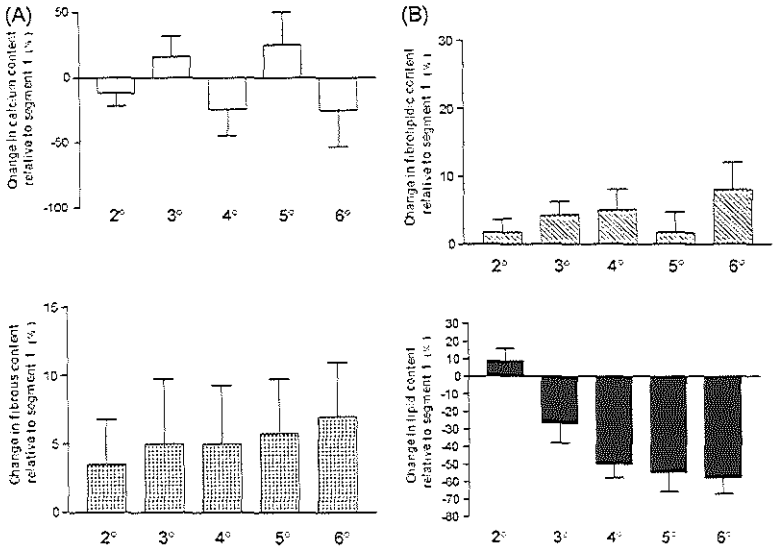

Figure 1 Relative change in plaque composition with respect to segment 1. Starting from segment 3, relative lipid content showed a progressive decrease with respect to ostial segment (segment 1) taken as a reference. Relative changes in segments 2 and 3 were calculated using model 1, whereas for the relative change in segments 4, 5, and 6, models 2, 3, and 4 were employed, respectively. All relative changes are expressed as mean value and standard deviation.

consecutive series of patients. Our findings support the concept that coronary plaques located in the proximal tract (≈20 mm) of coronary vessels are relatively richer in lipid content with respect to those more distally located, independently from clinical presentation. In this regard, the magnitude of lipid content appeared to be relatively higher in patients presenting with clinical instability but no interaction emerged in our model between clinical presentation and lipid content, suggesting that the relative change in plaque composition along the vessel is a well-preserved phenotype in both groups of patients. Moreover, distance from the coronary ostium resulted to be an independent predictor of relative lipid content along the vessel wall in our regression model, together with age, unstable presentation, presence of diabetes mellitus, and no use of statin.

Our current findings should be regarded as an attempt to extend the pathophysiological knowledge on plaque vulnerability, mainly because of the well-known linkage between plaque composition and risk of plaque rupture or erosion.[34–36] Thus, this might contribute to explain the higher likelihood for plaque erosion or rupture to occur proximally in the coronary tree. Moreover, the finding that coronary plaques show a relatively higher lipid content if proximally located along the longitudinal axis of the vessel with respect to those more distally located might elicit new methodological issues in future investigations. In particular, hypothesizing that plaque progression/regression studies accomplished through aggressive lipid-lowering regimen would mainly affect the lipid content in the plaque, it seems reasonable to believe that the relative effect of the tested medication observed at IVUS investigation in terms of overall plaque CSA, could differ in relation to the localization of ROI with respect to the coronary ostium. This could bear special hazard particularly in those studies having limited ROI length.[37]

An interesting finding of our study was that the percentage of stenosis did not differ in relation to the distance from the ostium, whereas plaque area was progressively smaller moving form proximal to distal segments. This might be explained by the interplay between the physiological proximal-distal tapering of the coronary vessel and the higher propensity of the proximal segments to undergo positive remodelling with respect to those located more distally. This seems to be in keeping with our recent findings that positive remodelling is indeed more pronounced in lipid-rich coronary segments.[38]

Limitations of the study

As exploratory-pilot investigation, our current findings should be regarded as provisional. In particular, to assess relatively minor changes in plaque composition along longitudinal vessel axis, such as that observed for fibrous tissue, or for highly dispersed data such as for relative calcium content, a bigger, properly powered, sample size is clearly needed. Similarly, the observed insignificant trends for fibrous tissue to be increased and fibrolipidic content to be decreased in stable vs. unstable patients may reflect a type-II error. Our results mainly apply to the first 40 mm of the three main coronary arteries, whereas the longitudinal pattern of shift in coronary plaque composition in coronary segments more distally located or in left main coronary artery should be evaluated in studies specifically designed for such an aim. In particular, in keeping with our primary endpoint, the only comparison for which this study was properly powered for is the one between the first and the

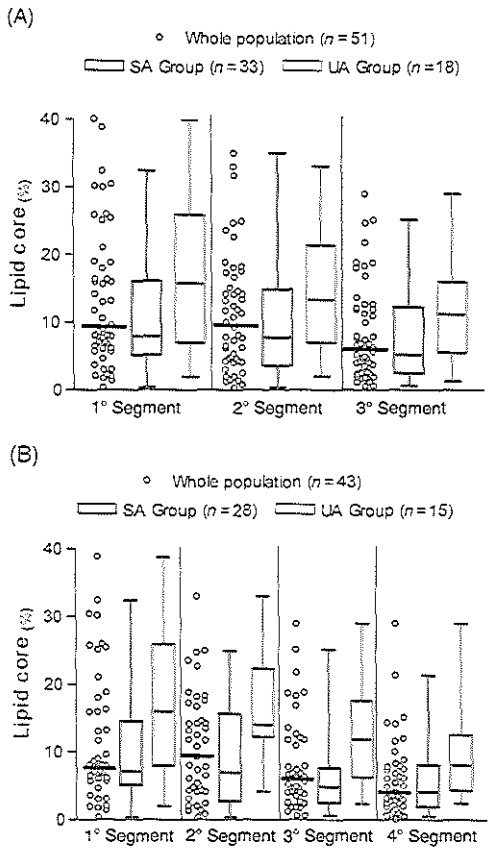

Figure 2 Per-segment distribution of relative lipid content in the study population. Per-segment distribution of relative lipid contents both in the whole population and stable vs. unstable patients in model 1 (*A*) and 2 (*B*). Bars indicate median values in the whole population. As shown in *Table 3*, relative lipid content significantly decreased in the whole population in segment 3 in model 1 and in segments 3 and 4 in model 2 with respect to segment 1 at *post hoc* analysis.

third segment in model 1. All other analyses, including the tests for four models and all *post hoc* comparisons should be regarded as exploratory. Despite careful examination of all angiograms, we cannot completely rule out the possibility that patients with a higher number of IVUS interrogated 10 mm segments had a more favourable coronary anatomy as compared with those in whom a long pull-back could not been obtained.

Relevant to this point, it is the fact that: (i) plaque composition in the first three coronary segments did not differ in patients with 30 mm pull back length as compared with those in whom a longer IVUS pull back was obtained; and (ii) the change in plaque composition along the study vessel was remarkably consistent in all the four models analysed.

We failed to find sex-related differences in the proximal-distal pattern of plaque composition. However, the great majority (88%) of patients enrolled were males, which

Table 4 Predictors of plaque lipid content at uni- and multivariate analysis in model 1

Variables	Beta-values	(95% CI)	*P*-values
Univariate analysis			
Age (years)	−0.12	−0.25, 0.008	0.069
Sex (M vs. F)	0.029	−0.101, 0.16	0.66
Smoking status	0.022	−0.108, 0.15	0.7
Previous history of			
Hypertension	0.048	−0.08, 0.16	0.48
CVD in the family	−0.038	−0.16, 0.082	0.56
Hypercholesterolaemia	0.08	−0.032, 0.197	0.21
Diabetes mellitus	0.14	0.023, 0.257	0.041
ACS	0.044	−0.086, 0.174	0.50
Coronary revascularization	−0.15	−0.2, −0.028	0.02
Coronary vessel[a]	0.038	−1.93, 2.008	0.5
ACS at presentation	0.25	0.11, 0.39	0.0032
LDL (mg/dL)	0.09	−0.04, 0.22	0.42
HDL (mg/dL)	−0.12	−0.25, 0.01	0.067
Triglycerides (mg/dL)	0.04	−0.09, 0.17	0.78
Use of statin	−0.25	−0.37, −0.12	0.0001
Distance from ostium[b]	−0.32	−0.45, −0.30	<0.0001
Multivariable analysis[c]			
Distance from ostium[b]	−0.28	−0.15, −41	<0.0001
Age (years)	−0.26	−0.12, −40	0.0004
ACS at presentation	0.16	0.03, 0.29	0.005
Use of statin	−0.18	−0.36, 0.004	0.057
Diabetes mellitus	0.21	0.07, 0.34	0.003
Coronary revascularization	−0.07	−0.02, 0.12	0.46
HDL (mg/dL)	−0.02	−0.05, 0.21	0.84

CVD, cardiovascular disease; LDL, low-density lipoprotein; HDL, high-density lipoprotein.

[a]Analysed as left anterior descending vs. circumflex vs. right coronary artery

[b]Analysed as segment 1 taken as a reference vs. segment 3.

[c]Adjusted $R^2 = 0.36$ for the model.

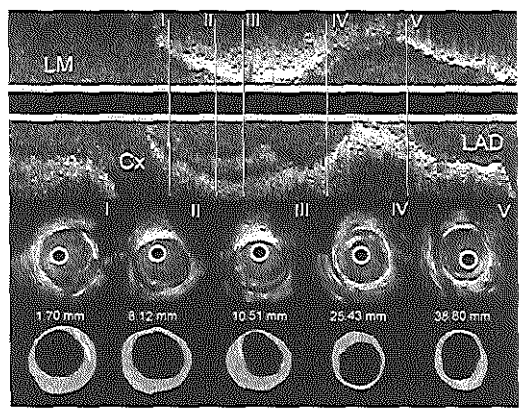

Figure 3 IVUS-VH CSA along a coronary vessel. IVUS-VH cross-sectional areas in a representative patient showing the change in plaque composition (calcium: white; fibrous: green; fibrolipidic: greenish-yellow; and lipid core: red) along the longitudinal axis of the vessel. LM, left main coronary artery; CFX, circumflex artery; LAD, left anterior descending artery. The distance between the cross-sectional area and the ostium of the vessel is reported in millimetres (mm).

calls for future studies with more balanced sex-distribution to properly address this gender issue.

Finally, it should not undergo unnoticed that the proportion of lipid core content predicted by our multivariable regression model, despite highly significant, was far from being optimal. This means that future investigations should probably aim to increase the capability to predict relative lipid content in coronary plaques taking a broader set of possible independent predictors into account.

Conclusion

Our study provides proof of concept for a non-uniform longitudinal distribution of plaque composition mainly in terms of lipid core content along the main coronary arteries *in vivo* in humans. The clinical and pathophysiological meaning of this observation and whether it could help explaining the non-uniform distribution of vulnerable plaques along the coronary vessel remains unclear. Future studies are needed to extend and possibly confirm our current findings.

Conflict of interest: none declared.

References

1. Burke AP, Farb A, Pestaner J, Malcom GT, Zieske A, Kutys R, Smialek J, Virmani R. Traditional risk factors and the incidence of sudden coronary death with and without coronary thrombosis in blacks. *Circulation* 2002;105:419–424.
2. Shah PK. Mechanisms of plaque vulnerability and rupture. *J Am Coll Cardiol* 2003;41:15S–22S.
3. Ambrose JA, Tannenbaum MA, Alexopoulos D, Hjemdahl-Monsen CE, Leavy J, Weiss M, Borrico S, Gorlin R, Fuster V. Angiographic progression of coronary artery disease and the development of myocardial infarction. *J Am Coll Cardiol* 1988;12:56–62.
4. Giroud D, Li JM, Urban P, Meier B, Rutishauer W. Relation of the site of acute myocardial infarction to the most severe coronary arterial stenosis at prior angiography. *Am J Cardiol* 1992;69:729–732.
5. Hackett D, Davies G, Maseri A. Pre-existing coronary stenoses in patients with first myocardial infarction are not necessarily severe. *Eur Heart J* 1988;9:1317–1323.
6. Lichtlen PR, Nikutta P, Jost S, Deckers J, Wiese B, Rafflenbeul W. Anatomical progression of coronary artery disease in humans as seen by prospective, repeated, quantitated coronary angiography. Relation to clinical events and risk factors. The INTACT Study Group. *Circulation* 1992;86:828–838.
7. Little WC, Constantinescu M, Applegate RJ, Kutcher MA, Burrows MT, Kahl FR, Santamore WP. Can coronary angiography predict the site of a subsequent myocardial infarction in patients with mild-to-moderate coronary artery disease? *Circulation* 1988;78:1157–1166.
8. Naghavi M, Libby P, Falk E, Casscells SW, Litovsky S, Rumberger J, Badimon JJ, Stefanadis C, Moreno P, Pasterkamp G, Fayad Z, Stone PH, Waxman S, Raggi P, Madjid M, Zarrabi A, Burke A, Yuan C, Fitzgerald PJ, Siscovick DS, de Korte CL, Aikawa M, Airaksinen KE, Assmann G, Becker CR, Chesebro JH, Farb A, Galis ZS, Jackson C, Jang IK, Koenig W, Lodder RA, March K, Demirovic J, Navab M, Priori SG, Rekhter MD, Bahr R, Grundy SM, Mehran R, Colombo A, Boerwinkle E, Ballantyne C, Insull W Jr, Schwartz RS, Vogel R, Serruys PW, Hansson GK, Faxon DP, Kaul S, Drexler H, Greenland P, Muller JE, Virmani R, Ridker PM, Zipes DP, Shah PK, Willerson JT. From vulnerable plaque to vulnerable patient: a call for new definitions and risk assessment strategies: Part II. *Circulation* 2003;108:1772–1778.
9. Gibson CM, Kirtane AJ, Murphy SA, Karha J, Cannon CP, Giugliano RP, Roe MT, Harrington RA, Ohman EM, Antman EM. Distance from the coronary ostium to the culprit lesion in acute ST-elevation myocardial infarction and its implications regarding the potential prevention of proximal plaque rupture. *J Thromb Thrombolysis* 2003;15:189–196.
10. Wang JC, Normand SL, Mauri L, Kuntz RE. Coronary artery spatial distribution of acute myocardial infarction occlusions. *Circulation* 2004; 110:278–284.
11. Buffon A, Biasucci LM, Liuzzo G, D'Onofrio G, Crea F, Maseri A. Widespread coronary inflammation in unstable angina. *N Engl J Med* 2002;347:5–12.
12. Valgimigli M, Agnoletti L, Curello S, Comini L, Francolini G, Mastrorilli F, Merli E, Pirani R, Guardigli G, Grigolato PG, Ferrari R. Serum from patients with acute coronary syndromes displays a proapoptotic effect on human endothelial cells: a possible link to pan-coronary syndromes. *Circulation* 2003;107:264–270.
13. Madjid M, Zarrabi A, Litovsky S, Willerson JT, Casscells W. Finding vulnerable atherosclerotic plaques: is it worth the effort? *Arterioscler Thromb Vasc Biol* 2004;24:1775–1782.
14. Maseri A, Fuster V. Is there a vulnerable plaque? *Circulation* 2003; 107:2068–2071.
15. VanderLaan PA, Reardon CA, Getz GS. Site specificity of atherosclerosis: site-selective responses to atherosclerotic modulators. *Arterioscler Thromb Vasc Biol* 2004;24:12–22.
16. Nair A, Kuban BD, Tuzcu EM, Schoenhagen P, Nissen SE, Vince DG. Coronary plaque classification with intravascular ultrasound radiofrequency data analysis. *Circulation* 2002;106:2200–2206.
17. Rodriguez-Granillo GA, Aoki J, Ong ATL, Valgimigli M, van Mieghem CAG, Regar E, McFadden E, de Feyter P, Serruys PW. Methodological considerations and approach to cross-technique comparisons using *in vivo* coronary plaque characterization based on intravascular radiofrequency data analysis: insights from the integrated Biomarker and Imaging Study (IBIS). *Int J Cardiovasc Interv* 2005;7:52–58.
18. Kåresen K. Deconvolution of sparse spike trains by iterated window maximization. *IEEE Trans Signal Process* 1997;45:1173–1183.
19. Kåresen KF BE. Blind deconvolution of ultrasonic traces accounting for pulse variance. *IEEE Trans Ultrason Ferroelectr Freq Contr* 1999; 46:564–573.
20. Mann JM, Davies MJ. Vulnerable plaque. Relation of characteristics to degree of stenosis in human coronary arteries. *Circulation* 1996; 94:928–931.
21. Draper NR, Smith H. *Applied Regression Analysis*. New York, NY: Wiley; 1981.
22. Diggle PJ, Heagerty PJ, Liang KY, Zeger SL. *Analysis of Longitudinal Data*. New York, NY: Oxford University Press; 2002.
23. Monroe VS, Kerensky RA, Rivera E, Smith KM, Pepine CJ. Pharmacologic plaque passivation for the reduction of recurrent cardiac events in acute coronary syndromes. *J Am Coll Cardiol* 2003;41:23S–30S.
24. Casscells W, Naghavi M, Willerson JT. Vulnerable atherosclerotic plaque: a multifocal disease. *Circulation* 2003;107:2072–2075.
25. Ambrose JA, D'Agate DJ. Classification of systemic therapies for potential stabilization of the vulnerable plaque to prevent acute myocardial infarction. *Am J Cardiol* 2005;95:379–382.
26. Balk EM, Karas RH, Jordan HS, Kupelnick B, Chew P, Lau J. Effects of statins on vascular structure and function: a systematic review. *Am J Med* 2004;117:775–790.
27. Nissen SE, Tsunoda T, Tuzcu EM, Schoenhagen P, Cooper CJ, Yasin M, Eaton GM, Lauer MA, Sheldon WS, Grines CL, Halpern S, Crowe T, Blankenship JC, Kerensky R. Effect of recombinant ApoA-I Milano on coronary atherosclerosis in patients with acute coronary syndromes: a randomized controlled trial. *JAMA* 2003;290:2292–2300.
28. Nissen SE, Tuzcu EM, Schoenhagen P, Brown BG, Ganz P, Vogel RA, Crowe T, Howard G, Cooper CJ, Brodie B, Grines CL, DeMaria AN. Effect of intensive compared with moderate lipid-lowering therapy on progression of coronary atherosclerosis: a randomized controlled trial. *JAMA* 2004;291:1071–1080.
29. Matsuzaki M, Hiramori K, Imaizumi T, Kitabatake A, Hishida H, Nomura M, Fujii T, Sakuma I, Fukami K, Honda T, Ogawa H, Yamagishi M. Intravascular ultrasound evaluation of coronary plaque regression by low density lipoprotein-apheresis in familial hypercholesterolemia: the Low Density Lipoprotein-Apheresis Coronary Morphology and Reserve Trial (LACMART). *J Am Coll Cardiol* 2002;40:220–227.
30. Lima JA, Desai MY, Steen H, Warren WP, Gautam S, Lai S. Statin-induced cholesterol lowering and plaque regression after 6 months of magnetic resonance imaging-monitored therapy. *Circulation* 2004;110: 2336–2341.
31. Malek AM, Alper SL, Izumo S. Hemodynamic shear stress and its role in atherosclerosis. *JAMA* 1999;282:2035–2042.
32. Kinlay S, Libby P, Ganz P. Endothelial function and coronary artery disease. *Curr Opin Lipidol* 2001;12:383–389.
33. Einav S, Bluestein D. Dynamics of blood flow and platelet transport in pathological vessels. *Ann NY Acad Sci* 2004;1015:351–366.

34. Kolodgie FD, Burke AP, Farb A, Gold HK, Yuan J, Narula J, Finn AV, Virmani R. The thin-cap fibroatheroma: a type of vulnerable plaque: the major precursor lesion to acute coronary syndromes. *Curr Opin Cardiol* 2001;16:285-292.
35. Fayad ZA, Fuster V. Clinical imaging of the high-risk or vulnerable atherosclerotic plaque. *Circ Res* 2001;89:305-316.
36. Kolodgie FD, Virmani R, Burke AP, Farb A, Weber DK, Kutys R, Finn AV, Gold HK. Pathologic assessment of the vulnerable human coronary plaque. *Heart* 2004;90:1385-1391.
37. Okazaki S, Yokoyama T, Miyauchi K, Shimada K, Kurata T, Sato H, Daida H. Early statin treatment in patients with acute coronary syndrome: demonstration of the beneficial effect on atherosclerotic lesions by serial volumetric intravascular ultrasound analysis during half a year after coronary event: the ESTABLISH Study. *Circulation* 2004;110: 1061-1068.
38. Rodriguez-Granillo GA, Serruys PW, Garcia-Garcia HM, Aoki J, Valgimigli M, van Mieghem CA, Mc Fadden E, de Jaegere PP, de Feyter P. Coronary artery remodelling is related to plaque composition. *Heart* 2005; doi:10.1136/hrt.2004.057810.

CHAPTER 3.4

Plaque composition and its relationship with acknowledged shear stress patterns in coronary arteries.

Rodriguez-Granillo GA, **Garcia-Garcia HM**, Wentzel J, Valgimigli M, Tsuchida K, van der Giessen W, de Jaegere P, Regar E, de Feyter PJ, Serruys PW.

J Am Coll Cardiol. 2006;47:884-5.

Plaque Composition and its Relationship With Acknowledged Shear Stress Patterns in Coronary Arteries

To the Editor: Several studies in coronary and peripheral arteries have demonstrated that atherosclerosis has a tendency to arise more frequently in low-oscillatory shear stress (LOSS) regions such as in inner curvature of nonbranching segments and opposite to the flow divider (FD) at bifurcations (1–3). In particular, atherosclerotic disease has certain predilection for the outer wall of the left main coronary artery bifurcation, sparing the FD (2). Intravascular ultrasound (IVUS) has been used to describe the extent, distribution, and profile of plaques in the proximal left anterior descending coronary artery (LAD) (2). Nevertheless, in vivo data regarding tissue composition of this region remain unknown. Furthermore, to date, no study has explored the characteristics of plaques located in the proximal LAD compared to the left main coronary artery (LMCA). In the present study, we sought to explore the morphologic and compositional characteristics of plaque located at an acknowledged LOSS area (outer wall of the ostial LAD [OLAD]) and compare them to the characteristics of plaque located at an average shear stress region (distal LMCA [DLMCA]).

This prospective investigators-driven study included patients where the LAD was interrogated before any intervention using IVUS radiofrequency data (RFD) analysis (IVUS-VH; Volcano Therapeutics, Rancho Cordova, California). The IVUS-VH uses spectral analysis of IVUS RFD to construct tissue maps that were correlated with a specific spectrum of the RFD and assigned color codes (Fig. 1) (4). The IVUS-VH was performed with 30-MHz (Ultracross; Boston Scientific, Santa Clara, California) and 20-MHz (Eagle Eye; Volcano Therapeutics) catheters, and contour detection was determined using previously reported methodology (5). Informed consent was obtained from all patients. Plaque eccentricity was defined as the ratio of maximal to minimal plaque thickness (1). Plaque burden was defined as $([EEM_{area} - lumen_{area}]/EEM_{area}) \times 100$. The carina of the bifurcation was identified as the frame immediately distal to the take-off of the circumflex.

The maximal plaque thickness (MPT) was calculated at this level and spatially located according to a circumference ranging from 0° to 360°, being the inner and opposite part of the carina at 0° and 180°, respectively. Lesions were therefore prospectively divided into two groups, according to their localization in the outer (from 91° to 271°) or inner (from 270° to 90°) hemisphere of the carina.

Two regions were prospectively identified and their morphology and composition compared. The OLAD was defined as the carina and the immediate 3-mm distal segment, because the flow in this area is still influenced by the bifurcation (6). Similarly, the DLMCA was identified as the 3-mm segment immediately

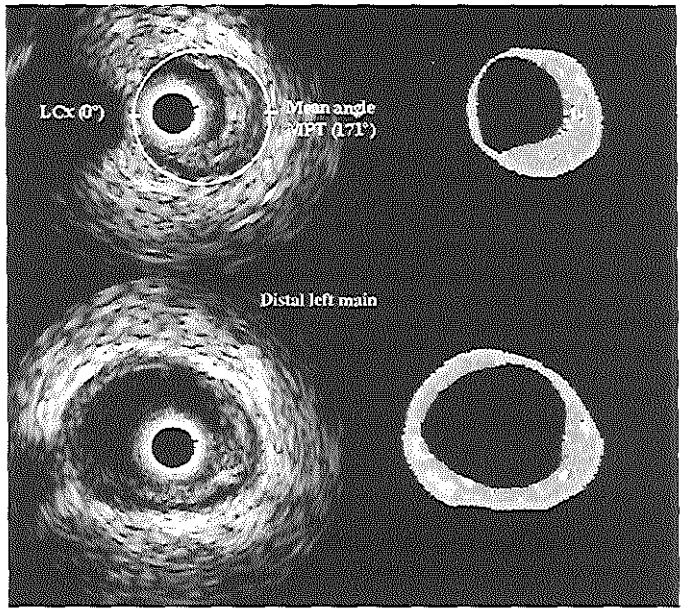

Figure 1. Intravascular ultrasound cross-section images from the carina of the left anterior descending coronary artery and of the left main coronary artery. The **left side** shows the reconstructed grayscale, and the **right side** shows the color-coded data (**green** = fibrous; **yellow-green** = fibrolipidic; **red** = necrotic core; **white** = calcium) provided by the IVUS-VH unit (Volcano Therapeutics, Rancho Cordova, California). LCx = left circumflex artery; MPT = maximal plaque thickness.

Table 1. Volumetrical and Compositional Comparative Results Between the Ostial Left Anterior Descending Coronary Artery (OLAD) and the Distal Left Main Coronary Artery (DLMCA)

	OLAD	DLMCA	p Value
Plaque burden (%)	45.5 ± 10.2	36.4 ± 10.8	<0.0001
Plaque eccentricity	14.5 ± 11.6	10.4 ± 7.6	0.05
Max. plaque thickness (mm)	1.24 ± 0.4	1.04 ± 0.3	0.002
Necrotic core (%)	12.4 ± 9.2	7.9 ± 8.6	<0.0001
Calcium (%)	4.1 ± 5.1	1.3 ± 2.0	<0.0001
Fibrous (%)	64.5 ± 13.6	64.9 ± 13.3	0.82
Fibrolipidic (%)	18.4 ± 11.8	24.9 ± 12.8	0.005

Values are presented as mean ± SD. Plaque eccentricity was defined as the ratio of maximal to minimal plaque thickness. Plaque burden was defined as $([EEM_{area} - lumen_{area}]/EEM_{area}) \times 100$.

proximal to the bifurcation. Compositional and geometrical data were expressed as mean percentages.

Discrete variables are presented as counts and percentages. Continuous variables are presented as mean ± SD. Differences in means among groups were analyzed by two-sample *t* test. A p value of <0.05 (two-sided) was considered to indicate statistical significance.

Forty-four patients were finally included in the analysis. The clinical presentation was stable angina in 23 patients (52.3%), unstable angina in 10 patients (22.7%) and acute myocardial infarction in 11 patients (5%); the mean age of the patients was 58.8 ± 11.5 years, and 33 patients (75%) were male. Geometric and compositional comparative results between the OLAD and the DLMCA are depicted in Table 1. Plaque burden was larger in the OLAD than in the DLMCA (45.5 ± 10.2% vs. 36.4 ± 10.8%; $p < 0.0001$). OLAD plaques presented more calcified (4.13 ± 5.1% vs. 1.28 ± 2.0%; $p < 0.0001$) and necrotic (12.36 ± 9.2% vs. 7.90 ± 8.6%, $p < 0.0001$) core content.

The MPT was located in the outer hemisphere of the carina in 77.3% (n = 34) of the cases and the mean angle was 170.7 ± 60.6°. Only one case presented the MPT at 0 degrees. Necrotic core content was larger in outer than in inner lesions (14.4 ± 10.0% vs. 6.3 ± 6.9%; $p = 0.02$).

The current investigation extends earlier findings on atheroma distribution in the LAD by comparing in vivo plaque burden and composition in acknowledged areas of low and average shear stress. It has been previously established that an inverse relationship exists between LOSS and thickness of the vessel wall (3). The pathophysiology of such phenomena can briefly be explained by the fact that LOSS induces a loss of the physiologic flow-oriented alignment of the endothelial cells, thus causing an enhancement of the expression of adhesion molecules and a weakening of cell junctions, ultimately leading to an increase in permeability to lipids and macrophages (3,7–9). The results of the present study are in line with histopathologic data, showing higher concentrations of necrotic core and calcium in an acknowledged area subject to LOSS. Such difference may be driven by the lipid leakage present in these areas (8). The high lipid load in addition to the eccentric characteristics of the atheroma would potentially render these plaques more susceptible to rupture (10). Conversely, the more stable phenotype observed in DLMCA lesions supports the low incidence of atherothrombotic events at this level (11). Finally, these results may provide another potential explanation for the higher risk of restenosis after percutaneous coronary intervention of bifurcation lesions.

In summary, we found that OLAD atherosclerotic plaques present larger plaque burden, eccentricity, and MPT than DLMCA plaques. In addition, a larger calcified and necrotic core content was found distal to the circumflex take-off. Lesions were predominantly located in the outer wall of the carina, and such location was associated with larger necrotic core content.

Gastón A. Rodriguez-Granillo, MD
Héctor M. García-García, MD
Jolanda Wentzel, PhD
Marco Valgimigli, MD
Keiichi Tsuchida, MD
Wim van der Giessen, MD, PhD
Peter de Jaegere, MD, PhD
Evelyn Regar, MD, PhD
Pim J. de Feyter, MD, PhD
***Patrick W. Serruys, MD, PhD, FACC**

*Thoraxcenter, Bd406
Dr. Molewaterplein 40
3015-GD Rotterdam
the Netherlands
E-mail: p.w.j.c.serruys@erasmusmc.nl

doi:10.1016/j.jacc.2005.11.027

REFERENCES

1. Jeremias A, Huegel H, Lee DP, et al. Spatial orientation of atherosclerotic plaque in nonbranching coronary artery segments. Atherosclerosis 2000;152:209–15.
2. Kimura BJ, Russo RJ, Bhargava V, McDaniel MB, Peterson KL, DeMaria AN. Atheroma morphology and distribution in proximal left anterior descending coronary artery: in vivo observations. J Am Coll Cardiol 1996;27:825–31.
3. Kornet L, Hocks AP, Lambregts J, Reneman RS. In the femoral artery bifurcation, differences in mean wall shear stress within subjects are associated with different intima-media thicknesses. Arterioscler Thromb Vasc Biol 1999;19:2933–9.
4. Nair A, Kuban BD, Tuzcu EM, Schoenhagen P, Nissen SE, Vince DG. Coronary plaque classification with intravascular ultrasound radiofrequency data analysis. Circulation 2002;106:2200–6.
5. Rodriguez-Granillo GA, Serruys PW, Garcia-Garcia HM, et al. Coronary artery remodelling is related to plaque composition. Heart 2005 Jun 17; [Epub ahead of print].
6. Gijsen F, Thury A, Lamers B, Wentzel JJ, Schuurbiers JCH, Serruys PW, Slager CJ. 3D plaque distribution and its relationship to shear stress in a human coronary artery bifurcation in vivo. Presented at: Summer Bioengineering Conference, June 22–26, 2005 Vail, Colorado.
7. Berceli SA, Warty VS, Sheppeck RA, Mandarino WA, Tanksale SK, Borovetz HS. Hemodynamics and low density lipoprotein metabolism. Rates of low density lipoprotein incorporation and degradation along medial and lateral walls of the rabbit aorto-iliac bifurcation. Arteriosclerosis 1990;10:686–94.
8. Kaazempur-Mofrad MR, Isasi AG, Younis HF, et al. Characterization of the atherosclerotic carotid bifurcation using MRI, finite element modeling, and histology. Ann Biomed Eng 2004;32:932–46.
9. Slager CJ, Wentzel J, Gijsen FJH, Schuurbiers JCH, van der Wal AC, van der Steen AFW, Serruys PW. The role of shear stress in the generation of rupture-prone vulnerable plaques. Nat Clin Pract 2005; 2:401–7.
10. Falk E, Shah PK, Fuster V. Coronary plaque disruption. Circulation 1995;92:657–71.
11. Wang JC, Normand SL, Mauri L, Kuntz RE. Coronary artery spatial distribution of acute myocardial infarction occlusions. Circulation 2004;110:278–84.

CHAPTER 3.5

Tissue Characterization of Atherosclerotic Plaque in Coronary Artery Bifurcations in Humans.

Han Seung Hwan, Puma J, **Garcia-Garcia HM**, Nasu K, Margolis P, Saito S, Leon M, Lerman A.

Submitted.

ABSTRACT

Objective: We assessed compositional characteristics of atherosclerotic plaque in coronary artery bifurcations with intravascular ultrasound radio frequency data analysis.

Background: Coronary artery bifurcations are prone to develop atherosclerotic plaque accumulation.

Methods: As global virtual histology registry (N=990), we analyzed the geometrical and compositional characteristics of plaque at the 3 segments at the sites of the major bifurcations, 5 mm proximal and distal segments to the bifurcation at different bifurcation sites. (N=258, left main (LM)-left anterior descending artery (LAD)=41, LM-left circumflex artery (LCX)=2, LAD-diagonal=128, LCX-obtuse marginal artery (OM)=34, right coronary artery (RCA)-acute marginal artery (AM)=53).

Results: The percent (%) necrotic core including media in just and distal segments of LM-LAD bifurcations was significantly greater than proximal segments (6.75 ± 5.07%, 7.36 ± 6.01% vs. 4.89 ± 4.78%, all $p<0.05$). In contrast, the % necrotic core in proximal segments of non-LM bifurcations was significantly greater than just and distal segments of bifurcations (8.08 ± 6.21% vs. 6.47 ± 5.11%, 6.28 ± 5.05%, all $p<0.001$). The % necrotic core in proximal and distal segments of LM-LAD bifurcations were significantly correlated with plaque+media (P+M) burden ($r=0.45$, $p=0.003$, $r=0.42$, $p=0.006$, respectively). The % necrotic core in each segment of non-LM bifurcations showed a significant positive correlation with P+M burden and negative correlation with lumen cross sectional area (CSA) ($0.51\leq r\leq 0.64$, all $p<0.001$ and $-0.35\leq r\leq -0.31$, all $p<0.001$, respectively).

Conclusions: The current study demonstrates that the bifurcation sites of LM-LAD had greater necrotic core at just and distal segments of the bifurcation, while non-LM showed greater necrotic core in proximal segment of bifurcation. The results may suggest a heterogeneous distribution of the atherosclerosis plaques in bifurcation lesions and may support a strategy of an imaging guided therapeutic for complex coronary plaques such as bifurcation lesions.

Key words: atherosclerosis; bifurcation; intracoronary ultrasound, virtual histology

CONDENSED ABSTRACT

We assessed geometrical and compositional characteristics of major coronary bifurcations with intravascular ultrasound radiofrequency data analysis. The % necrotic core including media at just and distal segments of left main-left anterior descending bifurcations were significantly greater than proximal segments, however, the % necrotic core including media in proximal segments of non-left main bifurcations were significantly greater than at just and distal segments of bifurcations. These results might support the strategy of imaging guided therapy for coronary artery disease in humans.

ABBREVIATIONS

IVUS, intravascular ultrasound
LM, left main coronary artery
LAD, left anterior descending coronary artery
LCX, left circumflex coronary artery
RCA, right coronary artery
OM, obtuse marginal coronary artery
AM, acute marginal coronary artery
P+M, plaque+media
RFD, radiofrequency data
VH, virtual histology, spectral analysis plaque characterization methodology

INTRODUCTION

Atherosclerotic plaques of the coronary artery are prone to develop at specific locations such as bifurcation and ostial locations [1-2]. Percutaneous coronary intervention of bifurcation lesions still remain a challenging lesion subset [3]. The differential lesion characteristics, different tissue composition and adaptive arterial remodeling at bifurcation sites may be derived from different geometric variation and additional factors such as shear stress, and vessel structure [4-6].

The ability to visualize and quantify the different components of atherosclerosis provides important information not only on the mechanism of coronary artery disease, but also on potential future therapeutic interventions to alter the disease process and optimize interventional outcome. A new spectral analysis of the intravascular ultrasound (IVUS) radiofrequency data (RFD) may be a useful tool [7,8] because it allows detailed assessment of plaque composition, with a high predictive accuracy of 93.1% to 96.7% in fibrous tissue, fibro-fatty, dense calcium, and necrotic core regions with sensitivities and specificities ranging from 72% to 99% [9]. In addition, rcecent studies demonstrated that in-vivo tissue characteristics of patients with coronary artery disease can be available and it is useful imaging tool in understanding the pathophysiology of the disease process [10-12].

Until now, the compositional characteristics at the bifurcation sites and proximal and distal segments of major bifurcation sites are not well investigated and not evaluated according to their coronary artery locations. Thus, the current study was designed to evaluate the geometrical and compositional characteristics of atherosclerotic lesions at the bifurcation sites among proximal, at the site and distal segments of bifurcations and their differential characteristics according to their anatomical locations.

METHODS

Study Subjects

To evaluate the compositional characteristics of atherosclerotic plaque in the coronary atherosclerosis, subjects who underwent IVUS-RFD analysis, virtual histology (VH) were prospectively enrolled to multicenter, international, global VH registry (N=990). To evaluate the geometrical and compositional characteristics of atherosclerotic plaque in coronary artery bifurcations, we analyzed the IVUS-RFD of major bifurcation sites (the diameter of side branch more than 2mm by IVUS) from this registry. The exclusion criteria of the present study

included the presence of intervening other major side branch and previous history of percutaneous coronary intervention within 10 mm of index bifurcation sites.

Intravascular Ultrasound Virtual Histology Examination

The methods of the IVUS-RFD analysis were described previously [8-13]. The IVUS-RFD analysis was performed with a dedicated IVUS-VH console (Volcano Therapeutics, Rancho Cordova, California) during the routine coronary angiography after intracoronary administration of 100 to 200 μg nitroglycerin. A 20-MHz, 2.9F monorail, electronic Eagle Eye Gold IVUS catheter (Volcano Therapeutics, Rancho Cordova, California) was advanced into the distal to the index sites, and automatic pullback at 0.5 mm/s was done to an proximal to the index sites. The IVUS-RFD image was recorded on a DVD-ROM and sent to the imaging core lab for offline analysis later.

Spectral Analysis of Intravascular Ultrasound Radiofrequency Data

These off line analyses were done with personal computer (PC) VH program software (Volcano Therapeutics, Rancho Cordova, California) by an examiner who was unaware of the clinical characteristics of the subjects. For both the lumen and the media-adventitia interface, semiautomatic contour detection was done for all the frames of the whole examined coronary segments. Then, the borders were manually corrected in all the frames [10-12]. For each frame, compositional tissue characteristics were expressed in colors, as previously described (green for fibrous tissue, green-yellow for fibro-fatty, white for dense calcium, and red for necrotic core area) [8]. We analyzed geometrical and compositional characteristics of the 5mm-proximal, just bifurcation and 5mm-distal segments at bifurcation sites, the number of frames correspond to their length were analyzed (Fig. 1.).

To evaluate the reference vessel we examined the single frame with the largest lumen and smallest plaque+media (P+M) burden % within 10mm proximal and distal to just bifurcation segments. Mean vessel cross sectional area (CSA), lumen CSA, P+M CSA, P+M burden %, remodeling index were calculated. P+M CSA was calculated as (vessel CSA - lumen CSA). % P+M burden was calculated as: (P+M CSA/vessel CSA) × 100. Proximal and distal remodeling index were calculated as (vessel CSA with most P+M burden %/average vessel CSA of proximal and distal reference vessel). In addition, compositional parameters such as mean dense calcium CSA (mm^2) and % (including media), fibrous tissue CSA (mm^2) and %, fibro-fatty CSA (mm^2) and %, necrotic core CSA (mm^2) and % were calculated. The definition of bifurcation lesion was P+M burden % on the frame which had

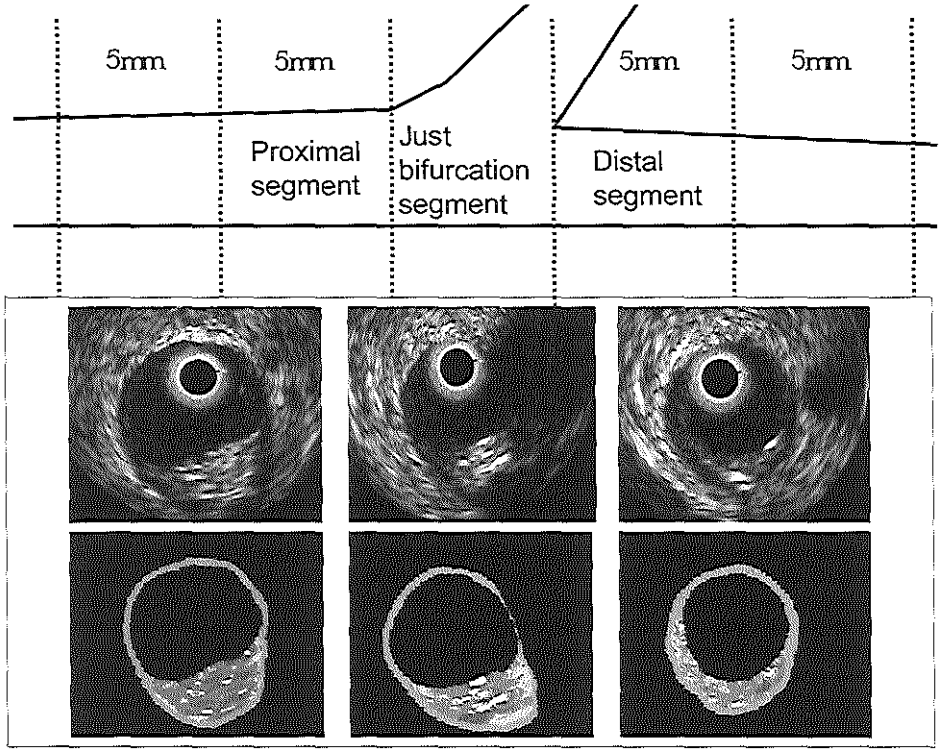

Fig. 1. The schematic definition of proximal, just bifurcation and distal segments of bifurcations (upper panel). Gray IVUS (middle panel) and VH-IVUS (lower panel) of each frame were analyzed. The proximal segment and distal segment of the bifurcation sites were analyzed in the 5 mm proximal and distal to bifurcation sites. The just bifurcation segment were analyzed in each segment length. The proximal and distal reference sites were analyzed in the frame which showed the least P+M % within 10 mm of the bifurcation site.

the largest P+M burden % had more than 75% of the vessel CSA. The types of bifurcation lesions were defined as proximal or distal type of bifurcation lesion if bifurcation lesion existed in the proximal or distal segments of bifurcations.

Statistical Analysis

All analyses were done using SPSS (version 12.0; SPSS Inc, Chicago, Illinois). Discrete variables are presented as counts and percentages. Continuous variables were summarized as mean ± SD. Pearson's chi-square or Fisher exact test, Student t test, and Wilcoxon rank-sum tests were performed, as indicated. The one-way repeated measures ANOVA was used to compare the geometrical and compositional characteristics of plaque among proximal, just bifurcation and distal segments of bifurcation sites. Mauchly's test of sphericity was done. If the sphericity assump-

tion was not met, sphericity assumption was corrected by Greenhouse-Geisser method. Post-hoc tests were performed by multiple comparisons for the means of all paired combinations of the three repeated measures condition, which were adjusted using Bonferroni method. The Spearman's correlation coefficient was used to assess associations between measured parameters. Statistical significance was accepted as p less than 0.05.

RESULTS

Baseline Characteristics of Subjects

239 subjects, 258 major bifurcation sites (left main (LM) and left anterior descending artery (LAD)=41, LM and left circumflex artery (LCX)=2, LAD and diagonal artery=128, LCX and obtuse marginal artery (OM)=34, right coronary artery (RCA) and acute marginal artery (AM)=53) which meet the inclusion and exclusion criteria of this study from global VH registry were analyzed.

Table 1. Baseline Characteristics of the Study Population

Variables	N=239
Age, yrs	61.1 ± 11.3
Male, %	184 (77.0)
Diabetes, %	49 (20.5%)
Hypertension, %	144 (60.3%)
Smoking	
Current	72 (30.1%)
Ex	55 (23.0%)
Non	112 (46.9%)
Hypercholesteronemia	141 (59.0%)
Clinical Presentation	
Stable angina	146 (61.1%)
Acute coronary syndrome	93 (38.9%)
Bifurcation site	**N=258**
LM to LAD	41 (15.9%)
LM to LCX	2 (0.8%)
LAD and Diagonal	128 (49.6%)
LCX and OM	34 (13.2%)
RCA and AM	53 (20.5%)
Bifurcation Lesion (P+M burden % > 75)	37 (14.3%)

Data are expressed as number (%).

LM: left main coronary artery, LAD: left anterior descending artery, LCX: left circumflex artery, OM: obtuse marginal artery,

AM: acute marginal artery, P+M: plaque+media

The baseline characteristics of the study subjects are shown in table 1. The mean age of study subjects was 60.8 ± 11.0 and male subjects were 75.7%.

The study subjects were presented as stable angina (61.2%) and acute coronary syndrome (38.8%).

The Baseline Characterization of left main bifurcations and non-left main bifurcations

In Table 2 is shown the baseline characteristics of subjects with LM-LAD bifurcations (N=41) and non-LM bifurcations (N=204). The subjects in LM-LAD bifurcation sites had a tendency to have diabetes (p=0.08) and significantly high

Table. 2. The Baseline Characteristics of Subjects Between Left Main and Non-Left Main Bifurcation Sites

Variables	Subjects (LM-LAD Bifurcation, N=41)	Subjects (Non-LM Bifurcation, N=204)	p
Age, yrs	62.7 ± 12.1	60.8 ± 11.0	0.31
Male, %	34 (82.9)	154 (75.5)	0.30
Diabetes, %	13 (31.7)	39 (19.1)	0.08
Hypertension, %	28 (68.3)	121 (59.3)	0.28
Smoking, %			
Non	19 (46.3)	95 (46.6)	0.27
Ex	13 (31.7)	44 (21.5)	
Current	9 (22.0)	65 (31.9)	
Clinical Presentation			
Stable angina	27 (65.9)	124 (60.8)	0.26
Acute coronary syndrome	14 (34.1)	80 (39.2)	
Total Cholesterol (mg/dL)	172.2 ± 57.4	183.7 ± 45.0	0.20
Triglyceride (mg/dL)	87.0 ± 79.6	93.0 ± 90.6	0.72
HDL-Cholesterol (mg/dL)	44.9 ± 17.2	47.9 ± 15.0	0.33
LDL-Cholesterol (mg/dL)	99.4 ± 42.1	109.3 ± 37.7	0.20
Medication			
Aspirin	35 (85.4)	181 (88.7)	0.54
Beta blocker	31 (75.6)	118 (57.8)	0.03
RAS blockade	14 (34.1)	89 (44.3)	0.26
Calcium channel antagonist	3 (7.3)	39 (19.1)	0.07
Statin	27 (65.9)	136 (66.7)	0.92
Bifurcation Lesion (P+M burden % > 75%)	4 (9.8)	35 (16.3)	0.30
Bifurcation Lesion type			
Proximal type	1 (2.4)	12 (5.6)	0.50
Distal type	3 (7.3)	9 (4.2)	

Data are expressed as number (%) or means ± SD.

RAS: rennin anigiotensin aldosteron system, P+M: plaque+media

proportion of taking beta-blockers (p=0.03). There were no significant differences in the proportion of bifurcation lesion and their types between two groups.

The Geometrical and Compositional Characteristics of LM-LAD and non-LM Bifurcation Sites

Table 3 and 4 showed differential geometrical and compositional characteristics among proximal, at the bifurcation and distal segments of LM-LAD and non-LM bifurcation sites. As expected, in LM-LAD bifurcations, the vessel CSA, lumen CSA, P+M CSA and % P+M burden of proximal were greater that those of distal bifurcation segment (all p<0.05). The % fibro-fatty of proximal and just bifurcation segment were significantly greater that that of distal segment in LM-LAD bifurcation sites (13.81 ± 8.66%, 14.60 ± 7.87% vs. 9.94 ± 6.83%, all p<0.05). Of interest, % necrotic core and dense calcium of at the bifurcation site and distal segments were greater than that of proximal bifurcation segment in LM-LAD bifurcation sites (6.75 ± 5.09%, 7.36 ± 6.01% vs. 4.89 ± 4.78% and 3.31 ± 2.9%, 3.73 ± 3.28% vs. 1.89 ± 2.1%, all p<0.05, Table 3, Fig. 2.).

Table 3. Geometrical and Compositional Characteristics in Left Main-LAD Bifurcation Sites (N=41)

Variables	Proximal (P)	Just Bifurcation (B)	Distal (D)	ANOVA			
Geometrical parameters					P/B	P/D	B/D
Vessel CSA (mm2)	26.83 ± 5.44	25.65 ± 6.44	18.51 ± 4.30	<0.001	NS	<0.001	<0.001
Lumen CSA (mm2)	16.05 ± 4.55	15.37 ± 5.73	9.85 ± 3.03	<0.001	NS	<0.001	<0.001
P+M CSA (mm2)	10.78 ± 3.64	10.28 ± 3.00	8.66 ± 3.20	<0.001	NS	<0.001	<0.001
Plaque CSA (mm2)	5.98 ± 3.66	6.14 ± 2.86	4.75 ± 3.07	0.001	NS	0.019	<0.001
P+M Burden (%)	40.40 ± 11.76	41.15 ± 11.01	46.55 ± 12.08	<0.001	NS	0.002	0.001
Remodeling Index	1.19 ± 0.18		0.85 ± 0.14	<0.001			
Compositional parameters					P/B	P/D	B/D
DC CSA (mm2)	0.22 ± 0.26	0.37 ± 0.36	0.36 ± 0.36	0.007	0.004	0.076	NS
DC (%)	1.89 ± 2.10	3.31 ± 2.87	3.73 ± 3.28	<0.001	<0.001	0.002	NS
FT CSA (mm2)	3.52 ± 2.18	3.43 ± 1.63	2.71 ± 1.78	0.006	NS	0.023	0.003
FT (%)	29.88 ± 10.66	31.81 ± 8.87	28.58 ± 10.91	NS			
FF CSA (mm2)	0.89 ± 0.80	1.07 ± 0.81	0.64 ± 0.58	<0.001	0.055	0.003	<0.001
FF (%)	13.81 ± 8.66	14.60 ± 7.87	9.94 ± 6.83	<0.001	NS	0.004	<0.001
NC CSA (mm2)	0.61 ± 0.77	0.76 ± 0.70	0.70 ± 0.64	NS			
NC (%)	4.89 ± 4.78	6.75 ± 5.09	7.36 ± 6.01	0.006	0.001	0.026	NS

Data are expressed as means ± SD. The proportions of compositional characteristics were derived from plaque area including media.

P/B=Proximal segment vs Bifurcation segment, P/D=Proximal segment vs distal segment, B/D= Bifurcation segment vs distal segment, CSA=Cross sectional area, P+M=Plaque+media,DC=Dense calcium, FT=Fibrous tissue, FF=Fibrous-fatty, NC=Necrotic core, NS=not significant.

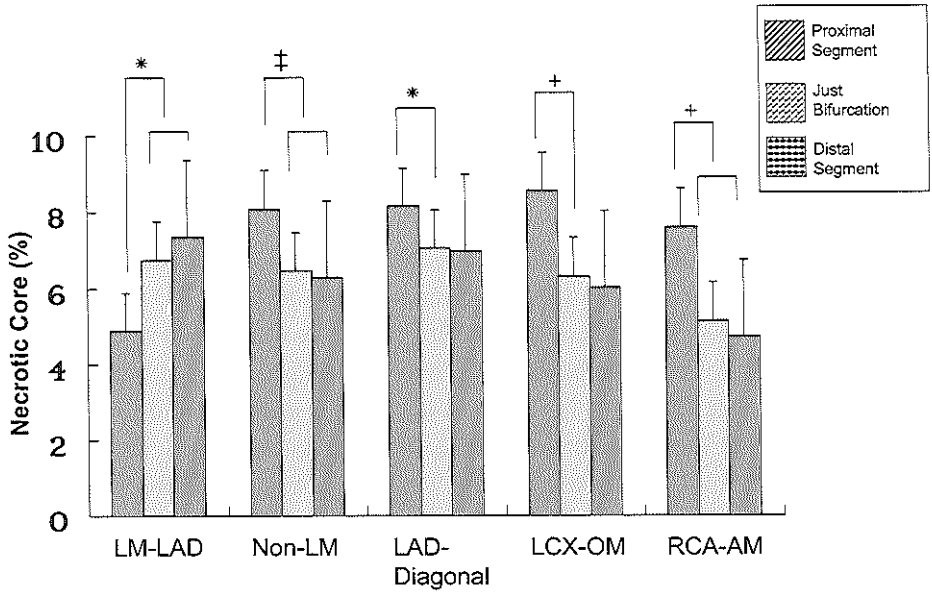

Fig. 2. The comparison of necrotic core % among the proximal, just bifurcation and distal segments of LM-LAD, non-LM (LAD-diagonal, LCX-OM, RCA-AM) bifurcations. Values are mean ± SEM. *P<0.05, +P<0.01, ‡P<0.001

In non-LM bifurcation sites (Table 4.), vessel CSA of the proximal and at the bifurcation segments were significantly greater than that of distal segments (all P<0.001). The % P+M burden of proximal segment was significantly greater than those of just at the bifurcation and distal bifurcation segments (all p<0.05). Remodeling index of proximal segment in non-LM bifurcations was significantly greater than that of distal segment (p<0.001). The % necrotic core and dense calcium of proximal segment were significantly greater than those of just bifurcation and distal bifurcation segments (8.08 ± 6.21 vs. 6.47 ± 5.11, 6.28 ± 5.05 and 4.57 ± 4.67 vs. 3.38 ± 3.44, 3.55 ± 3.74, all p<0.05, Table 4, Fig. 2.).

Table 5. showed geometrical and compositional characteristics of each coronary artery in non-LM bifurcations. Of interest, % necrotic core of proximal segment of LAD-diagonal, LCX-OM, RCA-AM bifurcation sites were significantly greater than those of at the bifurcation or distal segments of bifurcations (all p<0.05, Fig. 2.).

The Comparative Analysis of Compositional Characteristics Between LM-LAD and non-LM Bifurcation Sites

Table 6 showed the comparison of compositional characteristics between LM-LAD and non-LM bifurcation sites. LM-LAD bifurcation sites had significant

Table 4. Geometrical and Compositional Characteristics in Non-Left Main Bifurcation Sites (N=215)

Variables	Proximal (P)	Just Bifurcation (B)	Distal (D)	ANOVA			
Geometrical parameters					P/B	P/D	B/D
Vessel CSA (mm2)	17.82 ± 4.68	17.85 ± 4.63	13.75 ± 4.05	<0.001	NS	<0.001	<0.001
Lumen CSA (mm2)	9.12 ± 3.65	9.86 ± 3.72	7.31 ± 2.70	<0.001	<0.001	<0.001	<0.001
P+M CSA (mm2)	8.71 ± 2.89	7.99 ± 2.64	6.44 ± 2.42	<0.001	<0.001	<0.001	<0.001
P+M Burden %	49.41 ± 12.12	45.34 ± 11.21	46.80 ± 10.68	<0.001	<0.001	0.009	NS
Remodeling Index	1.15 ± 0.18		0.90 ± 0.15	<0.001			
Compositional parameters					P/B	P/D	B/D
DC CSA (mm2)	0.42 ± 0.46	0.30 ± 0.34	0.25 ± 0.29	<0.001	<0.001	<0.001	NS
DC (%)	4.57 ± 4.67	3.38 ± 3.44	3.55 ± 3.74	<0.001	<0.001	0.006	NS
FT CSA (mm2)	2.91 ± 1.73	2.61 ± 1.47	1.89 ± 1.30	<0.001	0.004	<0.001	<0.001
FT (%)	31.07 ± 10.20	30.46 ± 9.74	26.25 ± 10.94	<0.001	NS	<0.001	<0.001
FF CSA (mm2)	0.91 ± 0.78	1.03 ± 0.85	0.65 ± 0.64	<0.001	0.029	<0.001	<0.001
FF (%)	9.83 ± 6.93	12.02 ± 7.44	8.22 ± 6.47	<0.001	<0.001	<0.001	<0.001
NC CSA (mm2)	0.77 ± 0.74	0.57 ± 0.55	0.45 ± 0.45	<0.001	<0.001	<0.001	0.002
NC (%)	8.08 ± 6.21	6.47 ± 5.11	6.28 ± 5.05	<0.001	<0.001	<0.001	NS

Data are expressed as means ± SD. The proportions of compositional characteristics were derived from plaque area including media.
P/B=Proximal segment vs Bifurcation segment, P/D=Proximal segment vs distal segment, B/D= Bifurcation segment vs distal segment, CSA=Cross sectional area, P+M=Plaque+media,DC=Dense calcium, FT=Fibrous tissue, FF=Fibrous-fatty, NC=Necrotic core, NS=not significant.

lesser % dense calcium and necrotic core compare to non-LM bifurcation sites in the proximal bifurcation sites (1.89 ± 2.10% vs. 4.57 ± 4.67% and 4.89 ± 4.78% vs. 8.08 ± 6.20%, all p<0.001). The LM-LAD bifurcation sites had significant greater % fibro-fatty compare to non-LM bifurcation sites in just bifurcation segment (14.60 ± 7.87 vs. 12.02 ± 7.44, p=0.045).

The Correlation Between % Necrotic Core and Geometrical Parameters in LM-LAD and non-LM Bifurcation Sites

The % necrotic core of the proximal and distal segments in LM-LAD bifurcation sites significantly correlated with % P+M burden (r=0.45, p=0.003, and r=0.42, p=0.006, respectively, Fig. 3a.). There were no significant correlation between necrotic core % and lumen CSA in each segment of LM-LAD bifurcations (Fig. 3b.). The necrotic core % of each segment in non-LM bifurcation sites showed significant positive correlation with P+M burden % (proximal segments; r=0.51, p<0.001, just bifurcation segments; r=0.55, p<0.001, distal segments; r=0.64, p<0.001, Fig. 4a.) and negative correlation with lumen CSA (proximal segments; r=-0.35, p<0.001, just bifurcation segments; r=-0.35, p<0.001, distal segments;

Table 5. Geometrical and Compositional Characteristics in Each Non-Left main Bifurcation

Variables	Proximal Segment (P)	Just Bifurcation (B)	Distal Segment (D)	ANOVA			
LAD-Diagonal (N=128)							
Geometrical parameters					**P/B**	**P/D**	**B/D**
Vessel CSA (mm2)	17.68 ± 4.64	17.74 ± 4.57	13.52 ± 3.78	<0.001	NS	<0.001	<0.001
Lumen CSA (mm2)	8.91 ± 3.54	9.67 ± 3.59	6.99 ± 2.34	<0.001	0.004	<0.001	<0.001
P+M CSA (mm2)	8.76 ± 2.99	8.07 ± 2.78	6.52 ± 2.47	<0.001	0.002	<0.001	<0.001
P+M Burden %	50.06 ± 12.30	45.89 ± 11.67	47.88 ± 10.59	0.001	<0.001	NS	0.085
Remodeling Index	1.19 ± 0.17		0.91 ± 0.16	<0.001			
Compositional parameters					**P/B**	**P/D**	**B/D**
DC CSA (mm2)	0.46 ± 0.51	0.36 ± 0.38	0.30 ± 0.33	<0.001	0.023	0.001	NS
DC (%)	4.86 ± 4.94	3.97 ± 3.67	4.09 ± 4.02	0.055			
FT CSA (mm2)	2.89 ± 1.73	2.59 ± 1.49	1.91 ± 1.26	<0.001	0.038	<0.001	<0.001
FT (%)	30.59 ± 10.42	29.80 ± 9.86	26.45 ± 10.66	<0.001	NS	0.001	<0.001
FF CSA (mm2)	0.94 ± 0.82	1.05 ± 0.93	0.62 ± 0.70	<0.001	NS	<0.001	<0.001
FF (%)	10.00 ± 7.57	11.98 ± 7.96	8.22 ± 6.81	<0.001	0.001	0.007	<0.001
NC CSA (mm2)	0.78 ± 0.73	0.62 ± 0.55	0.50 ± 0.44	<0.001	0.006	<0.001	0.040
NC (%)	8.15 ± 6.01	7.05 ± 5.18	6.98 ± 5.20	0.029	0.028	NS	NS
LCX-OM (N=34)							
Geometrical parameters					**P/B**	**P/D**	**B/D**
Vessel CSA (mm2)	18.83 ± 4.50	18.38 ± 4.33	13.25 ± 3.40	<0.001	NS	<0.001	<0.001
Lumen CSA (mm2)	10.05 ± 3.95	10.62 ± 3.98	7.25 ± 2.70	<0.001	NS	<0.001	<0.001
P+M CSA (mm2)	8.78 ± 2.40	7.76 ± 1.92	5.99 ± 2.13	<0.001	0.014	<0.001	<0.001
P+M Burden %	47.68 ± 11.90	43.31 ± 10.06	45.60 ± 12.44	NS			
Remodeling Index	1.12 ± 0.19		0.89 ± 0.16	<0.001			
Compositional parameters					**P/B**	**P/D**	**B/D**
DC CSA (mm2)	0.37 ± 0.34	0.27 ± 0.32	0.21 ± 0.22	0.021	NS	0.067	NS
DC (%)	4.04 ± 3.62	3.24 ± 3.60	3.44 ± 3.84	NS			
FT CSA (mm2)	2.98 ± 1.54	2.50 ± 1.11	1.67 ± 1.32	<0.001	NS	<0.001	0.002
FT (%)	32.01 ± 11.21	30.82 ± 9.14	24.23 ± 12.35	<0.001	NS	0.009	0.006
FF CSA (mm2)	0.82 ± 0.55	0.89 ± 0.51	0.51 ± 0.46	<0.001	NS	0.003	<0.001
FF (%)	9.28 ± 5.55	11.19 ± 5.48	7.40 ± 5.44	<0.001	0.025	NS	<0.001
NC CSA (mm2)	0.83 ± 0.83	0.54 ± 0.50	0.40 ± 0.38	<0.001	0.007	0.015	NS
NC (%)	8.55 ± 6.99	6.32 ± 4.87	6.02 ± 4.99	0.044	0.007	NS	NS
RCA-AM (N=53)							
Geometrical parameters					**P/B**	**P/D**	**B/D**
Vessel CSA (mm2)	17.53 ± 4.89	17.77 ± 5.01	14.62 ± 4.91	<0.001	NS	<0.001	<0.001
Lumen CSA (mm2)	9.01 ± 3.70	9.82 ± 3.84	8.10 ± 3.32	<0.001	0.012	0.032	<0.001
P+M CSA (mm2)	8.53 ± 2.97	7.94 ± 2.72	6.52 ± 2.50	<0.001	NS	<0.001	<0.001
P+M Burden %	49.29 ± 11.94	45.31 ± 10.82	44.95 ± 9.49	0.002	0.007	0.007	NS
Remodeling Index	1.07 ± 0.18		0.90 ± 0.13	<0.001			
Compositional parameters					**P/B**	**P/D**	**B/D**
DC CSA (mm2)	0.38 ± 0.43	0.17 ± 0.20	0.16 ± 0.20	<0.001	<0.001	0.001	NS
DC (%)	4.20 ± 4.61	2.05 ± 2.21	2.34 ± 2.56	<0.001	<0.001	0.006	NS
FT CSA (mm2)	2.90 ± 1.84	2.72 ± 1.64	1.97 ± 1.40	<0.001	NS	<0.001	<0.001
FT (%)	31.63 ± 9.05	31.82 ± 9.84	27.07 ± 10.72	<0.001	NS	0.004	<0.001
FF CSA (mm2)	0.89 ± 0.80	1.07 ± 0.81	0.64 ± 0.58	<0.001	0.055	0.003	<0.001
FF (%)	9.77 ± 6.17	12.66 ± 7.28	8.75 ± 6.27	<0.001	<0.001	NS	<0.001
NC CSA (mm2)	0.69 ± 0.71	0.46 ± 0.57	0.35 ± 0.48	<0.001	0.001	0.001	NS
NC (%)	7.60 ± 6.22	5.14 ± 4.90	4.74 ± 4.41	<0.001	<0.001	0.001	NS

Data are expressed as means ± SD. The proportions of compositional characteristics were derived from plaque area including media.
LAD : left anterior descending artery, CSA: cross sectional area, P+M: plaque+media, P/B=Proximal segment vs Bifurcation segment, P/D=Proximal segment vs distal segment,
B/D= Bifurcation segment vs distal segment, DC=Dense calcium, FT=Fibrous tissue, FF=Fibrous-fatty, NC=Necrotic core, NS=not significant.
LCX : left circumflex artery, OM : obtuse marginal artery, RCA: right coronary artery, AM: acute marginal artery
NS=not significant.

Table 6. The Comparison of Compositional Characteristics Between LM-LAD and Non-LM Bifurcation Sites

	LM-LAD Bifurcation (N=41)	Non-LM Bifurcation (N=215)	p
Proximal Segment			
DC (%)	1.89 ± 2.10	4.57 ± 4.67	<0.001
FT (%)	29.88 ± 10.66	31.07 ± 10.20	0.50
FF (%)	13.81 ± 8.67	9.83 ± 6.93	0.008
NC (%)	4.89 ± 4.78	8.08 ± 6.20	<0.001
Just Bifurcation Segment			
DC (%)	3.31 ± 2.87	3.38 ± 3.44	0.90
FT (%)	31.81 ± 8.87	30.46 ± 9.74	0.41
FF (%)	14.60 ± 7.87	12.02 ± 7.44	0.045
NC (%)	6.75 ± 5.09	6.47 ± 5.11	0.75
Distal Segment			
DC (%)	3.73 ± 3.28	3.55 ± 3.74	0.78
FT (%)	28.58 ± 10.91	26.25 ± 10.94	0.21
FF (%)	9.94 ± 6.83	8.22 ± 6.47	0.12
NC (%)	7.36 ± 6.01	6.28 ± 5.05	0.22

Data are expressed as means ± SD. The proportions of compositional characteristics were derived from plaque area including media.
LM: left main artery, LAD: left anterior descending artery, DC=Dense calcium, FT=Fibrous tissue, FF=Fibrous-fatty, NC=Necrotic core

r=-0.31, p<0.001, Fig. 4b.). There were no significant correlation between % necrotic core and the remodeling index in LM-LAD (proximal segment: r=0.05, p=NS, distal segment: r=-0.01, p=NS) and non-LM bifurcation sites (proximal segment: r=0.14, p=0.06, distal segment: r=0.05, p=NS).

DISCUSSION

The current study demonstrates for the first time the geometrical and compositional characteristics of coronary atherosclerotic plaques at bifurcations sites in

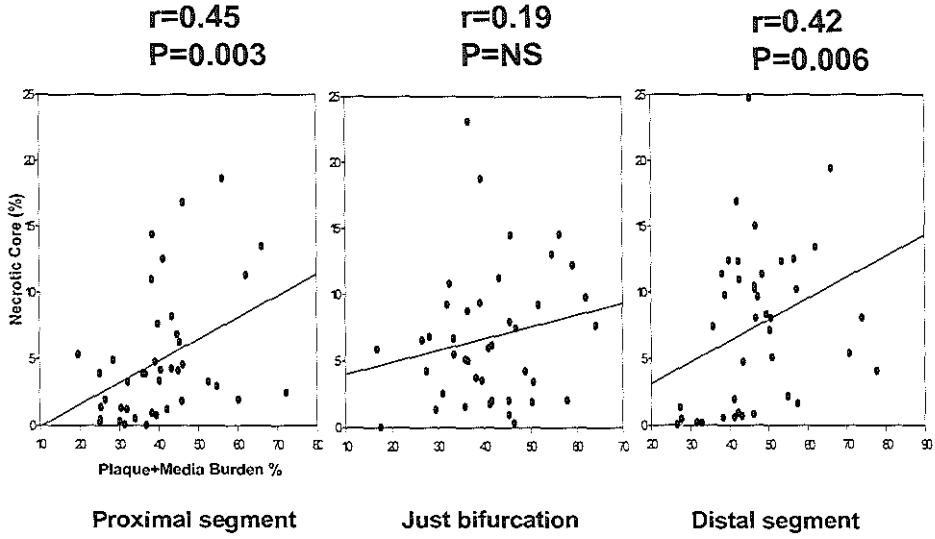

Fig. 3a. The correlations between necrotic core % and P+M burden % in each segment of LM-LAD bifurcations.

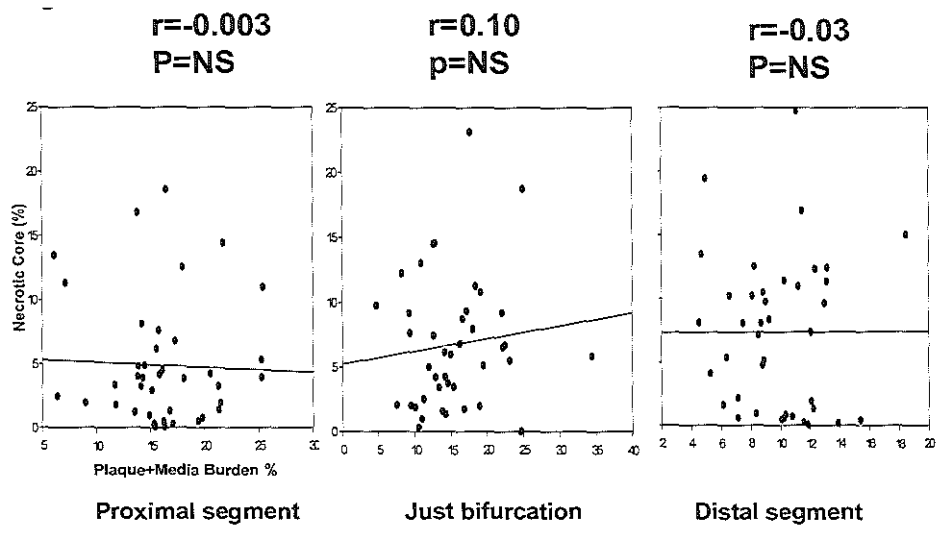

Fig. 3b. The correlations between necrotic core % and lumen CSA in each segment of LM-LAD bifurcations.

humans and demonstrated that bifurcation sites of LM-LAD have greater necrotic core at the site and distal segments of the bifurcation compared to proximal segments. In contrast, bifurcation sites of non-LM coronary arteries showed greater necrotic core in proximal segment of bifurcation. Secondly, there were significant positive correlations between % necrotic core and P+M burden in each segment

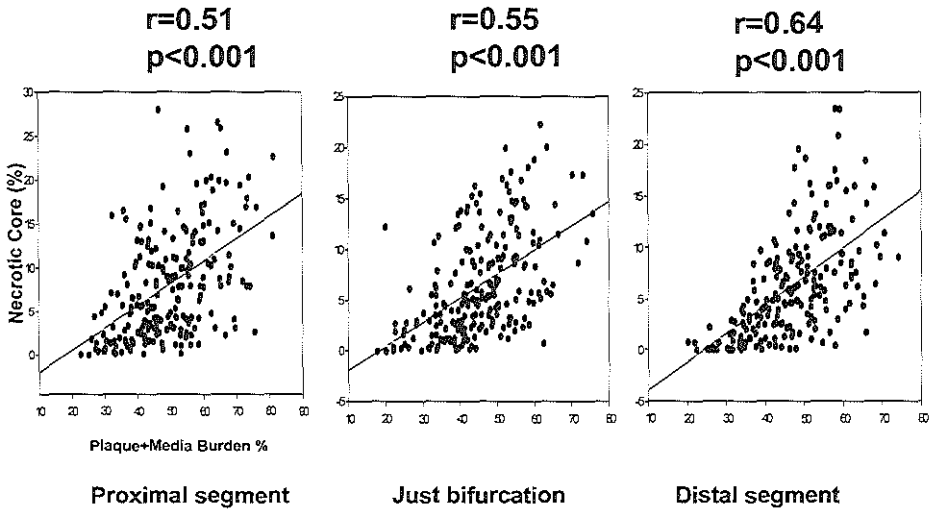

Fig. 4a. The correlations between necrotic core % and P+M burden % in each segment of non-LM bifurcations.

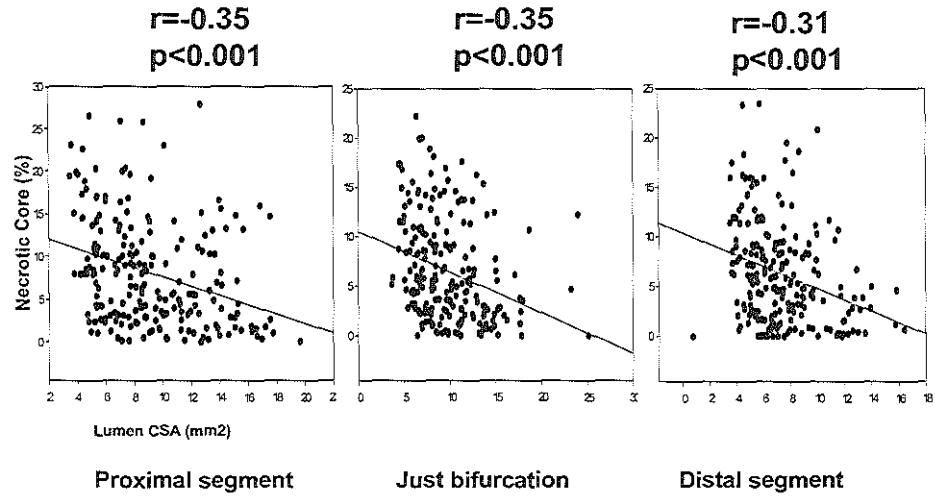

Fig. 4b. The correlations between necrotic core % and lumen CSA in each segment of non-LM bifurcations.

of coronary bifurcation sites, which might be derived by differential anatomical locations and additional factors such as shear stress, vessel structure of bifurcation sites. The current study suggests that there is a heterogonous mechanism and distribution of atherosclerotic plaques between bifurcation sites.

It is well known that vulnerable plaques and ruptured or prone to ruptured plaques are non-uniformly distributed along the coronary arteries [10, 14-17].

However, to our knowledge, there is no previous *in vivo* data regarding compositional tissue characteristics of atherosclerosis in the coronary bifurcations according to their anatomical locations. Thus, the current study may have implications on the imaging guided approach for the treatment of coronary artery disease.

Left Main-LAD Bifurcations

The previous histological and intravascular ultrasound studies of the LM coronary artery bifurcation have demonstrated that atherosclerotic plaques are localized exclusively on the non-flow dividing walls (opposite to carina) of the left anterior descending and left circumflex coronary artery [4,6,18]. Valgimigli et al. [19] recently reported that the amount of necrotic core increases significantly in the first, second, and third 6mm segment of LM-LAD, LM-LCX when compared with the LM trunk by IVUS-VH study. In addition, Rodriguez-Granillo et al. [20] recently reported that ostial LAD atherosclerotic plaques present larger plaque burden, eccentricity, and plaque thickness than distal LM coronary plaques. In this study, a larger calcified and necrotic core content by IVUS-RFD analysis was found distal to the LCX take-off in ostial LAD.

In the current study, the segments at the site of the bifurcation and distal to the bifurcations of the LM-LAD has greater % necrotic core and dense calcium compared to proximal segment of bifurcations. In addition, % P+M burden of distal segment in LM-LAD bifurcations was significantly greater than those of proximal and just bifurcation segments in LM-LAD bifurcations. Of interest, the necrotic core of proximal and distal segments in LM-LAD bifurcation sites correlated significantly with % P+M burden. These results indicated that distal segments of LM-LAD bifurcations have structurally larger atheroma burden and functionally also greater necrotic core in these segments. Our study extends previous observations and demonstrates the differential distribution of the component of the plaque in LM-LAD bifurcation sites.

Non-Left Main Bifurcations

Regarding Non-LM bifurcations, Badak et al. [21] reported the results of IVUS analysis in the LAD-diagonal and LCX-OM bifurcations. Volumetric analysis showed that vessel CSA, lumen CSA and P+M CSA were larger in the proximal segment of bifurcations than in the distal segment, where % P+M burden was similar between these segments. The data from the current study, is consistent with this previous observation study also reports the tissue characterization of these lesion. Moreover, in the current study we reported that

the % necrotic core and dense calcium in the proximal segment of non-LM bifurcations were greater than those of just bifurcation and distal segments. In the current study, the degree of necrotic core in each segment of non-LM bifurcation sites had significant positive correlation with P+M burden and negative correlation with lumen CSA. These observations support the role of the necrotic core in the lesion development and its contribution to remodeling process [22].

Clinical Implications

Large body of evidence have demonstrated a significant relationship between early atheroma development and low or oscillatory shear forces resulting from bifurcations of vessel [2, 20, 23-25]. These data suggest that differential anatomical location, shear forces at the bifurcationsites between LM-LAD and non-LM bifurcations might lead to the formation of atheroma at different predilection sites among proximal, just bifurcation and distal segments of bifurcations.

Post mortem data suggests also that plaque composition itself plays a pivotal role in determining plaque vulnerability [26]. Our results, which show differential geometrical and compositional characteristics between LM-LAD bifurcations and non-LM bifurcations, suggest a differential likelihood for plaque rupture to occur at LM and non-LM bifurcations.

Bifurcation coronary lesions remain a challenging lesion subset for interventional procedures even during drug eluting stent era [3]. It has been reported that the baseline plaque accumulation is related to the long-term outcome of interventional procedures [27]. Finn et al. suggested that a tendency for lesions with penetration of necrotic core by drug eluting stent struts to be associated with late stent thrombosis by their unpublished pathologic data [28]. The importance to characterized the plaque components is underscored by recent studies which demonstrated that, necrotic core rich lesion assessed by IVUS-RFD analysis was an important predictor of the risk of distal embolization after stent deployment in patients with myocardial infarction and in patents with elective percutaneous intervention [29, 30].

In the current study, necrotic core rich segment was observed in coronary bifurcations sites, this may suggest at least in part the less favorite outcome of intervention for bifurcation lesions as compared to non-bifurcation lesions. Furthermore, our results suggest that more effective treatment strategy of intervention, such as imaging guided or more specific drugs will be needed for the treatment of coronary bifurcations.

In addition, our results suggest that the main therapeutic target in the LM-LAD bifurcation should be just bifurcation and distal segment of the bifurcation and in the non-LM bifurcation should be the proximal segment of the bifurcation.

Study Limitations

Our study has some limitations. We did not evaluate the effects of side branch locations in terms of the orientation of side branch toward the myocardial or epicardial surface and the obliquity of the side branch take-off. In addition, we did not analyze the characteristic of flow divider and non-flow divider sides of bifurcation site.

In conclusions, the current study demonstrates that there is a heterogeneous distribution of atherosclerotic plaques and its components between different bifurcation sites. The bifurcation sites of LM-LAD had greater necrotic core at the bifurcation and distal segments of bifurcation opposite to bifurcation sites of non-LM. These results might be derived from differential morphology, anatomical locations (possible angle dependency) and additional factors such as shear stress and vessel structure (elastic vs. muscular) of bifurcation sites.

The current study supports the development of an imaging guided intervention for complex coronary artery disease such as bifurcation lesion.

REFERENCES

1. Nerem RM. Vascular fluid mechanics, the arterial wall, and atherosclerosis. J Biomech Eng 1992;114:274-82.
2. Glagov S, Zarins C, Giddens DP, Ku DN. Hemodynamics and atherosclerosis. Insights and perspectives gained from studies of human arteries. Arch Pathol Lab Med. 1988;112:1018-31.
3. Louvard Y, Lefèvre T, Morice MC. Percutaneous coronary intervention for bifurcation coronary disease. Heart 2004;90:713-22.
4. Svindland A. The localization of sudanophilic and fibrous plaques in the main left coronary bifurcation. Atherosclerosis 1983;48:139-45.
5. Grottum P, Svindland A, Walloe L. Localization of atherosclerotic lesions in the bifurcation of the main left coronary artery. Atherosclerosis 1983;47:55-62.
6. Kimura BJ, Russo RJ, Bhargava V, et al. Atheroma morphology and distribution in proximal left anterior descending coronary artery: in vivo observations. J Am Coll Cardiol 1996;27:825-31.
7. Nair A, Kuban BD, Obuchowski N, Vince DG. Assessing spectral algorithms to predict atherosclerotic plaque composition with normalized and raw intravascular ultrasound data. Ultrasound Med Biol. 2001;27:1319-31.
8. Nair A, Kuban BD, Tuzcu EM, Schoenhagen P, Nissen SE, Vince DG. Coronary plaque classification with intravascular ultrasound radiofrequency data analysis. Circulation. 2002;106:2200-6.
9. Nair A, Margolis P, Kuban B, Vince D. Automated coronary plaque characterization with intravascular ultrasound backscatter: ex vivo validation. EuroInterv 2007;3:113-20.
10. Rodriguez-Granillo GA, Garcia-Garcia HM, Mc Fadden EP, et al. In vivo intravascular ultrasound-derived thin-cap fibroatheroma detection using ultrasound radiofrequency data analysis. J Am Coll Cardiol. 2005;46:2038-42.
11. Fujii K, Carlier SG, Mintz GS, et al. Association of plaque characterization by intravascular ultrasound virtual histology and arterial remodeling. Am J Cardiol. 2005;96:1476-83.
12. Rodriguez-Granillo GA, Serruys PW, Garcia-Garcia HM, et al. Coronary artery remodeling is related to plaque composition. Heart. 2006;92:388-91.
13. Nasu K, Tsuchikane E, Katoh O, et al. Accuracy of in vivo coronary plaque morphology assessment. J Am Coll Cardiol 2006;47:2405-12.
14. Shah PK. Mechanisms of plaque vulnerability and rupture. J Am Coll Cardiol 2003;41 Supple S; 15S-22S.
15. von Birgelen C, Klinkhart W, Mintz GS, et al. Plaque distribution and vascular remodeling of ruptured and nonruptured coronary plaques in the same vessel: an intravascular ultrasound study in vivo. J Am Coll Cardiol 2001;37:1864-70.
16. Wang JC, Normand SL, Mauri L, Kuntz RE. Coronary artery spatial distribution of acute myocardial infarction occlusions. Circulation 2004;110:278-84.
17. Hong MK, Mintz GS, Lee CW, et al. The site of plaque rupture in native coronary arteries: a three-vessel intravascular ultrasound analysis. J Am Coll Cardiol 2005;46:261-5.

18. Ding Z, Biggs T, Seed WA, Friedman MH. Influence of the geometry of the left main coronary artery bifurcation on the distribution of sudanophilia in the daughter vessels. Arterioscler Thromb Vasc Biol 1997;17:1356-60.
19. Valgimigli M, Rodriguez-Granillo GA, Garcia-Garcia HM, et al. Plaque composition in the left main stem mimics the distal but not the proximal tract of the left coronary artery: influence of clinical presentation, length of the left main trunk, lipid profile, and systemic levels of C-reactive protein. J Am Coll Cardiol 2007;49:23-31.
20. Rodriguez-Granillo GA, Garcia-Garcia HM, Wentzel J, et al. Plaque composition and its relationship with acknowledged shear stress patterns in coronary arteries. J Am Coll Cardiol 2006;47:884-5.
21. Badak O, Schoenhagen P, Tsunoda T, et al. Characteristics of atherosclerotic plaque distribution in coronary artery bifurcations: an intravascular ultrasound analysis. Coron Artery Dis 2003;14:309-16.
22. García-García HM, Goedhart D, Serruys PW. Relation of plaque size to necrotic core in the three major coronary arteries in patients with acute coronary syndrome as determined by intravascular ultrasonic imaging radiofrequency. Am J Cardiol 2007;99:790-2.
23. Zarins CK, Giddens DP, Bharadvaj BK, Sottiurai VS, Mabon RF, Glagov S. Carotid bifurcation atherosclerosis. Quantitative correlation of plaque localization with flow velocity profiles and wall shear stress. Circ Res 1983;53:502-14.
24. Weydahl ES, Moore JE. Dynamic curvature strongly affects wall shear rates in a coronary artery bifurcation model. J Biomech 2001;34:1189-1196.
25. Chatzizisis YS, Coskun AU, Jonas M, et al. Role of endothelial shear stress in the natural history of coronary atherosclerosis and vascular remodeling : molecular, cellular, and vascular behavior. J Am Coll Cardiol 2007;49:2379-93.
26. Virmani R, Kolodgie FD, Burke AP, Farb A, Schwartz SM. Lessons from sudden coronary death: a comprehensive morphological classification scheme for atherosclerotic lesions. Arterioscler Thromb Vasc Biol 2000;20:1262-75.
27. Hoffmann R, Mintz GS, Mehran R, et al. Intravascular ultrasound predictors of angiographic restenosis in lesions treated with Palmaz-Schatz stents. J Am Coll Cardiol 1998;31:43-49.
28. Nakazawa G, Finn AV, Virmani R. Vascular pathology of drug-eluting stents. Herz 2007;274-80.
29. Kawaguchi R, Oshima S, Jingu M, et al. Usefulness of virtual histology intravascular ultrasound to predict distal embolization for ST-segment elevation myocardial infarction. J Am Coll Cardiol 2007;50:1641-6
30. Kawamoto T, Okura H, Koyama Y, et al. The relationship between coronary plaque characteristics and small embolic particles during coronary stent implantation. J Am Coll Cardiol 2007;50:1635-40.

CHAPTER 4.1

Synergistic Effect of Cardiovascular Risk Factors and Clinical Presentation on Necrotic Core in Coronary Arteries: A Report From the Global Intravascular Radiofrequency Data Analysis Registry.

García-García HM, Serruys PW, Mintz G, Saito S, Klaus V, Margolis MP, Carlier S, Goedhart D, Schwartz R.

J Am Coll Cardiol Img. 2009;2:629-36.

ABBREVIATIONS LIST

ACS- Acute coronary syndrome
IVUS- Intravascular ultrasound
NC – Necrotic core
RFD – Radiofrequency data analysis

ABSTRACT

Objectives: We explored whether an individual or a cluster of risk factors affects the extent of necrotic core (NC) assessed by IVUS-radiofrequency data (RFD) analysis.

Background: Several systemic diseases contribute to the development of coronary artery disease.

Methods: Volcano Registry was a prospective, multi-center and non-randomized study that enrolled 990 patients with coronary artery disease in whom one major coronary artery was imaged by IVUS-RFD. For the multivariable analysis, the population was divided into 4 classes: young females, young males (both ≤62 yrs), old females, and old males (>62 yrs). Mean NC area was categorized as 1: top quartile (≥ 0.62 mm^2) or as 0: lower three quartiles.

Results: Young patients had 0.40±0.36mm^2 of NC vs. 0.50±0.46mm^2 in old patients, p=0.0007. Non-diabetics had 0.43±0.41mm^2 of NC vs. 0.51±0.44mm^2 in diabetics, p=0.02. NC area measured 0.40±0.36mm^2 in normotensives vs. 0.48±0.44mm^2 in hypertensives, p=0.02. All significantly-associated variables in the bivariate analysis (age, hypertension, diabetes, and prior CABG) were introduced in the logistic regression model; but only age [OR 1.023 (1.009, 1.037), p=0.001] and diabetes [OR 1.636 (1.174, 2.279), p=0.004] remained statistically significant. In a per-class logistic regression analyses including only diabetes as covariate, in young females the OR was 2.1 (95%CI 0.77, 6.0), p=0.14; in young males the OR was 1.6 (95%CI 0.90, 2.7), p=0.11; in old females the OR was 2.3 (95%CI 1.09, 4.9), p=0.03; and in old males the OR was 1.6 (95%CI 0.96, 2.7), p=0.07. Further, when only patients with diabetes and hypertension were included, in young females the OR was 2.4 (95%CI 0.69, 8.6) p=0.17; in young males the OR was 2.0 (95%CI 1.03, 3.8) p=0.041; in old females the OR was 3.04 (95%CI 1.029.1) p=0.046; and in old males the OR was 2.2 (95%CI 1.1, 4.2) p=0.025.

Conclusion: Individually and collectively, age and diabetes mellitus are associated with an increase in necrotic core.

Key words: Cardiovascular Risk factors, Clinical presentation, Intravascular ultrasound, Plaque composition.

INTRODUCTION

Several systemic diseases contribute to the development of coronary artery disease (CAD). For example, in a very large international registry of patients with established CAD, 38.3% were diabetics, 80.3% were hypertensive, 77.0% were hypercholesterolemic, 45.4% were obese, and 13% were current smokers (1). These well-known cardiovascular risk factors not only modify coronary plaque composition (2), but also predispose patients to coronary plaque rupture or acute coronary thrombosis (3). Two of the chief modifiers of plaque morphology are age and gender (4).

A postmortem study showed that the necrotic core (NC) size and plaque burden are larger in diabetics compared to non-diabetics(2). Furthermore, the simultaneous presence of both diabetes mellitus and dyslipidemia was associated with an increase in necrotic core size when compared to patients with only diabetes(2). The purpose of the current analysis was to assess whether the extent of necrotic core in coronary arteries, as measured by intravascular ultrasound-radiofrequency data analysis (IVUS-RFD) analysis, is influenced by the presence of one or more cardiovascular risk factors in a worldwide registry of patients.

METHODS

Patient selection

The Volcano Global Registry is a prospective, multi-center (42 centers), non-randomized study of CAD patients admitted for coronary catheterization and undergoing analysis by IVUS-RFD; it started enrolment in March 2004, and the current analysis includes the first 990 patients enrolled. Patients, irrespective of their clinical presentation, older than 18 years old were eligible if at least one of their coronary vessels containing an atherosclerotic lesion by visual assessment was suitable for IVUS interrogation (absence of extensive calcification and/or severe vessel tortuosity). The selection of the investigated artery was left to the operator's decision; in the case report form the investigator reported the target lesion diameter stenosis by visual assessment and/or quantitative coronary angiography (QCA). Acute coronary syndrome (ACS) encompassed unstable angina (UA)

according to the Braunwald classification, non-ST-segment elevation myocardial infarction (NSTEMI), and ST-segment elevation myocardial infarction (STEMI). All the local ethical committees of the participant centers approved the protocol, and informed written consent was obtained from all patients.

Clinical definitions used in this study

Diabetes mellitus was defined if the patient had a fasting glucose ≥1.26 g/L, if this risk factor was documented in the medical record, or if the patient was receiving diet, oral drug, or insulin treatment.

Hypercholesterolemia was defined if the patient had a total cholesterol more than 200 mg/dl, if this risk factor was documented in the medical record, or if the patient was receiving any lipid-lowering treatment such as diet or pharmacological.

Arterial Hypertension was defined if systolic blood pressure was ≥140 mmHg or diastolic blood pressure was ≥90 mmHg, if this risk factor was documented in the medical record, or if the patient was receiving antihypertensive treatment.

IVUS-RFD Acquisition and Analysis

Image acquisition was performed during diagnostic coronary angiography, pre-intervention, post-balloon dilation, or post-stenting; however, the treated segment and 5mm of adjacent reference was not included in the analysis.

Details regarding the validation of the technique have been reported(5,6). Briefly, IVUS-RFD uses spectral analysis of IVUS radiofrequency data to build tissue maps that are correlated with a specific spectrum of the radiofrequency signal and assigned colour codes [fibrous (labelled green), fibrofatty (labelled greenish-yellow), necrotic core (labelled red) and calcium (labelled white)](5).

IVUS-RFD data was acquired using continuous catheter pullback (Eagle-Eye™ 20 MHz Volcano Therapeutics, Rancho Cordova, CA) and a dedicated IVUS-RFD console (Volcano Therapeutics, Rancho Cordova, CA). The IVUS-RFD data were stored on DVD and sent to the Corelab (Cardiovascular Research Foundation, NY, US; Erasmus Medical Center/Cardialysis, Rotterdam, The Netherlands, or Toyohashi Heart Center, Japan) for offline analysis. Data acquisition was ECG-gated and recorded during the automated withdrawal of the catheter using a mechanical pullback device (TrakBack II or R-100 Volcano Therapeutics, Rancho Cordova, CA) at a pullback speed of 0.5 mm/s. The IVUS-RFD sampling during pullback is gated to the peak R-wave and is therefore dependent on heart rate. For instance, during constant heart rate of 60 bpm, samples will be collected every 0.5 mm.

IVUS images were reconstructed from the RF data by customized software (pcVH 2.2, Volcano Therapeutics, Rancho Cordova, CA). Longitudinal and cross-sectional views were used to determine the contours. Manual contour detection of both the lumen and the media-adventitia interface was performed; and the radiofrequency data was normalized using a technique known as "Blind Deconvolution"(7), an iterative algorithm that deconvolves the catheter transfer function from the backscatter, thus accounting for catheter-to-catheter variability. Geometrical and compositional data were obtained for every slice. *Plaque burden* was calculated as EEM_{area}-$Lumen_{area}$/EEM_{area} X 100, where EEM refers to the external elastic membrane. For this study, the mean cross-sectional area (CSA) of necrotic core of the *entire vessel pullback* per patient was analyzed.

Statistical analysis

The distribution of the amount of necrotic core, expressed as the mean area in mm^2, was right skewed. Accordingly, non-parametric statistics were used to calculate p values for the comparison between groups. Bivariate analysis and multivariable logistic regression analyses were performed to identify predictors of necrotic core. To this aim, the study population was divided into two: i. patients (n=732) with a mean necrotic core area corresponding to the three lower quartiles (NC <0.62mm^2) of the overall NC distribution (coded as 0); and ii. patients (n=250) with a mean necrotic area corresponding to the upper quartile of the mean necrotic core area (NC ≥0.62mm^2), coded as 1. All variables significantly (p <0.10) associated with mean MC area on bivariate analysis were entered into subsequent models. Next, a logistic regression analysis with the *enter* method was performed for all pertinent covariates. The only two variables that remained statistically significant were age and diabetes. The Hosmer and Lemeshow Goodness-of-Fit test statistic was 0.14. This means that the model explains the variance in the dependent variable to a significant degree.

In a second approach the population was divided into four classes according to the age (the median age was 62 years; age therefore was stratified into two classes: ≤62 vs >62 years of age) and gender: i. young females (n=90), ii. young males (n=406), iii. old females (n=153), and iv. old males (n=333). Then, for each class a logistic regression analysis was performed including diabetes as a covariate because diabetes was the only variable that was statistically significant in the previous multivariable analysis. Afterwards, for each class a new logistic regression analysis was performed including a variable that identified the simultaneous presence of diabetes and hypertension (coded as 1) or their absence in a patient (coded 0).

Results of logistic regression analyses are reported as odds ratios with 95% confidence intervals and p values. All analyses were performed with SPSS version 12 statistical software (SPSS Inc., Chicago, Illinois).

RESULTS

This analysis includes the first 990 patients (990 vessels) enrolled in this global registry. The baseline characteristics are depicted in **table 1**. The studied vessel was the left anterior descending in 484 (49.3%) cases, the left circumflex in 171 (17.4%) patients, or the right coronary artery in 289 (29.4%) cases; in 38 (3.8%) patients other vessels were imaged, but 8 patients with imaging of a saphenous vein graft were excluded from the analysis. Image acquisition was performed during 425 diagnostic coronary angiography procedures; the others were acquired pre-intervention (n=355), after balloon dilation (n=62), or after stenting (n=126). The rest were acquired post-thrombectomy. The worst lesion diameter stenosis was 61.4±27.3% (visual assessment) or 63.2±20.3% (QCA).

Patient age was 62.1±11.4 years, and most patients were male (75.3%). Pullback length was 48.7±21.5mm. The mean EEM CSA was 15.6±4.8mm^2, the mean lumen CSA was 8.7±3.0mm^2, the mean plaque+media CSA (EEM minus lumen) was 6.8±2.7mm^2, and the mean plaque burden was 43.5±9.2%. Overall in this population, the mean CSA of the necrotic core was 0.45±0.41mm^2 (12.3%), the mean CSA of calcified tissue was 0.31±0.38mm^2 (8.5%), the mean CSA of fibrotic tissue was 2.2±1.4mm^2 (60.1%), and the mean CSA of fibrofatty tissue was 0.70±0.58mm^2 (19.1%). ACS comprised 40.9% of the total population; these patients had nearly the same amount of necrotic core (0.46±0.42mm^2) as non-ACS patients (0.44±0.41mm^2, p=0.74).

Cardiovascular risk factors and coronary plaque composition

Gender: male patients had a non-significant trend towards more necrotic core (0.46±0.43mm^2) than female patients (0.42±0.38mm^2, p=0.20). **Table 2.**

Age: necrotic core content increased with age; patients ≤62 years had mean NC CSA of 0.40±0.36mm^2 vs. 0.50±0.46mm^2 in patients >62 years, p=0.0007.

Diabetes Mellitus: non-diabetic patients had on average a mean NC CSA of 0.43±0.41mm^2 vs. 0.51±0.44mm^2 in diabetic patients, p=0.02. Of note, insulin-requiring diabetic patients had an even larger mean NC area (0.57±0.47mm^2, p=0.04) than the non-insulin-requiring diabetic population.

Table 1. Demographics and baseline characteristics, n=982

	n(%)
Age (years+SD)	62.1 (11.4)
Male	739 (75.3)
Prior cardiac history	585 (59.8)
Hypertension	625 (63.9)
Diabetes	240 (24.6)
Insulin user	61 (25.3)
Lipid disorder	639 (65.1)
Prior MI	269 (27.9)
Prior CABG	53 (5.4)
Family history of CAD	425 (47.2)
Current smoker	255 (25.8)
Previous smoker	253 (25.7)
Clinical presentation	
Non-ACS	581 (59.1)
ACS	401 (40.9)
Vessel imaged	
LAD	484 (49.3)
LCX	171 (17.4)
RCA	289 (29.4)
Other	38 (3.8)
Medication	
Statin	670 (68.2)
Aspirin	857 (87.6)
Beta-blocker	600 (61.5)
Ace inhibitor	405 (41.2)
Calcium channel blocker	185 (19.0)
Blood test	
Total cholesterol (mg/dl)	179.8 (45.4)
LDL cholesterol (mg/dl)	105.7 (36.7)
HDL cholesterol (mg/dl)	47.4 (14.8)
Triglycerides (mg/dl)	97.8 (98.3)
CK (U/L)	221.8 (402.5)
CK-MB (ug/L)	20.1 (49.3)
CRP (mg/dl)	35.8 (93.8)

SD, standard deviation; MI, myocardial infarction; CABG, coronary artery bypass graft; CAD, coronary artery disease; NSTEMI, non ST segment elevation myocardial infarction; STEMI, ST segment elevation acute myocardial infarction; ACS, acute coronary syndrome; LAD, left anterior descending; LCX, left circumflex; RCA, right coronary artery; SVG, saphenous vein graft; CK, creatine kinase;CRP, C-reactive protein.

Hypercholesterolemia: there was no difference between patients with this hypercholesterolemia than those without hypercholesterolemia.

Hypertension: mean NC CSA was 0.40±0.36mm^2 in normotensive patients vs. 0.48±0.44mm^2 in hypertensive patients, p=0.02.

Table 2. Content of necrotic core per cross-sectional area according to clinical presentation and cardiovascular risk factor status

	Mean	SD	p value
Gender			0.20
Female	0.42	0.38	
Male	0.46	0.43	
Age			0.0007
Younger than 62 years	0.40	0.36	
Older than 62 years	0.50	0.46	
Clinical presentation			0.74
Non-ACS	0.44	0.41	
ACS	0.46	0.42	
Diabetes			0.02
.-Yes	0.51	0.44	
.-No	0.43	0.41	
Lipid disorder			0.92
.-Yes	0.45	0.42	
.-No	0.45	0.41	
Hypertension			0.002
.-Yes	0.48	0.44	
.-No	0.40	0.36	
Prior cardiac history			0.0007
.-Yes	0.48	0.42	
.-No	0.41	0.40	
Prior MI			0.04
.-Yes	0.49	0.44	
.-No	0.43	0.41	
Prior CABG			0.04
.-Yes	0.61	0.65	
.-No	0.44	0.39	
Medication			
Ace inhibitor			0.03
.-Yes	0.42	0.43	
.-No	0.47	0.46	
Calcium channel blocker			0.01
.-Yes	0.50	0.41	
.-No	0.44	0.42	
Blood test			
Total cholesterol			0.98
>200 mg/dl	0.42	0.33	
<=200 mg/dl	0.45	0.42	
LDL cholesterol			0.83

	Mean	SD	p value
>100 mg/dl	0.44	0.39	
<=100 mg/dl	0.44	0.40	
HDL cholesterol			0.0001
< 50 mg/dl	0.48	0.41	
>= 50 mg/dl	0.38	0.35	
Triglycerides			0.30
>150 mg/dl	0.42	0.36	
<=150 mg/dl	0.45	0.38	
CRP			0.07
>3 mg/dl	0.43	0.40	
<=3 mg/dl	0.39	0.40	

ACS, acute coronary syndrome;.MI, myocardial infarction; CABG, coronary artery bypass grafting; CK, creatine kinase;CRP, C-reactive protein;

Prior cardiac history or an MI or CABG: patients with a history of cardiovascular disease had a larger mean NC CSA than their counterparts.

Smoking: neither previous smokers nor non-current smokers had a statistically significant larger mean NC CSA than non-smokers, p=0.23 and p=0.37 respectively.

Univariable and multivariable analysis of necrotic core area.

All significantly associated variables in the bivariate analysis (age, hypertension, diabetes, and prior CABG) were introduced in the logistic regression model; but only age [OR 1.023 (1.009,1.037), p=0.001] and diabetes [OR 1.636 (1.174,2.279), p=0.004] remained statistically significant.

In a per class logistic regression analyses including only diabetes as covariate, in young females the OR was 2.1 (95%CI 0.77,6.0), p=0.14; in young males the OR was 1.6 (95%CI 0.90,2.7), p=0.11; in old females the OR was 2.3 (95%CI 1.09,4.9), p=0.03; and in old males the OR was 1.6 (95%CI 0.96,2.7), p=0.07. Further, when only a variable that identified patients with diabetes and hypertension was included, in young females the OR was 2.4 (95%CI 0.69,8.6), p=0.17; in young males the OR was 2.0 (95%CI 1.03,3.8), p=0.041; in old females the OR was 3.04 (95%CI 1.02,9.1) p=0.046; and in old males the OR was 2.2 (95%CI 1.1,4.2), p=0.025. (**Table 3 and 4**).

Table 3. Logistic regression predictors for the top quartile measure of necrotic core area

Parameter	Beta coefficient	Wald	OR	95% CI		p value
Age, yrs	0.023	10.4	1.023	1.009	1.037	0.001
Hypertension (Y/N)	0.180	1.1	1.197	0.862	1.662	0.28
Diabetes Mellitus (Y/N)	0.492	8.5	1.636	1.174	2.279	0.004
Prior CABG (Y/N)	0.494	2.7	1.638	0.911	2.945	0.09
Constant	-2.8			-0.081	-0.012	0.007

Y, yes; N, no; CABG, coronary artery bypass graft.

Table 4. Logistic regression analysis

	Young females (≤62 yrs), n=90	Young males (≤62 yrs), n=406	Old females (>62 yrs), n=153	Old males (>62 yrs), n=333
Model 1: Patients with diabetes	OR 2.1 (95%CI 0.77,6.0) p = 0.14	OR 1.6 (95%CI 0.90,2.7) p = 0.11	OR 2.3 (95%CI 1.09,4.9) p = 0.03	OR 1.6 (95%CI 0.96,2.7) p = 0.07
Model 2: Patients with diabetes and hypertension	OR 2.4 (95%CI 0.69,8.6) p = 0.17	OR 2.0 (95%CI 1.03,3.8) p = 0.041	OR 3.04 (95%CI 1.02,9.1) p = 0.046	OR 2.2 (95%CI 1.1,4.2) p = 0.025

DISCUSSION

The main findings of this paper are the following: 1). The relative amount of necrotic core found in this *in vivo* study resembles that previously reported in pathological studies(8,9). 2). The presence of some individual cardiovascular risk factors is related to an increase in necrotic core. 3). In a per class logistic regression analysis it appears that some cardiovascular risk factors assert a synergistic effect on the amount of necrotic core in coronary atherosclerotic plaques.

The relevance of studying necrotic core lies in its role in the instability of atherosclerotic plaque. Rupture of TCFAs accounts for more than 60% of acute coronary events (4). Ruptured plaques are significantly more obstructive and contain larger necrotic cores, more macrophage infiltration, more calcium, fewer smooth muscles cells, and more positive remodeling than intact thin-cap fibroatheromas (TFCA) (10).

The individual and collective impact of many cardiovascular risk factors in terms of cardiac morbidity and mortality has been described. Individually, these risk factors can either affect the overall plaque composition or specifically the necrotic core (**figure 1**). Similarly, the synergistic effect of two or more cardiovascular risk factors can either affect the overall plaque composition or specifically the necrotic core; this more accurately reflects reality since a patient usually is diabetic and hypercholesterolemic, diabetic and hypertensive, etc. Consider a patient of

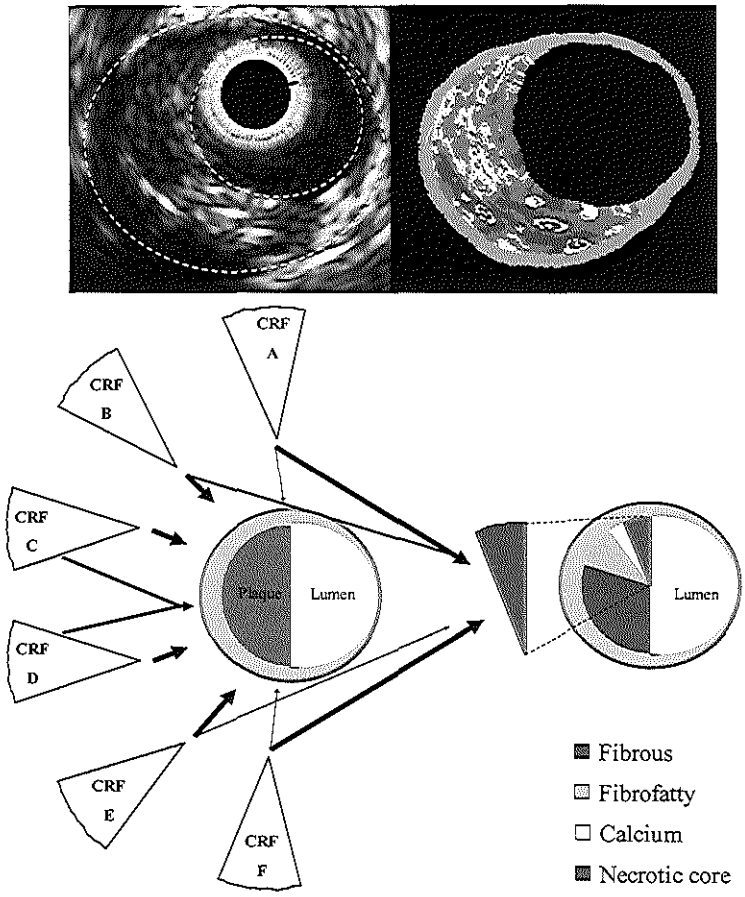

Figure 1. Top: Cross-sectional areas of the same coronary atherosclerotic plaque, on the left hand side a greyscale image and on the right hand side the corresponding IVUS radiofrequency data image. **Bottom:** Cardiovascular risk factors (CRF) act alone or in combination (biological interaction) to assert their effect on overall plaque composition. Note that the impact of these CRFs varies (thickness of the arrow). Their effect could exclusively be on overall plaque composition or simultaneously affect necrotic core, once again, individually or collectively.

any age, gender, and diabetes status (**figure 2**). When this patient is analyzed as a part of a given patient population, cardiovascular risk factor "A" could have no effect because the impact of this cardiovascular risk factor depends on the class to which the patient belongs even if this population is split by age, gender, or any other cardiovascular risk factor. How can this be tested statistically? One option is to introduce interaction terms in the multivariable analysis in order to assess the biological interaction among variables that compound the interaction term. However, this requires a complex statistical analyses that is difficult to put into perspective in clinical practice. Instead, we categorized the current population

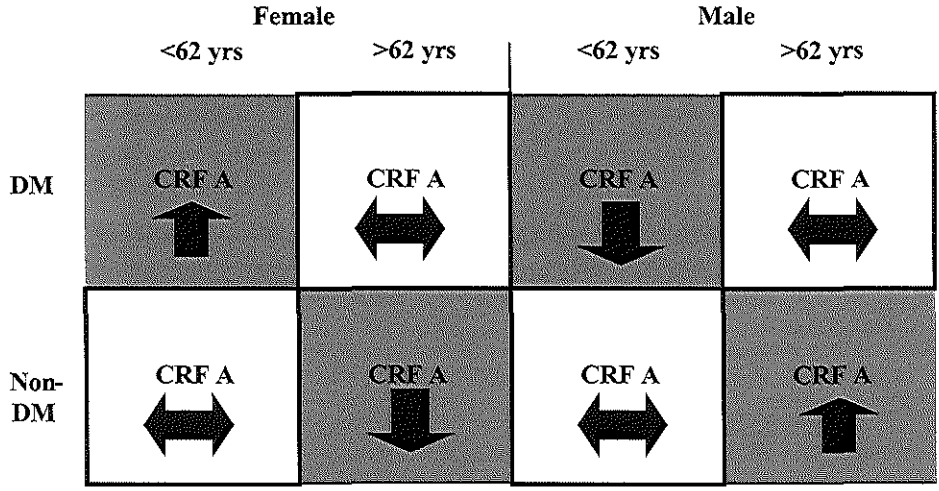

Figure 2. The population has been divided by age, gender and diabetes, resulting in eight categories. The same cardiovascular risk factor (CRF) "A" is assessed in each of them in terms of change in necrotic core. This CRF "A" can have not effect (horizontal arrow), increase (upward arrow) or decrease (downward arrow) the amount of necrotic core. When a population based analysis is conducted, either by age, gender or clinical presentation no effect can be found, although there is a significant change in some of the categories. DM, diabetes mellitus.

into four classes considering two variables that are intrinsic and not modifiable: age and gender. Eventually we had four groups – young females, young males, old females, and old males – in whom we assessed the effect of diabetes that was the only independent predictor of necrotic core area in the overall population. Diabetes was associated with an increase in necrotic core area in old females, and a strong trend was observed in old males. When a variable that identified patients with both diabetes and hypertension was entered into the logistic regression analysis per group, being diabetic and hypertensive was associated with an increase in necrotic core not only in old patients, but also in young males. Of note, in this second model all of the odds ratios were larger than in the first model where only diabetes was tested. Thus, the combined presence of diabetes and hypertension exerted a synergistic and differential effect across age/gender groups.

In post-mortem studies smoking was associated with acute thrombosis (OR 3.6, p=0.004) and low serum HDL cholesterol was associated with plaque rupture (p=0.008)(3). In our study the necrotic core was larger among patients with low HDL cholesterol levels, but this variable failed to be an independent predictor in the multivariable analysis. The rest of the cardiovascular risk factors correlated only mildly with the size of the necrotic core. The same group of pathologists later reported the plaque composition among diabetic patients(2). Type II diabetic patients had larger necrotic cores, more calcium, and more inflammation than

non-diabetics. Patients who were diabetic and hypercholesterolemic had larger necrotic cores compared to patients who were only diabetics while patients with diabetes and hypercholesterolemia had a larger macrophage infiltrate compared to patients with normal cholesterol and no diabetes mellitus. Although some of our results were in line with this pathological study, we refrained from a direct comparison between pathology and our in vivo study because these pathological studies defined cardiovascular risk factors based on clinical history and postmortem blood and sera analysis as well as by histology and IVUS-RFD is not pathology even though the predictive accuracy of necrotic core detection is reported to be 95.8%(6).

This study has many potential clinical implications. First, necrotic core is a pathological marker of atherosclerotic plaque instability. In future prospective studies aiming to describe the relation of necrotic core rich plaques to clinical events, an enrichment of the study population can be performed by increasing the number of hypertensive and diabetic males and older diabetic and hypertensive females, variables that were strongly associated with larger NC areas in this current study. Second, we are entering in a new IVUS era where not only size, but also qualitative plaque composition, specifically necrotic core, matters. In classical IVUS plaque regression studies not all patients in the treated arm were regressors, and some of them were even progressors(11). *In vivo* tissue characterization could help to evaluate the temporal changes of the plaque composition in addition to overall progression/regression. Third, previous epidemiological studies have studied only clinical, angiographic, tomographic, and biomarkers in relation to patient mortality and morbidity; IVUS-RFD allows assessment of actual plaque composition in relationship to patient outcomes. Fourth, the synergistic and additive presence of "traditional" cardiovascular risk factors on plaque composition can be prospectively analyzed with IVUS-RFD to understand the dynamic nature of the atherosclerosis disease.

Limitations

This study has several limitations. The most important is that external validity is limited because the studied population is still small and some of the cardiovascular risk factors, such as female gender and diabetes, are not extensively represented. Furthermore, we used analyses that were optimized based on the dataset, that is, we used the top quartile of necrotic core measures and age cutpoints (i.e. ≤62 years). The use of "optimized" analyses has the potential to be less generalizable to validated analyses.

Other metabolic, chemical, mechanical, and rheological factors that influence the behavior of a diseased coronary vessel wall were not measured; these are independent from plaque composition and are not investigated concurrently in this study.

Conclusions

Overall plaque composition as analyzed by IVUS-RFD is similar to pathology. Individually and collectively, specific cardiovascular risk factors are associated with an increase in necrotic core.

Funding/Support: This study was funded by Volcano Therapeutics.
Role of the Sponsor: The sponsor participated in discussions regarding study design and protocol development and provided logistical support during the trial.

Database was performed by a contract research organization, Pacific Data Design, California, US, under contract to the sponsor.

The manuscript was prepared by the first and corresponding authors and modified after consultation with the other authors. The sponsor reviewed the manuscript, but the final decision on content was exclusively retained by the authors.

Independent Statistical Analysis: This was performed by Dick Goedhart, PhD from an independent Corelab, Cardialysis, BV, Rotterdam, The Netherlands. The statistician did not receive compensation for his statistical services.

VOLCANO REGISTRY Investigators and participating centers:
United States: Jason Rogers, MD, UC Davis Medical Center, Sacramento, CA; Steve Marso, MD, Mid-America, Kansas City, MO; Jim Margolis, MD, Miami Heart, Miami, FL; Amir Lerman, MD, Mayo Clinic, Minneapolis, MN; Juan Pittaluga, MD, Winchester Medical Winchester, VA; George Revtyak, MD, St. Francis Hospital, Beech Grove, IN; Ed O'Leary, MD, Nebraska Heart, Omaha, NE; Murat Tuzcu, MD, Cleveland Clinic Foundation Cleveland, OH; Nabil Dib, MD, Arizona Heart, Phoenix, AZ; Rajesh Dave, MD, Pinnacle Health Harrisburg, PA; Morton Kern, MD, Saint Louis University, Saint Louis, MO; John Hodgson, MD Saint Joseph's Hospital, Phoenix, AZ; Samer Kazziha, MD, Mount Clemens General, Mt. Clemens, MI; Greg Braden, MD, Forsyth Hospital, Forsyth, NC; Louis I. Heller, MD, Saint Joseph's Hospital, Atlanta, GA; Marty Leon, MD, Columbia Hospital, Columbia, NY; Joseph Puma, MD, New York Methodist, Brooklyn, NY.

Europe: V. Klauss, MD, Innenstadt, Munich; M. Pieper, MD, Herz-und Neurozentrum Kreuzlingen; D. Glogar, MD, AKH, Vienna; P. Oemrawsingh, MD, LUMC, Leiden; O. Bleie, MD, Haukeland Hospital, Bergen; D. Dudek, MD, Jagiellonian University, Krakow; Schiele, MD, CHU, Besancon; M. Sabate, MD, Hopital Clinico San Carlos, Madrid; Prof. P. Serruys, MD, Thoraxcenter, Rotterdam; R. Erbel, MD, Westdeutsches Herzzentrum, Essen; W. Wijns, MD, OLVZ, Aalst; Colman, MD, Valdecilla Hospital Santander; F. Prati, MD, San Giovannni Roma; P. Sganzerla, MD, Cliniche Gavazzeni, Bergamo; P. Presbitero, MD, Clinica Humanitas, Rozzano; Miller, MD, Ichilov, Tel Aviv; R. Kornowski, MD, Rabin Medical Center; Petah Tiqwa; A. Iniguez, MD, Meixoeiro, Vigo; E. Eeckhout, MD, CHUV, Lausanne; Harnek, MD, University Hospital, Lund; Quininha, MD, Hospital de Santa Marta, Lisbon.
Japan: Osamu Katoh, MD, Kenya Nasu, MD, Takahiko Suzuki, Toyohashi Heart Center, Toyohashi; Satoru Sumitsuji, MD, Rinku General Medical Center, Izumisano; Satoshi Saito, MD, Junko Honye, MD, Nihon University, Tokyo.

Author Contributions: Dr Garcia-Garcia had full access to all of the data in the study
Study concept and design: Garcia-Garcia, Serruys
Acquisition of data: Margolis
Analysis and interpretation of data: Garcia-Garcia, Serruys
Drafting of the manuscript: Garcia-Garcia, Serruys
Critical revision of the manuscript for important intellectual content: Garcia-Garcia, Serruys, Mintz. Saito, Klaus, Carlier, Margolis, Shwartz.
Statistical analysis: Goedhart, Garcia-Garcia, Serruys
Administrative, technical, or material support: Margolis
Study supervision: Garcia-Garcia, Serruys, Mintz. Saito, Klaus, Carlier, Margolis, Shwartz.

REFERENCES

1. Bhatt DL, Steg PG, Ohman EM, et al. International prevalence, recognition, and treatment of cardiovascular risk factors in outpatients with atherothrombosis. Jama 2006;295:180-9.
2. Burke AP, Kolodgie FD, Zieske A, et al. Morphologic findings of coronary atherosclerotic plaques in diabetics: a postmortem study. Arterioscler Thromb Vasc Biol 2004;24:1266-71.
3. Burke AP, Farb A, Malcom GT, Liang YH, Smialek J, Virmani R. Coronary risk factors and plaque morphology in men with coronary disease who died suddenly. N Engl J Med 1997;336:1276-82.
4. Virmani R, Kolodgie FD, Burke AP, Farb A, Schwartz SM. Lessons from sudden coronary death: a comprehensive morphological classification scheme for atherosclerotic lesions. Arterioscler Thromb Vasc Biol 2000;20:1262-75.
5. Nair A, Kuban BD, Tuzcu EM, Schoenhagen P, Nissen SE, Vince DG. Coronary plaque classification with intravascular ultrasound radiofrequency data analysis. Circulation 2002;106:2200-6.
6. Nair A MP, Kuban BD, Vince DG. Automated coronary plaque characterization with intravascular ultrasound backscatter: ex vivo validation. Eurointervention 2007;3:113-130.
7. Karesen KF BE. Blind deconvolution of ultrasonic traces accounting for pulse variance. IEEE Trans Ultrason Ferroelectr Freq Control 1999;46:564-573.
8. Kragel AH, Reddy SG, Wittes JT, Roberts WC. Morphometric analysis of the composition of atherosclerotic plaques in the four major epicardial coronary arteries in acute myocardial infarction and in sudden coronary death. Circulation 1989;80: 1747-56.
9. Falk E. Pathogenesis of atherosclerosis. J Am Coll Cardiol 2006;47:C7-12.
10. Kolodgie FD, Virmani R, Burke AP, et al. Pathologic assessment of the vulnerable human coronary plaque. Heart 2004;90:1385-91.
11. Nissen SE, Nicholls SJ, Sipahi I, et al. Effect of very high-intensity statin therapy on regression of coronary atherosclerosis: the ASTEROID trial. Jama 2006;295: 1556-65.

CHAPTER 4.2

Relationship Between Cardiovascular Risk Factors and Biomarkers with Necrotic Core and Plaque Size Measured by Intravascular Ultrasound Radiofrequency Data Analysis.

García-García HM, Klauss V, Gonzalo N, Onuma Y, van Es GA, Goedhart D, Hamm CW, Wijns W, Zalewski A, Serruys PW.

Submitted

ABSTRACT

Background. Few post-mortem studies compared plaque composition with available patient characteristics and no comprehensive correlations between these variables have been undertaken *in vivo*. Therefore, we explored the impact of patient demographics, anthropometric measures, CV risk factors, and soluble biomarkers on plaque composition and its overall size in patients with coronary heart disease (CHD).

Methods and Results. The Integrated Biomarkers and Imaging Study-2 trial enrolled patients with CHD (n=309). Baseline patient variables were entered in univariable and multivariable regression procedures along with necrotic core (NC) area and total plaque area, as measured by IVUS-RF. The set of variables with a p-value of ≤0.15 were used for the multivariable regression analyses. A backward selection approach was used; the stay criterion was set to 0.1. In the multivariable analysis, age, male gender, waist circumference and systolic blood pressure were positive, whereas urinary TxB2 negative, independent predictors of NC area; while only age and waist circumference were positively and urinary TxB2 were negatively associated with an increase in overall plaque size.

Conclusions. In non-culprit vessels, patient demographics (age, male gender), anthropometric measures (waist circumference), clinical risk factors (systolic blood pressure) are related plaque composition (larger necrotic core area) after multivariate adjustment. Accordingly, necrotic core, as assessed by IVUS-RF, could be viewed as a novel in situ/in vivo biomarker, potentially reflecting the long-term impact of cardiovascular risk on plaque phenotype.

Key words: Atherosclerosis, necrotic core, IVUS backscattering radiofrequency data analysis

INTRODUCTION

Cardiovascular (CV) disease remains the principal cause of death worldwide, with three-fourths of CV deaths attributed to atherosclerosis. Pathological studies in patients who died from coronary heart disease (CHD) showed an extensive coronary atherosclerosis.[1] The current paradigm asserts that the main cause of cardiac death is primarily due to rupture of an advanced atherosclerotic lesion.[2] Ruptured plaques contain the largest amount of necrotic core (NC) among the atherosclerotic lesions, suggesting a link between the amount of NC and their predisposition to rupture.[3]

The anthropometric measures and conventional cardiovascular (CV) risk factors relate to the risk of subsequent CV events as demonstrated by the original Framingham cohort and more recently the INTERHEART multiethnic study of the predictors of the first myocardial infarction.[4,5] Notwithstanding these observations, accurate prediction of major coronary events on the individual patient level, as opposed to population based studies, remains challenging. Therefore, there is an interest in additional markers of patient vulnerability that would enhance precision of risk estimation beyond that afforded by Framingham risk score or other conventional risk engines. The ability to quantify NC *in vivo* by the intravascular ultrasound radiofrequency (IVUS-RF) data analysis offers the opportunity to provide unique information about plaque type to enhance precision of clinical and laboratory variables used to assess CV risk. Although the ultimate validity of this measurement will require very large and long-term natural history studies, the first step is to examine the relationship between patient derived variables and NC. Accordingly, we sought to explore *in vivo* the relationship between patient demographics, anthropometric measures, CV risk factors, soluble biomarkers and plaque composition (NC area) or its overall size (plaque area).

METHODS

Study Design

The Integrated Biomarkers and Imaging Study-2 trial has been published elsewhere.[6] Briefly, it was an international, multicenter, randomized, double blind, placebo-controlled study in patients with confirmed CHD. Institutional review boards at each center approved the protocol, and patients provided written informed consent. From the original cohort of IBIS-2 patients, 309 patients

with complete information regarding baseline clinical characteristics, laboratory measurements and imaging data were selected for this study.

Patient Population

Patients 18 years of age or older undergoing cardiac catheterization for acute coronary syndrome (ACS - NSTEMI or STEMI) or non-ACS (eg, chronic stable angina or troponin-negative resting chest pain) were eligible. The protocol specified 50% of randomized patients to have troponin-positive ACS. The randomization was stratified according to ACS status and center. Key exclusion criteria were planned surgical revascularization, stroke in the past 6 months, chronic hepatic disorder or abnormal ALT, bilirubin (ALT >2.5 or bilirubin >1.5 upper limit of normal), serum creatinine >2.0 mg/dL, blood pressure >160/100 mm Hg, poorly controlled diabetes mellitus (HbA_{1c} >10%), severe heart failure or left ventricular ejection fraction <30%, and current life-threatening condition. Patients were ineligible if angiography demonstrated left main coronary stenosis >50% or coronary anatomy was inappropriate for IVUS.

IVUS Imaging

The ECG-gated IVUS-RF acquisition was performed using EagleEye catheter (20 MHz) at pullback speed of 0.5 mm/sec as described.[6] The quantitative IVUS analysis was performed by the Core Imaging Laboratory (Cardialysis, Rotterdam, The Netherlands) using customized software (pcVH 2.1, Volcano Therapeutics). The analyst selected the region of interest flanked by the presence of easily identifiable anatomical landmarks. Vessel and lumen areas data were obtained for every cross-section throughout the region of interest by semiautomatic planimetry of the leading edges of the luminal and external elastic membrane borders. The composition of coronary atheroma was assessed using spectral analysis of backscatter RF signals. Necrotic core was identified with autoregressive classification system that showed sensitivity and specificity of 92% and 97% for detection of necrotic core, respectively.[7,8] To assess intra- and interobserver variability of necrotic core measurements, 20 patients from the current study (2465 frames) were analyzed twice by two different analysts. The mean absolute difference for necrotic core area was 0.01 mm^2 (SD 0.06) for the intraobserver and 0.02 mm^2 (SD 0.08) for the interobserver variability, respectively.

Study End Point Definitions (IVUS-RF)

Plaque area contains both atherosclerotic plaque and media. This was obtained after planimetry was completed at the lumen/plaque boundary and at the media/adventitia boundary in each cross-section forming the region of interest. Plaque area was reported in mm^2.

The necrotic core area was automatically obtained in each cross-section forming the region of interest using dedicated software (pcVH 2.1, Volcano Therapeutics). Necrotic core values were expressed in mm^2.

Biomarkers

Plasma hsCRP was measured as described previously.[7] Plasma Lp-PLA_2 activity was measured by a colorimetric method.[7] Other biomarkers (IL-6, MPO, ICAM-1, and MMP-9 activity) were assayed using commercially available kits. Oxidized phospholipid content per particle of apoB (oxPL/apoB) was measured using murine monoclonal antibody E06 as described.[8] Platelet biomarkers were measured in plasma (P-selectin, CD40L) and urine (11-dehydro thromboxane B_2 normalized by urine creatine concentration [11-dehydro-TxB_2/mmol Cr]) as described.[7]

Statistical Analysis

Continuous variables were reported as mean±SD. Based on the plots of the residuals against the predicted values it was decided to log transform the necrotic core area and those continuous variables, from which the maximum z-score superseded the value 4. (The z-score was calculated for each continuous variable as the number of standard deviations change from its mean). All class variables except gender were coded [0,1] with 0 for absence or 1 for presence. Gender was coded 0 for females and 1 for males. In total 41 variables were entered into the univariable regression procedure. The set of thirteen variables with a p-value of <=0.15 were used for the multivariable regression procedure. A backward selection procedure was used, both the entry criterion for the forward and the stay criterion for the backward procedure were set to 0.1.

To further understand relationship between age and antropometric variables and imaging parameters, the population was categorized into classes according to the distribution of age in tertiles. First tertile ranged from 33 to 52 years, second tertile from 53 to 63 years and in the third tertile from 64 to 82 years. Further,

waist circumference was also categorized as follows: first tertile from 68 to 93 cm; second tertile from 94 to 101.5 and third tertile 102 to 131 cm.

Statistical analyses were performed with use of SAS V8.02.

RESULTS

Between November 16th, 2005 and August 16th, 2006, 330 patients were enrolled with 309 patients included in this analysis. The reasons for not including 21 patients (6%) included missing imaging data or suboptimal quality (6 patients did not undergo imaging, 14 had non-interpreatable IVUS images, and the image data of 1 patient was lost in the archiving/saving procedure). In **Table 1**, the

Table 1. Baseline Characteristics

	(n=309)
Clinical characteristics	
Age (y)	58.6±10.0
Males (n, %)	254 (82.2)
Waist circumference (cm)	97.6±11.0
Body-mass index (kg/m²)	27.7±3.9
Diabetes mellitus (n, %)	42 (13.6)
Hypertension (n, %)	188 (60.8)
Hypercholesterolemia (n, %)	181 (60.5)
Current smoker (n, %)	117 (37.9)
Metabolic syndrome (n, %)	71 (23)
Prior medical history (n, %)	
Prior myocardial infarction	94 (30.4)
Prior coronary revascularization	95 (30.8)
Prior stroke	8 (2.6)
Index hospitalization (n, %)	
ACS	154 (49.8)
Stable	155 (50.2)
Cardiovascular medications at randomization (n, %)	
Statins	100 (33.7)
Laboratory values	
Cholesterol (mg/dL)	
Total	184.6±46.3
LDL	105.6±40.1
HDL	47.5±11.9
Triglycerides (mg/dL)	
Median	136.3
IQR	(95.6, 196.5)
hsC-reactive protein (mg/L)	9.4±24.7
Blood pressure	
Systolic - mm Hg	127.1±16.4
Diastolic - mm Hg	75.4±9.7

baseline characteristics of patients with complete information regarding clinical and imaging data are shown. The mean age was 58.6±10.0, mostly men were included (82.2%). By design, 155 (50.2%) had stable CHD and 154 (49.8%) had troponin-positive acute coronary syndrome. The mean waist circumference was 97.6 cm and the mean systolic and diastolic blood pressure values were 127.1 and 75.4 mmHg, respectively. Overall, the mean LDL-cholesterol was 105.6 mg/dL and the mean HDL-cholesterol was 47.5 mg/dL.

Mean length of the IVUS pullbacks was 50.3±16.8mm. In total, 37,617 cross-sectional areas (CSAs) were included in this substudy. Out of these, 28620 (76.1%) were CSAs with necrotic core. Overall, the mean percent atheroma plaque was 40.2%.

Univariable association between baseline characteristics with necrotic core and plaque area

The following variables were strongly associated with necrotic core ($p \leq 0.05$): male gender, age, waist circumference, weight, height, body mass index, current smoker, systolic blood pressure, creatinine, HgA1C, urine 11-Dehydro TXB2 and % diameter stenosis by QCA; and the following with plaque size: male gender, age,

Table 2. List of variables (only with a p value < 0.15) and their univariable association with necrotic core area and plaque area

	ln Necrotic core area				Plaque area			
	Estimate	95%CI		p value	Estimate	95%CI		p value
Waist circumference (cm)	0.026	0.013	0.039	0.0001	0.007	0.003	0.012	0.0019
Weight (kg)	0.020	0.009	0.030	0.0003	0.006	0.003	0.010	0.0007
Diameter stenosis by QCA (%)	0.024	0.010	0.037	0.0005	0.007	0.002	0.011	0.0049
Systolic blood pressure (mmHg)	0.014	0.006	0.023	0.0012	0.004	0.001	0.007	0.0080
Body Mass Index	0.059	0.022	0.096	0.0018	0.017	0.004	0.029	0.0127
Current smoker	-0.410	-0.704	-0.116	0.0064	-0.118	-0.221	-0.014	0.0256
Age in years	0.018	0.004	0.031	0.0124	0.008	0.003	0.013	0.0009
Male gender	0.477	0.104	0.850	0.0124	0.145	0.014	0.276	0.0304
Creatinine	0.010	0.002	0.018	0.0161	0.003	0.001	0.006	0.0690
Height (cm)	0.017	0.001	0.035	0.0500	0.006	0.001	0.012	0.0513
Urine 11-Dehydro TXB2	-0.232	-0.467	0.003	0.0541	-0.087	-0.169	-0.005	0.0373
Glycosylated Hemoglobin A1C	1.196	-0.019	2.411	0.0546	0.417	-0.009	0.843	0.0560
Glucose	0.572	-0.031	1.175	0.0639	0.170	-0.041	0.382	0.1159
Oxidised Phospholipids/Apolipoprotein B100 ratio	0.163	-0.013	0.340	0.0701	0.057	-0.005	0.119	0.0714
Baseline eGFR value - ml/min/1.73 m²	-0.507	-1.113	0.099	0.1023	—	—	—	—
Hypertension	0.241	-0.053	0.535	0.1079	0.103	0.001	0.205	0.0502
Diastolic blood pressure (mmHg)	0.012	-0.003	0.027	0.1128	0.005	0.001	0.010	0.0662
Previous PCI or CABG	—	—	—	—	0.082	-0.027	0.191	0.1409
Mean lumen diameter (mm)	—	—	—	—	0.293	0.202	0.384	0.0001

waist circumference, weight, height, body mass index, current smoker, hypertension, systolic blood pressure, HgA1C, urine 11-Dehydro TXB2 and % diameter stenosis and mean lumen diameter by QCA (**Table 2).**

Other tested variables that failed to be statistically significant were: clinical presentation (acute coronary syndrome), diabetes, LDL-c, HDL-c and hs CRP. A complete table that included all tested variables is published online. (APPENDIX A)

Multivariable association between baseline characteristics with necrotic core and plaque area

In the multivariable analysis, age, male gender, waist circumference and systolic blood pressure were independent positive predictors of NC; while only age and waist circumference were positively associated with (increase in) plaque size. The urine 11-Dehydro TXB2 was an independent negative predictor for both necrotic core and plaque size. **Table 3.**

To further understand relationship between age, antropometric variables and imaging parameters, the population was categorized by age and waist circumference in tertiles.

Within the first and second age tertiles, the mean necrotic core area and mean plaque area were not different across different waist circumference groups. In contrast, in older patients (the third age tertile: >64 years), the mean necrotic core area and the mean plaque area were significantly higher with increasing degree of abdominal obesity tertiles (**Figure 1**).

Table 3. List of variables and their multivariable association with ln(Necrotic core area) and plaque area

A. NC predictors	Parameter Estimate	95% Confidence Limits		P value
Intercept	-5.25	-7.33	-3.16	<.0001
Urine 11-Dehydro TXB2	-0.233	-0.471	0.006	0.056
Systolic blood pressure	0.011	0.0009	0.021	0.033
Age	0.018	0.003	0.033	0.022
Waist circumference	0.021	0.007	0.034	0.003
Male gender	0.446	0.047	0.845	0.029

B. Plaque predictors	Parameter Estimate	95% Confidence Limits		P value
Intercept	0.944	0.287	1.599	0.005
Previous CABG and PCI	0.083	-0.031	0.196	0.154
Age	0.009	0.004	0.014	0.001
Waist circumference	0.007	0.0024	0.012	0.003
Urine 11-Dehydro TXB2	-0.094	-0.178	-0.009	0.030

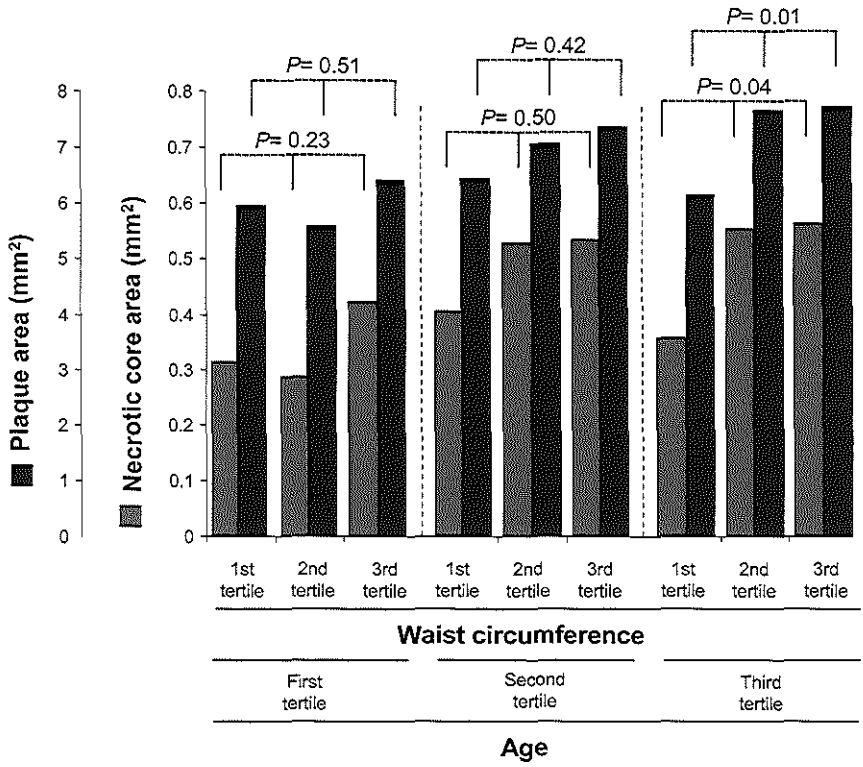

Figure 1. Stratification of mean plaque area and necrotic core area according to both age and waist circumference tertiles.

DISCUSSION

Our findings indicate that age, waist circumference, systolic blood pressure and urine 11-Dehydro TxB2 are independent predictors of necrotic core in the multivariable analysis, with fewer variables predictive of overall plaque size. This raises the possibility that the measurements of necrotic core may offer additional prognostic information in risk assessment of individual patients.

Necrotic Core and Cardiovascular Risk Factors in Pathological Studies

Prior attempts to correlate patients characteristics with plaque morphology assessed during post-mortem examination are limited by selection bias (only patients with fatal events due to coronary or no coronary causes are included) and often post-mortem ascertainment of laboratory values. History of smoking was associated with evidence of acute coronary thrombosis (OR 3.6, p=0.004) and low HDL-cholesterol levels were associated with plaque rupture (odds ratio

for each additional milligram per deciliter, 1.01).[9] Diabetes was shown to be associated with larger necrotic core and increased macrophage content consistent with clinically observed increased of CV events in these patients.[10] The differences with the current study may stem from the fact that our observations focused on non-culprit vessels. In addition, current algorithm for spectral analysis of IVUS-RF is unable to detect thrombus and lacks precision to detect inflammatory cell content. Post-mortem measurement of HDL-cholesterol is also fraught with potential confounding factors.

Plaque size by intravascular imaging and its relationship with CV risk factors

Several CV risk factors such as male gender, BMI, diabetes and prior coronary revascularization have been found strong predictors of atheroma volume measured by conventional IVUS.[11] As shown by Nicholls et al., atheroma volume in women is smaller even in the presence of more risk factors in secondary prevention trials.[12] Our study extends these observations showing independent impact of male gender on the size of necrotic core. We were unable to detect relationship between diabetes or prior coronary revascularization and IVUS measurements. These findings were unexpected and possibly related to too few diabetics enrolled in the current study (14%). It is noteworthy, however, that continuous measurements reflecting cardiometabolic risk (waist circumference, blood pressure, HgA1C), demonstrated stronger relationship with the size of necrotic core in either univariate or multivariate analysis in our dataset. Obesity is an important but complex contributor to CV morbidity and mortality.[13] Waist circumference, simple measure of visceral (abdominal) obesity, has a superior predictive value for the presence CHD or the risk of MI to that of BMI.[14] Large multiethnic INTERHEART study showed significant relationship between waist circumference or waist-to-hip ratio and risk of first MI even after full adjustment for other risk factors.[5] Furthermore, patients with low BMI but increased waist circumference have increased 1-year mortality.[15] In our study, increasing waist circumference was not only predictor of plaque size but more importantly an independent predictor of necrotic core area.

Despite favourable effects of cholesterol-lowering therapy with statins in primary and secondary prevention, single measurement of serum lipids did not correlate with IVUS measurements of atheroma size or necrotic core in univariate or multivariate analysis. These findings are consistent with those reported by others regarding conventional IVUS measures and do not contradict halting plaque progression or even its regression with intensive LDL cholesterol lowering. [16,17] In contrast to lipid measurements, systolic blood pressure was specifically related to larger necrotic core size. It is noteworthy that systolic blood pressure is an inde-

pendent predictor of plaque progression by IVUS and therapeutic intervention(s) lowering blood pressure below current guideline mandated thresholds may retard progression of atherosclerosis and reduce CV events.[18]

Study Limitations

This study is a cross-sectional analysis that has number of limitations. First, sample size was small thus possibly limiting full exploration of categorical variables (e.g., diabetes). Second, the measurements of biomarkers that entered into the model do not reflect chronic circulating levels as 50% of patients presented with ACS, which transiently alters inflammatory biomarkers. In addition, our data indicate that ACS status does not affect necrotic core size when assessed in non-culprit vessels. Although pan-coronary inflammation was reported in ACS patients, IVUS methodology is not well suited to measure such endpoints. Third, some of the measurements are confounded by concomitant treatments. For example, 99% of patients were receiving aspirin, thus the inverse relationship between urinary TxB2 and necrotic core or plaque size is clearly confounded by the impact of this therapy. Fourth, we wish to emphasize that all IVUS studies are limited to the analysis of a relatively short segment of coronary arterial tree that does not fully reflect disease characteristics elsewhere.

Conclusions

In non-culprit vessels, patient demographics, anthropometric measures, clinical CV risk factors are related not only to increase in plaque size but also its composition (increase in necrotic core) size after multivariate adjustment. Accordingly, necrotic core, as assessed by IVUS-RF, should be viewed as a novel in situ/in vivo biomarker, potentially reflecting the long-term impact of cardiovascular risk on plaque phenotype. Longitudinal studies with hard clinical endpoints are needed to fully assess clinical value of this measurement.

APPENDIX

Core Laboratories: Imaging (Cardialysis, Rotterdam, The Netherlands).
Participating Centers (number of patients enrolled): Austria: Hanusch Krankenhaus, Georg Gaul (6). Belgium: Centre Hospitalier Universitaire Sart-Tilman, Victor Legrand (10); ZNA Campus Middelheim, Stefan Verheye (25); Cardiovascular Center, Aalst, William Wijns (14). Czech Republic: Všeobecná Fakultní

Nemocnice, Michael Aschermann (23). Denmark: Skejby University Hospital, Hans Erik Bøtker (18). Germany: West German Heart Center, Raimund Erbel (7); Kerckhoff Klinik, Christian Hamm (7); Universitätsklinikum Heidelberg, Stefan Hardt, Helmut Kücherer (1); Universitätsklinikum München, Volker Klauss (14), Universitätsklinikum Ulm, Wolfgang Koenig (9); Segeberger Kliniken, Gert Richardt (3). The Netherlands: Medisch Spectrum Twente, Clemens von Birgelen (14); Medisch Centrum Leeuwarden, Adrianus Johannes van Boven (12); Catharina Hospital and Catherine R&D, Herman Rolf Michels (14), Erasmus Medical Center, Patrick Serruys (20); Medisch Centrum Rijnmond Zuid, Pieter Smits (11). Norway: Haukeland Sykehus, Oyvind Bleie (20). Poland: Upper Silesian Heart Center, Pawel Buszman (40); Szpital Uniwersytecki, Dariusz Dudek (19). Spain: Hospital Marques de Valdecilla, Thierry Colman (9); Hospital Clinico San Carlos, Carlos Macaya (9). Switzerland: Kantonsspital Luzern, Paul Erne (25).

DISCLOSURES

Andrew Zalewski is a GlaxoSmithKline employee.

FUNDING SOURCE

This study was funded by a research grant from GlaxoSmithKline.

REFERENCES

1. Virmani R, Kolodgie FD, Burke AP, Farb A, Schwartz SM. Lessons from sudden coronary death: a comprehensive morphological classification scheme for atherosclerotic lesions. *Arterioscler Thromb Vasc Biol.* 2000;20(5):1262-1275.
2. Davies MJ. Anatomic features in victims of sudden coronary death. Coronary artery pathology. *Circulation.* 1992;85(1 Suppl):I19-24.
3. Cheruvu PK, Finn AV, Gardner C, Caplan J, Goldstein J, Stone GW, Virmani R, Muller JE. Frequency and distribution of thin-cap fibroatheroma and ruptured plaques in human coronary arteries: a pathologic study. *J Am Coll Cardiol.* 2007;50(10):940-949.
4. Yusuf S, Hawken S, Ounpuu S, Dans T, Avezum A, Lanas F, McQueen M, Budaj A, Pais P, Varigos J, Lisheng L. Effect of potentially modifiable risk factors associated with myocardial infarction in 52 countries (the INTERHEART study): case-control study. *Lancet.* 2004;364(9438):937-952.
5. Yusuf S, Hawken S, Ounpuu S, Bautista L, Franzosi MG, Commerford P, Lang CC, Rumboldt Z, Onen CL, Lisheng L, Tanomsup S, Wangai P, Jr., Razak F, Sharma AM, Anand SS. Obesity and the risk of myocardial infarction in 27,000 participants from 52 countries: a case-control study. *Lancet.* 2005;366(9497):1640-1649.
6. Serruys PW, Garcia-Garcia HM, Buszman P, Erne P, Verheye S, Aschermann M, Duckers H, Bleie O, Dudek D, Botker HE, von Birgelen C, D'Amico D, Hutchinson T, Zambanini A, Mastik F, van Es GA, van der Steen AF, Vince DG, Ganz P, Hamm CW, Wijns W, Zalewski A. Effects of the Direct Lipoprotein-Associated Phospholipase A2 Inhibitor Darapladib on Human Coronary Atherosclerotic Plaque. *Circulation.* 2008.
7. Mohler ER, 3rd, Ballantyne CM, Davidson MH, Hanefeld M, Ruilope LM, Johnson JL, Zalewski A. The effect of darapladib on plasma lipoprotein-associated phospholipase A2 activity and cardiovascular biomarkers in patients with stable coronary heart disease or coronary heart disease risk equivalent: the results of a multicenter, randomized, double-blind, placebo-controlled study. *J Am Coll Cardiol.* 2008;51(17):1632-1641.
8. Tsimikas S, Brilakis ES, Miller ER, McConnell JP, Lennon RJ, Kornman KS, Witztum JL, Berger PB. Oxidized phospholipids, Lp(a) lipoprotein, and coronary artery disease. *N Engl J Med.* 2005;353(1):46-57.
9. Burke AP, Farb A, Malcom GT, Liang YH, Smialek J, Virmani R. Coronary risk factors and plaque morphology in men with coronary disease who died suddenly. *N Engl J Med.* 1997;336(18):1276-1282.
10. Burke AP, Kolodgie FD, Zieske A, Fowler DR, Weber DK, Varghese PJ, Farb A, Virmani R. Morphologic findings of coronary atherosclerotic plaques in diabetics: a postmortem study. *Arterioscler Thromb Vasc Biol.* 2004;24(7):1266-1271.
11. Nicholls SJ, Tuzcu EM, Crowe T, Sipahi I, Schoenhagen P, Kapadia S, Hazen SL, Wun CC, Norton M, Ntanios F, Nissen SE. Relationship between cardiovascular risk factors and atherosclerotic disease burden measured by intravascular ultrasound. *J Am Coll Cardiol.* 2006;47(10):1967-1975.

12. Nicholls SJ, Wolski K, Sipahi I, Schoenhagen P, Crowe T, Kapadia SR, Hazen SL, Tuzcu EM, Nissen SE. Rate of progression of coronary atherosclerotic plaque in women. *J Am Coll Cardiol.* 2007;49(14):1546-1551.
13. Barrett-Connor EL. Obesity, atherosclerosis, and coronary artery disease. *Ann Intern Med.* 1985;103(6 (Pt 2)):1010-1019.
14. Onat A, Avci GS, Barlan MM, Uyarel H, Uzunlar B, Sansoy V. Measures of abdominal obesity assessed for visceral adiposity and relation to coronary risk. *Int J Obes Relat Metab Disord.* 2004;28(8):1018-1025.
15. Zeller M, Steg PG, Ravisy J, Lorgis L, Laurent Y, Sicard P, Janin-Manificat L, Beer JC, Makki H, Lagrost AC, Rochette L, Cottin Y. Relation between body mass index, waist circumference, and death after acute myocardial infarction. *Circulation.* 2008;118(5):482-490.
16. Nissen SE, Tuzcu EM, Schoenhagen P, Brown BG, Ganz P, Vogel RA, Crowe T, Howard G, Cooper CJ, Brodie B, Grines CL, DeMaria AN. Effect of intensive compared with moderate lipid-lowering therapy on progression of coronary atherosclerosis: a randomized controlled trial. *Jama.* 2004;291(9):1071-1080.
17. Nissen SE, Nicholls SJ, Sipahi I, Libby P, Raichlen JS, Ballantyne CM, Davignon J, Erbel R, Fruchart JC, Tardif JC, Schoenhagen P, Crowe T, Cain V, Wolski K, Goormastic M, Tuzcu EM. Effect of very high-intensity statin therapy on regression of coronary atherosclerosis: the ASTEROID trial. *JAMA.* 2006;295(13):1556-1565.
18. Nissen SE, Tuzcu EM, Libby P, Thompson PD, Ghali M, Garza D, Berman L, Shi H, Buebendorf E, Topol EJ. Effect of antihypertensive agents on cardiovascular events in patients with coronary disease and normal blood pressure: the CAMELOT study: a randomized controlled trial. *Jama.* 2004;292(18):2217-2225.

CHAPTER 5.1

Virtual histology and remodeling index allow in vivo identification of allegedly high risk coronary plaques in patients with acute coronary syndromes: a three vessel intravascular ultrasound radiofrequency data analysis.

Garcia-Garcia HM, Goedhart D, Schuurbiers JC, Kukreja N, Tanimoto S, Daemen J, Morel MA, Bressers M, van Es GA, Wentzel JJ, Gijsen F, van der Steen AFW, Serruys PW.

Eurointervention. 2006;2:338-344.

EuroIntervention

Virtual histology and remodelling index allow *in vivo* identification of allegedly high-risk coronary plaques in patients with acute coronary syndromes: a three vessel intravascular ultrasound radiofrequency data analysis

Héctor M. García-García[1], MD; Dick Goedhart[2], PhD; Johan C.H. Schuurbiers[1], Bsc; Neville Kukreja[1], MRCP; Shuzou Tanimoto[1], MD; Joost Daemen[1], MD; Marie-Angele M. Morel[2], BSc; Marco Bressers[2], MSc; Gerrit-Ann van Es[2], PhD; Jolanda J. Wentzel[1], PhD; Frank Gijsen[1], PhD; Antonius F.W. van der Steen[1], PhD; Patrick W. Serruys[1]*, MD, PhD

1. Thoraxcenter, Erasmus MC, Rotterdam, The Netherlands; 2 Cardialysis BV, Rotterdam, The Netherlands

All authors have declared that there is no conflict of interest.

KEYWORDS
Atherosclerosis, imaging, coronary disease

Abstract

Background: Virtual histology (VH) uses intravascular ultrasound (IVUS) radiofrequency spectral analysis to locally identify the morphology and composition of atherosclerotic plaques. We sought to explore *in vivo* the relation between IVUS-derived thin cap fibro-atheroma (IDTCFA) and remodelling index in patients with acute coronary syndromes using IVUS-VH.

Methods and results: Twenty-one patients (63 vessels) were enrolled. When compared to cross sectional areas (CSAs) without necrotic core in contact with the lumen (NCCL), CSAs with NCCL had a larger plaque burden 42.8±11.5% vs. 32.8±11.5%, p<0.001; higher overall necrotic core content [13.8±10.7% vs. 2.3±7.9% (p<0.001)] and calcified tissue [4.7±6.5 vs. 0.66±2.1% (p<0.001)]. On average there were 2 IVUS-derived thin cap fibro-atheroma (IDTCFA) per patient. Nearly half of the IDTCFAs had positive remodelling.

Conclusions: CSAs with NCCL had worse morphological profiles than those with no NCCL. The simultaneous and more detailed assessment of IDTCFA and remodelling index identifies a reduced number of allegedly high-risk plaques. The findings of this study may have important clinical implications, since they shed light into a possible method of identifying potentially high-risk plaques suitable for pharmacological and/or local treatment.

* *Corresponding author: Thoraxcenter, Bd583a, Dr.Molewaterplein 40, 3015-GD Rotterdam, The Netherlands*
E-mail:p.w.j.c.serruys@erasmusmc.nl

Abbreviations and acronyms

ACS: Acute coronary syndrome
CSA: Cross sectional area
EEM: External elastic membrane
IDTCFA: IVUS-derived thin cap fibro-atheroma
IVUS: Intravascular ultrasound
NC: Necrotic core
NCCL: Necrotic core in contact with the lumen
NSTEMI: Non-ST segment elevation myocardial infarction
PB: Plaque burden
RI: Remodelling index
STEMI: ST segment elevation myocardial infarction
UA: Unstable angina
VH: Virtual Histology

Introduction

For the most part, acute coronary syndromes (ACS) are the consequence of the rupture of particular atherosclerotic plaques called thin-cap fibro-atheromas (TCFAs). These TCFAs have a thin fibrous cap, paucity of smooth muscle cells, heavy inflammatory infiltration of the cap, large necrotic core, positive remodelling and high strain[1-6]. Coronary plaque rupture is a frequent and unpredictable event that impacts the global burden of cardiovascular disease[7]. Indeed, coronary heart disease is expected to be the leading cause of disability-adjusted life-years in 2020[8]. Accordingly, many cutting-edge imaging techniques have recently been developed to help us better understand the atherosclerotic process. The first *in vivo* studies using such techniques were performed against the background of previous histopathological knowledge about morphological and compositional features related to plaques prone to rupture, so several studies have been published recently that mimic previous pathological findings[9-11]. Spectral analysis of the IVUS radiofrequency data (IVUS-VH) is emerging as a tool to assess plaque morphology and composition[12,13]. This combined assessment of remodelling and plaque characterisation might allow a more accurate and complete characterisation *in vivo* for allegedly high-risk plaques.

We thus sought to further explore *in vivo* the relation between compositional features of coronary atherosclerotic plaques, specifically IVUS-derived thin cap fibro-atheroma and remodelling index, in patients with acute coronary syndromes.

Methods

Patient selection

From January to May 2005, all patients with acute coronary syndromes admitted for coronary catheterisation and subsequent intervention were eligible if all three coronary vessels were suitable for IVUS interrogation (absence of extensive angiographic calcification and/or severe vessel tortuosity). Acute coronary syndrome encompasses unstable angina (UA) according to the Braunwald classification, non-ST-segment elevation myocardial infarction (NSTEMI) and ST-segment elevation myocardial infarction (STEMI). The three-vessel IVUS-VH acquisition timing was as follows: in patients with UA/NSTEMI, acquisition was performed just after the interventional treatment; in patients suffering from STEMI it was done when the patient was symptom-free, without ECG changes and haemodynamically stable (defined as systolic blood pressure >90 mmHg without vasopressor or inotropic support, and with a heart rate of between 60 and 100 bpm). Informed written consent was obtained from all patients. Our local Ethics Committee approved the protocol.

IVUS-VH acquisition and analysis

Details regarding the validation of the technique on explanted human coronary segments and *in vivo* post-atherectomy have previously been reported[12,13]. Briefly, IVUS-VH uses spectral analysis of IVUS radiofrequency data to construct tissue maps that are correlated with a specific spectrum of the radiofrequency signal and assigned colour codes (fibrous [labelled green], fibro-lipidic [labelled greenish-yellow], necrotic core [labelled red] and calcium [labelled white])[12].

The IVUS-VH sampling rate during pull-back is gated to peak R-wave and is therefore dependent on heart rate. For instance, during constant heart rate of 60 bpm, then data will be collected every 0.5 mm. IVUS B-mode images were reconstructed from the RF data by customised software (IVUSLab Version 4.4, Volcano Therapeutics, Rancho Cordova, CA, USA). Semi-automated contour detection of both lumen and the media-adventitia interface was performed, and the RF data was normalised using a technique known as "Blind Deconvolution", an iterative algorithm that deconvolves the catheter transfer function from the backscatter, thus accounting for catheter-to-catheter variability[14,15]. Compositional data was obtained for every slice and expressed as mean percent for each component.

Quantification of the necrotic core in contact with the lumen (NCCL) and its angle was performed using MATLAB® (MathWorks, Natick, MA, USA).

Definitions used in this study

Necrotic core tissue in contact with the lumen, is defined as the presence of necrotic core tissue in direct contact with the luminal space and with no detectable overlying fibrous tissue; this is reported as (i) a continuous variable in mm^2, (ii) as a percent of the total plaque composition and (iii) as a percent out of the total necrotic core, (iv) as a binary variable considering the presence or absence of NCCL. In addition, the major confluent pool of NCCL was selectively quantified in terms of area in mm^2 and as a percentage of both the total plaque composition and the total necrotic core. The angle (measured from the gravity centre of the lumen) occupied by the entire NCCL was measured as well as the specific angle occupied by the major confluent NCCL. (Figure 1)

Plaque burden (PB), is defined as EEM_{area}-$Lumen_{area}$/EEM_{area} X 100, where EEM refers to external elastic membrane.

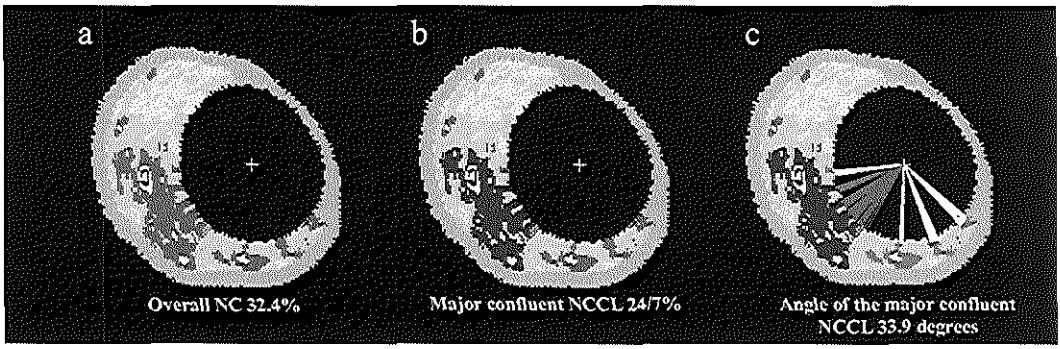

Figure 1. An example of selective quantification of the necrotic core in contact with the lumen. (a) The original IVUS-VH cross-sectional area; (b) Modification using the VH tool to selectively quantify the major confluent necrotic core that is in direct contact with the lumen. (c) Measurement of the angle occupied by the entire necrotic core in contact with the lumen (white and red lines) and specifically the angle occupied by the major confluent necrotic core in contact with the lumen (red lines).

Remodelling was assessed by means of the remodelling index (RI), expressed as the EEM CSA at the site of minimum luminal area divided by the reference EEM CSA as previously described[11,16,17].

The reference site was ≤10 mm proximal to the selected lesion[18]. There were no major side branches between the MLA and reference sites. We defined positive remodelling as RI ≥ 1.05 and negative remodelling as RI ≤ 0.95. Values in between were considered neutral (no remodelling). IVUS-derived TCFA (IDTCFA)[9], is defined as a lesion fulfilling the following criteria in at least 3 consecutive CSAs: 1) plaque burden ≥ 40%; 2) confluent necrotic core ≥ 10%[19] in direct contact with the lumen in the investigated CSA (Figure 2). All consecutive CSAs having the same morphologic characteristics were considered as part of the same IDTCFA lesion.

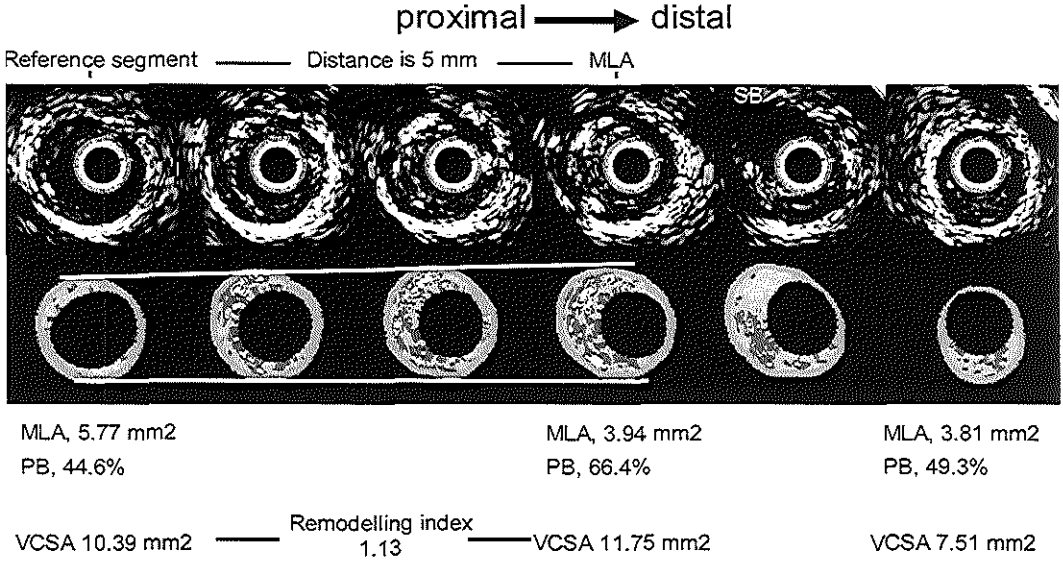

Figure 2. The figure shows the IVUS grey scale and the corresponding IVUS-VH frames of an IVUS derived thin cap fibro-atheroma (four central frames) and the proximal and distal reference segment in which the remodelling index was calculated. MLA, minimum luminal area; PB, plaque burden; VCSA, vessel cross sectional area.

Statistical analysis

Discrete variables are presented as counts and percentages. Continuous variables are presented as means ±SD. A two-sided p value of less than 0.05 indicated statistical significance. Assumptions for normality were checked after transformation based on a p-value >0.20 at Kolmogorov-Smirnov test and by visual assessment of Q-Q plots of residuals. Accordingly, log transformation was performed on the variables with skewed distribution.

To compare CSAs with and without NCCL, in a General Estimating Equations model, with binomial distribution and a logit link function, cases were regarded as a random factor (as we had multiple observations for each patient); we also allowed for an autoregressive correlation structure and the vessel was a fixed factor in the model. Statistical analyses were performed with use of SPSS software version 11.5.

Results

Twenty-one (63 vessels) consecutive patients were included in this study. The baseline characteristics of the patient population are depicted in Table 1. The mean age was 52.9±7.8 years, most being male patients (71.4%). Sixty-six percent of the patients presented with acute myocardial infarction. The culprit vessel was the left anterior descending (LAD) in 47.6%, the left circumflex (LCX) in 23.8% and the right coronary artery (RCA) in 28.6% of the patients. The mean length of the IVUS pull-back was 45.7±22.9 mm.

IVUS-VH findings

A total of 6,351 CSAs were analysed with IVUS-VH. Necrotic core in contact with the lumen was found in 71.7% (4556/6351) of CSAs. These CSAs had a mean area of necrotic core in contact with the lumen of 0.59±0.72 mm² which corresponds to 13.8±10.7% of the total plaque area; on average 53.8±35.2% of the total amount of necrotic core present in a CSA was in contact with the lumen and the angle occupied by the necrotic core in the luminal circumference was 30.3±34.8°. Nearly all the geometrical and compositional parameters of the CSA with NCCL were significantly different compared with CSAs without necrotic core in contact with the lumen (Table 2). Specifically, CSAs with NCCL had a higher plaque burden compared to CSAs without NCCL, 42.8±11.5% vs. 32.8±11.5%, p<0.001 and more necrotic core and calcified tissue compared to the ones without NC in contact with the lumen, 13.8±10.7% vs. 2.3±7.9% (p<0.001) and 4.6±6.4 vs. 0.59±2.1% (p<0.001) respectively.

Table 1. Baseline characteristics, n=21

Age, yrs (mean±SD)	52.9±7.8
Male %	71.4
Body mass index, kg/m² (mean±SD)	27.3±4.2
Diabetes mellitus %	33.3
Hypertension %	33.3
Family history of CHD %	42.9
Current smoking %	71.4
Hypercholesterolaemia %	33.3
Previous ACS %	14.3
Previous PCI %	28.6
Clinical presentation %	
Unstable angina/Non-ST-segment elevation MI	33.3
ST-elevation MI	66.7
Culprit vessel %, n=21	
Left anterior descending	47.6
Left circumflex	23.8
Right coronary artery	28.6

SD, standard deviation; CHD, cardiovascular heart disease; ACS, acute coronary syndrome; PCI, percutaneous coronary intervention; MI, myocardial infarction.

Table 2. Compositional and geometrical analysis of CSAs with necrotic core in contact with the lumen.

	NC No contact (1795 CSAs)		NC Contact (4556 CSAs)		
	Mean	SD	Mean	SD	p value
Calcified mm²	0.02	0.06	0.21	0.38	0.03
Calcified %	0.59	2.1	4.6	6.4	<0.001
Fibrous mm²	1.5	1.7	2.6	1.8	0.01
Fibrous %	66.3	17.4	62.7	12.0	0.03
Fibrolipid mm²	0.68	0.85	0.84	0.86	0.86
Fibrolipid %	30.7	18.0	18.9	11.6	0.60
Necrotic core mm²	0.04	0.12	0.59	0.72	0.005
Necrotic core %	2.27	7.9	13.8	10.7	<0.001
Vessel CSA mm²	16.7	5.6	18.0	6.6	0.24
Lumen CSA mm²	11.2	4.2	10.3	4.6	0.29
Plaque CSA mm²	5.5	2.9	7.6	3.4	0.006
Plaque eccentricity	0.11	0.12	0.18	0.16	0.65
Plaque burden %	32.5	11.2	42.8	11.5	<0.001

NC, necrotic core; CSA, cross sectional area.

Overall, there were 805 (12.7%) CSAs with confluent NCCL >10%; among these only 430 CSAs had a PB >40% (Table 3).

Table 3. Number of CSAs according to the amount of confluent necrotic core in contact with the lumen and plaque burden >40%.

	Overall, n=6351	CSAs with PB >40%, n=2886
Confluent NCCL >10%	805(12.7%)	430(14.9%)
Confluent NCCL >15%	385(6.1%)	198(6.9%)
Confluent NCCL >20%	218(3.4%)	105(3.6%)
Confluent NCCL >25%	125(2%)	44(1.5%)
Confluent NCCL >30%	73(1.1%)	23(0.8%)

NCCL, necrotic core in contact with the lumen; CSA, cross-sectional area; PB, plaque burden

IVUS-derived thin cap fibro-atheroma

A total of 42 IDTCFAs were detected in the 21 patients. However, 13 patients had at least one IDTCFA in their coronary tree (38.1% of the population did not have any IDTCFA). Thus, on average there were 2 IDTCFAs per patient. Seventeen IDTCFAs were found in the LAD, 12 in the LCX and 13 in the RCA. In 7 patients at least one

other IDTCFA was found in a different vessel and in 13 vessels more than one IDTCFA was found in the same vessel (Table 4).

Table 4. Description of the multifocal aspect of IDTCFA.

	IDTCFA n=42
No. patients with:	
One	13
Two	9
Three	8
Four or more	5
No. of vessels with:	
One	23
Two	13
Three	6
Four or more	1
No. of patients with one IDTCFA in at least one other vessel	7

CSA, cross-sectional area; IDTCFA, IVUS-derived thin cap fibro-atheroma

The mean IDTCFA lesion length was 4.8±2.8 mm (Range: 0.95-13.5 mm) and the remodelling index was 1.09±0.21. In three IDTCFAs it was not possible to measure the remodelling index due to lack of reference segment; two of them were located in the proximal LAD, so the only segment without disease proximal to the lesion was the left main artery. Five (11.9%) IDTCFAs had negative remodelling, 14 (33.3%) no remodelling and 20 (47.6%) had positive remodelling. The IDTCFAs were divided into three different categories according to the largest confluent necrotic core in contact with the lumen, largest confluent NCCL < 20%, NCCL between 20-30% and NCCL >30%. Subsequently, the remodelling index was plotted against these three categories (Figure 3). The overall mean necrotic core was 26.5±9.7%, and the major area of confluent NC that was in contact with the lumen was 12.2±8.0% which represented 44.9±21.2% of the total amount of NC present in the CSA. The circumference occupied by the confluent NCCL was 27.6±17.5°. The mean plaque burden was 50.3±8.5, whilst the vessel CSA and lumen CSA were15.4±6.2 mm2 and 7.6±3.3 mm^2 respectively (Table 5).

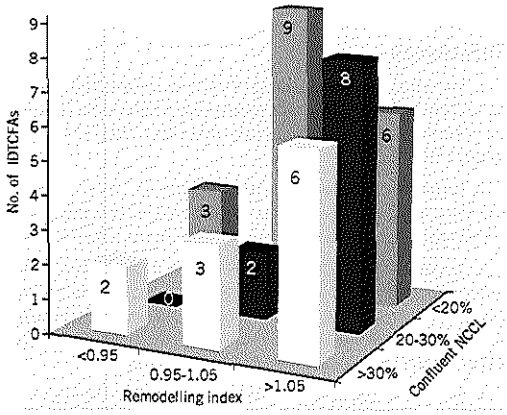

Figure 3. Bar graph shows the number of IVUS-derived thin cap fibro-atheroma according to the largest confluent necrotic core in contact with the lumen (NCCL) and the remodelling index. It seems that among the IDTCFAs there are different degrees of disease, possibly with different likelihoods of rupture.

Table 5. Characteristics of IVUS-derived thin cap fibro-atheroma.

	IDTCFA, n=42	
	Mean	**SD**
Calcified mm^2	0.35	0.38
Calcified %	7.6	7.0
Fibrous mm^2	2.5	1.7
Fibrous %	54.4	10.6
Fibrolipid mm^2	0.56	0.65
Fibrolipid %	11.5	8.5
Necrotic core mm^2	1.2	0.81
Necrotic core %	26.5	9.7
Major confluent NC in contact with the lumen		
– Area mm^2	0.68	0.58
– % out of the total NC	45.0	21.2
– % out of the total PCSA	12.2	8.0
– Angle of the NC (degrees)	27.6	17.5
Vessel CSA mm^2	15.4	6.2
Lumen CSA mm^2	7.6	3.3
Plaque CSA mm^2	7.8	3.4
Plaque eccentricity	0.21	0.16
Plaque burden %	50.3	8.5
Length (mm)	4.8	2.8
Remodelling index	1.1	0.21

NC, necrotic core; CSA, cross sectional area; PCSA, plaque CSA; SD, standard deviation.

Discussion

The main findings of this study that included 21 patients (63 vessels) with acute coronary syndrome are: 1) on average there were 2 IDTCFAs per patient; 2) after treatment of the culprit lesion, 38.1% of the population did not have any IDTCFA; 3) CSAs with NC in contact with the lumen were more obstructive and with larger vessel CSA than their counterparts without NC in contact with the lumen; 4) CSAs with NC in contact with the lumen had also larger necrotic core and calcified tissue compared to the ones without NC in contact with the lumen; 5) Nearly half of the IDTCFAs had positive remodelling.

To date, there is no single isolated marker of vulnerability that can accurately and precisely identify atherosclerotic plaques at risk of rupture. On the contrary, it seems that the *in vivo* simultaneous assessment of acknowledged high-risk atherosclerotic plaque characteristics may improve the accuracy to reliably identify vulnerable plaques. For the first time IDTCFA and remodelling index are assessed in an *in vivo* three vessel IVUS-VH based study in patients with acute coronary syndrome.

Trying to understand the atherosclerosis process has continued for more than a century, and while many paradigms have lost importance, others still remain. Specifically, although vast information with respect to the pathophysiology of acute coronary syndromes has been published, only a few concepts are today generally accepted. First, the former belief that acute coronary syndromes originate exclusively from flow-limiting stenoses has shifted to well-defined histological plaque phenotypes. These plaques have particular characteristics, such as large necrotic core, thin fibrous cap, inflammation within the cap and positive remodelling[4,12,20-22]. Nevertheless, to date, the natural history of lesions with these characteristics remains unknown and the limited knowledge about their eventual prognosis is provided by retrospective histopathological studies[7,23]. Second, inflammation plays an important part in the development and growth of such plaques, and most importantly in triggering unpredictable rupturing events[24]. Third, the multifocal distribution of vulnerable plaques has been proven by means of pathology[1], angiography[25], angioscopy[20], IVUS[26], palpography[27] and lately IVUS-VH[9]. This latter concept is once again demonstrated in this study, where in 33.3% (7/21) of the patients IDTCFAs were present in at least two vessels. Moreover, in 31.7% of the vessels, two or more IDTCFAs were detected.

Spectral analysis of IVUS radiofrequency data has been used as a tool to assess plaque composition and remodelling[11,12], since they are acquired in one single pull-back, simultaneous and complementary information can be retrieved. The previous manuscript from our group reporting the incidence of IDTCFA is essentially similar from the methodological point of view, but dramatically different from the quantitative point of view. So in the first report by Rodriguez-Granillo et al[9], one of the criteria was the presence of NC>10% in a CSA with some NC in contact with the lumen, without considering its distribution along the luminal circumference (spotty or confluent). Thus, the main difference with the approach used in this report is the fact that the CSAs were included only if the necrotic core was confluent and this pool of NC represented more than 10% of the tissue present in the CSA and was in direct contact with the lumen. This different methodology may impact on the reported incidence of vulnerable plaque, but it offers a definition which is closer to the pathological one. Nevertheless, the inability to precisely measure the thickness of the fibrous cap makes our observations a surrogate of the pathological TCFA.

Positive remodelling has been associated with an unstable clinical presentation[17,28] and with characteristic pathological[6] and IVUS-VH[11] lesion types. In line with these previous reports, the remodelling index found in this study shows the outward growth of these types of plaques. Some lipid lowering trials using conventional IVUS have suggested that there is a change in "composition" after a period of treatment[29], whilst another with a similar design reported a change in the remodelling index[18]. IVUS-VH offers the opportunity to follow-up these lesions and to correlate longitudinally and simultaneously the composition and the change in the remodelling index. It seems that among IDTCFAs there is different degree of disease. Not all of them have positive remodelling. The only opportunity to know if there is a different degree of risk among the same type of lesion is to look back into the pathological studies to learn which TCFAs have been undergone rupture. It is clear that ruptured plaque have more necrotic core, macrophage infiltration, calcification, less smooth muscles cells and more positive remodelling than TCFAs[30]. We can then conclude that those IDTCFAs having abundant necrotic core with positive remodelling have a higher risk, and it turns out that in this study these are few in number.

The clinical implications of these findings are manifold. First, the capability of simultaneously assessing more than one of the different acknowledged features of "high-risk" plaques could potentially enhance the prognostic value of the invasive detection of vulnerable plaque. Second, this combined assessment can potentially identify very high-risk plaques, thereby lowering the number of vulnerable plaques that deserve to be followed and ultimately treated.

Limitations

Although we have included all consecutive patients with three vessel IVUS assessment in a defined period of time, the sample size is small.

In general, the more severely diseased part of the vessel was stented before IVUS acquisition eliminating the analysis of potentially the most pathological region of interest.

The inferior axial resolution of IVUS-VH in comparison to histology remains a major handicap, but is partially compensated by the higher sampling rate of the ultrasonic approach when compared to the pathologic.

Conclusions

Cross sectional areas with necrotic core in contact with the lumen had a worse morphological profile than the ones without NC in contact with the lumen. The simultaneous assessment of IDTCFA and remodelling index identifies a reduced number of high-risk plaques. The findings of this study have potentially important clinical implications, since for the first time it sheds light into the possibility to follow these plaques after pharmacological treatment and/or to treat them locally.

References

1. Virmani R, Kolodgie FD, Burke AP, Farb A, Schwartz SM. Lessons from sudden coronary death: a comprehensive morphological classification scheme for atherosclerotic lesions. *Arterioscler Thromb Vasc Biol.* 2000;20:1262-75.

2. Davies MJ, Richardson PD, Woolf N, Katz DR, Mann J. Risk of thrombosis in human atherosclerotic plaques: role of extracellular lipid, macrophage, and smooth muscle cell content. *Br Heart J.* 1993;69:377-81.

3. Schaar JA, Muller JE, Falk E, Virmani R, Fuster V, Serruys PW, Colombo A, Stefanadis C, Ward Casscells S, Moreno PR, Maseri A, van der Steen AF. Terminology for high-risk and vulnerable coronary artery plaques. Report of a meeting on the vulnerable plaque, June 17 and 18, 2003, Santorini, Greece. *Eur Heart J.* 2004;25:1077-82.

4. Schaar JA, De Korte CL, Mastik F, Strijder C, Pasterkamp G, Boersma E, Serruys PW, Van Der Steen AF. Characterizing vulnerable plaque features with intravascular elastography. *Circulation.* 2003; 108: 2636-41.

5. Loree HM, Kamm RD, Stringfellow RG, Lee RT. Effects of fibrous cap thickness on peak circumferential stress in model atherosclerotic vessels. *Circ Res.* 1992;71:850-8.

6. Burke AP, Kolodgie FD, Farb A, Weber D, Virmani R. Morphological predictors of arterial remodeling in coronary atherosclerosis. *Circulation.* 2002;105:297-303.

7. Burke AP, Kolodgie FD, Farb A, Weber DK, Malcom GT, Smialek J, Virmani R. Healed plaque ruptures and sudden coronary death: evidence that subclinical rupture has a role in plaque progression. *Circulation.* 2001;103:934-40.

8. Murray CJ, Lopez AD. Alternative projections of mortality and disability by cause 1990-2020: Global Burden of Disease Study. *Lancet.* 1997;349:1498-504.

9. Rodriguez-Granillo GA, Garcia-Garcia HM, Mc Fadden EP, Valgimigli M, Aoki J, de Feyter P, Serruys PW. *In vivo* intravascular ultrasound-derived thin-cap fibroatheroma detection using ultrasound radiofrequency data analysis. *J Am Coll Cardiol.* 2005;46:2038-42.

10. Valgimigli M, Rodriguez-Granillo GA, Garcia-Garcia HM, Malagutti P, Regar E, de Jaegere P, de Feyter P, Serruys PW. Distance from the ostium as an independent determinant of coronary plaque composition *in vivo*: an intravascular ultrasound study based radiofrequency data analysis in humans. *Eur Heart J.* 2006;27:655-63.

11. Rodriguez-Granillo GA, Serruys PW, Garcia-Garcia HM, Aoki J, Valgimigli M, van Mieghem CA, McFadden E, de Jaegere PP, de Feyter P. Coronary artery remodelling is related to plaque composition. *Heart.* 2006;92:388-91.

12. Nair A, Kuban BD, Tuzcu EM, Schoenhagen P, Nissen SE, Vince DG. Coronary plaque classification with intravascular ultrasound radiofrequency data analysis. Circulation. 2002;106:2200-6.

13. Nasu K, Tsuchikane E, Katoh O, Vince DG, Virmani R, Surmely JF, Murata A, Takeda Y, Ito T, Ehara M, Matsubara T, Terashima M, Suzuki T. Accuracy of *in vivo* coronary plaque morphology assessment: a validation study of *in vivo* virtual histology compared with *in vitro* histopathology. *J Am Coll Cardiol.* 2006;47:2405-12.

14. Käresen KF BE. Blind deconvolution of ultrasonic traces accounting for pulse variance. *IEEE Trans Ultrason Ferroelectr Freq Control.* 1999; 46:564-573.

15. Nair A VD. 'Blind' data calibration of intravascular ultrasound data for automated tissue characterization. *IEEE ultrasonics symposium.* 2004:1126-1129.

16. Nakamura M, Nishikawa H, Mukai S, Setsuda M, Nakajima K, Tamada H, Suzuki H, Ohnishi T, Kakuta Y, Nakano T, Yeung AC. Impact of coronary artery remodeling on clinical presentation of coronary artery disease: an intravascular ultrasound study. *J Am Coll Cardiol.* 2001;37:63-9.

17. Schoenhagen P, Ziada KM, Kapadia SR, Crowe TD, Nissen SE, Tuzcu EM. Extent and direction of arterial remodeling in stable versus unstable coronary syndromes: an intravascular ultrasound study. *Circulation.* 2000;101:598-603.

18. Schoenhagen P, Tuzcu EM, Apperson-Hansen C, Wang C, Wolski K, Lin S, Sipahi I, Nicholls SJ, Magyar WA, Loyd A, Churchill T, Crowe T, Nissen SE. Determinants of arterial wall remodeling during lipid-lowering therapy: serial intravascular ultrasound observations from the Reversal of Atherosclerosis with Aggressive Lipid Lowering Therapy (REVERSAL) trial. *Circulation.* 2006;113:2826-34.

19. Virmani R, Burke AP, Kolodgie FD, Farb A. Vulnerable plaque: the pathology of unstable coronary lesions. *J Interv Cardiol.* 2002;15:439-46.

20. Asakura M, Ueda Y, Yamaguchi O, Adachi T, Hirayama A, Hori M, Kodama K. Extensive development of vulnerable plaques as a pan-coronary process in patients with myocardial infarction: an angioscopic study. *J Am Coll Cardiol.* 2001;37:1284-8.

21. Romer TJ, Brennan JF, 3rd, Fitzmaurice M, Feldstein ML, Deinum G, Myles JL, Kramer JR, Lees RS, Feld MS. Histopathology of human coronary atherosclerosis by quantifying its chemical composition with Raman spectroscopy. *Circulation.* 1998;97:878-85.

22. Jang IK, Tearney GJ, MacNeill B, Takano M, Moselewski F, Iftima N, Shishkov M, Houser S, Aretz HT, Halpern EF, Bouma BE. *In vivo* characterization of coronary atherosclerotic plaque by use of optical coherence tomography. *Circulation.* 2005;111:1551-5.

23. Burke AP, Farb A, Malcom GT, Liang YH, Smialek J, Virmani R. Coronary risk factors and plaque morphology in men with coronary disease who died suddenly. *N Engl J Med.* 1997;336:1276-82.

24. Mauriello A, Sangiorgi G, Fratoni S, Palmieri G, Bonanno E, Anemona L, Schwartz RS, Spagnoli LG. Diffuse and active inflammation occurs in both vulnerable and stable plaques of the entire coronary tree: a histopathologic study of patients dying of acute myocardial infarction. *J Am Coll Cardiol.* 2005;45:1585-93.

25. Goldstein JA, Demetriou D, Grines CL, Pica M, Shoukfeh M, O'Neill WW. Multiple complex coronary plaques in patients with acute myocardial infarction. *N Engl J Med.* 2000;343:915-22.

26. Rioufol G, Finet G, Ginon I, Andre-Fouet X, Rossi R, Vialle E, Desjoyaux E, Convert G, Huret JF, Tabib A. Multiple atherosclerotic plaque rupture in acute coronary syndrome: a three-vessel intravascular ultrasound study. *Circulation.* 2002;106:804-8.

27. Schaar JA, Regar E, Mastik F, McFadden EP, Saia F, Disco C, de Korte CL, de Feyter PJ, van der Steen AF, Serruys PW. Incidence of high-strain patterns in human coronary arteries: assessment with three-dimensional intravascular palpography and correlation with clinical presentation. *Circulation.* 2004;109:2716-9.

28. Pasterkamp G, Schoneveld AH, van der Wal AC, Haudenschild CC, Clarijs RJ, Becker AE, Hillen B, Borst C. Relation of arterial geometry to luminal narrowing and histologic markers for plaque vulnerability: the remodeling paradox. *J Am Coll Cardiol.* 1998;32:655-62.

29. Schartl M, Bocksch W, Koschyk DH, Voelker W, Karsch KR, Kreuzer J, Hausmann D, Beckmann S, Gross M. Use of intravascular ultrasound to compare effects of different strategies of lipid-lowering therapy on plaque volume and composition in patients with coronary artery disease. *Circulation.* 2001;104:387-92.

30. Kolodgie FD, Virmani R, Burke AP, Farb A, Weber DK, Kutys R, Finn AV, Gold HK. Pathologic assessment of the vulnerable human coronary plaque. *Heart.* 2004;90:1385-91.

CHAPTER 5.2

In vivo intravascular ultrasound-derived thin-cap fibroatheroma detection using ultrasound radiofrequency data analysis.

Rodriguez-Granillo GA, **Garcia-Garcia HM**, Mc Fadden EP, Valgimigli M, Aoki J, de Feyter P, Serruys PW.

J Am Coll Cardiol. 2005;46:2038-42.

In Vivo Intravascular Ultrasound-Derived Thin-Cap Fibroatheroma Detection Using Ultrasound Radiofrequency Data Analysis

Gastón A. Rodriguez-Granillo, MD, Héctor M. García-García, MD, Eugène P. Mc Fadden, MD, FRCPI, Marco Valgimigli, MD, Jiro Aoki, MD, Pim de Feyter, MD, PhD, Patrick W. Serruys, MD, PhD

Rotterdam, the Netherlands

OBJECTIVES The purpose of this study was to assess the prevalence of intravascular ultrasound (IVUS)-derived thin-cap fibroatheroma (IDTCFA) and its relationship with the clinical presentation using spectral analysis of IVUS radiofrequency data (IVUS-Virtual Histology [IVUS-VH]).

BACKGROUND Thin-cap fibroatheroma lesions are the most prevalent substrate of plaque rupture.

METHODS In 55 patients, a non-culprit, non-obstructive (<50%) lesion was investigated with IVUS-VH. We classified IDTCFA lesions as focal, necrotic core-rich (≥10% of the cross-sectional area) plaques being in contact with the lumen; IDTCFA definition required a percent atheroma volume (PAV) ≥40%.

RESULTS Acute coronary syndrome (ACS) (n = 23) patients presented a significantly higher prevalence of IDTCFA than stable (n = 32) patients (3.0 [interquartile range (IQR) 0.0 to 5.0] vs. 1.0 [IQR 0.0 to 2.8], p = 0.018). No relation was found between patient's characteristics such as gender (p = 0.917), diabetes (p = 0.217), smoking (p = 0.904), hypercholesterolemia (p = 0.663), hypertension (p = 0.251), or family history of coronary heart disease (p = 0.136) and the presence of IDTCFA. A clear clustering pattern was seen along the coronaries, with 35 (35.4%), 31 (31.3%), 19 (19.2%), and 14 (14.1%) IDTCFAs in the first 10 mm, 11 to 20 mm, 21 to 30 mm, and ≥31 mm segments, respectively, p = 0.008. Finally, we compared the severity (mean PAV 56.9 ± 7.4 vs. 54.8 ± 6.0, p = 0.343) and the composition (mean percent necrotic core 19.7 ± 4.1 vs. 18.1 ± 3.0, p = 0.205) of IDTCFAs between stable and ACS patients, and no significant differences were found.

CONCLUSIONS In this in vivo study, IVUS-VH identified IDTCFA as a more prevalent finding in ACS than in stable angina patients. (J Am Coll Cardiol 2005;46:2038–42) © 2005 by the American College of Cardiology Foundation

Sudden cardiac death or unheralded acute coronary syndromes (ACS) are common initial manifestations of coronary atherosclerosis, and most such events occur at sites of non-flow limiting coronary atherosclerosis (1,2). Autopsy data suggest that plaque composition is a key determinant of the propensity of atherosclerotic lesions to provoke clinical events. Thin-cap fibroatheroma (TCFA) plaques with large avascular, hypocellular lipid cores seem particularly prone to rupture and result in epicardial occlusion (3–5).

Careful systematic evaluation, in a large series of victims of sudden cardiac death, suggested that ruptured TCFA was the precipitating factor for 60% of acute coronary thrombi. Furthermore, 70% of those patients had other TCFAs that had not ruptured (5).

Intravascular ultrasound (IVUS) is the gold standard for evaluation of coronary plaque, lumen, and vessel dimensions (6,7). However, although visual interpretation of gray-scale IVUS can identify calcification within plaques, it cannot reliably differentiate lipid-rich from fibrous plaque (7). Recently, spectral analysis of IVUS radiofrequency data (IVUS-Virtual Histology [IVUS-VH]) has demonstrated potential to provide detailed quantitative information on plaque composition and morphology and has been validated in studies of explanted human coronary segments (8).

In the present study, we evaluated the prevalence of IVUS-derived TCFA (IDTCFA) in coronary artery segments with non-significant lesions on angiography using IVUS-VH.

METHODS

In 55 patients, a non-culprit, de novo, angiographically non-obstructive (<50%) lesion was investigated with IVUS-VH. Written informed consent was obtained from all patients.

IVUS-VH acquisition and analysis. Details regarding the validation of the technique on explanted human coronary segments have previously been reported (8). Briefly, IVUS-VH uses spectral analysis of IVUS radiofrequency data to construct tissue maps that classify plaque into four major components (fibrous [labeled green], fibrolipidic [labeled greenish-yellow], necrotic core [labeled red], and calcium [labeled white]) which were correlated with a specific spectrum of the radiofrequency signal and assigned color codes (8).

Intravascular Ultrasound-Virtual Histology data were acquired after intracoronary administration of nitrates using a continuous pullback (Ultracross 2.9-F 30-MHz catheter, Boston Scientific, Santa Clara, California), by a dedicated

From the Erasmus Medical Center, Thoraxcenter, Rotterdam, the Netherlands.

Manuscript received May 25, 2005; revised manuscript received June 24, 2005, accepted July 25, 2005.

Abbreviations and Acronyms

ACS	= acute coronary syndrome
IDTCFA	= intravascular ultrasound-derived thin-cap fibroatheroma
IQR	= interquartile range
IVUS	= intravascular ultrasound
IVUS-VH	= Intravascular Ultrasound-Virtual Histology
LAD	= left anterior descending coronary artery
LCX	= left circumflex artery
PAV	= percent atheroma
RCA	= right coronary artery
ROI	= region of interest
TCFA	= thin-cap fibroatheroma

IVUS-VH console (Volcano Therapeutics, Rancho Cordova, California). The IVUS-VH data were stored on a CD-ROM and sent to the imaging core lab for offline analysis. Intravascular ultrasound B-mode images were reconstructed from the radiofrequency data by customized software (IVUSLab, Volcano Therapeutics, Rancho Cordova, California). Manual contour detection of both the lumen and the media-adventitia interface was performed, and the radiofrequency data were normalized using a technique known as "blind deconvolution," an iterative algorithm that deconvolves the catheter transfer function from the backscatter, thus accounting for catheter-to-catheter variability (9). Geometric and compositional data were obtained for every slice and expressed as mean percent for each component. The plaque eccentricity index (EI) was calculated by dividing the minimum plaque thickness by the maximum plaque thickness. Percent atheroma volume (PAV) was defined as: $EEM_{area} - lumen_{area}/EEM_{area} \times 100$, where EEM refers to external elastic membrane.

Subsequently, we evaluated the presence of IDTCFA lesions along the interrogated vessels, and their incidence and characteristics were determined. Finally, the spatial distribution of IDTCFA along the coronaries was evaluated starting from the ostium and dividing the vessel in 10-mm segments, evaluating a minimal length of 30 mm.

Definition of IDTCFA. Two experienced, independent IVUS analysts defined IDTCFA as a lesion fulfilling the following criteria in at least three consecutive frames: 1) necrotic core ≥10% without evident overlying fibrous tissue (Fig. 1); and 2) PAV ≥40%.

We selected this cutoff value because TCFA lesions are very unlikely present in segments with <40% occlusion (10). Cross sections with non-uniform rotational distortion artifact were excluded from the analysis.

Statistical analysis. Discrete variables are presented as counts and percentages. Continuous variables are presented as medians (25th, 75th percentile) or mean values ± SD when indicated. Pearson's chi-square or Fisher exact test, Student *t* test, and Wilcoxon rank-sum tests were performed, as indicated. A two-sided p value of <0.05 indicated statistical significance. Logistic regression analysis was performed to identify potential predictors of the presence of IDTCFA. Statistical analyses were performed with use of 11.5 SPSS software (SPSS Inc., Chicago, Illinois).

RESULTS

The baseline characteristics of the patients (n = 55) we studied are presented in Table 1. Thirty-four (61.8%) patients had at least one IDTCFA in the region of interest (ROI).

The population was prospectively divided into two groups, stable patients and patients presenting with ACS (defined as unstable angina, non–ST-segment elevation myocardial infarction, or ST-segment elevation myocardial infarction).

IDTCFA incidence and predictors. Acute coronary syndrome patients had a significantly higher incidence of IDTCFA than stable patients (3.0 [interquartile range (IQR) 0.0 to 5.0] vs. 1.0 [IQR 0.0 to 2.8], p = 0.018). When corrected for the length of the ROI, the density of

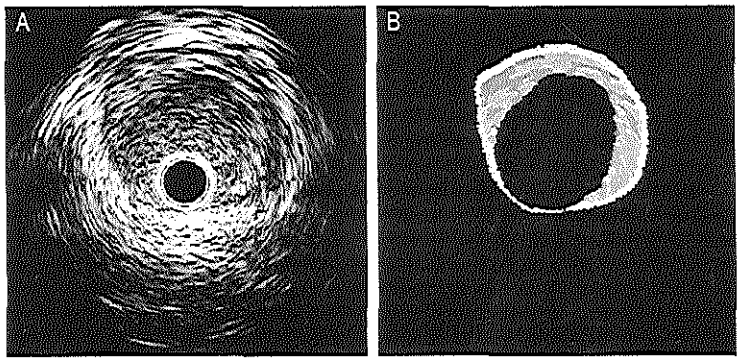

Figure 1. Left anterior descending artery depicted by Intravascular Ultrasound-Virtual Histology, where calcified, fibrous, fibrolipidic, and necrotic core regions are labeled **white**, **green**, **greenish-yellow**, and **red**, respectively. **Panel A** shows an intravascular ultrasound cross-sectional area reconstructed from backscattered signals. **Panel B** shows the corresponding tissue map depicting a necrotic core–rich plaque with necrotic core tissue in contact with the lumen.

Table 1. Baseline Characteristics (n = 55)

	n (%)
Age (yrs ± SD)	57.6 ± 9.5
Male gender	44 (80.0)
Diabetes	5 (9.1)
Hypertension	20 (36.4)
Current smoking	15 (27.3)
Previous smoking	14 (25.5)
Hypercholesterolemia	46 (83.6)
Family history of coronary disease	30 (54.5)
Vessel	
Right coronary artery	22 (40.0)
Left anterior descending	23 (41.8)
Left circumflex	10 (18.2)
Clinical presentation	
Stable	32 (58.2)
Acute coronary syndrome	23 (41.8)

IDTCFA remained statistically significant (0.7 [IQR 0.0 to 1.3] IDTCFA/cm vs. 0.2 [IQR 0.0 to 0.7] IDTCFA/cm, p = 0.031) (Table 2).

No relation was found between patient's characteristics such as gender (p = 0.917), diabetes (p = 0.217), smoking (p = 0.904), hypercholesterolemia (p = 0.663), hypertension (p = 0.251), or family history of coronary heart disease (p = 0.136) and the presence of IDTCFA.

Characteristics and location. We compared the severity (mean PAV 56.9 ± 7.4% vs. 54.8 ± 6.0%, p = 0.343) and the composition (mean percent necrotic core 19.7 ± 4.1% vs. 18.1 ± 3.0%, p = 0.205) of IDTCFAs between ACS and stable patients, and no significant differences were found. Although not significantly, the left anterior descending coronary artery (LAD) (73.9% of the LADs, n = 23) was the most frequent location, followed by the left circumflex artery (LCX) (60.0% of the LCXs, n = 10) and the right coronary artery (RCA) (50.0% of the RCAs, n = 22, p = 0.254).

Four patients were excluded from the spatial distribution subanalysis, three because the IVUS assessment of the ROI was shorter than 30 mm and the last one because the pullback did not reach the ostium. A total of 99 IDTCFA were present in vessels that met the aforementioned criteria. A clear clustering pattern was seen along the coronaries, with 35 (35.4%), 31 (31.3%), 19 (19.2%), and 14 (14.1%) IDTCFAs in the first 10 mm, 11 to 20 mm, 21 to 30 mm, and ≥31 mm segments, respectively, p = 0.008 (Fig. 2). The results showed a clear clustering pattern of the lesions along the coronaries, with 66 (66.7%) IDTCFA located in the first 20 mm, whereas further along the vessels the incidence was significantly lower (33, 33.3%, p = 0.008).

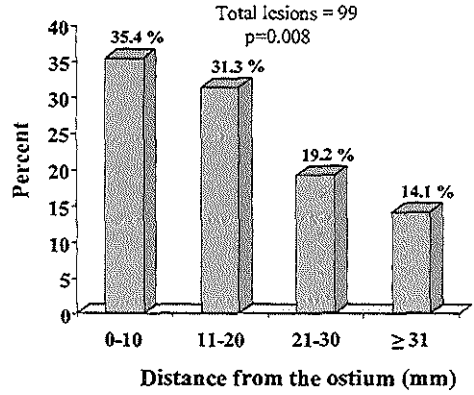

Figure 2. Bar graphs illustrating the frequency of intravascular ultrasound-derived thin-cap fibroatheroma (IDTFCA) starting from the ostium.

DISCUSSION

Post-mortem observations have documented several characteristic histological patterns that are substrates for sudden death related to epicardial coronary occlusion, of which the most common is TCFA (5,11,12). The same studies have demonstrated that plaque rupture at TCFAs may also occur without clinical consequences. The ability to identify TCFA in patients would both help clarify the natural history of TCFA and provide the means to assess the effects of pharmacological, or other, intervention.

Until recently, no technique could identify TCFA in vivo. However, spectral analysis of IVUS radiofrequency (IVUS-VH) data has demonstrated potential to provide detailed quantitative information both on overall plaque composition and on the anatomic relation of specific plaque components to the lumen of the vessel, and it has been validated in studies of explanted human coronary segments (8).

IDTCFA definition. It is well established that tissue shrinkage occurs during tissue fixation (13). Shrinkage of up to 60%, 15%, and 80% can occur during critical-point drying, free drying, and air drying, respectively (14). Furthermore, postmortem contraction of arteries is an additional confounding factor (15).

Although the most accepted threshold to define a cap as "thin" has been set at 65 μm (16), a number of important

Table 2. Incidence and Characteristics of IDTCFA Lesions in Stable and ACS Patients

	Length of ROI	IDTCFA	IDTCFA/cm	% PAV	% NC	EI
Stable (n = 32)	35.41 ± 11.6	1.0 (0.0, 2.8)	0.2 (0.0, 0.7)	54.8 ± 6.0	18.1 ± 3.0	0.23 ± 0.1
ACS (n = 23)	33.90 ± 15.0	3.0 (0.0, 5.0)	0.7 (0.0, 1.3)	56.8 ± 7.4	19.7 ± 4.1	0.27 ± 0.2
p value	0.684	0.018	0.031	0.343	0.205	0.35

Continuous variables are presented as medians (25th, 75th percentile) or mean values ± SD when indicated.

ACS = acute coronary syndrome; EI = plaque eccentricity index (defined as minimum plaque thickness divided by maximum plaque thickness); IDTCFA = intravascular ultrasound-derived thin-cap fibroatheroma; % PAV = percent atheroma volume (defined as EEM_{area} − $lumen_{area}$/EEM_{area} × 100, where EEM refers to external elastic membrane); ROI = region of interest; % NC = percent necrotic core of the cross-sectional area.

ex vivo studies have used higher (>200 μm) thresholds (4,17,18). Indeed, one of these studies identified a mean cap thickness of 260 and 360 μm for "vulnerable" and "non-vulnerable" plaques, respectively (18). Because the axial resolution of IVUS-VH is between 100 to 150 μm, we assumed that the absence of visible fibrous tissue overlying a necrotic core suggested a cap thickness of below 100 to 150 μm and used the absence of such tissue to define a thin fibrous cap (19). Figure 1 depicts a typical example of IDTCFA.

Incidence, characteristics, and distribution of IDTCFA. The major findings of our study were first that IVUS-VH findings, compatible with IDTCFA, were common in non-culprit lesions of patients undergoing percutaneous intervention in another vessel. Second, the prevalence of IDTCFA was significantly higher in patients who presented with ACS compared to stable patients. In addition, the distribution of IDTCFA lesions along the coronary vessels was clearly clustered. Finally, we found no significant correlation between the presence of conventional risk factors and the occurrence of IDTCFA.

In vivo studies established that a multifocal instability process is present in ACS (20,21). Rioufol et al. (20) found at least one plaque rupture remote from the culprit lesion in 80% of patients and from the culprit artery in 71% of patients (20). The significantly higher prevalence of IDTCFA in non-culprit coronaries of patients presenting with an ACS supports the theory that holds ACS as multifocal processes.

The distribution of the IDTCFA in the coronaries was in line with previous ex vivo and clinical studies, with a clear clustering pattern from the ostium, thus supporting the non-uniform distribution of vulnerable plaques along the coronary tree (22,23). Of note, the mean PAV and the mean necrotic core percentage of the IDTCFAs detected by IVUS-VH were also similar to previously reported histopathological data (55.9% vs. 59.6% and 19% vs. 23%, respectively) (10).

The large number of high-risk plaques found throughout the coronary tree by means of angiography, angioscopy, IVUS, and palpography, in addition to the unpredictability of the natural history of such lesions and the uncertainty about whether vulnerable plaque characteristics will subsequently lead to fatal or non-fatal ischemic events, suggests that potential local preventive strategies could not be cost-effective (12,20,21,24,25). On the contrary, a systemic "plaque stabilization" approach including statins and angiotensin-converting enzyme inhibitors could be capable of "cooling-down" the inflammatory burden.

To our knowledge, this is the first study to detect in vivo the presence of an IVUS surrogate of TCFA. This novel intravascular diagnostic tool could potentially aid the assessment of the effect of antiatherosclerotic drugs, and allow a more comprehensive pathophysiologic approach towards natural history studies.

Study limitations. The present was an observational study where we evaluated only one coronary artery per patient. The inferior axial resolution of IVUS-VH in comparison to histology could influence our results. This study does not directly assess the incremental value of IVUS-VH over visual identification of plaque characterization. The main finding of the study (IDTCFA) is only a surrogate of a histopathological finding. Besides, the lack of a direct comparison between IVUS-VH and histopathology renders our observation to some extent only exploratory. Accordingly, interpretation of our findings must be cautious. Prospective studies are needed in order to evaluate the prognostic value and natural history of such finding. The seemingly high prevalence of IDTCFA in comparison with histopathological studies is mainly driven by the sampling limitation of such studies and has previously been acknowledged (26).

Conclusions. In this in vivo study, IVUS-VH identified IDTCFA as a more prevalent finding in ACS than in stable angina patients. Prospective studies are needed in order to evaluate the prognostic value of such finding in natural history studies.

Reprint requests and correspondence: Dr. Patrick W. Serruys, Thoraxcenter, Bd406, Dr. Molewaterplein 40, 3015-GD Rotterdam, the Netherlands. E-mail: p.w.j.c.serruys@erasmusmc.nl.

REFERENCES

1. Ambrose JA, Tannenbaum MA, Alexopoulos D, et al. Angiographic progression of coronary artery disease and the development of myocardial infarction. J Am Coll Cardiol 1988;12:56–62.
2. Little WC, Constantinescu M, Applegate RJ, et al. Can coronary angiography predict the site of a subsequent myocardial infarction in patients with mild-to-moderate coronary artery disease? Circulation 1988;78:1157–66.
3. Davies MJ, Richardson PD, Woolf N, Katz DR, Mann J. Risk of thrombosis in human atherosclerotic plaques: role of extracellular lipid, macrophage, and smooth muscle cell content. Br Heart J 1993;69:377–81.
4. Felton CV, Crook D, Davies MJ, Oliver MF. Relation of plaque lipid composition and morphology to the stability of human aortic plaques. Arterioscler Thromb Vasc Biol 1997;17:1337–45.
5. Virmani R, Kolodgie FD, Burke AP, Farb A, Schwartz SM. Lessons from sudden coronary death: a comprehensive morphological classification scheme for atherosclerotic lesions. Arterioscler Thromb Vasc Biol 2000;20:1262–75.
6. Nishimura RA, Edwards WD, Warnes CA, et al. Intravascular ultrasound imaging: in vitro validation and pathologic correlation. J Am Coll Cardiol 1990;16:145–54.
7. Peters RJ, Kok WE, Havenith MG, Rijsterborgh H, van der Wal AC, Visser CA. Histopathologic validation of intracoronary ultrasound imaging. J Am Soc Echocardiogr 1994;7:230–41.
8. Nair A, Kuban BD, Tuzcu EM, Schoenhagen P, Nissen SE, Vince DG. Coronary plaque classification with intravascular ultrasound radiofrequency data analysis. Circulation 2002;106:2200–6.
9. Kåresen KF, Bølviken E. Blind deconvolution of ultrasonic traces accounting for pulse variance. IEEE Trans Ultrasoun Ferroelectr Freq Control 1999;46:564–73.
10. Virmani R, Burke AP, Kolodgie FD, Farb A. Vulnerable plaque: the pathology of unstable coronary lesions. J Interv Cardiol 2002;15:439–46.
11. Davies MJ, Thomas A. Thrombosis and acute coronary-artery lesions in sudden cardiac ischemic death. N Engl J Med 1984;310:1137–40.
12. Burke AP, Kolodgie FD, Farb A, et al. Healed plaque ruptures and sudden coronary death: evidence that subclinical rupture has a role in plaque progression. Circulation 2001;103:934–40.

13. Lee RM. A critical appraisal of the effects of fixation, dehydration and embedding of cell volume. In: Revel JP, Barnard T, Haggis GH, editors. The Science of Biological Specimen Preparation for Microscopy and Microanalysis. Scanning Electron Microscopy. Chicago, IL: AMF O'Hare, 1984:61–70.
14. Boyde A, Jones SJ, Tamarin A. Dimensional changes during specimen preparation for scanning electron microscopy. Scan Electron Microsc 1977;I:507–18.
15. Fishbein MC, Siegel RJ. How big are coronary atherosclerotic plaques that rupture? Circulation 1996;94:2662–6.
16. Burke AP, Farb A, Malcom GT, Liang YH, Smialek J, Virmani R. Coronary risk factors and plaque morphology in men with coronary disease who died suddenly. N Engl J Med 1997;336:1276–82.
17. Mann JM, Davies MJ. Vulnerable plaque. Relation of characteristics to degree of stenosis in human coronary arteries. Circulation 1996;94: 928–31.
18. Schaar JA, De Korte CL, Mastik F, et al. Characterizing vulnerable plaque features with intravascular elastography. Circulation 2003;108: 2636–41.
19. Nair ACD, Vince DG. Regularized autoregressive analysis of intravascular ultrasound data: improvement in spatial accuracy of plaque tissue maps. IEEE Trans Ultrason Ferroelectr Freq Control 2004;51: 420–31.
20. Rioufol G, Finet G, Ginon I, et al. Multiple atherosclerotic plaque rupture in acute coronary syndrome: a three-vessel intravascular ultrasound study. Circulation 2002;106:804–8.
21. Asakura M, Ueda Y, Yamaguchi O, et al. Extensive development of vulnerable plaques as a pan-coronary process in patients with myocardial infarction: an angioscopic study. J Am Coll Cardiol 2001;37: 1284–8.
22. Kolodgie FD, Burke AP, Farb A, et al. The thin-cap fibroatheroma: a type of vulnerable plaque: the major precursor lesion to acute coronary syndromes. Curr Opin Cardiol 2001;16:285–92.
23. Wang JC, Normand SL, Mauri L, Kuntz RE. Coronary artery spatial distribution of acute myocardial infarction occlusions. Circulation 2004;110:278–84.
24. Goldstein JA, Demetriou D, Grines CL, Pica M, Shoukfeh M, O'Neill WW. Multiple complex coronary plaques in patients with acute myocardial infarction. N Engl J Med 2000;343:915–22.
25. Schaar JA, Regar E, Mastik F, et al. Incidence of high-strain patterns in human coronary arteries: assessment with three-dimensional intravascular palpography and correlation with clinical presentation. Circulation 2004;109:2716–9.
26. Farb A, Tang AL, Burke AP, Sessums L, Liang Y, Virmani R. Sudden coronary death. Frequency of active coronary lesions, inactive coronary lesions, and myocardial infarction. Circulation 1995;92:1701–9.

CHAPTER 5.3

Global characterization of coronary plaque rupture phenotype using three-vessel intravascular ultrasound radiofrequency data analysis.

Rodriguez-Granillo GA, **Garcia-Garcia HM**, Valgimigli M, Vaina S, van Mieghem C, van Geuns RJ, van der Ent M, Regar E, de Jaegere P, van der Giesssen W, de Feyter P, Serruys PW.

Eur Heart J. 2006 Aug;27(16):1921-7

Global characterization of coronary plaque rupture phenotype using three-vessel intravascular ultrasound radiofrequency data analysis

Gastón A. Rodriguez-Granillo, Héctor M. García-García, Marco Valgimigli, Sophia Vaina, Carlos van Mieghem, Robert J. van Geuns, Maarten van der Ent, Evelyn Regar, Peter de Jaegere, Willem van der Giessen, Pim de Feyter, and Patrick W. Serruys*

Department of Cardiology of the Thoraxcenter, Erasmus MC, Bd-406, Dr Molewaterplein 40, PO Box 1738, 3015-GD Rotterdam, The Netherlands

Received 12 December 2005; revised 5 May 2006; accepted 26 May 2006; online publish-ahead-of-print 13 July 2006

See page 1889 for the editorial comment on this article (doi:10.1093/eurheartj/ehl129)

KEYWORDS
Plaque rupture;
Ultrasonography;
Atherosclerosis;
Vulnerable plaque

Aims To compare the global characteristics of patients with and without evidence of plaque rupture (PR) in their coronary tree and to evaluate the phenotype of ruptured plaques using intravascular ultrasound (IVUS) radiofrequency data analysis (IVUS-VH).

Methods and results Forty patients underwent three-vessel IVUS-VH interrogation. Twenty-eight PRs were diagnosed in 26 vessels (25.7% of the vessels studied) of 20 patients (50% of the population). Ruptures located in the left anterior descending were clustered in the proximal part of the vessel, whereas ruptures located in the right coronary artery were more distally located ($P = 0.02$). Patients with at least one PR presented larger body mass index (BMI) (28.4 ± 3.7 vs. 25.8 ± 2.6 kg/m^2, $P = 0.01$) and plaque burden (40.7 ± 7.6 vs. 33.7 ± 8.4%, $P = 0.01$) than patients without rupture, despite showing similar lumen cross-sectional area (9.6 ± 3.3 vs. 9.2 ± 2.3 mm^2, $P = 0.60$). Among current smokers, 66.7% presented a PR in their coronary tree. Finally, PR sites showed a higher content of necrotic core compared with minimum lumen area sites (17.48 ± 10.8 vs. 13.10 ± 6.5%, $P = 0.03$) and a trend towards higher calcified component.

Conclusion Patients with at least one PR in their coronary tree presented larger BMI and worse IVUS-derived characteristics compared with patients without PR.

Introduction

It has been established that coronary plaque rupture (PR) is the cause of death in a large proportion of sudden coronary death patients.[1] Despite its pre-conceived dire prognosis, retrospective studies have determined that PR is a common finding in both coronary and non-coronary sudden death patients.[1,2] In addition, clinically silent PR has been identified as a cause of plaque progression.[3,4] The fate of a given atherosclerotic plaque is thus linked not only to its severity but also to its histological composition, and the presence of a rich necrotic core has been consistently related to plaque fissuring.[5,6]

Intravascular ultrasound (IVUS) has been largely demonstrated to be an accurate diagnostic tool able to provide a high resolution, real-time, tomographic view of the coronary arteries. As such, several studies have portrayed the prevalence of PR in living patients by means of IVUS.[7,8] IVUS has, though, a suboptimal predictive value to estimate the composition of coronary arteries, particularly of lipid deposits.[9] In turn, spectral analysis of IVUS radiofrequency data has demonstrated improved accuracy for tissue characterization.[10] Besides, to date, no study has reported the global burden of the disease and its relationship with PR by means of IVUS.

The purpose of our study was two-fold: first, to compare the global characteristics of patients with and without evidence of PR in their coronary tree, and secondly, to evaluate the phenotype of ruptured against non-ruptured plaques using IVUS radiofrequency data analysis (IVUS-VH).

Methods

Patients

In this single-centre, investigators-driven, observational, prospective study, patients referred to our institution for elective or urgent PCI with the absence of extensive calcification, severe vessel tortuosity and haemodynamic instability and with suitable anatomy underwent IVUS interrogation of the three main epicardial coronary arteries. The patients included in this study, are part of published (IBIS-1)[11] and unpublished (LICO, BETAX) mono-centre studies conducted at our centre.

* Corresponding author. Tel: +31 10 4635260; fax: +31 10 4369154.
E-mail address: p.w.j.c.serruys@erasmusmc.nl

Patients with stable angina, unstable angina, and acute myocardial infarction (MI) were included. MI was diagnosed by an increase in the creatine kinase MB level to more than two-fold the normal limit. Acute coronary syndrome (ACS) patients encompassed patients presenting with unstable angina, non-ST-segment elevation MI, or ST-segment elevation MI. The institution's Ethics Committee approved the study protocol, which complies with the Declaration of Helsinki, and written informed consent was obtained from all patients.

Intravascular ultrasound

IVUS acquisition

The IVUS catheters used were commercially available mechanical and electronical catheters (Ultracross™ 30 MHz catheter, Boston Scientific, Santa Clara, USA; Eagle Eye™ 20 MHz catheter, Volcano Corporation, Rancho Cordova, USA). After administration of intracoronary nitrates, the IVUS catheter was introduced up to the distal coronary bed of the three coronary vessels. IVUS was aimed to be performed prior to any intervention. Using an automated pullback device, the transducer was withdrawn at a continuous speed of 0.5 mm/s until the ostium was seen. Cine runs, before and during contrast injection, were performed to define the position of the IVUS catheter before the pullback was started. IVUS-VH (Volcano Corporation) acquisition was ECG-gated using a dedicated console (Volcano Corporation). IVUS-VH data were stored on CD-ROM/DVD and sent to the imaging core lab for offline analysis.

IVUS-VH analysis

IVUS B-mode images were reconstructed from the RF data by customized software, and contour detection was performed using cross-sectional views with a semi-automatic contour detection software to provide geometrical and compositional output (IvusLab 3.0 for 30 MHz acquisitions and IvusLab 4.4 for 20 MHz acquisitions, respectively; Volcano Corporation). The RF data were normalized using a technique known as 'Blind Deconvolution', an iterative algorithm that deconvolves the catheter transfer function from the backscatter, thus accounting for catheter-to-catheter variablity.[11]

Details regarding the validation of IVUS-VH on explanted human coronary segments have previously been reported.[10] Briefly, IVUS-VH uses spectral analysis of IVUS radiofrequency data to construct tissue maps that classify plaque into four major components. In preliminary *in vitro* studies, four histological plaque components (fibrous, fibrolipidic, necrotic core, and calcium) were correlated with a specific spectrum of the radiofrequency signal.[10] These different plaque components were assigned colour codes. Calcified, fibrous, fibrolipidic, and necrotic core regions were labelled white, green, greenish-yellow, and red, respectively.

The contours of the external elastic membrane (EEM) and the lumen–intima interface enclosed an area that was defined as the coronary plaque plus media area. Plaque burden was calculated as $[(EEM_{area} - lumen_{area}/EEM_{area}) \times 100]$. Following a previously reported classification, PR was defined as a ruptured capsule with an underlying cavity (*Figure 1*) or plaque excavation by atheromatous extrusion with no visible capsule.[7,8] Rupture sites separated by at least 5 mm length of rupture-free vessel were considered as different ruptures. Screening for diagnosis of a PR required the independent review and agreement between two experienced IVUS observers (G.A.R.-G. and H.M.G.-G.), who had no knowledge about demographical data of the patients. Disagreement was solved by consensus between the observers. Lumen contour detection at the rupture site was performed following the intima–lumen interface, excluding the rupture cavity from the plaque cross-sectional area (CSA) calculation. Absolute geometrical data and absolute and relative compositional data were obtained for each CSA and an average was calculated for each coronary and for the total coronary tree. Finally, measurements were calculated in CSAs meeting criteria of PR and at the site of the minimum lumen area (MLA).

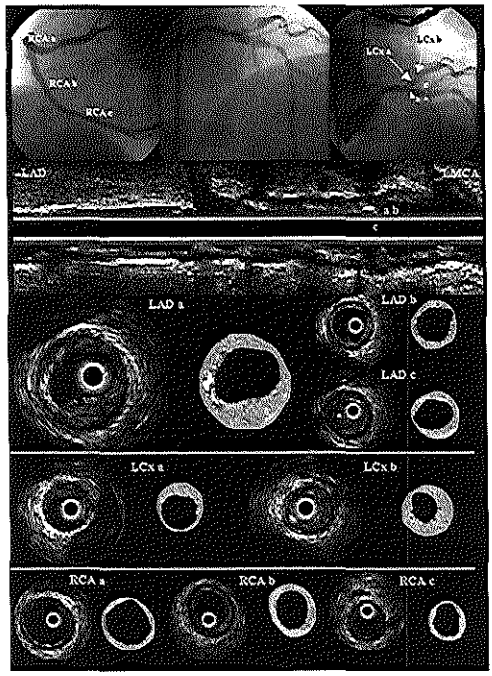

Figure 1 Three-vessel imaging using IVUS-VH (where calcified tissue is labelled as white, fibrous as green, fibrolipidic tissue as greenish-yellow, and necrotic core as red) in a 57-year-old male presenting with unstable angina. PR in the ostial LAD (LAD a). The underlying substrate of the cavity is rich in necrotic-core (red) and calcium (white), whereas the thrombus has migrated distally (LAD c, asterisk).

As pre-specified subanalysis, we compared the different geometrical and compositional characteristics of the three main epicardial coronaries. In addition, the difference between culprit/target and non-culprit/non-target vessels was assessed.

Statistical analysis

Discrete variables are presented as counts and percentages. Continuous variables are presented as means ± SD or medians (25th, 75th percentile) when indicated. On the basis of previous histopathological findings showing that ruptured plaques presented 34% of necrotic core, 10% more than non-ruptured plaques,[1] we calculated a sample size of 36 subjects to achieve a power of 80% to detect a true difference in population means, considering a type I error of 0.05 (two-sided) and a within group standard deviation of 15.

Comparisons between groups were performed using paired and independent Student's *t*-test, or χ^2 tests as indicated. For variables with a non-normal distribution, we used Kruskal–Wallis or Wilcoxon signed ranks tests as indicated. A two-sided *P*-value of less than 0.05 indicated statistical significance. Statistical analyses were performed with the use of SPSS software, version 13.0 (Chicago, IL, USA).

Results

Patients

Forty-six patients were included in the study protocol. Subsequently, six patients were excluded from the final analysis due to the absence of coronary plaque outside the

stented segment in one patient, and bad quality acquisition owed to non-continuous pullback in five patients. Accordingly, 40 non-consecutive patients were prospectively included in the study. IVUS interrogation of the three main coronaries was attempted in all patients. Two-vessel IVUS interrogation was achieved in all patients and three-vessel IVUS imaging was achieved in 31 (77.5%) cases. Five vessels were excluded from the analysis due to the lack of a diseased non-stented segment. Patient characteristics are provided in *Table 1*. The mean age was 55.7 ± 11.0 years. Twenty-nine (72.5%) patients were male. There was a low prevalence (10.0%) of diabetes. Thirteen (32.5%) patients presented with stable angina (SA), 12 (30.0%) with unstable angina, and 15 (37.5%) with AMI. The global geometrical and compositional characteristics of the coronary tree are presented in *Table 1*.

PR: prevalence and location

Twenty-eight PRs were diagnosed in 26 vessels (25.7% of the vessels studied) of 20 patients (50% of the population). Sixteen (59.3%) ACS patients presented at least one PR in their coronary tree, whereas such finding was observed in four (30.8%) stable patients. The tear was located in the shoulder of the plaque in 18 (64.3%) cases and in the centre of the plaque in 10 (35.7%) cases.

Ruptures were located in the left anterior descending (LAD) artery in 13 cases (34.2%), in the left circumflex (LCx) in seven cases (21.2%), and in the right coronary artery (RCA) in eight cases (24.2%). Ruptures located in the LAD were clustered in the proximal part of the vessel [median mm from the ostium (interquartile range, IQR): 14.16 (8.5–26.5)], ruptures located in the LCx were widely distributed [median (IQR): 21.9 (5.7–35.5)], and ruptures in the RCA were more distally located [median (IQR): 38.8 (28.8–60.0)]. PRs were located at the MLA in six cases (21.4%), proximal to the MLA in nine cases (32.1%) and distal to the MLA in 11 cases (39.3%). The MLA could not be identified accurately in two (7.1%) cases due to the presence of diffuse disease. Six (28.6%) of the culprit vessels of ACS contained a PR, whereas such finding was present in 16 (31.4%) of non-culprit vessels.

Multiple PR was present in six ACS patients (22% of all ACS patients). No multiple PR was identified in stable patients. Two patients presented two different ruptures in the same vessel.

Table 1 Baseline characteristics and average IVUS parameters ($n = 40$)

	n (%)
Age (years ± SD)	55.7 ± 11.0
Male sex	29 (72.5)
Diabetes	4 (10.0)
Hypertension	17 (42.5)
Current smoking	15 (37.5)
Previous smoking	6 (15.0)
Hypercholesterolaemia	20 (50.0)
Family history of coronary disease	19 (47.5)
Height (cm ± SD)	174.5 ± 9.2
Weight (kg ± SD)	82.8 ± 14.0
BMI (kg/m^2 ± SD)	27.1 ± 3.4
LDL (mmol/L ± SD)	2.70 ± 0.7
HDL (mmol/L ± SD)	1.20 ± 0.5
Clinical presentation	
SA	13 (32.5)
Unstable angina	12 (30.0)
Acute MI	15 (37.5)
IVUS-VH measurements	
Analysed length (mm)[a]	46.9 (33.9–59.8)
Geometrical parameters	
Lumen CSA (mm^2 ± SD)	9.4 ± 2.8
Vessel CSA (mm^2 ± SD)	15.1 ± 4.8
Plaque CSA (mm^2 ± SD)	5.8 ± 2.7
Plaque max. thickness (mm ± SD)	0.9 ± 0.2
Plaque burden (% ± SD)	37.2 ± 8.7
Compositional parameters	
Calcium CSA (mm^2 ± SD)	0.07 (0.03–0.14)
Calcium (% ± SD)	2.50 (1.45–3.53)
Fibrous CSA (mm^2 ± SD)	1.53 (0.81–2.11)
Fibrous (% ± SD)	57.84 (52.3–64.5)
Fibrolipidic CSA (mm^2 ± SD)	0.48 (0.26–0.77)
Fibrolipidic (% ± SD)	17.96 (13.9–21.9)
Necrotic core CSA (mm^2 ± SD)	0.26 (0.15–0.42)
Necrotic core (% ± SD)	10.13 (6.2–12.6)

Discrete variables are presented as counts and percentages. Continuous variables are presented as means ± SD or medians (25th, 75th percentile) when indicated.

[a]The average analysed length per coronary.

PR: demographical and IVUS-derived characteristics

Table 2 depicts the demographical characteristics and the IVUS-VH measurements of patients with and without the presence of PR in their coronary tree. Body mass index (BMI) was significantly higher in patients with rupture (28.4 ± 3.7 vs. 25.8 ± 2.6 kg/m^2, $P = 0.01$). Of note, 66.7% of current smokers presented a ruptured plaque in their coronary tree.

Patients with ruptured plaques in their coronary tree had globally more severe disease (plaque burden 40.7 ± 7.6 vs. 33.7 ± 8.4%, $P = 0.01$) (*Table 2*).

Finally, PR sites showed a higher relative content of necrotic core compared with MLA sites (16.7, 7.9–26.5 vs. 11.8, 8.4–17.1%, $P = 0.03$) (*Table 3*).

Differences between coronaries and culprit vs. non-culprit lesions

The LAD presented more severe plaques (plaque burden; LAD 42.2 ± 9.9 vs. LCx 33.17 ± 9.2% vs. RCA 33.96 ± 10.3), more calcified plaques (LAD 3.15; 1.74–4.91 vs. LCx 2.10; 1.17–3.79 vs. RCA 1.49; 0.39–2.53%), and showed larger necrotic core content (LAD 11.68; 5.3–15.8 vs. LCx 7.71; 4.15–13.6 vs. RCA 9.18; 3.87–13.3%) of plaques compared with the LCx and the RCA, respectively (*Table 4*).

There were no significant differences in IVUS-VH measurements between SA ($n = 13$) and ACS ($n = 27$) patients. IVUS-VH parameters other than mean plaque burden (40.62 ± 10.7% vs. 35.26 ± 10.2%, $P = 0.02$) did not differ significantly between culprit/target and non-culprit/non-target vessels. Furthermore, in ACS patients, geometrical and compositional characteristics did not differ significantly between culprit and non-culprit vessels, only showing trends for larger plaque burden (39.39 ± 10.0 vs. 34.60 ± 10.0%, $P = 0.07$) and relative necrotic core content (12.16; 5.4–16.6 vs. 9.66; 5.2–13.8%, $P = 0.17$) in culprit vessels.

Table 2 Demographical characteristics and IVUS-derived of patients with and without the presence of PR

	Rupture ($n = 20$)	No rupture ($n = 20$)	*P*-value
Age (years ± SD)	53.0 ± 11.4	58.5 ± 10.1	0.12
BMI (kg/m^2 ± SD)	28.4 ± 3.7	25.8 ± 2.6	0.01
Sex			
Male (% within RF)	17 (58.6)	12 (41.4)	0.08
Female (% within RF)	3 (27.3)	8 (72.7)	
Diabetes (% within RF)	2 (50.0)	2 (50.0)	0.99
Hypertension (% within RF)	10 (58.8)	7 (41.2)	0.34
Current smoking (% within RF)	10 (66.7)	5 (33.3)	0.09
Hypercholesterolemia (% within RF)	11 (55.0)	9 (45.0)	0.53
Family history of coronary disease (% within RF)	8 (42.1)	11 (57.9)	0.34
LDL (mmol/L ± SD)	2.72 ± 0.5	2.69 ± 0.9	0.92
HDL (mmol/L ± SD)	1.19 ± 0.6	1.21 ± 0.3	0.91
Clinical presentation			
SA	4 (30.8)	9 (69.2)	0.09[a]
ACS	16 (59.3)	11 (40.7)	
IVUS-VH measurements			
Geometrical parameters			
Lumen CSA (mm^2)	9.6 ± 3.3	9.2 ± 2.3	0.60
Vessel CSA (mm^2)	16.5 ± 6.0	13.8 ± 2.7	0.08
Plaque CSA (mm^2)	6.9 ± 3.3	4.6 ± 1.4	0.01
Plaque max. thickness (mm)	1.0 ± 0.2	0.8 ± 0.2	0.02
Plaque burden (%)	40.7 ± 7.6	33.7 ± 8.4	0.01
Compositional parameters			
Calcium CSA (mm^2)	0.09 (0.06–0.16)	0.04 (0.02–0.11)	0.01
Calcium (%)	2.53 (2.09–3.53)	2.06 (0.67–3.58)	0.14
Fibrous CSA (mm^2)	1.94 (1.31–3.49)	1.00 (0.70–1.68)	0.003
Fibrous (%)	62.3 (55.9–64.8)	54.2 (47.0–63.8)	0.04
Fibrolipidic CSA (mm^2)	0.58 (0.34–1.08)	0.34 (0.22–0.55)	0.03
Fibrolipidic (%)	17.8 (15.0–22.5)	18.9 (12.8–21.9)	0.95
Necrotic core CSA (mm^2)	0.30 (0.22–0.51)	0.22 (0.06–0.37)	0.02
Necrotic core (%)	10.74 (7.7–12.5)	9.22 (4.1–13.02)	0.26

Values are expressed as means ± SD.
[a]Across groups. Comparisons between groups were performed using independent Student's *t*-test, χ^2 or Kruskall–Wallis test as indicated.

Table 3 Focal characteristics of ruptured plaques and MLA controls ($n = 28$)

	Rupture site	MLA site	*P*-value
Geometrical parameters			
Lumen CSA (mm^2)	9.47 ± 6.3	6.76 ± 4.2	<0.001
Vessel CSA (mm^2)	19.09 ± 9.3	19.15 ± 9.8	0.95
Plaque CSA (mm^2)	9.63 ± 4.2	12.38 ± 6.9	0.01
Plaque max. thickness (mm)	1.38 ± 0.3	1.71 ± 0.5	0.002
Plaque burden (%)	51.32 ± 10.6	64.06 ± 10.1	<0.001
Compositional parameters[a]			
Calcium CSA (mm^2)	0.25 (0.05–0.55)	0.27 (0.05–0.49)	0.50
Calcium (%)	4.75 (1.22–7.83)	2.97 (0.87–7.18)	0.14
Fibrous CSA (mm^2)	3.65 (1.67–5.67)	4.09 (3.18–6.89)	0.008
Fibrous (%)	60.3 (50.1–67.9)	58.3 (55.6–66.2)	0.53
Fibrolipidic CSA (mm^2)	0.94 (0.40–1.82)	1.40 (0.93–3.25)	0.001
Fibrolipidic (%)	15.4 (10.9–22.6)	20.5 (13.5–28.6)	0.005
Necrotic core CSA (mm^2)	0.83 (0.41–1.52)	0.92 (0.54–1.64)	0.35
Necrotic core (%)	16.7 (7.9–26.5)	11.8 (8.4–17.1)	0.03

[a]Values are expressed in means ± SD or median (IQR) as indicated. Comparisons between groups were performed using paired Student's *t*-test and Wilcoxon signed ranks test.

Table 4 Differences between the coronaries ($n = 101$)

	LAD ($n = 37$)	LCx ($n = 32$)	RCA ($n = 32$)
Analysed length (mm ± SD)	42.37 ± 17.7	48.85 ± 20.9	51.76 ± 16.6
Geometrical parameters			
Lumen CSA (mm^2)	8.53 ± 2.6	9.26 ± 3.2	11.07 ± 4.6
Vessel CSA (mm^2)	14.94 ± 4.6	14.18 ± 5.6	16.81 ± 6.8
Plaque CSA (mm^2)	6.43 ± 2.8	4.92 ± 3.3	5.74 ± 3.0
Plaque max. thickness (mm)	1.05 ± 0.3	0.84 ± 0.3	0.85 ± 0.3
Plaque burden (%)	42.2 ± 9.9	33.17 ± 9.2	33.96 ± 10.3
Compositional parameters			
Calcium CSA (mm^2)	0.11 (0.04–0.22)	0.05 (0.02–0.14)	0.04 (0.01–0.09)
Calcium (%)	3.15 (1.74–4.91)	2.10 (1.17–3.79)	1.49 (0.39–2.53)
Fibrous CSA (mm^2)	1.82 (1.12–3.13)	0.90 (0.59–1.55)	1.12 (0.68–2.52)
Fibrous (%)	62.1 (54.0–68.2)	56.5 (42.5–66.0)	59.5 (52.2–68.0)
Fibrolipidic CSA (mm^2)	0.52 (0.30–1.01)	0.31 (0.16–0.49)	0.34 (0.18–0.83)
Fibrolipidic (%)	17.6 (12.8–23.0)	15.2 (12.7–21.0)	18.6 (13.5–23.6)
Necrotic core CSA (mm^2)	0.28 (0.19–0.57)	0.14 (0.07–0.30)	0.21 (0.05–0.38)
Necrotic core (%)	11.68 (5.3–15.8)	7.71 (4.15–13.6)	9.18 (3.87–13.3)

Values are expressed in means ± SD or median (IQR) as indicated.

Discussion

Several histopathological and, more recently, IVUS studies have described the distinctive morphological features present in PR sites. Nevertheless, none has prospectively compared the clinical and IVUS-derived characteristics of patients with and without the presence of PR in their coronary tree.

In the present prospective three-vessel IVUS study, patients with at least one PR in their coronary tree presented larger BMI and overall worse IVUS-derived (geometrical and compositional) characteristics compared with patients without evidence of PR. In addition, PR sites had a worse phenotype than the MLA sites of the same vessels.

Coronary PR is the ultimate consequence of the progressive accumulation of lipid-rich atheroma and fibrous cap thinning, commonly involving haemodynamically non-significant lesions.[13] For decades, the corollary of such event has been deemed an acute occlusion of the corresponding artery with the subsequent ACS and its inherent dire prognosis. *Ex vivo* studies have challenged such concept by providing evidence that subclinical rupture is not rare in sudden death patients.[2,4] Furthermore, recent IVUS studies have reported a prevalence of PR of 20–30% in SA patients.[7,12,14] In agreement with such previous reports, we identified PR in 30.8% of SA patients, whereas 59.3% of the ACS patients presented PR.

Patients with at least one PR in their coronary tree (50% of the population) showed a larger BMI and were more likely current smokers. These findings have a physiopathological basis because both high body weight[15] and smoking[16] are associated with an increase in the expression of matrix-metalloproteinases, enzymes involved in the collagen breakdown of fibrous caps.[17] Patients with PR also showed more severe burden of the disease and larger calcium, fibrous, and necrotic content of plaques than patients without rupture.

Several studies showed increased inflammatory marker levels, larger lipid cores, and pronounced medial thinning in positive remodelled vessels.[18–20]

Our study extends those earlier findings and establishes a link between PR and coronary remodelling. Despite larger mean plaque CSAs, patients with the presence of at least one PR in their coronary tree showed similar lumen CSAs. The lack of lumen encroachment despite a significant increase in plaque burden was probably driven by a positive remodelling phenomenon, clearly shown as a significant increase in vessel CSA.

At site-specific locations, ruptured sites showed an overall worse phenotype than MLA sites. In particular, ruptured sites showed a higher necrotic core content (16.7; 7.9–26.5 vs. 11.8; 8.4–17.1%, $P = 0.03$). These results were in line with histopathological findings supporting the role of the atheromatous core as the most thrombogenic component of atherosclerotic plaques.[21] Of interest, and in agreement with Farb *et al.*[22] who frequently found calcium in ruptured plaques, ruptured sites showed a larger calcium content than the MLA sites and the overall population.

It is noteworthy yet confirmatory of a previous *ex vivo* study[23] that there was no significant difference in plaque composition between culprit and non-culprit vessels, supporting the validity of the interrogation of a single vessel to estimate the global burden of the disease.[24] Nevertheless, several differences were detected between the three major epicardial arteries. Interestingly, the LAD showed more severe lesions and a worse phenotype than the LCx and RCA. In addition, ruptures located in the LAD were clustered in the proximal part of the vessel, ruptures located in the RCA were more distally located, and ruptures in the LCx showed no apparent site specificity. A recent IVUS study found a similar distribution throughout the coronary tree.[25] Overall, these findings might potentially explain the higher re-stenosis rates seen in the LAD, particularly in the proximal LAD, compared with the LCx and RCA, respectively.[26]

Clinical and *ex vivo* studies have conclusively established that there is commonly a delay between the rupture of a plaque and its clinical consequence, if any.[14,27,28] Indeed, Rittersma *et al.*[28] have recently studied thrombectomy material of STEMI patients and found that 51% of the patients had day-to-week-old thrombotic material. Thrombotic occlusion of a vessel seems to be an episodic event[4] and the underlying prevailing composition of the

cavity (*Figure 1*) might potentially have a prognostic value in identifying plaques at higher risk of occlusion. Large prospective studies using IVUS-VH might shed light into this question.

Limitations

All analyses and comparisons performed in the present manuscript beyond the assessment of the necrotic core content in ruptured vs. non-ruptured plaques should be regarded as exploratory and hypothesis-generating because we cannot rule out the possibility that inflation of type I error due to multiple comparisons may have confounded our results. The relatively small population included may limit this study. Small ruptures, ruptures masked by overlying thrombus and the lack of assessment of minor branches may lead to an underestimation of the prevalence of such finding. Finally, prioritizing patient's safety, the decision to perform pre-intervention and three-vessel IVUS was at the discretion of the operator, potentially inducing a selection bias.

Conclusions

The present study extends earlier findings about the prevalence, distribution, and morphology of PR in the coronary tree. In this prospective three-vessel IVUS study, patients with at least one PR in their coronary tree had larger BMI and overall worse IVUS-derived characteristics compared with patients without evidence of PR. In addition, PR sites had a worse phenotype than the MLA sites of the same vessels.

Acknowledgements

We thank Mrs Inés Dávalos Michel for her generous contribution to the study. We declare that G.A.R.-G. has received a research grant from Volcano Corp.

Conflict of interest: none declared.

References

1. Virmani R, Kolodgie FD, Burke AP, Farb A, Schwartz SM. Lessons from sudden coronary death: a comprehensive morphological classification scheme for atherosclerotic lesions. *Arterioscler Thromb Vasc Biol* 2000;20:1262–1275.
2. Arbustini E, Grasso M, Diegoli M, Morbini P, Aguzzi A, Fasani R, Specchia G. Coronary thrombosis in non-cardiac death. *Coron Artery Dis* 1993;4:751–759.
3. Mann J, Davies MJ. Mechanisms of progression in native coronary artery disease: role of healed plaque disruption. *Heart* 1999;82:265–268.
4. Burke AP, Kolodgie FD, Farb A, Weber DK, Malcom GT, Smialek J, Virmani R. Healed plaque ruptures and sudden coronary death: evidence that subclinical rupture has a role in plaque progression. *Circulation* 2001;103:934–940.
5. Davies MJ, Richardson PD, Woolf N, Katz DR, Mann J. Risk of thrombosis in human atherosclerotic plaques: role of extracellular lipid, macrophage, and smooth muscle cell content. *Br Heart J* 1993;69:377–381.
6. Gertz SD, Roberts WC. Hemodynamic shear force in rupture of coronary arterial atherosclerotic plaques. *Am J Cardiol* 1990;66:1368–1372.
7. Ge J, Chirillo F, Schwedtmann J, Gorge G, Haude M, Baumgart D, Shah V, von Birgelen C, Sack S, Boudoulas H, Erbel R. Screening of ruptured plaques in patients with coronary artery disease by intravascular ultrasound. *Heart* 1999;81:621–627.
8. Rioufol G, Finet G, Ginon I, Andre-Fouet X, Rossi R, Vialle E, Desjoyaux E, Convert G, Huret JF, Tabib A. Multiple atherosclerotic plaque rupture in acute coronary syndrome: a three-vessel intravascular ultrasound study. *Circulation* 2002;106:804–808.
9. Peters RJ, Kok WE, Havenith MG, Rijsterborgh H, van der Wal AC, Visser CA. Histopathologic validation of intracoronary ultrasound imaging. *J Am Soc Echocardiogr* 1994;7:230–241.
10. Nair A, Kuban BD, Tuzcu EM, Schoenhagen P, Nissen SE, Vince DG. Coronary plaque classification with intravascular ultrasound radiofrequency data analysis. *Circulation* 2002;106:2200–2206.
11. Kåresen K. Deconvolution of sparse spike trains by iterated window maximization. *IEEE Trans Signal Process* 1997;45:1173–1183.
12. Hong MK, Mintz GS, Lee CW, Kim YH, Lee SW, Song JM, Han KH, Kang DH, Song JK, Kim JJ, Park SW, Park SJ. Comparison of coronary plaque rupture between stable angina and acute myocardial infarction: a three-vessel intravascular ultrasound study in 235 patients. *Circulation* 2004;110:928–933.
13. Falk E, Shah PK, Fuster V. Coronary plaque disruption. *Circulation* 1995;92:657–671.
14. Maehara A, Mintz GS, Bui AB, Walter OR, Castagna MT, Canos D, Pichard AD, Satler LF, Waksman R, Suddath WO, Laird JR Jr, Kent KM, Weissman NJ. Morphologic and angiographic features of coronary plaque rupture detected by intravascular ultrasound. *J Am Coll Cardiol* 2002;40:904–910.
15. Laimer M, Kaser S, Kranebitter M, Sandhofer A, Muhlmann G, Schwelberger H, Weiss H, Patsch JR, Ebenbichler CF. Effect of pronounced weight loss on the nontraditional cardiovascular risk marker matrix metalloproteinase-9 in middle-aged morbidly obese women. *Int J Obes (Lond)* 2005;29:498–501.
16. Kangavari S, Matetzky S, Shah PK, Yano J, Chyu KY, Fishbein MC, Cercek B. Smoking increases inflammation and metalloproteinase expression in human carotid atherosclerotic plaques. *J Cardiovasc Pharmacol Ther* 2004;9:291–298.
17. Shah PK, Falk E, Badimon JJ, Fernandez-Ortiz A, Mailhac A, Villareal-Levy G, Fallon JT, Regnstrom J, Fuster V. Human monocyte-derived macrophages induce collagen breakdown in fibrous caps of atherosclerotic plaques. Potential role of matrix-degrading metalloproteinases and implications for plaque rupture. *Circulation* 1995;92:1565–1569.
18. Pasterkamp G, Schoneveld AH, van der Wal AC, Haudenschild CC, Clarijs RJ, Becker AE, Hillen B, Borst C. Relation of arterial geometry to luminal narrowing and histologic markers for plaque vulnerability: the remodeling paradox. *J Am Coll Cardiol* 1998;32:655–662.
19. Varnava AM, Mills PG, Davies MJ. Relationship between coronary artery remodeling and plaque vulnerability. *Circulation* 2002;105:939–943.
20. Burke AP, Kolodgie FD, Farb A, Weber D, Virmani R. Morphological predictors of arterial remodeling in coronary atherosclerosis. *Circulation* 2002;105:297–303.
21. Fernandez-Ortiz A, Badimon JJ, Falk E, Fuster V, Meyer B, Mailhac A, Weng D, Shah PK, Badimon L. Characterization of the relative thrombogenicity of atherosclerotic plaque components: implications for consequences of plaque rupture. *J Am Coll Cardiol* 1994;23:1562–1569.
22. Farb A, Burke AP, Tang AL, Liang TY, Mannan P, Smialek J, Virmani R. Coronary plaque erosion without rupture into a lipid core. A frequent cause of coronary thrombosis in sudden coronary death. *Circulation* 1996;93:1354–1363.
23. Kragel AH, Reddy SG, Wittes JT, Roberts WC. Morphometric analysis of the composition of atherosclerotic plaques in the four major epicardial coronary arteries in acute myocardial infarction and in sudden coronary death. *Circulation* 1989;80:1747–1756.
24. Rodriguez-Granillo GA, McFadden EP, Valgimigli M, van Mieghem CAG, Regar E, de Feyter PJ, Serruys PW. Coronary plaque composition of non-culprit lesions, assessed by *in vivo* intracoronary ultrasound radio frequency data analysis, is related to clinical presentation. *Am Heart J* 2006;151:1020–1024.
25. Hong MK, Mintz GS, Lee CW, Lee BK, Yang TH, Kim YH, Song JM, Han KH, Kang DH, Cheong SS, Song JK, Kim JJ, Park SW, Park SJ. The site of plaque rupture in native coronary arteries: a three-vessel intravascular ultrasound analysis. *J Am Coll Cardiol* 2005;46:261–265.
26. Ashby DT, Dangas G, Mehran R, Lansky AJ, Narasimaiah R, Iakovou I, Polena S, Satler LF, Pichard AD, Kent KM, Stone GW, Leon MB. Comparison of clinical outcomes using stents vs no stents after percutaneous coronary intervention for proximal left anterior descending versus proximal right and left circumflex coronary arteries. *Am J Cardiol* 2002;89:1162–1166.
27. Ojio S, Takatsu H, Tanaka T, Ueno K, Yokoya K, Matsubara T, Suzuki T, Watanabe S, Morita N, Kawasaki M, Nagano T, Nishio I, Sakai K,

Nishigaki K, Takemura G, Noda T, Minatoguchi S, Fujiwara H. Considerable time from the onset of plaque rupture and/or thrombi until the onset of acute myocardial infarction in humans: coronary angiographic findings within 1 week before the onset of infarction. *Circulation* 2000;102: 2063–2069.

28. Rittersma SZ, van der Wal AC, Koch KT, Piek JJ, Henriques JP, Mulder KJ, Ploegmakers JP, Meesterman M, de Winter RJ. Plaque instability frequently occurs days or weeks before occlusive coronary thrombosis: a pathological thrombectomy study in primary percutaneous coronary intervention. *Circulation* 2005;111:1160–1165.

Clinical vignette

doi:10.1093/eurheartj/ehi765
Online publish-ahead-of-print 2 February 2006

Isolated ventricular non-compaction with restrictive cardiomyopathy

Claudio Rapezzi[1]*, Ornella Leone[2], Marinella Ferlito[1], Elena Biagini[1], Fabio Coccolo[1], and Giorgio Arpesella[3]

[1]Institute of Cardiology, University of Bologna and S. Orsola-Malpighi Hospital, Via Massarenti 9, 40138 Bologna, Italy; [2]Department of Pathology, University of Bologna and S. Orsola-Malpighi Hospital, Bologna, Italy and [3]Department of Cardiovascular Surgery, University of Bologna and S. Orsola-Malpighi Hospital, Bologna, Italy

* Corresponding author. Tel: +39 051349858; fax: +39 051344859. *E-mail address*: crapezzi@aosp.bo.it

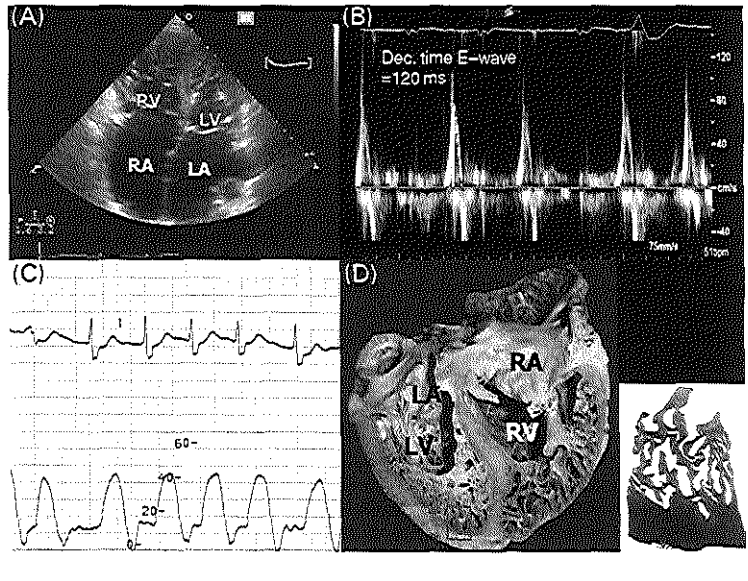

A 42-year-old man with chronic heart failure and permanent atrial fibrillation was referred to our cardiology institute for diagnostic assessment and therapy. The patient denied any known family history of heart disease. No clinical/echocardiographic sign of heart disease was detected among living first-degree relatives. Atrial fibrillation and progressively worsening effort dyspnoea had started at age 25. Physical examination showed moderate bilateral leg oedema, marked hepatomegaly, and raised jugular venous pressure and gallop rhythm. ECG showed atrial fibrillation with right bundle branch block and left anterior hemiblock. Cardiomegaly and chronic interstitial lung oedema were apparent on chest X-ray. Echocardiography revealed a normally sized, mildly hypokinetic left ventricle (ejection fraction = 45%) and an enlarged, mildly hypokinetic right ventricle, accompanied by massive right and left atrial enlargement and severe tricuspid regurgitation. The apical portions of both ventricles had a coarsely trabeculated, spongy appearance suggestive of non-compaction (Panel A). E-wave deceleration time was abnormally shortened in the echo-Doppler profile at transmitral level (Panel B). Coronary arteries were normal at angiography. At the right heart catheterization, restrictive physiology was evident (Panel C). Pulmonary artery pressures were 40/20/22 mmHg; mean pulmonary capillary wedge and right atrial pressures were 22 and 15 mmHg, respectively; cardiac index was 2.1 L/min/m^2. The patient was submitted to heart transplantation, which was successfully performed. The explanted heart (Panel D) provided definitive confirmation of biventricular non-compaction and restrictive cardiomyopathy (without signs of infiltrating myocardial diseases or desmin accumulation). Ventricular non-compaction has been shown to occur in the context of congenital anomalies, otherwise normal hearts or, most often, dilated cardiomyopathy. To our knowledge, the present case provides the first documentation of (bi)ventricular non-compaction in the context of a restrictive cardiomyopathy. This observation is in line with the concept that isolated ventricular non-compaction is more likely to be a morphological trait that can be found within different types of cardiomyopathy rather than a distinct cardiomyopathy.

Panel A. Two-dimensional echocardiography in four-chamber view shows huge biatrial dilation, a normally sized left ventricle, and a moderately enlarged right ventricle. The apical portions of both ventricles have a coarsely trabeculated, spongy appearance, suggestive of ventricular non-compaction.

Panel B. Transmitral echo-Doppler profile indicates very short deceleration time, suggesting restrictive physiology.

Panel C. Right ventricular catheterization trace (bottom) shows 'square-root' morphology in the diastolic portion of the curve accompanied by protodiastolic pressure above zero, confirming restrictive physiology.

Panel D. Macroscopic longitudinal section of the explanted heart (lacking the upper portion of the atrial cuff) clearly shows biventricular non-compaction with coarse apical trabeculation and deep inter-trabecular recesses. The non-compacted portions of both ventricles are predominant, drastically limiting cavity volumes. The histological detail (inset) after Mallory's trichrome staining additionally shows mild fibrotic endocardial thickening and moderate interstitial fibrosis.

CHAPTER 5.4

Coronary artery remodelling is related to plaque composition.

Rodriguez-Granillo GA, Serruys PW, **Garcia-Garcia HM**, Aoki J, Valgimigli M, van Mieghem C, Mc Fadden EP, de Jaegere, de Feyter P.

Heart. 2006;92:388-91.

Coronary artery remodelling is related to plaque composition

G A Rodriguez-Granillo, P W Serruys, H M Garcia-Garcia, J Aoki, M Valgimigli, C A G van Mieghem, E McFadden, P P T de Jaegere, P de Feyter

Heart 2006;**92**:388–391. doi: 10.1136/hrt.2004.057810

See end of article for authors' affiliations

Correspondence to: Professor Patrick W Serruys, Thoraxcentre, Bd-406, Dr Molewaterplein 40, 3015-GD Rotterdam, Netherlands; p.w.j.c.serruys@erasmusmc.nl

Accepted 13 June 2005
Published Online First 17 June 2005

Objective: To assess the potential relation between plaque composition and vascular remodelling by using spectral analysis of intravascular ultrasound (IVUS) radiofrequency data.

Methods and results: 41 coronary vessels with non-significant (< 50% diameter stenosis by angiography), ⩽ 20 mm, non-ostial lesions located in non-culprit vessels underwent IVUS interrogation. IVUS radiofrequency data obtained with a 30 MHz catheter, were analysed with IVUS virtual histology software. A remodelling index (RI) was calculated and divided into three groups. Lesions with RI ⩾ 1.05 were considered to have positive remodelling and lesions with RI ⩽ 0.95 were considered to have negative remodelling. Lesions with RI ⩾ 1.05 had a significantly larger lipid core than lesions with RI 0.96–1.04 and RI ⩽ 0.95 (22.1 (6.3) *v* 15.1 (7.6) *v* 6.6 (6.9), $p < 0.0001$). A positive correlation between lipid core and RI ($r = 0.83$, $p < 0.0001$) and an inverse correlation between fibrous tissue and RI ($r = -0.45$, $p = 0.003$) were also significant. All of the positively remodelled lesions were thin cap fibroatheroma or fibroatheromatous lesions, whereas negatively remodelled lesions had a more stable phenotype, with 64% having pathological intimal thickening, 29% being fibrocalcific lesions, and only 7% fibroatheromatous lesions ($p < 0.0001$).

Conclusions: In this study, in vivo plaque composition and morphology assessed by spectral analysis of IVUS radiofrequency data were related to coronary artery remodelling.

Glagov *et al*[1] described vascular remodelling as a compensatory enlargement of the coronary arteries in response to an increase in plaque area. This concept has further evolved into a dynamic theory whereby vessels may also shrink in response to plaque growth.[2] This remodelling modality has been related to a more stable phenotype and clinical presentation,[3–6] whereas several studies showed an increase in inflammatory marker concentrations, larger lipid cores, and pronounced medial thinning in positively remodelled vessels.[4 5 7]

Recently, retrospective pathological studies have identified morphological and compositional features characteristic of plaque rupture.[8 9] This has led to a new classification of coronary lesions that more comprehensively illustrates plaque progression.[9]

Grey scale intravascular ultrasound (IVUS) is of limited value for identification of specific plaque components.[10] However, spectral analysis of IVUS radiofrequency data (IVUS virtual histology (VH)) has the potential to provide detailed quantitative information on plaque composition and has been validated in explanted human coronary segments.[11]

In this study, we sought to evaluate in vivo the relation between plaque composition and coronary artery remodelling by using ultrasound radiofrequency data analysis. In addition, we classified lesions with respect to their morphology and evaluated the potential relation between lesion type and coronary remodelling.[9]

METHODS

Patients

Forty one consecutive patients were retrospectively selected after screening a 54 patient database where non-culprit, angiographically non-obstructive (<50%), ⩽ 20 mm, non-ostial lesions were investigated with IVUS. Patients were excluded if they had diffusely diseased vessels or lacked a lesion occluding ⩾ 40% of the cross sectional area (CSA). Lesions located in proximal and mid segments of a coronary artery were included in the study.

Major exclusion criteria were coronary anatomy that precluded safe IVUS examination of a suitable region of interest. Informed, written consent was obtained from all the patients.

IVUS-VH acquisition and analysis

Details regarding the validation of the technique on explanted human coronary segments have previously been reported.[11] Briefly, IVUS-VH uses spectral analysis of IVUS radiofrequency data to construct tissue maps that classify plaque into four major components. In preliminary in vitro studies, four histological plaque components (fibrous, fibrolipidic, lipid core, and calcified) were correlated with a specific spectrum of the radiofrequency signal.[11] These plaque components were assigned colour codes. Calcified, fibrous, fibrolipidic, and lipid core regions were labelled white, green, greenish yellow, and red, respectively.

IVUS-VH data were acquired after intracoronary administration of nitrates by means of a continuous pullback (0.5 mm/s) with a commercially available mechanical sector scanner (Ultracross 2.9 French, 30 MHz catheter; Boston Scientific, Santa Clara, California, USA) by a dedicated IVUS-VH console (Volcano Therapeutics, Rancho Cordova, California, USA). The IVUS-VH data were stored on a CD ROM and sent to the imaging core laboratory for offline analysis. IVUS B mode images were reconstructed from the radiofrequency data by customised software (IVUSLab, Volcano Therapeutics). Subsequently, contours of both the lumen and the media–adventitia interface were detected

Abbreviations: CSA, cross sectional area; IVUS, intravascular ultrasound; MLA, minimum lumen area; RI, remodelling index; VH, virtual histology

manually. To account for catheter to catheter variability the acquired radiofrequency data were normalised by a technique known as "blind deconvolution". Blind deconvolution is an iterative algorithm that deconvolves the catheter transfer function from the backscatter, thus enabling automated data normalisation.[12 13] Compositional data of the minimum lumen area (MLA) were expressed as percentage of the plaque CSA corresponding to each plaque component.

The MLA site and a reference site ⩽ 10 mm proximal to the lesion were selected. There were no major side branches between the MLA and reference sites.

Remodelling was assessed by means of the remodelling index (RI), expressed as the external elastic membrane CSA (MLA site) divided by the reference external elastic membrane CSA as previously described.[9 14 15].

We defined positive remodelling as RI ⩾ 1.05 and negative remodelling as RI ⩽ 0.95. Values in between were considered neutral (no remodelling). Percentage stenosis of the MLA site was defined as:

$$vessel_{area}MLA - lumen_{area}MLA/vessel_{area}MLA \times 100.$$

In accordance with previously reported data, we classified lesions as pathological intimal thickening (mainly fibrotic–fibrolipidic tissue, with the lipid core constituting 0% to ⩽ = 3% of the CSA), fibrocalcific lesions (featuring mainly fibrotic plaques, with some calcification and a lipid core occupying between 3–10% of the CSA), fibrous cap atheroma (lipid rich (> 10% CSA) plaques with overlying fibrous tissue), and thin cap fibroatheroma (lipid-rich (> 10% CSA) plaques with no overlying fibrous tissue). Figure 1 depicts examples of this classification. To classify lesions, these criteria had to be met in the MLA site plus the immediate distal and proximal cross sections. Since the axial resolution of this technique is between 100–150 μm, we assumed that the absence of fibrous tissue overlying a lipid core suggested a cap thickness of below 100–150 μm.[16]

Statistical analysis

Discrete variables are presented as counts and percentages. Continuous variables are presented as mean (SD). We looked for correlations between the RI and both plaque components and percentage stenosis MLA by using Pearson correlation coefficients. Differences in means between groups were analysed by a two sided t test or by one way analysis of variance. We compared frequencies by means of the χ^2 test. A probability value of $p < 0.05$ indicated significance. Data were statistically analysed with SPSS software version 11.5 (SPSS Inc, Chicago, Illinois, USA).

RESULTS

Table 1 shows patient characteristics. Mean age was 55.9 (10.9). Most patients were men (83%) with a low prevalence of diabetes (7.3%). The study vessel was the right coronary artery in 19 patients (46.3%), the left anterior descending in 16 patients (39.0%), and the left circumflex in six patients (14.6%).

Lesions with positive remodelling had significantly larger lipid core percentages than lesions with no remodelling or negative remodelling (22.1 (6.3)% *v* 15.1 (7.6)% *v* 6.6 (6.9)%, respectively, $p < 0.0001$). Negative remodelling lesions tended to have larger fibrous tissue percentages than lesions with no remodelling and positive remodelling (68.6 (13.7)% *v* 62.9 (9.5)% *v* 58.1 (12.9)%, $p = 0.13$). Table 2 shows these results.

Table 3 presents Pearson correlation coefficients between the RI and both plaque components and percentage stenosis MLA. The positive co.relation between the lipid core and the RI was significant ($r = 0.83$, $p < 0.0001$) (fig 2). Moreover, fibrous tissue was inversely correlated with the RI ($r = -0.45$, $p = 0.003$) (fig 3). Lastly, the percentage stenosis of the MLA and the RI were non-significantly inversely related ($r = -0.27$, $p = 0.09$).

With regard to lesion type, thin cap fibroatheroma and fibroatheromatous lesions comprised 100% of the positively

Table 1 Baseline characteristics (n=41)

Age (years)	55.9 (10.9)
Men	19 (83%)
Diabetes	3 (7.3%)
Hypertension*	12 (29.3%)
Current smoking	8 (19.5%)
Previous smoking	15 (36.6%)
Hypercholesterolaemia†	32 (78%)
Family history of coronary disease	19 (46.3%)
Previous myocardial infarction	6 (14.6%)
Artery	
Right coronary	19 (46.3%)
Left anterior descending	16 (39%)
Left circumflex	6 (14.6%)
Clinical presentation	
No angina‡	11 (26.8%)
Stable angina	14 (34.1%)
Unstable angina	6 (14.6%)
Myocardial infarction	10 (24.4%)

Data are mean (SD) or number (%).
*Blood pressure >160/95 mm Hg or treatment for hypertension; †total cholesterol >5.57 mmol/l or treatment for hypercholesterolemia; ‡these patients were studied at scheduled follow up angiography.

Table 2 Geometrical and compositional data of the minimum lumen area (MLA) site

	Remodelling index			
	<0.95	0.96–1.04	>1.05	p Value
Number	29 (70.7%)	3 (7.3%)	9 (22%)	
Stenosis (%)	63.1 (7.5)	69.1 (8.6)	59.9 (9.9)	0.24
Calcific CSA (%)	1.38 (2.7)	2.07 (3.2)	1.67 (1.6)	0.88
Fibrous CSA (%)	68.6 (13.7)	62.9 (9.5)	58.1 (12.9)	0.13
Fibrolipidic CSA (%)	23.5 (9.9)	19.9 (6.9)	18.1 (12.6)	0.39
Lipid core CSA (%)	6.6 (6.9)	15.1 (7.6)	22.1 (6.3)	<0.0001

Data are mean (SD).
Percentage stenosis of the MLA site is calculated as $vessel_{area}MLA - lumen_{area}MLA/vessel_{area}MLA \times 100$. Remodelling index (RI) is defined as MLA of the external elastic membrane (EEM) cross sectional area (CSA)/reference EEM CSA.

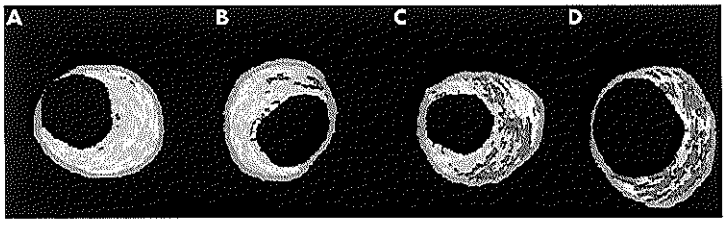

Figure 1 Minimum lumen area (MLA) sites depicting the progression of atherosclerotic disease. The plaque components were assigned colour codes. Calcified, fibrous, fibrolipidic, and lipid core regions were labelled white, green, greenish yellow, and red, respectively. MLA sites feature (A) pathological intimal thickening and (B) fibrocalcific, (C) fibroatheromatous, and (D) thin cap fibroatheromatous lesions.

Table 3 Relations between remodelling index (RI), percentage stenosis of the MLA, and plaque composition of the MLA site

	RI	p Value
Lipid core CSA (%)	0.83	<0.0001
Fibrous CSA (%)	−0.45	0.003
Percentage stenosis MLA	−0.27	0.09
Calcific CSA (%)	0.12	0.47
Fibrolipidic CSA (%)	−0.17	0.28

Data are Pearson correlation coefficients.

remodelled lesions, whereas negative remodelling lesions had a more stable phenotype: 64% had pathological intimal thickening, 29% were fibrocalcific, and only 7% were fibroatheromatous lesions ($p < 0.0001$) (fig 4).

DISCUSSION

Recently, the relation between vascular remodelling and plaque composition was assessed by IVUS.[17–20] This catheter based diagnostic tool provides an accurate tomographic view of the coronary arteries and in vitro validation studies have shown a high correlation with histological samples.[21–23] Nevertheless, accurate plaque characterisation with visual interpretation of grey scale IVUS, particularly of lipid rich plaques, remains unresolved.[22] On the contrary, spectral analysis of IVUS radiofrequency data (IVUS-VH) has the potential to provide detailed quantitative information on plaque composition and has been validated in studies of explanted human coronary segments.[11]

The results of the present study confirm in vivo the relation between plaque composition and coronary remodelling. Lipid core size was significantly larger in positively remodelled coronary lesions than in those with vessel shrinkage. Furthermore, the fibrotic burden of the plaque was significantly and inversely correlated with the RI.

Lastly, positively remodelled lesions had a higher risk phenotype, with 56% of them being classified as thin cap fibroatheroma, the lesion type most likely to rupture.[24] On the contrary, negative remodelling was associated with a more stable phenotype: 64% had pathological intimal thickening and no evidence of thin cap fibroatheroma. Fibrocalcific lesions, a potential hallmark of the end stage of atheromatous plaque rupture or erosion with healing and calcification, were found in 29% of negatively remodelled lesions.[9]

Overall, these findings support the importance of the histological composition of atherosclerotic plaque as a major contributor to its fate as described by Davies *et al*,[4] who showed that plaques with a large lipid core harbour a higher risk of rupture and subsequent thrombosis. The lipid core is a source of metalloproteinases, a group of proteolytic enzymes that have an important function in vascular remodelling mechanisms and whose most common locations are foam cell accumulation areas and shoulder regions.[25 26]

Conversely, negatively remodelled vessels consisted predominantly of fibrotic plaques. In addition, in line with previously reported data, negatively remodelled lesions had a higher degree of stenosis.[2 17 27] The findings of this study are consistent with previous pathological findings in patients after sudden death.[3] However, such postmortem studies do not have implications in the natural history of high risk plaques and thus in the clinical outcome of patients. On the contrary, we strongly believe that the identification of these high risk plaques in vivo may provide more insights into the prognosis and natural history of such lesions and into the

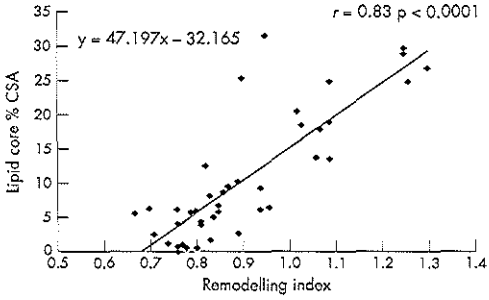

Figure 2 Linear regression plot showing positive correlation between lipid core and remodelling. CSA, cross sectional area. Remodelling index is defined as MLA of the external elastic membrane (EEM) CSA/reference EEM CSA.

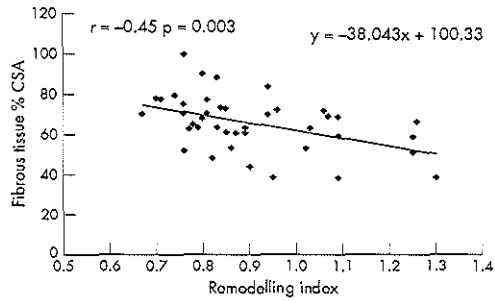

Figure 3 Linear regression plot showing an inverse relation between fibrous tissue and remodelling.

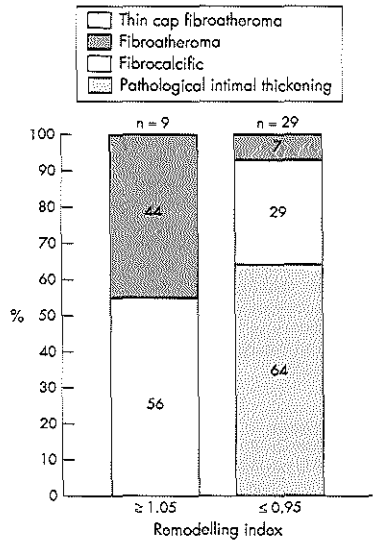

Figure 4 Bar graphs illustrating the lesion type frequencies according to remodelling modality. All of the high risk plaques had positive remodelling (56% were thin cap fibroatheroma and 44% fibroatheromatous lesions). Negatively remodelled lesions had a more stable phenotype, with 93% being low risk lesions and only 7% fibroatheromatous lesions.

effect of conventional and emerging anti-atherosclerotic pharmacological interventions.

Limitations

Since this was a cross sectional study and atherosclerosis is usually a diffuse disease, finding a fully non-diseased reference site is not guaranteed. Therefore, we cannot rule out the early presence of remodelling in the reference site. In addition, this was a pilot study that needs further confirmation in a larger population. Moreover, classifying lesion types by this technique lacks the accuracy of histopathological classification, since resolution is inferior. Nevertheless, a significant relation was found by using this arbitrary classification. Although histopathological classification remains the ideal, spectral analysis of IVUS radiofrequency data has the potential to provide real time accurate information regarding tissue characterisation and plaque morphology.

Conclusions

In this small clinical study, in vivo plaque composition and morphology assessed by spectral analysis of IVUS radiofrequency data were related to coronary artery remodelling, supporting the role of plaque composition in the mechanisms of vessel remodelling. Lipid core size was significantly larger in positively remodelled coronary lesions than in those with vessel shrinkage. Furthermore, the fibrotic burden of the plaque was significantly and inversely correlated with the RI. The findings of this study are consistent with previous pathological findings. However, postmortem studies do not have the potential to provide prospective information about the natural history of high risk plaques. On the contrary, we strongly believe that the identification of these high risk plaques in vivo may provide more insights into the prognosis and natural history of such lesions and into the effect of conventional and emerging anti-atherosclerotic pharmacological interventions.

Authors' affiliations

G A Rodriguez-Granillo, P W Serruys, H M Garcia-Garcia, J Aoki, M Valgimigli, C A G van Mieghem, E McFadden, P P T de Jaegere, P de Feyter, Thoraxcentre, Erasmus Medical Centre, Rotterdam, the Netherlands

No author has any conflict of interest.

All authors have approved the final manuscript, which has not been published and is not under consideration elsewhere.

REFERENCES

1 **Glagov S**, Weisenberg E, Zarins CK, *et al.* Compensatory enlargement of human atherosclerotic coronary arteries. *N Engl J Med* 1987;**316**:1371–5.
2 **Pasterkamp G**, Wensing PJ, Post MJ, *et al.* Paradoxical arterial wall shrinkage may contribute to luminal narrowing of human atherosclerotic femoral arteries. *Circulation* 1995;**91**:1444–9.
3 **Smits PC**, Pasterkamp G, Quarles van Ufford MA, *et al.* Coronary artery disease: arterial remodelling and clinical presentation. *Heart* 1999;**82**:461–4.
4 **Pasterkamp G**, Schoneveld AH, van der Wal AC, *et al.* Relation of arterial geometry to luminal narrowing and histologic markers for plaque vulnerability: the remodeling paradox. *J Am Coll Cardiol* 1998;**32**:655–62.
5 **Varnava AM**, Mills PG, Davies MJ. Relationship between coronary artery remodeling and plaque vulnerability. *Circulation* 2002;**105**:939–43.
6 **Nakamura M**, Nishikawa H, Mukai S, *et al.* Impact of coronary artery remodeling on clinical presentation of coronary artery disease: an intravascular ultrasound study. *J Am Coll Cardiol* 2001;**37**:63–9.
7 **Burke AP**, Kolodgie FD, Farb A, *et al.* Morphological predictors of arterial remodeling in coronary atherosclerosis. *Circulation* 2002;**105**:297–303.
8 **Davies MJ**, Richardson PD, Woolf N, *et al.* Risk of thrombosis in human atherosclerotic plaques: role of extracellular lipid, macrophage, and smooth muscle cell content. *Br Heart J* 1993;**69**:377–81.
9 **Virmani R**, Kolodgie FD, Burke AP, *et al.* Lessons from sudden coronary death: a comprehensive morphological classification scheme for atherosclerotic lesions. *Arterioscler Thromb Vasc Biol* 2000;**20**:1262–75.
10 **Peters RJ**, Kok WE, Havenith MG, *et al.* Histopathologic validation of intracoronary ultrasound imaging. *J Am Soc Echocardiogr* 1994;**7**:230–41.
11 **Nair A**, Kuban BD, Tuzcu EM, *et al.* Coronary plaque classification with intravascular ultrasound radiofrequency data analysis. *Circulation* 2002;**106**:2200–6.
12 **Kåreson K.** Deconvolution of sparse spike trains by iterated window maximization. *IEEE Trans Signal Process* 1997;**45**:1173–83.
13 **Karesen KF**, Bolviken E. Blind deconvolution of ultrasonic traces accounting for pulse variance. *IEEE Trans Ultrason Ferroelectr Freq Control* 1999;**46**:564–73.
14 **Schoenhagen P**, Ziada KM, Kapadia SR, *et al.* Extent and direction of arterial remodeling in stable versus unstable coronary syndromes: an intravascular ultrasound study. *Circulation* 2000;**101**:598–603.
15 **Gussenhoven EJ**, Geselschap JH, van Lankeren W, *et al.* Remodeling of atherosclerotic coronary arteries assessed with intravascular ultrasound in vitro. *Am J Cardiol* 1997;**79**:699–702.
16 **Nair A**, Calvetti D, Vince DG. Regularized autoregressive analysis of intravascular ultrasound data: improvement in spatial accuracy of plaque tissue maps. *IEEE Trans Ultrason, Ferroelectr Freq Control* 2004;**51**:420–31.
17 **Mintz GS**, Kent KM, Pichard AD, *et al.* Contribution of inadequate arterial remodeling to the development of focal coronary artery stenoses: an intravascular ultrasound study. *Circulation* 1997;**95**:1791–8.
18 **Tauth J**, Pinnow E, Sullebarger JT, *et al.* Predictors of coronary arterial remodeling patterns in patients with myocardial ischemia. *Am J Cardiol* 1997;**80**:1352–5.
19 **Sabate M**, Kay IP, de Feyter PJ, *et al.* Remodeling of atherosclerotic coronary arteries varies in relation to location and composition of plaque. *Am J Cardiol* 1999;**84**:135–40.
20 **Fuessl RT**, Kranenberg E, Kiausch U, *et al.* Vascular remodeling in atherosclerotic coronary arteries is affected by plaque composition. *Coron Artery Dis* 2001;**12**:91–7.
21 **Tobis JM**, Mallery JA, Gessert J, *et al.* Intravascular ultrasound cross-sectional arterial imaging before and after balloon angioplasty in vitro. *Circulation* 1989;**80**:873–82.
22 **Potkin BN**, Bartorelli AL, Gessert JM, *et al.* Coronary artery imaging with intravascular high-frequency ultrasound. *Circulation* 1990;**81**:1575–85.
23 **Nishimura RA**, Edwards WD, Warnes CA, *et al.* Intravascular ultrasound imaging: in vitro validation and pathologic correlation. *J Am Coll Cardiol* 1990;**16**:145–54.
24 **Farb A**, Tang AL, Burke AP, *et al.* Sudden coronary death: frequency of active coronary lesions, inactive coronary lesions, and myocardial infarction. *Circulation* 1995;**92**:1701–9.
25 **Galis ZS**, Khatri JJ. Matrix metalloproteinases in vascular remodeling and atherogenesis: the good, the bad, and the ugly. *Circ Res* 2002;**90**:251–62.
26 **Galis ZS**, Sukhova GK, Lark MW, *et al.* Increased expression of matrix metalloproteinases and matrix degrading activity in vulnerable regions of human atherosclerotic plaques. *J Clin Invest* 1994;**94**:2493–503.
27 **Pasterkamp G**, Wensing PJ, Hillen B, *et al.* Impact of local atherosclerotic remodeling on the calculation of percent luminal narrowing. *Am J Cardiol* 1997;**79**:402–5.

CHAPTER 6.1

Diagnosis and treatment of coronary vulnerable plaques.

Garcia-Garcia HM, Gonzalo N, Granada JF, Regar E, Serruys PW.

Expert Rev Cardiovasc Ther. 2008;6:209-22.

EXPERT REVIEWS

Diagnosis and treatment of coronary vulnerable plaques

Expert Rev. Cardiovasc. Ther. 6 (1), 209–222 (2008)

Héctor M García-García, Nieves Gonzalo, Juan F Granada, Evelyn Regar and Patrick W Serruys†

†Author for correspondence
Thoraxcenter, Ba-583, Erasmus MC, Dr. Molewaterplein 40, 3015 GD Rotterdam, The Netherlands
Tel.: +31 104 635 260
Fax: +31 104 369 154
p.w.j.c.serruys@erasmusmc.nl

Thin-capped fibroatheroma is the morphology that most resembles plaque rupture. Detection of these vulnerable plaques *in vivo* is essential to being able to study their natural history and evaluate potential treatment modalities and, therefore, may ultimately have an important impact on the prevention of acute myocardial infarction and death. Currently, conventional grayscale intravascular ultrasound, virtual histology and palpography data are being collected with the same catheter during the same pullback. A combination of this catheter with either thermography capability or additional imaging, such as optical coherence tomography or spectroscopy, would be an exciting development. Intravascular magnetic resonance imaging also holds much promise. To date, none of the techniques described above have been sufficiently validated and, most importantly, their predictive value for adverse cardiac events remains elusive. Very rigorous and well-designed studies are compelling for defining the role of each diagnostic modality. Until we are able to detect *in vivo* vulnerable plaques accurately, no specific treatment is warranted.

KEYWORDS: acute coronary syndrome • atherosclerosis • plaque rupture • thin-capped fibroatheroma

Unheralded acute coronary syndromes (ACS) are common initial manifestations of coronary atherosclerosis and are frequently caused by plaque ruptures [1]. Histopathological studies have identified several plaque morphologies associated with ACS and sudden cardiac death, such as calcified nodule, plaque erosion and thin-capped fibroatheroma (TCFA). The plaques that are at increased risk of thrombosis and rapid progression of lumen encroachment are referred to as high-risk or vulnerable lesions [2]. However, the natural history of these lesions remains unknown and the limited knowledge about their eventual prognosis is provided by retrospective histopathological studies [3]. Detection of these vulnerable plaques *in vivo* is essential to study their natural history and to evaluate potential treatment modalities and, therefore, may ultimately have an important impact on the prevention of acute myocardial infarction (AMI) and death. Coronary angiography offers valuable information on the long-term behavior of the complex lesions. Goldstein *et al.* reported that patients with ST-segment elevation myocardial infarction (STEMI) and multiple complex lesions during the year after STEMI had an increased incidence of recurrent ACS compared with patients with single complex lesions (19.0 vs 2.6%; $p < 0.001$, respectively) and repeated angioplasty, particularly of noninfarct-related lesions (32.0 vs 12.4%; $p < 0.001$) [4]. However, angiography is limited to fully evaluate the vessel wall. Therefore, there are currently several diagnostic invasive imaging techniques aiming at specifically evaluating indicators of plaque vulnerability [5]. These techniques can provide information on the vessel, lumen and wall size, tissue composition, and the status of inflammation. This article aims to review the current histopathological definitions, state-of-the-art of invasive imaging techniques and treatment of coronary vulnerable plaques, with focus on TCFAs.

Histopathological vulnerable plaque definitions

The 'classical', most described phenotype of a vulnerable plaque is a TCFA [6], which has a large necrotic core with an overlying thin cap infiltrated by macrophages. Smooth muscle cells in the cap are absent or few. The thickness of the fibrous cap near the rupture site measures 23 ± 19 μm, with 95% of the caps measuring less than 65 μm [1,7]. Rupture of a TCFA with exposure of the thrombogenic necrotic core to circulating platelets could be responsible for 60% of all ACS [1]. Macrophage infiltration of the thin cap with release of matrix metalloproteinases and local inflammation can cause extracellular matrix degradation

and subsequent plaque rupture [8,9]. Excessive mechanical strain, particularly at the junction of the TCFA and the normal vessel wall is another factor contributing to rupture [10,11].

Chevuru *et al.* reported new pathological evidence on TCFA characterization [12]. The prevalence of TCFA and ruptured TCFA is low (0.46 ± 0.95 and 0.38 ± 0.70 per heart, respectively), focal and located in the proximal segments of the coronaries. In earlier studies, up to three TCFA were found per heart [13]. Necrotic core size was relatively small for both, TCFA (1.6 ± 1.8 mm^2; length: 2.7 ± 2.0 mm) and ruptured plaques (2.2 ± 1.9 mm^2; length: 1.9 ± 3.6 mm). In previous studies, the size of necrotic core in TCFAs was 1.7 ± 1.1 mm^2 with a length of 8 mm (range: 2–17 mm), and in ruptured plaques 3.8 ± 5.5 mm^2, with a length of 9 mm (range: 2.5–22 mm) [14].

The second recognized phenotype of vulnerable plaque, accounting for approximately 40% of coronary thromboses in pathology series, is plaque erosion in lesions consisting of either pathological intimal thickening or thick-capped fibroatheroma [15]. These lesions typically have a high smooth muscle cell content, are rich in proteoglycans and are more common in young women and smokers, but are not associated with other conventional risk factors, such as hypercholesterolemia [1,16].

Third, there are calcified nodules, which may protrude into the vessel lumen and comprise up to 5% of lesions in pathological series. These lesions are characterized by an absence of endothelium and inflammatory cells [1]. In addition, intraplaque hemorrhage secondary to leakage from the vasa vasorum may also play a role [17].

Imaging of vulnerable plaques

Coronary angiography

Although coronary angiography represents the standard modality for visualization of the coronary artery disease, there is a clear discrepancy between the appearance of the opacified vascular lumen and the actual extent of atherosclerosis (FIGURE 1). Additionally, the percentage diameter stenosis of a lesion does not provide reliable information concerning the risk for myocardial infarction and death [18,19]. Large randomized lipid-lowering trials using both angiographic and clinical assessment have shown minimal or no improvement of angiographic lumen diameter but a much more impressive reduction in clinical endpoints, including myocardial infarction [20]. In fact, the 'luminogram' is unable to provide information on the composition of the artery wall and is therefore unable to distinguish between stable and high-risk, vulnerable plaques.

Angioscopy

Intracoronary angioscopy (CAS) is a well-established technique that allows direct visualization of the plaque surface and intraluminal structures. It enables assessment of the plaque color (white, red or yellow), and can illuminate plaque complications, such as rupture, intimal tears and thrombosis with a higher sensitivity than angiography [21–24]. Angioscopically, normal artery segments appear as glistening white, whereas atherosclerotic plaques can be categorized based on their angioscopic color as yellow or white. Platelet-rich thrombus at the site of plaque rupture is characterized as white granular material and fibrin/erythrocyte-rich thrombus as an irregular, red structure protruding into the lumen. Yellow plaques are associated with ACS and thrombosis [25,26]. They have also been correlated with other features of vulnerability, such as positive remodeling and increased distensibility [27].

The major limitation of angioscopy is that it requires a blood-free field during image acquisition, which can be obtained either by complete vessel occlusion or by continuous saline flushing in front of the angioscope. Specifically, nowadays, CAS (Vecmova®, Clinical Supply Co., Gifu, Japan) can be made while blood is cleared away from view by the injection of 5–10 ml saline. Furthermore, only a limited part of the coronary tree can be investigated (i.e., vessels > 2 mm in diameter) and assessment of stenotic lesions may prove difficult. Finally, angioscopy only images the luminal surface and, although changes in the vessel wall are reflected on the surface, this might not be sufficiently sensitive to detect subtle alterations in plaque composition or plaque burden in the presence of positive remodeling [28].

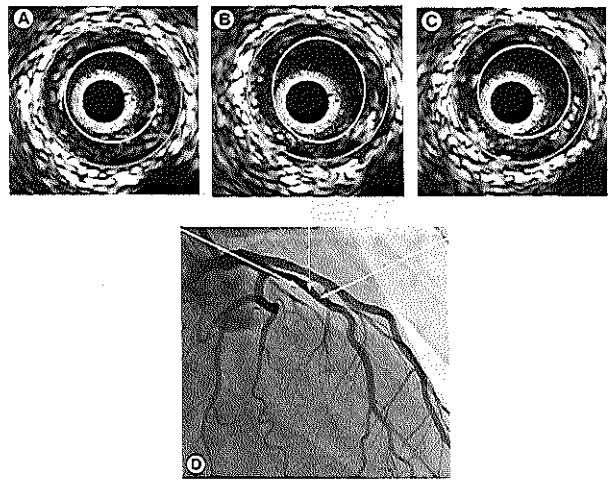

Figure 1. (A, B & C) show three consecutive intravascular ultrasound images of the proximal left anterior descending **(D)**, which is disease-free angiographically. Note that the intravascular ultrasound images show a plaque burden of 50%.

Kubo *et al.* reported the ability of optical coherence tomography (OCT) for assessment of the culprit lesion morphology in AMI in comparison with intravascular ultrasound (IVUS) and CAS [24]. The incidence of plaque rupture observed by OCT was 73%, 47% by CAS (p = 0.035) and 40% by IVUS, (p = 0.009). Furthermore, OCT (23%) was superior to CAS (3%; p = 0.022) and IVUS (0%; p = 0.005) in the detection of fibrous cap erosion. The intracoronary thrombus was observed in all cases by OCT and CAS, but it was identified in 33% by IVUS (vs OCT; p < 0.001).

Intravascular ultrasound

Currently, the gold standard for intracoronary imaging is IVUS. Positive vessel remodeling can readily be evaluated with IVUS [29–31]. In addition to the lumen and vessel borders, IVUS examination can provide real-time, high-resolution images of the plaque (FIGURE 2). Visual assessment of plaque echogenicity provides semiquantitative tissue characterization [32]. Calcification can be identified with a sensitivity and specificity of approximately 90%, as bright echo signals with acoustic shadowing [33]. Lipid deposits, visualized as echolucent zones, can be detected with high sensitivity (78–95%), but low specificity (30%) [34,35]. Moreover, the axial resolution of IVUS is in the range of 100–150 µm, whereas the fibrous cap of a TCFA is thinner than 65 µm and, therefore, cannot be visualized by IVUS. Despite these limitations, large eccentric plaques containing an echolucent zone by IVUS were associated with the development of ACS in a prospective study [36]. Microbubble contrast-enhanced IVUS can measure activity and inflammation within atherosclerotic plaques by imaging vasa vasorum density, which is increasingly considered as a strong marker for plaque vulnerability [37]. A few limitations of IVUS can be improved by analyzing the backscattered ultrasound signal using more sophisticated techniques for tissue characterization [38].

Intravascular ultrasound radiofrequency analysis: virtual histology

IVUS gray-scale imaging is formed by the envelope (amplitude) of the radiofrequency signal, discarding a considerable amount of information lying beneath and between the peaks of the signal. The frequency and power of the signal commonly differ between tissues, regardless of similarities in the amplitude. IVUS-virtual histology (IVUS-VH, Volcano Corp., Rancho Cordoba, USA) involves spectral analysis of the data and evaluates different spectral parameters (e.g., Y-intercept, minimum power, maximum power, mid-band power, frequency at minimum power, frequency at maximum power, slope) to construct

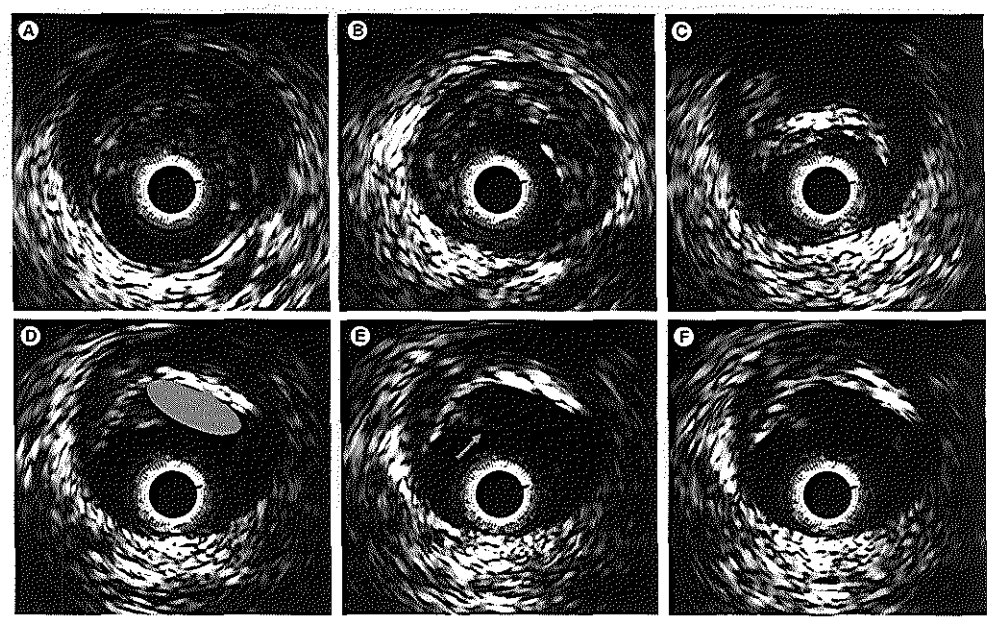

Figure 2. IVUS plaque types. These IVUS images, taken from distal to proximal in the same vessel **(A–F)**, represent different IVUS gray scale plaque types. **(A)** shows a soft plaque, large plaque burden and positive remodeling. On the contrary, **(B)** shows a fibrotic plaque (similar echogenicity to adventitia). **(C)** Depicts a superficial calcified plaque (see shadowing). **(D–F)**, a plaque rupture is illustrated; a large empty cavity (red oval, **[D]**) with the remnant of fibrous cap is overhanging the lumen (arrow, **[E]**).

tissue maps that classify plaque into four major components (fibrous, fibrolipidic, necrotic core and calcium). Different plaque components are assigned different color codes: calcified (white), fibrous (green), fibrolipidic (greenish–yellow) and necrotic core (red) [39]. Although this classification was initially evaluated *in vitro*, more recently IVUS-VH pre- and post-procedure has also been correlated with pathological specimens obtained by atherectomy with good correlation for all four tissue types [40]. As assessed by IVUS-VH, the sensitivity and specificity for fibrous tissue was 86 and 90.5%, fibrofatty 79.3 and 100%, necrotic core 67.3 and 92.9%, and dense calcium 50 and 98.9%, respectively.

IVUS-VH data are currently acquired using a commercially available 64-element phased-array catheter (Eagle Eye™ 20 MHz catheter, Volcano Corporation, Rancho Cordova, USA). Using an automated pullback device, the transducer is withdrawn at a continuous speed of 0.5 mm/s up to the ostium. IVUS-VH acquisition is ECG-gated at the R-wave peaks using a dedicated console.

IVUS B-mode images are reconstructed by customized software and contour detection is performed using cross-sectional views with semi-automatic contour detection software to provide quantitative geometrical and compositional measurements. Due to the unreliability of manual calibration, the radiofrequency data is normalized using a technique known as 'blind deconvolution', an iterative algorithm that deconvolves the catheter transfer function from the backscatter, thus accounting for catheter-to-catheter variability [41–43].

It has been our observation that in the near field an excessive amount of necrotic core was present. The developers have accounted for this and a proper correction was introduced in the current version of classification tree.

Our group recently evaluated the incidence of IVUS-derived TCFA (IDTCFA) using IVUS-VH [44]. Two independent IVUS analysts defined IDTCFA as a lesion fulfilling the following criteria in at least three consecutive cross-sectional areas (CSAs): necrotic core of 10% or more without evident overlying fibrous tissue, and lumen obstruction greater than or equal to 40%. In this study, 62% of patients had at least one IDTCFA in the interrogated vessels. ACS patients had a significantly higher incidence of IDTCFA than stable patients (3.0 [interquartile range: 0.0–5.0] IDTCFA/coronary vs 1.0 [interquartile range: 0.0–2.8] IDTCFA/coronary; $p = 0.018$) Finally, a clear clustering pattern was seen along the coronaries, with 66.7% of all IDTCFAs located in the first 20 mm, whereas further along the vessels the incidence was significantly lower (33.3%; $p = 0.008$). This distribution of IDTCFAs is consistent with previous *ex vivo* and clinical studies, with a clear clustering pattern from the ostium demonstrating a nonuniform distribution of vulnerable plaques along the coronary tree [45]. Patients presenting with ACS had a significantly higher prevalence of IDTCFA even in nonculprit vessels, supporting the concept of a multifocal process [46]. Of note, the lesion percent area stenosis and the mean necrotic core areas of the IDTCFAs detected by IVUS-VH were also similar to previously reported histopathological data (55.9 vs 59.6% and 19 vs 23%, respectively) [14].

It is worth mentioning that, although the most accepted threshold to define a cap as 'thin' has previously been set at less than 65 µm, this was based on postmortem studies that looked at ruptured plaques [7]. Extrapolation of such criteria to *in vivo* studies requires caution. It is well established that tissue shrinkage occurs during tissue fixation [47]. Shrinkage (particularly of collagen tissue, the main component of fibrous caps) of up to 60, 15 and 80% can occur during critical-point-drying, free-drying and air-drying, respectively [48]. Furthermore, postmortem contraction of arteries is an additional confounding factor [49,50]. Since the axial resolution of IVUS-VH is 246 µm, we assumed that the absence of visible fibrous tissue overlying a necrotic core suggested a cap thickness of below 246 µm and used the absence of such tissue to define a thin fibrous cap [51].

We have recently developed software to quantify the amount of necrotic core in contact with the lumen, enabling refinement of our analysis. Our current definition of an IVUS-derived TCFA (IDTCFA) is a lesion fulfilling the following criteria in at least three consecutive CSAs:

- Plaque burden greater than or equal to 40%;
- Confluent necrotic core of 10% or more in direct contact with the lumen (i.e., no visible overlying tissue) in the investigated CSA;
- All consecutive CSAs having the same morphologic characteristics are considered as part of the same IDTCFA lesion [53].

In a recent study, using this refined definition of TCFA as assessed by IVUS-VH, in patients with ACS underwent IVUS of all three epicardial coronaries, on average, there were two IDTCFA per patient with half of them showing outward remodeling [52] (FIGURE 3).

The potential value of IVUS-VH in the prediction of adverse coronary events is currently under evaluation in two international multicenter prospective studies (the PROSPECT study and the Integrated Biomarker and Imaging Study [IBIS] II trial).

Intravascular ultrasound radiofrequency analysis: palpography

This technique allows the assessment of local mechanical tissue properties. For a defined pressure difference, soft tissue (e.g., lipid-rich) components will deform more than hard tissue components (e.g., fibrous, calcified) [53,54]. Radiofrequency data obtained at different pressure levels are compared to determine the local tissue deformation.

Each palpogram represents the strain information for a certain cross section over the full cardiac cycle. The longitudinal resolution of the acquisitions depends on heart rate and pullback speed. With a heart rate of 60 bpm and a pullback speed of 1.0 mm/s, the longitudinal resolution is 1.0 mm. Palpograms are acquired using a 20-MHz phased array IVUS catheter (Eagle Eye). Digital radiofrequency data are acquired using a custom-designed workstation.

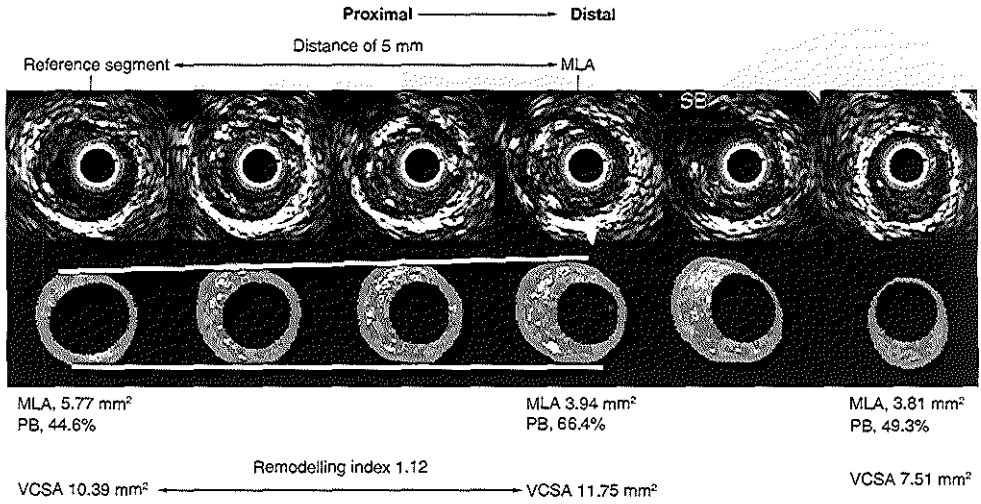

Figure 3. Intravascular ultrasound (IVUS) gray-scale frames and their corresponding virtual histology frames of an IVUS-derived thin-cap fibroatheroma (four central frames) and the proximal and distal reference segment in which the remodeling index was calculated.
MLA: Minimum luminal area; PB: Plaque burden; VCSA: Vessel cross-sectional area.
Virtual histology color code: green is fibrous, greenish is fibrofatty, red is necrotic core and white is dense calcium.

The local strain is calculated from the gated radiofrequency traces using cross-correlation analysis and displayed, color-coded, from blue (for 0% strain) to red to yellow (for 2% strain) [55]. Plaque strain values are assigned a Rotterdam classification (ROC) score ranging from I–IV (ROC I = 0 to <0.6%; ROC II = 0.6 to <0.9%; ROC III = 0.9 to <1.2%; ROC IV > 1.2%) (FIGURE 4) [56]. A region is defined as a high-strain spot when it has a ROC III–IV that spans an arc of at least 12° at the surface of a plaque (identified on the IVUS recording) adjacent to low-strain regions (<0.5%). Our group has demonstrated that palpography has a high sensitivity (88%) and specificity (89%) to detect vulnerable plaques *in vitro* [53]. Postmortem coronary arteries were investigated with intravascular elastography and subsequently processed for histology. There was a positive correlation between the presence of high strain and the amount of macrophages ($p < 0.006$) and an inverse relation between the amount of smooth muscle cells and strain ($p < 0.0001$). Vulnerable plaques identified by palpography had a thinner cap than nonvulnerable plaques ($p < 0.0001$). In a subsequent study, 55 patients with stable angina, unstable angina or AMI were analyzed. Among patients with stable angina, the prevalence of deformable plaques per vessel was significantly fewer (0.6 ± 0.6) than in unstable angina patients (1.6 ± 0.7; $p = 0.0019$) or AMI patients (2.0 ± 0.7; $p < 0.0001$). In IBIS I study, on palpography, both the absolute number of high-strain spots (grade 3/4) in the ROI ($p = 0.009$) and their density per centimeter ($p = 0.012$) decreased significantly between baseline and follow-up. This decrease in the overall population was largely driven by changes in the subgroup of patients with STEMI; this group had both the highest number of high-strain spots at baseline and the most marked relative decrease during follow-up, compared with patients with other clinical presentations. At 6-month follow-up, the density of high-strain spots (1.2 ± 1.4/cm) was comparable among clinical subgroups [57].

Optical coherence tomography

Optical coherence tomography (OCT) is an optical analogue of ultrasound; however, it uses light instead of sound to create an image [58,59]. For OCT imaging, low coherence, near infrared (NIR) light with a wavelength around 1300 nm is used since it minimizes the energy absorption in the light beam caused by protein, water, hemoglobin and lipids. The light waves are reflected by the internal microstructures within biological tissues as a result of their differing optical indices.

This technique provides a resolution of 10–20µm *in vivo*: this level of detail is well beyond the level of resolution of IVUS (100–150 µm) [60,61]. OCT has been demonstrated to be highly sensitive and specific for characterizing atherosclerotic plaques *in vitro* when compared with histological analysis [62–64] with a sensitivity and specificity of 71–79% and 97–98% for fibrous plaques, 95–96% and 97% for fibrocalcific plaques, and 90–94% and 90–92% for lipid-rich plaques, respectively. In addition, the interobserver and intraobserver reliabilities of

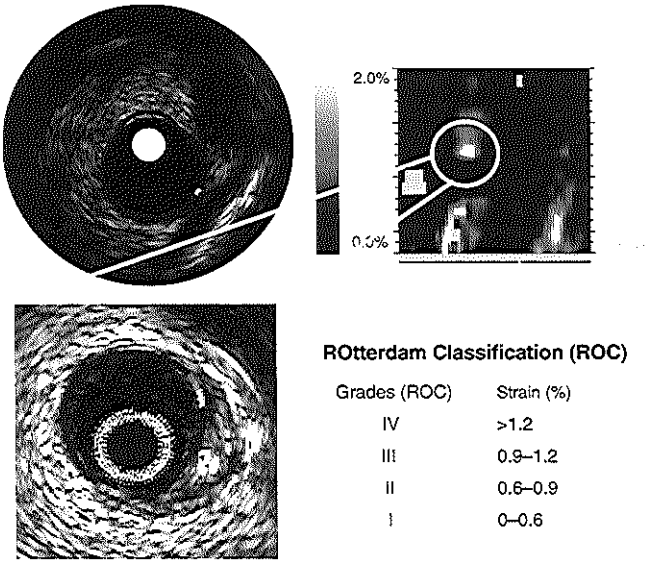

Figure 4. IVUS palpography. The local strain is calculated from the gated radiofrequency traces using cross-correlation analysis and displayed, color-coded, from blue (for 0% strain) to red to yellow (for 2% strain).
Plaque strain values are assigned a Rotterdam Classification (ROC) score ranging from 1 to 4 (ROC I= 0 to <0.6%; ROC II= 0.6 to <0.9%; ROC III= 0.9 to <1.2%; ROC IV >1.2%).

OCT assessment were high (κ values of 0.88 and 0.91, respectively) [64]. *In vitro* comparison of OCT with IVUS demonstrated superior delineation by OCT of structural details such as thin caps, lipid pools or tissue proliferation [65]. An *in vitro* comparison of OCT, integrated backscatter IVUS (similar methodology to IVUS-VH) and conventional IVUS found that OCT had the best potential for tissue characterization of coronary plaques, with higher sensitivity and specificity compared with the other imaging modalities [66]. However, a recent study comparing OCT with histopathology reported a lower sensitivity for plaque components. Misclassification occurred in 41% of lesions, predominantly due to a combination of incomplete penetration depth into the vessel wall and the inability to distinguish calcium deposits from lipid pools [67].

In a pilot clinical study, our group performed *in vivo* OCT analysis of the coronary arterial wall in patients who were undergoing percutaneous coronary interventions. Imaging was possible in all patients and the entire vessel circumference was visualized at all times. A wide spectrum of different plaque morphologies was observed. OCT allowed for differentiation of the normal artery wall and inhomogeneous, mixed plaques, as well as TCFAs with inhomogeneous, low-reflecting necrotic cores, covered by highly reflecting thin fibrous caps [61].

As a result of its high axial resolution, there is no doubt that OCT is the *in vivo* gold standard for identifying and measuring the thickness of the fibrous cap (FIGURE 5): an *in vivo* study found a significant difference in minimal cap thickness between AMI and stable angina patients, with median (interquartile range) values of 47.0 µm (25.3–184.30) and 102.6 µm (22.0–291.1), respectively (p = 0.02) [68]. On top of its reliability as a tool to measure the thickness of the cap *in vivo*, recent postmortem and *in vivo* studies have shown that OCT is capable of evaluating the macrophage content of infiltrated fibrous caps [69,70].

Kubo *et al.* evaluated the ability of intracoronary OCT to assess culprit lesions during primary PCI in patients with AMI. The thickness of the remnants of the fibrous cap after symptomatic rupture measured *in vivo* was 49 ± 21 µm [24].

The main limitation of OCT is the shallow penetration depth (2 mm) into the tissue, which hampers imaging of the entire vessel wall in large vessels and light absorbance by blood that currently needs to be overcome by saline infusion and balloon occlusion, thereby precluding interrogation of long and proximal segments of the coronary tree, which may limit the clinical applications of this technique.

Thermography

Atherosclerosis is accompanied by inflammation, and vulnerable plaques have been associated with increased macrophage activity, metabolism and inflammation [71]. Activated macrophages produce thermal energy, which might be detected on the surface of these atherosclerotic lesions using specially designed catheters equipped with thermistor sensors at the distal tip [72]. A rise in temperature can be found in atherosclerotic plaques compared with disease-free coronary segments. Temperature differences between an atherosclerotic plaque and normal vessel wall increase progressively from patients with stable angina to patients with AMI with a maximum temperature difference to the background temperature of 1.5 ± 0.7°C [73]. In a prospective study, the same investigators reported an association between temperature heterogeneity and the incidence of adverse events at follow-up in patients with coronary artery disease undergoing a successful percutaneous intervention [74]. In addition, treatment with statins seems to affect the thermographic results: in nonculprit lesions the temperature difference was lower in the group treated with statins compared with the untreated group (0.06 ± 0.05°C vs 0.11 ± 0.10°C; p = 0.05) [75].

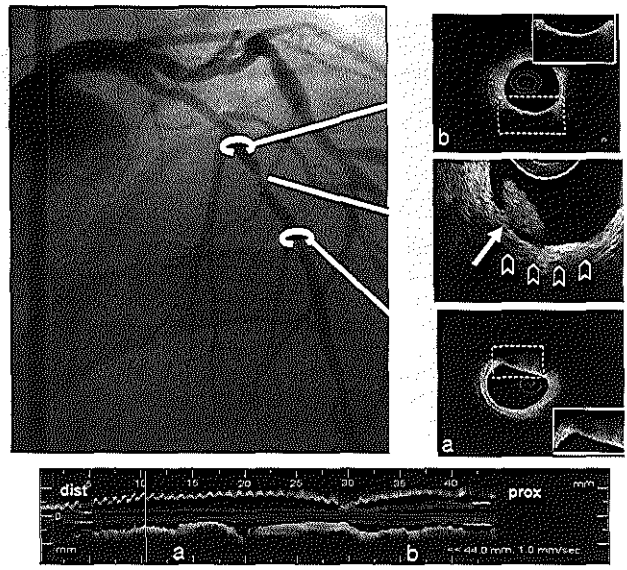

Figure 5. OCT and standard coronary angiography correlation. Angiography shows a complex lesion in the mid left anterior descending. The optical coherence tomography image shows a ruptured plaque with thrombus at that site (white arrow). Proximally and distally to the culprit lesion, thin-capped fibroatheroma lesions are present (**[B]** and **[A]** respectively).

However, there are several different aspects that deserve further investigation. The prevalence and distribution of inflammatory cells in stable and unstable atherosclerotic plaque is unclear, and the predictive value of 'warm' lesions remains elusive. Furthermore, the impact of different coronary flow conditions on plaque temperature ('cooling effect') is still not completely understood [76,77]. Simulations have revealed that the correct interpretation of intravascular thermographic measurements requires data on the flow and on the morphologic characteristics of the atherosclerotic plaque [78].

There are a few limitations to the routine use of thermography in the catheterization laboratory:

- Most of the catheters used still comprise over-the-wire systems;
- Accurate temperature assessment requires direct contact of the thermistors with the vessel wall, with the associated potential risk of endothelial damage;
- Since the temperature within the vessel changes rapidly with fluid application, any intracoronary injection of contrast dye, flush or medication has to be avoided before and during measurements [79].

Intravascular magnetic resonance

Magnetic resonance (MR) is a nonionizing diagnostic tool exploiting the spins of the nuclear protons in a strong magnetic field. For intravascular diagnosis, two different approaches have been introduced.

The first, conventional approach visualizes the anatomical structure by using a coil placed in a catheter or wire in combination with an external magnet (MR imaging [MRI]). While this approach has been (10 years ago) [80] principally shown to be able to provide detailed information on structure and composition of the arterial wall and plaque, the procedure has yet to be performed in a MR magnet, not in a cardiac catheterization laboratory. The accuracy for MRI differentiation of plaque components has been validated *in vitro* and feasibility demonstrated *in vivo* [81]. The 0.030-inch intravascular (IV)-MRI coil had a sensitivity and specificity of 73 and 85%, respectively, for lipid, 83 and 81%, respectively, for fibrous tissue and 100 and 97%, respectively, for calcification. Subsequently, the same system was applied in human iliac arteries *in vivo* using a 1.5-T magnet with a resolution of 312 μm. Complete vessel wall analysis was possible in all 25 patients and required 20 min for an arterial segment of 20 mm length. Compared to IVUS, mean lumen diameters were similar, but the outer wall area was overestimated by IVMRI (mean 116.4 ± 4.7 mm^2 vs 86.6 ± 5.8 mm^2; p = 0.0001). However, interobserver agreements for IVMRI were much higher (κ: 0.68–0.79) than for IVUS (κ: 0.21).

The other, novel approach analyses the chemical composition by placing both, the coils and miniaturized magnets on the tip of a catheter, without the need of external magnets (MR spectroscopy) and can be performed in the cardiac catheterization laboratory [82].

MR spectroscopy can identify fibrous and lipid-rich tissue by measuring differential water diffusion in a field of view. Acquired data are displayed as color-code sectors based on the lipid fraction index for each zone of the field of view. Blue indicates no lipid, gray corresponds to intermediate lipid content and yellow indicates high lipid content (Figure 6). Clinical fesibility of cather-based, self-contained IV MR spectroscopy has been demonstrated recently in patients scheduled for coronary catheterization [83].

Preclinical trials employing this technology demonstrated its capability to differentiate plaque composition of human aortas, coronary and carotid arteries *in vitro*. IVMR spectroscopy could accurately detect different components (fibrous cap, smooth muscle cells, organizing thrombus, fresh thrombus, edema, lipid and calcium) with sensitivities and specificities ranging from 84 to 100%. Agreement with histology for

grading the extent of intraplaque lipid accumulation was 74% for grading of intimal thickness 80%. Further analysis revealed high correlation to histological analysis of a wide spectrum of plaque types in 15 of 16 (94%) aortic lesions and 16 of 18 (89%) coronary lesions (sensitivity: 100%; specificity: 89%), including one plaque rupture, three TCFAs, seven thick cap fibrous atheromas, four fibrocalcific plaques, two intimal xanthomas and one adaptive intimal thickening [84].

Current limitations include the limited field of view, the size of the catheter, the need for direct vessel wall contact and the time required for acquisition. In the past, the use of an auto-perfusion balloon during data acquisition has been proposed to limit ischemia [85].

Clearly, IVMR diagnostics remain an exciting area still under development. Catheter-based systems will further increase the user friendliness, their sample volume and allow for scanning of longer arterial segments. Upcoming developments include the improvement MR plaque differentiation by the use of contrast agents, such as paramagnetic gadolinium-based contrast or supraparamagnetic contrast agents (iron oxide nanoparticles), that can accumulate in macrophages [86,87]. There are still a few unanswered questions, including the effect of the thermal energy generated on small arteries and on coronary artery stents, although conventional MRI appears safe in this setting [88]. In addition, the presence of a permanent pacemaker is a contra-indication for any MRI imaging due to reports of arrhythmias and death.

Raman & near-infrared spectroscopy

A number of spectroscopic intravascular imaging techniques have been developed recently and are still under investigation [89]. Spectroscopy can provide qualitative and quantitative information about chemical plaque composition. The Raman effect is created when incident laser light (typically 750–850 nm wavelength) excites molecules in a tissue sample, which scatter light at a different wavelength. This change in wavelength, called the Raman effect is dependent on the chemical components of the tissue sample [90,91] and can therefore provide quantitative information about molecular composition [92–94]. Raman spectroscopy has shown acceptable correlation compared with histology (r = 0.68 for cholesterol and r = 0.71 calcification) and with IVUS *in vitro* [94,95].

Alternatively, NIR molecular vibrational transitions can be measured in the NIR region (750–2500 nm) and laser spectroscopy using wavelengths of 360–510 nm has been evaluated *in vitro* [95,96].

In near-infrared spectroscopy, it is observed how different substances absorb and scatter NIR light to different degrees at various wavelengths. An NIR spectrometer emits light into a sample and measures the proportion of light that is returned over a wide range of optical wavelengths. The return signal is then plotted as a graph of absorbance (y-axis) at different wavelengths (x-axis) called a spectrum.

In aortic and coronary artery autopsy, specimens have confirmed the ability of the technique to identify lipid-rich TCFAs through blood [97]. A catheter-based system has been developed to address the challenges of access to the coronary artery, blood, motion and the need to scan, which must be overcome for use in patients. Initial clinical experience in six patients with stable angina demonstrates that high-quality NIR spectra can be safely obtained [89]. Additional studies are planned to validate the ability of the technique to identify lipid-rich coronary artery plaques and ultimately link chemical characterization with subsequent occurrence of an ACS (FIGURE 7) [98,99].

Treatment

Treatment of asymptomatic, nonobstructive coronary lesions may be a desirable pursuit, but the pre-emptive strike may be a risky, time-consuming and expensive proposition. Assumptions include:

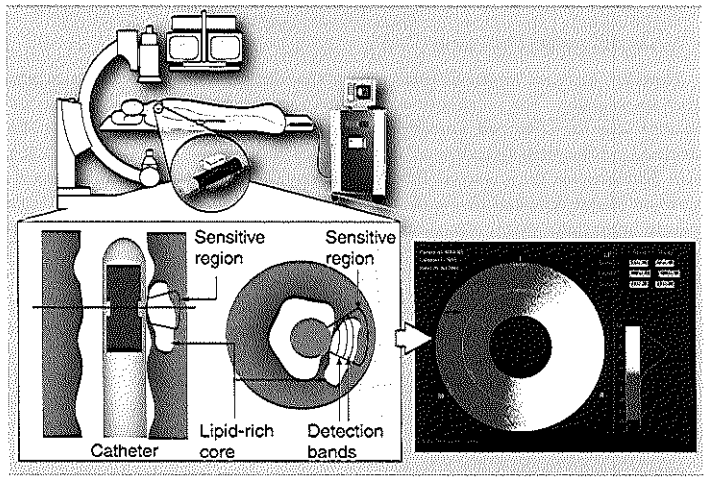

Figure 6. Intravascular magnetic resonance. The magnetic fields generated by the probe located at the tip of the catheter, create a FOV with a sector shape, looking sideways into the artery wall. The FOV has a lateral resolution of 60°, a longitudinal length of 2 mm and a depth of 200 µm. It makes the analysis for the area comprised between 50 and 200 µm from the lumen.
Acquired data is displayed as color-code sectors based of the lipid fraction index for each zone of the FOV. Blue indicates no lipid, gray correspond to intermediate lipid content and yellow indicates high lipid content.
FOV: Field of view.

- Accepting that the specific pathology can be defined in living subjects
- Presuming that this particular pathology is responsible for future clinical events
- The 'fingerprint' of this pathology can be reliably detected
- These findings are predictive of future adverse clinical events [3]

Based on these assumptions, initial risk stratification of asymptomatic patients drawn from the general population will be required, probably using an early screening method able to detect nonobstructive suspicious lesions. Then, patients will have to be further stratified based on noninvasive/invasive imaging ('regional stratification tool'). Once a suspect lesion is identified, focal treatment will be based on a prediction model to prove both safety and efficacy, assuming the endovascular detection modality was correct. Among symptomatic patients (non-obstructive, non-culprit lesion in the setting of an ACS), a regional stratification strategy may be sufficient to justify therapy in the future. The main question still remains as if the therapy should focus on the entire segment containing the lesion or the 'focal' area in which the TCFA is identified.

Segmental therapy

Treating all three major coronary arteries or their proximal parts requires a technology capable of delivering the therapeutic effect across long segments without the need for multiple interventions or guidance to a particular lesion. Current stenting technology is simply not up to the task to consider so-called 'full-metal-jacket' stenting of an entire vessel [100]. Until further improvements in vascular prosthesis are made, the industry is seeking methods for passivating at-risk vessels through therapeutic applications of drugs and energy. The merge between targeted nanoparticles and local drug delivery are of special interest as potential therapeutic alternatives capable of treating large vascular territories [101].

Sonotherapy directs energy in the form of ultrasonic vibrations to the lesion and vessel wall and has been shown to decrease cell proliferation and smooth muscle cell migration *in vitro*, but very little clinical experience exists. Cryotherapy involves the therapeutic application of heat removal or hyperthermia in a segment to induce a passivation effect on the intima to halt disease progression [102,103]. Photodynamic therapy utilizes pharmaceutical compounds, which are activated locally to reduce damage outside of the treatment zone [104]. A more selective approach to photo-angioplasty is a cell targeting technique known as selective photothermolysis, which targets particular cells (e.g., macrophages) for apoptosis using nanomarkers, limiting damage to nearby structures. The other directed energy techniques are still in early stage research and there are not available data on their safety and efficacy.

Focal therapy

Myocardial infarctions are typically the result of focal complex or vulnerable lesions, and it is quite reasonable that many interventionalists have suggested treating high-risk plaques with the same tools currently employed for these symptomatic lesions (bare metal stents or drug-eluting stents). Balloon-expandable metallic scaffoldings provide substantial radial forces for dilating hard, obstructive plaques leading to the unavoidable and uncontrollable disruption of the vascular structures intended to treat. Restenosis after treating a lesion with a bare metal stent has been curbed by slow-release antiproliferative drug coatings applied directly to the stent. Unfortunately, recent clinical evidence points to increased risk of late thrombosis as a result of the drug and its affect on endothelial cell functioning and vascular healing, especially in the setting of ACS [105] Based on these risks, these devices, in their current form, do not appear to be a proper approach to pre-emptive treatment of vulnerable or at-risk plaques.

It is clear that current practices and available technologies in focal treatment are primarily focused on improving luminal diameter in occlusive plaques and are not well suited for treatment of vulnerable plaques. More focus is needed on achieving the main objectives of focal therapy: mechanical stabilization, promotion of vascular healing and reduction of inflammation. If mechanical stabilization is the objective, the proposed device must find a point of equilibrium its intrinsic expansive force radial force and its capability to induce excessive vascular injury. Computational finite element and fluid structure interaction models are critical in the development of these devices. Recently, it has been shown that geometrical changes in the shape of the lumen may affect unfavorably or favorably the distribution of local stress, either leading to plaque rupture or reinforcing of the thin fibrous cap [106,107]. Preliminary data using self-expandable nitinol-based devices designed with the objective of inducing reinforcement of the cap and necrotic core compression but not cap rupture have been published [108,109]. Conceptually, these devices must reinforce the fibrous cap, reshape the necrotic core and mechanically stabilize the lesion at risk of disruption. Another important aspect of device development is the possibility of *in situ*

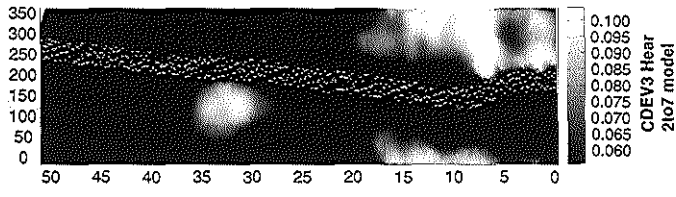

Figure 7. Near infra-red spectroscopy. Demonstration of spectral findings in the left anterior descending coronary artery of an autopsy specimen (unpublished data, on file InfraReDx, Inc., Burlington, Massachusetts). The panel shows the results of the scan, with distance along the lumen on the x-axis and arc of rotation on the y-axis. As indicated by the yellow signal, the scan successfully detected lipid necrotic core rich areas. Image courtesy of James E Muller.

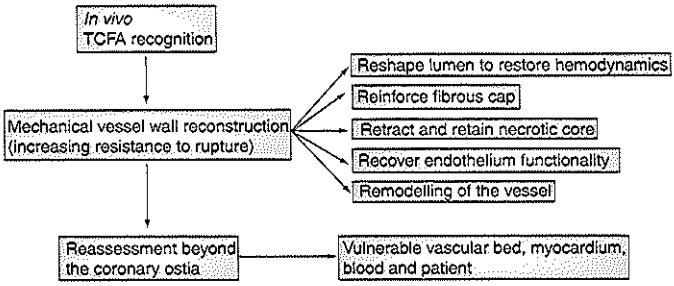

Figure 8. Treatment of coronary vulnerable plaques.

promoting tissue regeneration. Specifically, the regeneration of the endothelium and recovery of its functionality by means of passive or active endothelial cell attraction is also under development [110]. Ideally, drug elution specifically targeting the inflammatory components of the plaque must be required to mitigate inflammation with the use of these devices. Although still early for human application, several technologies specifically designed to passivate vulnerable plaques are under validation phases in animal models. Their potential as therapeutic alternatives will probably depend on the development of accurate risk stratification strategies and the validation of device safety in the appropriate clinical setting.

Conclusion

Several invasive imaging techniques are currently under development to detect vulnerable coronary plaques in human coronary arteries *in vivo*. To date, none of the techniques described previously have been sufficiently validated and, most importantly, their predictive value for adverse cardiac events remains elusive. Intravascular palpography and virtual histology, based on conventional IVUS catheters, appear to be very promising and their predictive role is presently under investigation in a large international trial.

Very rigorous and well-designed studies are compelling for defining the role of each imaging modality. Noninvasive techniques and the assessment of humoral and genetic factors comprise complementary and important tools in this direction.

At present, the main purpose of all these evolving techniques is to improve our understanding of atherosclerotic disease and to define its natural history. Ultimately, the aims are to identify patients at high risk for future cardiovascular events and to evaluate the benefit from either local or systemic therapeutic interventions.

Expert commentary & five-year view

Unheralded ACS are common initial manifestations of coronary atherosclerosis and are frequently caused by plaque ruptures. TCFA is the morphology that most resembles plaque rupture. However, the natural history of these high-risk or vulnerable lesions remains unknown and the limited knowledge about their eventual prognosis is provided by retrospective histopathological studies. Detection of these vulnerable plaques *in vivo* is essential to study their natural history and to evaluate potential treatment modalities and, therefore, may ultimately have an important impact on the prevention of AMI and death. Several invasive imaging techniques are currently under development to detect vulnerable coronary plaques in human coronary arteries *in vivo*. The optimal device for imaging vulnerable plaque would combine several techniques, overcoming the deficiencies of each and providing information on different aspects of vulnerability. Currently, conventional grayscale IVUS, IVUS-VH and palpography are imaged with the same catheter during the same pullback. A combination of this catheter with either thermography capability or alternative imaging such as OCT or spectroscopy would be an exciting development. IVMRI also holds much promise. To date, none of the techniques described previously have been sufficiently validated and, most importantly, their predictive value for adverse cardiac events remains elusive. Very rigorous and well-designed studies are compelling for defining the role of each imaging modality. Noninvasive techniques and the assessment of biohumoral and genetic factors comprise complementary and important tools in this direction.

Financial & competing interests disclosure

The authors have no relevant affiliations or financial involvement with any organization or entity with a financial interest in or financial conflict with the subject matter or materials discussed in the manuscript. This includes employment, consultancies, honoraria, stock ownership or options, expert testimony, grants or patents received or pending, or royalties.

No writing assistance was utilized in the production of this manuscript.

Key issues

- The natural history of the so-called vulnerable plaque is unknown.
- There is not a single imaging technique able to fully characterize vulnerable plaques.
- Combination of some of these techniques may improve accuracy on vulnerable plaque detection.
- Ongoing studies using these techniques would provide better understanding of this intrincate process.

References

Papers of special note have been highlighted as:

- • of interest
- •• of considerable interest

1 Virmani R, Kolodgie FD, Burke AP, Farb A, Schwartz SM. Lessons from sudden coronary death: a comprehensive morphological classification scheme for atherosclerotic lesions. *Arterioscler. Thromb. Vasc. Biol.* 20, 1262–1275 (2000).

2 Schaar JA, Muller JE, Falk E *et al.* Terminology for high-risk and vulnerable coronary artery plaques. Report of a meeting on the vulnerable plaque, June 17th to 18th 2003, Santorini, Greece. *Eur. Heart J.* 25, 1077–1082 (2004).

3 Serruys PW, Garcia-Garcia HM, Regar E. From postmortem characterization to the *in vivo* detection of thin-capped fibroatheromas: the missing link toward percutaneous treatment: what if Diogenes would have found what he was looking for? *J. Am. Coll. Cardiol.* 50, 950–952 (2007).

4 Goldstein JA, Demetriou D, Grines CL, Pica M, Shoukfeh M, O'Neill WW. Multiple complex coronary plaques in patients with acute myocardial infarction. *N. Engl. J. Med.* 343, 915–922 (2000).

5 Waxman S, Ishibashi F, Muller JE. Detection and treatment of vulnerable plaques and vulnerable patients: novel approaches to prevention of coronary events. *Circulation* 114, 2390–2411 (2006).

6 Kolodgie FD, Burke AP, Farb A *et al.* The thin-cap fibroatheroma: a type of vulnerable plaque: the major precursor lesion to acute coronary syndromes. *Curr. Opin. Cardiol.* 16, 285–292 (2001).

7 Burke AP, Farb A, Malcom GT, Liang YH, Smialek J, Virmani R. Coronary risk factors and plaque morphology in men with coronary disease who died suddenly. *N. Engl. J. Med.* 336, 1276–1282 (1997).

8 Moreno PR, Falk E, Palacios IF, Newell JB, Fuster V, Fallon JT. Macrophage infiltration in acute coronary syndromes. Implications for plaque rupture. *Circulation* 90, 775–778 (1994).

9 Ross R. Atherosclerosis – an inflammatory disease. *N. Engl. J. Med.* 340, 115–126 (1999).

10 Loree HM, Kamm RD, Stringfellow RG, Lee RT. Effects of fibrous cap thickness on peak circumferential stress in model atherosclerotic vessels. *Circ. Res.* 71, 850–858 (1992).

11 Richardson PD, Davies MJ, Born GV. Influence of plaque configuration and stress distribution on fissuring of coronary atherosclerotic plaques. *Lancet* 2, 941–944 (1989).

12 Cheruvu PK, Finn AV, Gardner C *et al.* Frequency and distribution of thin-cap fibroatheroma and ruptured plaques in human coronary arteries: a pathologic study. *J. Am. Coll. Cardiol.* 50, 940–949 (2007).

13 Kolodgie FD, Virmani R, Burke AP *et al.* Pathologic assessment of the vulnerable human coronary plaque. *Heart* 90, 1385–1391 (2004).

14 Virmani R, Burke AP, Kolodgie FD, Farb A. Vulnerable plaque: the pathology of unstable coronary lesions. *J. Interv. Cardiol.* 15, 439–446 (2002).

15 Farb A, Burke AP, Tang AL *et al.* Coronary plaque erosion without rupture into a lipid core : a frequent cause of coronary thrombosis in sudden coronary death. *Circulation* 93, 1354–1363 (1996).

16 Arbustini E, Dal Bello B, Morbini P *et al.* Plaque erosion is a major substrate for coronary thrombosis in acute myocardial infarction. *Heart* 82, 269–272 (1999).

17 Kolodgie FD, Gold HK, Burke AP *et al.* Intraplaque hemorrhage and progression of coronary atheroma. *N. Engl. J. Med.* 349, 2316–2325 (2003).

18 Ambrose JA, Tannenbaum MA, Alexopoulos D *et al.* Angiographic progression of coronary artery disease and the development of myocardial infarction. *J. Am. Coll. Cardiol.* 12, 56–62 (1988).

19 Little WC, Constantinescu M, Applegate RJ *et al.* Can coronary angiography predict the site of a subsequent myocardial infarction in patients with mild-to-moderate coronary artery disease? *Circulation* 78, 1157–1166 (1988).

20 Topol EJ, Nissen SE. Our preoccupation with coronary luminology. The dissociation between clinical and angiographic findings in ischemic heart disease. *Circulation* 92, 2333–2342 (1995).

21 Mizuno K, Satomura K, Miyamoto A *et al.* Angioscopic evaluation of coronary-artery thrombi in acute coronary syndromes. *N. Engl. J. Med.* 326, 287–291 (1992).

22 Sherman CT, Litvack F, Grundfest W *et al.* Coronary angioscopy in patients with unstable angina pectoris. *N. Engl. J. Med.* 315, 913–919 (1986).

23 de Feyter PJ, Ozaki Y, Baptista J *et al.* Ischemia-related lesion characteristics in patients with stable or unstable angina: a study with intracoronary angioscopy and ultrasound. *Circulation* 92, 1408–1413 (1995).

24 Kubo T, Imanishi T, Takarada S *et al.* Assessment of culprit lesion morphology in acute myocardial infarction: ability of optical coherence tomography compared with intravascular ultrasound and coronary angioscopy. *J. Am. Coll. Cardiol.* 50, 933–939 (2007).

25 Thieme T, Wernecke KD, Meyer R *et al.* Angioscopic evaluation of atherosclerotic plaques: validation by histomorphologic analysis and association with stable and unstable coronary syndromes. *J. Am. Coll. Cardiol.* 28, 1–6 (1996).

26 Ueda Y, Ohtani T, Shimizu M, Hirayama A, Kodama K. Assessment of plaque vulnerability by angioscopic classification of plaque color. *Am. Heart J.* 148, 333–335 (2004).

27 Takano M, Mizuno K, Okamatsu K, Yokoyama S, Ohba T, Sakai S. Mechanical and structural characteristics of vulnerable plaques: analysis by coronary angioscopy and intravascular ultrasound. *J. Am. Coll. Cardiol.* 38, 99–104 (2001).

28 Smits PC, Pasterkamp G, de Jaegere PP, de Feyter PJ, Borst C. Angioscopic complex lesions are predominantly compensatory enlarged: an angioscopy and intracoronary ultrasound study. *Cardiovasc. Res.* 41, 458–464 (1999).

29 Nakamura M, Nishikawa H, Mukai S *et al.* Impact of coronary artery remodeling on clinical presentation of coronary artery disease: an intravascular ultrasound study. *J. Am. Coll. Cardiol.* 37, 63–69 (2001).

30 Maehara A, Mintz GS, Bui AB *et al.* Morphologic and angiographic features of coronary plaque rupture detected by intravascular ultrasound. *J. Am. Coll. Cardiol.* 40, 904–910 (2002).

31 Kotani J, Mintz GS, Castagna MT *et al.* Intravascular ultrasound analysis of infarct-related and non-infarct-related arteries in patients who presented with an acute myocardial infarction. *Circulation* 107, 2889–2893 (2003).

32 Aoki J, Abizaid AC, Serruys PW *et al.* Evaluation of four-year coronary artery response after sirolimus-eluting stent implantation using serial quantitative intravascular ultrasound and computer-

assisted grayscale value analysis for plaque composition in event-free patients. *J. Am. Coll. Cardiol.* 46, 1670–1676 (2005).

33 Di Mario C, The SH, Madretsma S *et al.* Detection and characterization of vascular lesions by intravascular ultrasound: an *in vitro* study correlated with histology. *J. Am. Soc. Echocardiogr.* 5, 135–146 (1992).

34 Potkin BN, Bartorelli AL, Gessert JM *et al.* Coronary artery imaging with intravascular high-frequency ultrasound. *Circulation* 81, 1575–1585 (1990).

35 Rasheed Q, Dhawale PJ, Anderson J, Hodgson JM. Intracoronary ultrasound-defined plaque composition: computer-aided plaque characterization and correlation with histologic samples obtained during directional coronary atherectomy. *Am. Heart J.* 129, 631–637 (1995).

36 Yamagishi M, Terashima M, Awano K *et al.* Morphology of vulnerable coronary plaque: insights from follow-up of patients examined by intravascular ultrasound before an acute coronary syndrome. *J. Am. Coll. Cardiol.* 35, 106–111 (2000).

37 Carlier S, Kakadiaris IA, Dib N *et al.* Vasa vasorum imaging: a new window to the clinical detection of vulnerable atherosclerotic plaques. *Curr. Atheroscler. Rep.* 7, 164–169 (2005).

38 Jeremias A, Kolz ML, Ikonen TS *et al.* Feasibility of *in vivo* intravascular ultrasound tissue characterization in the detection of early vascular transplant rejection. *Circulation* 100, 2127–2130 (1999).

39 Nair A, Kuban BD, Tuzcu EM, Schoenhagen P, Nissen SE, Vince DG. Coronary plaque classification with intravascular ultrasound radiofrequency data analysis. *Circulation* 106, 2200–2206 (2002).

40 Nasu K, Tsuchikane E, Katoh O *et al.* Accuracy of *in vivo* coronary plaque morphology assessment: a validation study of *in vivo* virtual histology compared with *in vitro* histopathology. *J. Am. Coll. Cardiol.* 47, 2405–2412 (2006).

41 Rodriguez-Granillo GA, Aoki J, Ong AT *et al.* Methodological considerations and approach to cross-technique comparisons using *in vivo* coronary plaque characterization based on intravascular ultrasound radiofrequency data analysis: insights from the Integrated Biomarker and Imaging Study (IBIS). *Int. J. Cardiovasc. Intervent.* 7, 52–58 (2005).

42 Kaaresen K. Deconvolution of sparse spike trains by iterated window maximization. *IEEE Trans. Signal Process* 45, 1173–1183 (1997).

43 Kaaresen K, Bolviken E. Blind deconvolution of ultrasonic traces accounting for pulse variance. *IEEE Trans. Ultrason. Ferroelectr. Freq. Control* 46, 564–573 (1999).

44 Rodriguez-Granillo GA, Garcia-Garcia HM, Mc Fadden EP *et al. In vivo* intravascular ultrasound-derived thin-cap fibroatheroma detection using ultrasound radiofrequency data analysis. *J. Am. Coll. Cardiol.* 46, 2038–2042 (2005).

45 Wang JC, Normand SL, Mauri L, Kuntz RE. Coronary artery spatial distribution of acute myocardial infarction occlusions. *Circulation* 110, 278–284 (2004).

46 Rioufol G, Finet G, Ginon I *et al.* Multiple atherosclerotic plaque rupture in acute coronary syndrome: a three-vessel intravascular ultrasound study. *Circulation* 106, 804–808 (2002).

47 Lowder ML, Li S, Carnell PH, Vito RP. Correction of distortion of histologic sections of arteries. *J. Biomech.* 40(2), 445–450 (2007).

48 Boyde A, Jones SJ, Tamarin A. Dimensional changes during specimen preparation for scanning electron microscopy. *Scan. Electron Microsc.* 1, 507–518 (1977).

49 Fishbein MC, Siegel RJ. How big are coronary atherosclerotic plaques that rupture? *Circulation* 94, 2662–2666 (1996).

50 Siegel RJ, Swan K, Edwalds G, Fishbein MC. Limitations of postmortem assessment of human coronary artery size and luminal narrowing: differential effects of tissue fixation and processing on vessels with different degrees of atherosclerosis. *J. Am. Coll. Cardiol.* 5, 342–346 (1985).

51 Nair A , Calvetti D, DG V. Regularized autoregressive analysis of intravascular ultrasound data: improvement in spatial accuracy of plaque tissue maps. *IEEE Trans. Ultrason. Ferroelectr. Freq. Control* 51, 420–431 (2004).

52 Garcia-Garcia HM, Goedhart D, Schuurbiers JC *et al.* Virtual histology and remodeling index allow *in vivo* identification of allegedly high risk coronary plaques in patients with acute coronary syndromes: a three vessel intravascular ultrasound radiofrequency data analysis. *Eurointervention* 2, 338–344 (2006).

53 Schaar JA, de Korte CL, Mastik F *et al.* Characterizing vulnerable plaque features with intravascular elastography. *Circulation* 108, 2636–2641 (2003).

54 Schaar JA, Regar E, Mastik F *et al.* Incidence of high-strain patterns in human coronary arteries: assessment with three-dimensional intravascular palpography and correlation with clinical presentation. *Circulation* 109, 2716–2719 (2004).

55 de Korte CL, Carlier SG, Mastik F *et al.* Morphological and mechanical information of coronary arteries obtained with intravascular elastography: feasibility study *in vivo*. *Eur. Heart J.* 23, 405–413 (2002).

56 van Mieghem CAG, Bruining N, Schaar JA *et al.* Rationale and methods of the integrated biomarker and imaging study (IBIS): combining invasive and non-invasive imaging with biomarkers to detect subclinical atherosclerosis and assess coronary lesion biology. *Int. J. Cardiovasc. Imaging* 21, 425–441 (2005).

57 Van Mieghem CA, McFadden ER de Feyter PJ *et al.* Noninvasive detection of subclinical coronary atherosclerosis coupled with assessment of changes in plaque characteristics using novel invasive imaging modalities: the Integrated Biomarker and Imaging Study (IBIS). *J. Am. Coll. Cardiol.* 47, 1134–1142 (2006).

58 Regar E vLA, Serruys PW. *Optical Coherence Tomography in Cardiovascular Research*. Informa Healthcare, London, UK (2007).

59 Huang D, Swanson EA, Lin CP *et al.* Optical coherence tomography. *Science* 254, 1178–1181 (1991).

60 Brezinski ME, Tearney GJ, Bouma BE *et al.* Imaging of coronary artery microstructure (*in vitro*) with optical coherence tomography. *Am. J. Cardiol.* 77, 92–93 (1996).

61 Regar E, Schaar JA, Mont E, Virmani R, Serruys PW. Optical coherence tomography. *Cardiovasc. Radiat. Med.* 4, 198–204 (2003).

62 Jang IK, Bouma BE, Kang DH *et al.* Visualization of coronary atherosclerotic plaques in patients using optical coherence tomography: comparison with intravascular ultrasound. *J. Am. Coll. Cardiol.* 39, 604–609 (2002).

63 Patwari P, Weissman NJ, Boppart SA *et al.* Assessment of coronary plaque with optical coherence tomography and high-frequency ultrasound. *Am. J. Cardiol.* 85, 641–644 (2000).

64 Yabushita H, Bouma BE, Houser SL *et al.* Characterization of Human Atherosclerosis by Optical Coherence Tomography. *Circulation* 106, 1640–1645 (2002).

65 Brezinski ME, Tearney GJ, Weissman NJ *et al.* Assessing atherosclerotic plaque morphology: comparison of optical coherence tomography and high frequency intravascular ultrasound. *Heart* 77, 397–403 (1997).

66 Kawasaki M, Bouma BE, Bressner J *et al.* Diagnostic accuracy of optical coherence tomography and integrated backscatter intravascular ultrasound images for tissue characterization of human coronary plaques. *J. Am. Coll. Cardiol.* 48, 81–88 (2006).

67 Manfrini O, Mont E, Leone O *et al.* Sources of error and interpretation of plaque morphology by optical coherence tomography. *Am. J. Cardiol.* 98, 156–159 (2006).

68 Jang IK, Tearney GJ, MacNeill B *et al.* *In vivo* characterization of coronary atherosclerotic plaque by use of optical coherence tomography. *Circulation* 111, 1551–1555 (2005).

69 Tearney GJ, Yabushita H, Houser SL *et al.* Quantification of macrophage content in atherosclerotic plaques by optical coherence tomography. *Circulation* 107, 113–119 (2003).

70 MacNeill BD, Jang IK, Bouma BE *et al.* Focal and multi-focal plaque macrophage distributions in patients with acute and stable presentations of coronary artery disease. *J. Am. Coll. Cardiol.* 44, 972–979 (2004).

71 Fuster V. Human lesion studies. *Ann. NY Acad. Sci.* 811, 207–224, discussion 224–225 (1997).

72 Casscells W, Hathorn B, David M *et al.* Thermal detection of cellular infiltrates in living atherosclerotic plaques: possible implications for plaque rupture and thrombosis. *Lancet* 347, 1447–1451 (1996).

73 Stefanadis C, Diamantopoulos L, Vlachopoulos C *et al.* Thermal heterogeneity within human atherosclerotic coronary arteries detected *in vivo*: a new method of detection by application of a special thermography catheter. *Circulation* 99, 1965–1971 (1999).

74 Stefanadis C, Toutouzas K, Tsiamis E *et al.* Increased local temperature in human coronary atherosclerotic plaques: an independent predictor of clinical outcome in patients undergoing a percutaneous coronary intervention. *J. Am. Coll. Cardiol.* 37, 1277–1283 (2001).

75 Toutouzas K, Drakopoulou M, Mitropoulos J *et al.* Elevated plaque temperature in non-culprit *de novo* atheromatous lesions of patients with acute coronary syndromes. *J. Am. Coll. Cardiol.* 47, 301–306 (2006).

76 Stefanadis C, Toutouzas K, Tsiamis E *et al.* Thermal heterogeneity in stable human coronary atherosclerotic plaques is underestimated *in vivo*: the 'cooling effect' of blood flow. *J. Am. Coll. Cardiol.* 41, 403–408 (2003).

77 Diamantopoulos L, Liu X, De Scheerder I *et al.* The effect of reduced blood-flow on the coronary wall temperature: are significant lesions suitable for intravascular thermography? 10.1016/S0195–668X(03)00440–00448. *Eur. Heart J.* 24, 1788–1795 (2003).

78 ten Have AG, Gijsen FJ, Wentzel JJ, Slager CJ, van der Steen AF. Temperature distribution in atherosclerotic coronary arteries: influence of plaque geometry and flow (a numerical study). *Phys. Med. Biol.* 49, 4447–4462 (2004).

79 Verheye S, De Meyer GRY, Krams R *et al.* Intravascular thermography: Immediate functional and morphological vascular findings. *Eur. Heart J.* 25, 158–165 (2004).

80 Correia LC, Atalar E, Kelemen MD *et al.* Intravascular magnetic resonance imaging of aortic atherosclerotic plaque composition. *Arterioscler. Thromb. Vasc. Biol.* 17, 3626–3632 (1997).

81 Larose E, Yeghiazarians Y, Libby P *et al.* Characterization of human atherosclerotic plaques by intravascular magnetic resonance imaging. *Circulation* 112, 2324–2331 (2005).

82 Blank A, Alexandrowicz G, Muchnik L *et al.* Miniature self-contained intravascular magnetic resonance (IVMI) probe for clinical applications. *Magn. Reson. Med.* 54, 105–112 (2005).

83 Regar E HB, Grube E, Halon D, Wilensky RL, Virmani R, Schneiderman J, Sax S, Friedmann H, Serruys PW, Wijns W. First-in-man application of a miniature self-contained intracoronary magnetic resonance probe. A multi-centre safety and feasibility trial. *Eurointervention* 2, 77–83 (2006).

84 Schneiderman J, Wilensky RL, Weiss A *et al.* Diagnosis of thin-cap fibroatheromas by a self-contained intravascular magnetic resonance imaging probe in *ex vivo* human aortas and *In situ* coronary arteries. *J. Am. Coll. Cardiol.* 45, 1961–1969 (2005).

85 Quick HH, Ladd ME, Hilfiker PR, Paul GG, Ha SW, Debatin JF. Autoperfused balloon catheter for intravascular MR imaging. *J. Magn. Reson. Imaging* 9, 428–434 (1999).

86 Barkhausen J, Ebert W, Heyer C, Debatin JF, Weinmann HJ. Detection of atherosclerotic plaque with Gadofluorine-enhanced magnetic resonance imaging. *Circulation* 108, 605–609 (2003).

87 Kooi ME, Cappendijk VC, Cleutjens KB *et al.* Accumulation of ultrasmall superparamagnetic particles of iron oxide in human atherosclerotic plaques can be detected by *In Vivo* magnetic resonance imaging. *Circulation* 107, 2453–2458 (2003).

88 Porto I, Selvanayagam J, Ashar V, Neubauer S, Banning AP. Safety of magnetic resonance imaging one to three days after bare metal and drug-eluting stent implantation. *Am. J. Cardiol.* 96, 366–368 (2005).

89 Moreno PR, Muller JE. Identification of high-risk atherosclerotic plaques: a survey of spectroscopic methods. *Curr. Opin. Cardiol.* 17, 638–647 (2002).

90 Brennan JF 3rd, Romer TJ, Lees RS, Tercyak AM, Kramer JR Jr, Feld MS. Determination of human coronary artery composition by Raman spectroscopy. *Circulation* 96, 99–105 (1997).

91 Baraga JJ, Feld MS, Rava RP. *In situ* optical histochemistry of human artery using near infrared fourier transform raman spectroscopy. *Proc. Natl Acad. Sci. USA* 89, 3473–3477 (1992).

92 Romer TJ, Brennan JF, Fitzmaurice M *et al.* Histopathology of human coronary atherosclerosis by quantifying its chemical composition with raman spectroscopy. *Circulation* 97, 878–885 (1998).

93 Romer TJ, Brennan JF, Puppels GJ *et al.* Intravascular ultrasound combined with raman spectroscopy to localize and quantify cholesterol and calcium salts in atherosclerotic coronary arteries. *Arterioscler. Thromb. Vasc. Biol.* 20, 478–483 (2000).

94 van de Poll SWE, Kastelijn K, Schut TCB *et al.* On-line detection of cholesterol and calcification by catheter based Raman spectroscopy in human atherosclerotic plaque *ex vivo*. *Heart* 89, 1078–1082 (2003).

95 Wang J, Geng YJ, Guo B *et al.* Near-infrared spectroscopic characterization of human advanced atherosclerotic plaques. *J. Am. Coll. Cardiol.* 39, 1305–1313 (2002).

96 Marcu L, Fishbein MC, Maarek JM, Grundfest WS. Discrimination of human coronary artery atherosclerotic lipid-rich lesions by time-resolved laser-induced fluorescence spectroscopy. *Arterioscler. Thromb. Vasc. Biol.* 21, 1244–1250 (2001).

97 Moreno PR, Lodder RA, Purushothaman KR, Charash WE, O'Connor WN, Muller JE. Detection of lipid pool, thin fibrous cap, and inflammatory cells in human aortic atherosclerotic plaques by near-infrared spectroscopy. *Circulation* 105, 923–927 (2002).

98 Caplan JD, Waxman S, Nesto RW, Muller JE. Near-infrared spectroscopy for the detection of vulnerable coronary artery plaques. *J. Am. Coll. Cardiol.* 47, C92–C96 (2006).

99 Waxman S, Ishibashi F, Caplan JD. Rationale and use of near-infrared spectroscopy for detection of lipid-rich and vulnerable plaques. *J. Nucl. Cardiol.* 14, 719–728 (2007).

100 Aoki J, Ong AT, Rodriguez Granillo GA *et al.* 'Full metal jacket' (stented length > or =64 mm) using drug-eluting stents for de novo coronary artery lesions. *Am. Heart J.* 150, 994–999 (2005).

101 Wickline SA, Neubauer AM, Winter PM, Caruthers SD, Lanza GM. Molecular imaging and therapy of atherosclerosis with targeted nanoparticles. *J. Magn. Reson. Imaging* 25, 667–680 (2007).

102 Serruys PW, Hoye A, Grollier G, Colombo A, Symons J, Mudra H. A European multi-center trial investigating the anti-restenotic effect of intravascular sonotherapy after stenting of de novo lesions (EUROSPAH: European Sonotherapy Prevention of Arterial Hyperplasia). *Int. J. Cardiovasc. Intervent.* 6, 53–60 (2004).

103 Kandzari DE, Chu A, Brodie BR *et al.* Feasibility of endovascular cooling as an adjunct to primary percutaneous coronary intervention (results of the LOWTEMP pilot study). *Am. J. Cardiol.* 93, 636–639 (2004).

104 Chou TM, Woodburn KW, Cheong WF *et al.* Photodynamic therapy: applications in atherosclerotic vascular disease with motexafin lutetium. Catheter Cardiovasc Interv 57, 387–394 (2002).

105 Finn AV, Nakazawa G, Joner M *et al.* Vascular responses to drug eluting stents: importance of delayed healing. *Arterioscler. Thromb. Vasc. Biol.* 27, 1500–1510 (2007).

106 Slager CJ, Wentzel JJ, Gijsen FJ *et al.* The role of shear stress in the generation of rupture-prone vulnerable plaques. *Nat. Clin. Pract. Cardiovasc. Med.* 2, 401–407 (2005).

107 Slager CJ, Wentzel JJ, Gijsen FJ *et al.* The role of shear stress in the destabilization of vulnerable plaques and related therapeutic implications. *Nat. Clin. Pract. Cardiovasc. Med.* 2, 456–464 (2005).

108 Moreno PR, Kilpatrick D, Purushothaman KR, Coleman L, O'Connor WN. Stenting vulnerable plaques improves fibrous cap thickness and reduces lipid content: understanding alternatives for plaque stabilization. *TCT* (2002).

109 Kaluza G, Alviar CL, Tellez A, Kolodgie F, Virmani R, Granada JF. First *in-vivo* experience with a novel low-pressure self-expanding intraarterial shield: a one-month study comparing to balloon expandable stents in porcine coronary arteries. *TCT* (2007).

110 Aoki J, Serruys PW, van Beusekom H *et al.* Endothelial progenitor cell capture by stents coated with antibody against CD34: the HEALING-FIM (Healthy Endothelial Accelerated Lining Inhibits Neointimal Growth-First In Man) Registry. *J. Am. Coll. Cardiol.* 45, 1574–1579 (2005).

Affiliations

- Héctor M García-García MD, MSc
  Thoraxcenter, Erasmus MC, Rotterdam, The Netherlands
  Tel.: +31 104 632 917
  Fax: +31 104 633 292
  h.garciagarcia@erasmusmc.nl
- Nieves Gonzalo MD
  Thoraxcenter, Erasmus MC, Rotterdam, The Netherlands
  Tel.: +31 104 632 917
  Fax: +31 104 633 292
  m.gonzalolopez@erasmusmc.nl
- Evelyn Regar MD, PhD
  Thoraxcenter, Erasmus MC, Rotterdam, The Netherlands
  Tel.: +31 107 035 729
  Fax: +31 107 032 357
  e.regar@erasmusmc.nl
- Juan F Granada
  Skirball Center for Cardiovascular Translational Research, The Cardiovascular Research Foundation, New York, NY, USA
  jgranada@crf.org
- PW Serruys, MD, PhD
  Professor, Thoraxcenter, Ba-583, Erasmus MC, Dr. Molewaterplein 40, 3015 GD Rotterdam, The Netherlands
  Tel.: +31 104 635 260
  Fax: +31 104 369 154
  p.w.j.c.serruys@erasmusmc.nl

CHAPTER 6.2

From postmortem characterization to the in vivo detection of thin-capped fibroatheromas: the missing link toward percutaneous treatment: what if Diogenes would have found what he was looking for?

Serruys PW, **Garcia-Garcia HM**, Regar E.

J Am Coll Cardiol. 2007;50:950-2.

EDITORIAL COMMENT

From Postmortem Characterization to the In Vivo Detection of Thin-Capped Fibroatheromas: The Missing Link Toward Percutaneous Treatment

What If Diogenes Would Have Found What He Was Looking For?*

Patrick W. Serruys, MD, PhD, FACC,
Hector M. Garcia-Garcia, MD, MSc, FACC,
Evelyn Regar, MD, PhD

Rotterdam, the Netherlands

In this issue of the *Journal,* Kubo et al. (1) and Cheruvu et al. (2) provide essential anatomical information about plaques that cause acute coronary thrombotic occlusion and their postulated precursors, thin-capped fibroatheromas (TCFAs). Histopathological assessment (Cheruvu et al. [2]) of the epicardial vascular tree revealed that the incidence of TCFAs and ruptured plaques is low and their spatial distribution is focal. An in vivo investigation of patients with acute myocardial infarction (Kubo et al. [1]) confirmed that, indeed, ruptured TCFA is the predominant morphologic substrate. Linking these observations together can cast light on possible options for treatment of such coronary lesions.

See pages 933 and 940

From Postmortem Observations to the In Vivo "Hot Plaque" Characterization

The current paradigm postulates a particular morphology for so-called vulnerable plaques, including a thin fibrous cap overlying a necrotic-rich core. However, it is difficult to translate postmortem findings into a prospective, prognostically relevant concept for patients.

When is a fibrous cap considered thin? Pioneering pathology studies applied various criteria regarding study population, region of interest, and cap definition. Mann and Davies (3) reported on 160 coronary plaques obtained from 31 subjects who died of sudden cardiac death. Mean cap thickness was 250 μm (range 20 to 1,140 μm) in types IV and V plaques. Burke et al. (4) sectioned coronaries at 3-mm intervals. Only cross sections with more than 50% lumen narrowing were analyzed. In ruptured plaques, fibrous cap thickness was 23 ± 19 μm, and in 95% of these plaques cap thickness was <65 μm. This value of cap thickness of *ruptured plaques* has been used—maybe inappropriately—for the definition of *nonruptured* TCFA (5), despite the fact that TCFAs have less necrotic core, less cholesterol clefts, and less macrophage infiltration compared with ruptured plaque.

The present reports use the <65-μm criterion to define TCFA. However, there is no consensus among clinicians and pathologists regarding the critical threshold for cap thickness that would reliably predict imminent plaque rupture. The criticism of clinicians stems from the fact that application of absolute histomorphometric values can be misleading due to anisotropic tissue shrinkage and to the lack of longitudinal data. In addition, the absence of a technique able to provide an accurate cap assessment in vivo has resulted in a lack of knowledge on the natural history of such plaques.

Optical coherence tomography (OCT), the optical analogue to pulse-echo ultrasound imaging, can directly visualize a thin fibrous cap. Currently, intracoronary OCT systems work with a resolution of 10 to 15 μm. Cilingiroglu et al. (6) demonstrated that OCT is able to accurately visualize thin fibrous caps in vivo (7). Optical coherence tomography can evaluate the macrophage content (7–9) and the collagen composition of a fibrous cap (7). In the current issue, Kubo et al. (1) evaluated the ability of intracoronary OCT to assess culprit lesions during primary percutaneous coronary intervention in patients with acute myocardial infarction. Optical coherence tomography was superior in detecting plaque rupture and erosion as compared with intravascular ultrasound (IVUS) and angioscopy. The study is remarkable in several respects. Obviously, it demonstrates the feasibility of a complex imaging protocol including IVUS, angioscopy, and OCT in the acute setting. Secondly, it confirms the pathology-driven hypothesis of the prominent role of TCFA rupture in acute coronary thrombotic occlusion. Third, it allows for the first time in vivo estimation of critical cap thickness in patients. The thickness of the remnants of the fibrous cap after symptomatic rupture measured in vivo was 49 ± 21 μm. These observations represent a very encouraging step toward a prospective, in-vivo evaluation of "hot" plaques at high risk for acute coronary events. However, the results should be interpreted with caution. The incidence of plaque rupture cannot be generalized, as there was considerable selection bias in the

*Editorials published in the *Journal of the American College of Cardiology* reflect the views of the authors and do not necessarily represent the views of *JACC* or the American College of Cardiology.

From the Thoraxcenter, Rotterdam, the Netherlands.

study cohort. Optical coherence tomography differentiation of necrotic-rich core from calcified plaque by visual assessment of the gray scale image can be difficult (10). Therefore, it would important to know the actual intra- and interobserver variability of Kubo et al. (1) to assess the accurateness of their results.

When Distribution and Frequency Matters

As atherosclerosis is a systemic disease, plaque rupture is considered a ubiquitous process that may be clinically silent or symptomatic in different regions of the vascular system. In patients with acute coronary syndrome (ACS), Rioufol et al. (11) reported at least 1 plaque rupture remote from the culprit lesion in 80% and remote from the culprit artery in 71% of their patients. A meta-analysis described that more than 20% of ACS patients have more than 1 ruptured plaque (12). Likewise, a high prevalence of rupture-prone lesions throughout the coronary tree has been reported by angiography (13), angioscopy (14), and palpography (15).

The report of Cheruvu et al. (2) is at variance with previous reported data. First, the prevalence of TCFA and ruptured plaques is *low* (0.46 ± 0.95 and 0.38 ± 0.70 per heart, respectively), *focal*, and located in the *proximal segments* of the coronaries. In earlier studies, up to 3 TCFA were found per heart (16). Explanations for this might be demographic differences in studied population and in methods, namely *longitudinal* instead of cross-sectional cutting of the coronaries. Second, necrotic core size was relatively *small* for both, TCFA (1.6 ± 1.8 mm^2; length 2.7 ± 2.0 mm) and ruptured plaques (2.2 ± 1.9 mm^2; length 1.9 ± 3.6 mm). In previous studies, the size of necrotic core in TCFAs was 1.7 ± 1.1 mm^2 with a length of 8 mm (range 2 to 17 mm), and in ruptured plaques 3.8 ± 5.5 mm^2, with a length of 9 mm (range 2.5 to 22 mm) (5). The difference in length is striking. Therefore, we may wonder whether the intrinsic risk varies among the type of lesions that are labeled by the same morphologic term "TCFA."

The Cheruvu et al. (2) findings have potentially important clinical implications, since maybe only TCFA that are proximally located, with large necrotic core and outward remodeling, should be considered for local treatment. Unfortunately, remodeling index is not reported, likely due to the methodology (longitudinal cut in 4 quadrants).

To date, there is no single marker that can accurately identify the risk of rupture for an individual plaque. But it has been suggested that assessment of several plaque characteristics (morphologic, biochemical, and mechanical) may improve the ability to correctly diagnose vulnerable plaques. Radiofrequency IVUS data analysis (e.g., virtual histology, palpography) has emerged as a tool to potentially detect TCFAs in vivo. In a recent study, patients with ACS underwent IVUS-VH analysis of all 3 epicardial coronaries. On average, there were 2 IVUS-derived TCFA per patient with half of them showing outward remodeling (17). Interestingly, the size of the necrotic core (1.2 ± 0.8 mm^2) is in line with the Cheruvu et al. (2) histopathological data. Another interesting approach is the combination of VH and palpography. Both datasets can be simultaneously acquired during one single IVUS pullback, allowing for the assessment of both morphologic and biomechanical properties of a particular plaque. Assessing several characteristics of a given plaque could potentially enhance invasive risk stratification by identifying very high-risk plaques, thereby lowering the number of vulnerable plaques that deserve to be followed over time and ultimately treated.

What If Diogenes Would Have Found What He Was Looking For?

The cynic Greek philosopher Diogenes walked through Athens in broad daylight carrying a lighted lamp, looking for an honest man. Needless to say, he never found one.

What if we ever *became* able *to identify* in vivo the uncommon TCFAs on the verge of imminent rupture? Vessel wall *re*inforcement should be considered mandatory. Ideally, lesion coverage and cap *re*inforcement by a dedicated shield with thin and dense struts (permanent or preferably absorbable) strong enough to progressively change the geometry of the lumen by self-expansion without rupturing the cap would be appealing. Computational finite element and fluid dynamics taught us that geometrical changes in lumen shape can affect local mechanics unfavorably or favorably, either leading to plaque rupture or to *re*inforcement of the thin fibrous cap (18,19). Finally, having acutely constrained the necrotic core, it should subsequently be reduced by a pharmacologic agent or mechanically. Furthermore, *re*generation of the endothelium and *re*covery of its functionality, possibly by passive or active endothelial cell attraction, would heal the endothelial lining, while drugs specifically targeting the necrotic core could be released abluminally. Such newly designed absorbable stents are currently contemplated as future focal treatment for vulnerable plaque.

Reprint requests and correspondence: Dr. Patrick W. Serruys, Thoraxcenter, Ba583, Dr. Molewaterplein 40, 3015-GD Rotterdam, the Netherlands. E-mail: p.w.j.c.serruys@erasmusmc.nl.

REFERENCES

1. Kubo T, Imanishi T, Takarada S, et al. Assessment of culprit lesion morphology in acute myocardial infarction: ability of optical coherence tomography compared with intravascular ultrasound and coronary angioscopy. J Am Coll Cardiol 2007;50:933–9.
2. Cheruvu PK, Finn AV, Gardner C, et al. Frequency and distribution of thin-cap fibroatheroma and ruptured plaques in human coronary arteries: a pathologic study. J Am Coll Cardiol 2007;50:940–9.
3. Mann JM, Davies MJ. Vulnerable plaque. Relation of characteristics to degree of stenosis in human coronary arteries. Circulation 1996;94: 928–31.
4. Burke AP, Farb A, Malcom GT, Liang Y-H, Smialek J, Virmani R. Coronary risk factors and plaque morphology in men with coronary disease who died suddenly. N Engl J Med 1997;336:1276–82.
5. Virmani R, Burke AP, Kolodgie FD, Farb A. Vulnerable plaque: the pathology of unstable coronary lesions. J Interv Cardiol 2002; 15:439–46.

6. Cilingiroglu M, Oh JH, Sugunan B, et al. Detection of vulnerable plaque in a murine model of atherosclerosis with optical coherence tomography. Cathet Cardiovasc Intervent 2006;67:915–23.
7. Regar E, van Leeuwen AMGJ, Serruys PW. Optical Coherence Tomography in Cardiovascular Research. London: Informa Healthcare, 2007.
8. Tearney GJ, Yabushita H, Houser SL, et al. Quantification of macrophage content in atherosclerotic plaques by optical coherence tomography. Circulation 2003;107:113–9.
9. MacNeill BD, Jang IK, Bouma BE, et al. Focal and multi-focal plaque macrophage distributions in patients with acute and stable presentations of coronary artery disease. J Am Coll Cardiol 2004;44:972–9.
10. Manfrini O, Mont E, Leone O, et al. Sources of error and interpretation of plaque morphology by optical coherence tomography. Am J Cardiol 2006;98:156–9.
11. Rioufol G, Finet G, Ginon I, et al. Multiple atherosclerotic plaque rupture in acute coronary syndrome: a three-vessel intravascular ultrasound study. Circulation 2002;106:804–8.
12. Libby P. Act local, act global: inflammation and the multiplicity of "vulnerable" coronary plaques. J Am Coll Cardiol 2005;45:1600–2.
13. Goldstein JA, Demetriou D, Grines CL, Pica M, Shoukfeh M, O'Neill WW. Multiple complex coronary plaques in patients with acute myocardial infarction. N Engl J Med 2000;343:915–22.
14. Asakura M, Ueda Y, Yamaguchi O, et al. Extensive development of vulnerable plaques as a pan-coronary process in patients with myocardial infarction: an angioscopic study. J Am Coll Cardiol 2001;37:1284–8.
15. Schaar JA, Regar E, Mastik F, et al. Incidence of high-strain patterns in human coronary arteries: assessment with three-dimensional intravascular palpography and correlation with clinical presentation. Circulation 2004;109:2716–9.
16. Kolodgie FD, Virmani R, Burke AP, et al. Pathologic assessment of the vulnerable human coronary plaque. Heart 2004;90:1385–91.
17. Garcia-Garcia HM, Goedhart D, Schuurbiers JC, et al. Virtual histology and remodeling index allow in vivo identification of allegedly high risk coronary plaques in patients with acute coronary syndromes: a three vessel intravascular ultrasound radiofrequency data analysis. Eurointervention 2006;2:338–44.
18. Slager CJ, Wentzel JJ, Gijsen FJ, et al. The role of shear stress in the generation of rupture-prone vulnerable plaques. Nat Clin Pract Cardiovasc Med 2005;2:401–7.
19. Slager CJ, Wentzel JJ, Gijsen FJ, et al. The role of shear stress in the destabilization of vulnerable plaques and related therapeutic implications. Nat Clin Pract Cardiovasc Med 2005;2:456–64.

CHAPTER 7.1

The Effects of the Direct Lipoprotein-associated Phospholipase A_2 Inhibitor Darapladib on Human Coronary Atherosclerotic Plaque.

Serruys PW, **García-García HM**, Buszman P, Erne P, Verheye S, Aschermann M, Duckers H, Bleie O, Dudek D, Bøtker HE, von Birgelen C, D'Amico D, Hutchinson T, Zambanini A, Mastik F, van Es GA, van der Steen AFW, Vince DG, Ganz P, Hamm CW, Wijns W, Zalewski A.

Circulation. 2008 Sep 9;118(11):1172-82

Effects of the Direct Lipoprotein-Associated Phospholipase A_2 Inhibitor Darapladib on Human Coronary Atherosclerotic Plaque

Patrick W. Serruys, MD, PhD; Héctor M. García-García, MD, MSc; Pawel Buszman, MD, PhD; Paul Erne, MD, PhD; Stefan Verheye, MD, PhD; Michael Aschermann, MD; Henrikus Duckers, MD, PhD; Oyvind Bleie, MD; Dariusz Dudek, MD; Hans Erik Bøtker, MD; Clemens von Birgelen, MD, PhD; Don D'Amico, MA; Tammy Hutchinson, MSc; Andrew Zambanini, MD; Frits Mastik; Gerrit-Anne van Es, PhD; Antonius F.W. van der Steen, PhD; D. Geoffrey Vince, PhD; Peter Ganz, MD; Christian W. Hamm, MD; William Wijns, MD, PhD; Andrew Zalewski, MD, PhD; for the Integrated Biomarker and Imaging Study-2 Investigators

Background—Lipoprotein-associated phospholipase A_2 (Lp-PLA_2) is expressed abundantly in the necrotic core of coronary lesions, and products of its enzymatic activity may contribute to inflammation and cell death, rendering plaque vulnerable to rupture.

Methods and Results—This study compared the effects of 12 months of treatment with darapladib (an oral Lp-PLA_2 inhibitor, 160 mg daily) or placebo on coronary atheroma deformability (intravascular ultrasound palpography) and plasma high-sensitivity C-reactive protein in 330 patients with angiographically documented coronary disease. Secondary end points included changes in necrotic core size (intravascular ultrasound radiofrequency), atheroma size (intravascular ultrasound gray scale), and blood biomarkers. Background therapy was comparable between groups, with no difference in low-density lipoprotein cholesterol at 12 months (placebo, 88±34 mg/dL; darapladib, 84±31 mg/dL; P=0.37). In contrast, Lp-PLA_2 activity was inhibited by 59% with darapladib (P<0.001 versus placebo). After 12 months, there were no significant differences between groups in plaque deformability (P=0.22) or plasma high-sensitivity C-reactive protein (P=0.35). In the placebo-treated group, however, necrotic core volume increased significantly (4.5±17.9 mm^3; P=0.009), whereas darapladib halted this increase (−0.5±13.9 mm^3; P=0.71), resulting in a significant treatment difference of −5.2 mm^3 (P=0.012). These intraplaque compositional changes occurred without a significant treatment difference in total atheroma volume (P=0.95).

Conclusions—Despite adherence to a high level of standard-of-care treatment, the necrotic core continued to expand among patients receiving placebo. In contrast, Lp-PLA_2 inhibition with darapladib prevented necrotic core expansion, a key determinant of plaque vulnerability. These findings suggest that Lp-PLA_2 inhibition may represent a novel therapeutic approach. (***Circulation.*** **2008;118:1172-1182.**)

Key Words: atherosclerosis ■ drugs ■ imaging ■ lipoprotein-associated phospholipase A_2

Despite intensive management of conventional risk factors, many patients continue to experience recurrent coronary events.[1] Most acute coronary events arise from initially non–flow-limiting stenoses that often are underestimated by angiography.[2,3] The salient features of culprit lesions resulting in fatal myocardial infarction include the

Received February 8, 2008; accepted May 23, 2008.

From Thoraxcenter, Erasmus MC, Rotterdam, the Netherlands (P.W.S., H.M.G.-G., H.D., F.M., A.F.W.v.d.S.); Cardialysis, Rotterdam, the Netherlands (H.M.G.-G., G.-A.v.E.); Upper Silesian Heart Center, Katowice, Poland (P.B.); Abteilung Kardiologie Kantonsspital, Lucerne, Switzerland (P.E.); ZNA Campus Middelheim, Antwerp, Belgium (S.V.); Všeobecná Fakultní Nemocnice, Prague, Czech Republic (M.A.); Haukeland Sykehus, Bergen, Norway (O.B.); Szpital Uniwersytecki, Krakow, Poland (D. Dudek); Skejby Sygehus, Aarhus, Denmark (H.E.B.); Medisch Spectrum Twente, Enschede, the Netherlands (C.v.B.); GlaxoSmithKline, Philadelphia, Pa (D. D'Amico, A. Zalewski); GlaxoSmithKline, Harlow, Essex, UK (T.H.); GlaxoSmithKline, Greenford, Middlesex, UK (A. Zambanini); Volcano Corp, Rancho Cordova, Calif (D.G.V.); San Francisco General Hospital, University of California, San Francisco (P.G.); Kerckhoff Klinik, Bad Nauheim, Germany (C.W.H.); Cardiovascular Center, Aalst, Belgium (W.W.); and Thomas Jefferson University, Philadelphia, Pa (A. Zalewski).

The online Data Supplement can be found with this article at http://circ.ahajournals.org/cgi/content/full/CIRCULATIONAHA.108.771899/DC1.

Guest Editor for this article was Thomas F. Lüscher, MD.

Clinical trial registration information—URL: ttp://www.clinicaltrials.gov/ct2/show/NCT00268996?term=darapladib&rank=5. Unique identifier: NCT00268996.

Correspondence to Professor P.W. Serruys, MD, PhD, Thoraxcenter, Ba583, Erasmus MC, Rotterdam, Netherlands. E-mail p.w.j.c.serruys@erasmusmc.nl

Circulation **is available at http://circ.ahajournals.org** **DOI: 10.1161/CIRCULATIONAHA.108.771899**

disruption of a thin fibrous cap, the presence of a large lipid-rich necrotic core, and an extensive inflammatory cell infiltrate.[4] Recent intravascular ultrasound (IVUS)–based regression trials could not address these important lesion characteristics because of inherent limitations in IVUS technology, although they have demonstrated a relationship between changes in the overall plaque volume and plasma low-density lipoprotein cholesterol (LDL-C) levels.[5,6] Because the current standard of care for high-risk cardiovascular patients already mandates intensive LDL-C lowering, intravascular imaging that could assess changes in plaque biomechanical or compositional characteristics may be particularly helpful in evaluating the mechanisms of future events or the efficacy of new pharmacological agents that act via novel mechanisms.[7]

Editorial p 1120
Clinical Perspective p 1182

Lipoprotein-associated phospholipase A_2 (Lp-PLA_2) is a circulating enzyme produced and secreted by inflammatory cells centrally involved in atherosclerosis,[8–11] bound predominantly to apolipoprotein B–containing lipoproteins, and highly expressed in the necrotic core of atherosclerotic lesions.[12,13] Although this enzyme was first described as the platelet-activating factor acetylhydrolase, it has much broader substrate specificity.[14] Lp-PLA_2 rapidly degrades oxidatively modified phospholipids in LDL-C, leading to formation of proinflammatory and cytotoxic products.[8,15,16] Because enhanced cell death and impaired clearance of apoptotic bodies are thought to be key mechanisms for necrotic core expansion,[17] Lp-PLA_2 inhibition may favorably affect rupture-prone lesions.

The objective of this study was to explore the effects of treatment with a direct Lp-PLA_2 inhibitor (darapladib) on coronary plaque deformability, composition, and size. In addition, the effects of Lp-PLA_2 inhibition on several biomarkers and clinical safety parameters were assessed.

Methods

Study Design

The Integrated Biomarkers and Imaging Study-2 trial was an international, multicenter, randomized, double-blind, placebo-controlled study of patients with angiographically confirmed coronary heart disease. The trial was designed by the Steering Committee (Appendix) in collaboration with the sponsor. Institutional review boards at each center approved the protocol, and patients provided written informed consent.

Patient Population

Patients ≥18 years of age undergoing cardiac catheterization for acute coronary syndrome (ACS: ST-segment elevation myocardial infarction or non–ST-segment elevation myocardial infarction) or non-ACS (eg, chronic stable angina or troponin-negative resting chest pain) were eligible. The protocol specified 50% of randomized patients to have troponin-positive ACS. Key exclusion criteria were planned surgical revascularization, stroke in the past 6 months, chronic hepatic disorder or abnormal alanine aminotransferase, bilirubin (alanine aminotransferase >2.5 or bilirubin >1.5 times the upper limit of normal), serum creatinine >2.0 mg/dL, blood pressure >160/100 mm Hg, poorly controlled diabetes mellitus (HbA_{1c} >10%), severe heart failure or left ventricular ejection fraction <30%, and current life-threatening condition. Patients were ineligible if angiography demonstrated left main coronary stenosis >50% or their coronary anatomy was inappropriate for IVUS. Within 10 days of qualifying cardiac catheterization, eligible patients were randomized to oral doses of darapladib 160 mg (GlaxoSmithKline, King of Prussia, Pa) or placebo once daily (1:1 ratio) for the 12-month treatment. The randomization was stratified according to ACS status and center.

IVUS Imaging

After intracoronary nitroglycerin administration, the vessel was imaged with a 20-MHz IVUS catheter (Eagle-Eye, Volcano Therapeutics, Rancho Cordova, Calif) during a 0.5-mm/s continuous motorized pullback (R-100 pullback device). The nonintervened studied segment had to be at least 40 mm long and exhibit <50% stenosis by angiography. All imaging data were stored digitally in a dedicated console (In-Vision Gold, Volcano Therapeutics, Rancho Cordova, Calif). Patients who received at least 1 dose of the investigational agent were scheduled to undergo IVUS of the same study vessel at 12 months. Patients who required urgent cardiac catheterization <12 months but >6 months after randomization had their imaging data included in the analysis. Details regarding imaging methodologies are provided in the online Data Supplement and are illustrated schematically in Figure 1.

IVUS-Based End-Point Definitions

IVUS-Based Palpography

The density of high strain per 10 mm (the coprimary end point) was defined as the number of cross sections with strain values ≥0.9% divided by the number of all analyzable cross sections in the region of interest and normalized for 10 mm.[7]

IVUS-Based Radiofrequency Analysis

The necrotic core volume was calculated by multiplying the mean necrotic core area of the region of interest by its length. Necrotic core values were expressed in cubic millimeters or as the percent of total radiofrequency (RF)-derived plaque volume. Other components of the plaque (dense calcium, fibrofatty tissue, and fibrous tissue) were calculated in the same manner.

IVUS Gray Scale

Total atheroma volume and percent atheroma volume were calculated. The latter was derived by dividing the total atheroma volume by the total vessel volume and multiplying by 100. Of note, total atheroma volume derived from IVUS gray scale contains both atherosclerotic plaque and media.

Biomarkers

Blood samples were collected at baseline and after randomization. Plasma high-sensitivity C-reactive protein (hsCRP; coprimary end point) was measured as described previously.[18] Plasma Lp-PLA_2 activity was measured by a colorimetric method with an intra-assay precision of 1.7% and interassay precision of 4.8%.[11,18] Details regarding other biomarkers are provided in the online Data Supplement.

Clinical Safety

Patient safety was assessed through adverse event reporting, physical examinations, ECG monitoring, and clinical laboratory tests. After randomization, patients visited the study centers at 1 and 3 months and every 3 months thereafter.

To detect any potential signal of harm, the Independent Data Monitoring Committee met every 3 months, by teleconference or in person, to review the unblinded safety data. The Independent Data Monitoring Committee deliberations took place entirely separately and independently of the Steering Committee or the sponsor (Appendix).

Statistical Analysis

Continuous variables for imaging end points were reported as mean±SD. Within-treatment-group changes from baseline were

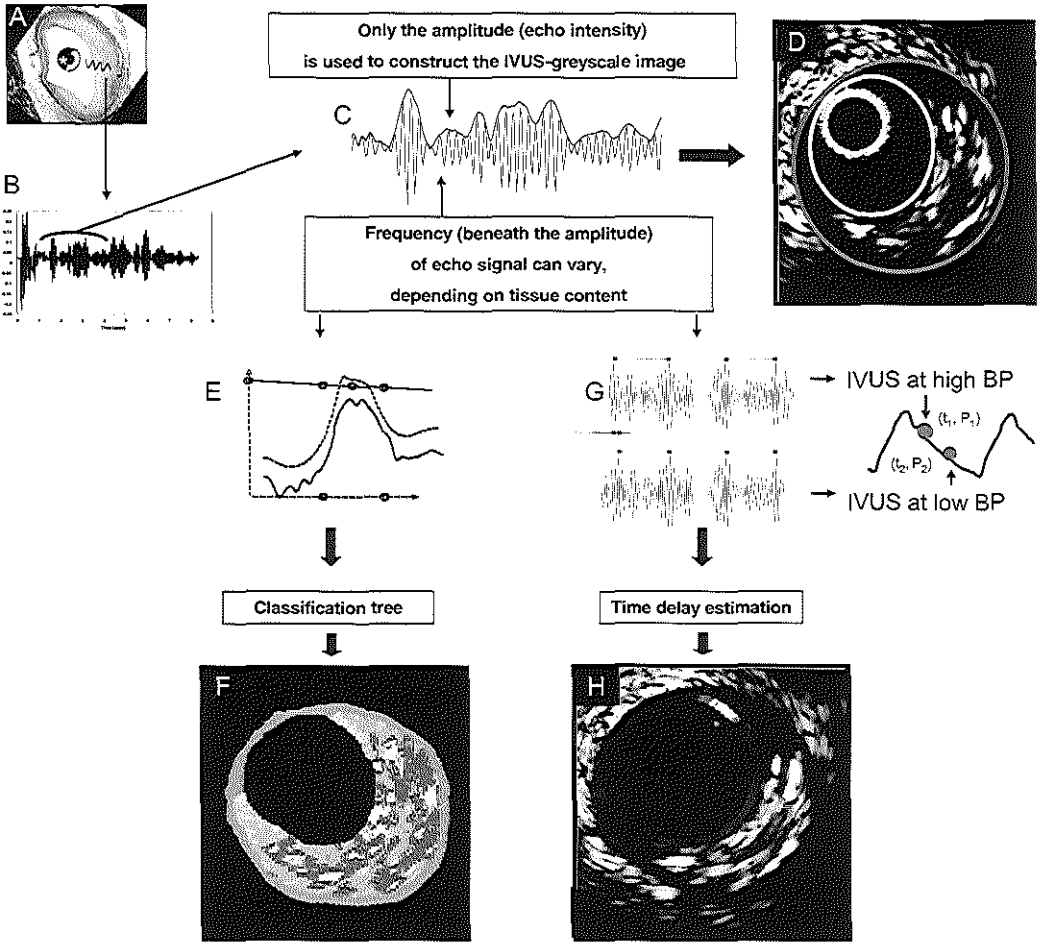

Figure 1. A, The ultrasound signal is generated in a piezoelectric crystal (*) that transmits and receives sound waves. B, Ultrasound reflected by the tissue deforms crystal, generating RF signal. C, Gray-scale IVUS is derived from the amplitude of RF signal, discarding information beneath the peaks of the signal. D, Changes in the electric field of the piezoelectric crystal caused by ultrasound reflection are used to generate a gray-tone image. E, IVUS RF analysis uses several additional spectral parameters to identify 4 plaque components. F, Plaque components that are identified are dense calcium (white), fibrous (green), fibrofatty (greenish-yellow), and necrotic core (red). G, IVUS palpography takes advantage of RF signals generated by the artery being deformed by blood pressure (BP). Using analysis of RF signals at "low" and "high" BP, the strain (deformation) in the inner layer of atheroma is determined. H, This strain is quantified and superimposed on the IVUS image at the lumen/vessel wall boundary. Note that high strain (yellow) is found at the shoulders of the eccentric plaque.

evaluated by paired *t* tests, and treatment comparisons of changes from baseline in IVUS were analyzed with ANCOVA adjusted for ACS status, pooled country, baseline value, and segment length. Treatment differences were expressed as the adjusted mean, 95% CI, and probability value. Biomarkers were log transformed and analyzed with last-observation-carried-forward ANCOVA and repeated-measures mixed modeling adjusted for ACS status, pooled country, visit, and interaction between visit and treatment. Treatment differences were expressed as adjusted percentage change, 95% CI, and probability value. No multiplicity adjustments were applied; all probability values are presented 2 sided.

The sample size was determined with an estimation approach because the effects of an Lp-PLA_2 inhibitor on novel imaging parameters were unknown. The SDs of changes for high-strain density (IVUS palpography) and hsCRP in a similar patient population were used, with additional consideration given to the expected number of nonevaluable IVUS imagings.[7] With this approach, by recruiting ≈300 patients, the study could estimate the treatment effects on the reduction of plaque deformability or hsCRP with good precision; reductions of ≈20% were anticipated to reach statistical significance.

The authors had full access to and take full responsibility for the integrity of the data. All authors have read and agree to the manuscript as written.

Results

Between November 16, 2005, and August 16, 2006, we randomized 330 patients. We assigned 155 patients to pla-

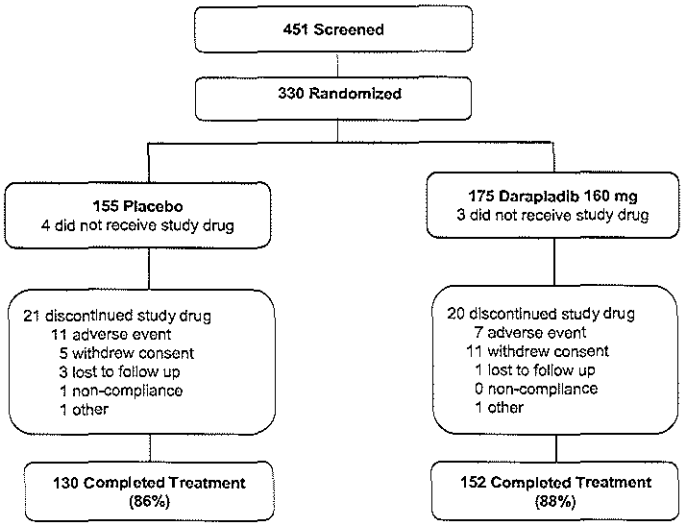

Figure 2. Patient disposition flow chart. Completed treatment refers to patients who received ≥11 months of treatment.

cebo and 175 patients to darapladib (Figure 2). As shown in Table 1, both groups were well matched except for a higher prevalence of hypertension among those receiving darapladib. At randomization, there was a high level of adherence to guideline-mandated treatments, including statin use in ≈90% of patients.

Imaging Efficacy Results

Of randomized patients who received at least 1 dose of placebo or darapladib, those with analyzable baseline and follow-up IVUS after a minimum of 6 months of treatment constituted the imaging population. The median time to follow-up IVUS was 364 days in the placebo and 364 days in the darapladib group, with repeat IVUS at ≥11 months after randomization in 97% and 96% patients, respectively.

IVUS Palpography

At baseline, the density of high strain per 10 mm was comparable between placebo-treated (n=115) and darapladib-treated (n=131) patients (0.44±0.64 versus 0.43±0.63, respectively). At follow-up, the between-group comparison of the change from baseline in density of high strain (coprimary end point) was not statistically significant (−0.08; 95% CI, −0.21 to 0.05; P=0.22). Details regarding prespecified sensitivity analysis, including only vessels with high strain at baseline, are provided in the online Data Supplement.

In the 10-mm subsegments with the highest baseline density of high strain per 10 mm (placebo, 1.22±1.56; darapladib, 1.21±1.62), both groups showed significant reductions after 12 months (placebo, 35%, P=0.001; darapladib, 33%, P=0.002), but the difference between groups was not significant (P=0.87).

IVUS RF Analysis

At baseline, necrotic core volume measurements were comparable between treatment groups in the entire region of interest and in the worst 10-mm subsegment (Table 2).

In the entire region of interest, necrotic core volume increased significantly during the study period among those receiving placebo (4.5±17.9 mm^3; P=0.009) but remained unchanged in the darapladib group (−0.5±13.9 mm^3; P=0.71 for within-group comparison). When the change from baseline was compared between groups, there was a significant treatment effect in favor of darapladib (−5.2 mm^3; 95% CI, −9.2 to −1.1; P=0.012). The nominal changes in necrotic core expressed as percent of RF-derived atheroma volume showed consistent treatment effects (Table 2).

In the 10-mm subsegment containing the largest necrotic core volume, there also was a significant treatment effect in favor of darapladib (−2.2 mm^3; 95% CI, −3.6 to −0.8; P=0.003; Table 2).

Figure 3 illustrates the high degree of consistency in treatment effect of darapladib compared with placebo in several important clinical subgroups.

When the individual plaque components were analyzed as a percent of IVUS RF–derived atheroma, an increase in necrotic core was paralleled by a decrease in fibrous tissue. In a comparison of the 2 groups, the differences in necrotic core (P=0.047) were accompanied by the reciprocal changes in fibrous tissue (P=0.021) (Figure 4). These findings suggest that in the placebo group a larger amount of fibrous tissue was converted into necrotic core, whereas in the darapladib group this process was significantly attenuated. The Table in the online Data Supplement provides data for all plaque components.

Gray-Scale IVUS

At baseline, total atheroma volume was comparable between the placebo-treated (n=118) and darapladib-treated (n=143) groups (placebo, 313±149 mm^3; darapladib, 327±189 mm^3; P=0.51). At 12 months, atheroma volume decreased by −4.9±32.7 mm^3 in the placebo group (P=0.10) and −5.0±28.0 mm^3 in the darapladib group (P=0.033).

Table 1. Baseline Characteristics

	Placebo (n=151)	Darapladib (n=172)
Clinical characteristics		
Age, y	57.3±10.9	59.4±9.8
Men, n (%)	126 (83)	140 (81)
Body mass index, kg/m^2	27.8±3.8	27.5±4.0
Diabetes mellitus, n (%)	22 (15)	22 (13)
Hypertension, n (%)	89 (59)	115 (67)
Low HDL cholesterol (<40 mg/dL), n (%)	40 (26)	45 (26)
Hypercholesterolemia, n (%)	95 (63)	108 (63)
Current smoker, n (%)	57 (38)	64 (37)
Prior medical history, n (%)		
Prior myocardial infarction	49 (32)	51 (29)
Prior coronary revascularization	47 (31)	50 (29)
Peripheral artery disease	7 (5)	17 (10)
Prior stroke	3 (2)	4 (2)
Index hospitalization, n (%)		
ACS	74 (49)	87 (51)
STEMI	35 (23)	40 (23)
Non-STEMI	39 (26)	47 (27)
PCI during index hospitalization	122 (81)	130 (76)
Cardiovascular medications at randomization, n (%)		
Aspirin	138 (91)	149 (87)
Clopidogrel or ticlopidine	122 (81)	136 (79)
Any antiplatelet medication	150 (>99)	170 (99)
ACE inhibitors or ARBs	88 (58)	101 (59)
β-Blockers	119 (79)	138 (80)
Statins	134 (89)	157 (91)
Laboratory values		
Cholesterol, mg/dL		
Total	187.3±47.6	182.3±43.2
LDL	108.2±41.4	103.6±37.4
HDL	46.8±11.2	48.0±12.4
Triglycerides, mg/dL		
Median	141	136
IQR	97–202	96–193
hsCRP, mg/L		
Geometric mean	2.4	2.4
95% CI	1.9, 3.1	1.9, 3.0
Lp-PLA$_2$ activity, μmol · min^{-1} · L^{-1}		
Geometric mean	159	160
95% CI	152, 167	153, 167
Blood pressure, mm Hg		
Systolic	125.7±16.9	128.0±16.1
Diastolic	75.2±10.1	75.6±9.9
Study vessel*		
LAD, n (%)	44 (36)	56 (39)
LCx, n (%)	32 (26)	37 (26)
RCA, n (%)	45 (37)	51 (35)
Diameter stenosis, %†	28.0 (10.5)	26.6 (10.3)
Mean lumen diameter, mm†	2.9±0.5	3.0±0.6

HDL indicates high-density lipoprotein; STEMI, ST-segment–elevation myocardial infarction; PCI, percutaneous coronary intervention; ACE, angiotensin-converting enzyme; ARB, angiotensin receptor blocker; IQR, interquartile range; LAD, left anterior descending artery; LCx, left circumflex artery; and RCA, right coronary artery. Values are presented as mean±SD unless otherwise specified. To convert to mmol/L, multiply values of cholesterol by 0.02586 and triglycerides by 0.0113.

*Imaging evaluable population: placebo, 121 patients; darapladib, 146 patients.

†Quantitative coronary angiography: placebo, 121 patients; darapladib, 144 patients.

Table 2. Necrotic Core Measurements Based on IVUS RF Analysis

	Placebo (n=110)	Darapladib (n=129)	P
Region of interest, mm	48±16	49±16	
Necrotic core volume, mm³*			
Baseline			
Mean±SD	21.5±21.9	22.8±24.5	
Median	14.8	13.6	
Interquartile range	6.1 to 28.2	7.3 to 32.4	
Follow-up			
Mean±SD	26.0±25.3	22.4±25.8	
Median	15.7	16.3	
Interquartile range	8.1 to 36.4	5.6 to 27.1	
Change from baseline			
Mean±SD	4.5±17.9	−0.5±13.9	
P†	0.009	0.71	
Least-squares mean (95% CI)‡	−5.2 (−9.2 to −1.1)		0.012
Necrotic core of total plaque, %*			
Baseline			
Mean±SD	13.1±7.6	13.4±6.5	
Median	12.6	12.5	
Interquartile range	6.8 to 16.8	9.1 to 17.5	
Follow-up			
Mean±SD	15.7±8.8	13.9±7.7	
Median	14.7	12.6	
Interquartile range	8.5 to 22.1	7.8 to 18.7	
Change from baseline			
Mean±SD	2.5±9.6	0.5±7.6	
P†	0.006	0.453	
Least-squares mean (95% CI) ‡	−2.0 (−3.9 to −0.0)		0.047
Necrotic core in the worst 10 mm, mm³			
Baseline			
Mean±SD	9.2±8.1	9.1±7.6	
Median	7.2	6.8	
Interquartile range	3.5 to 11.8	3.2 to 12.7	
Follow-up			
Mean±SD	10.1±9.2	7.9±6.7	
Median	7.3	5.7	
Interquartile range	3.3 to 16.0	2.7 to 11.2	
Change from baseline			
Mean±SD	0.9±6.6	−1.2±4.9	
P†	0.162	0.008	
Least-squares mean (95% CI)‡	−2.2 (−3.6 to −0.8)		0.003

*Values denote measurements in the entire region of interest.
†Paired *t* test (within-group comparison).
‡ANCOVA adjusted for ACS, pooled country, baseline value, and matched segment length (between-group comparison).

The between-group comparison of change from baseline was not significant (P=0.95). The percent atheroma volume also was similar between groups (placebo, 42.2±10.0%; darapladib, 40.7±10.1%; P=0.24) at baseline. The within-group changes and between-group differences were not significant (P=0.90). Likewise, atheroma volume showed no treatment effect in the worst 10-mm subsegment (data not shown).

Biomarkers and Other Laboratory Assessments

At 12 months, hsCRP was 1.0 mg/L (95% CI, 0.8 to 1.2) among those receiving placebo (n=140) and 0.9 mg/L (95% CI, 0.8 to 1.1) in the darapladib group (n=162). Nonsignificant reductions in hsCRP were observed with repeated-measures analysis (−15%; 95% CI, −36 to 11; P=0.22). These results were consistent with the last-observation-carried-forward analysis and observed data at 12 months (hsCRP was lower in the darapladib group by −12% [95% CI, −32 to 15; P=0.35] and −22% [95% CI, −41 to 3; P=0.08], respectively). A significantly higher percentage of patients, however, achieved very low levels of hsCRP (<1 mg/L) on darapladib (62%) than did those on placebo (45%) (odds ratio, 1.99; 95% CI, 1.22 to 3.24; P<0.008).

Plasma Lp-PLA_2 activity was significantly reduced by darapladib at all time points. At 12 months, Lp-PLA_2 activity was 153 $\mu mol \cdot min^{-1} \cdot L^{-1}$ (95% CI, 147 to 159) in the placebo and 62 $\mu mol \cdot min^{-1} \cdot L^{-1}$ (95% CI, 58 to 65) in the darapladib group. This corresponds to −59% (95% CI, −62 to −56; P<0.001) inhibition of Lp-PLA_2 activity compared with placebo (repeated-measures analysis and last-observation-carried-forward analysis). The concentrations of other biomarkers (interleukin-6, myeloperoxidase, intracellular adhesion molecule-1, oxidized phospholipid/apolipoprotein B, and matrix metalloproteinase-9 activity) did not change significantly.

Approximately 94% patients continued statins at the end of the treatment period. The 12-month LDL-C was 88±34 mg/dL in the placebo group and 84±31 mg/dL in the darapladib group (P=0.37). Plasma high-density lipoprotein cholesterol also was unaffected by treatment (48±11 mg/dL in the placebo; 50±13 mg/dL in the darapladib group; P=0.18).

Adverse Events, Clinical Safety, and Outcomes

Table 3 summarizes adverse events in both treatment groups. A higher incidence of malodor (mainly feces or urine) was reported with darapladib (16%) compared with placebo (3%) but was an uncommon cause of withdrawal from the study (darapladib, 2%).

Vital signs were similar except for the mean on-treatment systolic blood pressure, which was higher in the darapladib group by 3.0 mm Hg (95% CI, 0.3 to 5.7; P=0.031) when analyzed with the repeated-measures analysis adjusted for baseline values. After 12 months, systolic blood pressure was 129.6±17.2 mm Hg in the placebo and 133.3±18.5 mm Hg in the darapladib group. A posthoc analysis of the intraaortic blood pressure at the time of follow-up cardiac catheterization showed no differences between groups (placebo,

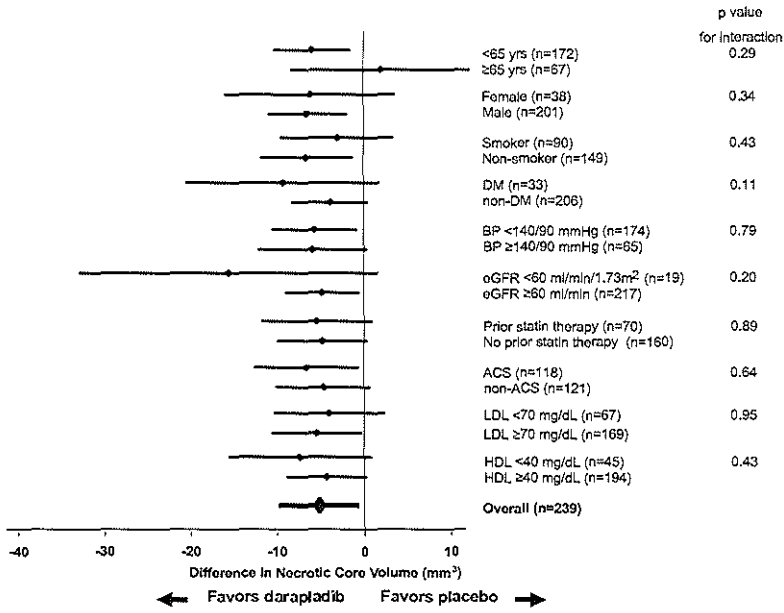

Figure 3. Treatment differences in necrotic core volume across clinical subgroups. The results are displayed as adjusted mean treatment difference and 95% CI. LDL-C and high-density lipoprotein (HDL) cholesterol values refer to on-treatment levels. DM indicates diabetes mellitus; eGFR, estimated glomerular filtration rate.

124.1±23.8 mm Hg; darapladib, 121.8±23.0 mm Hg; P=0.19).

There was no evidence of significant differences in platelet biomarkers (P-selectin, sCD40L, and urinary 11-dehydro-thromboxane B_2) measured at multiple time points (3, 6, and 12 months) except for higher levels of CD40L at 12 months (placebo, 181 pg/mL [95% CI, 150 to 217]; darapladib, 258 pg/mL [95% CI, 208 to 320]; P=0.024). No imbalance in clinical events related to increased platelet activity was observed (Table 3).

Discussion

The main finding of this study was that darapladib, a direct Lp-PLA_2 inhibitor, prevented necrotic core expansion, whereas patients receiving placebo showed significant progression despite standard-of-care treatment, with average LDL-C levels <90 mg/dL. The results suggest that human coronary atherosclerosis is a dynamic process with potential for replacement of fibrous tissue by necrotic core. Prolonged Lp-PLA_2 inhibition halted this process, indicating a direct effect on human atheroma that is distinct from current pharmacological therapies.

Lp-PLA_2 and Necrotic Core Formation

The mere presence of Lp-PLA_2 in high-risk plaques does not necessarily establish its causal role in lesion propensity for rupture. However, Lp-PLA_2 inhibition, with the subsequent reduction of its product, lysophosphatidylcholine, has reduced inflammation and cell death in studies in vitro.[12,15,16] Furthermore, darapladib decreased intraplaque lysophosphatidylcholine content, attenuated the expression of inflammatory genes, and reduced necrotic core in a porcine model of coronary atherosclerosis.[19] In humans, treatment with darapladib not only inhibited intraplaque Lp-PLA_2 activity but also reduced activity of the intracellular proteases (caspase-3 and caspase-8) that are responsible for apoptotic cell death.[20] Therefore, the finding from the present study, that darapladib interferes with necrotic core expansion, is consistent with the overall biological hypothesis and supports a proatherogenic role for Lp-PLA_2.

Intravascular Imaging of Coronary Atherosclerosis

Until recently, no intravascular imaging modality has been capable of assessing the composition of coronary atheroma in a precise manner. IVUS RF analysis has been validated in postmortem pressure-perfused human coronary arteries and in the specimens retrieved by coronary atherectomy and carotid endarterectomy.[21–24] The present study provides the first longitudinal observation of the atherosclerotic process among patients receiving standard-of-care treatment. We demonstrate continued necrotic core expansion in patients receiving placebo, whereas darapladib halted this process, with a consistent effect across several subgroups. Because atherosclerosis is a highly heterogeneous process, we also confirmed statistically significant regression of necrotic core volume in the worst 10-mm subsegments (Table 2).

The IVUS palpography failed to detect a significant effect on biomechanical properties of coronary plaques during darapladib treatment. An unexpectedly high percentage of patients without high strain (37%) at baseline may have

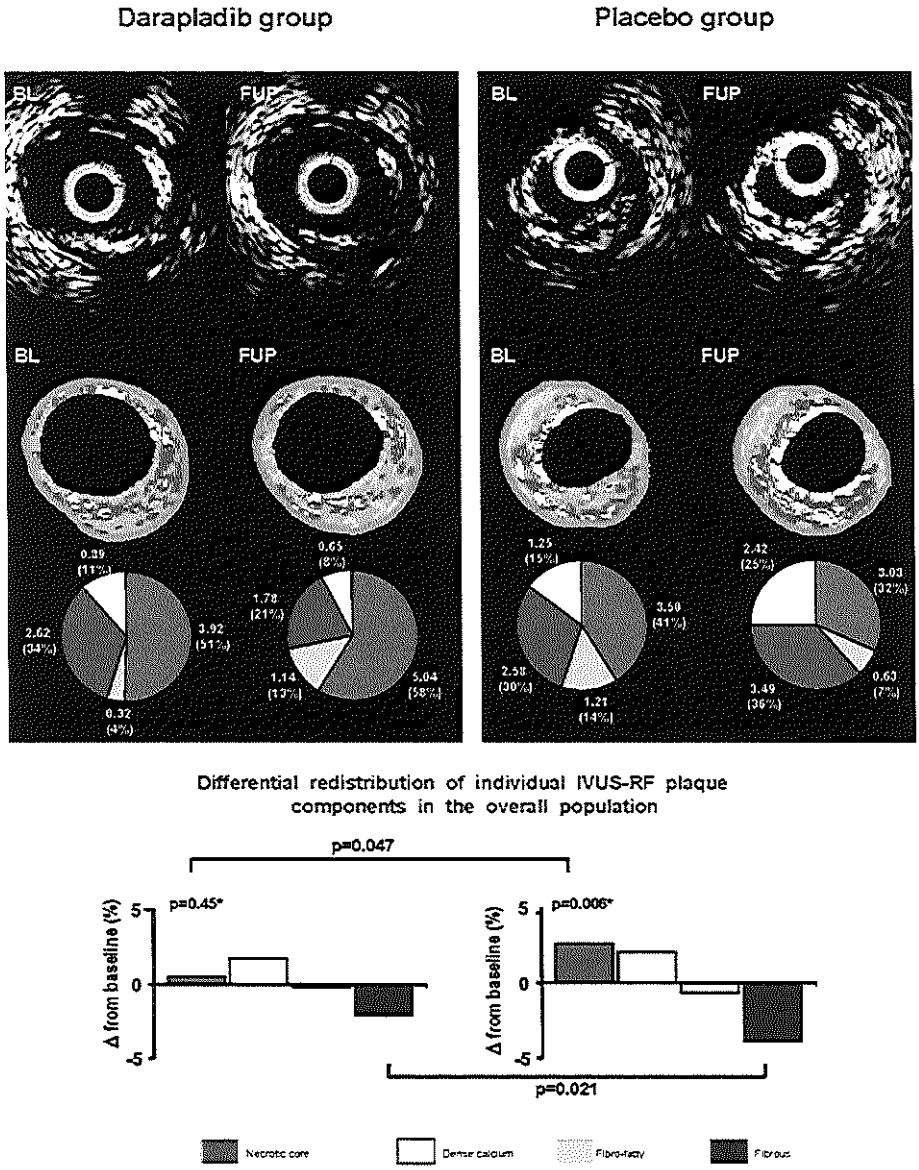

Figure 4. Top, Representative examples of plaque composition in the darapladib- and placebo-treated groups. The gray-scale frames and corresponding IVUS RF frames are shown. The pie charts provide quantitative display of individual plaque components in the cross sections. Values are in millimeters squared (and percent of RF-derived atheroma area). In the darapladib-treated patient, a decrease in necrotic core is seen. In the placebo-treated patient, an increase in necrotic core is demonstrated. Bottom, Differential changes in plaque components from IVUS RF analysis in the overall placebo and darapladib groups. Results are expressed as mean change from baseline (BL), with individual components expressed as percent of RF-derived atheroma volume. FUP indicates follow-up. *Within-group change from baseline.

reduced the statistical power needed to demonstrate significant differences between treatment groups.[7] Supporting this hypothesis is the prespecified sensitivity analysis demonstrating a significant reduction in high strain in the darapladib group ($P=0.009$) when only patients with highly deformable plaque at baseline were analyzed.

Despite the relatively short treatment duration, the changes in volumetric measurements using IVUS gray scale were

Table 3. Adverse Events, Clinical Outcomes, and Laboratory Abnormalities

Variable	Placebo (n=151)	Darapladib (n=172)
Adverse events,* n (%)		
Serious adverse event	46 (30)	49 (28)
Any adverse event	109 (72)	121 (70)
Any adverse event leading to withdrawal	11 (7)	7 (4)
MACE event, n (%)		
Composite of first MACE (CV death, MI, stroke, coronary revascularization)	29 (19)	29 (17)
All components of MACE,† n (%)		
Death	0	0
Myocardial infarction	7 (5)	4 (2)
Stroke	1 (<1)	1 (<1)
Coronary revascularization	29 (19)	28 (16)
Other CV events,† n (%)		
Coronary restenosis	20 (13)	18 (10)
In-stent thrombosis	2 (1)	1 (<1)
Hospitalization for myocardial ischemia	13 (9)	11 (6)
Blood pressure–related events, n (%)		
Investigator-reported hypertensive adverse events	4 (3)	3 (2)
Blood pressure ≥140/90 mm Hg	95 (63)	117 (68)
Systolic blood pressure ≥140 mm Hg	89 (59)	112 (65)
Laboratory abnormalities,‡ n (%)		
Alanine aminotransferase ≥3 times ULN	1 (<1)	2 (1)
Aspartate aminotransferase ≥3 times ULN	0	1 (<1)
Total bilirubin ≥1.5 times ULN	5 (3)	1 (<1)
Alkaline phosphatase ≥2 times ULN	0	0

MACE indicates major adverse cardiac events; CV, cardiovascular; MI, myocardial infarction; and ULN, upper limit of normal. Adverse events were collected during treatment phase and up to 28 days after discontinuation of the study medication.

*The safety population consisted of patients who received at least 1 dose of placebo or darapladib.

†Patients with >1 event are counted more than once.

‡All counts refer to number of patients.

comparable to those observed in other regression trials with similar on-treatment LDL-C values.[25] IVUS gray scale has been recognized as an established method to assess regression/progression of atherosclerosis, but it relies exclusively on plaque volume measurements.[5,6,25] The present study demonstrates that IVUS RF analysis detects changes in atheroma composition in the absence of detectable overall plaque volume changes. We cannot exclude the possibility that a longer treatment duration (eg, >12 months) may have allowed an even more pronounced effect on necrotic core and ultimately atheroma volume.

Darapladib and Biomarker Response

hsCRP, a broad marker of systemic inflammatory burden, showed only trends toward lower values in the darapladib group, similar to a recent report.[18] The noxious effects of Lp-PLA_2 depend on intraplaque concentrations of its substrate (ie, oxidized phospholipid in modified LDL-C) and in situ Lp-PLA_2 concentration, which may explain the predominantly local effects of darapladib without a more profound systemic impact.[26] A high adherence to statin therapy also contributed to lowering hsCRP (and other inflammatory biomarkers), thus minimizing the opportunity for further reductions with darapladib.

Clinical Safety

Although the study was underpowered to address the effects of darapladib on cardiovascular outcomes, there was no imbalance in reported clinical outcomes. The higher sCD40L level in the darapladib group at 12 months is probably not of clinical relevance because only much higher values predict ischemic events.[27] Of note, other platelet biomarkers (P-selectin and 11-dehydro-thromboxane B_2) did not differ between treatment groups. Importantly, there was no excess of clinical events associated with increased platelet reactivity.

Higher systolic blood pressure in the darapladib group was not consistent with the results of a prior clinical study and requires careful attention in future studies.[18] Additional comparison of the intraarterial blood pressure also revealed no differences between groups.

Study Limitations

This was an exploratory study that used novel imaging IVUS modalities to assess plaque deformability, composition, and size. The clinical relevance of plaque compositional changes observed with sustained, long-term Lp-PLA_2 inhibition requires confirmation in event-driven outcomes trials.

Our observations focus on a small segment of the coronary arterial tree and might not fully represent disease progression elsewhere. Finally, the approach undertaken in this and other IVUS trials has not assessed changes in the precise plaque phenotype that may portend clinical risk (eg, thin-cap fibroatheroma).

Conclusions

This study demonstrated that necrotic core expansion occurs despite contemporary cardiovascular therapies, even in the absence of overall plaque size increase. This unabated necrotic core expansion could be responsible, in part, for the recurrent cardiovascular events in high-risk patients. Lp-PLA_2 inhibition with darapladib halted this process and therefore may represent a new approach for the treatment of atherosclerosis if the benefit of this intervention is confirmed by the results of future event-driven outcomes trials.

Appendix

Integrated Biomarker and Imaging Study-2 Steering Committee: Patrick W. Serruys (chairman; Rotterdam, the Netherlands), Gerrit-Anne van Es (Rotterdam, the Netherlands), Christian Hamm (Bad Nauheim, Germany), William Wijns (Aalst, Belgium), Andrew Zalewski (nonvoting member; King of Prussia, Pa), and Andrew Zambanini (nonvoting member; Middlesex, UK).

Independent Data Monitoring Committee: Peter Ganz (chairman; Boston, Mass), Charles S. Abrams (Philadelphia, Pa), Richard Cairns (Nottingham, UK), Barry R. Davis (ex officio; Houston, Tex), Marian Fisher (Madison, Wis), James Shepherd (Glasgow, Scotland), and Sidney Smith (Chapel Hill, NC).

Core laboratories: imaging (Cardialysis, Rotterdam, the Netherlands); clinical biochemistry/hematology (Quest Diagnostics, Van

Nuys, Calif); biomarkers (Quest Diagnostics, Van Nuys, Calif; Boston Children's Hospital, Boston, Mass; Prognostix, Inc, Cleveland, Ohio; University of California at San Diego, San Diego).

Participating centers (number of patients enrolled): Austria: Hanusch Krankenhaus, Georg Gaul (6). Belgium: Centre Hospitalier Universitaire Sart-Tilman, Victor Legrand (10); ZNA Campus Middelheim, Stefan Verheye (25); Cardiovascular Center, Aalst, William Wijns (14). Czech Republic: Všeobecná Fakultní Nemocnice, Michael Aschermann (23). Denmark: Skejby University Hospital, Hans Erik Bøtker (18). Germany: West German Heart Center, Raimund Erbel (7); Kerckhoff Klinik, Christian Hamm (7); Universitätsklinikum Heidelberg, Stefan Hardt, Helmut Kücherer (1); Universitätsklinikum München, Volker Klauss (14), Universitätsklinikum Ulm, Wolfgang Koenig (9); Segeberger Kliniken, Gert Richardt (3). The Netherlands: Medisch Spectrum Twente, Clemens von Birgelen (14); Medisch Centrum Leeuwarden, Adrianus Johannes van Boven (12); Catharina Hospital and Catherine R&D, Herman Rolf Michels (14), Erasmus Medical Center, Patrick Serruys (20); Medisch Centrum Rijnmond Zuid, Pieter Smits (11). Norway: Haukeland Sykehus, Oyvind Bleie (20). Poland: Upper Silesian Heart Center, Pawel Buszman (40); Szpital Uniwersytecki, Dariusz Dudek (19). Spain: Hospital Marques de Valdecilla, Thierry Colman (9); Hospital Clinico San Carlos, Carlos Macaya (9). Switzerland: Kantonsspital Luzern, Paul Erne (25).

Acknowledgments

We express our gratitude to the study participants and research personnel for their involvement in this study. We also would like to recognize Bianca Backx and Marie-Angele Morel (Cardialysis) and Angela Richter (Volcano Corp) for providing technical assistance.

Source of Funding

This study was funded by a research grant from GlaxoSmithKline.

Disclosures

D. D'Amico, T. Hutchinson, Dr Zambanini, and Dr Zalewski are GlaxoSmithKline employees. Dr Vince is employed by and owns equity in Volcano Corp. The other authors report no conflicts.

References

1. Cannon CP, Braunwald E, McCabe CH, Rader DJ, Rouleau JL, Belder R, Joyal SV, Hill KA, Pfeffer MA, Skene AM. Intensive versus moderate lipid lowering with statins after acute coronary syndromes. *N Engl J Med*. 2004;350:1495–1504.
2. Glagov S, Weisenberg E, Zarins CK, Stankunavicius R, Kolettis GJ. Compensatory enlargement of human atherosclerotic coronary arteries. *N Engl J Med*. 1987;316:1371–1375.
3. Ambrose JA, Tannenbaum MA, Alexopoulos D, Hjemdahl-Monsen CE, Leavy J, Weiss M, Borrico S, Gorlin R, Fuster V. Angiographic progression of coronary artery disease and the development of myocardial infarction. *J Am Coll Cardiol*. 1988;12:56–62.
4. Virmani R, Kolodgie FD, Burke AP, Farb A, Schwartz SM. Lessons from sudden coronary death: a comprehensive morphological classification scheme for atherosclerotic lesions. *Arterioscler Thromb Vasc Biol*. 2000; 20:1262–1275.
5. Nissen SE, Nicholls SJ, Sipahi I, Libby P, Raichlen JS, Ballantyne CM, Davignon J, Erbel R, Fruchart JC, Tardif JC, Schoenhagen P, Crowe T, Cain V, Wolski K, Goormastic M, Tuzcu EM. Effect of very high-intensity statin therapy on regression of coronary atherosclerosis: the ASTEROID trial. *JAMA*. 2006;295:1556–1565.
6. Nissen SE, Tuzcu EM, Schoenhagen P, Brown BG, Ganz P, Vogel RA, Crowe T, Howard G, Cooper CJ, Brodie B, Grines CL, DeMaria AN. Effect of intensive compared with moderate lipid-lowering therapy on progression of coronary atherosclerosis: a randomized controlled trial. *JAMA*. 2004;291:1071–1080.
7. Van Mieghem CA, McFadden EP, de Feyter PJ, Bruining N, Schaar JA, Mollet NR, Cademartiri F, Goedhart D, de Winter S, Granillo GR, Valgimigli M, Mastik F, van der Steen AF, van der Giessen WJ, Sianos G, Backx B, Morel MA, van Es GA, Zalewski A, Serruys PW. Noninvasive detection of subclinical coronary atherosclerosis coupled with assessment of changes in plaque characteristics using novel invasive imaging modalities: the Integrated Biomarker and Imaging Study (IBIS). *J Am Coll Cardiol*. 2006;47:1134–1142.
8. MacPhee CH, Moores KE, Boyd HF, Dhanak D, Ife RJ, Leach CA, Leake DS, Milliner KJ, Patterson RA, Suckling KE, Tew DG, Hickey DM. Lipoprotein-associated phospholipase A_2, platelet-activating factor acetylhydrolase, generates two bioactive products during the oxidation of low-density lipoprotein: use of a novel inhibitor. *Biochem J*. 1999;338: 479–487.
9. O'Donoghue M, Morrow DA, Sabatine MS, Murphy SA, McCabe CH, Cannon CP, Braunwald E. Lipoprotein-associated phospholipase A_2 and its association with cardiovascular outcomes in patients with acute coronary syndromes in the PROVE IT-TIMI 22 (Pravastatin or Atorvastatin Evaluation and Infection Therapy–Thrombolysis in Myocardial Infarction) trial. *Circulation*. 2006;113:1745–1752.
10. Oei HH, van der Meer IM, Hofman A, Koudstaal PJ, Stijnen T, Breteler MM, Witteman JC. Lipoprotein-associated phospholipase A_2 activity is associated with risk of coronary heart disease and ischemic stroke: the Rotterdam Study. *Circulation*. 2005;111:570–575.
11. Koenig W, Twardella D, Brenner H, Rothenbacher D. Lipoprotein-associated phospholipase A_2 predicts future cardiovascular events in patients with coronary heart disease independently of traditional risk factors, markers of inflammation, renal function, and hemodynamic stress. *Arterioscler Thromb Vasc Biol*. 2006;26:1586–1593.
12. Zalewski A, Macphee C. Role of lipoprotein-associated phospholipase A_2 in atherosclerosis: biology, epidemiology, and possible therapeutic target. *Arterioscler Thromb Vasc Biol*. 2005;25:923–931.
13. Kolodgie FD, Burke AP, Skorija KS, Ladich E, Kutys R, Makuria AT, Virmani R. Lipoprotein-associated phospholipase A_2 protein expression in the natural progression of human coronary atherosclerosis. *Arterioscler Thromb Vasc Biol*. 2006;26:2523–2529.
14. Davis B, Koster G, Douet LJ, Scigelova M, Woffendin G, Ward JM, Smith A, Humphries J, Burnand KG, Macphee CH, Postle AD. Electrospray ionization mass spectrometry identifies substrates and products of lipoprotein-associated phospholipase A_2 in oxidized human low density lipoprotein. *J Biol Chem*. 2008;283:6428–6437.
15. Carpenter KL, Dennis I, Challis IR, Osborn DP, Macphee CH, Leake DS, Arends MJ, Mitchinson MJ. Inhibition of lipoprotein-associated phospholipase A_2 diminishes the death-inducing effects of oxidised LDL on human monocyte-macrophages. *FEBS Lett*. 2001;505:357–363.
16. Shi Y, Zhang P, Zhang L, Osman H, Mohler ER 3rd, Macphee C, Zalewski A, Postle A, Wilensky RL. Role of lipoprotein-associated phospholipase A_2 in leukocyte activation and inflammatory responses. *Atherosclerosis*. 2007;191:54–62.
17. Tabas I. Consequences and therapeutic implications of macrophage apoptosis in atherosclerosis: the importance of lesion stage and phagocytic efficiency. *Arterioscler Thromb Vasc Biol*. 2005;25: 2255–2264.
18. Mohler ER 3rd, Ballantyne CM, Davidson MH, Hanefeld M, Ruilope LM, Johnson JL, Zalewski A. The effect of darapladib on plasma lipoprotein-associated phospholipase A_2 (Lp-PLA_2) activity and cardiovascular biomarkers in patients with stable coronary heart disease (CHD) or CHD-risk equivalent. *J Am Coll Cardiol*. 2008;51:1632–1641.
19. Wilensky RL, Shi Y, Zalewski A, Mohler ER III, Hamamdzic D, Li JU, Pelcovitz D, Webb C, Burgert ME, Walker MC, Macphee CH. Darapladib, a selective inhibitor of Lp-PLA_2, reduces coronary atherosclerosis in diabetic, hypercholesterolemic swine. *Circulation*. 2007; 116(suppl):II-33. Abstract.
20. Shi Y, Zalewski A, Macphee C, Dawson M. Selective inhibition of lipoprotein-associated phospholipase A_2 attenuates markers of plaque vulnerability in humans. *Circulation*. 2007;116(suppl):II-108. Abstract.
21. Nair A, Kuban BD, Tuzcu EM, Schoenhagen P, Nissen SE, Vince DG. Coronary plaque classification with intravascular ultrasound radiofrequency data analysis. *Circulation*. 2002;106:2200–2206.
22. Nair A, Margolis P, Kuban BD, Vince DG. Automated coronary plaque characterization with intravascular ultrasound backscatter: ex vivo validation. *Eurointervention*. 2007;3:113–130.
23. Nasu K, Tsuchikane E, Katoh O, Vince DG, Virmani R, Surmely JF, Murata A, Takeda Y, Ito T, Ehara M, Matsubara T, Terashima M, Suzuki T. Accuracy of in vivo coronary plaque morphology assessment: a validation study of in vivo virtual histology compared with in vitro histopathology. *J Am Coll Cardiol*. 2006;47:2405–2412.
24. Diethrich EB, Margolis P, Reid DB, Burke A, Rumaiah V, Rodriguez-Lopez JA, Wheatley G, Olsen D, Virmani R. Virtual histology intravascular ultrasound assessment of carotid artery disease: the Carotid Artery Plaque Virtual Histology Evaluation (CAPITAL) study. *J Endovasc Ther*. 2007;14:676–686.

25. Nissen SE, Tuzcu EM, Brewer HB, Sipahi I, Nicholls SJ, Ganz P, Schoenhagen P, Waters DD, Pepine CJ, Crowe TD, Davidson MH, Deanfield JE, Wisniewski LM, Hanyok JJ, Kassalow LM. Effect of ACAT inhibition on the progression of coronary atherosclerosis. *N Engl J Med*. 2006;354:1253–1263.
26. Lavi S, McConnell JP, Rihal CS, Prasad A, Mathew V, Lerman LO, Lerman A. Local production of lipoprotein-associated phospholipase A_2 and lysophosphatidylcholine in the coronary circulation: association with early coronary atherosclerosis and endothelial dysfunction in humans. *Circulation*. 2007;115:2715–2721.
27. Kinlay S, Schwartz GG, Olsson AG, Rifai N, Sasiela WJ, Szarek M, Ganz P, Libby P. Effect of atorvastatin on risk of recurrent cardiovascular events after an acute coronary syndrome associated with high soluble CD40 ligand in the Myocardial Ischemia Reduction With Aggressive Cholesterol Lowering (MIRACL) Study. *Circulation*. 2004;110:386–391.

CLINICAL PERSPECTIVE

Despite intensive management of conventional risk factors, coronary events continue to recur at an unacceptably high rate. Thus, novel therapeutic options for treating coronary heart disease are needed. Inhibition of the enzyme lipoprotein-associated phospholipase A_2 (Lp-PLA_2) with darapladib has emerged as a potential approach to addressing residual risk of cardiovascular events by directly targeting high-risk coronary atheroma. This multicenter study used intravascular ultrasound–derived techniques to characterize coronary atheroma in patients receiving a standard-of-care treatment. The results demonstrate that the necrotic core, a key determinant of plaque vulnerability, continued to increase among patients receiving placebo despite a high level of adherence to recommended therapies. This result is consistent with a proatherogenic role for Lp-PLA_2 that is postulated to contribute to plaque vulnerability. In contrast, treatment with the direct Lp-PLA_2 inhibitor darapladib added to standard of care prevented necrotic core expansion. Pharmacological intervention with darapladib exerted favorable effects on coronary atheroma consistent with plaque stabilization. These findings suggest that direct Lp-PLA_2 inhibition may represent a novel therapeutic approach to reducing residual risk in patients with coronary heart disease.

CHAPTER 7.2

Phospholipase A_2 Inhibitors.

García-García HM, Serruys PW.

Current Opinion in Lipidology. 2009 Aug. In press.

INTRODUCTION

Atherosclerosis is the main cause of ischemic heart disease. At present, ischemic heart disease is the leading cause of death worldwide and it is predicted that it will continue to be the first in the world in 2030.[1] Although for long time atherosclerosis was regarded as a lipid-driven disease, it is now clear that it is an intricate process that involves also the simultaneous and combined effect of inflammatory and immunological factors[2-4]. A critical primary step is the accumulation and oxidation of low-density lipoprotein (LDL) particles. Oxidized-LDL favors leukocyte recruitment and their activation, as well as cell death. This leads to generation of complex atherosclerotic plaques.[5] These high-risk atherosclerotic plaques have a particular phenotype that is characterized by a high content of necrotic core, a thin inflamed fibrous cap (intense accumulation of macrophages) and scarce presence of smooth muscle cells. In the necrotic core underlying the thin fibrous cap are commonly found hemorrhage, calcification and intraplaque vasa vasorum.[6,7] These lesions have been identified as vulnerable plaques, inferring to their association with cardiovascular clinical events.

THE PHOSPHOLIPASE A_2 (PLA_2) SUPERFAMILY

This family of enzymes currently comprises 15 groups, a number of subgroups and five types of enzymes [i.e. the secreted PLA_2s ($sPLA_2$), the cytosolic PLA_2s ($cPLA_2$), the Ca^{2+} independent PLA_2s ($iPLA_2$), the platelet-activating factor acetylhydrolases (PAF-AH), and the lysosomal PLA_2s].[8] Of these five, the secreted PLA_2s and the platelet-activating factor acetylhydrolases (or lipoprotein-associated phospholipase A_2 - Lp-PLA_2) have been associated with atherogenesis and its complications. Therefore, we focus our review on these two enzymes.

Secreted phospholipase A_2

The secreted PLA_2s hydrolyze the *sn*-2 position of glycerol-phospholipids to produce two biologically active lipids, namely arachidonic acid and lysophospholipids.[8] Out of the ten different members of the $sPLA_2$, group IIA ($sPLA_2$ - IIA) is not only found in atherosclerotic lesions, but also is closely implicated with a number of atherosclerosis pathways. It has been linked to hydrolysis of LDL, therefore it is thought to be a contributor of atherogenesis. Specifically, modified LDL by $sPLA_2$ confers high affinity to proteoglycans, this results in accumulation of LDL particles that are thereafter cleared by macrophages, thereby increasing foam cell

formation.[9] In addition, hydrolyzed LDL particles by sPLA2 caused spontaneous LDL aggregation which is proportional to the degree of LDL hydrolysis. Thus, sPLA2 may play an important role in atherogenesis by modifying LDL particles in the arterial wall, thereby enhancing their aggregation, retention, and macrophage uptake.

In different clinical presentation settings, epidemiological studies have linked increased plasma levels of sPLA2 IIA and risk of cardiovascular events [10-13]. In the EPIC-Norfolk cohort[13], a total of 991 subjects that were followed during 6 years were compared to 1806 controls, matched by age and sex. Although the risk of incident coronary artery disease was associated with increasing quartiles of $sPLA_2$ activity (P<0.001), the combination of $sPLA_2$ activity and CRP values was more useful to detect incident risk of CAD than either biomarker alone. Subjects in the highest quartiles of $sPLA_2$ activity and CRP had an adjusted odds ratio of 2.89 (95% CI, 1.78 to 4.68; P<0.001) for CAD vs. those with the lowest quartiles of both markers.

Lipoprotein-associated phospholipase A_2

Lipoprotein-associated phospholipase A_2 ($Lp\text{-}PLA_2$) is produced and secreted by inflammatory cells involved in atherogenesis,[14-17] it is also bound predominantly to apoB-containing lipoproteins, and highly expressed in the necrotic core of atherosclerotic lesions.[18-20] Although this enzyme was first described as platelet activating factor acetylhydrolase (or type VIIA PLA_2), it has much broader substrate specificity.[21] $Lp\text{-}PLA_2$ rapidly degrades oxidatively modified phospholipids in, for example, modified LDL leading to formation of proinflammatory and cytotoxic products [i.e. lysophosphatidylcholine (LPC) and oxidized nonesterified fatty acids (oxNEFAs)].[14, 22, 23] LPC promotes recruitment and activation of leukocytes, initiation of apoptosis and impaired clearance of apoptotic bodies.[18] A pathological study showed that $Lp\text{-}PLA_2$ staining in pathologic intimal thickening plaques was nearly absent; while in complex lesions such as thin-cap fibroatheromas and ruptured plaques an intense $Lp\text{-}PLA_2$ expression within necrotic cores and surrounding macrophages including those in the fibrous cap was shown. The degree of macrophage apoptosis was greater in thin-cap fibroatheroma and ruptured plaques compared with pathologic intimal thickening plaques.[19] This may imply that derived cytotoxic compounds from $Lp\text{-}PLA_2$ play an important role in plaque vulnerability. These observations, therefore, suggest that $Lp\text{-}PLA_2$ inhibition may favorably affect rupture-prone lesions.

In epidemiological studies, increased concentrations of $Lp\text{-}PLA_2$ predict future cardiovascular events. In a study that included 466 patients with stable coronary

heart disease the prognostic value of Lp-PLA_2 has been studied.[24] Patients were followed-up for a median of 4.0 years. Higher Lp-PLA_2 levels were associated with a greater risk of events: the hazard ratio per SD was 1.28 (P=0.009), after adjusting for clinical and lipid variables and C-reactive protein. Koening et al.,[17] reported the prognostic value of plasma concentrations and activity of Lp-PLA_2 in 1051 patients with coronary heart disease. In multivariable analyses, Lp-PLA_2 mass and activity were strongly associated with cardiovascular events after controlling for traditional risk factors, severity of CHD, statin treatment, cystatin C, and N-terminal proBNP.

SELECTIVE PHOSPHOLIPASE A2 INHIBITORS

Secretory phospholipase A2 inhibitors

Initially, scientists from Lilly and Shionogi reported that substituted indoles and indolizines were the most potent sPLA2 inhibitors, such as the indolizine Indoxam and the substituted indoles Me-Indoxam and 1 [LY315920 or varespladib sodium (sodium 2-(1-benzyl-2-ethyl-3-oxamoylindol-4-yl) oxyacetate;A-001). More recently, some other substituted indoles, 6,7-benzoindoles, and indolizines derived from LY315920 have been tested. [25]

$sPLA_2$ potent inhibitors include: 1. varespladib methyl (1-H-indole-3-glyoxamide;A-002) with selectivity towards sPLA2- IIA, sPLA2-V and sPLA2-X; 2. LY311727 (3-[1-benzyl-3-carbamoylmethyl)-2-ethyl-indol-5-yl]-oxypropylphosphonic acid; and 3. LY374388 ([3-aminnooxalyl-1-benzyl-2-ethyl-6-methyl-1H-indol-4-yloxy]-acetic acid methyl ester).

In the PLASMA study, varespladib methyl (1-H-indole-3-glyoxamide; A-002 Anthera Pharmaceuticals, San Mateo, CA, USA) has been evaluated. This compound has specificity towards sPLA2-IIA, sPLA2-V, and sPLA2-X enzymes. [26] The PLASMA study was a phase II, randomized, double-blind, placebo controlled parallel arm dose-ranging study of four doses (50, 100, 250 or 500 mg) of varespladib methyl in 393 patients with stable coronary heart disease (NCT00455546). The primary objective was to examine the effects of A-002 on sPLA2 concentration and activity and on plasma lipoproteins and inflammatory biomarkers following 8 weeks of treatment.

More than 10% of the patients did not reached the primary endpoint, eventually 348 patients were studied (A-002 n=278, placebo n=70). Mean sPLA2-IIA concentration fell by 86·7%, (from 15·7 pmol/L to 2·1 pmol/L), in the treatment group, vs. 4·8%, (from 15·7 pmol/L to 14·3 pmol/L), in the placebo group

(p<0·0001). The reductions in sPLA2-IIA concentration in the A-002 groups were dose dependent. In addition, oxidized LDL and C-reactive protein were reduced, as well as quantitative and qualitative lipoprotein changes were observed. Particularly, in the A-002 treatment group, the mean difference from baseline in oxidized LDL was -3.8%±23.6 mU/L. The absolute reduction differed from placebo only for treatment doses of 100 and 250 mg. Mean C-reactive protein concentrations reduced from baseline significantly in the A-002 treated group (p<0.0001), however it was not different as compared to placebo (p=0.477).

Interestingly, in 259 patients that were taking a statin, [the baseline LDL cholesterol was lower (range 1.9–2.0 mmol/L) than in the total study population (0.7–4.7 mmol/L)], the mean reduction in LDL cholesterol was similar to that seen in the total study population. This drug was in general well tolerated, in patients taking statins there was no evidence of hepatotoxicity. Only one patient had a serious adverse event (exacerbation of underlying chronic obstructive pulmonary disease), in the 500 mg A-002 treatment group.[26]

The PLASMA II is a bio-equivalence study, double-blind, parallel assignment, placebo control and randomized (NCT00525954). This study examined the effects of 2 different doses (250 mg, 500 mg) of A-002 compared with placebo, on enzyme levels ($sPLA_2$ mass) and activity after 8 weeks of treatment. In addition, the effect of treatment on inflammatory markers of cardiovascular risk (C-reactive protein [CRP]), lipid levels and lipoprotein subclasses and other soluble biomarkers (e.g., ICAM-1, VCAM-1, TNF, MCP-1 etc) were assessed. As of this writing, although the study has been completed, no results have been posted so far.

Another interesting context in which secretory phospholipase A_2 inhibitors may play an important role, it is in the setting of an acute myocardial infarction. The $sPLA_2$ has been found in the limits of the infarcted myocardium by immunohistochemistry[27]. It has been shown that $sPLA_2$ products, specifically lysophospholipids, are ligands for C-reactive protein. These are related to complement-mediated tissue damage in acute myocardial infarction. [28] The FRANCIS-ACS Trial is currently enrolling patients with acute coronary syndromes to study the safety and efficacy of A-002. (NCT00743925). This is a double-blind randomized parallel group placebo controlled study. Subjects will be randomized to receive either, 1. A-002 500 mg once daily (QD) plus Atorvastatin (80 mg QD); 2. or placebo tablets in addition to 80 mg atorvastatin QD.

The primary objective is the comparison of the mean percent changes in LDL hs-CRP, sPLA2 and other biomarkers between the two groups at 8 weeks. All enrolled subjects will remain on treatment until all subjects have been treated for a minimum of 24 weeks or until the occurrence of a Major Adverse Cardiac Event (MACE). At that point, all active subjects (those who have not early withdrawn

or those that have not already had a MACE) will be brought in for a final study visit. Subjects who complete the final study visit may be eligible to enroll in an open-label extension study for up to 2 years total study drug exposure.

As of this writing, the varespladib (A-002) is also being tested in the context of percutaneous coronary intervention (PCI). The sPLA 2 Inhibition to Decrease Enzyme Release after PCI (SPIDER-PCI trial) is a also double blind (subject, caregiver, investigator, outcomes assessor), parallel assignment, placebo control, prevention, randomized, safety/efficacy study. The primary endpoint is the incidence of myocardial injury as evidenced by elevation of CK-MB or troponin I above the upper limit of normal at 8 hours and 18-24 hours post-angioplasty. Patients in the active treatment group take 250mg tablets BID beginning 3-5 days pre-angioplasty and for 5 days post-angioplasty.

Key exclusion criteria are: 1. patients with ST elevation MI or any troponin elevation (non-STEMI) within preceding 10days; and 2. elevation of CK-MB or troponin I at baseline.

Selective lipoprotein-associated phospholipase A2 inhibitors

In the past, there was considerable discussion over whether Lp-PLA_2 primarily had a pro-inflammatory (generation of lysophosphatidylcholine) or anti-inflammatory (degradation of PAF or PAF-like lipids) role in atherogenesis. With the advent of a selective and extremely potent and substrate-competitive inhibitors of this enzyme, it became clearer that Lp-PLA_2 had a predominantly pro-inflammatory role in atherogenesis.[14] Two inhibitors are being tested as therapeutical options, namely darapladib and rilapladib (GlaxoSmithKline, Philadelphia PA).

In animal studies, selective lipoprotein-associated phospholipase A2 inhibitors (i.e. darapladib) have shown reduced development of advanced coronary atherosclerosis in diabetic and hypercholesterolemic swine.[20] Specifically, darapladib treatment resulted in a considerable decrease in plaque area and necrotic core area, and reduced medial destruction, resulting in fewer lesions with an unstable phenotype. The mean plaque area (± s.e.m.) in the left anterior descending coronary artery was 0.178 ± 0.046 mm^2 versus 0.636 ± 0.212 mm^2 in the treated group compared to the control group. The mean necrotic core area (± s.e.m.) from the arterial section with the greatest plaque area was significantly reduced from 0.87 ± 0.33 mm^2 to 0.03 ± 0.003 mm^2 (p =0.015) with treatment. Overall, the mean medial destruction score for control coronary vessels was 2.4 ± 0.027; whereas in the treatment group, the score was reduced (1.2 ± 0.24, p =0.003).

More advanced coronary lesions (i.e. thin fibrous cap atheroma) were found in the control group as compared to treated group (41 vs. 10%, p=0.05)

The mean ratio of macrophages to total intimal and medial area was 1.78 ± 0.44% in the control group, 0.71 ± 0.18% in the treated group (p = 0.036).

In a multicenter, randomized, double-blind, placebo-controlled study in 959 patients with coronary heart disease or CHD-risk equivalent subjects receiving atorvastatin 20 or 80 mg, the effects of 12-week darapladib treatment (40 mg, 80 mg, and 160 mg oral) on Lp-PLA2 activity and mass, biomarkers and oxidized lipids was evaluated (NCT00269048).[29] Darapladib 40, 80, and 160 mg inhibited Lp-PLA_2 activity by approximately 43%, 55%, and 66% compared with placebo (p < 0.001 at week12), and mass by mass measured in a 9.6%, 12.9%, and 9.3% by darapladib 40, 80, and 160 mg, respectively, (p < 0.001 for all doses at week 12 compared with placebo). Sustained dose-dependent inhibition was noted overall in both atorvastatin groups and at different baseline LDL-C (≥70 vs. <70 mg/dl) and HDL-C (<40 vs. ≥40 mg/dl). Interesting of note, at week 12, there was no significant interaction between atorvastatin and darapladib on change in Lp-PLA_2 activity (p = 0.60). Likewise, there was no interaction between baseline LDL-C (<70 mg/dl vs. ≥70 mg/dl) or HDL-C (<40 mg/dl vs. ≥40 mg/dl) and the change in Lp-PLA_2 activity at 12 weeks for all darapladib doses (p = 0.12 and p = 0.13, respectively).

Although hs-CRP at baseline was low due to intensive background atorvastatin therapy, treatment with darapladib 160 mg (n = 161) produced a 20.2% (p = 0.003; within group comparison) and a 13.0% reduction with placebo (p = 0.15; between groups comparison).

Patients treated with darapladib 160 mg (n = 150) had a 21.5% reduction in interleukin-6 (p < 0.001; within group comparison), it was also statistically significant compared with placebo (p = 0.028).

The Integrated Biomarkers and Imaging Study-2 trial was an international, multicenter, randomized, double blind, placebo-controlled study in 330 patients with angiographically confirmed coronary heart disease (NCT00268996).[30] At 12 months, there was no difference in LDL-cholesterol (placebo: 88±34 and darapladib: 84±31 mg/dL, p=0.37). The primary endpoint was coronary atheroma deformability (IVUS-palpography) and plasma hs-CRP. Secondary end points included changes in necrotic core size (IVUS-radiofrequency), atheroma size (IVUS-greyscale), and blood biomarkers. The Lp-PLA_2 activity was inhibited by 59% with darapladib (p<0.001 versus placebo). After 12 months, there were no significant differences between groups in plaque deformability (p=0.22) or plasma hsCRP (*p*=0.35). hsCRP was 1.0 mg/L (95% CI, 0.8 to 1.2 mg/L) among those receiving placebo (n=140) and 0.9 mg/L (95% CI, 0.8 to 1.1 mg/L) in the darapladib group (n=162). However, a significantly higher percentage of patients, achieved very low levels of hsCRP (<1 mg/L) on darapladib (62%) than

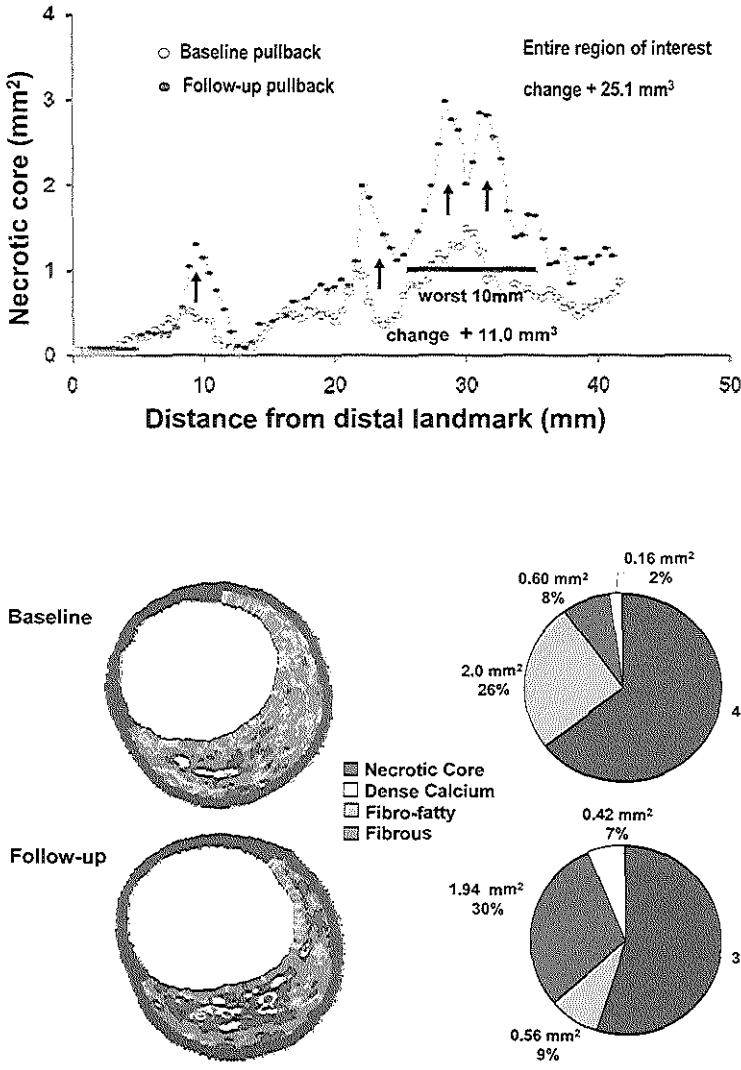

Figure 1. Temporal changes in necrotic core in a patient treated with placebo in the IBIS 2 study

Top: graph displayed the necrotic core (NC) areas in all consecutive cross-sections in this patient, the increase of necrotic core in placebo treated patient is apparent at several locations of the pullback, as highlighted by the arrows. In the entire analyzed region, there was increase in necrotic core volume of 25.1 mm^3 after one year, while in the worst 10 mm segment, an increase of 11 mm^3 in NC was observed.

Bottom: In these two sequential cross-sections from the same anatomical location, there is evidence of progression of necrotic core area (depicted in red) at the expense of fibrous tissue (depicted in green).

Overall, this graph illustrates changes in IVUS virtual histologgy as typically seen in placebo-treated patients between baseline and follow-up.

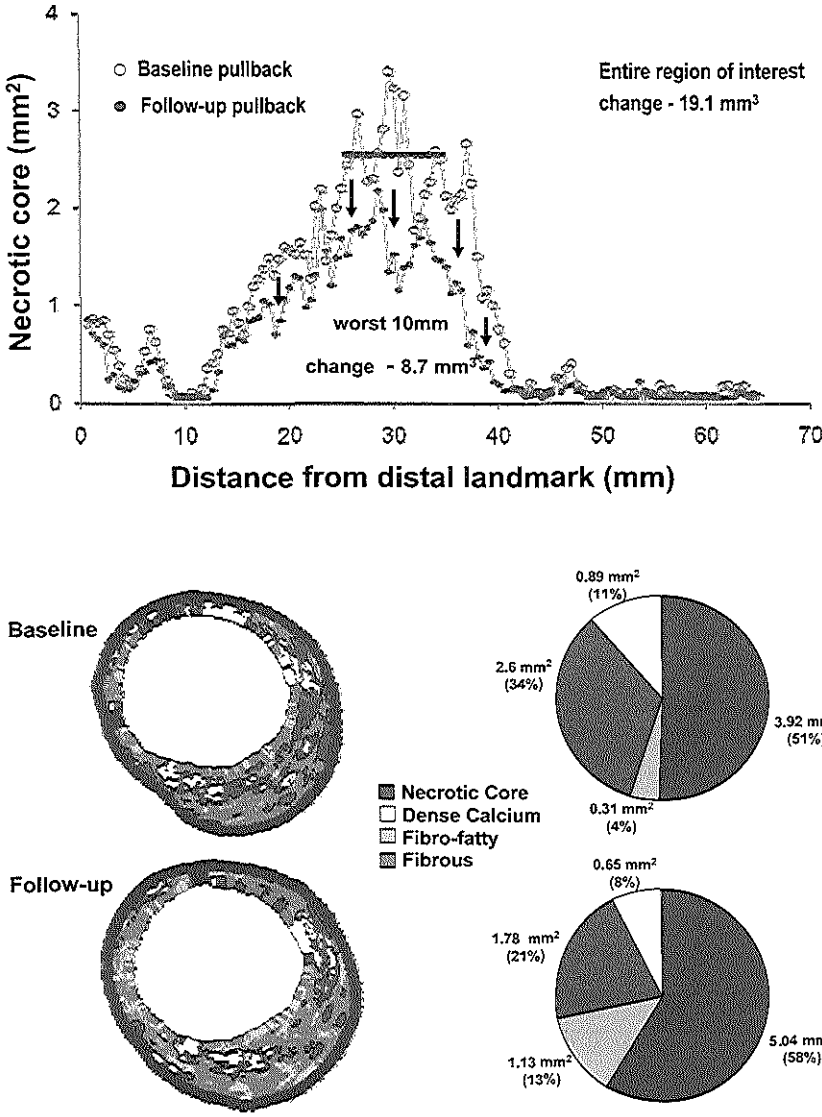

Figure 2. Temporal changes in necrotic core in a patient treated with an Lp-PLA2 inhibitor (darapladib) in the IBIS 2 study

Top: graph displayed the necrotic core (NC) areas in all consecutive cross-sections in this patient, a decrease of necrotic core in darapladib treated patient is apparent at several locations of the pullback, as highlighted by the arrows. In the entire analyzed region, there was increase in necrotic core volume of 19.1 mm^3 after one year, while in the worst 10 mm segment, a decrease of 8.7 mm^3 in NC was observed.

Bottom: In contrast to placebo, two cross-sections from the darapladib-treated patient demonstrate reduction in necrotic core area depicted in red. Of note, concomitant increase in fibrous tissue (in green) is consistent with plaque stabilization effect.

did those on placebo (45%) ($p<0.008$). In the placebo-treated group, however, necrotic core volume increased significantly (4.5±17.9 mm^3, $p=0.009$), whereas darapladib halted this increase (-0.5±13.9 mm^3, $p=0.71$), resulting in a significant treatment difference of -5.2 mm^3 ($p=0.012$). Figure 1 and 2. These intra-plaque compositional changes occurred without a significant treatment difference in total atheroma volume ($p=0.95$).

The Stabilization of Atherosclerotic Plaque by Initiation of Darapladib Therapy Trial (STABILITY, NCT00799903) is a clinical outcome study of darapladib versus placebo in patients with chronic coronary heart disease to compare the incidence of major adverse cardiovascular events (CV death [death due to a cardiovasacular cause], non-fatal myocardial infarction, non-fatal stroke). Patients will remain in the study until a specified number of MACE events have occurred. It is anticipated that patients will be in the study about 3 years. This study is currently recruiting participants.

In conclusion, despite of standard of care treatment, patients with coronary artery disease continue to have recurrent cardiovascular events. Phospholipase A2 inhibition may represent a new approach for the treatment of atherosclerosis if the benefit of this intervention is confirmed by the results of on-going event-driven outcomes trials.

REFERENCES

1. http://www.who.int/whosis/whostat/EN_WHS08_Full.pdf.
2. Segers D G-GH, Cheng C, de Crom R, Krams R, Wentzel JJ, van der Steen AFW, Serruys PW, Leenen PJM, Laman JM. A primer on the inmune system in the pathogenesis and treatment of atherosclerosis. *Eurointervention.* 2008;4:378-390.
3. Ross R. Atherosclerosis--an inflammatory disease. *N Engl J Med.* 1999;340(2):115-126.
4. Hansson GK, Libby P. The immune response in atherosclerosis: a double-edged sword. *Nat Rev Immunol.* 2006;6(7):508-519.
5. Virmani R, Kolodgie FD, Burke AP, Farb A, Schwartz SM. Lessons from sudden coronary death: a comprehensive morphological classification scheme for atherosclerotic lesions. *Arterioscler Thromb Vasc Biol.* 2000;20(5):1262-1275.
6. Burke AP, Farb A, Malcom GT, Liang Y, Smialek JE, Virmani R. Plaque rupture and sudden death related to exertion in men with coronary artery disease. *JAMA.* 1999;281(10):921-926.
7. Burke AP, Farb A, Malcom GT, Liang YH, Smialek J, Virmani R. Coronary risk factors and plaque morphology in men with coronary disease who died suddenly. *N Engl J Med.* 1997;336(18):1276-1282.
8. Schaloske RH, Dennis EA. The phospholipase A2 superfamily and its group numbering system. *Biochim Biophys Acta.* 2006;1761(11):1246-1259.
9. Wooton-Kee CR, Boyanovsky BB, Nasser MS, de Villiers WJ, Webb NR. Group V sPLA2 hydrolysis of low-density lipoprotein results in spontaneous particle aggregation and promotes macrophage foam cell formation. *Arterioscler Thromb Vasc Biol.* 2004;24(4):762-767.
10. Kugiyama K, Ota Y, Takazoe K, Moriyama Y, Kawano H, Miyao Y, Sakamoto T, Soejima H, Ogawa H, Doi H, Sugiyama S, Yasue H. Circulating levels of secretory type II phospholipase A(2) predict coronary events in patients with coronary artery disease. *Circulation.* 1999;100(12):1280-1284.
11. Liu PY, Li YH, Tsai WC, Chao TH, Tsai LM, Wu HL, Chen JH. Prognostic value and the changes of plasma levels of secretory type II phospholipase A2 in patients with coronary artery disease undergoing percutaneous coronary intervention. *Eur Heart J.* 2003;24(20):1824-1832.
12. Kugiyama K, Ota Y, Kawano H, Soejima H, Ogawa H, Sugiyama S, Doi H, Yasue H. Increase in plasma levels of secretory type II phospholipase A(2) in patients with coronary spastic angina. *Cardiovasc Res.* 2000;47(1):159-165.
13. Mallat Z, Benessiano J, Simon T, Ederhy S, Sebella-Arguelles C, Cohen A, Huart V, Wareham NJ, Luben R, Khaw KT, Tedgui A, Boekholdt SM. Circulating secretory phospholipase A2 activity and risk of incident coronary events in healthy men and women: the EPIC-Norfolk study. *Arterioscler Thromb Vasc Biol.* 2007;27(5):1177-1183.
14. MacPhee CH, Moores KE, Boyd HF, Dhanak D, Ife RJ, Leach CA, Leake DS, Milliner KJ, Patterson RA, Suckling KE, Tew DG, Hickey DM. Lipoprotein-associated phospholipase A2, platelet-activating factor acetylhydrolase, generates two bioactive products during the oxidation of low-density lipoprotein: use of a novel inhibitor. *Biochem J.* 1999;338 (Pt 2):479-487.

15. O'Donoghue M, Morrow DA, Sabatine MS, Murphy SA, McCabe CH, Cannon CP, Braunwald E. Lipoprotein-associated phospholipase A2 and its association with cardiovascular outcomes in patients with acute coronary syndromes in the PROVE IT-TIMI 22 (PRavastatin Or atorVastatin Evaluation and Infection Therapy-Thrombolysis In Myocardial Infarction) trial. *Circulation.* 2006;113(14): 1745-1752.
16. Oei HH, van der Meer IM, Hofman A, Koudstaal PJ, Stijnen T, Breteler MM, Witteman JC. Lipoprotein-associated phospholipase A2 activity is associated with risk of coronary heart disease and ischemic stroke: the Rotterdam Study. *Circulation.* 2005;111(5):570-575.
17. Koenig W, Twardella D, Brenner H, Rothenbacher D. Lipoprotein-associated phospholipase A2 predicts future cardiovascular events in patients with coronary heart disease independently of traditional risk factors, markers of inflammation, renal function, and hemodynamic stress. *Arterioscler Thromb Vasc Biol.* 2006;26(7):1586-1593.
18. Zalewski A, Macphee C. Role of lipoprotein-associated phospholipase A2 in atherosclerosis: biology, epidemiology, and possible therapeutic target. *Arterioscler Thromb Vasc Biol.* 2005;25(5):923-931.
19. Kolodgie FD, Burke AP, Skorija KS, Ladich E, Kutys R, Makuria AT, Virmani R. Lipoprotein-associated phospholipase A2 protein expression in the natural progression of human coronary atherosclerosis. *Arterioscler Thromb Vasc Biol.* 2006;26(11): 2523-2529.
20. Wilensky RL, Shi Y, Mohler ER, 3rd, Hamamdzic D, Burgert ME, Li J, Postle A, Fenning RS, Bollinger JG, Hoffman BE, Pelchovitz DJ, Yang J, Mirabile RC, Webb CL, Zhang L, Zhang P, Gelb MH, Walker MC, Zalewski A, Macphee CH. Inhibition of lipoprotein-associated phospholipase A2 reduces complex coronary atherosclerotic plaque development. *Nat Med.* 2008;14(10):1059-1066.
21. Davis B, Koster G, Douet LJ, Scigelova M, Woffendin G, Ward JM, Smith A, Humphries J, Burnand KG, Macphee CH, Postle AD. Electrospray Ionization Mass Spectrometry Identifies Substrates and Products of Lipoprotein-associated Phospholipase A2 in Oxidized Human Low Density Lipoprotein. *J Biol Chem.* 2008;283(10):6428-6437.
22. Carpenter KL DI, Challis IR, Osborn DP, Macphee CH, Leake DS, Arends MJ, Mitchinson MJ. Inhibition of lipoprotein-associated phospholipase A2 diminishes the death-inducing effects of oxidised LDL on human monocyte-macrophages. *FEBS Lett.* 2001;505:357-363.
23. Shi Y, Zhang P, Zhang L, Osman H, Mohler ER, 3rd, Macphee C, Zalewski A, Postle A, Wilensky RL. Role of lipoprotein-associated phospholipase A2 in leukocyte activation and inflammatory responses. *Atherosclerosis.* 2007;191(1):54-62.
24. Brilakis ES, McConnell JP, Lennon RJ, Elesber AA, Meyer JG, Berger PB. Association of lipoprotein-associated phospholipase A2 levels with coronary artery disease risk factors, angiographic coronary artery disease, and major adverse events at follow-up. *Eur Heart J.* 2005;26(2):137-144.
25. Oslund RC, Cermak N, Gelb MH. Highly specific and broadly potent inhibitors of mammalian secreted phospholipases A2. *J Med Chem.* 2008;51(15):4708-4714.

26. Rosenson RS, Hislop C, McConnell D, Elliott M, Stasiv Y, Wang N, Waters DD. Effects of 1-H-indole-3-glyoxamide (A-002) on concentration of secretory phospholipase A2 (PLASMA study): a phase II double-blind, randomised, placebo-controlled trial. *Lancet.* 2009;373(9664):649-658.
27. Nijmeijer R, Lagrand WK, Baidoshvili A, Lubbers YT, Hermens WT, Meijer CJ, Visser CA, Hack CE, Niessen HW. Secretory type II phospholipase A(2) binds to ischemic myocardium during myocardial infarction in humans. *Cardiovasc Res.* 2002;53(1): 138-146.
28. Nijmeijer R, Lagrand WK, Visser CA, Meijer CJ, Niessen HW, Hack CE. CRP, a major culprit in complement-mediated tissue damage in acute myocardial infarction? *Int Immunopharmacol.* 2001;1(3):403-414.
29. Mohler ER, 3rd, Ballantyne CM, Davidson MH, Hanefeld M, Ruilope LM, Johnson JL, Zalewski A. The effect of darapladib on plasma lipoprotein-associated phospholipase A2 activity and cardiovascular biomarkers in patients with stable coronary heart disease or coronary heart disease risk equivalent: the results of a multicenter, randomized, double-blind, placebo-controlled study. *J Am Coll Cardiol.* 2008; 51(17):1632-1641.
30. Serruys PW, Garcia-Garcia HM, Buszman P, Erne P, Verheye S, Aschermann M, Duckers H, Bleie O, Dudek D, Botker HE, von Birgelen C, D'Amico D, Hutchinson T, Zambanini A, Mastik F, van Es GA, van der Steen AF, Vince DG, Ganz P, Hamm CW, Wijns W, Zalewski A. Effects of the Direct Lipoprotein-Associated Phospholipase A2 Inhibitor Darapladib on Human Coronary Atherosclerotic Plaque. *Circulation.* 2008.

CHAPTER 8.1

Greyscale Intravascular Ultrasound and IVUS-Radiofrequency Tissue Characterization to Improve Understanding of the Mechanisms of Coronary Stent Thrombosis in Drug-eluting Stents.

Garcia-Garcia HM, Gonzalo N, Kukreja N, Alfonso F.

EuroIntervention. 2008 Aug;4 Suppl C:C33-8.

EuroIntervention

Greyscale intravascular ultrasound and IVUS-radiofrequency tissue characterisation to improve understanding of the mechanisms of coronary stent thrombosis in drug-eluting stents

Hector M. Garcia-Garcia[1]*, MD, MSc; Nieves Gonzalo[1], MD; Neville Kukreja[1], MRCP; Fernando Alfonso[2], MD

1. Thoraxcenter, Erasmus MC, Rotterdam, The Netherlands; 2. Instituto Cardiovascular, Hospital Clinico "San Carlos", Madrid, Spain

The authors have no conflict of interest to declare.

KEYWORDS
radiofrequency data analysis, incomplete stent apposition, necrotic core

Abstract

Stent thrombosis is one of the major concerns after drug-eluting stent implantation. Multiple mechanical causes (i.e. stent under-expansion, edge dissection, geographic miss, residual stenosis, incomplete stent apposition and aneurysm) have been postulated. These features are easily identifiable by intravascular ultrasound. However, it is uncertain which of them are inextricably related to stent thrombosis, primarily due to the low number of such patients studied by IVUS in case control studies.

Complementary to greyscale IVUS, tissue characterisation by IVUS radiofrequency data (RFD) analysis has the potential to add valuable information on the pathogenesis of stent thrombosis by providing information on plaque composition, specifically on the amount of necrotic core and its location (superficial or deep). However, the clinical utility of IVUS-RFD analysis in this context has yet to be demonstrated.

* *Corresponding author: Thorax Center, ErasmusMC, 's-Gravendijkwal 230 3015 CE Rotterdam, The Netherlands*
E-mail:hgarciagarcia@erasmusmc.nl

Introduction

In current practice, one of the most important concerns for the interventionalist is stent thrombosis, primarily of drug-eluting stents (DES)[1-5]. Among the multiple postulated causes, there is a large group encompassed in so-called mechanical causes (i.e. stent under-expansion, edge dissection, geographic miss, residual stenosis, incomplete stent apposition [ISA] and aneurism [extreme ISA]). These were also formerly related to thrombosis of bare metal stents (BMS). In fact, for this stent type, it has been reported that in 78% of the patients with stent thrombosis at least one mechanical cause is present using greyscale intravascular ultrasound (IVUS)[6]. Furthermore, ISA at long-term follow-up seems to be more frequent after sirolimus-eluting stent (SES) implantation than after BMS implantation[7]. Extreme positive remodelling after DES implantation is one of the main processes involved in cases with late acquired ISA. More importantly, ISA has recently been linked to thrombotic coronary events[4,8].

Complementary to greyscale IVUS, tissue characterisation by IVUS radiofrequency data (RFD) analysis has the potential to add valuable information on the pathogenesis of stent thrombosis by providing information on plaque composition, specifically on the amount of necrotic core (NC) and its location (superficial or deep). Although IVUS-RFD analysis is a new technique and there is a long way ahead to prove its clinical value in the context of stent thrombosis, in this report we describe pathological findings that have been related to stent thrombosis that are identifiable by IVUS-RFD.

We also describe the current evidence that relates greyscale IVUS findings with stent thrombosis.

Definitions of the mechanical causes of stent thrombosis (Figure 1)

Stent under-expansion index, defined as minimum stent cross-sectional area (CSA) ÷ mean of proximal and distal reference areas[4,8].

Significant residual reference segment stenosis, defined as the combination of a reference segment minimum lumen CSA <4 mm^2 plus a plaque burden >70%[9].

Geographical miss, defined as a mismatch of intended lesion and balloon-injured targets with subsequent stent deployment sites[10]. Unlike previous definition, geographical miss also refers to balloon-injured areas left untreated.

Incomplete stent apposition, defined as the lack of contact of at least one stent strut with the vessel wall, not encompassing a side branch. This can be detected immediately after stent implantation (acute or post-stenting ISA) or at follow-up (six months and beyond - late acquired ISA). (Figure 2).

Edge dissection, defined as the presence of a flap in close proximity to stent edges.

Aneurysm, defined as an enlargement of both the external elastic membrane (EEM) and lumen area >50% of the proximal reference segment[11].

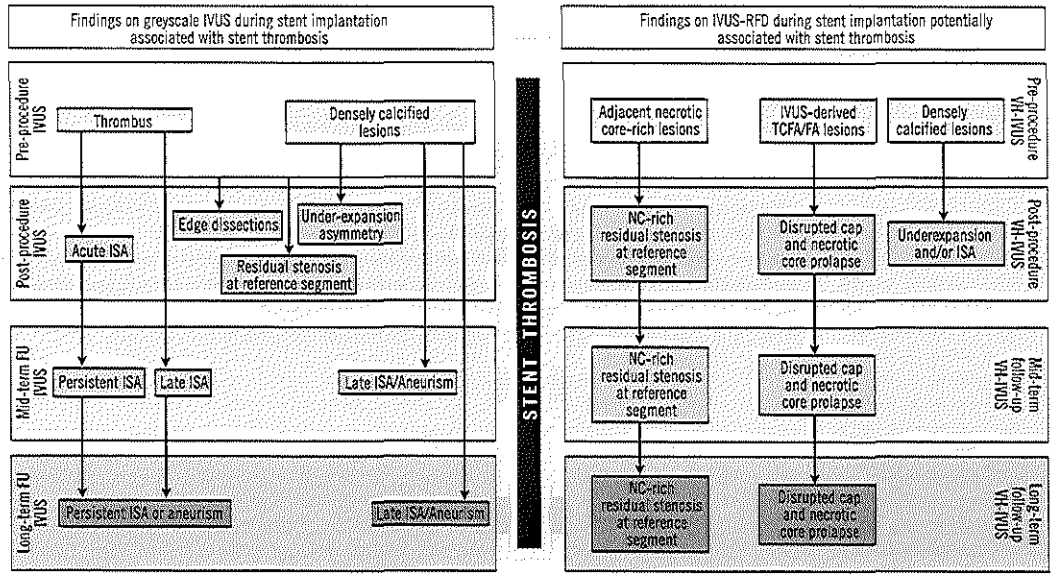

Figure 1. This illustration displays the potential use of greyscale IVUS and IVUS-radiofrequency data (RFD) analysis across the different stages of the interventional procedure and imaging follow-up of the patients. Greyscale IVUS can categorise plaque types and the acute result of the intervention, as well as provide useful information on some characteristics that have been related to stent thrombosis such as incomplete stent apposition (ISA), edge dissection, residual stenosis, under-expansion and thrombus. IVUS-RFD could provide valuable information on the intact plaque, especially on necrotic core (NC) amount and location.

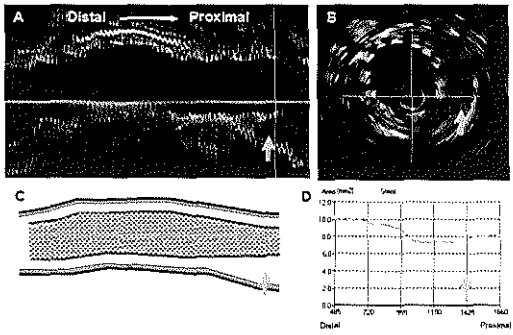

Figure 2. Panel A shows a longitudinal view of an IVUS pullback. The arrow points to a proximal segment that is not apposed to the vessel wall. Panel B is the corresponding cross-sectional area (CSA). The arrow shows multiple stent struts that are not apposed. Panel C is a diagrammatic representation of the longitudinal view. Notice the lack of stent apposition signalled by the arrow. Panel D indicates the stent CSA throughout the segment. An important decrease in stent area is seen at the proximal part.

Greyscale IVUS

Incomplete stent apposition has been postulated to be one of the potential causes of stent thrombosis. Yet, is ISA truly highly prevalent in patients with stent thrombosis after DES implantation? Or is stent thrombosis a rare event among patients with ISA? This is not clear, the reported prevalence of ISA post-stenting among DES studies (sirolimus, paclitaxel ([PES]) and everolimus-eluting stents (EES]) varies from 2.4 to 34.4%[12-18]. On the other hand, although late-acquired ISA has, by definition, the same IVUS appearance as post-stenting ISA, its postulated mechanisms are completely different including progressive expansion of the vessel wall, thrombus resolution and lack of tissue growth around the stent struts[17]. In the literature, the incidence ranges from 0.0 to 16.7%[12-14,16-21]. Possible explanatory reasons for the wide spread of occurrence across all reported stent studies are the following: i) lesion-related (calcified, eccentric, chronic total occlusions or thrombus)[17]; ii) procedure-related (absence of postdilatation and IVUS-guidance); iii) device-related (DES > BMS); and iv) corelab-related (inter-analyst and inter-corelab variability). Of note, no clinical events related to ISA have been reported in these trials.

The STLLR trial documented that geographical miss occurred in 66.5% of implantations and was an additional risk for late acute coronary events following drug-eluting stent implantation[10]. Thus, this suggests that angiographic-guided implantation of DES may be not satisfactory. In this regard, IVUS easily identifies incomplete lesion coverage, stent under expansion and ISA, yet remains infrequently used (approximately 7% of cases in the United States)[22]. Although IVUS-guided stenting could potentially improve stent implantation, the cost-effectiveness of routine IVUS use in this context has yet to be evaluated. More importantly, whether this approach would impact the incidence of late stent-related clinical events is unknown. However, we do not think all cases are suitable for IVUS-guided stenting. In this era of more liberal DES use, interventionalists frequently have to treat vessels with complex anatomy (e.g. severe tortuosity), in which even with IVUS-guided stenting, complete apposition may not be fully ensured. Thus, a careful analysis of the coronary anatomy prior to stent implantation may help operators to select cases in which IVUS imaging is safe and the information useful.

Clinical studies of patients with stent thrombosis and intravascular ultrasound imaging

Fujii et al[9] compared 15 patients treated with SES who experienced early stent thrombosis with 45 patients who had no evidence of SES thrombosis. Incomplete stent apposition was found in 13% of patients with SES thrombosis vs. 16% of controls. The minimum stent CSA was 4.3±1.6 mm^2 in patients with SES thrombosis compared with 6.2±1.9 mm^2 in controls ($p<0.001$); the stent under-expansion index was smaller in SES thrombosis (0.65±0.18 vs. 0.85±0.14; $p<0.001$), and the residual reference segment stenosis was 67% in the SES thrombosis group vs. 9% in the controls, $p<0.001$. In another case control study of 13 patients (14 DES with early thrombosis)[23], the minimum stent CSA was also smaller as compared to controls (4.6±1.1 vs. 5.6±1.7 mm^2; $p<0.05$), with 11 of 14 stents (79%) having a minimum stent CSAs ≤ 5.0 mm^2 compared with 12 of 30 (40%) in the control group ($p=0.04$). These authors also found larger residual reference segment stenosis in patients with thrombosis.

Mintz et al[21] reported the comparison of 15 cases of DES with early thrombosis with 45 cases of DES restenosis. In line with the above-mentioned reports, the minimum stent CSA was smaller in DES thrombosis lesions (3.7±0.8 vs. 4.9±1.8 mm^2; $p=0.01$). Independent predictors of stent thrombosis were diffuse stent under-expansion (odds ratio [OR], 1.5; $p=0.03$) and proximal location of the site of minimum stent CSA (OR, 12.7; $p=0.04$).

Siquiera et al[24] reported late-acquired incomplete stent apposition in 10 out of 195 patients (seven with SES, three with PES) studied with IVUS at six months; two out of these 10 patients with late-acquired ISA had stent thrombosis at 331 (PES) and 1,152 days (SES).

A report of two cases with DES thrombosis (one SES and one PES) revealed extensive positive remodelling (increase in vessel volume of 19.7 and 38.6%) leading to large areas of late-acquired incomplete stent apposition in both cases by means of serial angiography and IVUS[25].

More recently, Cook et al[8] reported 11 patients with very late DES thromboses and compared them with 198 controls that had undergone routine IVUS follow-up but did not develop stent thrombosis. Incomplete stent apposition was present at the time of thrombosis in 77% of patients with very late DES thromboses vs. 12% of controls imaged during routine follow-up; $p<0.0001$. The authors suggested that incomplete stent apposition may play a role in the pathogenesis of this adverse event.

The latest report available in the literature is by Alfonso et al[4] who reported 26 patients with DES thrombosis out of 1,974 patients treated with DES during the same period, resulting in a two-year stent thrombosis incidence of 1.3%. Only 12 were included in the IVUS substudy. Thrombotic occlusion was seen in all patients by IVUS. Severe stent under-expansion and significant residual

reference segment stenosis were again the common denominators in this series. Incomplete stent apposition was detected in 50% of the patients (three subacute, three late thrombosis), and major side branches jailed by the stent were seen in 67% of the patients. According to the Multicentre Ultrasound Stenting in Coronaries Study (MUSIC) criteria[26], deployment of the stents was suboptimal in all patients with stent thrombosis. In contrast with other studies, the minimum stent area was not small (9±3 mm^2). After re-intervention, residual thrombus was present in all patients (17±7% of stent volume post-intervention vs. 51±22% pre-intervention, p= 0.001).

We can therefore conclude that incomplete stent apposition is highly prevalent among patients with DES thrombosis that have been studied by IVUS. In addition, stent under-expansion and residual reference segment stenosis were also constantly associated with DES thrombosis.

Table 1 summarises the IVUS findings that have been reported among patients with stent thrombosis.

Table 1. IVUS findings in patients with stent thrombosis.

EEM CSA, mm^2	28.6	Mean[a]
Increase in EEM volume over time,%	19.7-38.6	Range[b]
ISA,%	50-100	Range[abc]
Maximal ISA CSA, mm^2	2.0-24	Range[a]
Maximal ISA length, mm	6.3	Mean[a]
Calcium arc, °	360	Mean[a]
Stent underexpansion index	0.39-1.00	Range[ac]
Stent asymmetry	0.77-0.90	Range[c]
Minimum stent CSA, mm^2	3.7; 4.3; 4.6	Mean[def]

EEM: external elastic membrane; CSA: cross-sectional area; ISA: incomplete stent apposition; [a] Cook et al; [b] Feres et al; [c] Alfonso et al; [d] Mintz et al; [e] Fujii et al; [f] Okabe et al

IVUS Radiofrequency data analysis

Our knowledge of the pathophysiology of late DES thrombosis is derived from pathologic samples[27-30]. It has been demonstrated that DES cause substantial delayed healing (the most common cause of late DES thrombosis at autopsy) characterised by the lack of complete re-endothelialisation and persistence of fibrin when compared with BMS[31]. This cannot be assessed by any IVUS modality due to its limited axial resolution (100 µm).

Other proposed pathological mechanisms of coronary stent thrombosis are stenting of necrotic core-rich plaques with extensive tissue prolapse and plaque disruption in the proximity of the stented arterial segment[27,31]. (Figure 3). IVUS-RFD is able to characterise necrotic core with high sensitivity and specificity[32]. This technique also provides geometrical analysis of each frame, allowing us to have the combined assessment of necrotic core and plaque size; indeed this relationship has been tested in 25 patients with acute coronary syndromes in whom an increment in plaque size was followed by an increase in the NC[33]. Thus, pre-stenting imaging using IVUS-RFD can give us an insight not only into the extent of plaque but also on the extent of necrotic core within and beyond the intended stenting segment. This latter assessment is important since stenting has been lately performed, under conventional angiography guidance, from "normal to normal" arterial segments;

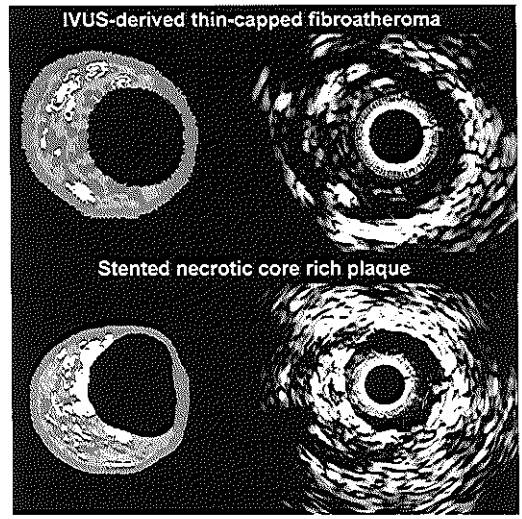

Figure 3. Greyscale IVUS frame and its corresponding IVUS-radiofrequency data frames of an IVUS derived thin cap fibro-atheroma (two upper frames). At the bottom, a stented necrotic core-rich plaque is shown. Notice the presence of stent struts at the lumen in the color picture as "dense calcium" on top of a confluent area of necrotic core. Virtual histology color code: green is fibrous, greenish is fibro-fatty, red is necrotic core and white is dense calcium.

however, disruption of adjacent necrotic core-rich areas that are angiographically disease-free could be avoided by IVUS-RFD pre-stenting investigation. In this context, we studied 24 patients in whom 26 stented segments (by angiography stenting was performed from "normal to normal" coronary segments) using IVUS-RFD were assessed. We observed that necrotic core rich areas were left unstented (5mm-proximal edge mean necrotic core 17.0±13.5% and 5 mm-distal edge 18.5±16.5%); however, no stent thrombosis has been observed in this small cohort of patients at six months follow-up. It has yet to be determined in a larger population whether incomplete coverage of necrotic core-rich coronary plaques or disruption of adjacent necrotic core areas by DES impact on long-term clinical events.

Bifurcation lesions are the preferable location of TCFAs; in clinical studies this subset of lesions has been related to stent thrombosis[4]; we therefore hypothesised that the evaluation of the location and amount of the necrotic core is crucial. Thus, not only may the bifurcation stenting technique change accordingly, mainly by avoiding overlapping segments on these NC-rich areas, but also the stent used to treat these lesions. The desirable objective is a device that offers: a) mechanical stabilisation, b) promotion of vascular healing and c) reduction of inflammation. Nevertheless, it is worth mentioning that although related to a different physiopathological process and other arterial segment – restenosis following carotid stenting – the dissection of a lipid-rich, inflammatory plaque has been recently associated with reduced risk of restenosis.[34]

Theoretically, IVUS-RFD enables us to characterise *in vivo* TCFA - IVUS-derived thin-capped fibro-atheroma (IDTCFA); these lesions

may pose a distinctive high risk of stent thrombosis, due to the fact that they contain large amount of necrotic core located superficially. We have recently developed software to quantify the amount of necrotic core in contact with the lumen, enabling refinement of our analysis. Our current definition of an IDTCFA is a lesion fulfilling the following criteria in at least three CSAs: 1) plaque burden ≥40%; 2) confluent necrotic core ≥10% in direct contact with the lumen (i.e., no visible overlying tissue) in the investigated CSA; all consecutive CSAs having the same morphologic characteristics are considered as part of the same IDTCFA lesion[35]. In a recent study, using this refined definition of TCFA as assessed by IVUS-RFD, in patients with ACS who underwent IVUS imaging of all three epicardial coronaries, on average, there were two IDTCFAs per patient, half of which showed outward remodelling[35] (Figure 3).

Post-stenting analysis by IVUS radiofrequency data analysis is limited since this technique lacks proper validation in this respect. An approach to get around this limitation could be to perform pre-stenting and post-stenting IVUS-RFD to assess the acute changes in terms of composition and relate this to the follow-up findings. Thus an IVUS-RFD clinical study that investigates the relationship between plaque composition of the intended stent segment (including its 10 mm proximal and distal segments) and development of stent thrombosis is still to be scheduled.

Conclusions

Although there are several potential mechanical causes of stent thrombosis that can be detected during the index procedure by greyscale IVUS as well as by repeated imaging at follow-up, it is uncertain which of them are inarguably related to stent thrombosis, primarily due to the low number of patients with stent thrombosis studied by IVUS in case control studies where causality is difficult to assess. A longitudinal and prospective study, adequately powered to demonstrate the mechanical factors potentially identifiable by IVUS and related to stent thrombosis is still awaited.

References

1. Iakovou I, Schmidt T, Bonizzoni E, Ge L, Sangiorgi GM, Stankovic G, Airoldi F, Chieffo A, Montorfano M, Carlino M, Michev I, Corvaja N, Briguori C, Gerckens U, Grube E, Colombo A. Incidence, predictors, and outcome of thrombosis after successful implantation of drug-eluting stents. *JAMA.* 2005;293(17):2126-2130.

2. Garcia-Garcia HM, Vaina S, Tsuchida K, Serruys PW. Drug-eluting stents. *Arch Cardiol Mex.* 2006;76(3):297-319.

3. Daemen J, Wenaweser P, Tsuchida K, Abrecht L, Vaina S, Morger C, Kukreja N, Juni P, Sianos G, Hellige G, van Domburg RT, Hess OM, Boersma E, Meier B, Windecker S, Serruys PW. Early and late coronary stent thrombosis of sirolimus-eluting and paclitaxel-eluting stents in routine clinical practice: data from a large two-institutional cohort study. *Lancet.* 2007;369(9562):667-678.

4. Alfonso F, Suarez A, Perez-Vizcayno MJ, Moreno R, Escaned J, Banuelos C, Jimenez P, Bernardo E, Angiolillo DJ, Hernandez R, Macaya C. Intravascular ultrasound findings during episodes of drug-eluting stent thrombosis. *J Am Coll Cardiol.* 2007;50(21):2095-2097.

5. Ong AT, McFadden EP, Regar E, de Jaegere PP, van Domburg RT, Serruys PW. Late angiographic stent thrombosis (LAST) events with drug-eluting stents. *J Am Coll Cardiol.* 2005;45(12):2088-2092.

6. Cheneau E, Leborgne L, Mintz GS, Kotani J, Pichard AD, Satler LF, Canos D, Castagna M, Weissman NJ, Waksman R. Predictors of subacute stent thrombosis: results of a systematic intravascular ultrasound study. *Circulation.* 2003;108(1):43-47.

7. Hoffmann R, Morice MC, Moses JW, Fitzgerald P, Mauri L, Breithardt G, Schofer J, Serruys P, Stoll HP, Leon M. Impact of Late Incomplete Stent Apposition After Sirolimus-Eluting Stent Implantation on 4-Year Clinical Events. Intravascular Ultrasound Analysis from the Multicenter, Randomized, RAVEL, E-SIRIUS and SIRIUS Trials. *Heart.* 2007.

8. Cook S, Wenaweser P, Togni M, Billinger M, Morger C, Seiler C, Vogel R, Hess O, Meier B, Windecker S. Incomplete stent apposition and very late stent thrombosis after drug-eluting stent implantation. *Circulation.* 2007;115(18):2426-2434.

9. Fujii K, Carlier SG, Mintz GS, Yang YM, Moussa I, Weisz G, Dangas G, Mehran R, Lansky AJ, Kreps EM, Collins M, Stone GW, Moses JW, Leon MB. Stent underexpansion and residual reference segment stenosis are related to stent thrombosis after sirolimus-eluting stent implantation: an intravascular ultrasound study. *J Am Coll Cardiol.* 2005;45(7):995-998.

10. Costa MA. Treatment of drug-eluting stent restenosis. *Am Heart J.* 2007;153(4):447-449.

11. Mintz GS, Nissen SE, Anderson WD, Bailey SR, Erbel R, Fitzgerald PJ, Pinto FJ, Rosenfield K, Siegel RJ, Tuzcu EM, Yock PG. American College of Cardiology Clinical Expert Consensus Document on Standards for Acquisition, Measurement and Reporting of Intravascular Ultrasound Studies (IVUS). A report of the American College of Cardiology Task Force on Clinical Expert Consensus Documents. *J Am Coll Cardiol.* 2001;37(5):1478-1492.

12. Aoki J, Colombo A, Dudek D, Banning AP, Drzewiecki J, Zmudka K, Schiele F, Russell ME, Koglin J, Serruys PW. Peristent remodeling and neointimal suppression 2 years after polymer-based, paclitaxel-eluting stent implantation: insights from serial intravascular ultrasound analysis in the TAXUS II study. *Circulation.* 2005;112(25):3876-3883.

13. Weissman NJ, Koglin J, Cox DA, Hermiller J, O'Shaughnessy C, Mann JT, Turco M, Caputo R, Bergin P, Greenberg J, Kutcher M, Wong SC, Strickland W, Mooney M, Russell ME, Ellis SG, Stone GW. Polymer-based paclitaxel-eluting stents reduce in-stent neointimal tissue proliferation: a serial volumetric intravascular ultrasound analysis from the TAXUS-IV trial. *J Am Coll Cardiol.* 2005;45(8):1201-1205.

14. Tanabe K, Serruys PW, Degertekin M, Grube E, Guagliumi G, Urbaszek W, Bonnier J, Lablanche JM, Siminiak T, Nordrehaug J, Figulla H, Drzewiecki J, Banning A, Hauptmann K, Dudek D, Bruining N, Hamers R, Hoye A, Ligthart JM, Disco C, Koglin J, Russell ME, Colombo A. Incomplete stent apposition after implantation of paclitaxel-eluting stents or bare metal stents: insights from the randomized TAXUS II trial. *Circulation.* 2005;111(7):900-905.

15. Ako J, Morino Y, Honda Y, Hassan A, Sonoda S, Yock PG, Leon MB, Moses JW, Bonneau HN, Fitzgerald PJ. Late incomplete stent apposition after sirolimus-eluting stent implantation: a serial intravascular ultrasound analysis. *J Am Coll Cardiol.* 2005;46(6):1002-1005.

16. Kimura M, Mintz GS, Carlier S, Takebayashi H, Fujii K, Sano K, Yasuda T, Costa RA, Costa JR, Jr., Quen J, Tanaka K, Lui J, Weisz G, Moussa I, Dangas G, Mehran R, Lansky AJ, Kreps EM, Collins M, Stone GW, Moses JW, Leon MB. Outcome after acute incomplete sirolimus-eluting stent apposition as assessed by serial intravascular ultrasound. *Am J Cardiol.* 2006;98(4):436-442.

17. Hong MK, Mintz GS, Lee CW, Park DW, Park KM, Lee BK, Kim YH, Song JM, Han KH, Kang DH, Cheong SS, Song JK, Kim JJ, Park SW, Park SJ.

Late stent malapposition after drug-eluting stent implantation: an intravascular ultrasound analysis with long-term follow-up. *Circulation.* 2006;113(3):414-419.

18. Hong YJ, Jeong MH, Hwang SH, Yun NS, Lim SY, Lee SR, Hong SN, Kim KH, Park HW, Kim JH, Kim W, Ahn YK, Cho JG, Park JC, Kang JC. Impact of postprocedure minimum stent area on long-term results following abciximab-coated stent implantation: an intravascular ultrasound analysis. *Int J Cardiol.* 2007;123(1):23-28.

19. Serruys PW, Ruygrok P, Neuzner J, Piek J, Seth A, Schofer J, Richardt G, Wiemer M, Carrie D, Thuesen L, Boone E, Miquel-Herbert K, Daemen J. A randomised comparison of an everolimus-eluting coronary stent with a paclitaxel-eluting coronary stent: the SPIRIT II trial. *Eurointervention.* 2006;2:286-294.

20. Escolar E, Mintz GS, Popma J, Michalek A, Kim SW, Mandinov L, Koglin J, Stone G, Ellis SG, Grube E, Dawkins KD, Weissman NJ. Meta-analysis of angiographic versus intravascular ultrasound parameters of drug-eluting stent efficacy (from TAXUS IV, V, and VI). *Am J Cardiol.* 2007;100(4):621-626.

21. Mintz GS. Features and parameters of drug-eluting stent deployment discoverable by intravascular ultrasound. *Am J Cardiol.* 2007;100(8B):26M-35M.

22. Hodgson JM, Stone GW, Lincoff AM, Klein L, Walpole H, Bottner R, Weiner BH, Leon MB, Feldman T, Babb J, Dehmer GJ. Late stent thrombosis: considerations and practical advice for the use of drug-eluting stents: a report from the Society for Cardiovascular Angiography and Interventions Drug-eluting Stent Task Force. *Catheter Cardiovasc Interv.* 2007;69(3):327-333.

23. Okabe T, Mintz GS, Buch AN, Roy P, Hong YJ, Smith KA, Torguson R, Gevorkian N, Xue Z, Satler LF, Kent KM, Pichard AD, Weissman NJ, Waksman R. Intravascular ultrasound parameters associated with stent thrombosis after drug-eluting stent deployment. *Am J Cardiol.* 2007;100(4):615-620.

24. Siqueira D AA, Feres F, Mattos LA, Staico R, Maia J, Tanajura LFL, Abizaid AC, Chaves AJ, Sousa AGMR, Sousa JE. Late-acquired incomplete apposition after drug-eluting stents: frequency and potential for late stent thrombosis [abstract]. *J Am Coll Cardiol.* 2006;47.

25. Feres F, Costa JR, Jr., Abizaid A. Very late thrombosis after drug-eluting stents. *Catheter Cardiovasc Interv.* 2006;68(1):83-88.

26. de Jaegere P, Mudra H, Figulla H, Almagor Y, Doucet S, Penn I, Colombo A, Hamm C, Bartorelli A, Rothman M, Nobuyoshi M, Yamaguchi T, Voudris V, DiMario C, Makovski S, Hausmann D, Rowe S, Rabinovich S, Sunamura M, van Es GA. Intravascular ultrasound-guided optimized stent deployment. Immediate and 6 months clinical and angiographic results from the Multicenter Ultrasound Stenting in Coronaries Study (MUSIC Study). *Eur Heart J.* 1998;19(8):1214-1223.

27. Farb A, Burke AP, Kolodgie FD, Virmani R. Pathological mechanisms of fatal late coronary stent thrombosis in humans. *Circulation.* 2003;108(14):1701-1706.

28. Virmani R, Farb A, Guagliumi G, Kolodgie FD. Drug-eluting stents: caution and concerns for long-term outcome. *Coron Artery Dis.* 2004;15(6):313-318.

29. Virmani R, Guagliumi G, Farb A, Musumeci G, Grieco N, Motta T, Mihalcsik L, Tespili M, Valsecchi O, Kolodgie FD. Localized hypersensitivity and late coronary thrombosis secondary to a sirolimus-eluting stent: should we be cautious? *Circulation.* 2004;109(6):701-705.

30. Virmani R, Kolodgie FD, Farb A. Drug-eluting stents: are they really safe? *Am Heart Hosp J.* 2004;2(2):85-88.

31. Finn AV, Nakazawa G, Joner M, Kolodgie FD, Mont EK, Gold HK, Virmani R. Vascular responses to drug eluting stents: importance of delayed healing. *Arterioscler Thromb Vasc Biol.* 2007;27(7):1500-1510.

32. Nair A MP, Kuban BD, Vince DG. Automated coronary plaque characterization with intravascular ultrasound backscatter: ex vivo validation. *Eurointervention.* 2007;3:113-130.

33. Garcia-Garcia HM, Goedhart D, Serruys PW. Relation of plaque size to necrotic core in the three major coronary arteries in patients with acute coronary syndrome as determined by intravascular ultrasonic imaging radiofrequency. *Am J Cardiol.* 2007;99(6):790-792.

34. Hellings WE, Moll FL, De Vries JP, Ackerstaff RG, Seldenrijk KA, Met R, Velema E, Derksen WJ, De Kleijn DP, Pasterkamp G. Atherosclerotic plaque composition and occurrence of restenosis after carotid endarterectomy. *JAMA.* 2008;299(5):547-554.

35. Garcia-Garcia HM, Goedhart D, Schuurbiers JC, Kukreja N, Tanimoto S, Daemen J, Morel MA, Bressers M, van Es GA, Wentzel J, Gijsen F, van der Steen AF, Serruys PW. Virtual histology and remodeling index allow in vivo identification of allegedly high risk coronary plaques in patients with acute coronary syndromes: a three vessel intravascular ultrasound radiofrequency data analysis. *Eurointervention.* 2006;2:338-344.

CHAPTER 8.2

Tissue Characterization of the Edge Effects of Paclitaxel-Eluting Stents as Assessed by Serial Intravascular Ultrasound Radiofrequency Data Analysis: BETAX (BEside TAXus) study.

García-García HM, Gonzalo N, Tanimoto S, Meliga E, de Jaegere P, Serruys PW.

Rev Esp Cardiol. 2008 Oct;61(10):1013-9.

Characterization of Edge Effects With Paclitaxel-Eluting Stents Using Serial Intravascular Ultrasound Radiofrequency Data Analysis: The BETAX (BEside TAXus) Study

Héctor M. García-García, Nieves Gonzalo, Shuzou Tanimoto, Emanuele Meliga, Peter de Jaegere, and Patrick W. Serruys

Thoraxcenter, Erasmus MC, Rotterdam, The Netherlands

Introduction and objectives. At present, the effect of paclitaxel on tissue structure at the edges of Taxus® stents is unknown. The objective of this study was to investigate in vivo the temporal changes occurring at the edges of paclitaxel-eluting stents using intravascular ultrasound radiofrequency (IVUS-RF) data analysis.

Methods. The study included 24 patients who had a total of 26 paclitaxel-eluting stented segments. In all patients, IVUS-RF imaging was performed 5 mm proximally and 5 mm distally to the stent edges 6 months after stent implantation. For subsequent analysis, proximal and distal segments were divided into five 1-mm subsegments.

Results. In the first 2 subsegments adjacent to the proximal edge of the stent, the vessel wall had grown to compensate for plaque growth without affecting the vessel lumen, while in the remaining three subsegments there was overcompensation (ie, the vessel wall increased to greater than the plaque size). Consequently, the lumen had increased in size. At the distal edge of the stent, overcompensation was observed in all five subsegments and the lumen had increased in size. In general, proximal and distal growth was due to an increase in fibrolipid plaque ($P<.001$ and $P<.001$, respectively) along with a decrease in the necrotic core ($P=.014$ and $P<.001$, respectively) and the presence of dense calcium ($P<.001$ and $P<.001$, respectively).

Conclusions. Serial expansive vascular remodeling was observed at proximal and distal stent edges. Remodeling occurred in response to tissue growth, which was mainly due to increased fibrofatty tissue.

Key words: *Restenosis. Imaging. Drug-eluting stents. Coronary disease.*

SEE EDITORIAL ON PAGES 1001-6

Correspondence: Dr. P.W. Serruys,
Thoraxcenter, Bd583a,
Dr. Molewaterplein 40, 3015-GD, Rotterdam, The Netherlands
E-mail:p.w.j.c.serruys@erasmusmc.nl

Received November 30, 2007.
Accepted for publication March 13, 2008.

Caracterización de los efectos tisulares en los segmentos adyacentes a los stents liberadores de paclitaxel según el análisis de datos de radiofrecuencia procedentes de ecocardiografía intravascular seriada: estudio BETAX (BEside TAXus)

Introducción y objetivos. En la actualidad se desconoce el efecto de paclitaxel en la composición tisular en los segmentos adyacentes (bordes) del *stent* Taxus®. El objetivo de este estudio fue investigar in vivo los cambios temporales que se producen en los bordes del *stent* liberador de paclitaxel según un análisis de los datos de radiofrecuencia procedentes de ecografía intravascular (EIV).

Métodos. En total participaron 24 pacientes (26 segmentos con *stents* liberadores de paclitaxel). Se obtuvieron imágenes con EIV de los 5 mm proximales y los 5 mm distales de los bordes del *stent* transcurridos 6 meses del implante. Para realizar un análisis posterior, los segmentos proximales y distales se fraccionaron en cinco subsegmentos de 1 mm cada uno.

Resultados. En los primeros dos subsegmentos adyacentes al *stent* del borde proximal, la pared del vaso crece para compensar el crecimiento de la placa sin que ello afecte a la luz, mientras en los siguientes 3 subsegmentos se observó una sobrecompensación (la pared del vaso aumentó más que el tamaño de la placa). Por lo tanto, aumentó el tamaño luminal. En el borde distal, se observó sobrecompensación en todos los subsegmentos, seguida de un aumento del tamaño luminal. En general, el crecimiento proximal y distal se basó en un aumento de la placa fibrolipídica ($p < 0,001$ y $p < 0,001$ respectivamente), con una disminución del núcleo necrótico ($p = 0,014$ y $p < 0,001$ respectivamente) y un contenido denso de calcio ($p < 0,001$ y $p < 0,001$ respectivamente).

Conclusiones. Se observó un remodelado vascular expansivo y seriado en los bordes proximal y distal del *stent*, para acomodar un crecimiento tisular principalmente debido al aumento del tejido fibrolipídico.

Palabras clave: *Reestenosis. Técnicas de imagen.* Stents *farmacoactivos. Enfermedad coronaria.*

ABREVIATIONS

CSA: cross-sectional area
IVUS: intravascular ultrasound
RFD: radiofrequency data

INTRODUCTION

Stent use has been one of the major breakthroughs in the treatment of patients with coronary artery disease.[1] Together with its many advantages some associated pitfalls are restenosis and stent thrombosis.[2-9] Regarding the vascular responses after stenting (ie, restenosis and remodeling), a response-to-injury pattern of wound healing occurs, mainly characterized by an increase in smooth muscle cells and extracellular matrix.[10]

In the Taxus II study a significant reduction in lumen size was observed at the proximal edge in both paclitaxel eluting stent and bare metal stent groups, while at the distal edge the reduction was only present in the bare metal stent group. This was mainly due to an augment in plaque size not fully compensated by vessel wall remodeling.[11]

Nowadays spectral analysis of the intravascular ultrasound (IVUS) radiofrequency data (RFD) analysis[12,13] is emerging as a tool to assess tissue composition in the coronary arteries. Thus, not only serial geometrical changes can be analyzed, but also its composition.

However, in stented vessels this can only be performed at the edges of the stent, because the actual stent area and its surroundings cannot be analyzed with IVUS-RFD, due to: *a)* misclassification of the stent struts as "dense calcium": *b)* lack of proper validation of IVUS-RFD in this context; and *c)* potential interference of the superficial stent struts on the backscattering of the tissue behind them.

We hypothesized that the tissue involved in the increase of plaque at the edges of the stent, as assessed by IVUS-RFD, is mainly fibro-fatty tissue, which has been described as loosely packed bundles of collagen fibers with regions of lipid deposit and extracellular matrix without necrotic areas.[14]

We thus sought in vivo the temporal geometrical and tissue composition changes at the edge of paclitaxel-eluting stent as assessed by IVUS-RFD analysis.

METHODS

Patient Selection

The BEside TAXus® (BETAX) study was a longitudinal and prospective cohort of non-consecutive patients who had a clinical indication for coronary intervention and were treated with Taxus® stent (Taxus® Express²™; Boston Corporation, Natick, MA, USA) in at least one of their coronary arteries. Only patients who gave informed written consent were included in the study. Patients with stable angina and acute coronary syndromes were included. Acute coronary syndromes comprise unstable angina, non-ST segment elevation myocardial infarction and ST-segment elevation myocardial infarction. IVUS-RFD imaging was performed at post-stenting and at 6 months. Our local Ethics Committee approved the protocol.

IVUS-RFD Acquisition and Analysis

Details regarding the validation of the technique, on explanted human coronary segments and in vivo post-atherectomy, have previously been reported.[12-14] Briefly, IVUS-RFD uses spectral analysis of IVUS radiofrequency data to construct tissue maps that are correlated with a specific spectrum of the radiofrequency signal and assigned color codes (fibrous [labeled green], fibrofatty [labeled greenish-yellow], necrotic core [labeled red], and dense calcium [labeled white]).[12,13]

IVUS-RFD was acquired using a continuous pullback (Eagle-Eye™ 20 MHz Volcano Therapeutics, Rancho Cordova, CA, USA) by a dedicated IVUS-RFD console (Volcano Therapeutics, Rancho Cordova, CA, USA). The IVUS-RFD recordings were stored on a DVD and sent to Corelab (Erasmus Medical Center/Cardialysis, Rotterdam, The Netherlands) for offline analysis.

The 5-mm proximal (p) and 5-mm distal (d) segments adjacent to the stent were subsequently divided into 1-mm 5 subsegments (ss) (Figure).

The IVUS-RFD sampling rate during pullback is gated to peak R-wave and is therefore dependent on heart rate. For instance, during constant heart rate of 60 bpm, data will be collected every 0.5 mm.

Compositional and geometrical data were obtained for every cross-sectional area (CSA) and expressed as mean areas and percent for each IVUS-RFD component.

Statistical Analysis

Discrete variables are presented as counts and percentages. Continuous variables are presented as means (SD). A P value (2-sided) less than .05 was considered significant. Assumptions for normality were checked after transformation based on a P value >.20 at Kolmogorov-Smirnov test and by visual assessment of Q-Q plots of residuals. Accordingly, log transformation was performed on the variables with skewed distribution.

The comparison between baseline and follow-up was performed using paired Student t test.

Statistical analyses were performed with use of SPSS software version 11.5.

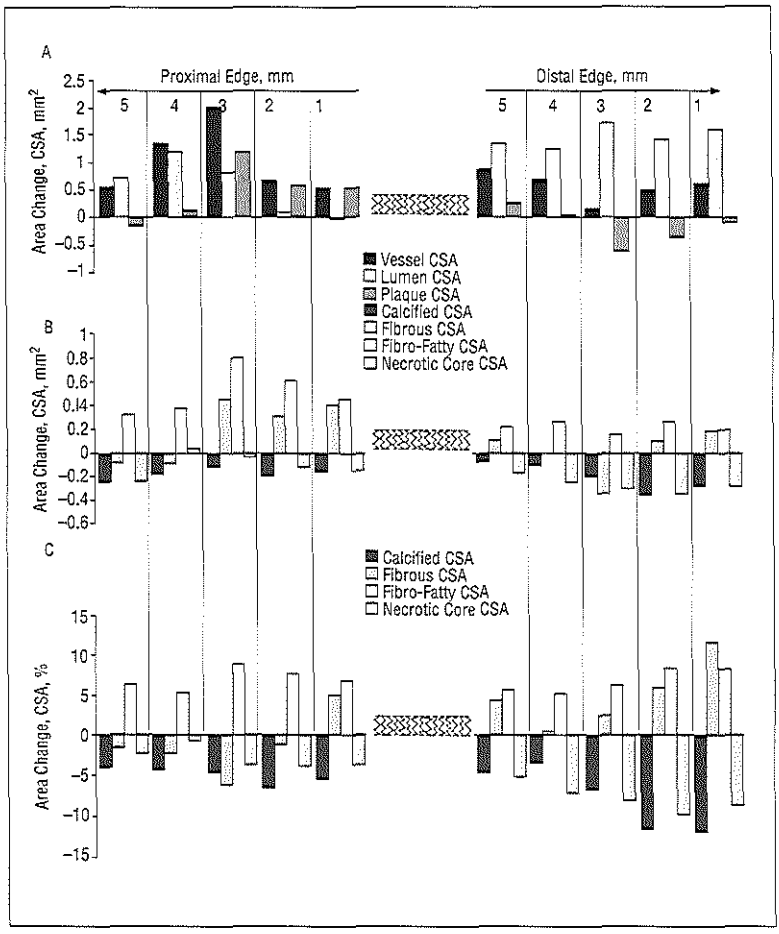

Figure. A: area changes in geometrical measurements at the proximal and distal 5-mm of the Taxus stent. B and C: absolute and relative temporal changes in plaque composition. CSA indicates cross-sectional area.

RESULTS

Overall, 30 patients were included in this study, but only 24 (26 stented segments) patients were ultimately analyzed. Two patients refused angiographic follow-up and in other 4 patients the IVUS image quality was poor (non-continuous pullback and presence of IVUS artifacts). The baseline characteristics of the patient population are depicted in Table 1. The mean age was 57.6 (11.2) years, most being male patients (75%) and 66% of the patients presented with stable angina. The studied vessel was the left anterior descending in 46.2 %, the left circumflex in 26.9 %, and the right coronary artery in 26.9 % of the cases. The mean number of stent per patient was 1.5 (0.7). No stent thrombosis has been observed so far.

IVUS-RFD Findings. Changes From Baseline to Follow-up in Geometrical and Compositional Parameters Within and Between the Proximal and Distal Segments.

At baseline, the mean vessel CSA (16.5 [4.9] vs 11.5 [4.0] mm^2; $P<.001$), plaque CSA (7.7 [3.6] vs 5.3 [2.7] mm^2; $P<.001$), and lumen CSA (8.8 [2.6] vs 6.2 [1.7] mm^2; $P<.001$) of the entire 5-mm edge segment in the proximal edge were larger than their counterparts in the distal segment. The same holds at follow-up for the measurements of the mean vessel CSA (17.5 [5.9] vs 12.8 [4.0] mm^2; $P<.001$), plaque CSA (8.2 [4.4] vs 5.1 [2.6] mm^2; $P<.001$), and lumen CSA (9.3 [3.0] vs 7.7 [4.0] mm^2; $P<.001$) (Table 2).

TABLE 1. **Demographic, Medication, and Procedure Characterisitics (n=24)**[a]

Age, mean (SD), y	57.6 (11.2)
BMI, mean (SD), kg/m²	28.1 (3.8)
Male18	(75)
Hypertension	10 (41.7)
Diabetes mellitus	6 (25)
Hypercholesterolemia	10 (41.7)
Current smoker	4 (16.7)
Previous cardiac history	5 (20.8)
Previous CABG	0
Previous ACS	3 (12.5)
Family history of CAD	11 (45.8)
Clinical presentation	
Stable angina	16 (66.6)
ACS	9 (37.4)
Medication	
Aspirin	
Baseline	17 (70.8)
6 Months follow-up	24 (100)
Clopidogrel	
Baseline	5 (20.8)
6 Months follow-up	24 (100)
Beta-blockers	
Baseline	7 (29.2)
6 Months follow-up	19 (79.2)
ACE inhibitor	
Baseline	5 (20.8)
6 Months follow-up	12 (50)
Calcium channel blocker	
Baseline	3 (12.5)
6 Months follow-up	1 (4.2)
Statins	
Baseline	12 (50)
6 Months follow-up	21 (87.5)
Studied vessel (n=26)	
LAD	12 (46.2)
LCX	7 (26.9)
RCA	7 (26.9)
Procedure characteristics	
Stent length, mean (SD), mm	16.6 (4.1)
Stent diameter, mean (SD), mm	3 (0.41)
Balloon pre-dilatation	11 (42.3)
Balloon length/stent length ratio, mean (SD)	0.97 (0.27)
Stent implantation pressure, mean (SD), atm	19.6 (3.24)

[a]ACS indicates acute coronary syndrome; BMI, body mass index; CABG, coronary artery bypass graft; CAD, coronary artery disease; LAD, left anterior descending; LCX, left circumflex; RCA, right coronary artery.
Data are expressed as n (%) or median (SD).

At the proximal and distal edges, a serial expansive vascular remodeling was observed at follow-up, with a significant increase in mean vessel CSA of the entire proximal (P=.031) and trend towards an increase in the distal segment (P=.06).

TABLE 2. **IVUS Virtual Histology Tissue Composition and Geometrical Data in the Entire 5 mm Segments**

	Calcified, mm²	Calcified, %	Fibrotic, mm²	Fibrotic, %	Fibrofatty, mm²	Fibrofatty, %	Necrotic Core, mm²	Necrotic Core, %	Vessel Cross Sectional Area, mm²	Lumen Cross Sectional Area, mm²	Plaque Cross Sectional Area, mm²	Plaque Burden, %
Proximal edge												
Baseline	0.52 (0.63)	10.7 (11.5)	2.6 (2.1)	57.9 (19.3)	0.52 (0.71)	11.7 (11.9)	0.74 (0.69)	17 (13.5)	16.5 (4.9)	8.8 (2.6)	7.7 (3.6)	45.4 (11.9)
Follow-up	0.32 (0.49)	5.8 (8.2)	2.8 (2.5)	56.9 (18.4)	1.02 (1.15)	18.7 (13.4)	0.63 (0.77)	14.2 (13.8)	17.5 (5.9)	9.3 (3)	8.2 (4.4)	45.1 (12.6)
P	<.0001	<.001	.48	.49	<.001	<.001	.014	.002	.031	.043	.54	.95
Distal Edge												
Baseline	0.29 (0.48)	11 (14.2)	1.4 (1.4)	47.8 (29.2)	0.21 (0.33)	7 (9.3)	0.52 (0.86)	18.5 (16.5)	11.5 (4)	6.2 (1.7)	5.3 (2.7)	43.5 (10)
Follow-up	0.09 (0.17)	3.3 (6.3)	1.4 (1.4)	53 (28.7)	0.43 (0.54)	13.7 (13.1)	0.26 (0.32)	0.8 (12.6)	12.8 (4)	7.7 (4)	5.1 (2.6)	40.2 (10.7)
P	<.001	<.001	.99	.18	<.001	<.001	<.001	<.001	.063	<.001	.69	.001
Baseline												
Proximal versus distal edge, P	<.001	.8	<.001	<.001	<.001	<.001	<.001	.23	<.001	<.001	<.001	.038
Follow-up												
Proximal versus distal edge, P	<.001	<.001	<.001	<.001	<.001	<.001	<.001	<.001	<.001	<.001	<.001	<.001

Since plaque CSA hardly increases, this remodeling resulted in a significant increase in mean lumen CSA was observed (Table 2).

In terms of tissue composition, at baseline, in the proximal segment as compared to the distal, the percentage of calcified tissue was not different (10.7% [11.5%] vs 11.0% [14.2%]; *P*=.80), the same was true for the necrotic core (17.0% [13.5%] vs 18.5% [16.5%]; *P*=.23); on the contrary significantly larger percentage of fibrous (57.9% [19.3%] vs 47.8% [29.2%]; *P*<.001), and fibrofatty tissue (11.7% [11.9%] vs 7.0% [9.3%]; *P*<.001) were observed.

At follow-up, all tissue types were larger in the proximal segment than in the distal, calcified (5.8% [8.2%] vs 3.3% [6.3%]; *P*<.001), necrotic core (14.2% [13.8%] vs 10.8% [12.6%]; *P*<.001), fibrous (56.9% [18.4] vs 53.0% [28.7%]; *P*<.001), and fibrofatty tissue (18.7% [13.4%] vs 13.7% [13.1%]; *P*<.001) (Table 2).

Overall, in the proximal and distal segments a significant increase of fibrofatty tissue was observed, whereas a decrease of calcified and necrotic core over the time was present. Fibrous tissue did not show significant temporal changes (Table 2).

Subsegmental Analysis of Longitudinal Changes at 5-mm Edge Segment of Proximal and Distal Edges

The mean absolute difference vessel CSA (follow-up – baseline) was positive throughout the proximal and distal segments: this was accompanied by a positive mean absolute difference in lumen CSA: the most prominent increase in plaque CSA (although not significant) was documented in first three proximal subsegments. (Figure). In particular, at the proximal edge, in the first 2 millimeters the vessel wall grew to compensate for the plaque growth (1-mm pss, Δ+0.52 and Δ+0.54 mm^2; 2-mm pss, Δ+0.65 and Δ+0.58 mm^2; vessel area change and plaque area change respectively) without affecting the lumen size (1-mm pss, Δ-0.02 mm^2; 2-mm pss, Δ+0.07 mm^2 in lumen area change), while in the following 3 subsegments overcompensation was observed, that is the vessel wall grew more than the plaque (3-mm pss, Δ+1.98 and Δ+1.18 mm^2; 4-mm pss, Δ+1.32 and Δ+0.12 mm^2; 5-mm pss, Δ+0.54 and Δ+0.14 in vessel area change and plaque area change respectively), resulting in an increase in lumen size (3-mm pss, Δ+0.81 mm^2; 4-mm pss, Δ+1.21 mm^2; and 5-mm pss, Δ+0.69 mm^2). At the distal edge, overcompensation was observed in all 5 subsegments, resulting in an increase in lumen size (1-mm dss, Δ+0.88; Δ+0.23 and Δ+1.35 mm^2; 2-mm dss, Δ+0.67; Δ+0.04 and Δ+1.24 mm^2; 3-mm dss, Δ+0.17; Δ-0.63 and Δ+1.72 mm^2; 4-mm dss, Δ+0.51; Δ-0.36 and Δ+1.42 mm^2; 5-mm dss, Δ+0.63; Δ-0.10 and Δ+1.61mm^2 in vessel, plaque and lumen area change respectively).

At 6-month follow-up, the percentage of fibrofatty tissue increased in all subsegments, while fibrous tissue showed a more heterogeneous behavior, with calcified tissue and necrotic core being decreased throughout the ten subsegments analyzed. (Figure).

DISCUSSION

The main findings of this study were the following: *a)* at the proximal and distal edge, a serial expansive vascular remodeling was observed, with an increase in mean vessel area and mean lumen area of the entire edge from baseline to follow-up; *b)* in the first 3 subsegments adjacent to the proximal part of the stent the most prominent increase in mean plaque area was observed. This is in line with the results of Taxus II and IV studies[11,15]; and *c)* overall, in the proximal and distal segment a significant increase of fibrofatty tissue was observed, while a decrease of calcified tissue and necrotic core over time was present.

The serial changes in tissue composition at the edges of the stent could vary depending on the location (proximal vs distal edge), the shear stress conditions,[16] the morphological baseline characteristics (degree of obstruction) of the segment as well as the baseline tissue composition. Last but not least, the degree of vessel wall injury after dilatation plays a role.[17] In animal and human pathological studies the response-to-injury process after stenting has been extensively described.[10] Restenosis occurs secondary to accumulation of smooth muscle cells and extracellular matrix, which consists of proteoglycans, hyaluronan and collagen (Type I and III). This extracellular matrix modulates neointimal growth and remodeling.[10] The IVUS-RFD tissue type that correlates with extracellular matrix is the fibro-fatty tissue, which happened to be the one that mostly increased in this study and, positive remodeling was also observed at both stent edges at 6 months. Serial remodeling has been proposed as the best approach to evaluate the geometrical vessel wall changes[18]. In this regard other previous Taxus® stent studies have described this phenomenon at the edges. In particular, in TAXUS II[11] a positive remodeling was only observed at the distal edge in both slow and moderate release Taxus group due to an increase in plaque size and hardly not change in lumen size; while in TAXUS IV[15] almost no change was observed in vessel size at proximal edge and a trend towards negative remodeling was observed at the distal edge. It is difficult to put in perspective these three studies, since they all have different sample size, in TAXUS IV authors acknowledged potential selection bias. So, although this study has a small sample size, a more complete characterization of the serial changes has been achieved.

In the present study, necrotic core rich areas were left unstented (proximal edge 17% [13.5%] and distal

edge 18.5% [16.5%]), however no stent thrombosis has been observed in this small cohort of patients. Proposed pathological mechanisms of stent thrombosis are stenting of necrotic core-rich plaques with extensive tissue prolapse and plaque disruption in the proximity of the stented arterial segment.[19,20] IVUS-RFD is not only able to characterize necrotic core with high sensitivity and specificity,[14] it also provides geometrical analysis of each frame, allowing us to have the combined assessment of necrotic core and plaque size. Thus, pre-stenting imaging using IVUS-RFD can give us an insight into the extent of plaque and necrotic core within and beyond the intended stenting segment. This latter assessment is important since stenting has been lately performed from "normal to normal" arterial segments in angiography; however, disruption of adjacent necrotic core-rich areas that are angiographically disease-free should be avoided. Indeed, it has been reported that incomplete coverage of coronary atherosclerotic plaques with drug-eluting stents may impact on long-term clinical events, especially in necrotic-core rich plaques.[19] Nevertheless, in this study, a decrease in necrotic core was showed at both edges at follow-up. Whether this is related to the presence of stent or even more to the drug type eluted on the stent remains to be elucidated.

The limitations of this study are various, firstly only a small cohort of patients has been included, since the study was considered mainly exploratory and without formal statistical hypothesis. Secondly, it would have been ideal to study completely the stent segment plus the edge effects, however as mentioned earlier, there is not validation of the tissue characterization behind the stent struts which may themselves interfere with the process of ultrasound backscattering of the tissue located behind the struts. Six-month follow-up may be a relatively short period of time to fully evaluate the tissue changes at the edges of the stent considering the fact that longer angiographic follow-up has been suggested to better evaluate the vascular responses at these locations.

CONCLUSIONS

Serial expansive vascular remodeling was observed at the proximal and distal edge of the stent, to accommodate a tissue growth mainly due to an increase in fibrofatty tissue.

REFERENCES

1. Serruys PW, Kutryk MJ, Ong AT. Coronary-artery stents. N Engl J Med. 2006;354:483-95.
2. McFadden EP, Stabile E, Regar E, Cheneau E, Ong AT, Kinnaird T, et al. Late thrombosis in drug-eluting coronary stents after discontinuation of antiplatelet therapy. Lancet. 2004;364: 1519-21.
3. Spaulding C, Daemen J, Boersma E, Cutlip DE, Serruys PW. A pooled analysis of data comparing sirolimus-eluting stents with bare-metal stents. N Engl J Med. 2007;356:989-97.
4. Stone GW, Moses JW, Ellis SG, Schofer J, Dawkins KD, Morice MC, et al. Safety and efficacy of sirolimus- and paclitaxel-eluting coronary stents. N Engl J Med. 2007;356:998-1008.
5. Kastrati A, Mehilli J, Pache J, Kaiser C, Valgimigli M, Kelbaek H, et al. Analysis of 14 trials comparing sirolimus-eluting stents with bare-metal stents. N Engl J Med. 2007;356:1030-9.
6. Lagerqvist B, James SK, Stenestrand U, Lindback J, Nilsson T, Wallentin L. Long-term outcomes with drug-eluting stents versus bare-metal stents in Sweden. N Engl J Med. 2007;356:1009-19.
7. Mauri L, Hsieh WH, Massaro JM, Ho KK, D'Agostino R, Cutlip DE. Stent thrombosis in randomized clinical trials of drug-eluting stents. N Engl J Med. 2007;356:1020-9.
8. Dibra A, Kastrati A, Mehilli J, Pache J, Schuhlen H, Von Beckerath N, et al. Paclitaxel-eluting or sirolimus-eluting stents to prevent restenosis in diabetic patients. N Engl J Med. 2005;353:663-70.
9. Windecker S, Remondino A, Eberli FR, Juni P, Raber L, Wenaweser P, et al. Sirolimus-eluting and paclitaxel-eluting stents for coronary revascularization. N Engl J Med. 2005; 353:653-62.
10. Farb A, Kolodgie FD, Hwang JY, Burke AP, Tefera K, Weber DK, et al. Extracellular matrix changes in stented human coronary arteries. Circulation. 2004;110:940-7.
11. Serruys PW, Degertekin M, Tanabe K, Russell ME, Guagliumi G, Webb J, et al. Vascular responses at proximal and distal edges of paclitaxel-eluting stents: serial intravascular ultrasound analysis from the TAXUS II trial. Circulation. 2004;109:627-33.
12. Nair A, Kuban BD, Tuzcu EM, Schoenhagen P, Nissen SE, Vince DG. Coronary plaque classification with intravascular ultrasound radiofrequency data analysis. Circulation. 2002; 106:2200-6.
13. Nasu K, Tsuchikane E, Katoh O, Vince DG, Virmani R, Surmely JF, et al. Accuracy of in vivo coronary plaque morphology assessment: a validation study of in vivo virtual histology compared with in vitro histopathology. J Am Coll Cardiol. 2006;47:2405-12.
14. Nair A MP, Kuban BD, Vince DG. Automated coronary plaque characterization with intravascular ultrasound backscatter: ex vivo validation. Eurointervention. 2007;3:113-30.
15. Weissman NJ, Koglin J, Cox DA, Hermiller J, O'Shaughnessy C, Mann JT, et al. Polymer-based paclitaxel-eluting stents reduce in-stent neointimal tissue proliferation: a serial volumetric intravascular ultrasound analysis from the TAXUS-IV trial. J Am Coll Cardiol. 2005;45:1201-5.
16. Wentzel JJ, Gijsen FJ, Stergiopulos N, Serruys PW, Slager CJ, Krams R. Shear stress, vascular remodeling and neointimal formation. J Biomech. 2003;36:681-8.
17. Wilcox JN, Okamoto EI, Nakahara KI, Vinten-Johansen J. Perivascular responses after angioplasty which may contribute to postangioplasty restenosis: a role for circulating myofibroblast precursors? Ann N Y Acad Sci. 2001;947:68-90.
18. Mintz GS, Nissen SE, Anderson WD, Bailey SR, Erbel R, Fitzgerald PJ, et al. American College of Cardiology Clinical Expert Consensus Document on Standards for Acquisition, Measurement and Reporting of Intravascular Ultrasound Studies (IVUS). A report of the American College of Cardiology Task Force on Clinical Expert Consensus Documents. J Am Coll Cardiol. 2001;37:1478-92.

19. Farb A, Burke AP, Kolodgie FD, Virmani R. Pathological mechanisms of fatal late coronary stent thrombosis in humans. Circulation. 2003;108:1701-6.

20. Finn AV, Nakazawa G, Joner M, Kolodgie FD, Mont EK, Gold HK, et al. Vascular responses to drug eluting stents: importance of delayed healing. Arterioscler Thromb Vasc Biol. 2007;27:1500-10.

CHAPTER 8.3

Assessment of the Absorption Process, Temporal Changes in Strain Values and Tissue Composition Following Bioabsorbable Everolimus-Eluting Stent Implantation: An Intravascular Ultrasound Radiofrequency Data Analysis Study.

García-García HM, Gonzalo N, Pawar R, Kukreja N, Dudek D, Thuesen L, Ormiston JA, Regar E, Serruys PW.

EuroIntervention. 2008;4:443-448

EuroIntervention

Assessment of the absorption process following bioabsorbable everolimus-eluting stent implantation: temporal changes in strain values and tissue composition using intravascular ultrasound radiofrequency data analysis A substudy of the ABSORB clinical trial

Héctor M. García-García[1,2], MD, MSc; Nieves Gonzalo[1], MD; Ravindra Pawar[2], BSc; Neville Kukreja[1], MRCP; Dariusz Dudek[3], MD; Leif Thuesen[4], MD; John A. Ormiston[5], MD; Evelyn Regar[1], MD, PhD; Patrick W. Serruys[1]*, MD. PhD

1. Thoraxcenter. Erasmus MC, Rotterdam, The Netherlands; 2. Cardialysis BV, Rotterdam, The Netherlands; 3. Jagiellonian University, Krakow, Poland; 4. Skejby Sygehus, Aarhus, Denmark; 5. Auckland City Hospital, Auckland, New Zealand

None of the authors have a conflict of interest to declare.

KEYWORDS
Bioabsorbable stent, palpography, IVUS-VH

Abstract

Aims: The main objective was to use IVUS-backscatter radiofrequency (IVUS-RF) to assess the degradation of a bioabsorbable stent by measuring serial changes in dense calcium (DC) and necrotic core (NC) as assessed by intravascular ultrasound-Virtual Histology™ (IVUS-VH) and in the strain as assessed by palpography.

Methods and results: In the ABSORB trial, 27 patients treated with a single bioabsorbable everolimus-eluting stent (BVS, Abbott Vascular, Santa Clara, CA, USA) were all imaged with IVUS-RF post-stenting and at 6-month follow-up, and 13 and 12 patients were also investigated pre-stenting with IVUS-VH and palpography respectively.

From pre- to post-stenting, with VH (n=13), there was an increase in mean "DC" (9.8 vs. 25.4%, p=0.0002) and "NC" (15.5 vs. 30.5%, p=0.0002). In palpography (n=12), the mean number of frames with Rotterdam Classification (ROC) III/IV per cm decreased from 1.22±1.91 to 0.12±0.31 (p= 0.0781) and the mean cumulative strain values (all frames with ROC I-IV scores) changed from 0.50±0.27 to 0.20±0.10% (p= 0.0034).

Comparing post-stenting with follow-up (n=27), VH showed a decrease in "DC" (29.7% vs. 21.1%, p=0.0001). "NC" also decreased (26.9 vs. 21.5%, p=0.0027). For palpography (n=25 patients), an increase in the mean number of frames with ROC III/IV per cm was observed from 0.09±0.26 to 0.22±0.36 (p=0.1563) while the mean cumulative strain values (all frames with ROC I-IV scores) changed from 0.15±0.10 to 0.26±0.12% (p<0.0001).

Conclusions: IVUS-VH changes at 6 months suggest alteration of the BVS with reduction of RF backscattering by polymeric struts. Strained plaques on the palpograms were almost abolished following stent implantation. However, strain values reappeared within 6 months suggesting an increase in endoluminal deformability of the stented vessel.

* *Corresponding author: Department of Cardiology, Erasmus Medical Center, Thoraxcenter, Ba583a, Erasmus MC, 's-Gravendijkwal 230, 3015 CE Rotterdam, The Netherlands*
E-mail:p.w.j.c.serruys@erasmusmc.nl

Introduction

Metal stent use has been one of the major breakthroughs in the treatment of patients with coronary artery disease.[1] However, the many advantages are somewhat counterbalanced by associated pitfalls such as restenosis, the persistent metal presence that may preclude late surgical revascularisation of the treated vessel, and jailing of side branches.[2-9] The advent of a new bioabsorbable everolimus-eluting stent[10] promises to overcome some of these disadvantages. The *in vivo* serial changes in its structural conformation (polymer degradation profile) were established in a porcine coronary artery model. Mass loss was approximately 30% at 12 months with a further reduction to 60% mass loss by 18 months after implantation[10]. However, in human coronary arteries the bio-absorption process has never been explored. Hence in the ABSORB trial all clinically available and potentially useful invasive coronary imaging techniques to assess bio-absorption of polymeric struts were used (i.e. echogenicity, intravascular ultrasound [IVUS] – radiofrequency [RF] data analysis: Virtual Histology™ [VH] and palpography and optical coherence tomography). Nevertheless, none of these techniques have been specifically designed to assess bio-absorption. Specifically, IVUS-VH[11,12] is a tool developed to assess the tissue composition of intact native coronary arteries. The analysis of the actual stent area and its surroundings by IVUS-VH identified the stent struts as "dense calcium" and "necrotic core" (white and red colour in the VH colour-code), which correspond to a specific backscattered radiofrequency of the polymeric strut structures (highly echogenic). Palpography is an IVUS-based technique that assesses the local mechanical deformation of the vessel wall by measuring the relative alteration of backscattered radiofrequency signals at two different blood pressure levels. For instance, lipid-rich vulnerable plaques ha ve greater deformation and higher strain values compared to calcific or fibrous plaques.[13] The main objective was twofold: i) to use IVUS-VH to follow-up the degradation of a bio-absorbable everolimus-eluting stent by measuring the temporal changes in IVUS-VH characteristics at pre-, post-stenting and at 6 months; and ii) to evaluate the temporal changes in palpographic strain values in the stented segment.

Methods

Study design

The study design for the prospective, open label ABSORB trial has already been published elsewhere.[10] Briefly, this was a single arm study that enrolled 30 patients at 4 participating sites between March and July 2006. Patients were older than 18 years, with a diagnosis of stable, unstable or silent ischaemia. All treated lesions were single, *de novo* in a native coronary artery of 3.0 mm, shorter than 8 mm for the 12 mm stent or ≤14 mm for the 18 mm stent (only two patients received an 18 mm stent), with a % diameter stenosis ≥50% and <100% and a thrombolysis in myocardial infarction (TIMI) flow grade of ≥1. Major exclusion criteria were patients presenting with an acute myocardial infarction, unstable arrhythmias or patients who had left ventricular ejection fraction <30%, restenotic lesions, lesions located in the left main coronary artery, lesions involving a side branch >2 mm in diameter, and the presence of thrombus or another clinically significant stenosis in the target vessel.

The study was approved by the ethics committee at each participating institution and each patient gave written informed consent before inclusion.

Study device

The BVS stent has a polymer backbone of Poly-L (racemic)-lactic Acid (PLLA) coated with a Poly-D (racemic), L-lactic acid (PDLLA) polymer that contains and controls the release of the anti-proliferative drug everolimus. Both PLLA and PDLLA are fully absorbable. The absorption process occurs via hydrolysis: the long chains of PLLA/PDLLA become shorter as bonds between the repeating units are hydrolysed, producing lactic acid which is metabolised via the Krebs cycle, and small particles <2 microns diameter that are phagocytosed by macrophages. The time for complete absorption of the polymer backbone is predicted from preclinical studies to be about 2-3 years whereas the polymer coating is absorbed in approximately 9 months.

Stenting procedure

Lesions were treated with routine interventional techniques that included mandatory pre-dilatation using a balloon shorter than the study device and 0.5 mm less in diameter. The BVS stent was implanted at a pressure not exceeding the rated burst pressure (16 atm). All patients were pretreated with aspirin and a loading dose of at least 300 mg of clopidogrel was administered according to local hospital practice. After the procedure, all patients were to receive aspirin ≥75 mg daily for the study duration (5 years) and clopidogrel 75 mg daily for a minimum of 6 months. Anticoagulation and glycoprotein IIb/IIIa inhibitor use was according to local hospital practice.

Imaging procedure

Pre-stenting IVUS-VH (n=13) and pre-stenting palpography (n=12) imaging were obtained in a subgroup of patients treated at the Thoraxcenter, Erasmus MC, Rotterdam, The Netherlands. The purpose of these analyses was to observe the acute changes after the implantation of the BVS stent. Subsequently, in the entire population IVUS-RF was obtained post-stenting and at follow-up. Both imaging techniques were acquired simultaneously with a phased array 20 MHz intravascular ultrasound catheter (EagleEye™; Volcano Corporation, Rancho Cordova, CA, USA) using automated pullback at 0.5 mm per second. Four tissue components (necrotic core – red; dense calcium – white; fibrous – green; and fibro-fatty – light green) were identified with autoregressive classification systems.[11,14] Each individual tissue component was quantified and colour coded in all IVUS cross sections as previously described. In a previous post-mortem validation study, RF analysis demonstrated sensitivity and specificity for detection of necrotic core of 92% and 97%, respectively.[14] All IVUS- VH analyses were performed offline using pcVH 2.1 (Volcano Corporation, Rancho Cordova, CA, USA) by an independent clinical research organisation (Cardialysis, Rotterdam, The Netherlands). For each cross section, polymeric stent struts were detected as areas of apparent "dense calcium" and "necrotic core". We used the change in quantitative analyses of these characteristics between implantation and follow-up as a surrogate assessment of the polymer bio-absorption process. IVUS-based palpography assesses deformability of the plaque. The underlying principle is that softer tissue is more readily deformed

compared with harder tissue when force (eg, pulsatile arterial pressure) is applied.[13] The deformability of coronary plaque is quantified using the analysis of radiofrequency signals at different diastolic pressure levels. The strain is normalised to a pressure difference of 2.5 mm Hg per frame. This allows the construction of a 'strain' image in which harder (low strain) and softer (high strain) regions of the coronary arteries can be identified, with radial strain values ranging between 0% and 2%.[13] In post-mortem coronary arteries that were investigated with histology and IVUS palpography, the sensitivity and specificity of palpography to detect high strain values were 88% and 89%, respectively.[13]

Plaque strain values were assigned a Rotterdam Classification (ROC) score ranging from I to IV (ROC I: 0% to 0.6%; ROC II: 0.6% to <0.9%; ROC III: 0.9% to <1.2%; ROC IV: >1.2%) as previously described.[15] All IVUS- palpography analyses were performed by an independent clinical research organisation (Cardialysis, Rotterdam, The Netherlands).

The clinical and geometrical analysis in the ABSORB study has already been reported.[10] Thus, in this paper, we exclusively report changes in tissue composition and plaque deformability.

Statistical analysis

As stated in the main ABSORB Study, the sample size was not defined on the basis of an endpoint hypothesis but rather to provide information about device efficacy and safety. Therefore, the present substudy should be seen as hypothesis-generating.

Discrete variables are presented as counts and percentages. Continuous variables are presented as means ± SD, quartiles and ranges. A two-sided p-value of less than 0.05 indicated statistical significance. Due to the exploratory nature of these analyses, p values were unadjusted for multiple comparisons in this manuscript.

The density of high-strain spots per 10 mm was defined as the number of cross-sections with strain values ≥0.9% (i.e. ROC III or IV) divided by the number of all analysable cross sections in the region of interest and normalised for 10 mm.

Paired comparisons between pre-procedure, post-procedure and follow-up were done by the Wilcoxon signed rank test. Statistical analyses were performed with use of SAS 9.1.

Results

Overall, 30 patients were included in the ABSORB study. The mean age was 62±9 years, most being male patients (60.0%), while 70.0% of the patients presented with stable angina, 26.7% and 3.3% had unstable angina and silent ischaemia respectively. The studied vessel was the left anterior descending in 46.7%, the left circumflex in 30.0% and the right coronary artery in 23.3% of the patients.

Intravascular ultrasound Virtual Histology™

Changes between pre- and post-stenting

In 13 patients, IVUS-VH was performed pre- and post-stenting (Table 1 and Figure 1). The mean percentage of "dense calcium" increased from 9.8% to 25.4% (p=0.0002) and "necrotic core" went from 15.5% to 30.5% (p=0.0002). Fibrous tissue, the major component of the vessel wall when expressed as mean area did not demonstrate statistically significant changes post-stenting, however its

Table 1. Acute changes in IVUS-VH in 13 patients.

	Pre stenting	Post stenting	p value
Dense calcium (mm²)			0.0002
Mean ± SD (N)	0.42±0.44 (13)	1.23±0.68 (13)	
Median	0.27	1.12	
(Q1-Q3)	(0.06, 0.89)	(0.87, 1.51)	
Range (min, max)	(0.01, 1.14)	(0.39, 2.90)	
Dense Calcium (%)			0.0002
Mean±SD (N)	9.83±9.64 (13)	25.42±11.27 (13)	
Median	6.19	27.09	
(Q1-Q3)	(4.26, 15.06)	(16.79, 31.78)	
Range (min, max)	(0.25, 34.66)	(9.91, 46.87)	
Fibrous (mm²)			0.1099
Mean±SD (N)	2.52±1.37 (13)	2.12±1.17 (13)	
Median	2.43	2.37	
(Q1-Q3)	(1.40, 3.62)	(1.05, 2.88)	
Range (min, max)	(0.17, 4.40)	(0.32, 4.08)	
Fibrous (%)			0.0002
Mean±SD (N)	60.75±13.06 (13)	38.98±10.47 (13)	
Median	64.40	37.14	
(Q1-Q3)	(52.32, 72.71)	(31.73, 45.35)	
Range (min, max)	(35.31, 76.90)	(24.88, 58.28)	
Fibrofatty (mm²)			0.0034
Mean±SD (N)	0.63±0.46 (13)	0.29±0.25 (13)	
Median	0.67	0.19	
(Q1-Q3)	(0.32, 0.94)	(0.10, 0.43)	
Range (min, max)	(0.01, 1.50)	(0.01, 0.81)	
Fibrofatty (%)			0.0002
Mean±SD (N)	13.89±8.31 (13)	5.07±3.92 (13)	
Median	13.22	3.76	
(Q1-Q3)	(8.76, 14.47)	(2.45, 5.48)	
Range (min, max)	(4.50, 34.16)	(1.44, 14.31)	
Necrotic Core (mm²)			0.0002
Mean±SD (N)	0.74±0.62 (13)	1.66±0.86 (13)	
Median	0.60	1.70	
(Q1-Q3)	(0.28, 1.24)	(0.89, 2.28)	
Range (min, max)	(0.03, 1.92)	(0.29, 2.88)	
Necrotic Core (%)			0.0002
Mean±SD (N)	15.53±8.43 (13)	30.54±6.16 (13)	
Median	14.10	31.56	
(Q1-Q3)	(9.86, 21.31)	(28.39, 33.62)	
Range (min, max)	(1.19, 33.01)	(17.50, 41.82)	

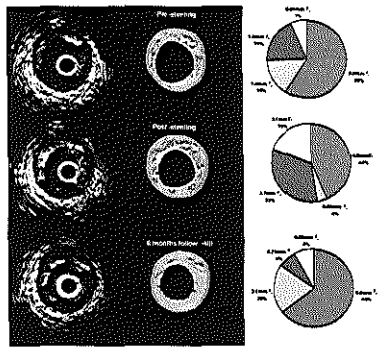

Figure 1. Serial changes in the stent struts as assessed by IVUS Virtual Histology™ (VH). On the left hand side, greyscale IVUS images are shown at pre-, post-stenting and follow-up. In the central part, their corresponding colour code VH images are depicted. On the right hand side, per-cross section quantification in absolute and relative terms is shown. Of note, increases in "dense calcium" (white) and "necrotic core" (red) are noted after stenting. At follow-up, a change in the stent strut appearance in greyscale IVUS is noted and decreases in the "dense calcium" and "necrotic core" contents in IVUS- VH are detected. Fibrous - green; and fibro-fatty - light green.

relative contribution to the stented vessel wall decreased significantly (60.8% vs. 39.0%, p=0.0002). In a similar fashion the percentage of fibro-fatty tissue decreased (13.9% vs. 5.1%, p=0.0002).

Changes from post-stenting to follow-up

Overall, in patients (n=27) with post-stenting and follow-up VH, a significant decrease in "dense calcium" (29.7% vs. 21.1%, p=0.0001) was shown. In 21 out of 27 patients, there was a regression in the "calcified" pattern (Table 2 and Figure 2). The content of "necrotic core" also decreased (26.9% vs. 21.5%, p=0.0027). In turn, both fibro-fatty and fibrous tissue increased in terms of both mean areas and percentages (Table 2 and Figure 1).

Intravascular ultrasound palpography

CHANGES FROM PRE- TO POST-STENTING

In 12 patients, IVUS-palpography was performed pre- and post-stenting (Figure 3 and 4). The mean number of frames with ROC III/IV per cm decreased from 1.22±1.91 to 0.12±0.31 (p=0.0781). The mean cumulative strain values in all frames with ROC I-IV scores changed from 0.50±0.27 to 0.20±0.10% (p= 0.0034).

CHANGES FROM POST-STENTING TO FOLLOW-UP

In patients (n=25) with post-stenting and follow-up palpography, a slight increase in the mean number frames with ROC III/IV per cm from 0.09±0.26 to 0.22±0.36 (p=0.1563) was observed, while the mean cumulative strain values in all frames with ROC I-IV scores increased significantly from 0.15±0.10 to 0.26±0.12% (p<0.0001) (Figure 3 and 4).

Discussion

In this substudy of the ABSORB clinical trial the main findings in IVUS-VH were an important increase in "dense calcium" and "necrotic core" immediately after stent implantation and a subsequent decrease of these tissue surrogates at 6 months follow-up; this decrease potentially reflects echogenic alteration of the BVS stent struts. On the palpograms, the almost complete initial abolition of the high strain regions was decreased six months following stent implantation: presumably after partial stent absorption the mean strain values increased again.

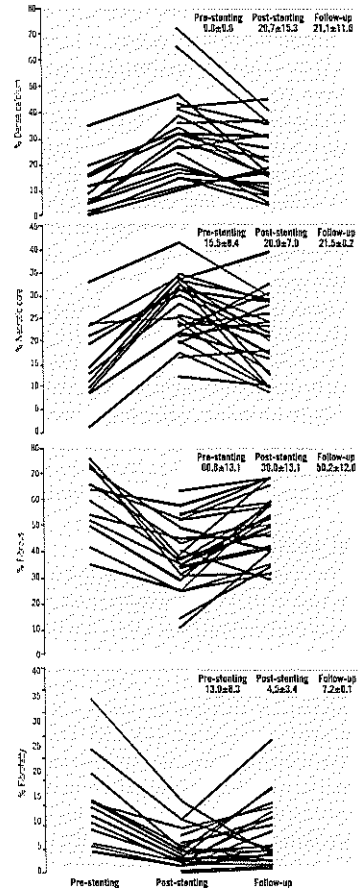

Figure 2. Temporal changes in virtual histology tissue types. From top to bottom, the mean percentage of "dense calcium", "necrotic core", fibrous tissue and fibro-fatty tissue is reported. Thirteen patients were imaged at pre-, post-stenting and follow-up (red solid lines). A further 14 patients were only imaged at post-stenting and follow-up (black dotted lines).

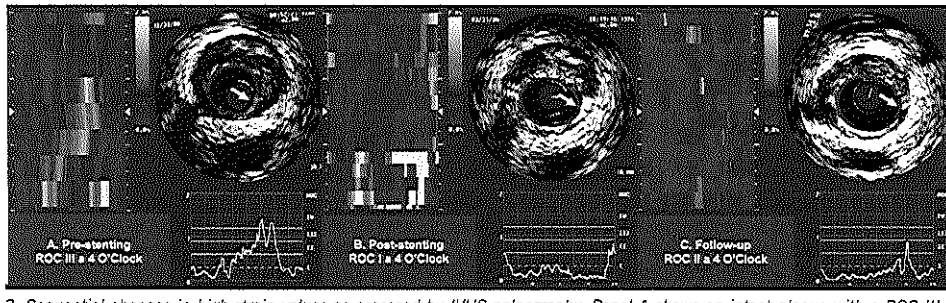

Figure 3. Sequential changes in high-strain values as assessed by IVUS-palpography. Panel A shows an intact plaque with a ROC III spot at 4 o'clock (white arrow). Panel B depicts abolition of this high strain spot following stenting (ROC I). In panel C a slight increase in plaque deformability was documented (ROC II).

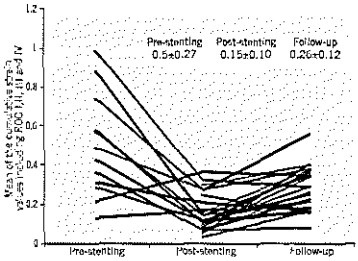

Figure 4. Temporal changes in strain values. The mean cumulative strain values in all frames with ROC I-IV scores are shown. Twelve patients were imaged at pre-, post-stenting and follow-up (red solid lines). Another 13 patients were only imaged at post-stenting and follow-up (black dotted lines). After stenting, abolition of the strain values was noted; however a higher level of plaque deformability was present at follow-up.

Table 2. Changes from post -procedure to 6-months.

	Post stenting	Follow-up	p value
Dense Calcium (mm²)			0.6065
Mean±SD (N)	0.97±0.59 (27)	0.88±0.61 (27)	
Median	0.89	0.86	
(Q1-Q3)	(0.49, 1.25)	(0.31, 1.22)	
Range (min, max)	(0.28, 2.90)	(0.17, 2.82)	
Dense Calcium (%)			0.0001
Mean±SD (N)	29.66±15.25 (27)	21.13±11.58 (27)	
Median	27.09	18.49	
(Q1-Q3)	(18.22, 38.44)	(10.86, 30.80)	
Range (min, max)	(9.91, 72.10)	(4.66, 44.91)	
Fibrous (mm²)			<0.0001
Mean±SD (N)	1.65±1.23 (27)	2.42±1.37 (27)	
Median	1.47	2.53	
(Q1-Q3)	(0.69, 2.57)	(1.19, 3.36)	
Range (min, max)	(0.06, 4.08)	(0.17, 4.93)	
Fibrous (%)			<0.0001
Mean±SD (N)	39.02±13.07 (27)	50.20±12.55 (27)	
Median	37.79	50.71	
(Q1-Q3)	(30.70, 49.81)	(40.26, 59.24)	
Range (min, max)	(10.85, 63.69)	(29.26, 68.95)	
Fibro-fatty (mm²)			0.0040
Mean±SD (N)	0.21±0.23 (27)	0.38±0.42 (27)	
Median	0.11	0.22	
(Q1-Q3)	(0.04, 0.33)	(0.12, 0.48)	
Range (min, max)	(0.00, 0.81)	(0.01, 1.72)	
Fibro-fatty (%)			0.0096
Mean±SD (N)	4.47±3.36 (27)	7.22±6.12 (27)	
Median	3.32	4.72	
(Q1-Q3)	(2.45, 5.65)	(2.57, 11.16)	
Range (min, max)	(0.54, 14.31)	(1.21, 26.18)	
Necrotic core (mm²)			0.4815
Mean±SD (N)	1.14±0.86 (27)	1.01±0.73 (27)	
Median	0.89	0.90	
(Q1-Q3)	(0.33, 1.77)	(0.58, 1.23)	
Range (min, max)	(0.10, 2.88)	(0.13, 3.07)	
Necrotic core (%)			0.0027
Mean±SD (N)	26.85±6.97 (27)	21.45±8.17 (27)	
Median	25.53	21.80	
(Q1-Q3)	(21.85, 33.11)	(13.61, 28.59)	
Range (min, max)	(12.30, 41.82)	(8.87, 39.70)	

In a previous study by Tamai et al,[16] PLLA stents analysed by greyscale IVUS at 6 months seemed to maintain their scaffolding properties and apparently did not exhibit changes in echogenicity as a sign of biodegradation. In the ABSORB trial, a reduction of the stent area was observed suggesting a mild recoil of the polymeric stent structures.[10] Implantation of polymeric struts resulted in the appearance in the vessel wall of highly echogenic structures with radiofrequency backscattering similar to calcific structures (Figure 1). Indeed, in this study using IVUS-VH, an increase in absolute "dense calcium" (Δ0.82 mm², p=0.0002) from pre- to post-stenting was observed. This dramatic and sudden change in "DC" may be attributed to the introduction of polymeric struts and might correspond to the VH fingerprint of the polymeric struts.

Following BVS stent implantation, the mean fibrous tissue area showed a slight decrease that failed to reach statistical significance (from 2.5 to 2.1 mm², p=0.1099). The mean fibro-fatty tissue area decreased significantly, although the change is numerically very small, and might be an artefact. From the ultrasonic point of view, the introduction of these highly echogenic structures might affect ultrasound penetration and therefore the backscattering of other tissue components located behind the struts, since potentially less acoustic signals are reaching the tissue.

Although we acknowledge that the classification tree of the IVUS radiofrequency analysis has not been validated for polymeric stent struts, the radiofrequency backscattering is expected to increase with the reduction in the echogenicity of the implanted stent. It is reasonable to assume that the hydrolysis of the polymer which affects its molecular weight and mass, will also alter its acoustic properties. The BVS stent is constituted of PLLA (backbone) and PDLLA (coating) which are both fully bio-absorbable. During bio-absorption, the long chains of PLLA and PDLLA are progressively shortened and ultimately phagocytosed by macrophages.[10] At follow-up, these pseudo-dense calcific structures shrink by nearly 30% (in absolute terms, an 8.6 % reduction in "dense calcium" from 29.7% to 21.1%), which is consistent with the reduction in mass of the BVS polymeric struts observed in animals. These observations are at variance with the previous report by Tamai et al where no signs of biodegradation were observed.[16] A possible explanation is that the speed of bioabsorption of a polylactic polymer is greatly influenced by its purity, crystallinity and relative composition of L and D isomers.

The changes in the physical properties of an artery can be described in terms of stiffness, ability to distend and compliance. These characteristics are dependent on the composition of the vascular wall.[17] Deployment of a stent against the vessel wall undoubtedly modifies the physical properties of the endoluminal surface. The near-abolition of the high strain values (ROC III/IV) immediately post-stenting reflects major changes in deformability of the plaque and the observed reductions in high strain values may be due to a real decrease in deformability of the scaffolded vessel wall. Alternatively, it may also reflect an ultrasonic artefact, namely the incapability of palpography to measure intrinsic changes in strain of the vessel due to the acoustic properties of the stent struts preventing a proper propagation of radiofrequency signal behind them. The loss of mass observed over time in the porcine model may cause the reappearance of high strain values on the endoluminal surface of the vessel wall. All these observations are indirect indicators of the modifications in strut structure. Although

IVUS-VH and palpography have not been validated to detect change in the integrity of polymeric stents, they seem to change acutely and chronically with the introduction and subsequent bio-absorption of the polymeric struts.

These new imaging techniques allow a better understanding of the effect of different therapeutic modalities.

Among the many clinical implications of the use of a biobasorbable stent, the most relevant pertains to the possibility to avoid potentially deadly events such as late stent thrombosis, providing the stent is fully absorbed in a reasonable period of time. Ideally, bio-absorption must occur after neointimal growth has been modulated. Knowing that this occurs mainly during the first 6 months after stent implantation, we have assessed bio-absorption using IVUS radiofrequency data analysis over this period of time. The results of the present substudy are unique findings since the *in vivo* bio-absorption rate in diseased human arteries is not known.

Limitations

In the context of stent studies, IVUS radiofrequency data analysis faces the following issues: i) misclassification of the stent struts as "dense calcium" and "necrotic core" in VH; ii) with both techniques – VH and palpography – the lack of proper validation to assess polymeric stents and; iii) the potential interference of the superficial stent struts on the backscattering from the tissue behind them. However, these techniques have corroborated other observations of polymer alteration documented with light transmission. In other words, changes in optical coherence of the struts reported elsewhere confirm the ultrasonic modifications reported here.

Conclusions

The quantitative assessment of the IVUS-VH changes at 6 months suggests early strut alteration of the BVS stent with reduction of radiofrequency backscattering. High-strain plaques seen on the palpograms were almost abolished following stent implantation. However, strain values reappeared at 6 months in some patients also suggesting an increase in deformability on the luminal surface of the stented vessel.

Acknowledgements

Authors are grateful to Jurgen Ligthart, Senior IVUS technician in Thoraxcenter, Erasmus MC and Monique Schuijer, ABSORB trial project manager at Cardialysis NL. Authors also thank Susan Veldhof from Abbott Vascular.

References

1. Serruys PW, Kutryk MJ, Ong AT. Coronary-artery stents. *N Engl J Med* 2006;354:483-95.

2. McFadden EP, Stabile E, Regar E, Cheneau E, Ong AT, Kinnaird T, Suddath WO, Weissman NJ, Torguson R, Kent KM, Pichard AD, Satler LF, Waksman R, Serruys PW. Late thrombosis in drug-eluting coronary stents after discontinuation of antiplatelet therapy. *Lancet* 2004;364:1519-21.

3. Spaulding C, Daemen J, Boersma E, Cutlip DE, Serruys PW. A pooled analysis of data comparing sirolimus-eluting stents with bare-metal stents. *N Engl J Med* 2007;356:989-97.

4. Stone GW, Moses JW, Ellis SG, Schofer J, Dawkins KD, Morice MC, Colombo A, Schampaert E, Grube E, Kirtane AJ, Cutlip DE, Fahy M, Pocock SJ, Mehran R, Leon MB. Safety and efficacy of sirolimus- and paclitaxel-eluting coronary stents. *N Engl J Med* 2007;356:998-1008.

5. Kastrati A, Mehilli J, Pache J, Kaiser C, Valgimigli M, Kelbaek H, Menichelli M, Sabaté M, Suttorp MJ, Baumgart D, Seyfarth M, Pfisterer ME, Schömig A. Analysis of 14 trials comparing sirolimus-eluting stents with bare-metal stents. *N Engl J Med* 2007;356:1030-9.

6. Lagerqvist B, James SK, Stenestrand U, Lindback J, Nilsson T, Wallentin L. Long-term outcomes with drug-eluting stents versus bare-metal stents in Sweden. *N Engl J Med* 2007;356:1009-19.

7. Mauri L, Hsieh WH, Massaro JM, Ho KK, D'Agostino R, Cutlip DE. Stent thrombosis in randomized clinical trials of drug-eluting stents. *N Engl J Med* 2007;356:1020-9.

8. Dibra A, Kastrati A, Mehilli J, Pache J, Schühlen H, von Beckerath N, Ulm K, Wessely R, Dirschinger J, Schömig A; ISAR-DIABETES Study Investigators. Paclitaxel-eluting or sirolimus-eluting stents to prevent restenosis in diabetic patients. *N Engl J Med* 2005;353:663-70.

9. Windecker S, Remondino A, Eberli FR, Jüni P, Räber L, Wenaweser P, Togni M, Billinger M, Tüller D, Seiler C, Roffi M, Corti R, Sütsch G, Maier W, Lüscher T, Hess OM, Egger M, Meier B. Sirolimus-eluting and paclitaxel-eluting stents for coronary revascularization. *N Engl J Med* 2005;353:653-62.

10. Ormiston JA, Serruys PW, Regar E, Dudek D, Thuesen L, Webster MW, Onuma Y, Garcia-Garcia HM, McGreevy R, Veldhof S. A bioabsorbable everolimus-eluting coronary stent system for patients with single de-novo coronary artery lesions (ABSORB): a prospective open-label trial. *The Lancet* 2008;371:899-907.

11. Nair A, Kuban BD, Tuzcu EM, Schoenhagen P, Nissen SE, Vince DG. Coronary plaque classification with intravascular ultrasound radiofrequency data analysis. *Circulation* 2002;106:2200-6.

12. Nasu K, Tsuchikane E, Katoh O, Vince DG, Virmani R, Surmely JF, Murata A, Takeda Y, Ito T, Ehara M, Matsubara T, Terashima M, Suzuki T. Accuracy of in vivo coronary plaque morphology assessment: a validation study of in vivo virtual histology compared with in vitro histopathology. *J Am Coll Cardiol* 2006;47:2405-12.

13. Schaar JA, De Korte CL, Mastik F, Strijder C, Pasterkamp G, Boersma E, Serruys PW, Van Der Steen AF. Characterizing vulnerable plaque features with intravascular elastography. *Circulation* 2003;108:2636-41.

14. Nair A MP, Kuban BD, Vince DG. Automated coronary plaque characterization with intravascular ultrasound backscatter: ex vivo validation. *Eurointerv* 2007;3:113-130.

15. Van Mieghem CA, McFadden EP, de Feyter PJ, Bruining N, Schaar JA, Mollet NR, Cademartiri F, Goedhart D, de Winter S, Granillo GR, Valgimigli M, Mastik F, van der Steen AF, van der Giessen WJ, Sianos G, Backx B, Morel MA, van Es GA, Zalewski A, Serruys PW.Noninvasive detection of subclinical coronary atherosclerosis coupled with assessment of changes in plaque characteristics using novel invasive imaging modalities: the Integrated Biomarker and Imaging Study (IBIS). *J Am Coll Cardiol* 2006;47:1134-42.

16. Tamai H, Igaki K, Kyo E, Kosuga K, Kawashima A, Matsui S, Komori H, Tsuji T, Motohara S, Uehata H. Initial and 6-month results of biodegradable poly-l-lactic acid coronary stents in humans. *Circulation* 2000;102:399-404.

17. Wada T, Fujishiro K, Fukumoto T, Yamazaki S. Relationship between ultrasound assessment of arterial wall properties and blood pressure. *Angiology* 1997;48:893-900.

CHAPTER 8.4

Ultrasonic and pathological evidence of a neo-intimal plaque rupture in patients with bare metal stent.

Ramcharitar S, **García-García HM**, Nakazawa G, Kukreja N, Ligthart J, Virmani R, Serruys PW.

EuroIntervention. 2007.3:290-291.

EuroIntervention

Ultrasonic and pathological evidence of a neo-intimal plaque rupture in patients with bare metal stents

Steve Ramcharitar[1], MRCP, DPhil; Hector M. Garcia-Garcia[1], MD, MSc; Gaku Nakazawa[2], MD; Neville Kukreja[1], MRCP; Jurgen Ligthart[1], BSc; Renu Virmani[2], MD, PhD; Patrick W. Serruys[1]*, MD, PhD

1. Thoraxcenter, Erasmus Medical Center, Rotterdam, The Netherlands; 2. CVPath Institute, Inc, Gaithersburg, Maryland, USA

The authors have no conflict of interest to declare.

Case 1

A 58-year-old man was admitted to our coronary care with troponin negative unstable angina. His risk factors included, being an ex-smoker for a year, treated hypertension and dyslipidaemia. Medication on admission was aspirin and a statin. ECG showed T-wave inversion laterally. Nine years previously he had a bare metal stent implanted in his circumflex artery following a lateral infarction the preceding year. Angiography done during his acute presentation revealed an in-stent restenosis in the previously treated circumflex artery and a diffusely diseased marginal branch. The left anterior decending coronary (LAD) was normal and the right coronary artery (RCA) had a non-flow limiting lesion in the mid-vessel with a fractional flow reserve (FFR) of 0.79. Intravascular ultrasound (IVUS) of the circumflex artery was performed using a 20 MHz Eagle eye IVUS catheter (Volcano Therapeutics, Rancho Cordova, CA, USA). The length of the stented segment was 30mm and had a minimal luminal area (MLA) 4.6 mm^2. Neo-intimal formation was visible throughout the stent (Figure 1). This gave a neo-intimal hyperplasia (NIH) volume of 80.3 mm^3. The NIH on virtual histology had a tissue composition of necrotic core (NC) 13.6%, (0.08 mm^2, 2.4 mm^3), calcified tissue 16.8%, (0.10 mm^2, 3.0 mm^3), fibrofatty 5.8%, (0.03 mm^2, 1.04 mm^3), fibrotic tissue 63.9%, (0.38 mm^2, 11.5 mm^3). Distal to the MLA at distance of 18 mm IVUS revealed an eccentric soft neo-intimal ruptured plaque[1,2] (Figure 1C) within the stent. The necrotic core was 22% with remnant plaque burden of 54% at the plaque rupture site (Figure 1 C'). Just distal to ruptured plaque the vessel wall was intact and the plaque burden was higher 65% with no necrotic core in contact with the lumen (Figure 1D").

This ruptured lesion was subsequently managed with a drug eluting stent (DES) that also covered the MLA. The histological findings of a similar plaque rupture are illustrated in Case 2.

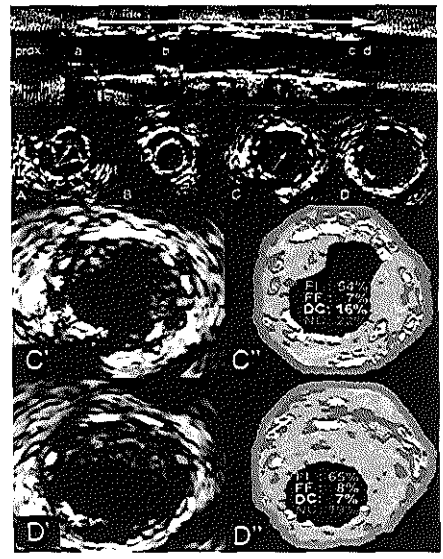

Figure 1. IVUS pullback. The top panel shows the longitudinal reconstruction. The double-headed arrow indicates the location of the stent. The characters "a" through "d" indicate the position of the cross sectional panels "A" through "D". Panel A: proximal part of the stent, arrows indicatestent malapposition. Panel B : minimal luminal area within the stent (MLA 4.6 mm^2). Panel C: eccentric plaque rupture (arrowed). Panel D: directly distal, intact eccentric neo-intimal plaque. Panel C" (magnified frame): IVUS VH of ruptured plaque within the neo-intima. Panel D" (magnified frame): immediately after the rupture. Panels C" and D" show a majority of fibrous tissue. Of note IVUS-VH analysis included the stents' struts that were seen as spots of calcium and necrotic core. FI, fibrotic tissue; FF, fibrofatty; DC, dense calcium; NC, necrotic core.

* *Corresponding author: Thoraxcenter, Bd 406, Dr Molewaterplein 40, 3015-GD Rotterdam, The Netherlands*
E-mail: p.w.j.c.serruys@erasmusmc.nl

Case 2

A 43-year-old obese male underwent percutaneous coronary intervention (PCI) with MINI-CROWN bare metal stent (BMS) implantation in 1999 for a severe lesion in the proximal left anterior descending coronary artery. He was a heavy smoker with a body mass index 26.4 but no diabetes or hyperlipidaemia. His past history includes peripheral vascular disease with intermittent claudication. He was found dead at his friend's house following a party approximately seven years after stent implantation. At autopsy, the heart showed biventricular hypertrophy with a healed subendocardial infarction in anteroseptal and lateral left ventricle. The coronary system was left dominant and middle left circumflex coronary artery had a 95% luminal narrowing without evidence of plaque rupture. However, there was an occlusive platelet-rich thrombus at the site of the stent in the LAD that was implanted just proximal to origin of the first left diagonal branch. The histological examination revealed a large ruptured atherosclerotic plaque with an underlying occlusive platelet thrombus. This ruptured plaque was composed of a NC rich in cholesterol cleft and an overlying fibrous cap was infiltrated by foamy macrophages (Figure 2).

These images are the first reported examples of a plaque rupture within the neo-intima induced by a stent and illustrate progression in the pathological process of atherosclerosis[3].

Currently there are concerns about late stent thrombosis in DES due to delayed endothelialisation. However, these two cases of very late BMS thrombosis highlight that it can occur despite full stent coverage.

References

1. Al-Sergani HS, Fitzpatrick PJ, Waxman S. Angiographic and ultrasonic Evidence of Plaque Rupture Causing Myocardial Infarction. *Circulation.* 1998; 98:1348

2. Rodriguez-Granillo GA. Garcia-Garcia HM, Valgimigli M, Vaina S, van Mieghem C, van Geuns RJ, van der Ent M, Regar E, de Jaegere P, van der Giessen W, de Feyter P, Serruys PW. Global characterization of coronary plaque rupture phenotype using three-vessel intravascular ultrasound radiofrequency data analysis. *European Heart Journal.* 2006;27(16): 1921-1927.

3. Farb A, Burke AP, Kolodgie FD, Virmini R. Pathological Mechanisms of Fatal Late Coronary Stent Thrombosis in Humans. *Circulation.* 2003; 108: 1701-1706

Online data supplement

AVI File 1. IVUS pullback along the stent to reveal the ruptured plaque.

AVI File 2. IVUS-VH superimposed on pullback along the stent to reveal the ruptured plaque.

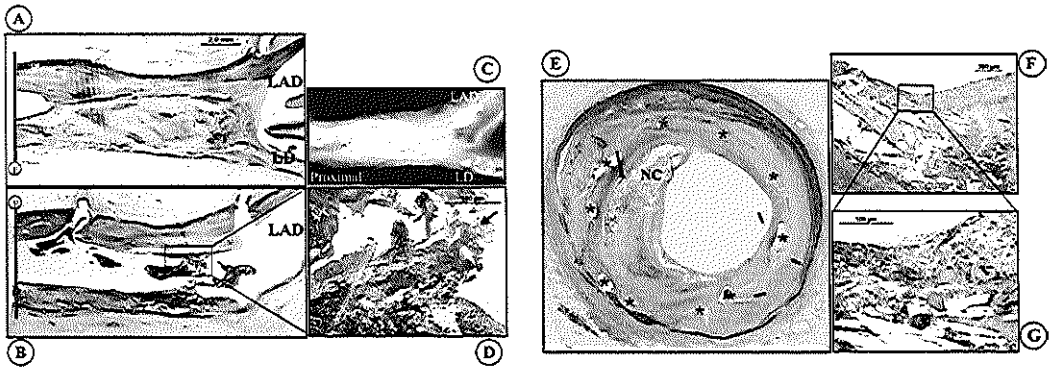

Figure 2. Histology of the case (Movat Pentachrome). A, B: Longitudinal section of the stent. The distal part of the stent shows site of plaque rupture and a superimposed platelet-rich adherent thrombus. C: X-ray of stented artery just above the bifurcation of LAD and left diagonal branch. D: High magnification image of the rupture site (*) and overlying platelet-rich thrombus is identified by the black arrow. E: The cross section of the proximal portion of the LAD stent. (corresponds to the black lines in panel A and B). Note the presence of a thin-cap fibroatheroma (vulnerable plaque) within the stent site (*). F, G: The fibrous cap is extremely thin and infiltrated by foamy macrophages with an underlying necrotic core (NC).

CHAPTER 9.1

Clinical Expert Consensus Document on Standards for Acquisition, Measurement and Reporting of Intravascular Ultrasound Regression/Progression Studies.

Mintz G, **García-García HM**, Nicholls S, Weissman N, Bruining N, Tardiff JC, Morel MA, van Es G, Crowe T, Serruys PW.

Submitted

RATIONALE FOR A CONSENSUS DOCUMENT

Atherosclerotic cardiovascular disease is a leading cause of morbidity and mortality despite the widespread use of established medical therapies. This has prompted the search to identify new therapeutic approaches to achieve more effective prevention of cardiovascular events. Considerable interest has focused on the role of surrogate markers of therapeutic efficacy in the early evaluation of novel anti-atherosclerotic therapies.

Monitoring changes in the extent of coronary atherosclerosis with intravascular ultrasound (IVUS) has been increasingly employed in clinical trials to assess progression and regression of atherosclerosis. This is based on the pivotal role that atherosclerotic plaque plays in the natural history of cardiovascular disease and the acceptance of validated arterial imaging approaches including coronary angiography and carotid intimal-medial thickness by regulatory authorities. The ability to generate high resolution imaging of the entire thickness of the coronary artery wall permits evaluation of the entire burden of atherosclerotic plaque.

In order to understand the differences, similarities, limitations and pitfalls of the IVUS technique among different academic core laboratories, a number of meetings of representatives from these groups were convened in 2007 and 2008. This document is the result of those IVUS methodology meetings that assembled experts from core laboratories to discuss standards for image acquisition, definitions, criteria, analyses, and primary and secondary endpoints.

EQUIPMENT

Early studies that employed coronary IVUS imaging typically involved the use of one imaging system in terms of both catheter and console. With technological advances a number of systems and catheters are now available that permit high resolution imaging within the coronary arteries. Given that studies often involve a large network of sites, there is likely to be marked heterogeneity in terms of imaging systems available among institutions and within each catheterization laboratory. As a result, there is now a much greater risk that an individual subject is imaged with different systems at different time points. It is critical that every possible effort is made to ensure that an individual is imaged with the same equipment (catheters and consoles and pullback devices) for baseline and follow-up studies.

It is the responsibility of the core laboratory to qualify and specify the systems, catheters, and pullback devices used in each study. While multivariate analysis

may be used to adjust for differences in cases where different systems are used within a single study, it remains to be determined whether this has any impact on the results. Regardless, every effort should be undertaken to include only imaging systems that have been demonstrated to produce high resolution imaging permitting precise measurements to a standard deemed appropriate for use by the core lab.

Consoles and catheters. Current rotating element IVUS catheters operate at frequencies between 30-45MHz (most commonly 40MHz); electronic phased array catheters operate at a center-frequency of approximately 20MHz. However, since the transducer manufacturing is difficult and performed under conditions of extremely high temperatures, the true center frequency of individual ultrasound elements may deviate from published specifications. It is unknown whether this has any impact on measurements. Given the higher resolution imaging that is generated with higher ultrasound frequency, rotational catheters are more often used in studies that evaluate the impact of medical therapies on progression of atheroma volume.

The higher the frequency, the higher the resolution, but the lower the penetration[1,2]. However, recent improvements in transducer design have minimized the negative impact of higher frequencies on penetration. Improvement in the resolution of transducers is to be encouraged since it is expected that such improvements will decrease variability and improve reproducibility in the core lab analysis[3]. Manufacturers should report resolution, beam profile, bandwidth, and other technical data such as the variability between catheters and consoles and provide this data to the core laboratories. Manufacturers should also report the speed of sound used by the ultrasound consoles to produce the actual images. This speed of sound setting is important because it is the cornerstone of all dimensional measurements and is necessary to test phantoms and other standardizations. In the past speed of sound was used to develop an algorithm to correct for in vivo measurement inaccuracies using the 30MHz BostonScientific catheter connected to a ClearView console.[4].

Measurements made with rotating vs. electronic array transducers or even with different rotating transducers made by the same or different manufacturers can vary significantly[5]. This is the reason that it is critical that the same equipment (catheters and consoles and pullback devices) be used for baseline and follow-up studies. Different clinical sites can use different systems as long as same equipment and settings are used for each individual patient.

At the start of a study, the core laboratory or sponsor must contract with each of the IVUS companies to insure that an adequate supply of the same IVUS catheters be available for the duration of the study and that technical support for

existing consoles be maintained until the last patient has completed follow-up. In situations in which many patients have been imaged without standardizing baseline and follow-up equipment, a mathematical transformation of the data can be considered; however, this should be revealed in the methodology of the final report. Alternatively, subjects imaged with different systems at baseline and follow-up can be considered major protocol deviators, a factor to be employed in subsequent per protocol analyses of data. Where sites have multiple imaging systems it should also be considered whether the site is designated to use one specific system at the commencement of the study to facilitate consistency of imaging systems for patients at different time points. In addition, it is advisable that the same "major" machine settings – especially, the "zoom" and frame rate – be standardized for baseline and follow-up studies. Finally, it is ideal – but, of course, not practical – that the same technical personnel be involved in the baseline and follow-up studies.

Experience has taught us that the performance of measurement software systems be evaluated in an objective and uniform manner. For example, quantitative coronary angiography (QCA) profoundly altered our approach to the assessment of percutaneous coronary interventions and strategies aimed to prevent recurrence and progression of stenoses. In one study 10 QCA systems at core laboratories in North America and Europe were validated. Cine films were made from phantom stenoses of known diameter (0.5 to 1.9mm) under 4 different experimental conditions. The cine films were analyzed by each automated QCA system without observer interaction. Accuracy and precision were taken as the mean and SD of the signed differences between the phantom stenoses; and the measured minimal luminal diameters and the correlation coefficient (r), the SEE, the y intercept, and the slope were derived by their linear regression. Performance of the 10 QCA systems ranged widely: accuracy, +0.07 to +0.31mm; precision, +/- 0.14 to +/- 0.24mm; correlation (r), .96 to .89; SEE, +/- 0.11 to +/- 0.16mm; intercept, +0.08 to +0.31mm; and slope, 0.86 to 0.64.[6]

We do not have similar accuracy and precision data from various IVUS measurement software, especially ones that use different edge detection algorithms. Power calculations and study design should be adjusted for the precision of the off-line IVUS analysis systems and reproducibility of measurements within the core laboratory in order to avoid the risk of failing to detect small differences in patient populations. Phantom studies for all new equipment – hardware and software – should be performed and reported before the equipment is used in clinical practice or in clinical trials.

Pullback methodology for image acquisition. Automatic motorized pullback is mandatory usually at a rate of 0.5 or 1mm/sec. Pullback accuracy is affected by

factors apart from the pullback devices themselves especially comparing sheath-based versus non-sheath based catheters.[7] In case of non-sheath catheters, the pitfalls of automatic pullback include presence of catheter slack outside the patient and friction in the coronary artery and guiding catheter during pullback affecting heterogeneity of pullback speed. Conversely, we believe that sheath-based, mechanical catheter systems allow smoother and more uniform pullbacks during image acquisition and are more precise in terms of length measurement. However, this is counterbalanced by the appearance of NURD (non-uniform rotation distortion) that is unique to mechanical, rotating, sheath-based transducer catheters. NURD can occur for a number of reasons and can be difficult to recognize. To minimize or eliminate NURD, the following are recommended: (1) Straighten the IVUS catheter. (2) Make sure that the hemostatic valve is not too tight. (3) Make sure that the guiding catheter is not too small or has too tight of a radius curve. (4) Select the least tortuous coronary segment for interrogation. If these are not effective and NURD persists, then the IVUS catheter should be changed.

The method of delivering power to an automatic pullback device potentially affects accuracy and consistency of the pullback speed. There are 3 different ways to deliver power and control the pullback device: battery, console that is not computer-controlled, and computer-controlled console. Tanaka K et al[7] evaluated the accuracy of 4 IVUS pullback systems by studying 180 patients (45 in each group) who had been treated with a single stent of known length ranging from 8 to 33mm. The correlations between known stent length and IVUS-measured stent length were 0.92 for CVIS, 0.83 for BostonScientific Galaxy, 0.63 for Endosonics Track-Back, and 0.69 for Volcano Model R-l00 research pullback device. At a pullback speed of 0.5mm/s, the authors reported that a 10% error would cause a 30mm length of artery to be measured as 27 to 33mm in length. It is important to make sure that batteries of a battery-powered pullback device are always at least 20% full to insure uniform pullback speed and to avoid having the pullback device fail in the middle of a run. Pullback devices should be tested from time to time either in a waterbed or against a single implanted stent of known length in a straight coronary segment. The pullback device is least accurate at the beginning of an imaging run (in the distal artery) and most accurate in the proximal artery. It is recommended that the pullback start at least 10mm distal to the distal anatomical landmark (fiduciary point) - the most distal side branch accessible for the IVUS probe. It is also recommended that slack be removed from the IVUS catheter before starting automatic pullback. Ideally, the same pullback device should be used at baseline and follow-up

Validation. Core laboratories should take part in validation studies of new imaging systems to insure that the imaging consoles and catheters employed in

their studies generate high resolution imaging required for accurate measurement of disease burden. This is often performed with the use of a phantom model employing a range of lumen dimensions. This will enable accurate validation of new imaging systems for potential use in future studies. Validation data should be available for review by trial sponsors and regulatory agencies.

IMAGE ACQUISITION

Site Experience and Training. It is important to select experienced IVUS operators and sites with research experience, infrastructure, and demonstrated recruitment and retention of patients during follow-up. The corelab should be involved in this selection process. Ideally, participating centers should have enrolled and followed up patients in other recent IVUS studies. The number of enrolled patients, quality of the recordings (ratio between enrolled patients and analyzable IVUS), and the follow-up rate should be considered in site selection. Equipment, imaging standards, and imaging protocols should be defined prior to the start of the study. It is advisable that each site perform test runs of their processes prior to patient enrollment. There should be meetings with the IVUS investigators to discuss these issues both before the start of the study (before any baseline studies are acquired) and again before the start of the round of follow-up IVUS studies; test cases should be discussed at such meetings. Training of the sites is crucial, especially for sites that are working with the core laboratory for the first time. While it is possible for the ultrasound companies to provide some support, it is essential that training be supervised and directed by the core laboratory to insure that the imaging details required for the study are provided to and followed by the sites. During the course of the study, feedback to the clinical sites and investigators is crucial and should not be delayed. An example of a feedback form is shown in Appendix A.

Selection of patients. The natural history of coronary atherosclerosis involves progression with an increase in atheroma burden. To insure a cohort with disease progression, patients are selected for inclusion on the basis of established obstructive disease on a coronary angiogram performed for a clinical indication. Most groups typically require the presence of at least one lumen stenosis >20% by angiography. It has been established that such patients have diffuse coronary artery atherosclerosis that increases in severity over time. This enables assessment of therapies that might potentially slow disease progression. Patients with normal coronary angiograms are typically excluded as this will include some subjects with either no plaque or minimal disease. Patients with severe left main arterial disease

or significant lumen stenoses of all three major epicardial coronary arteries are typically excluded due the high likelihood that they will require intervention during the course of the study and not be available for imaging at follow-up.

Selection of Vessel for Imaging. The study vessel should be selected based on standard angiographic findings. As the imaging resolution of non-invasive techniques such as computed tomography continues to improve, it will likely become possible to select the target vessel for invasive imaging on the basis of non-invasive findings. Some groups mandate that the vessel selected for IVUS imaging should include at least one diameter stenosis >20% by visual assessment of the angiogram and be the longest and least angulated vessel segment. Some groups require there to be a minimum plaque burden (atheroma area divided by external elastic membrane area) of 40% by IVUS. Other groups have not employed a minimal threshold of disease. However, from a practical standpoint, patients with no angiographic stenosis >20% are typically not randomized in these studies. Conversely, because the intent of the study is to evaluate the impact of medical therapies on the natural history of disease progression, vessels are usually excluded if they have undergone previous revascularization.

Segment length. Given that there is an increase in variability when short segments are analyzed, a minimum threshold of 10-15mm is typically employed. However, all groups recommend the acquisition of at least 30mm of analyzable IVUS length, advising investigators to acquire a segment that is as long as possible. Increasing measured segment lengths has been one of the factors contributing to the reduction in measurement variability in more recent studies. In case of dysfunction of the equipment or poor acquisition due to technical difficulties (signal disappearing, spasm, ischemia, etc) the run should be repeated. Imaging should always continue until the aorta is visualized. The entire imaging run should be recorded onto digital media to send to the core laboratory.

Measured pullback lengths of the same segment studied at baseline and follow-up are not always the same. This is one of the major determinants of reproducibility. Reasons include not starting the catheter distal enough so that slack is removed prior to reaching the distal fiduciary point, too small of a guiding catheter or too tight of a hemostatic valve so that there is resistance to transducer withdrawal, anatomic considerations such as tortuosity or a bendpoint or a tight proximal stenosis, problems with the pullback device itself, wrong pullback speed, battery power being too low, etc. Some groups apply a pre-specified threshold difference between baseline and follow-up measured segment lengths that automatically excludes a specific patient in the study with a recommendation that a 15% difference in length between baseline and follow-up is the maximum acceptable. If the difference between baseline and follow-up length is <15%, volumes should be

calculated using the mean length from the two studies. In other groups algorithms are applied to normalize the ratio between image number and segment length. Regardless of the approach, it is imperative that any pullback that clearly indicates an erratic rate of pullback or catheter hangup that results in a gross discordance between the two studies should be excluded from analysis. Accordingly, every effort should be made by the imaging physician to meticulously observe the images during pullback to detect any concern that would jeopardize its use for analysis and to repeat the pullback if required.

Use of Adjunct pharmacology. Today most diagnostic coronary angiograms are performed without anticoagulation. When performing IVUS imaging, it is important to give the patient an anticoagulant (unfractionated or low molecular weight heparin, bivalrudin, etc.) before inserting the IVUS catheter into a coronary artery. Otherwise, there is a risk of thrombosis. It is also advisable to give intracoronary nitroglycerine (100-200 micrograms) before imaging to avoid catheter-induced spasm and minimize ischemia; the dose should be limited only by the patient's blood pressure.

Option for ECG gating. Motorized transducer pullback is critical for studies assessing progression and regression of atherosclerosis. However, all motorized pullback devices assume no cardiac motion. This is, of course, not correct; one previous study of 59 measurements in 31 patients showed that longitudinal catheter motion between systole and diastole averaged 1.50 ± 0.80mm (range 0.5 to 5.5 mm)[8]. This could result in a non-anatomically correct order (or scrambling) of the image slices during pullback[9]. However, at end-diastole the ultrasound catheter always returns to the same longitudinal location inside the coronary artery. ECG-gated image acquisition makes use of this periodic phenomenon.

ECG-gated IVUS image acquisition[10,11] or co-registration of the ECG and IVUS images to select near end-diastolic beats (Volcano method developed for VH-IVUS) can resolve motion-induced artefacts allowing analyses using so-called longitudinal views without the typical saw-tooth shaped vessel appearance that makes contour detection difficult or even impossible[10,11]. However, ECG-gated image acquisition never gained munch enthusiasm since a dedicated workstation and pullback device were necessary occupying valuable cath lab space and severely prolonging the IVUS examination possibly causing discomfort for the patient. Furthermore, there is a lack of convincing data to suggest that ECG gating results in more accurate assessment of atheroma burden.

To overcome this problem an image-based, retrospective computer algorithm called the Intelligate® method[9] has been developed; it is capable of fully automatic selection of near end-diastolic frames from a non-gated continuous speed pullback IVUS. The algorithm has been validated against the hardware ECG-gated

IVUS image acquisition method and takes on average 20 minutes to complete a single processing[9]. This approach eliminates scrambled frames caused by catheter motion, saw-tooth shaped appearance of the vessel wall when longitudinally reconstructed, etc. The method has been and is applied successfully in several studies[12-15,9]. While there is little difference in mean values, contour detection is easier in the longitudinal view, and standard deviation of the measurements is improved. However, there is no data that these improvements influence the final outcomes of large-scale studies; and most large-scale studies have not used this approach.

Safety of the IVUS Procedure. Hausman et al[16] reported 2207 patients from 28 centers (including 915 patients studied for diagnostic purposes).[17] There were no complications in 2034 patients (92.2%). In 87 patients (3.9%), complications were judged to be unrelated to IVUS imaging. In 63 patients (2.9%) transient spasm occurred during imaging. In 9 patients (0.4%) complications were judged to have a "certain" relationship to IVUS (five acute occlusions, two dissections, one embolism, and one dissection). In 14 patients (0.6%) complications were judged to have an "uncertain" relationship to IVUS (five acute occlusions, three dissections, and one arrhythmia). Major events (acute myocardial infarction or emergency bypass surgery) occurred in three of nine and five of 14 of these patients, respectively. The complication rate was higher in patients with unstable angina or acute myocardial infarction and in patients undergoing intervention (as apposed to just diagnostic imaging).

Batkoff et al.[18] reported 718 IVUS "examinations" performed at 12 centers. There were eight events (1.1%), but no adverse clinical consequences; all occurred in patients with unstable angina undergoing percutaneous intervention. There were four cases of transient vessel spasm, two cases of dissection, and two cases of wire entrapment. Gorge reported 7085 IVUS studies from 51 centers.[19] Spasm occurred in 3% of all studies. Major complications (dissection, thrombosis, ventricular fibrillation, and refractory spasm) occurred in 10 (0.14%). There was only one major event.

The long-term safety of IVUS has been reported by Ramassubu et al[20] who studied transplant recipients imaged one or more times with IVUS and followed by coronary angiography at least one year after the last IVUS exam. Overall, 548 coronary arteries in 226 patients were imaged by IVUS and compared to 130 arteries that were not imaged by IVUS. Subsequent angiographic stenoses were observed in 19.5% (107/548) of imaged arteries vs 16.2% (21/130) of non-imaged arteries (p=0.4). The arterial diameters of non-imaged and imaged arteries were not significantly different (p=0.07) regardless of the number of IVUS exams and duration of follow-up. In a subgroup analysis of 31 patients, angiographic

lumen diameters were measured at baseline (within 8 weeks of transplantation) and at follow-up (after 2, 3, or 4 IVUS exams). There was a significant decrease in vessel lumen diameter over time in non-imaged as well as imaged arteries with no difference in the magnitude of the diameter decrease between the two groups

Guedes et al.[21] used quantitative coronary angiographic analysis to compare IVUS-imaged and non-IVUS-imaged arteries in 525 patients at baseline and at 18 to 24 months. The coronary change score (per-patient mean of minimum lumen diameter changes for all lesions measured) was -0.06 ± 0.23mm versus -0.05 ± 0.21 mm for IVUS-imaged and non-IVUS-imaged arteries, respectively (p=0.35). The increase in percent diameter stenosis from baseline to follow-up was 0.8 ± 6.7% and 1.2 ± 7.0% in the IVUS-imaged and non-IVUS-imaged arteries (p=0.29). New lesions occurred in 3.6% and 3.9% of IVUS-imaged and non-IVUS-imaged arteries, respectively (p=0.84). When all coronary lesions were considered, the incidence of lesion progression was not significantly different between IVUS-imaged (11.6%) and non-IVUS-imaged (9.8%) arteries. Coronary spasm occurred in 1.9% of IVUS procedures, and there was one case of acute occlusion with no long-term sequelae.

Thus, IVUS has been performed safely in a large number of subjects enrolled in research studies with no apparent increase in incidence of adverse effects. There is no evidence from studies that have employed serial imaging within the coronary arteries that this approach has any influence in terms of accelerating disease progression.

STORAGE AND TRANSFER OF IMAGES

Storage of the full dataset is important, and back-up digital storage is advisable to ensure longevity of the information. Analogue videotape - the medium of the past - was standardized, but is likely to be unavailable for use with more modern imaging systems. Accordingly, every effort has been made to store data in a digital manner. The lack of full standardization of both CD-ROM and DICOM provide challenges for digital storage of images.

Unfortunately, audio recording has become problematic with the advent of the CD-ROM. While DICOM allows for audio overlay that is already implemented in some of today's consoles, the IVUS community has been advised not to enable this feature because a DICOM file that includes audio overlay cannot be 'read' by all equipment and software analysis packages – especially, equipment and software used clinically. However, core laboratory view stations should be able to

read audio overlay. Audio archiving is currently supported in the BostonScientific DICOM - Basic Voice Audio Waveform Storage.

It is also possible to install a DICOM reader on the individual CD-ROM disks as done by angiographic companies. The IVUS manufacturers should be encouraged to implement this approach as long as the core laboratories are also able to override this feature as necessary.

The full pullback should be stored on the digital medium. It is up to the corelab, not the clinical sites to select the segment of interest. Improvements in electronic transfer of digital information will allow for immediate submission of imaging directly from the site to the core laboratory. This already occurs in research studies that have employed other imaging modalities. While the file size of data to be transferred is substantial, there are likely to be ongoing developments in terms of uploading, transfer, and storing of digital data which will result in a more efficient transmission of images to the core laboratory.

IMAGE ANALYSIS

Paired analysis is highly recommended, preferably during the same session by the same analyst who is blinded to treatment assignment and where baseline vs follow-up imaging have been de-identified. If the follow-up recording is not analyzable, it is recommendable that the baseline recording still be analyzed so that the patients are included in baseline population and demographics.

Common language and definitions. We recommend the nomenclature proposed by the American College of Cardiology Clinical Expert Consensus Document on Standards for Acquisition, Measurement and Reporting of Intravascular Ultrasound Studies (IVUS).[22] A report of the American College of Cardiology Task Force on Clinical Expert Consensus Documents: (1) external elastic membrane (EEM), (2) lumen, (3) atheroma (or plaque&media) calculated as EEM minus lumen, and (4) % atheroma area (or plaque area) or atheroma burden (or plaque burden calculated as plaque&media divided by EEM). Atheroma (or plaque&media) thickness is also reported variably in some regression/progression studies.

Corelab personnel qualifications. The corelab manager is responsible for training new employees and assessing his/her qualifications and competencies for corelab functions. After some tutorial sessions on the use of analysis software and understanding the anatomy and basic principles of the atherosclerosis disease process, new personnel can begin to analyze IVUS studies under supervision of a

senior analyst until the new analyst is considered to be able to perform independently.

Each corelab should maintain a library of IVUS recordings that can be used to assess the performance of qualified personnel including reproducibility and inter and intraobserver variability. These known IVUS recordings should be given to the new analyst. The total, mean, and standard deviations of the vessel and lumen areas should be used for comparison. In addition, frame-level measurements that are >2 times the standard deviation for the entire reference group should be discussed.

Corelab personnel performance and continuing education. To maintain the qualification of personnel, it is necessary to have systematic ongoing training. It is advisable that each corelab analyst measure known IVUS recordings twice each year. The region of interest should be the same for all analysts. Similarly, the total mean and standard deviations of the vessel and lumen areas should be used for comparison between qualified analysts. In some labs, the results of such quality control processes are provided for sponsors during the course of the study. Finally, it is recommended that there be monthly conferences in which interesting and difficult cases are discussed.

Detection of Disease Borders. Cross-sectional measurements are fundamental to quantitative IVUS analysis. There are many computed-assisted methods that help with cross-sectional contour detection of the lumen and EEM. Software should be carefully assessed by each core laboratory before implementation. Given that each image needs to be reviewed by an analyst to confirm that the correct leading edges have been detected, it remains to be determined whether current automatic software packages provide any benefit compared with manual planimetry by a trained analyst.

Longitudinal image reconstruction and analysis can be incorporated into both semiautomatic, and user-defined contour detection can be used interactively with cross-sectional contour detection; however, every cross-section should still be checked. Antegrade-retrograde, side-to-side, and systolic-diastolic catheter motion (greater in the RCA and LCX than in the LAD) causes a saw-tooth appearance to the longitudinal images. Longitudinal contours can be drawn at the peak, middle, or valley "of the "saw-tooth" and are analyst dependent; therefore, a standardized protocol is necessary. It is suggested that longitudinal contour detection be performed after gating in order to get a smooth appearance of the boundaries.

Selection of Anatomical landmarks and Segment for Analysis. The same proximal and distal fiduciary points must be used to identify the analysis segment on baseline and follow-up studies such as clearly identifiable proximal and distal sidebranches at baseline and follow-up using the proximal part of the distal

sidebranch and the distal part of the proximal sidebranch. The priority for the fiduciary point when imaging the RCA should be the aorto-ostial junction, then the conus branch or a proximal atrial branch, and finally a distal side branch. For the left coronary system, the carina is the most recommended fiduciary point. However, every attempt should be made to continue to image while withdrawing the catheter into the aorta to permit imaging within the left main arterial segment. The analysis segment should be chosen using the two fiduciary points that have the most similar lengths between the baseline and follow-up studies.

Analysis segment selection. Atherosclerosis is a diffuse disease. It is recommended to analyze very long proximal segments compared to shorter distal segments because atherosclerosis is more proximally distributed and events occur in more proximal segments. Bifurcation segments are interesting for analysis. However, analyzing bifurcations produces its own challenges. Since sidebranch-containing cross-sections do not display the artery as a "circle," some rules are necessary for defining the contours of the EEM and lumen. (1) The EEM contour should be interpolated to follow the main vessel cross-sections just proximal and distal to the sidebranch. (2) The lumen contour should be drawn on top of the EEM contour at the mouth of the sidebranch. (3) Rules for excluding the sidebranch-containing cross-sections should follow the rules for excluding cross-sections containing calcium (see below).

Imaging Artifacts. NURD is unique to mechanical catheter systems and results from mechanical binding of the drive cable that rotates the transducer[23]. Any cross-sections with a recognizable NURD that precludes accurate definition of the leading edge of the outer vessel wall border should be eliminated following the same rules as for calcium. The core laboratory must be also sensitive to any other artifacts such as side lobes. In the training set of IVUS pullbacks, these artifacts should be included. Presence of EEM out of view, loss of image due to bubbles, or any other artefact that prevents complete analysis of a single frame should be treated as calcium.

Calcium. Calcium is a strong reflector of ultrasound, shadows deeper arterial structures including the EEM contour, and hampers visualization and analysis of the vessel wall. At the present time we do not know the relationship between IVUS calcium detection and IVUS detectable progression and regression. The amount of calcium in an artery is influenced by the presence of a stenosis, the amount of plaque burden, and vessel size. On one hand, excluding calcified segments can make studies less applicable to a general patient population; on the other hand, excluding calcified segments can provide results with more specific information. However, from a practical standpoint, patients studied in progression/regression studies do not have severe stenoses and calcification; therefore, (from experience)

while only approximately 2% of patients are voided because of calcium, this tends to be one of the leading reasons for exclusion of patients from studies.

Therefore, we do not know whether calcium segments should or should not be included in the analysis. However, from a practical standpoint and in order to calculate changes in the plaque volume we are forced to deal with this confounding factor. The issues are as follows. (1) How much calcium precludes accurate assessment of EEM contours? (2) Which technique should be used to extrapolate contours behind calcium in either cross-sectional or longitudinal views? (3) When should individual cross-sections be excluded, and when should entire patients be excluded because of the extension of the calcium?

Using the longitudinal approach, extrapolation is allowed if there is EEM shadowing <45° (cross-sectional analysis) or if there is EEM shadowing of 45-90°, but <5mm in length. Using cross-sectional analysis, a single deposit with an arc of calcium >45° or multiple small arcs that add up to >180° voids an individual cross-section, but the length of calcium is not a consideration. When eliminating cross-sections, the same cross-sections should be eliminated at baseline and at follow-up. If after eliminating cross-sections, the "residual" length is less then 10mm, the entire case should be eliminated. It is advisable to document the number of frames and % of length eliminated due to the presence of calcium.

STATISTICAL APPROACHES

Selection of progression/regression endpoints. A number of endpoints are possible: (1) nominal change in Percent Atheroma Volume from baseline to follow-up, (2) nominal change in Total (absolute) Atheroma Volume from baseline to follow-up, and (3) percent change in Total (absolute) Atheroma Volume from baseline to follow-up. These endpoints can be reported for the total analysis segment and/or for the most-diseased segment. It is recommended to report all three endpoints so that the totality of the data can be used to understand the results, but there is a preference to use the absolute change in Percent Atheroma Volume (from baseline to follow-up) as the primary endpoint, largely due to the smaller variability of this endpoint for analysis. Conversely, even though the most-diseased 10mm subsegments contain the largest mean plaque burden, we do not recommend this as a primary endpoint because (1) the most-diseased subsegment lacks independent proximal and distal fiduciary points, (2) the minimum lumen area, the maximum plaque burden, and the most-diseased segment can shift during follow-up, (3) the length of the worst segment at follow-up can vary considerably due to the heterogeneity of the pullback speed, and (4) the variability of measurements in-

creases when the segment length is short. However, if analyzed, the most-diseased subsegment should contain at least one fiduciary point that is independent of lumen dimensions or plaque burden.

Selection of remodeling endpoints. Remodeling is conventionally assessed by comparing lesion site EEM to reference segment EEM. However, for serial studies involving volumetric characterization within an arterial segment, such a static definition is not recommended. Instead, remodeling should be assessed as EEM at follow-up minus EEM at baseline where an increase in EEM is positive remodeling, no change in EEM is absence of remodeling, and a decrease in EEM is negative remodeling. Furthermore, vessel segments with positive remodeling should be subdivided as expansive (overcompensatory) where ΔEEM/Δatheroma >1 or incomplete where ΔEEM/Δatheroma is between 0 and 1.0.

Normalization for length. Normalization for segment length is very important for assessing total atheroma volume, but is less important for assessing percent atheroma volume (plaque burden). A common way of normalization is to multiply the mean atheroma area by the median or mean length for all patients completing the trial or by use of a fixed adjustment factor. This adjusts for differing segment lengths across patients, thereby providing equal weighting of each patient in the calculation of atheroma volume.

EMERGING DEVELOPMENTS

With improved pharmacology it is anticipated that quantitative changes in atheroma burden will become less and less. Therefore, it is also anticipated that qualitative changes in plaque morphology or lesion phenotype will become more important. Examples of technologies that have been developed to assess plaque composition include virtual histology (VH)-IVUS and integrated backscatter (IB)-IVUS. Finally, it is possible that in the future IVUS will be integrated with other modalities such as optical coherence tomography or spectroscopy that could also provide qualitative data.

REFERENCES

1. Lockwood GR, Ryan LK, Hunt JW, Foster FS. Measurement of the ultrasonic properties of vascular tissues and blood from 35-65 MHz. *Ultrasound Med Biol.* 1991;17(7):653-666.
2. Bridal SL, Fornes P, Bruneval P, Berger G. Parametric (integrated backscatter and attenuation) images constructed using backscattered radio frequency signals (25-56 MHz) from human aortae in vitro. *Ultrasound Med Biol.* 1997;23(2):215-229.
3. Elliott MR, Thrush AJ. Measurement of resolution in intravascular ultrasound images. *Physiol Meas.* 1996;17(4):259-265.
4. Bruining N, Hamers R, Teo TJ, de Feijter PJ, Serruys PW, Roelandt JR. Adjustment method for mechanical Boston scientific corporation 30 MHz intravascular ultrasound catheters connected to a Clearview console. Mechanical 30 MHz IVUS catheter adjustment. *Int J Cardiovasc Imaging.* 2004;20(2):83-91.
5. Fort S, Freeman NA, Johnston P, Cohen EA, Foster FS. In vitro and in vivo comparison of three different intravascular ultrasound catheter designs. *Catheter Cardiovasc Interv.* 2001;52(3):382-392.
6. Keane D, Haase J, Slager CJ, Montauban van Swijndregt E, Lehmann KG, Ozaki Y, di Mario C, Kirkeeide R, Serruys PW. Comparative validation of quantitative coronary angiography systems. Results and implications from a multicenter study using a standardized approach. *Circulation.* 1995;91(8):2174-2183.
7. Tanaka K, Carlier SG, Mintz GS, Sano K, Liu X, Fujii K, de Ribamar Costa J, Jr., Lui J, Moses JW, Stone GW, Leon MB. The accuracy of length measurements using different intravascular ultrasound motorized transducer pullback systems. *Int J Cardiovasc Imaging.* 2007;23(6):733-738.
8. Arbab-Zadeh A, DeMaria AN, Penny WF, Russo RJ, Kimura BJ, Bhargava V. Axial movement of the intravascular ultrasound probe during the cardiac cycle: implications for three-dimensional reconstruction and measurements of coronary dimensions. *Am Heart J.* 1999;138(5 Pt 1):865-872.
9. De Winter SA, Hamers R, Degertekin M, Tanabe K, Lemos PA, Serruys PW, Roelandt JR, Bruining N. Retrospective image-based gating of intracoronary ultrasound images for improved quantitative analysis: the intelligate method. *Catheter Cardiovasc Interv.* 2004;61(1):84-94.
10. Bruining N, von Birgelen C, de Feyter PJ, Ligthart J, Li W, Serruys PW, Roelandt JR. ECG-gated versus nongated three-dimensional intracoronary ultrasound analysis: implications for volumetric measurements. *Cathet Cardiovasc Diagn.* 1998;43(3):254-260.
11. von Birgelen C, de Vrey EA, Mintz GS, Nicosia A, Bruining N, Li W, Slager CJ, Roelandt JR, Serruys PW, de Feyter PJ. ECG-gated three-dimensional intravascular ultrasound: feasibility and reproducibility of the automated analysis of coronary lumen and atherosclerotic plaque dimensions in humans. *Circulation.* 1997;96(9):2944-2952.
12. Aoki J, Abizaid AC, Serruys PW, Ong AT, Boersma E, Sousa JE, Bruining N. Evaluation of four-year coronary artery response after sirolimus-eluting stent implantation using serial quantitative intravascular ultrasound and computer-assisted grayscale

value analysis for plaque composition in event-free patients. *J Am Coll Cardiol.* 2005;46(9):1670-1676.

13. Van Mieghem CA, McFadden EP, de Feyter PJ, Bruining N, Schaar JA, Mollet NR, Cademartiri F, Goedhart D, de Winter S, Granillo GR, Valgimigli M, Mastik F, van der Steen AF, van der Giessen WJ, Sianos G, Backx B, Morel MA, van Es GA, Zalewski A, Serruys PW. Noninvasive detection of subclinical coronary atherosclerosis coupled with assessment of changes in plaque characteristics using novel invasive imaging modalities: the Integrated Biomarker and Imaging Study (IBIS). *J Am Coll Cardiol.* 2006;47(6):1134-1142.
14. Rodriguez-Granillo GA, de Winter S, Bruining N, Ligthart JM, Garcia-Garcia HM, Valgimigli M, de Feyter PJ. Effect of perindopril on coronary remodelling: insights from a multicentre, randomized study. *Eur Heart J.* 2007;28(19):2326-2331.
15. Ormiston JA, Serruys PW, Regar E, Dudek D, Thuesen L, Webster MWI, Onuma Y, Garcia-Garcia HM, McGreevy R, Veldhof S. A bioabsorbable everolimus-eluting coronary stent system for patients with single de-novo coronary artery lesions (ABSORB): a prospective open-label trial. *The Lancet.*371(9616):899-907.
16. Hausmann D, Erbel R, Alibelli-Chemarin MJ, Boksch W, Caracciolo E, Cohn JM, Culp SC, Daniel WG, De Scheerder I, DiMario C, et al. The safety of intracoronary ultrasound. A multicenter survey of 2207 examinations. *Circulation.* 1995;91(3):623-630.
17. Hausmann D, Erbel R, Alibelli-Chemarin M-J, Boksch W, Caracciolo E, Cohn J, Culp S, Daniel W, De Scheerder I, DiMario C, III FJ, Fitzgerald P, Friedrich G, Ge J, Gorge G, Hanrath P, Hodgson JM, Isner J, Jain S, Maier-Rudolph W, Mooney M, Moses J, Mudra H, Pinto F, RW S, Talley D, Tobis J, Walter P, Weidinger F, Werner G, Yeung A, Yock P. The safety of intracoronary ultrasound: A multicenter survey of 2207 examinations. *Circulation.* 1995;91:623-630.
18. Batkoff BW, Linker DT. Safety of intracoronary ultrasound: data from a Multicenter European Registry. *Cathet Cardiovasc Diagn.* 1996;38(3):238-241.
19. Gorge G, Peters R, Pinto F, Distante A, Visser C, Fraser A, Erbel R. Intravascular ultrasound: Safety and indications for use in 7085 consecutive patients studied in 32 centers in Europe and Israel. *J Am Coll Cardiol.* 1996;27:155A (abstract).
20. Ramasubbu K, Schoenhagen P, Balghith MA, Brechtken J, Ziada KM, Kapadia SR, Hobbs RE, Rincon G, Nissen SE, Tuzcu EM. Repeated intravascular ultrasound imaging in cardiac transplant recipients does not accelerate transplant coronary artery disease. *J Am Coll Cardiol.* 2003;41(10):1739-1743.
21. Guedes A, Keller PF, L'Allier PL, Lesperance J, Gregoire J, Tardif JC. Long-term safety of intravascular ultrasound in nontransplant, nonintervened, atherosclerotic coronary arteries. *J Am Coll Cardiol.* 2005;45(4):559-564.
22. Mintz GS, Nissen SE, Anderson WD, Bailey SR, Erbel R, Fitzgerald PJ, Pinto FJ, Rosenfield K, Siegel RJ, Tuzcu EM, Yock PG. American College of Cardiology Clinical Expert Consensus Document on Standards for Acquisition, Measurement and Reporting of Intravascular Ultrasound Studies (IVUS). A report of the American College of Cardiology Task Force on Clinical Expert Consensus Documents. *J Am Coll Cardiol.* 2001;37(5):1478-1492.
23. ten Hoff H, Korbijn A, Smith TH, Klinkhamer JF, Bom N. Imaging artifacts in mechanically driven ultrasound catheters. *Int J Card Imaging.* 1989;4(2-4):195-199.

APPENDIX A. CORELAB FEEDBACK LETTER

To :
Clinic :
From :

Subject :

Date :

Dear ....,

We received your IVUS recording for ..... trial.

Please find below our summary findings:

☐ IVUS pullbacks are of good quality

The recordings are in agreement with the protocol requirements and acquisition guidelines.

☐ IVUS pullbacks needs some improvement. You are kindly requested to forward a new testrun/pullback.

...

☐ IVUS pullbacks are non analyzable

The recordings are not in agreement with the protocol requirements and acquisition guidelines.

For further details see next page.
Yours sincerely,
Corelab Director

Please tick when applicable:

- _____ All images were obtained using a motorized pullback system.
- _____ Pullback speed of 0.5 mm/sec
- _____ Gain- and zoom-settings were carefully optimized before the pullback is started.
- _____ The IVUS procedure was preceded by the administration of 0.2 mg IC nitroglycerin (NTG) (check angiography views containing plates indicating NTG injection).
- _____ Pullback started at least 1cm distal from the distal target segment and was performed up to 1cm proximal of the proximal target segment.
- _____ An angiographic film with AND without contrast injection must be performed to indicate the IVUS catheter position before pullback.
- _____ If IVUS studies recorded on videotape, an audio commentary is recorded in the tape clearly describing the ongoing IVUS examination in English. The investigator should audio record the following: Position of probe, i.e. coronary segment (LAD, LCX, or RCA); Pull-back speed; Start time of pull-back (time visible at IVUS screen); End of pullback time.
- _____ The local time, displayed on the video screen should be filled out in the Technician's WorkSheet (not the video recorder time).
- _____ If tape acquisition, the calibration grid was recorded.
- _____ The pullback was continued until the transducer is in the guiding catheter.
- _____ Is the EEM out of view in more than 1/3 of the pullback
- _____ Is the EEM out of view in more than 2/3 of the pullback
- _____ The pullback is non continuous in more than 1/3 of the length of the pullback
- _____ The pullback is non continuous in more than 2/3 of the length of the pullback
- _____ Is the pullback too dark?
- _____ Is the pullback too bright?

CHAPTER 9.2

Effect of Rosiglitazone on Progression of Coronary Atherosclerosis in Patients with Type 2 Diabetes and Coronary Artery Disease: The APPROACH trial.

Gerstein HC, Ratner RE, Cannon CP, Serruys PW, **García-García HM**, van Es G, Kolatkar NS, Kravitz BG, Miller DM, Huang C, Nesto W, and the APPROACH study group.

Submitted.

ABSTRACT

Context: Rosiglitazone has several properties which may reduce the progression of atherosclerosis.

Objective: To determine the effect of the thiazolidinedione rosiglitazone on coronary atherosclerosis as assessed by intravascular ultrasound compared to the sulfonylurea glipizide.

Design: The APPROACH study was a randomized double-blind controlled study of rosiglitazone versus glipizide at a dose blindly titrated to achieve an A1C ≤ 7%. It was conducted between 2005 and 2008; mean follow-up was 16 months.

Setting: 92 ambulatory sites located in academic and community settings in 19 countries.

Patients: 672 patients aged 30–80 years with established type 2 diabetes treated by lifestyle, 1 oral agent or submaximal doses of 2 oral agents who had at least one atherosclerotic plaque with 10–50% luminal narrowing in a non-intervened coronary artery during a clinically indicated coronary angiography or percutaneous coronary intervention.

Intervention: Up to 15 mg of glipizide and 8 mg of rosiglitazone was provided to participants.

Main Outcome Measure: Change in percent atheroma volume (PAV) in the longest and least angulated non-intervened epicardial coronary artery. Secondary outcomes were the change in normalized total atheroma volume (TAV_N) and the change in total atheroma volume in the most diseased baseline 10-mm segment.

Results: PAV did not significantly change in patients allocated to glipizide (0.43%, 95% CI -0.22, 1.08; p=0.19) or rosiglitazone (-0.21%, 95% CI -0.86, 0.44; p=0.53), and rosiglitazone did not significantly reduce PAV compared to glipizide (-0.64%, 95% CI -1.46, 0.17; p=0.12). TAV_N did not significantly change on glipizide (1.2 mm^3, 95% CI -2.7, 5.1; p=0.54), but significantly decreased by 3.9 mm^3 (95% CI -7.8, -0.02; p=0.049) on rosiglitazone and rosiglitazone significantly reduced TAV_N by 5.1 mm^3 (95% CI -10.0, -0.3; p=0.04) compared to glipizide. Atheroma volume within the 10 mm most diseased baseline segment decreased by 3.6 mm^3 (95% CI -5.3, -1.8; p<0.0001) on glipizide and by 5.3 mm^3 (95% CI -7.0, -3.5; p<0.0001) on rosiglitazone; however rosiglitazone did not significantly reduce atheroma volume within the 10 mm most diseased baseline segment more than glipizide (-1.7 mm^3, 95% CI -3.9, 0.5; p=0.13).

Conclusions: Rosiglitazone did not significantly reduce progression of coronary atherosclerosis compared to glipizide in patients with type 2 diabetes and coronary atherosclerosis.

Trial Registration: Clinicaltrials.gov NCT00116831

INTRODUCTION

Type 2 diabetes (T2DM) is a strong independent risk factor for cardiovascular diseases[1] and epidemiologic studies have shown that this risk is progressively related to the degree of hyperglycemia as measured by the A1C [2]. Whereas recent trials of more versus less intensive glucose-lowering with a menu of drugs did not detect a clear cardiovascular benefit[3;4] the observation of reduced myocardial infarction and all-cause mortality in metformin-treated obese subjects during active therapy in the United Kingdom Prospective Diabetes Study[5], and in all participants following a further 8.5 years of passive follow-up [6] suggests that specific glucose-lowering drugs may have cardiovascular benefits. Prior to completing long-term cardiovascular outcome studies, such an effect would be supported if these drugs reduced coronary atherosclerosis.

Coronary atherosclerosis forms the substrate for vulnerable plaque which leads to clinical coronary events. Coronary atherosclerosis can be directly assessed using intravascular ultrasonography (IVUS), and progression of IVUS-determined atherosclerosis has been correlated with an increased risk of coronary events [7;8]. Furthermore, reductions in IVUS-detected plaque volume have been demonstrated in response to antihypertensive[9] and lipid-lowering therapies[10-13] that also reduce the incidence of coronary events.

Thiazolidinediones (TZDs) have effects on cardiovascular risk factors, including insulin sensitivity,[14;15] inflammatory biomarkers,[16] endothelial function,[17] coagulability,[16;18;19] plaque instability,[16] and blood pressure,[20] that may slow the progression of coronary atherosclerosis. Active-controlled trials of both thiazolidinediones (rosiglitazone and pioglitazone) in patients with T2DM have suggested a favorable effect of these agents on carotid atherosclerosis[21] and in-stent restenosis[22], however, the applicability of these data to native vessel coronary disease is uncertain. Moreover, a recent large randomized trial of one TZD (pioglitazone) demonstrated that it reduced progression of coronary atherosclerosis in non-intervened arteries more than glimepiride[23]. To date, comparable data using rosiglitazone have not been available.

The Assessment on the Prevention of Progression by Rosiglitazone on Atherosclerosis in diabetes patients with Cardiovascular History (APPROACH) trial was designed to compare the effect of rosiglitazone and glipizide - agents that reduce glucose through different mechanisms - on progression of coronary atherosclerosis. Importantly, the trial was designed to provide comparable glycemic control between treatment arms and to evaluate the treatment effect on a background of optimized contemporary therapy for secondary prevention of coronary disease including statins, anti-platelet agents, and antihypertensive medications.

METHODS

Study Design & Eligibility Criteria

A detailed description of the APPROACH trial has been previously published[24]. APPROACH was a prospective multicenter, double-blind, randomized, active-controlled trial (Figure 1) of 672 patients from 92 centers in 19 countries, who were aged 30–80 years with established T2DM and who had clinically indicated coronary angiography or percutaneous coronary intervention (PCI) between February 2005 and January 2007. Patients were included if they had at least one atherosclerotic plaque with 10–50% luminal narrowing in a non-intervened coronary artery, and if their diabetes was treated with either lifestyle approaches alone (with an A1C >7% and ≤ 10%), or with oral agents comprising 1 oral agent at any dose, or 2 oral agents where each was prescribed at ≤50% of its

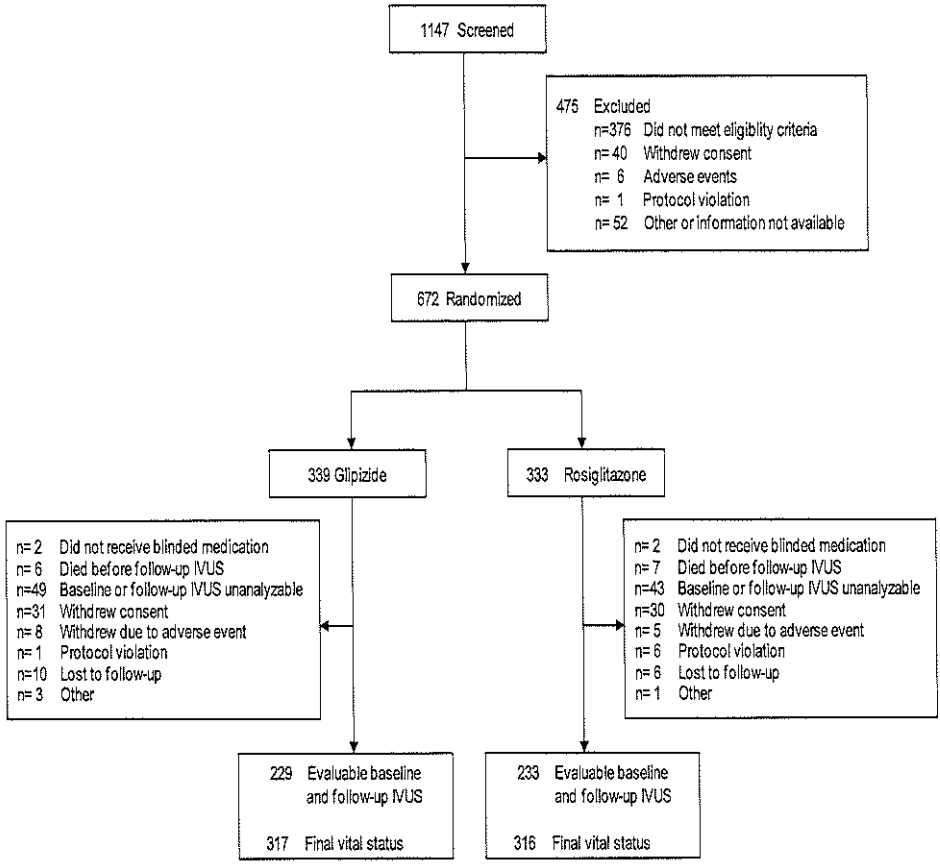

Figure 1. Disposition of APPROACH participants

maximal dose (with an A1C >6.5% and ≤ 8.5%). Exclusion criteria were: ST-segment elevation myocardial infarction in the prior 30 days; coronary artery bypass graft surgery; severe valvular heart disease; left ventricular ejection fraction <40%; any heart failure (New York Heart Association class I–IV); uncontrolled hypertension (systolic blood pressure >170 mmHg or diastolic blood pressure >100 mmHg); renal insufficiency (serum creatinine ≥1.5 mg/dL for men or ≥1.4 mg/dL for women); and active liver disease. Participant safety was monitored by an Independent Data Monitoring Committee who periodically reviewed rates of clinical outcomes according to unmasked therapy. The study protocol and consent forms were reviewed by the institutional review board at each site and all patients provided written informed consent. Study design, implementation, and analysis were performed under the supervision of the steering committee, which was composed of seven members from external, academic institutions and two from the sponsor. Data analysis was performed according to a prespecified plan that was developed with the approval of the steering committee.

Management of Glycemia and Follow-up

Patients were randomized in a 1:1 ratio to receive masked rosiglitazone (4 mg/day) or glipizide (5 mg/day) in one pill. At the time of randomization the doses of other oral antidiabetic drugs were reduced by 50% and were discontinued during a visit 1 month later. At that time and after 2 and 3 months, the dose of masked study drug was increased if tolerated and if the mean daily glucose level calculated from the patient's logbook of capillary tests in the 3 days prior to the visit was ≥ 126 mg/dl (7.0 mmol/l). If more than 1 titration was required, 2 pills per day were given. Titration doses of rosiglitazone at the 1st, 2nd and 3rd titration comprised 4 mg/day (1 pill – unchanged dose), 8 mg/day (as 2 pills with active drug in the morning and placebo in the evening), and 4 mg bid respectively; glipizide dosing at these visits comprised 10 mg/day (1 pill), 10 mg in the morning and 5 mg in the evening (as 2 pills) and this same dose as the 3rd titration respectively. Open-label metformin (maximal total daily dose 2550 mg) and then once-daily basal insulin, or both was added after the first 3 months if needed to maintain a HbA1c ≤ 7% using a glycemic titration algorithm designed to provide comparable glycemic control between treatment groups. Nonstudy drugs were reduced before study drugs in the event of hypoglycemia requiring dose reductions. Unless informed consent was formally withdrawn, all patients were followed until 18 months from randomization and clinical status ascertained regardless of whether they continued to take study medication.

Intravascular Ultrasound Examination and Image Analysis

The longest and least angulated non-intervened epicardial coronary artery was selected for IVUS examination. After intracoronary administration of nitroglycerin, an ultrasound catheter (2.5F Atlantis SR Pro Imaging 40 MHz) connected to a Galaxy G2 digital imaging console (Boston Scientific, Natick, MA) was advanced into the target vessel. The imaging transducer was positioned just distal to an identifiable side branch, and then motorized pullback of the transducer was performed at 0.5 mm/s. Follow-up IVUS examination was performed at study completion in all patients providing informed consent (irrespective of whether they continued to take study medication) with imaging of the same coronary artery segment identified at the baseline examination. If a participant required cardiac catheterization for a clinical indication between 9 and 18 months, follow-up IVUS examination could be performed at that time instead of at study completion.

Intravascular Ultrasound Outcomes

Core laboratory personnel (Cardialysis, Rotterdam, The Netherlands) who were blinded to treatment assignment analyzed all IVUS images using validated software (Curad, version 3.1, Wijk bij Duurstede, The Netherlands), that facilitates detection of luminal and external elastic membrane (EEM) boundaries in reconstructed longitudinal planes. In order to obtain a smooth appearance of the vessel wall structures in the longitudinal views, the Intelligate™ image-based gating method was applied [25;26]. The primary IVUS outcome is the change in percent atheroma volume (PAV) [9;27] calculated as PAV = $(\Sigma[EEM_{CSA} - LUMEN_{CSA}] / \Sigma EEM_{CSA}) \times 100$ where EEM_{CSA} is the external elastic membrane cross-sectional area (CSA) and $LUMEN_{CSA}$ is the luminal cross-sectional area. A secondary IVUS outcome is the change in normalized total atheroma volume (TAV_N), calculated as the product of the mean atheroma area and the median segment length in the entire population as follows: $TAV_N = (\Sigma[EEM_{CSA} - LUMEN_{CSA}]/N) \times$ overall median segment length. This calculation adjusts for differing segment lengths across patients, thereby providing equal weighting of each patient in the calculation of atheroma volume. An additional secondary IVUS outcome is the change in total atheroma volume in the most diseased baseline 10-mm segment. This was calculated as the follow-up – baseline difference in the total atheroma volume within the 10-mm contiguous segment with the greatest atheroma volume at baseline. Intraobserver variability was assessed using IVUS recordings from 20 randomly selected patients. Baseline and follow-up IVUS examinations were each analyzed twice. The mean (SD) differences were 0.09 (0.18) mm^2 for vessel area, and -0.02 (0.23) mm^2 for lumen

area. To evaluate variability between IVUS analysis methods, the same patients were analyzed twice longitudinally and twice cross-sectionally[10]. The mean (SD) differences (in mm^2) were 0.10 (0.36) mm^2 for vessel area and 0.001 (0.46) mm^2 for lumen area. Finally, to assess variability between core laboratories, the same patients were analyzed twice cross-sectionally at different core laboratories (Cardialysis, Rotterdam, The Netherlands and MedStar Research Institute, Division of Cardiology, Washington, DC). The mean (SD) differences (in mm^2) were 0.53 (0.37) mm^2 for vessel area and -0.07 (0.45) mm^2 for lumen area.

Clinical Cardiovascular Outcomes

Investigators submitted endpoint forms for any event which could potentially represent a myocardial ischemic event or heart failure. An independent endpoint committee blinded to treatment assignment prospectively adjudicated these cardiovascular events, which included cardiovascular and noncardiovascular death, nonfatal myocardial infarction and stroke, coronary revascularization, hospitalization for recurrent myocardial ischemia and heart failure.

Statistical Methods

Continuous variables are expressed as mean and standard deviation, or median and interquartile range if non-normally distributed, with categorical variables reported as percentage. IVUS outcomes were analyzed using analysis of covariance with terms for treatment group, baseline value, geographic region, gender, entry cardiac procedure (angiography or PCI), and prior oral antidiabetic medication. The change in PAV for each allocated group was calculated by estimating the model-adjusted mean change in PAV across the cohort. All p values are 2-sided and not adjusted for multiple testing, with p-values ≤ 0.05 considered significant. A worst-rank sensitivity analysis was performed as previously described to assess the potential influence on the primary endpoint of randomized patients who did not complete the follow-up IVUS examination due to a cardiovascular event[28]. For this analysis, all patients with evaluable baseline and follow-up IVUS examinations were assigned a rank value based on their change in PAV (ordered from least to greatest). Patients without a follow-up IVUS as noted above were assigned a rank value that was worse than that of the patient with the greatest increase in PAV. The rank value for these patients was first assigned based on a pre-specified hierarchy determined by the Steering Committee accounting for both clinical severity and relationship of the event to coronary atherosclerosis as follows (lowest to highest rank): congestive heart failure, hospitalization for recurrent myocardial ischemia,

coronary revascularization, noncardiovascular death, nonfatal stroke, nonfatal myocardial infarction, and cardiovascular death. Within each event category, the final rank was determined by the time to event, with earlier events assigned a worse (higher) rank. The worst-rank analysis compared the distribution of rank values between treatment groups using a univariate Wilcoxon-Mann-Whitney test.

Analysis of the primary IVUS outcome in pre-specified subgroups including region, angiography versus PCI, prior oral agent use (drug naïve, sulfonylurea, metformin, dual therapy), age (≤ 60 versus >60), gender, systolic blood pressure (≤ 130 mm Hg versus >130), statin use, body mass index, diabetes duration, and baseline high sensitivity C-reactive protein (hsCRP), A1C, HDL, LDL, triglycerides and PAV (≤ the median versus > the median value) was performed using ANCOVA with a test for treatment-by-subgroup interaction. The effect of treatment allocation on time to first occurrence of the various cardiovascular outcomes was estimated using a Cox proportional hazard model.

Sample size calculations determined that 206 patients per group with evaluable baseline and follow-up IVUS examinations were required to provide 90% power using a 2-sided α of 0.05 to detect a treatment difference between the groups of 1.6%, assuming a 5.0% standard deviation for the primary IVUS outcome. These assumptions were based on prior IVUS studies of lipid-lowering therapies in patients with diabetes[10]. Given prior noncompletion rates among patients with T2DM in contemporary IVUS studies ranging from 25-35% [9;10;23;27] a total sample size of 634 randomized patients was required under the worst-case assumption of a 35% noncompletion rate. All analyses were performed using SAS version 9.1 (SAS Institute, Cary, NC). Finally, to ensure the accuracy of the analyses, data for the primary and secondary endpoints were provided to an external biostatistician (Dr. Todd A. MacKenzie, Dartmouth Medical School) who independently repeated and confirmed all of the findings reported herein.

RESULTS

Participants

Of 1147 people who were screened, 672 (68% men) of mean (SD) age 61 (9) years median diabetes duration of 4.8 years and mean A1C of 7.2 (0.9) % were randomized to either glipizide (N=339) or rosiglitazone (N=333) from 92 sites in 19 countries (Figure 1). Baseline characteristics by treatment group are noted in Table 1; by chance, patients allocated to rosiglitazone versus glipizide were slightly older and had a slightly higher serum creatinine and lower systolic blood pressure.

Table 1: Baseline Characteristics of Randomized Patients

	Glipizide (N=339)	Rosiglitazone (N=333)	P value
Age, mean (SD), years	60.2 (9.0)	61.8 (8.4)	0.03
Male, number (%)	223 (65.8%)	233 (70.0%)	0.25
Current smoker, number (%)	57 (16.8%)	55 (16.5%)	1.00
Duration of diabetes, median [IQR], yrs	4.6 [1.7-8.9]	5.0 [2.2-7.9]	0.90
Hypertension, number (%)	272 (80.2%)	266 (79.9%)	0.92
Dyslipidemia, number (%)	227 (67.0%)	232 (70.0%)	0.46
Prior myocardial infarction, number (%)	82 (24.2%)	81 (24.3%)	1.00
Presenting condition, number (%)			
Acute coronary syndrome	130 (38.3%)	128 (38.4%)	1.00
Elective procedure	209 (61.7%)	205 (61.6%)	
Baseline procedure, number (%)			
Coronary angiography	171 (50.4%)	166 (49.8%)	0.94
Percutaneous coronary intervention	168 (49.6%)	167 (50.2%)	
Medication use, number (%)			
Aspirin	279 (82.3%)	280 (84.1%)	0.61
Other antiplatelet	195 (57.5%)	196 (58.9%)	0.75
Beta-blocker	223 (65.8%)	241 (72.4%)	0.07
ACE inhibitor or ARB	238 (70.2%)	237 (71.2%)	0.80
Nitrates	137 (40.4%)	125 (37.6%)	0.48
Statin	262 (77.3%)	248 (74.5%)	0.42
Fibrate or other lipid-lowering agent	24 (7.1%)	34 (10.2%)	0.17
Weight, mean (SD), kg	83.8 (18.5)	82.0 (19.1)	0.22
Body mass index, mean (SD), kg/m2	29.8 (5.3)	29.3 (5.5)	0.14
Blood Pressure, mean (SD), mmHg			
Systolic	131.0 (15.1)	127.9 (16.1)	0.004
Diastolic	76.3 (10.0)	75.2 (10.2)	0.16
Serum creatinine, mean (SD), mg/dL	0.98 (0.22)	1.02 (0.25)	0.02
A1C, mean (SD), %	7.2 (0.9)	7.1 (0.8)	0.08
BNP*, median [IQR], pg/mL	25 [12-53]	25 [11-58]	0.98
Fasting insulin*, median [IQR], µU/mL	13.0 [8.6-18.1]	13.0 [8.6-20.7]	0.49
LDL cholesterol, mean (SD), mg/dL	91.2 (35.5)	89.6 (35.9)	0.63
HDL cholesterol, mean (SD), mg/dL	42.7 (10.7)	42.4 (11.1)	0.77
Triglycerides, median [IQR], mg/dL	159.3 [122.1-204.9]	162.0 [122.1-211.5]	0.93
hsCRP, median [IQR], mg/L	5.4 [2.5-11.0]	4.9 [2.2-11.3]	0.54
MMP-9, median [IQR], µg/L	86.9 [43.8-195.1]	88.6 [44.1-221.6]	0.44

*Performed in a subset of patients (BNP N=464; Fasting insulin N=435); Abbreviations: ACE, angiotensin-converting enzyme; BNP, B-natriuretic peptide; ARB, angiotensin II receptor blocker; BMI, body mass index, HbA1c, hemoglobin A1c; HDL, high-density lipoprotein; hsCRP, high-sensitivity C-reactive protein; IQR, interquartile range; LDL, low-density lipoprotein; MMP-9, matrix metalloproteinase 9. SI conversion factors: to convert fasting plasma glucose to mmol/L, multiply by 0.0555, low-density lipoprotein and high-density lipoprotein cholesterol values to mmol/L, by 0.0259; triglyceride values to mmol/L, by 0.0113; serum creatinine to µmol/L, by 88.4; fasting insulin to pmol/L, by 6.945; c-reactive protein to nmol/L by 9.524

As randomization was stratified by the cardiac procedure, 50% of enrolled patients had diagnostic coronary angiography and 50% had a percutaneous coronary intervention. A total of 38% presented with acute coronary syndrome, and 76% were

on statins. A total of 229/339 patients (67.5%) allocated to glipizide and 233/333 (70%) allocated to rosiglitazone had an evaluable baseline and follow-up IVUS. Compared to participants who did not have 2 evaluable IVUS exams, those who did had a slightly lower diastolic blood pressure (P=0.05), were more likely to be from South America (P=0.001), were less likely to be on 2 oral antidiabetic agents (P=0.004), and were more likely to have had a stent inserted (P=0.006). An assessment of vital status at the 18 month final visit was available in 317 (93.5%) patients allocated to glipizide and 316 (94.9%) patients allocated to rosiglitazone.

Patients were followed for a median of 18.6 months (IQR 18.2-18.9) and a mean (SD) of 16 (6) months; Patients allocated to glipizide were adherent (took ≥80% and ≤120% of their study medications) at 90.7% of visits and those allocated to rosiglitazone were adherent at 92.7% of visits. Adverse effects that were either of interest based on prior studies, that occurred in more than 5% of participants in either group, or that significantly differed in frequency between groups are noted in Table 2. Compared to patients in the glipizide group, those allocated to rosiglitazone had less hypoglycemia and more anemia. No between-group difference was noted in the rate of cardiovascular events (all adjudicated) which occurred infrequently during the trial (Table 3); 5 of the cardiovascular events in the rosiglitazone group (1 revascularization, 2 nonfatal myocardial infarctions, 1 nonfatal stroke, and 1 cardiovascular death) occurred within 5 days of the baseline cardiac catheterization and were classified as procedure-related.

Table 2: Major Adverse Events in All Randomized Patients

Patients with an Event, N (%)	Glipizide (N=339)	Rosiglitazone (N=333)	P value
Events requiring change or stop in study medication			
Peripheral edema	1 (<1%)	2 (<1%)	0.62
Hypoglycemia	12 (4%)	0 (0%)	0.0004
Peripheral edema	24 (7%)	29 (9%)	0.48
Severe hypoglycemia (requiring external assistance)	3 (<1%)	0 (0%)	0.25
Hypoglycemia	96 (28%)	27 (8%)	<0.0001
Bone Fracture	2 (<1%)	6 (2%)	0.17
Hemoglobin decrease > 3 g/dL from baseline	10 (3%)	26 (8%)	0.006
Angina pectoris	35 (10%)	31 (9%)	0.69
Chest Pain	17 (5%)	12 (4%)	0.45
Cough	22 (6%)	13 (4%)	0.17
Diarrhea	17 (5%)	12 (4%)	0.45
Dizziness	18 (5%)	17 (5%)	1.00
Fatigue	14 (4%)	18 (5%)	0.47
Headache	23 (7%)	15 (5%)	0.24
Hypertension	22 (6%)	14 (4%)	0.23

Adverse events requiring changes in study drug, reported in ≥ 5% of patients in either group, significantly differed between groups, or were of interest based on other studies are listed.

Table 3: Adjudicated Clinical Cardiovascular Outcomes in All Randomized Patients

Patients with an event, n (%)	Glipizide (N=339)	Rosiglitazone (N=333)	P value*
Composite of all-cause death, nonfatal myocardial infarction, nonfatal stroke, coronary revascularization, or hospitalization for myocardial ischemia	38 (11.2%)	39 (11.7%)	0.58
Composite of cardiovascular death, nonfatal myocardial infarction, or nonfatal stroke	10 (2.9%)	14 (4.2%)	0.31
All-cause death	7 (2.1%)	8 (2.4%)	0.72
Cardiovascular death	3 (0.9%)	4 (1.2%)	0.50
Myocardial infarction			
Nonfatal	6 (1.8%)	7 (2.1%)	0.71
Fatal	1 (0.3%)	1 (0.3%)	0.89
Stroke			
Nonfatal	1 (0.3%)	5 (1.5%)	0.13
Fatal	0 (0%)	0 (0%)	–
Coronary revascularization	27 (8.0%)	26 (7.8%)	0.82
Hospitalization for myocardial ischemia	7 (2.1%)	11 (3.3%)	0.25
Congestive heart failure	3 (0.9%)	8 (2.4%)	0.14

*All p-values calculated using Cox proportional hazard model using time to first event

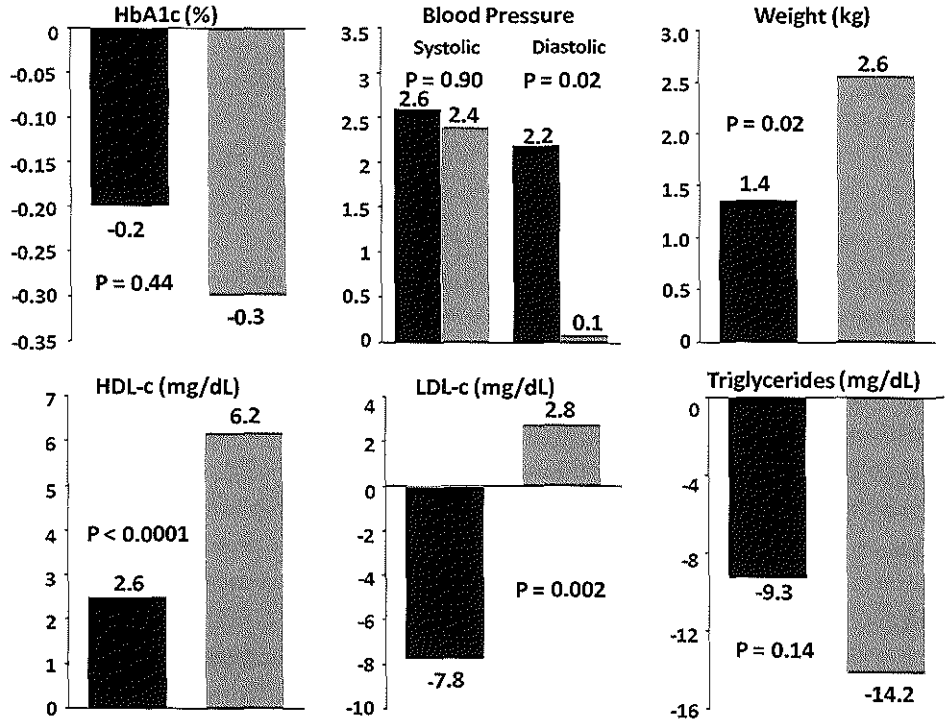

Figure 2. Effect of rosiglitazone versus glipizide on mean change in A1C, blood pressure, weight, HDL, and LDL level and on median change in triglyceride level in patients with 2 evaluable intravascular ultrasound measures. P values refer to differences of the change between groups. Gray bars depict the change for the rosiglitazone group and black bars depict the change for the glipizide group.

Table 4: Post-randomization Values and Medication Use at Final Visit

Measurement	Patients with Evaluable IVUS		
	Glipizide (N=229)	Rosiglitazone (N=233)	P
Continuous Variables			
Mean A1C (95% CI) %	6.9 (6.8, 7.0)	7.0 (7.0, 7.1)	0.01
Mean Blood Pressure (95% CI), mmHg			
Systolic	131.1 (129.6, 132.6)	130.7 (129.3, 132.2)	0.71
Diastolic	76.7 (75.8, 77.7)	75.4 (74.5, 76.4)	0.03
Mean LDL (95% CI), mg/dL	84.9 (80.7, 89.1)	95.3 (91.0, 99.6)	0.0001
Mean HDL (95% CI), mg/dL	45.5 (44.3, 46.7)	48.7 (47.5, 49.9)	<0.0001
Median Triglycerides (95% CI), mg/dL	156.2 (150.4, 164.6)	146.5 (138.9, 151.3)	0.14
Median hsCRP (95% CI), mg/L	1.9 (1.7, 2.1)	0.9 (0.8, 1.0)	<0.0001
Median MMP-9 (95% CI), ug/L	56.8 (54.2, 61.0)	47.9 (44.4, 50.8)	<0.0001
Mean weight (95% CI), kg	83.6 (83.1, 84.1)	84.0 (83.5, 84.5)	0.22
Final Visit Medication Use			
Aspirin	190 (83.0%)	199 (85.4%)	0.52
Other antiplatelet	93 (40.6%)	82 (35.2%)	0.25
Beta-blocker	152 (66.4%)	158 (67.8%)	0.77
ACE inhibitor or ARB	166 (72.5%)	176 (75.5%)	0.46
Nitrates	78 (34.1%)	76 (32.6%)	0.77
Statin	179 (78.2%)	190 (81.5%)	0.42
Fibrate or other lipid-lowering agent	27 (11.8%)	35 (15.0%)	0.34
Metformin	153 (66.8%)	152 (65.2%)	0.77
Any insulin	21 (9.2%)	14 (6.0%)	0.22

P values pertain to between-group differences in variables after randomization, and in medication use at the final visit. hsCRP, high-sensitivity C-reactive protein; LDL, low-density lipoprotein; HDL, high-density lipoprotein, MMP-9, matrix metalloproteinase 9; ARB, angiotensin II receptor blocker

The mean (SD) dose of study drug for patients who had a baseline and follow-up IVUS was 12.3 (4.3) mg for glipizide and 6.8 (1.8) mg for rosiglitazone. Of these patients, 220 (96.1%) of allocated to glipizide and 220 (94.4%) allocated to rosiglitazone had their follow-up IVUS done 17 or more months after the baseline IVUS. During the first 3 months of therapy when rosiglitazone or glipizide was substituted for other oral agents, HbA1c levels were higher on rosiglitazone. Subsequently A1C levels were the same and the final A1C levels did not differ between groups however the fluctuations resulted in the average post-randomization A1C value on rosiglitazone being slightly higher on rosiglitazone versus glipizide (7.0% versus 6.9% respectively, p=0.01). Figure 2 illustrates the change from baseline in A1C, blood pressure, lipids and weight for each group, and Table 4 lists the post-randomization mean or median values for these and other variables, as well the final use of concomitant medications by treatment group. Compared to patients on glipizide, those on rosiglitazone had a significantly lower post-randomization diastolic blood pressure, high sensitivity C-reactive protein, and matrix metalloproteinase 9 and significantly higher post-randomization A1C, LDL cholesterol and HDL cholesterol.

Effect on Intravascular Ultrasound Endpoints

Table 5 notes the effect of allocated therapy on the primary and secondary IVUS endpoints. During the course of the study, PAV (the primary outcome) did not significantly change from baseline in patients allocated to glipizide (0.43%, 95% CI -0.22, 1.08; p=0.19) or in patients allocated to rosiglitazone (-0.21%, 95% CI -0.86, 0.44; p=0.53). Moreover, rosiglitazone did not significantly reduce PAV compared to glipizide (-0.64%, 95% CI -1.46, 0.17; p=0.12). Similar findings were noted: a) when the data were analyzed after adjusting for baseline differences in age, creatinine and systolic blood pressure (-0.60%, 95% CI -1.43, 0.23; p=0.15); and b) when the data were analyzed using a worst rank analysis comprising 243 (72%) glipizide and 247 (74%) rosiglitazone patients, in which the 28 patients (14 per group) who did not have 2 evaluable IVUS examinations due to a cardiovascular event were assigned a rank based on their event as described above (P =0.20). The key secondary endpoint of total atheroma volume normalized for median segment length (TAV_N) did not significantly change in patients allocated to glipizide (1.2 mm^3, 95% CI -2.7, 5.1; p=0.54) and significantly decreased by 3.9 mm^3 (95% CI -7.8, -0.02; p=0.049) in patients allocated to rosiglitazone. Compared to glipizide, rosiglitazone significantly reduced TAV_N by 5.1 mm^3 (95% CI -10.0, -0.3; p=0.04). Atheroma volume within the 10 mm most diseased baseline segment was the other key secondary IVUS endpoint and decreased from baseline by 3.6 mm^3 (95% CI -5.3, -1.8; p<0.0001) in patients allocated to

Table 5: Intravascular Ultrasound Endpoints

Mean Value of IVUS Measurement (SD)	Glipizide			Rosiglitazone			Treatment Difference (95% CI)
	Baseline	Follow-up	Change† (95% CI)	Baseline	Follow-up	Change† (95% CI)	
Mean (SD) percent atheroma volume*	40.6 (11.0)	41.0 (11.2)	0.43 (-0.22, 1.08)	40.4 (11.8)	40.2 (11.4)	-0.21 (-0.86, 0.44)	**-0.64 (-1.46, 0.17)[a]**
Mean (SD) normalized total atheroma volume (mm^3)[¶]	232.8 (115.2)	233.2 (116.5)	1.2 (-2.68, 5.08)	226.1 (100.6)	221.6 (100.7)	-3.9 (-7.82, -0.02)[b]	**-5.12 (-9.98, -0.26)[c]**
Mean (SD) atheroma volume in the most diseased 10 mm segment (mm^3)[¶]	75.6 (32.6)	72.2 (33.3)	-3.6 (-5.31, -1.80)[d]	71.0 (30.0)	66.0 (30.7)	-5.3 (-7.04, -3.51)[d]	**-1.7 (-3.93, 0.49)**

SD – Standard Deviation; CI - Confidence Interval; *Primary IVUS Outcome; ¶Key IVUS secondary Outcomes; †change from baseline for each allocated group was estimated using analysis of covariance with terms for treatment group, baseline value, geographic region, gender, entry cardiac procedure (angiography or PCI), and prior oral antidiabetic medication. [a]P=0.12; [b]P=0.049; [c]P=0.04; [d]P<0.0001;[e]P=0.02;[f]P=0.01; *¶ similar P values were obtained for these outcomes when reanalyzed using a non-parametric test on rank-transformed data.

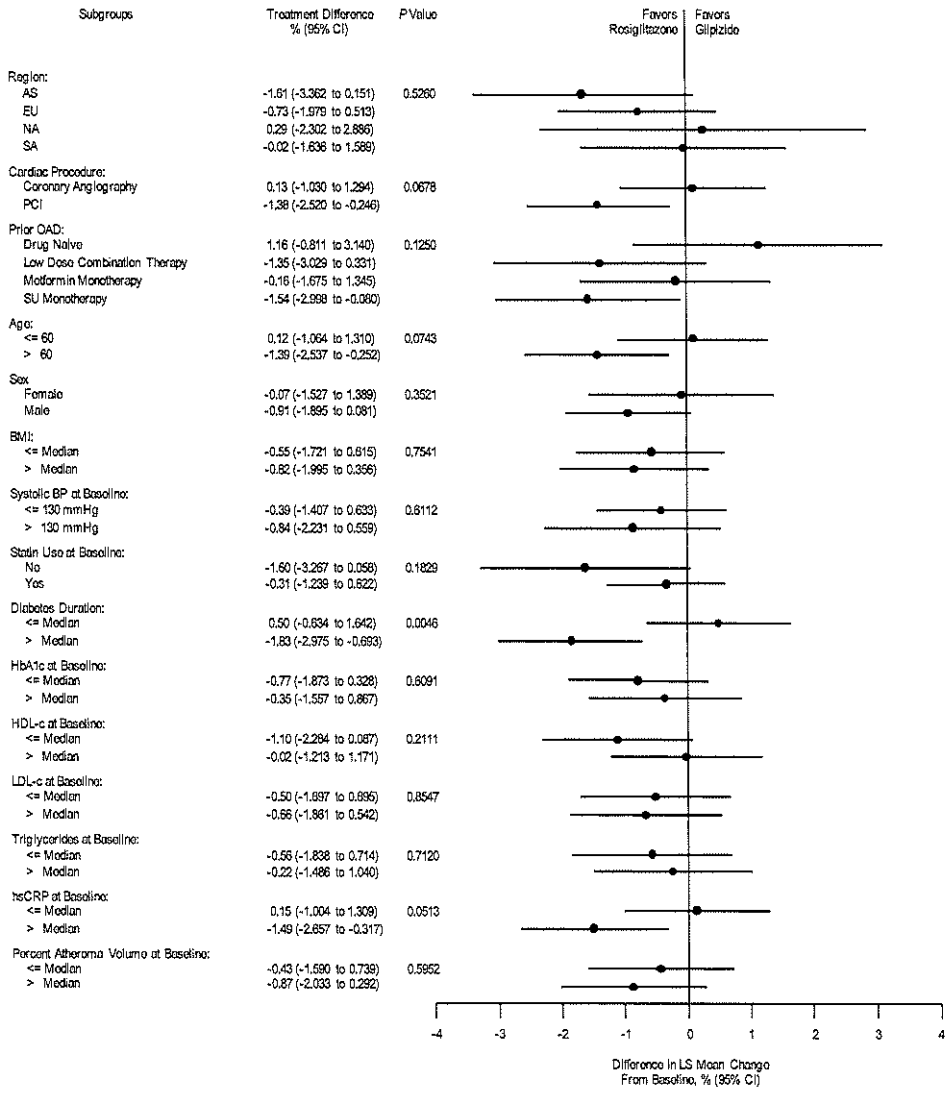

Figure 3. Effect of rosiglitazone versus glipizide on the primary outcome of change in percent atheroma volume according to predefined subgroups in patients with 2 evaluable intravascular ultrasound measures. P values reflect the test for an interaction between the subgroups and allocation to rosiglitazone versus glipizide. Median values are: BMI 28.9 kg/m^2; Diabetes duration 4.9 years; HbA1c 7.1%; HDL 42.5 mg/dl; LDL 87.0 mg/dl; Triglycerides 165.0 mg/dl; hs CRP 5.2mg/l; PAV 41.3%.

glipizide and by 5.3 mm^3 (95% CI -7.0, -3.5; p<0.0001) in patients allocated to rosiglitazone; however the effect of rosiglitazone did not significantly differ from that of glipizide (-1.7 mm^3, 95% CI -3.9, 0.5; p=0.13).

When analyzed according to prespecified subgroups (Figure 3), there was a clear interaction between treatment allocation and diabetes duration (P = 0.005) such that rosiglitazone reduced the PAV more than glipizide in patients with diabetes duration longer than the median duration of 4.9 years (i.e. a 1.8% decrease versus a 0.5% increase in those with a shorter diabetes duration). This analysis also suggested a trend favoring a greater effect of rosiglitazone allocation on patients with a higher baseline hsCRP and those who had a stent inserted versus angiography alone (P = 0.05 and 0.07 respectively).

DISCUSSION

In this 1.5 year study of the effect of rosiglitazone versus glipizide on coronary atherosclerosis a significant difference in the primary IVUS endpoint of PAV was not achieved. The observation that the trend towards reduced PAV volume reached significance within the prespecified subgroups of longer diabetes duration suggests that rosiglitazone may have an anti-atherosclerotic effect in sicker patients with a longer history of exposure to hyperglycemia, but should be viewed as hypothesis generating due to the many subgroups tested. These findings, and the observations that rosiglitazone significantly reduced the TAV_N more than glipizide support the hypothesis that rosiglitazone may reduce atherosclerotic plaque progression. Whether the rosiglitazone-mediated reduction in diastolic blood pressure, triglycerides, hsCRP and MMP-9 and the increase in weight and LDL cholesterol were responsible for these findings remains unknown.

These findings are consistent with those of a similar study in which another thiazolidinedione (pioglitazone) was compared to glimepiride[23]. In that 18 month study PAV significantly increased by 0.73% on glimepiride and nonsignificantly decreased by 0.16% on pioglitazone, with a significant difference between groups (P=0.002). Pioglitazone also decreased the TAV_N by 5.5 mm^3 versus a nonsignificant decrease of 1.5 mm^3 on glimepiride with no significant difference between groups (P=0.06). Indeed the effects of pioglitazone and rosiglitazone on IVUS indices and other metabolic and vascular markers were remarkably similar and are listed in Table 6. The absence of a statistically significant effect of rosiglitazone in this study may be due to the fact that the PAV in the glipizide control group only increased modestly whereas the increase in PAV in the glimepiride controls in the pioglitazone study was greater. These observations and reports of similar beneficial effects of these 2 drugs on carotid intima-media thickness [21;29] and need for revascularization following percutaneous intervention[30], as well as the adverse effect profile of these 2 drugs suggest that they have similar effects on atheroscle-

Table 6: Comparison of APPROACH and PERISCOPE

Measurement	Rosiglitazone (APPROACH)		Pioglitazone (PERISCOPE)	
	Baseline (SD or IQR)	Change (95% CI)	Baseline (SD or IQR)	Change (95% CI)
Mean (SD) percent atheroma volume	40.4 (11.8)	-0.21 (-0.86, 0.44)	40.6 (8.4)	-0.16 (-0.57, 0.25)
Mean (SD) normalized total atheroma volume (mm^3)	226.1 (100.6)	-3.9 (-7.82, -0.02)	207.5 (83.8)	-5.5 (-8.67, -2.38)
Mean (SD) atheroma volume in the most diseased 10 mm segment (mm^3)	71.0 (30.0)	-5.3 (-7.04, -3.51)	62.7 (28.1)	-2.0 (-3.33, -0.67)
Mean HbA1c (SD), %	7.1 (0.8)	-0.3 (-0.4, -0.2)	7.4 (1.0)	-0.55 (-0.68, -0.42)
Mean Systolic BP (SD), mm	127.6 (16.9)	2.4 (0.2, 4.6)	127.8 (16.6)	0.1 (-1.4, 1.5)
Mean Diastolic BP (SD), mm	74.7 (10.3)	0.1 (-1.2, 1.5)	75.7 (10.7)	-0.9 (-1.7, -0.01)
Mean Weight (SD), kg	81.9 (17.9)	2.6 (1.8, 3.4)	94.3 (19.5)	3.6 (2.8, 4.4)
Mean LDL (SD), mg/dL	90.5 (36.6)	2.8 (-2.4, 8.0)	93.5 (30.7)	2.1 (-1.5, 5.8)
Mean HDL (SD), mg/dL	42.4 (10.8)	6.2 (4.8, 7.6)	40.8 (11.5)	5.7 (4.4, 7.0)
Median TG* [IQR], mg/dL	162.8 [123.9-215.0]	-14.2 (-23.0, -3.5)	139 [104-198]	-16.3 (-27.7, -11.0)
Median Fasting insulin [IQR], µU/mL	13.0 [8.6-20.7]	-2.6 (-3.5, -0.9)	21.0 [16.0-33.0]	-5.0 (-7.0, -4.0)
Median BNP [IQR], pg/mL	24 [11-56]	5.0 (2.0, 11.0)	22.0 [11-52]	8.0 (5.0, 10.5)
Median hsCRP [IQR], mg/L	4.7 [2.2-10.5]	-3.2 (-4.0, -2.4)	2.6 [1.2-6.5]	-1.0 (-1.5, -0.8)

SD – Standard Deviation; CI - Confidence Interval; IQR – Interquartile Range; BP - blood pressure; PERISCOPE - Pioglitazone Effect on Regression of Intravascular Sonographic Coronary Obstruction Prospective Evaluation

rosis. However, whether they have similar or different effects on cardiovascular outcomes remains uncertain.

Strengths of this study are the large sample size, the use of masked therapies, high adherence rates, achievement of similar levels of cardiovascular risk factors in both groups, and careful validated measurements of IVUS indices. These findings are limited by the fact that 32.5% of patients allocated to glipizide and 30% of patients allocated to rosiglitazone did not have 2 evaluable IVUS measurements. Moreover, the observation that patients without 2 evaluable IVUS measurements were less likely to have had a stent inserted at baseline and were on fewer antidiabetic agents than those who had the 2 IVUS measurements suggests that the patients who did have the 2 IVUS measurements were those with more advanced atherosclerosis at baseline. However, the findings of the worst rank analysis which include 490 of the 672 (73%) randomized participants who received at least 1 dose of blinded medication, and which was similar to the analysis of patients with the 2 evaluable IVUS measurements suggests that it is unlikely that data from these individuals would have substantively altered the findings. These findings are also limited by the observation that rosiglitazone participants had a higher A1C level and that glipizide-treated patients had a lower LDL level after randomization despite blinded adjustment of medications designed to achieve similar levels of A1C and LDL.

In summary, this study supports but does not prove the hypothesis that rosiglitazone has a greater anti-atherosclerotic effect than glipizide in patients with type 2 diabetes, and suggests that that rosiglitazone may be more anti-atherosclerotic in patients with more advanced diabetes or higher risk for cardiovascular disease. Ongoing analyses will evaluate which factors relate to changes in atherosclerosis as measured by IVUS and will explore rosiglitazone's effects on atherosclerosis and plaque in more detail.

ACKNOWLEDGMENTS

Steering Committee: R. Ratner, P. Fitzgerald (co-chairs), C. Cannon, H. Gerstein, R. Nesto, P. Serruys, G-A Van Es, A. Zalewski.
Statistical Data and Analysis Center: Axio Research, Seattle, WA. L. Shemanski, A. Slee.
Endpoint Adjudication Committee: M. Savage (chair), H. Weitz, I. Ahmed.
APPROACH Study Management Team: R.P.Aftring, N. Kolatkar, B. Kravitz, A. Wolstenholme, K. Saarinen, R. Fowler, Janet Hoffman, D. Steele-Norwood, R. Russell,S. Young and former team members Hubert Chou, Steve McMorn, Courtney Kirsch, Bonnie Louridas, Teresa Olivieria, and Debra Mattioli.
APPROACH Statistics and Data Management Team: D. Miller, C. Huang, C. Nguyen, L. Jahnke.
Investigators- Argentina: Liliana Grinfeld, Daniel Nul, Graciela Gili, Sandra Silveiro, Silvina Ramos, Sonia Hermida, Hugo Torres, Estevan Zuanich, Pablo Severino, Ramiro Costello, Silvio Severino, Pablo Czerniuk, Liliana Grinfeld, Carlos Rojas Matas, Marcelo Halac, Alejandro Fernandez, José Gabay, Daniel Berrocal, Jorge Bluguerman, Daniel Mauro, Rodolfo Zazzali, Oscar Carlevaro, Jorge Alvarinas, Julia Blanco, Aristóbulo Balestrini, Arnoldo Girotti, Mario Principato, Susana Righi, Norma Del Hoyo, Pedro Tesone, Marcelo Mule, Jorge Belardi, Lucio Padilla, Mariano Albertal, Fernando Cura, Carlos Dall´asta, Guillermo Bortman, Pablo Czerniuk, Martin Gabriel Nicolini, Jorge Novas, Jorge Pinzetta Martinez, Marcos Litvak, Sebastián Schanz Estrada, Carlos Busso, Alejandro Cueto, Máximo Senesi, Francisco Gadaleta, Graciela Pedrale, Sandra Geraci, Carlos Wechsler, Edith Guerra, Elsa Ramirez de Martini, Susana Llois, Hugo Londero, Eugenio Trucco, Leandro Martinez Riera, Jose Pozzi, Silvana Solis, Jorge Waitman, María Cabrera, Francisco Paoletti, Daniel Mercado, Horacio Jure, Maria Pepe, Carolina Nadaya, Gabriela Morra, Jose Tibaldi, Cecilia Luquez, Alberto Villamil, Daniel Bekier, Judith Zilberman, Fabian Contreras, Paulo Reisin, Santiago Bruzone, Adriana Osorio, Sergio Kuznicki, Natalia Souto, Daniel Ricón,

Sebastian Rizzone, Maria Jimena Soutelo, Gabriel Sumay, Marcelo Masuelli, Sergio Chekherdenian, León Litwak, Ventura Simonovich, Lina Capurro, Ricardo Rey, Daniel Seinhart, Laura Brescacin, Pedro Forcada, Oscar Montaña, Christian Ponce, Alberto Marani, Jose Spolidoro, Virginia Visco, Claudia Mahfoud, Silvia Orio, Carlos Damico, Gustavo Costa, Simon Salzberg, Gustavo Alfredo Leiva, Miguel Oscar Payaslian, Ricardo Basile, Karina Crotto, Patricia Gibelman, Sonia Sassone, Fernando Mario Krinsky, Pablo Perez Baliño, Jorge Said Nisi, Felipe Martinez, Oscar Alfredo Allall, Sergio Rafael Tamiozzo, Rodolfo Sarjanovich, Viviana Arias, Marcela Giacometti, Marcela Giacometti, Victorino José Fuentealba, Moises Azize, Jimena María Martinez, Pablo Nicolas Guzman, Gabriel Sumay, Hugo Luquez. **Brazil:** Fábio de Brito Jr, Marco Perin, Breno Almeida, João Sá, Alexandre Abizaid, Luiz Tanajura, Luiz Mattos, Amanda Sousa, Roselei Graebin, José Sousa, Galo Andrade, Rodolfo Staico, Fausto Feres, Áurea Chaves, Denise Franco, Carlos Eduardo Soares, Felipe Maia, Ricardo Costa, José Júnior, Henry Zatz, Moysés Lima Filho, Geraldo Figueiredo, José Antonio Marin Neto, Ingrid Dick de Paula, Maria Cristina Freitas, Raul dos Santos, Expedito Silva, Pedro Horta, Eulógio Filho, Marcio Miname, Pedro Neto, Luiz César, Ana Paula Chacra, Wilson Filho, Carolina Chrisman. **Canada:** Jeff Pang, Harinda Wijeysundera, John Graham, Eric Cohen, Sam Radhakrishnan, Dennis Ko, Manu Prabhakar, Ram Vijayaraghavan, Salim Naqvi, Ivy Fettes, Jaffer Syed, Alexander Dick, Mina Madan, Asim Cheema, Bradley Strauss, Jason Burstein, Thierry Charron, Tej Sheth, Michael Kutryk, Warren Cantor, Robert Chisholm, Ruth McManus, Kumar Sridhar, David Almond, Patrick Teefy, Madhu Natarajan, Dominic Raco, James Velianou, Tej Sheth, David Crosby, Shamir Mehta, Michael Rokoss, Nicholas Valettas, William Harper, Ally Prebtani. **Czech Republic:** Josef Stasek, Irma Dresslerova, Pavel Polansky, Josef Bis, Dusan Cernohorsky, Miroslav Brtko, Jan Vojacek, Jaroslav Dusek. **France:** Bernard Vialettes, Catherine Mattei, Jean Louis Bonnet, Hervé Le Breton, Anne-Marie Leguerrier, Guillaume Lecoq, Dominique Boulmier, Marc Bedossa, Catherine Petit, Guillaume Charpentier, David Pesenti-Rossi, Christophe Caussin. **Germany:** Gabriele von Bergmann, Guenter Boehm, Iris Donati-Hirsch, Klaus Busch, Horst-Michael Frick, Susanne Hoeltz, Eckart Lohr, Ludwig Merker, I. Kreuzer, Michael Mikolaiczik, Adolf Trautmann, Raimund Erbel, Sebastian Alexander Philipp, Igor Kordish, Dirk Boese, Stefan Sack, Achim Gutersohn, Karl-Eugen Hauptmann, Herbert Dasch, B. Gestrich, Anne-Marie Ley, Gerrit Schneider, Bruno Sontag, Bernd Liesenfeld, Helmut Kuecherer, Stefan Hardt, Celine Johanssen, G. Korosoglou, Alexander Hansen, Raffi Bekeredjian, Andreas Muegge, Harald Klein, Antje Wagner, Tusgut Brodherr, Michael Lindstaedt, Alfried Germing, Eckard Rau, Christian Stute, Johannes Brachmann, Harald Rittger, Klaus-Juergen Gutleben, Guido Ritscher, Kai Koegler,

Hasan Alawi, Ilka Simon-Wagner, Georg Plassmann, Dirk Weber, Martin List. **Hong Kong:** John Sanderson, Cheuk-Man Yu, Pui Wai Lee, Juliana Chan, Eugene Wu, Norman Chan, Wing Bun Chan, Alice Kong, Leo Kum, Edmond Wong, Wilson Chan, Linda Lam, Wai-Hong Chen, Stephen Lee, Wing-Sun Chow, Annette Tso, Pui-Yin Lee, Chu-Pak Lau, Raymond Miu, Ryan Ko, Chi Sang Hung, Man Wo Tsang, Tai Pang Ip, Shing Chung Siu, Wai-Hong Chen, Michael Lee, Chiu Lai Fu, Steven LI, Duncan Ho, Cheung Hei Choi, Sau Cheung Tiu, Kam Tim Chan. **India:** Ajit Mullasari, Arpandev Bhattacharyya, Rajiv Passey, Balram Bhargava, Anil Dhall, Naveen Aggrawal, Sachin Khandelwal, M K Garg, N K Mahesh, Naveen Aggrawal, Anupam Goel, Ashok Seth, Dhiraj kapoor, Rajesh Saxena, Praveen Kumar Chandra. **Italy:** Giorgio Morocutti, Laura Tonutti, Guglielmo Bernardi, Claudio Noacco, Leonardo Spedicato, Patrizia Presbitero, Stefano Genovese, Silvia Rebuzzini, Dennis Zavalloni Parenti. **Korea:** Hyo-Soo Kim, HyunJae Kang, Bon-Kwon Koo, Young Min Cho, Sang Ho Jo, Hae Sung Kim, Soo Lim, Hyun-Jae Kang, Jin Wook Chung, Kyong Soo Park, Eun-Jung Lee, You Jin Lee, Mi-Yeon Kang, Cheol-Whan Lee, Cheol-Whan Lee, Young Hak Kim, Jung-Min Koh, DongHoon Choi, Bong-Soo Cha, Yang Soo Jang, Se-Eun Park, SeungJea Tahk, Byoung Joo Choi, Joon-Han Shin, Soo-Jin Kang, So-Yeon Choi, Hong-Seok Lim, Myoung Ho Yoon, Hae-Jin Kim, Dae-Jung Kim, Kwan-Woo Lee. **Latvia:** Valdis Pirags, Andrejs Erglis, Irina Kutajeva, Agnis Zvaigzne, Karlis Trusinskis, Indulis Kumsars, Sanda Jegere, Dace Sondore, Inga Narbute, Sandra Steina, Inga Balcere, Rota Ritenberga. **Mexico:** Guillermo Gonzalez-Galvez, Emilia Susana Pelayo-Orozco, Blanca Leticia Sánchez-Michel, Armando García-Castillo, Fernando Lavalle-González, Violeta Imelda Gallardo-Montejano, Arturo Abundes-Velasco. **Netherlands:** H.R. Michels, R.S.W. Entjes, B. Bravenboer, K. Krasznai, P.W. Serruys, Martin van der Ent, A.H. Bootsma, P.C. Smits, L.J.D.M. Schelfhout. **Poland:** Henryk Wysocki, Agnieszka Rutkowska, Dagmara Przymuszala, Mieczyslaw Dziarmaga, Janusz Tarchalski, Agnieszka Trawczynska, Jan Peruga, Ewa Mazurek, Malgorzata Sporna, Aleksander Jachniewicz, Adam Witkowski, Lukasz Kalinczuk, Jerzy Pregowski, Bozena Norwa-Otto, Andrzej Ciszewski, Zbigniew Chmielak, Witold Ruzyllo, Pawel Buszman, Agata Gruszka, Leszek Stachaczyk, Marcin Debinski, Stanislaw Trznadel, Aleksander Zurakowski, Krzysztof Milewski. **Russian Federation:** Ludmila Nedosugova, Bagrat Alekyan, Simon Matskeplishvili, Yuriy Buziashvili, Inna Klefortova, Samson Madoyan, Igor Shuvaev, Dzhamshed Kamardinov, Marat Aripov, Nino Tsereteli, Elvina Tugeeva, Natalya Trubitsina, Leonid Kokov, Andrey Ardashev, Svetlana Voloshko, Andrey Shavarov, Dmitriy Mangutov, Elena Potekhina, Vasiliy Chestukhin, Anna Sibyakina, Alexander Pokatilov, Alexey Mironkov. **Spain:** Carlos Macaya, Luis Azcona Varela, Mª Luz Capote Toledo, Fernando Alfonso Manterola, Manuel

Sabaté, Alfonso Suárez, Ángel Díaz, Javier Goicolea, José Ramón Domínguez Puente, Raymundo Ocaranza Sánchez, Juan Francisco Oteo, Alberto Simal, Arturo García Touchard, Víctor Castro, Amadeo Betriu, Mónica Masotti, Rafael Ruiz, Sergio Rueda, Enric Esmatjes, Vicente Mainar, Juan Miguel Ruiz Nodar, Javier Pineda, José Valencia, Pascual Bordes, Óscar Moreno, Antonio Pico, Alberto Berenguer, Enric Domingo, Josep Guindo, Adriana Soto, Jorge Mesa, Eladio José Losada Grande, Inocencio Anivarro, Juan Ángel, Edgardo Kaplinsky, Imanol Otaegui, Bruno García del Blanco, Nuria Batalla, Antonio Espolita, Iñigo Lozano, César Morís, Pablo Avanzas, Juan Rondán Murillo, Concepción Suárez Suárez, Elías Delgado, Angel Cequier, Joan Antoni Gomez Hospital, Francesc Jara, Jaume Maristany, Marcelo Jiménez, Eduard Montanya, Emili Iraculis, José María Hernández, María José Picón, Juan Alonso Briales, Manuel Jiménez Navarro, Araceli Frutos García, Pilar Carrillo, Vicente Bertomeu, Francisco José Pomares Gómez, José Ramón Domínguez Escribano, Ramón López Palop, Fina Mauri, Andreu Nubiola Calonge, Vicente Valle Tudela, Gerardo Aguilar, Oriol Rodríguez Leor, Eduardo Fernández Nofredias. **Sweden:** Bertil Wennerblom, Thomas Hedner, Inga-Britt Kling, Eva Dahl, Per Albertsson, Lars Grip, Asa Dahl, Staffan Svensson, Stanko Skrtic, Farshad Tahmasebiepour, Tage Nilsson, Karin Astrom Olsson, Marie Escar, Thomas Hedner, Bjorn Wahlstrand, Göran Matejka, Per Tornvall, Kerstin Hoglund, Camilla Hage, Eva Arnqvist-Gustafsson. **Thailand:** Srun Kuanprasert, Ampica Mangklabruks, Supawan Buranapin, Kaset Chimplee, Natapong Kosachunhanun, Padiporn Vasinanukorn, Sarat Sunthornyothin, Surapun Sitthisook, Jarkarpun Chaipromprasit, Sompongse Suwanwalaikorn. **United States:** Steven Bailey, Bogdana Ioana Balas, Barbara Walz, Ralph DeFronzo, Devang Patel, Marc Feldman, Robert Chilton, Umesh Arora, Michael Ball, Catherine Bain, Gregory Eisner, Matthew French, Edward Fry, John Fry, Jack Hall, James Hermiller, Zachary Hodes, Elaine Moen, Charles Orr, Kirk Parr, Thomas Peters, Ali Rizvi, Donald Rothbaum, Charles Taylor, James VanTassel, Joseph Barrera, Daniel Kulick, Arthur Loussararian, Mim Mulford, Venkatesh Nadar, Stanley Lewin, Renu Joshi, Robert Chadband, Harold Settle, Michael Simpson, Michael Rowland, Robert Foster, Van Reeder, Andrew Kronenberg, Andrew Brian, Brian Snoddy, Rachel Wilkinson, Arthur Chernoff, Catherine Garrison, Dennis Morris, Catherine Anastasopoulou, Shahriar Yazdanfar, Robert Chow, Robert Ferrera, Robert Schott, Linda Morrow, Sailesh Shah, Burritt Haag, Kamal Shoukri, Michael LeMay, Margaret Sharron, Ayesha Parvoz, Vasantha Reddy, Vilma Carlone, Marc Schweiger, Ibitoro Osakwe, Dominica Kelley, Gregory Guigliano, Satyendra Giri, Gopal Gododia, Shashin Desai, Nikhita Dhruv, Rajesh Desai, Theodore Heierman, Nancy Parker, Lucia Lilien, Laura Bryan, Henry Lui, Keith Atkins, Eie Hage-Korbin, Michelle Magee, Robert Rat-

ner, Asha Thomas, Angela Silverman, Wayman Cheatham, Gabriel Uwaifo, Debra Wells, Ron Waksman, Jennifer Holst, Kenneth Kent, John Laird, Augusto Pichard, Lowell Satler, John Sharretts, William Suddath, Marc Mitchell, Scott Eberly, Allen Geltzer, Thomas Amidon, Christopher Kozlowski, James Leggett, Joseph Doucette, Neal Perlmutter, Jorge Calles-Escandon, Talal Baki, William Little, Robert Applegate, Michael Kutcher, Sanjay Gandhi, Renato Santos, George Dangas, Mark Apfelbaum, Michael Collins, Daniel Donovan, Edward Kreps, Martin Leon, Roxana Mehran, Jeffrey Moses, Issam Moussa, Leroy Rabbani, Gregg Stone, Hal Wasserman, Judah Weinberger, Giora Weisz, Charles Whitcomb, Jason Rogers, Thomas Aoki, Todd Brown, Ann Munson, Jon Resar, Julie Miller, Alan Heldman, Kathleen Citro, Mary Ellen Ehlers, Jan Houghton, William Georgitis, Christopher Lang, David Kinnard, Steven Resnick, Albert Tseng, William Herzog, Michael Silverman, George Groman, Keith Friedman, Alexander Chudnovsky, Gebreye Rufael, Marie Gregory, Stephen Hippler, Craig Kurtz, Alan Chu, Robert Crawford, Ronald Rabjohns, David Best, Darrel Gumm, John Rashid, Barry Clemson, S. Craig Kurtz, Paul Schmidt, Stephen Schneider, Alpesh Patel, Jai Agarwal, Sheri Funderburk, Mark Moshiyakhov, Lilliana Cohen, Abel Moreyra, Gretchen Perilli, Anthony Lombardo, Shelley Greenhaus, Lisa Motivalli, Tudor Vaganescu, William Schafranek, Pirouz Parang, Ajay Chander, Anthony Messina, Syed Hussassian, Chirag Shah, Louis Amorosa, Rita Louard, Ray Matthews, Thomas Shook, Steven Burstein, Guy Mayeda, David Shavelle, Mariola Ficinski, Jane Reusch, Irene Schauer, Sarah Bull, John Messenger, Cecilia Wang, Rocio Pereira, Ivan Casserly, Stacey Mitchell, Kylie Carson, Barbara Watson, Paul Rosenblit, Reynaldo Mulingtapang, John Sullebarger, Robyn Aydelott, Nancy Grove, Huy Khuu, Beth Major, Manuel Sainz de la Pena, John Sullebarger, Fadi Martar, Marc Taylor, Anthony Morrison, Joel Strom, Reynaldo Mulingtapang, Tywaun Tillman, MaryAnn Yarborough, Helen Taylor, Cynthia Williams, Benjamin Rosin, Laryenth Lancaster, Veronica Piziak, David Robertson, Charles Wilmer, Charles Wickliffe, Kenneth Taylor, Spencer King III, William Jacobs, Mina Jacob, John Hurst Jr., Harold Carlson, Charles Brown III, William Blincoe, William Ballard, Scott Anderson, John Tayek, David Shavelle, Matthew Budoff, Gul Khawar, Edward Kosinski, Jeffrey Lins, Jay Zdunek, Alexander Kalenak, Tammy Outly, Richard Begg, Minn Mach, Daniel Eisenberg, Roger On, Joseph Lee, Eric Lee, A. Farfel, Khakloun Sroujieh, Augusta Silva, Bharat Shah, Boris Larreta, Sako Chen, Douglas Schreck, David Sato, Barry Rosen, William Gifford, Shawna Weisler, Tony DeMartini, Norman Soler, Linda L McCall, Romesh Kahdori, Gabor Matos, Frank Aguirre, Vincent Zuck, Wilfred Lam, Raymond Kacich, Ziad Issa, John Gill, Mansura Ghani, Chandhiran Rangaswamy, Nasar Nallamothu, Brian Miller, James Leibsohn, Beth Lalande, Catherine Zyniecki, John

Patterson, Michael Sollenberger, David Bohle, Jaime Zapata, Davidson Givens, Charles Harris, John McCabe, Usman Khawaja, Gary Reynaldo, Gregory Ledger, Thomas Rossiter, Anthony Giglio, Kelvin VanOsdol, David Cochran, Donald Myears, Robert Merritt, John Hawkins, Osvaldo Brusco, Srikanth Damaraju, John Pappas, Greg Arsenis, R. Kiesz, Thomas Rossiter, Alexander Shepherd, Krishnaswami Vijayaraghavan, W. Scott Robertson, Fuad Ibrahim, Alan Tenaglia, Mehrdad Saririan, Bradley Oswood, Leslie Barnett-Avery.

Independent Data Monitoring Committee-G. Mintz, J. Lachin (co-chairs), M. Abrahamson, P. Carson, P. Jones.

REFERENCE LIST

(1) Huxley R, Barzi F, Woodward M. Excess risk of fatal coronary heart disease associated with diabetes in men and women: meta-analysis of 37 prospective cohort studies. *BMJ* 2006;332:73-78.

(2) Selvin E, Marinopoulos S, Berkenblit G et al. Meta-analysis: glycosylated hemoglobin and cardiovascular disease in diabetes mellitus. *Ann Intern Med* 2004;141:421-431.

(3) Patel A, Macmahon S, Chalmers J et al. Intensive blood glucose control and vascular outcomes in patients with type 2 diabetes. *N Engl J Med* 2008;358:2560-2572.

(4) Action to Control Cardiovascular Risk in Diabetes Study Group., Gerstein HC, Miller ME et al. Effects of intensive glucose lowering in type 2 diabetes. *N Engl J Med* 2008;358:2545-2559.

(5) UK Prospective Diabetes Study (UKPDS) Group. Effect of intensive blood glucose control with metformin on complications in overweight patients with type 2 diabetes (UKPDS 34). *Lancet* 1998;352:854-865.

(6) Holman RR, Paul SK, Bethel MA, Matthews DR, Neil HA. 10-Year Follow-up of Intensive Glucose Control in Type 2 Diabetes. *N Engl J Med* 2008.

(7) Ricciardi MJ, Meyers S, Choi K, Pang JL, Goodreau L, Davidson CJ. Angiographically silent left main disease detected by intravascular ultrasound: a marker for future adverse cardiac events. *Am Heart J* 2003;146:507-512.

(8) von Birgelen C., Hartmann M, Mintz GS et al. Relationship between cardiovascular risk as predicted by established risk scores versus plaque progression as measured by serial intravascular ultrasound in left main coronary arteries. *Circulation* 2004;110:1579-1585.

(9) Nissen SE, Tuzcu EM, Libby P et al. Effect of antihypertensive agents on cardiovascular events in patients with coronary disease and normal blood pressure: the CAMELOT study: a randomized controlled trial. *JAMA* 2004;292:2217-2225.

(10) Nissen SE, Tuzcu EM, Schoenhagen P et al. Effect of intensive compared with moderate lipid-lowering therapy on progression of coronary atherosclerosis: a randomized controlled trial. *JAMA* 2004;291:1071-1080.

(11) Okazaki S, Yokoyama T, Miyauchi K et al. Early statin treatment in patients with acute coronary syndrome: demonstration of the beneficial effect on atherosclerotic lesions by serial volumetric intravascular ultrasound analysis during half a year after coronary event: the ESTABLISH Study. *Circulation* 2004;110:1061-1068.

(12) Schartl M, Bocksch W, Koschyk DH et al. Use of intravascular ultrasound to compare effects of different strategies of lipid-lowering therapy on plaque volume and composition in patients with coronary artery disease. *Circulation* 2001;104:387-392.

(13) Takagi T, Yoshida K, Akasaka T, Hozumi T, Morioka S, Yoshikawa J. Intravascular ultrasound analysis of reduction in progression of coronary narrowing by treatment with pravastatin. *Am J Cardiol* 1997;79:1673-1676.

(14) Tiikkainen M, Hakkinen AM, Korsheninnikova E, Nyman T, Makimattila S, Yki-Jarvinen H. Effects of rosiglitazone and metformin on liver fat content, hepatic insulin resistance, insulin clearance, and gene expression in adipose tissue in patients with type 2 diabetes. *Diabetes* 2004;53:2169-2176.

(15) Kahn SE, Haffner S, Heise MA et al. Glycemic durability of rosiglitazone, metformin, or glyburide monotherapy. *N Engl J Med* 2006;355:2427-2443.
(16) Haffner SM, Greenberg AS, Weston WM, Chen H, Williams K, Freed MI. Effect of rosiglitazone treatment on nontraditional markers of cardiovascular disease in patients with type 2 diabetes mellitus. *Circulation* 2002;106:679-684.
(17) Natali A, Baldeweg S, Toschi E et al. Vascular effects of improving metabolic control with metformin or rosiglitazone in type 2 diabetes. *Diabetes Care* 2004;27:1349-1357.
(18) Derosa G, Gaddi AV, Piccinni MN et al. Antithrombotic effects of rosiglitazone-metformin versus glimepiride-metformin combination therapy in patients with type 2 diabetes mellitus and metabolic syndrome. *Pharmacotherapy* 2005;25:637-645.
(19) Kelly AS, Thelen AM, Kaiser DR, Gonzalez-Campoy JM, Bank AJ. Rosiglitazone improves endothelial function and inflammation but not asymmetric dimethylarginine or oxidative stress in patients with type 2 diabetes mellitus. *Vasc Med* 2007;12:311-318.
(20) Qayyum R, Adomaityte J. A meta-analysis of the effect of thiazolidinediones on blood pressure. *J Clin Hypertens* 2006;8:19-28.
(21) Mazzone T, Meyer PM, Feinstein SB et al. Effect of pioglitazone compared with glimepiride on carotid intima-media thickness in type 2 diabetes: a randomized trial. *JAMA* 2006;296:2572-2581.
(22) Rosmarakis ES, Falagas ME. Effect of thiazolidinedione therapy on restenosis after coronary stent implantation: a meta-analysis of randomized controlled trials. *Am Heart J* 2007;154:144-150.
(23) Nissen SE, Nicholls SJ, Wolski K et al. Comparison of pioglitazone vs glimepiride on progression of coronary atherosclerosis in patients with type 2 diabetes: the PERISCOPE randomized controlled trial. *JAMA* 2008;299:1561-1573.
(24) Ratner RE, Cannon CP, Gerstein HC et al. Assessment on the Prevention of Progression by Rosiglitazone on Atherosclerosis in diabetes patients with Cardiovascular History (APPROACH): Study design and baseline characteristics. *Am Heart J* 2008;In Press.
(25) De Winter SA, Hamers R, Degertekin M et al. Retrospective image-based gating of intracoronary ultrasound images for improved quantitative analysis: the intelligate method. *Catheter Cardiovasc Interv* 2004;61:84-94.
(26) Rodriguez-Granillo GA, Vos J, Bruining N et al. Long-term effect of perindopril on coronary atherosclerosis progression (from the perindopril's prospective effect on coronary atherosclerosis by angiography and intravascular ultrasound evaluation [PERSPECTIVE] study). *Am J Cardiol* 2007;100:159-163.
(27) Nissen SE, Nicholls SJ, Sipahi I et al. Effect of very high-intensity statin therapy on regression of coronary atherosclerosis: the ASTEROID trial. *JAMA* 2006;295:1556-1565.
(28) Lachin JM. Worst-rank score analysis with informatively missing observations in clinical trials. *Control Clin Trials* 1999;20:408-422.
(29) Stocker DJ, Taylor AJ, Langley RW, Jezior MR, Vigersky RA. A randomized trial of the effects of rosiglitazone and metformin on inflammation and subclinical atherosclerosis in patients with type 2 diabetes. *Am Heart J* 2007;153:445-446.

(30) Riche DM, Valderrama R, Henyan NN. Thiazolidinediones and risk of repeat target vessel revascularization following percutaneous coronary intervention: a meta-analysis. *Diabetes Care* 2007;30:384-388.

CHAPTER 9.3

Meta-analysis of the studies assessing temporal changes in coronary plaque volume using intravascular ultrasound.

Rodriguez-Granillo GA, Agostoni P, **Garcia-Garcia HM**, Biondi-Zoccai GGL, Mc Fadden E, Amoroso G, de Jaegere P, Bruining N, de Feyter P, Serruys PW.

Am J Cardiol. 2007;99:5-10.

Meta-Analysis of the Studies Assessing Temporal Changes in Coronary Plaque Volume Using Intravascular Ultrasound

Gastón A. Rodriguez-Granillo, MD, PhD[a,c,*], Pierfrancesco Agostoni, MD[d], Héctor M. Garcia-Garcia, MD[a], Giuseppe G.L. Biondi-Zoccai, MD[e], Eugène Mc Fadden, MD[a], Giovanni Amoroso, MD, PhD[d], Peter de Jaegere, MD, PhD[a], Nico Bruining, PhD[a], Pim de Feyter, MD, PhD[a], and Patrick W. Serruys, MD, PhD[a]

To assess the temporal effect of statin therapy on coronary atherosclerotic plaque volume measured by intravascular ultrasound (IVUS), we searched PubMed for eligible studies published between 1990 and January 2006. Inclusion criteria for retrieved studies were (1) IVUS volume analysis at baseline and follow-up and (2) statin therapy in ≥1 group of patients. All data of interest were abstracted in prespecified structured collection forms. Statistical analysis was performed with Review Manager 4.2. Random-effect weighted mean difference (WMD) was used as summary statistics for comparison of continuous variables. Nine studies of 985 patients (with 11 statin treatment arms) were selected. After a mean follow-up of 9.8 ± 4.9 months, we found a significant decrease in coronary plaque volume (WMD −5.77 mm^3, 95% confidence interval −10.36 to −1.17, p = 0.01), with no significant heterogeneity across studies (p = 0.47). Prespecified subgroup analyses showed similar trends. Studies in which the achieved low-density lipoprotein (LDL) cholesterol level was <100 mg/dl showed a trend for plaque regression (WMD −7.88 mm^3, 95% confidence interval −16.31 to 0.55, p = 0.07), whereas studies in which the achieved level of LDL cholesterol was ≥100 mg/dl, the trend was less evident (WMD −4.22 mm^3, 95% confidence interval −10.27 to 1.82, p = 0.17). Plaque volume remained essentially unchanged in patients not treated with statins (WMD 0.13 mm^3, 95% confidence interval −4.42 to 4.68, p = 0.96). In conclusion, statin therapy, particularly when achieving the target LDL level, appears to promote a significant regression of coronary plaque volume as measured by IVUS. (Am J Cardiol 2007;99:5–10)

We performed a meta-analysis of all clinical studies that assessed intravascular ultrasound (IVUS)-based progression/regression of coronary atherosclerosis to evaluate whether treatment with statins can promote coronary plaque regression over time.

Methods

Two trained investigators (GARG and PA) searched PubMed for eligible studies in peer-reviewed journals published between January 1990 and January 2006. Search key words included "reduc*" or "regres*" or "progress*" and "IVUS" or "intravascular ultrasound," where * denotes a wildcard, which is a symbol used to search all words beginning with the written root. PubMed was searched using the method described by Biondi-Zoccai et al.[1] No language restriction was used. Cross references were checked, and experts were contacted to identify other relevant trials.

Citations initially selected by systematic search were first retrieved as title and/or abstract and screened independently by 2 reviewers (GARG and PA). Potentially relevant reports were then retrieved as complete publications and assessed for compliance to inclusion and exclusion criteria.

Inclusion criteria for retrieved studies were (1) IVUS volume analysis in native coronary arteries at baseline and follow-up and (2) statin therapy in ≥1 group of patients.

Exclusion criteria were (1) no volumetric output (only cross-sectional area analysis) and (2) studies in vessels different from coronary arteries.

All data of interest were abstracted in prespecified structured collection forms. Every study used the same IVUS imaging catheter at baseline and follow-up. All IVUS investigations were performed after intracoronary administration of nitrates. Cine runs, before and during contrast injection, were performed to define the position of the catheter distal to an identifiable side branch. Using an automated pull-back device, the transducer was withdrawn at a continuous speed of 0.5 mm/s, and IVUS data were stored on super-VHS for subsequent analysis. Our primary end point of interest was progression/regression of coronary atherosclerotic burden evaluated by IVUS volumetric analysis. According to the different studies included in the analysis, plaque volume was calculated as $^{n}\Sigma_{m=1}$ ($vessel_{area}$ − $lumen_{area}$) × d, where n refers to number

[a]Department of Cardiology, Thoraxcenter, Erasmus Medical Center, Rotterdam; and [b]Onze Lieve Vrouw Gasthuis, Amsterdam, The Netherlands; [c]Department of Cardiovascular Imaging, Otamendi Hospital, Buenos Aires, Argentina; [d]Antwerp Cardiovascular Center Middelheim, Antwerp, Belgium; and [e]Haemodynamics and Cardiovascular Radiology Service, Policlinico San Donato, Milan, Italy. Manuscript received April 18, 2006; revised manuscript received and accepted July 13, 2006.

*Corresponding author: Tel: 54-11-4964-8721; fax: 54-11-4964-8721.

E-mail address: grodriguezgranillo@gmail.com (G.A. Rodriguez-Granillo).

Table 1
Characteristics of studies included in the meta-analysis

Study	Year	Design	n (%)*	Treatment	Follow-up Mean (%)	Age (yrs)	Men	LDL at Follow-up (mg/dl)
GAIN[21]	2001	MC	48 (6)	Atorvastatin	12 mos	61	85	86 ± 30
ESTABLISH[20]	2004	SC	24 (3)	Atorvastatin	6 mos	61	86	70 ± 25
REVERSAL[28]	2004	MC	253 (32)	Atorvastatin	18 mos	56	71	79 ± 30
REVERSAL[28]	2004	MC	249 (32)	Pravastatin	18 mos	57	73	110 ± 26
Petronio et al.[24]	2005	SC	36 (5)	Simvastatin	12 mos	63	72	94 ± 9
Kawasaki et al.[26]	2005	SC	17 (2)	Atorvastatin	6 mos	66	71	95 ± 15
Kawasaki et al.[26]	2005	SC	18 (2)	Pravastatin	6 mos	67	72	102 ± 13
Nishioka et al.[23]	2005	SC	22 (3)	Statin	6 mos	66	77	106 ± 20
Jensen et al.[22]	2004	SC	40 (5)	Simvastatin	12 mos	58	100	40 ± 10
Yokoyama et al.[25]	2005	SC	29 (4)	Atorvastatin	6 mos	62	90	87 ± 29
Tani et al.[27]	2005	SC	52 (7)	Pravastatin	6 mos	63	75	104 ± 20

* Number of patients in treatment arm.
MC = multicenter; SC = single center.

of images, m to image, and d to distance between images. In case these data were not provided in the published report, the authors were contacted to obtain these values.

We compared baseline with follow-up plaque volume in patients receiving statins and control subjects (when present). In addition, as sensitivity analyses, we stratified the studies according to achieved low-density lipoprotein (LDL) cholesterol levels and time to follow-up, seeking an enlightenment of results.

Statistical analysis was performed with Review Manager 4.2.2 Continuous variables are reported as mean ± SD unless otherwise specified. Random-effect weighted mean difference (WMD) with 95% confidence intervals was used as summary statistics for comparison of continuous variables; this analysis is used when the unit of measurement of the variable under analysis remains constant across different studies.[3] The currently recommended inverse variance-weighting method, according to Dersimonian and Laird, was used for random-effect comparison.[3] Reported values were 2-tailed and results were considered statistically significant at $p < 0.05$. Statistical heterogeneity (i.e., between-study discrepancy in effect size estimates) was assessed with the Cochran Q test. This test strongly suggests underlying statistical heterogeneity for p values <0.10, even if other causes of heterogeneity, such as clinical differences between treatments, follow-up duration, or patient population, are not dismissed. Appraisal of statistical heterogeneity is pivotal to meta-analysis because some authorities have advocated statistical pooling of different trials only in the presence of statistical homogeneity.[3] To assess the risk of small-study bias (including publication bias), we built a funnel plot by graphically showing the relation between effect size and statistical weight for each study. A symmetric and funnel-shaped plot supports the lack of significant small-study bias, whereas a strongly asymmetric plot suggests the underlying presence of small-study or publication bias (i.e., where smaller studies reporting positive outcomes are more likely to be published than equally small studies reporting negative or nonsignificant results). Publication bias, if not recognized and acknowledged, can lead to meta-analyses with biased and overly optimistic findings and should thus be actively investigated and appraised.[3]

Results

PubMed queries permitted the retrieval of 977 citations. Most publications were excluded because they were editorials, reviews, or studies addressing the role of IVUS as an adjunctive tool to percutaneous coronary interventions. Eighteen publications were assessed for compliance to inclusion and exclusion criteria, leading to further exclusion of 9 studies. One study was not included because only area measurements and not volume analyses were reported.[4] One study did not include a treatment arm.[5] Three other studies were excluded because they evaluated IVUS in femoral arteries and transplant-associated arteriosclerosis.[6–8] One study used antihypertensive agents and 3 others used lipid-lowering therapies different from statins.[9–12] Therefore, 9 published studies were selected.[10,13–20]

These 9 studies included 985 patients. Most studies were randomized comparisons of a statin versus placebo, aside from a study by Jensen et al.[15] which was a single-arm observational study. In the randomized Reversal of Atherosclerosis with Aggressive Lipid Lowering (REVERSAL) trial, the 2 arms received statins, but different molecules; in a study by Kawasaki et al.[19] 2 groups received 2 different statins and 1 received placebo. Thus, overall, 788 patients were allocated to statin treatment in 11 different groups (Table 1).

All studies used absolute change in plaque volume in a matched region of interest evaluated at the longest available follow-up as an imaging end point, apart from a study by Petronio et al.[17] which reported change in plaque volume adjusted for analyzed vessel length. We contacted the authors to obtain the absolute change in plaque volume.

In the German Atorvastatin Intravascular Ultrasound (GAIN) study, patients were allocated to atorvastatin in an increasing dose to achieve a LDL cholesterol level <100 mg/dl or placebo.[14] For the Early Statin Treatment in Patients With Acute Coronary Syndrome (ESTABLISH) study, 20 mg/day of atorvastatin versus placebo was administrated.[13] In contrast, the REVERSAL investigators compared an intensive with a moderated lipid-lowering therapy (80 mg/day of ator-

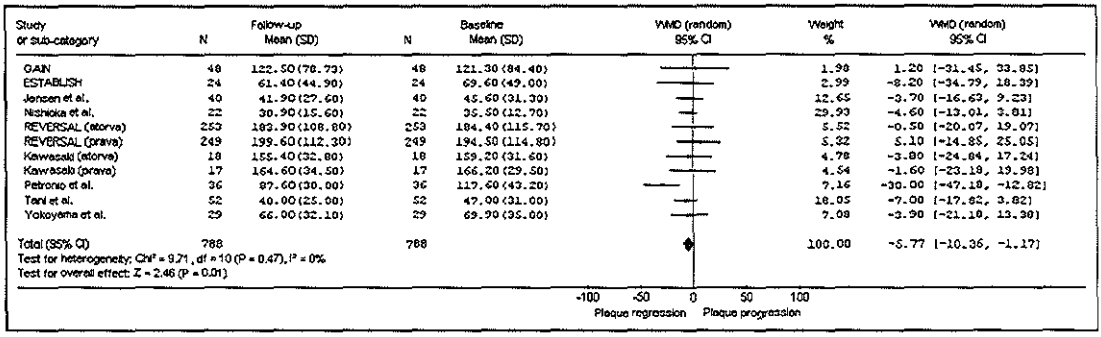

Figure 1. WMD with 95% confidence interval (CI) of difference in plaque volume between follow-up and baseline in the statin arm of the included studies.

Table 2
Stratification of change in plaque volume according to length of follow-up

Follow-up 6 mos (n = 158)		Follow-up >6 mos (n = 626)	
Study	WMD (95% CI)	Study	WMD (95% CI)
ESTABLISH[20]	−8.20 (−34.79 to 18.39)	GAIN[21]	1.20 (−31.45 to 33.85)
Nishioka et al[23]	−4.60 (−13.01 to 3.81)	Jensen et al[22]	−3.70 (−16.63 to 9.23)
Kawasaki et al[26] (atorvastatin)	−3.80 (−24.84 to 17.24)	REVERSAL[28] (atorvastatin)	−0.50 (−20.07 to 19.07)
Kawasaki et al[26] (pravastatin)	−1.60 (−23.18 to 19.98)	REVERSAL[28] (pravastatin)	5.10 (−14.85 to 25.05)
Tani et al[27]	−7.00 (−17.82 to 3.82)	Petronio et al[24]	−30.00 (−47.18 to −12.82)
Yokohama et al[25]	−3.90 (−21.18 to 13.38)	Total	−6.67 (−19.62 to 6.28)
Total	−5.07 (−10.67 to 0.53)	p Value	0.31
p Value	0.08		

CI = confidence interval.

Table 3
Stratification of change in plaque volume according to low-density lipoprotein cholesterol levels at follow-up

Follow-up LDL Cholesterol Levels <100 mg/dl (n = 443)		Follow-up LDL Cholesterol Levels ≥100 mg/dl (n = 341)	
Study	WMD (95% CI)	Study	WMD (95% CI)
GAIN[21]	1.20 (−31.45 to 33.85)	Nishioka et al[23]	−4.60 (−13.01 to 3.81)
ESTABLISH[20]	−8.20 (−34.79 to 18.39)	Kawasaki et al[26] (pravastatin)	−1.60 (−23.18 to 19.98)
Jensen et al[22]	−3.70 (−16.63 to 9.23)	REVERSAL[28] (pravastatin)	5.10 (−14.85 to 25.05)
REVERSAL[28] (atorvastatin)	−0.50 (−20.07 to 19.07)	Tani et al[27]	−7.00 (−17.82 to 3.82)
Kawasaki et al[26] (atorvastatin)	−3.80 (−24.84 to 17.24)	Total	−4.22 (−10.27 to 1.82)
Petronio et al[24]	−30.00 (−47.18 to −12.82)	p Value	0.17
Yokohama et al[25]	−3.90 (−21.18 to 13.38)		
Total	−7.88 (−16.31 to 0.55)		
p Value	0.07		

Abbreviation as in Table 2.

vastatin vs 40 mg/day of pravastatin).[21] Kawasaki et al[19] compared 20 mg/day of atorvastatin with 20 mg/day of pravastatin with placebo. Petronio et al[17] compared 20 mg/day of simvastatin with placebo. Yokoyama et al[18] compared 10 mg/day of atorvastatin with placebo control. Nishioka et al[16] compared the administration of different statin regimens (10 mg/day of pravastatin, 10 mg/day of atorvastatin, 5 mg/day of simvastatin, or 20 mg/day of fluvastatin) with placebo control. Tani et al[20] compared 10 mg/day of pravastatin in patients whose LDL cholesterol level was <140 mg/dl with 20 mg/day in patients whose LDL cholesterol level was >140 mg/dl versus controls. Patients in an observational study by Jensen et al[15] received increasing doses of simvastatin to reach a LDL cholesterol level of <3.0 mmol/L.

Except for 2 studies,[13,16] all investigations excluded patients presenting with an acute coronary syndrome.

Figure 1 shows WMD in plaque volume between follow-up and baseline with respective 95% confidence intervals at a mean follow-up of 9.8 ± 4.9 months. There was a significant decrease in coronary plaque volume over time (WMD −5.77 mm^3, 95% confidence interval −10.36 to −1.17, p = 0.01), with no significant heterogeneity between studies (p = 0.47).

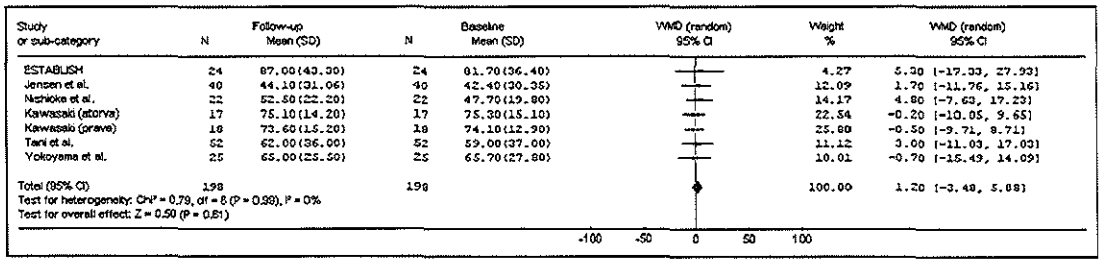

Figure 2. WMD with 95% confidence interval of difference in lumen volume between follow-up and baseline in the statin arm of the included studies. Abbreviation as in Figure 1.

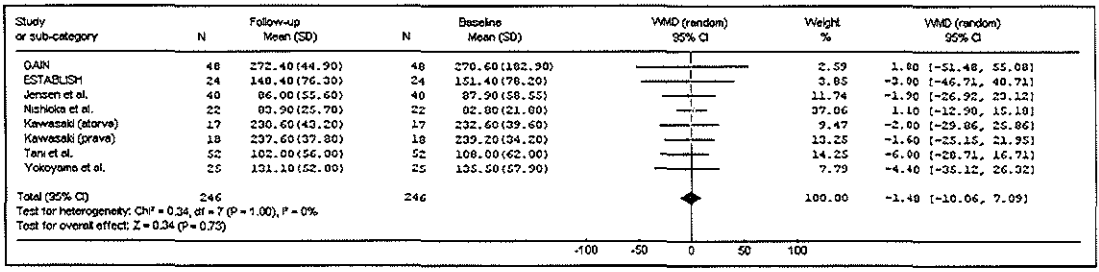

Figure 3. WMD with 95% confidence interval of difference in vessel volume between follow-up and baseline in the statin arm of the included studies. Abbreviation as in Figure 1.

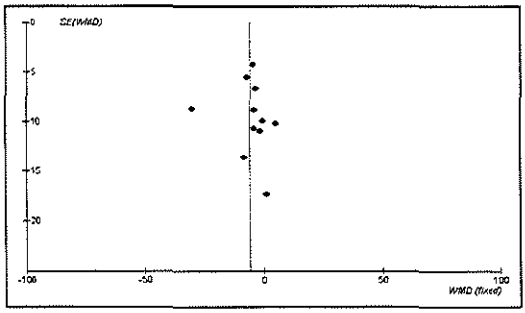

Figure 4. Funnel plot shows no asymmetry, so there is no publication bias present in the meta-analysis.

According to prespecified subgroup analyses evaluating studies according to length of follow-up (Table 2), similar trends were noted in studies with a 6-month follow-up and in studies with longer follow-up, although significant plaque regression did not occur, possibly due to a smaller sample. No significant heterogeneity ($p = 1.00$) between studies was found for the former subgroup analysis, whereas a significant heterogeneity between studies was present for the latter ($p = 0.06$).

Studies in which the achieved LDL cholesterol level was <100 mg/dl showed a strong trend for plaque regression. Conversely, studies in which the achieved LDL cholesterol level was >100 mg/dl showed that the trend toward plaque regression (Table 3) was less evident. Also, in these subgroup analyses, no significant heterogeneity between studies ($p = 0.23$ and 0.76, respectively) was noted.

After a mean follow-up of 7.7 ± 2.9 months, plaque volume remained substantially unchanged when evaluating control groups not receiving statin therapy (7 groups, 206 patients, WMD 0.13 mm^3, 95% confidence interval −4.42 to 4.68, $p = 0.96$), with no heterogeneity between studies ($p = 0.83$).

Figures 2 and 3 show WMD between follow-up and baseline in lumen and vessel volume, respectively, in patients receiving statin therapy. There was no significant change in coronary lumen volume or vessel volume over time. The funnel plot showed no evidence of publication bias (Figure 4).

Discussion

In the present systematic overview, statins were found to promote significant coronary plaque regression as assessed by IVUS. Nine studies and 11 statin arms were included in this meta-analysis in which, after a follow-up of approximately 10 months, a significant regression of coronary atherosclerotic plaque volume was evident. Our data are further supported by the substantial statistical homogeneity across the included studies.

Atherosclerotic plaque regression after onset of an intensive statin therapy strategy has been previously reported in the peripheral circulation.[22–24] Mechanisms involved in such a process are still not fully elucidated, having been ascribed thus far to changes in LDL and high-density lipoprotein cholesterol.[11,22,25] It has been suggested that, by decreasing the lipid content of plaques

and promoting a shift toward a more stable phenotype, statins may induce a "plaque stabilization" effect. Three studies included in the present meta-analysis found significant differences in surrogates of plaque composition despite no significant changes in plaque volume.[14,18,19] Further, statins have been found to decrease the inflammatory burden of plaques and to improve endothelial function.[26–28]

It is likely therefore that the antiatherosclerotic effect of statins is pleomorphic and effective against the 2 major mechanisms of atherosclerotic plaque progression.

The results of our meta-analysis are indirectly further reinforced by a lack of regression in patients assigned to placebo. In these patients, no substantial modification of plaque volume was noted over time.

Although IVUS is a highly accurate tool to measure changes in the vessel wall, factors such as intra- and interobserver variabilities, severely calcified vessels, and artifacts can impair the reproducibility of serial measurements.[29,30] It is therefore important to establish new standards regarding the acquisition, analysis, and reporting of IVUS clinical studies.

This meta-analysis was not based on individual data. Further, only 1 vessel was interrogated with IVUS and thus may not be representative of the total burden of the entire coronary tree. Although no significant heterogeneity was present across studies, bias adjudicated to small trials cannot be fully disregarded. Moreover, minor differences regarding IVUS methodology might have influenced our findings.

1. Biondi-Zoccai GG, Agostoni P, Abbate A, Testa L, Burzotta F. A simple hint to improve Robinson and Dickersin's highly sensitive PubMed search strategy for controlled clinical trials. *Int J Epidemiol* 2005;34:224–225.
2. 4.2. Review Manager. The Cochrane Collaboration. Available at: *http://www.cochrane.org*. Accessed November 29, 2004.
3. Clarke MOA. Cochrane reviewer's handbook 4.2.0. Updated March 2003. *Cochrane Database Syst Rev* 2003:2.
4. Takagi T, Yoshida K, Akasaka T, Hozumi T, Morioka S, Yoshikawa J. Intravascular ultrasound analysis of reduction in progression of coronary narrowing by treatment with pravastatin. *Am J Cardiol* 1997; 79:1673–1676.
5. von Birgelen C, Hartmann M, Mintz GS, Baumgart D, Schmermund A, Erbel R. Relation between progression and regression of atherosclerotic left main coronary artery disease and serum cholesterol levels as assessed with serial long-term (≥12 months) follow-up intravascular ultrasound. *Circulation* 2003;108:2757–2762.
6. Hagenaars T, Gussenhoven EJ, Kranendonk SE, Blankensteijn JD, Honkoop J, van der Linden E, van der Lugt A. Early experience with intravascular ultrasound in evaluating the effect of statins on femoropopliteal arterial disease: hypothesis-generating observations in humans. *Cardiovasc Drugs Ther* 2000;14:635–641.
7. Fang JC, Kinlay S, Beltrame J, Hikiti H, Wainstein M, Behrendt D, Suh J, Frei B, Mudge GH, Selwyn AP, Ganz P. Effect of vitamins C and E on progression of transplant-associated arteriosclerosis: a randomised trial. *Lancet* 2002;359:1108–1113.
8. Kapadia SR, Nissen SE, Ziada KM, Rincon G, Crowe TD, Boparai N, Young JB, Tuzcu EM. Impact of lipid abnormalities in development and progression of transplant coronary disease: a serial intravascular ultrasound study. *J Am Coll Cardiol* 2001;38:206–213.
9. Matsuzaki M, Hiramori K, Imaizumi T, Kitabatake A, Hishida H, Nomura M, Fujii T, Sakuma I, Fukami K, Honda T, et al. Intravascular ultrasound evaluation of coronary plaque regression by low density lipoprotein-apheresis in familial hypercholesterolemia: the Low Density Lipoprotein-Apheresis Coronary Morphology and Reserve Trial (LACMART). *J Am Coll Cardiol* 2002;40:220–227.
10. Nissen SE, Tuzcu EM, Libby P, Thompson PD, Ghali M, Garza D, Berman L, Shi H, Buebendorf E, Topol EJ. Effect of antihypertensive agents on cardiovascular events in patients with coronary disease and normal blood pressure: the CAMELOT study: a randomized controlled trial. *JAMA* 2004;292:2217–2225.
11. Nissen SE, Tsunoda T, Tuzcu EM, Schoenhagen P, Cooper CJ, Yasin M, Eaton GM, Lauer MA, Sheldon WS, Grines CL, et al. Effect of recombinant ApoA-I Milano on coronary atherosclerosis in patients with acute coronary syndromes: a randomized controlled trial. *JAMA* 2003;290:2292–2300.
12. Tardif JC, Gregoire J, L'Allier PL, Anderson TJ, Bertrand O, Reeves F, Title LM, Alfonso F, Schampaert E, Hassan A, et al. Effects of the acyl coenzyme A: cholesterol acyltransferase inhibitor avasimibe on human atherosclerotic lesions. *Circulation* 2004; 110:3372–3377.
13. Okazaki S, Yokoyama T, Miyauchi K, Shimada K, Kurata T, Sato H, Daida H. Early statin treatment in patients with acute coronary syndrome: demonstration of the beneficial effect on atherosclerotic lesions by serial volumetric intravascular ultrasound analysis during half a year after coronary event: the ESTABLISH Study. *Circulation* 2004; 110:1061–1068.
14. Schartl M, Bocksch W, Koschyk DH, Voelker W, Karsch KR, Kreuzer J, Hausmann D, Beckmann S, Gross M. Use of intravascular ultrasound to compare effects of different strategies of lipid-lowering therapy on plaque volume and composition in patients with coronary artery disease. *Circulation* 2001;104:387–392.
15. Jensen LO, Thayssen P, Pedersen KE, Stender S, Haghfelt T. Regression of coronary atherosclerosis by simvastatin: a serial intravascular ultrasound study. *Circulation* 2004;110:265–270.
16. Nishioka H, Shimada K, Kataoka T, Hirose M, Asawa K, Hasegawa T, Yamashita H, Ehara S, Kamimori K, Sakamoto T, et al. Impact of HMG-CoA reductase inhibitors for non-treated coronary segments. *Osaka City Med J* 2004;50:61–68.
17. Petronio AS, Amoroso G, Limbruno U, Papini B, De Carlo M, Micheli A, Ciabatti N, Mariani M. Simvastatin does not inhibit intimal hyperplasia and restenosis but promotes plaque regression in normocholesterolemic patients undergoing coronary stenting: a randomized study with intravascular ultrasound. *Am Heart J* 2005; 149:520–526.
18. Yokoyama M, Komiyama N, Courtney BK, Nakayama T, Namikawa S, Kuriyama N, Koizumi T, Nameki M, Fitzgerald PJ, Komuro I. Plasma low-density lipoprotein reduction and structural effects on coronary atherosclerotic plaques by atorvastatin as clinically assessed with intravascular ultrasound radio-frequency signal analysis: a randomized prospective study. *Am Heart J* 2005;150(2): e1–e287.
19. Kawasaki M, Sano K, Okubo M, Yokoyama H, Ito Y, Murata I, Tsuchiya K, Minatoguchi S, Zhou X, Fujita H, Fujiwara H. Volumetric quantitative analysis of tissue characteristics of coronary plaques after statin therapy using three-dimensional integrated backscatter intravascular ultrasound. *J Am Coll Cardiol* 2005;45: 1946–1953.
20. Tani S, Watanabe I, Anazawa T, Kawamata H, Tachibana E, Furukawa K, Sato Y, Nagao K, Kanmatsuse K, Kushiro T, Surugadai Atherosclerosis Regression Investigators. Effect of pravastatin on malondialdehyde-modified low-density lipoprotein levels and coronary plaque regression as determined by three-dimensional intravascular ultrasound. *Am J Cardiol* 2005;96:1089–1094.
21. Nissen SE, Tuzcu EM, Schoenhagen P, Brown BG, Ganz P, Vogel RA, Crowe T, Howard G, Cooper CJ, Brodie B, et al. Effect of intensive compared with moderate lipid-lowering therapy on progression of coronary atherosclerosis: a randomized controlled trial. *JAMA* 2004;291:1071–1080.
22. Lima JA, Desai MY, Steen H, Warren WP, Gautam S, Lai S. Statin-induced cholesterol lowering and plaque regression after 6 months of magnetic resonance imaging-monitored therapy. *Circulation* 2004;110: 2336–2341.
23. Corti R, Fuster V, Fayad ZA, Worthley SG, Helft G, Chaplin WF, Muntwyler J, Viles-Gonzalez JF, Weinberger J, Smith DA, et al. Effects of aggressive versus conventional lipid-lowering therapy by simvastatin on human atherosclerotic lesions: a prospective, randomized, double-blind trial with high-resolution magnetic resonance imaging. *J Am Coll Cardiol* 2005;46:106–112.

24. Yonemura A, Momiyama Y, Fayad ZA, Ayaori M, Ohmori R, Higashi K, Kihara T, Sawada S, Iwamoto N, Ogura M, et al. Effect of lipid-lowering therapy with atorvastatin on atherosclerotic aortic plaques detected by noninvasive magnetic resonance imaging. *J Am Coll Cardiol* 2005;45:733–742.
25. Nolting PR, de Groot E, Zwinderman AH, Buirma RJ, Trip MD, Kastelein JJ. Regression of carotid and femoral artery intima-media thickness in familial hypercholesterolemia: treatment with simvastatin. *Arch Intern Med* 2003;163:1837–1841.
26. Toutouzas K, Vaina S, Tsiamis E, Vavuranakis M, Mitropoulos J, Bosinakou E, Toutouzas P, Stefanadis C. Detection of increased temperature of the culprit lesion after recent myocardial infarction: the favorable effect of statins. *Am Heart J* 2004;148:783–788.
27. Furman C, Copin C, Kandoussi M, Davidson R, Moreau M, McTaggiart F, Chapman MJ, Fruchart JC, Rouis M. Rosuvastatin reduces MMP-7 secretion by human monocyte-derived macrophages: potential relevance to atherosclerotic plaque stability. *Atherosclerosis* 2004;174:93–98.
28. Landmesser U, Bahlmann F, Mueller M, Spiekermann S, Kirchhoff N, Schulz S, Manes C, Fischer D, de Groot K, Fliser D, et al. Simvastatin versus ezetimibe: pleiotropic and lipid-lowering effects on endothelial function in humans. *Circulation* 2005;111:2356–2363.
29. Hagenaars T, Gussenhoven EJ, van Essen JA, Seelen J, Honkoop J, van der Lugt A. Reproducibility of volumetric quantification in intravascular ultrasound images. *Ultrasound Med Biol* 2000;26:367–374.
30. Gaster AL, Korsholm L, Thayssen P, Pedersen KE, Haghfelt TH. Reproducibility of intravascular ultrasound and intracoronary Doppler measurements. *Catheter Cardiovasc Interv* 2001;53:449–458.

CHAPTER 9.4

Long-term effect of perindopril on coronary atherosclerosis progression (from the perindopril's prospective effect on coronary atherosclerosis by angiography and intravascular ultrasound evaluation [PERSPECTIVE] study).

Rodriguez-Granillo GA, Vos J, Bruining N, **Garcia-Garcia HM**, de Winter S, Ligthart J, Deckers J, Bertrand M, Simoons ML, Ferrari R, Fox KM, Remme W, de Feyter P on behalf of the Investigators of the EUROPA study.

Am J Cardiol. 2007;100:159-63.

Long-Term Effect of *Perindopril* on Coronary Atherosclerosis Progression (from the PERindopril's Prospective Effect on Coronary aTherosclerosis by Angiography and IntraVascular Ultrasound Evaluation [PERSPECTIVE] Study)

Gastón A. Rodriguez-Granillo, MD, PhD[a], Jeroen Vos, MD[c], Nico Bruining, PhD[a], Hector M. Garcia-Garcia, MD, MSc[a], Sebastiaan de Winter, BSc[a], Jurgen M.R. Ligthart, BSc[a], Jaap W. Deckers, MD, PhD[a], Michel Bertrand, MD[d], Maarten L. Simoons, MD[a], Roberto Ferrari, MD[e], Kim M. Fox, MD[f], Willem Remme, MD[b], and Pim J. De Feyter, MD[a,*], on behalf of the Investigators of the EUROPA Study

The multicenter EUROPA trial of 12,218 patients showed that perindopril decreased adverse clinical events in patients with established coronary heart disease. The PERSPECTIVE study, a substudy of the EUROPA trial, evaluated the effect of perindopril on coronary plaque progression as assessed by quantitative coronary angiography and intravascular ultrasound (IVUS). In total 244 patients (mean age 57 years, 81% men) were included. Evaluable paired quantitative coronary angiograms were obtained from 96 patients randomized to perindopril and from 98 patients to placebo. Concomitant treatment at baseline consisted of aspirin (90%), lipid-lowering agents (70%), and β blockers (60%). The primary and secondary end point was the difference of minimum and mean lumen diameters (quantitative coronary angiography) or mean plaque cross-sectional area (IVUS) measured at baseline and 3-year follow-up between the perindopril and placebo groups. After a median follow-up of 3.0 years (range 1.9 to 4.1), no differences in change in quantitative coronary angiographic or IVUS measurements were detected between the perindopril and placebo groups (minimum and mean luminal diameters -0.07 ± 0.4 vs -0.02 ± 0.4 mm, $p = 0.34$; mean luminal diameter -0.05 ± 0.2 vs -0.05 ± 0.3 mm, $p = 0.89$; mean plaque cross-sectional area -0.18 ± 1.2 vs -0.02 ± 1.2 mm^2, $p = 0.48$). In conclusion, we found no progression in coronary artery disease by quantitative coronary angiography and IVUS with long-term administration of perindopril or placebo, possibly because most patients were on concomitant treatment with a statin. (Am J Cardiol 2007;100:159–163)

Several preclinical and clinical studies have shown that angiotensin-converting enzyme (ACE) inhibitors exert an antiatherosclerotic effect.[1–6] Recent studies have shown that overall ACE inhibitors decrease adverse cardiovascular events.[7–12] No data are available of the efficacy of ACE inhibitors on progression of coronary atherosclerosis. The purpose of the PERindopril's Prospective Effect on Coronary aTherosclerosis by IntraVascular ultrasound Evaluation (PERSPECTIVE), a substudy of the EUROPA trial, was to evaluate the effect of long-term administration of perindopril on coronary plaque size as assessed by quantitative coronary angiography and intracoronary ultrasound (IVUS).

Methods

The EUROPA trial evaluated the effect of ACE inhibitor perindopril on the prevention of cardiovascular events in 12,218 patients with stable coronary artery disease. The methods of the EUROPA trial has been extensively described elsewhere.[8] In the run-in period, enrolled patients received oral perindopril 4 mg/day for 2 weeks in addition to their normal medication, followed by 8 mg/day for 2 weeks if the initial dose was tolerated. At the end of the run-in period, patients were randomly assigned to perindopril 8 mg/day or placebo for ≥3 years. The efficacy outcome was the combined end point of cardiovascular mortality, nonfatal myocardial infarction, and cardiac arrest with successful resuscitation.

Patients included in the main EUROPA trial in whom a coronary angiogram was indicated were eligible for the PERSPECTIVE study. In addition to EUROPA's inclusion

[a]Department of Cardiology, Thoraxcenter, Erasmus MC, and [b]Stichares Cardiovascular Research Foundation, Rotterdam, and [c]Amphia Ziekenhuis, Locatie Molengracht, Breda, The Netherlands; [d]Lille Heart Institute, Lille, France; [e]University of Ferrara and Cardiovascular Pathophysiology Research Centre, Salvatore Maugeri Foundation, IRCCS, Gussago (Brescia), Italy; and [f]Cardiology Department, National Heart and Lung Institute and Royal Brompton Hospital, London, United Kingdom. Manuscript received December 12, 2006; revised manuscript received and accepted February 22, 2007.

This study was supported by Servier, France. Drs. Fox and Simoons were supported by Servier, Paris, France.

*Corresponding author: Tel: 31-10-463-5071; fax: 31-10-463-2686.
E-mail address: p.j.defeyter@erasmusmc.nl (P.J. De Feyter).

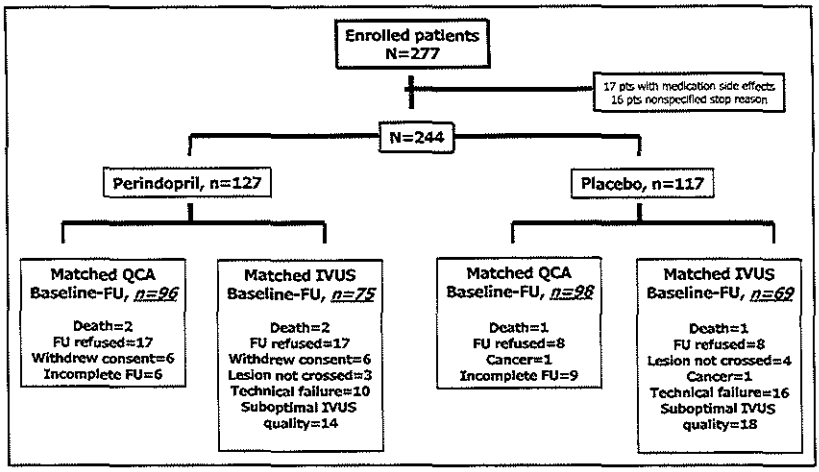

Figure 1. Flowchart of the PERSPECTIVE study. FU = follow-up; pts = patients; QCA = quantitative coronary angiogram.

and exclusion criteria, vessels anatomically suitable for the quantitative coronary angiographic/IVUS substudy were required.

Institutional ethics committees of all participating centers approved the study protocol and informed written consent was obtained from all patients.

Coronary angiograms were obtained at baseline before medication was started and at follow-up after ≥3 years. At least 3 orthogonal projections of the region of interest were filmed at baseline, and the same projections were repeated at follow-up. Quantitative coronary angiographic analysis was performed by an independent core laboratory (Cardialysis BV, Rotterdam, The Netherlands) as previously described with a validated computer-based edge-detection system (CAAS II, Pie Medical, Maastricht, The Netherlands).[13] The catheter tip was cleared of contrast for accurate calibration. Interpolated reference diameter, minimal lumen diameter, mean lumen diameter, and diameter stenosis were measured at the 2 time points using the "worst" view of an end-diastolic frame.

A noninfarct–related or percutaneously treated vessel was selected for investigation.

IVUS was acquired using 20-, 30-, or 40-MHz imaging catheters after coronary angiography. The catheter was advanced distally to an anatomically identifiable landmark allow evaluation of a segment of ≥30 mm. Cine runs before and during contrast injection were performed to define the position of the IVUS catheter before pullback was started. Using an automated pullback device, the transducer was withdrawn at a continuous speed of 0.5 mm/s until the ostium. IVUS data were acquired after intracoronary administration of nitroglycerin and stored on S-VHS videotape. At follow-up angiography, patients underwent repeat IVUS examination of the same region of interest by using an identical IVUS imaging catheter.

Quantitative coronary ultrasound analysis was performed by an independent core laboratory (Cardialysis BV) using validated semiautomatic contour detection software (Curad 3.1, Wijk bij Duurstede, The Netherlands). The IntelliGate image-based gating method was applied to eliminate motion artifacts by retrospectively selecting end-diastolic frames.[14] Cross-sectional areas of the lumen and vessel (defined as the external elastic membrane) were calculated for each cross-sectional image. Contours of the vessel and lumen-intima interface enclosed an area that was defined as the coronary plaque-plus-media area. On the baseline IVUS study a region of interest was identified using landmarks such as side branches and the coronary ostium. At follow-up, the same region of interest was identified using the same landmarks.

The primary end point was the difference in change of minimum and mean lumen diameters (quantitative coronary angiography) measured at baseline and 3-year follow-up between the perindopril and placebo groups. Prespecified secondary end points were the difference in change of mean plaque cross-sectional area (square millimeters) and of plaque volume (cubic millimeters) as measured by IVUS at baseline and at follow-up between groups. Development of new lesions (≥20% decrease in minimum lumen diameter) was another prespecified secondary end point.

Discrete variables were presented as counts and percentages or as medians (interquartile ranges) when indicated. Continuous variables were presented as means ± SDs.

Based on a previous quantitative coronary angiographic progression/regression trial,[15] we calculated a sample of 99 paired subjects to achieve a power of 80%, considering a type I error probability of 0.05 (2-sided), a difference (between groups) in minimum lumen diameter of 0.08, and a within-group SD of 0.20. In this calculation a drop-out rate of 15% nonanalyzable patients was included. Differences between groups were assessed by paired and unpaired Student's *t* test when applicable. For comparison between categorical variables, chi-square test was used. A 2-sided p value <0.05 was required for statistical significance. All analyses were performed using SAS 6.12 (SAS Institute, Cary, North Carolina).

Table 1
Baseline characteristics of population

	Perindopril (n = 96)	Placebo (n = 98)	Difference	95% CI	EUROPA (overall) (n = 12,218)
Variables					
Age (yrs)	57.5 ± 9.3	56.1 ± 9.0	1.3	−1.3 to 3.9	60 ± 9
Men	77 (80)	80 (82)	−1.4	−13 to 9.6	10,439 (86)
Diabetes mellitus	8 (8.3)	8 (8.2)	0.2	−7.6 to 7.9	1,502 (13)
Hypertension*	19 (20)	24 (25)	−4.7	−17 to 7.0	3,312 (27)
Smoker	24 (25)	22 (23)	2.6	−9.4 to 15	1,869 (16)
Hypercholesterolemia†	75 (78)	79 (81)	−2.5	−14 to 8.9	7,737 (63)
Peripheral vascular disease	2 (2.1)	4 (4.1)	−2.0	−6.8 to 2.9	883 (7.2)
Previous myocardial infarction	44 (46)	53 (54)	−8.2	−23 to 5.8	7,910 (65)
Previous percutaneous coronary intervention	83 (87)	92 (94)	−7.4	−16 to 0.9	3,573 (30)
Previous coronary artery bypass grafts	1 (1.0)		1.0	−1.0 to 3.1	3,587 (30)
Systolic blood pressure (mm Hg)	133 ± 16.0	13.1 ± 14	1.5	−2.7 to 5.8	137 (15)
Diastolic blood pressure (mm Hg)	80.0 ± 7.6	81 ± 12	1.8	−0.3 to 4.0	82 (8)
Weight (kg)	79 ± 12	81	−2.6	−5.9 to 0.8	82 (12)
Heart rate	70 ± 11	67 ± 7.8	3	0.4–5.8	68 (10)
Anginal status (CCS class)					
I	82 (86)	81 (83)	2.8	−7.5 to 13	NA (81)
II	12 (13)	15 (16)	−2.8	−13 to 6.9	NA (17)
III	2 (2.1)	2 (2.0)	0.0	−4.0 to 4.0	NA (2)
IV	0 (0.0)	0 (0.0)	0.0	0.0–0.0	
Other medications					
Platelet inhibitors	92 (96)	96 (98)	−2.1	−7.0 to 2.8	11,278 (93)
β Blockers	55 (58)	62 (64)	−6.0	20–7.8	7,535 (62)
Nitrates	39 (31)	20 (17)	14.9	3.3–27	5,242 (43)
Calcium channel blockers	52 (41)	41 (35)	6.9	−6.6 to 21	3,826 (32)
Lipid-lowering agents	93 (73)	86 (74)	−5.7	−18 to 6.5	7,033 (58)
At follow-up					
Systolic blood pressure (mm Hg)	131 ± 18	134 ± 15	−2.7	−7.3 to 1.9	NA
Change in systolic pressure (mm Hg)	−1.9 ± 18	2.8 ± 15	−4.7	−9.2 to 0.3	NA
Diastolic blood pressure (mm Hg)	76 ± 8.1	78 ± 8.5	−1.9	−4.2 to 0.4	NA
Change in diastolic pressure (mm Hg)	−3.4 ± 9.2	−0.3 ± 9.2	−3.2	−5.7 to 0.6	NA

Values are means ± SDs or numbers of patients (percentages).
* Blood pressure >160/95 mm Hg or antihypertension treatment.
† Cholesterol level >6.5 mmol/L or lipid-lowering therapy.
CI = confidence interval; CCS = Canadian Cardiovascular Society; NA = not available.

Results

Of 244 patients who were included in PERSPECTIVE and received randomized treatment, 194 had complete matched baseline and follow-up angiograms. Reasons for incomplete angiographic follow-up are presented in Figure 1. Baseline characteristics of the study population are presented in Table 1. Coronary risk factors and baseline blood pressure were well balanced, showing no significant differences between groups. At baseline and during the study period, >70% of patients received lipid-lowering treatment, >95% received platelet inhibitors, and ~60% were on β-blocker treatment.

At a median follow-up of 3.4 years (range 1.5 to 4.3), the rate of cardiac death, myocardial infarction, and cardiac resuscitation was not statistically different between the perindopril and placebo groups (6, 6.2%, vs 7, 7.1%) and slightly lower than the event rate reported in the EUROPA trial (8.0% vs 9.9%) at 4.2 years of follow-up. Follow-up angiography was performed after a median of 3.0 years (range 1.9 to 4.1). No significant changes were apparent in reference diameter, minimal lumen diameter, or diameter stenosis (Table 2). Differences in minimum and mean lumen diameters between baseline and follow-up in the perindopril group did not differ from that observed in the placebo group. There was no difference in the occurrence of new lesions between groups. In total 144 matched evaluable IVUS images were available at follow-up. Thirty-two patients were excluded due to suboptimal IVUS quality (caused by severely calcified vessels, severe image artifacts, or absence of clear anatomic landmarks). No significant differences were apparent over time in vessel area, plaque area, or plaque volume between groups (Table 3).

Discussion

Patients studied in the PERSPECTIVE substudy were stable, with a low adverse event rate of ~2% per year. They received intensive background pharmacologic treatment with aspirin and statins throughout the study to achieve a total cholesterol level of 4.8 mmol/L and a low-density lipoprotein cholesterol level of 2.8 mmol/L. They were normotensive, with mean systolic and diastolic blood pressures of 132 ± 8 and 77 ± 88 mm Hg, respectively. The PERSPECTIVE substudy demonstrated no beneficial effect on progression of atherosclerosis during 3.5 years of treat-

Table 2
Quantitative coronary angiographic results

Variable	Perindopril (n = 96)	Placebo (n = 98)
Length (mm)		
Baseline	32 ± 17	32 ± 15
Follow-up	31 ± 16	31 ± 14
Nominal change	−0.72 ± 3	−0.36 ± 3
Reference diameter (mm)		
Baseline	3.09 ± 0.6	2.96 ± 0.6
Follow-up	3.04 ± 0.7	2.93 ± 0.6
Nominal change	−0.05 ± 0.4	−0.03 ± 0.3
Minimal lumen diameter (mm)		
Baseline	2.19 ± 0.5	2.14 ± 0.7
Follow-up	2.11 ± 0.6	2.13 ± 0.6
Nominal change	−0.07 ± 0.4	−0.02 ± 0.4
Mean lumen diameter (mm)		
Baseline	2.92 ± 0.5	2.88 ± 0.6
Follow-up	2.87 ± 0.5	2.83 ± 0.6
Nominal change	−0.05 ± 0.2	−0.05 ± 0.3
Diameter stenosis (%)		
Baseline	29 ± 13	28 ± 15
Follow-up	29 ± 17	27 ± 15
Nominal change	0.42 ± 12	−0.56 ± 13
Development of new lesions (%)*	12 (12.5)	7 (7.1)

* At least 20% decrease in minimal lumen diameter.

Table 3
Intravascular ultrasound results

Mean Cross-Sectional Area (mm^2)	Perindopril (n = 75)	Placebo (n = 69)
Length (mm)		
Baseline	31 ± 14	31 ± 15
Follow-up	31 ± 14	31 ± 15
Vessel		
Baseline	15.5 ± 4.5	15.8 ± 4.7
Follow-up	15.3 ± 4.4	15.9 ± 4.6
Nominal change	−0.2 ± 2.0	0.1 ± 1.7
Lumen		
Baseline	9.1 ± 3.3	9.6 ± 3.9
Follow-up	9.1 ± 3.3	9.8 ± 4.1
Nominal change	0.1 ± 1.5	0.2 ± 1.7
Plaque		
Baseline	6.4 ± 2.7	6.2 ± 2.3
Follow-up	6.2 ± 2.6	6.1 ± 2.5
Nominal change	−0.2 ± 1.6	−0.1 ± 1.2
Plaque volume (mm^3)		
Baseline	192 ± 115	190 ± 108
Follow-up	190 ± 114	186 ± 105
Nominal change	−2 ± 55	−4 ± 37

ment with perindopril versus placebo as assessed with quantitative coronary angiography and intracoronary ultrasound. There are several reasons to explain the lack of effect of perindopril on coronary plaque size in our substudy. First, it is noteworthy that there was no progression of atherosclerosis in the placebo and perindopril groups of whom >70% had received statin therapy before and during the study. This is in keeping with previous studies demonstrating no progression of coronary artery disease as assessed by quantitative coronary angiography or intracoronary ultrasound in patients with intensive lipid-lowering treatment.[15–17] Because there was no progression of disease in the 2 groups, we could not demonstrate an effect of perindopril on plaque size because a potential effect would have become evident only if perindopril had induced regression of plaque size. Thus far, plaque regression has been shown to decrease only by aggressive lipid-lowering treatment after intensive treatment with statins.[18] Second, the number of patients studied in the PERSPECTIVE substudy was lower than anticipated to demonstrate an effect of perindopril. We had calculated a sample of 99 paired subjects based on an SD of 0.2 mm in the quantitative coronary angiographic measurements, but the actual SD in the study was 0.5 mm, which would require an even larger sample to demonstrate an effect; in addition, a rather large proportion of patients was excluded from analysis due to poor image quality.

Third, we cannot exclude the possibility that perindopril induced a change in the histologic composition of the plaque, which was not assessed in this study. However, it appears more likely that the beneficial clinical effect of perindopril found in the EUROPA study was related to an improvement in endothelial function and the effect that may have had on plaque stability rather than on absolute plaque size. This latter effect will be addressed in 2 separate substudies of the EUROPA trial.[19,20] Fourth, another mechanism may have played a role in which perindopril decreased cardiovascular events and could not be detected by IVUS. Fifth, it may be speculated that perindopril has no effect on coronary plaques compared with a beneficial effect of ACE inhibitors on carotid plaques shown in the Study to Evaluate Carotid Ultrasound Changes in Patients Treated With Ramipril and Vitamin E (SECURE) study.[11] However, other reasons may also explain difference in outcome between these 2 studies. In the PERSPECTIVE study, the follow-up period was shorter, the population was at lower risk (adverse events rate 6% vs 14%), and intensive lipid-lowering medical therapy was more frequent than in the SECURE study.

The present study has a number of limitations. A substantial number of patients was excluded from IVUS analysis due to suboptimal image quality and severe calcification precluding accurate plaque size assessment. This resulted in a rather small study sample. Larger studies may be required, using IVUS as a primary end point, to conclusively determine the efficacy of ACE inhibitors on progression of atherosclerosis. Different IVUS catheters with different specifications were used over a 3-year period, which may have induced small variations in measurements and thus may have obscured potential subtle changes in plaque measurements, although measurements obtained with the various 30-MHz catheters were adjusted according to a previously reported mathematical algorithm.[21]

Appendix

List of primary investigators in the PERSPECTIVE substudy: BELGIUM: Prof. W. van Mieghem, Ziekenhuis Oost Limburg, Genk; Dr. P.H.F. Materne, CHR de la Citadelle, Liège; Prod. V. Legrand, CHU Sart Tilman, Liège; Dr. G.R. Heyndrickx, Onze Lieve Vrouwe Ziekenhuis, Aalst.

GERMANY: Prof. R. Simon, Klinik für Kardiologie, Kiel; Prof. Dr. W. Rutsch, Klinik Charité der Humboldt Universitat, Berlin; Dr. B.R. Winkelmann, Herzzentrum Ludwigshafen, Ludwigshafen.

SPAIN: Prof. C. Macaya, Hospital Clinico San Carlos, Madrid; Dr. A.R. Cequier, Hospital de Bellvitge, Barcelona; Dr. J.M. Augé, Hospital de Sant Pau, Barcelona; Dr. R. Bros Caimari, Ciutat Sanitaria de Bellvitge, Barcelona.

FRANCE: Prof. J.P. Bassand, Hopital Jean Minjoz, Besancon. GREECE: Dr. V. Voudris, Onassis Cardiac Surgery Center, Athens.

PORTUGAL: Prof. R. Seabra-Gomes, Instituto Do, Linda-A-Velha.

SWITZERLAND: Dr. M. Pieper, Herzzentrum Bodensee, Kreuzlingen.

THE NETHERLANDS: Dr. F. Kiemeneij, Onze Lieve Vrouwe Gasthuis, Amsterdam; Dr. M.J. Suttorp, Sint Antonius Ziekenhuis, Nieuwegein; Prof. J.J. Piek, Academisch Medisch Centrum, Amsterdam.

1. Hornig B, Kohler C, Drexler H. Role of bradykinin in mediating vascular effects of angiotensin-converting enzyme inhibitors in humans. *Circulation* 1997;95:1115–1118.
2. Candido R, Jandeleit-Dahm KA, Cao Z, Nesteroff SP, Burns WC, Twigg SM, Dilley RJ, Cooper ME, Allen TJ. Prevention of accelerated atherosclerosis by angiotensin-converting enzyme inhibition in diabetic apolipoprotein E–deficient mice. *Circulation* 2002;106:246–253.
3. Powell JS, Clozel JP, Muller RK, Kuhn H, Hefti F, Hosang M, Baumgartner HR. Inhibitors of angiotensin-converting enzyme prevent myointimal proliferation after vascular injury. *Science* 1989;245:186–188.
4. Hayek T, Hamoud S, Keidar S, Pavlotzky E, Coleman R, Aviram M, Kaplan M. Omapatrilat decreased macrophage oxidative status and atherosclerosis progression in atherosclerotic apolipoprotein E–deficient mice. *J Cardiovasc Pharmacol* 2004;43:140–147.
5. Lonn E, Yusuf S, Dzavik V, Doris C, Yi Q, Smith S, Moore-Cox A, Bosch J, Riley W, Teo K. Effects of ramipril and vitamin E on atherosclerosis: the study to evaluate carotid ultrasound changes in patients treated with ramipril and vitamin E (SECURE). *Circulation* 2001;103:919–925.
6. Hosomi N, Mizushige K, Ohyama H, Takahashi T, Kitadai M, Hatanaka Y, Matsuo H, Kohno M, Koziol JA. Angiotensin-converting enzyme inhibition with enalapril slows progressive intima-media thickening of the common carotid artery in patients with non–insulin-dependent diabetes mellitus. *Stroke* 2001;32:1539–1545.
7. Yusuf S, Sleight P, Pogue J, Bosch J, Davies R, Dagenais G. Effects of an angiotensin-converting-enzyme inhibitor, ramipril, on cardiovascular events in high-risk patients. The Heart Outcomes Prevention Evaluation Study Investigators. *N Engl J Med* 2000;342:145–153.
8. Fox KM. Efficacy of perindopril in reduction of cardiovascular events among patients with stable coronary artery disease: randomised, double-blind, placebo-controlled, multicentre trial (the EUROPA study). *Lancet* 2003;362:782–788.
9. Braunwald E, Domanski MJ, Fowler SE, Geller NL, Gersh BJ, Hsia J, Pfeffer MA, Rice MM, Rosenberg YD, Rouleau JL. Angiotensin-converting-enzyme inhibition in stable coronary artery disease. *N Engl J Med* 2004;351:2058–2068.
10. Naccarella F, Naccarelli GV, Maranga SS, Lepera G, Grippo MC, Melandri F, Gatti M, Pazzaglia S, Spinelli G, Angelini V, et al. Do ACE inhibitors or angiotensin II antagonists reduce total mortality and arrhythmic mortality? A critical review of controlled clinical trials. *Curr Opin Cardiol* 2002;17:6–18.
11. Garg R, Yusuf S. Overview of randomized trials of angiotensin-converting enzyme inhibitors on mortality and morbidity in patients with heart failure. Collaborative Group on ACE Inhibitor Trials. *JAMA* 1995;273:1450–1456.
12. Flather MD, Yusuf S, Kober L, Pfeffer M, Hall A, Murray G, Torp-Pedersen C, Ball S, Pogue J, Moye L, Braunwald E. Long-term ACE-inhibitor therapy in patients with heart failure or left-ventricular dysfunction: a systematic overview of data from individual patients. ACE-Inhibitor Myocardial Infarction Collaborative Group. *Lancet* 2000;355:1575–1581.
13. Reiber JH, Serruys PW, Kooijman CJ, Wijns W, Slager CJ, Gerbrands JJ, Schuurbiers JC, den Boer A, Hugenholtz PG. Assessment of short-, medium-, and long-term variations in arterial dimensions from computer-assisted quantitation of coronary cineangiograms. *Circulation* 1985;71:280–288.
14. De Winter SA, Hamers R, Degertekin M, Tanabe K, Lemos PA, Serruys PW, Roelandt JR, Bruining N. Retrospective image-based gating of intracoronary ultrasound images for improved quantitative analysis: the intelligate method. *Catheter Cardiovasc Interv* 2004;61:84–94.
15. Effect of simvastatin on coronary atheroma: the Multicentre Anti-Atheroma Study (MAAS). *Lancet* 1994;344:633–638.
16. Nissen SE, Tuzcu EM, Schoenhagen P, Brown BG, Ganz P, Vogel RA, Crowe T, Howard G, Cooper CJ, Brodie B, Grines CL, DeMaria AN. Effect of intensive compared with moderate lipid-lowering therapy on progression of coronary atherosclerosis: a randomized controlled trial. *JAMA* 2004;291:1071–1080.
17. Balk EM, Karas RH, Jordan HS, Kupelnick B, Chew P, Lau J. Effects of statins on vascular structure and function: a systematic review. *Am J Med* 2004;117:775–790.
18. Nissen SE, Nicholls SJ, Sipahi I, Libby P, Raichlen JS, Ballantyne CM, Davignon J, Erbel R, Fruchart JC, Tardif JC, et al. Effect of very high-intensity statin therapy on regression of coronary atherosclerosis: the ASTEROID trial. *JAMA* 2006;295:1556–1565.
19. The Scientific Committee of the PERTINENT Sub-Study on behalf of the EUROPA-PERTINENT Investigators. PERTINENT—perindopril-thrombosis, inflammation, endothelial dysfunction and neurohormonal activation trial: a sub-study of the EUROPA study. *Cardiovasc Drugs Ther* 2003;17:83–91.
20. Bots ML, Remme WJ, Luscher TF, Grobbee DE. PERindopril-Function of the Endothelium in Coronary Artery Disease Trial: the PERFECT study—sub study of EUROPA: rationale and design. *Cardiovasc Drugs Ther* 2002;16:227–236.
21. Bruining N, Hamers R, Teo TJ, de Feijter PJ, Serruys PW, Roelandt JR. Adjustment method for mechanical Boston scientific corporation 30 MHz intravascular ultrasound catheters connected to a Clearview console. Mechanical 30 MHz IVUS catheter adjustment. *Int J Cardiovasc Imaging* 2004;20:83–91.

CHAPTER 9.5

Effect of perindopril on coronary remodelling: insights from a multicentre, randomized study.

Rodriguez-Granillo GA, de Winter S, Bruining N, Ligthart J, **Garcia-Garcia HM**, Valgimigli M, de Feyter P on behalf of EUROPA/PERSPECTIVE Investigators.

Eur Heart J. 2007;28:2326-31.

Effect of perindopril on coronary remodelling: insights from a multicentre, randomized study

Gastón A. Rodriguez-Granillo[1,2]*, Sebastiaan de Winter[1], Nico Bruining[1], Jurgen M.R. Ligthart[1], Héctor M. García-García[1], Marco Valgimigli[1], and Pim J. de Feyter[1] on behalf of the EUROPA/PERSPECTIVE Investigators

[1]*Department of Interventional Cardiology, Thoraxcenter, Erasmus MC, Rotterdam, The Netherlands; and* [2]*Department of Cardiovascular Imaging, Otamendi Hospital, Azcuénaga 870, C1115AAB Buenos Aires, Argentina*

Received 8 February 2007; revised 3 May 2007; accepted 18 May 2007; online publish-ahead-of-print 31 August 2007

See page 2299 for the editorial comment on this article (doi:10.1093/eurheartj/ehm276)

KEYWORDS
ACE-inhibitor;
Progression;
Remodelling;
Atherosclerosis;
Regression;
EUROPA

Aims This study sought to evaluate the effect of perindopril in coronary remodelling.
Methods and results In this sub-study of a double-blind, multicentre trial, patients without clinical evidence of heart failure were randomized to perindopril 8 mg/day or placebo for at least 3 years and IVUS investigation was performed at both time-points. Positive and negative remodelling were defined as a relative increase (positive remodelling) or decrease (negative remodelling) of the mean vessel cross-sectional area (CSA) >2 SD of the mean intra-observer difference. A total of 118 matched evaluable IVUS (711 matched 5 mm segments) were available at follow-up. After a median follow-up of 3.0 (inter-quartile range 1.9, 4.1) years, there was no significant difference in the change of plaque CSA between perindopril (360 segments) and placebo (351 segments) groups, $P = 0.27$. Conversely, the change in vessel CSA was significantly different between groups (perindopril -0.18 ± 2.4 mm^2 vs. placebo 0.19 ± 2.4, $P = 0.04$). Negative remodelling occurred more frequently in the perindopril than in the placebo group (34 vs. 25%, $P = 0.01$). In addition, the placebo group showed a larger, although not significant, mean remodelling index (RI) than the perindopril group (1.03 ± 0.2 vs. 1.00 ± 0.2, $P = 0.06$). The temporal change in vessel dimensions assessed by the RI was significantly correlated with the change in plaque dimensions ($r = 0.48$, $P < 0.0001$).
Conclusion In this sub-analysis of a multicentre, controlled study, long-term administration of perindopril was associated with a constrictive remodelling pattern without affecting the lumen.

Introduction

By preventing encroachment of the lumen and hence coronary flow, outward (positive) remodelling of coronary vessels was initially regarded as beneficial.[1] Notwithstanding, several studies have shown increased levels of inflammatory markers, larger lipid cores and pronounced medial thinning in positive remodelled vessels; being all factors related to the tendency of plaques to undergo rupture.[2–5]

Angiotensin-converting enzyme (ACE) inhibitors have demonstrated their efficacy in reducing mortality in both high- and low-risk patients.[6,7] In parallel, ACE-inhibitors inhibit progressive left ventricular remodelling, a critical factor that determines life expentancy.[8,9] More recently, ACE-inhibitors have shown to be effective in reversing vascular remodelling in the peripheral circulation.[10,11]

Atherosclerosis is a highly dynamic and multifocal disease, and coronary remodelling occurs diffusely within a vessel, even in seemingly healthy references.[12] Accordingly, longitudinal studies have been recognized as the gold-standard for remodelling assessment.[13]

Driven by the significant regression of coronary atherosclerosis induced by lipid-lowering therapies,[14] the PERindopril's Prospective Effect on Coronary aTherosclerosis by IntraVascular ultrasound Evaluation (PERSPECTIVE) trial evaluated the effect of long-term administration of perindopril on coronary plaque progression as assessed by angiography and intravascular ultrasound (IVUS) and demonstrated that the clinical benefit of ACE-inhibitors cannot be attributed to their effect on plaque size.[15] We performed a *post hoc* analysis of the PERSPECTIVE study to assess the effect of perindopril in coronary remodelling. In addition, we evaluated the effect of perindopril on a surrogate of plaque composition.

Methods

The EUROPA was a multicentre, randomized, double-blind, placebo-controlled study that evaluated the effect of perindopril on prevention of cardiovascular events in patients with coronary artery disease on 12 218 patients. PERSPECTIVE was a sub-study of the EUROPA trial that sought to explore the effect of perindopril on atherosclerosis progression/regression using coronary angiography and IVUS.

* Corresponding author. Tel/fax: +54 11 49648721.
E-mail address: grodriguezgranillo@gmail.com

The methodology of the EUROPA trial has been extensively described elsewhere.[7] In brief, patients were eligible if they were aged ≥18 years, without clinical evidence of heart failure and with evidence of coronary heart disease documented by previous myocardial infarction (>3 months before screening), percutaneous or surgical coronary revascularization (>6 months before screening), or angiographic evidence of at least 70% narrowing of one or more major coronary arteries.

In addition, for the IVUS sub-analysis patients required anatomically suitable vessels for the angiography/IVUS sub-study.

In a run-in period, enrolled patients received 4 mg/day oral perindopril for 2 weeks in addition to their normal medication, followed by 8 mg/day for 2 weeks if the initial dose was tolerated. At the end of the run-in period, patients were randomly assigned to perindopril 8 mg/day or placebo for 3 years.

The institutional ethics committees of all participating centres approved the study protocol and informed written consent was obtained from all patients.

Intravascular ultrasound acquisition

IVUS was acquired using 20, 30, and 40 MHz imaging catheters following coronary angiography. The catheter was advanced distal to an anatomically identifiable landmark, allowing the evaluation of a segment of at least 30 mm. Cine runs, before and during contrast injection, were performed to define the position of the IVUS catheter before the pullback was started. Using an automated pullback device, the transducer was withdrawn at a continuous speed of 0.5 mm/s until the ostium. IVUS data were acquired after the intracoronary administration of nitroglycerin and stored on S-VHS videotape. The videotapes were digitized on a computer system, transformed into the DICOM medical image standard and stored on an IVUS Picture Archiving and Communications System (PACS). After a 3-year follow-up period, patients underwent repeat catheterization and IVUS examination of the same region of interest (ROI) using an identical frequency IVUS imaging catheter.

Intravascular ultrasound analysis

Quantitative coronary ultrasound analysis was performed by an independent core laboratory (Cardialysis BV, Rotterdam, The Netherlands) using validated semi-automatic contour detection software (Curad, version 3.1, Wijk bij Duurstede, The Netherlands). The IntelliGate™ image-based gating method was applied to eliminate catheter-induced image artifacts, by retrospectively selecting end-diastolic frames.[16]

In order to avoid the significant impact of inter-observer variability,[17] contour detection was performed by a single experienced IVUS analyst who was blinded for the randomization allocation and time-point of the study. Longitudinal and cross-sectional views were used to determine the contours.

The contours of the external elastic membrane (EEM) and the lumen-intima interface enclosed an area that was defined as the coronary plaque plus media area. Plaque burden (PB) was defined as $[(EEM_{area} - Lumen_{area})/EEM_{area}] \times 100$. Direct measurements [lumen and vessel cross-sectional area (CSA)] were also determined. In the baseline IVUS study, a ROI was identified using identifiable landmarks such as side-branches and the coronary ostium. At 3-year follow-up, the same matched ROI was identified using the original anatomical landmarks to determine the lumen and vessel dimensional changes over time and consequently to calculate the impact on plaque changes. In order to assess more precisely the heterogeneous remodelling pattern within a vessel, the ROIs were subsequently subdivided in matched 5 mm sub-segments independently of the length of the pullback in the original IVUS study. Segments with a PB <10% were excluded.

Coronary remodelling was assessed using continuous and categorical variables. The remodelling index (RI) was defined as EEM_{area} at follow-up divided by the EEM_{area} at baseline.

Finally, we evaluated the number of segments presenting positive remodelling (defined as a relative increase in vessel CSA >2 SD from the mean relative intra-observer difference) and negative remodelling (defined as a relative temporal decrease >2 SD from the mean relative intra-observer difference).

IVUS tissue characterization

We used a computer-aided, in-house developed gray-scale value analysis programme for plaque characterization.[18] Using the mean gray level of the adventitia as a threshold, plaque was classified as more (hyperechogenic) or less (hypoechogenic) bright in relation to the adventitia. Upper and calcified tissue was defined as tissue that has a mean gray value higher than the mean adventitial intensity plus two times its standard deviation. The echogenicity software calculated the distribution of the gray-values present in the adventitia layer. When this distribution was not normal (severely calcified vessels), the data were excluded for IVUS analysis since the acoustic shadowing obscures the media-adventitia interface thus introducing serious inaccuracy in the contour detection.

Statistical analysis

Discrete variables are presented as counts and percentages. Continuous variables are presented as means ± SD or medians (inter-quartile range) as indicated. Pearson correlation coefficients were performed in order to estimate correlations between measurements.

Differences between groups were assessed by paired and unpaired Student's *t*-test when applicable. Fisher's exact test was used for categorical variables. A two-sided *P*-value <0.05 was required for statistical significance. All analyses were performed using SPSS version 13.0 software (Chicago, IL, USA).

Results

Study population

A total of 118 patients who had completed IVUS investigation at baseline and follow-up were included in the study. Populations were well matched (*Table 1*). The mean age was 56.6 ± 8.9, 100 (83.3%) were male, 11 (9.2%) had diabetes mellitus, 59 (49.2%) had history of prior myocardial infarction and 30 (25.0%) had hypertension. With regards to concomitant baseline medication, 115 (95.8%) were on aspirin, 67 (55.8%) were receiving beta-blockers, 32 (26.7%) were receiving nitrates, 46 (38.3%) were on calcium channel blocker therapy and 91 (75.8%) were on lipid-lowering therapy. Coronary risk factors and baseline blood pressure were well balanced between groups (*Table 1*).

At a median follow-up of 3.0 (range 1.9, 4.1) years, the rate of adverse events was minimal. Coronary revascularization [2 (3.3%) vs. 4 (6.9%), $P = 0.38$] and acute myocardial infarction [1 (1.7%) vs. 3 (5.2%), $P = 0.30$] rates were not statistically significant between perindopril and placebo groups. No deaths, strokes or admissions for heart failure were reported.

IVUS intra-observer variability

Fifteen cases (678 frames) were re-analysed by the same observer yielding minor differences between the 2 measurements. Relative differences for lumen, vessel, and plaque CSA were 1.43 ± 4.2%, 1.01 ± 3.4%, and 3.50 ± 8.5%, respectively. In addition, lumen ($r^2 = 0.99$, $P < 0.0001$), vessel ($r^2 = 0.99$, $P < 0.0001$), and plaque ($r^2 = 0.87$, $P < 0.0001$) CSA measurements were highly correlated.

Table 1 Study population

	Perindopril ($n = 60$)	Placebo ($n = 58$)	*P*-value
Baseline characteristics			
Age (years ± SD)	57.9 ± 9.2	55.2 ± 8.5	0.09
Male sex	50 (83.3)	50 (86.2)	0.67
Diabetes	4 (6.7)	7 (12.1)	0.32
Hypertension	12 (20.0)	18 (31.0)	0.17
Smoking	15 (25.0)	11 (19.0)	0.43
Hypercholesterolemia	51 (85.0)	47 (81.0)	0.57
Family history of CHD	16 (26.7)	17 (29.3)	0.75
Previous MI	32 (53.3)	27 (46.6)	0.47
Previous PTCA	53 (88.3)	57 (98.3)	0.03
Previous CABG	1 (1.7)	0 (0.0)	0.33
Systolic BP	130.6 ± 14.2	132.4 ± 13.6	0.48
Diastolic BP	78.9 ± 6.9	79.2 ± 7.5	0.78
BMI	26.5 ± 2.6	27.4 ± 3.1	0.91
Heart rate	68.5 ± 10.1	65.7 ± 7.1	0.09
Anginal status			
CCS I	50 (83.3)	45 (77.6)	0.44
CCS II	8 (13.3)	12 (20.7)	0.29
CCS III	2 (3.3)	1 (1.7)	0.58
CCS IV	0 (0.0)	0 (0.0)	NA
Other medications			
Platelet inhibitors	58 (96.7)	57 (98.3)	0.58
Beta-blockers	32 (53.3)	35 (60.3)	0.45
Nitrates	20 (33.3)	12 (20.7)	0.13
Ca-channel blockers	26 (43.3)	20 (34.5)	0.33
Lipid lowering agents	46 (76.7)	45 (77.6)	0.91
At 3-year follow-up			
Systolic BP	130.2 ± 16.5	131.1 ± 14.1	0.66
Diastolic BP	76.5 ± 8.5	79.0 ± 8.4	0.12
Other medications			
Platelet inhibitors	53 (88.3)	52 (89.7)	0.82
Beta-blockers	37 (61.7)	36 (62.1)	0.97
Nitrates	12 (20.0)	11 (19.0)	0.89
Ca-channel blockers	20 (33.3)	21 (36.2)	0.75
Lipid lowering agents	52 (86.7)	47 (81.0)	0.41

Hypercholesterolemia defined as cholesterol >6,5 mmol/L or on lipid-lowering therapy.
Blood pressure (BP) >160/95 mmHg or receiving antihypertensive treatment.
CCS, Canadian Cardiovascular Society.

Table 2 Intravascular ultrasound quantitative analysis

Mean cross-sectional area (mm^2)	Treatment ($n = 360$)	Placebo ($n = 351$)	*P*-value
Vessel			
Baseline	15.60 ± 5.0	15.82 ± 5.1	0.57
Follow-up	15.42 ± 4.8	16.01 ± 4.9	
Nominal change	−0.18 ± 2.4	0.19 ± 2.4	0.04
Relative change	−1.18 ± 17.0	1.20 ± 15.7	
P-value compared with baseline	0.15	0.13	
Lumen			
Baseline	9.21 ± 3.9	9.76 ± 4.1	0.07
Follow-up	9.17 ± 3.9	9.96 ± 4.4	
Nominal change	−0.04 ± 1.9	0.20 ± 2.4	0.14
Relative change	−0.42 ± 23.4	2.03 ± 26.6	
P-value compared with baseline	0.70	0.12	
Plaque			
Baseline	6.39 ± 2.8	6.06 ± 2.6	0.10
Follow-up	6.25 ± 2.7	6.05 ± 2.8	
Nominal change	−0.15 ± 1.7	−0.01 ± 1.7	0.27
Relative change	−2.28 ± 28.2	−0.09 ± 32.6	
P-value compared with baseline	0.11	0.95	
Plaque burden (%)			
Baseline	41.29 ± 13.1	39.01 ± 12.8	0.02
Follow-up	40.81 ± 13.4	38.55 ± 14.3	
Nominal change	−0.48 ± 8.1	−0.47 ± 9.5	0.98
Relative change	−1.16 ± 22.9	−1.20 ± 29.9	
P-value compared with baseline	0.26	0.36	
Hypoechogenicity			
Baseline	5.87 ± 2.6	5.66 ± 2.4	0.29
Follow-up	5.56 ± 2.4	5.56 ± 2.5	
Nominal change	−0.30 ± 1.7	−0.11 ± 1.7	0.12
Relative change	−5.19 ± 32.2	−1.90 ± 34.5	
P-value compared with baseline	0.001	0.23	

Intravascular ultrasound measurements

A total of 118 matched evaluable IVUS (711 matched 5 mm segments) were available at follow-up. Fifty-eight patients were excluded from the final analysis (29 from each group) due to sub-optimal IVUS quality (due to severely calcified vessels, severe artifacts or absence of clear anatomical landmarks). Quantitative IVUS results are shown in *Table 2*.

In the perindopril group, the temporal change in mean plaque CSA compared with baseline was $-0.15 \pm 1.7\ mm^2$ ($P = 0.11$). For the placebo group, the change was $-0.01 \pm 1.7\ mm^2$ ($P = 0.95$), with a *P*-value of 0.27 between groups. The temporal change in mean vessel CSA was $-0.18 \pm 2.4\ mm^2$ in the perindopril group and $0.19 \pm 2.4\ mm^2$ in the placebo group, with a *P*-value of 0.04 between groups. With regards to plaque hypoechogenicity, no significant difference was present between groups (perindopril $-0.30 \pm 1.7\ mm^2$ vs. placebo $-0.11 \pm 1.7\ mm^2$, $P = 0.12$). Both groups showed a highly heterogeneous remodelling pattern along the coronary segments (*Figure 1*). Nevertheless, the placebo group showed a larger mean RI than the perindopril group (1.03 ± 0.2 vs. 1.00 ± 0.2, $P = 0.06$). Of interest, negative remodelling was present in 124 (34.4%) segments in the perindopril group and in 86 (24.5%) segments in the placebo group. Conversely, positive remodelling was observed in 102 (28.3%) segments in the perindopril group and in 110 (31.3%) segments in the placebo group, with a significant (χ^2) difference between groups ($P = 0.01$). These changes are depicted in *Table 3*.

Linear regression analysis

The temporal change in vessel dimensions assessed by the RI was significantly correlated to the change in plaque dimensions ($r = 0.48$, $P < 0.0001$). The degree of such correlation was higher in the perindopril group than in the placebo group ($r = 0.58$, $P < 0.0001$ and $r = 0.36$, $P < 0.0001$,

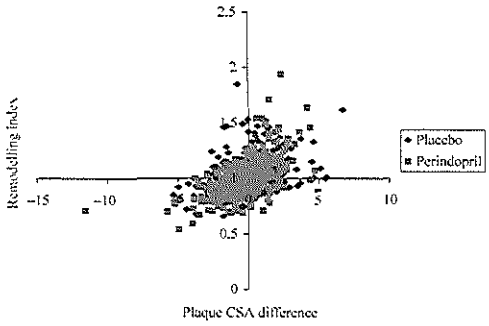

Figure 1 Linear regression scatter plot between the remodelling index and the difference in plaque cross-sectional area. See online supplementary material for colour version of this figure.

Table 3 Frequency of 5 mm segments with different remodelling patterns with perindopril and placebo, respectively

	Perindopril, *n* (%) (*n* = 360)	Placebo, *n* (%) (*n* = 351)	*P*-value (χ^2 across group)
Neutral	134 (37.2)	155 (44.2)	0.01
Positive remodelling[a]	102 (28.3)	110 (31.3)	
Negative remodelling[b]	124 (34.4)	86 (24.5)	

[a]Defined as a relative increase in vessel CSA >2 SD from the mean relative intra-observer difference.

[b]Defined as a relative temporal decrease >2 SD from the mean relative intra-observer difference.

respectively). As expected, the change in hypoechogenic content was highly related to the change in plaque ($r = 0.95$, $P < 0.001$) and vessel ($r = 0.45$, $P < 0.001$) CSA.

A strong relationship was found between changes in plaque and changes in vessel size (perindopril $r = 0.62$, $P < 0.0001$ and placebo $r = 0.35$, $P < 0.0001$). Such relation became stronger with increasing levels of PB at baseline (*Figure 2A*). In parallel, the placebo group showed a significant inverse relationship between the change in plaque and lumen CSA that was stronger at earlier stages of the disease (*Figure 2B*).

Discussion

The importance of coronary remodelling as a factor that has a major impact in the maintenance of lumen dimensions has been undoubtedly established.[1] Recently, several investigators have linked this originally deemed protective compensatory response of the vessel to the presence of a more unstable phenotype and plaque rupture.[2–5,19] Conversely, a paradoxical negative remodelling pattern has been associated with a more stable clinical presentation and lesion phenotype.[2,20] To date, most studies have assessed coronary remodelling at a single time-point and focally within the vessel, using proximal and distal references as surrogates of vessel size before it becomes diseased. However, coronary atherosclerosis is commonly a diffuse disease and finding a healthy reference is hard to attain. Moreover, such diffuse pattern implies a heterogeneous behaviour of atherosclerotic disease within a single vessel. Yet, although the assessment of coronary remodelling using serial determinations is highly required it has been scarcely exploited.[13,21]

The findings of the present longitudinal *in vivo* study offer several insights towards the better understanding of the long-term effect that ACE-inhibitors have on coronary atherosclerosis.

Overall, no significant differences regarding the temporal changes in plaque and lumen size were present between patients assigned to perindopril and placebo. Nevertheless, there was a significant difference between groups regarding the change in vessel size.

Negative remodelling occurred more frequently in the perindopril group than the placebo group. It is noteworthy though that, as a result of a parallel non-significant plaque regression effect, this slight constrictive effect had no impact on the lumen size. Similarly, the placebo group showed a larger mean RI than the perindopril group and a trend towards an enlargement of the coronaries with no change in plaque size, resulting in a non-significant increase of the lumen area.

The observed effect of perindopril on vessel remodelling might potentially be owed to the reduction in metalloproteinase levels induced by ACE-inhibitors,[22] since these enzymes have a central role in the pathophysiology of vessel remodelling.[12] Lipid lowering therapy with statins has recently shown to promote negative remodelling. The pathophysiology of such finding might be attributed to the inhibition of matrix metalloproteinase production.[23] Statins and ACE-inhibitors thus have a common inflammatory target related to coronary remodelling and plaque stabilization.

Contrasts with histopathology

Coronary remodelling has been long believed a vessel response to accommodate increasing burden of plaque without affecting the lumen patency.[1] In his study, Glagov made a static assessment of the correlation between plaque and vessel size in explanted left main coronary arteries. Our results are in line with the study of Glagov with respect to the fact that coronary remodelling is a phenomenon that occurs from very early stages of the disease and is mainly driven by the progressive accumulation of plaque within the vessel wall. Nevertheless, in our study, the strength of the relationship between changes in plaque CSA and changes in lumen CSA decreased with increasing levels of stenosis at baseline (*Figure 1*). Conversely, Glagov established that the positive correlation between vessel size and plaque size was stronger in sections with stenoses ≤20% and that an abrupt drop in lumen area was evident only after the obstruction reached 30–40%.[1] In brief, our results contradict Glagov's in the sense that control group patients showed higher remodelling capacity (and lumen manteinance) when the baseline severity of the disease was higher. It is noteworthy, however, that Glagov's seminal investigation was performed in the left main coronary artery, a coronary segment with a more benign plaque composition,[24] whereas it has previously been shown that the remodelling pattern of plaques is highly related to the underlying composition of plaques.[5]

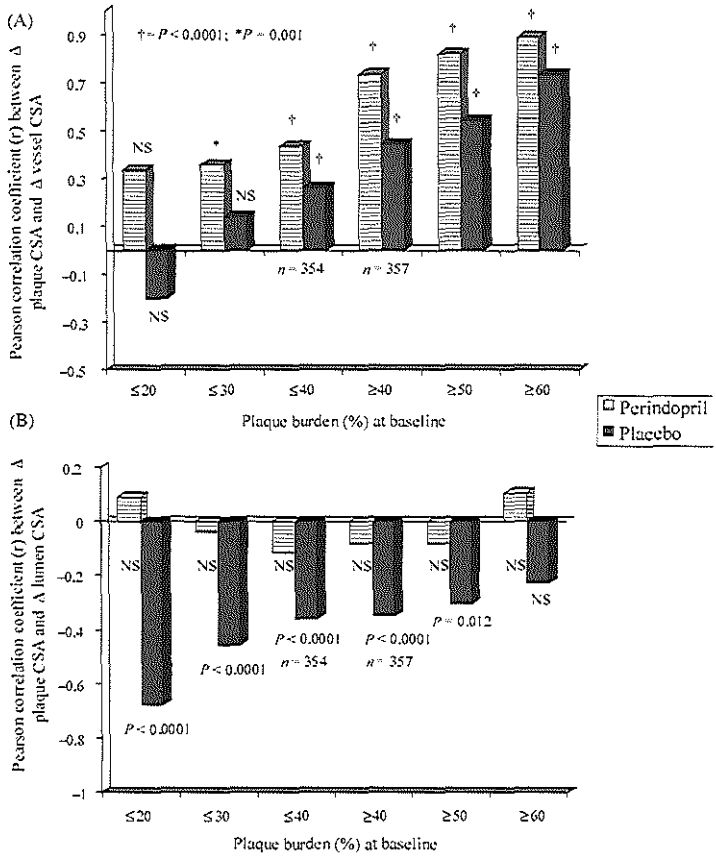

Figure 2 Bar graphs illustrating (*A*) the relationship between Δ plaque size and Δ vessel size and (*B*) the relationship between Δ plaque size and Δ lumen size. See online supplementary material for colour version of this figure.

It should be emphasized as well that statins, which have been shown to have a significant effect on plaque[14] and vessel[23] size, are currently administrated in an almost unrestricted fashion to cardiovascular patients, whereas two decades ago they were limited to patients with hypercholesterolemia. Finally, it is worth mentioning that, although there was no significant difference between groups regarding the change of hypoechogenic tissue, the administration of perindopril induced a significant beneficial shift in the echogenicity of plaques compared with baseline.

The findings of the present study confirm that coronary atherosclerosis is a highly dynamic disease. Moreover, the constrictive, yet lumen-preserving, effect shown has previously been associated with a more stable phenotype of lesions and better clinical presentation, suggesting that this pattern is associated with plaque stabilization.

Study limitations

A substantial number of vessels were excluded from the analysis due to sub-optimal image quality, principally due to the presence of severely calcified vessels. Nevertheless, we want to emphasize that this was essential to have a highly accurate assessment of the vessel contours. Only a single coronary artery was assessed by IVUS potentially being not representative of the entire coronary tree. Moreover, different IVUS catheters and consoles were used over a 3-year period, potentially influencing the results. Nevertheless, individual serial assessments were performed using identical IVUS catheters. To correct for any dimensional discrepancies, the results of the 30 MHz catheter were adjusted using a previously reported mathematical algorithm.[25] Larger studies in higher risk patients using IVUS as primary endpoint might conclusively determine the role of ACE-inhibitors in atherosclerosis natural history.

Conclusion

Our findings convey the relationship between plaque progression and coronary remodelling. In this study, perindopril was associated with a constrictive remodelling pattern without affecting the lumen, suggesting that this pattern is associated with plaque stabilization.

Acknowledgement

The PERSPECTIVE study was supported by Servier, France. The sponsor was not involved in the data collection and/or data analyses.

Supplementary material

Supplementary material is available at *European Heart Journal* online.

Conflict of interest: none declared.

References

1. Glagov S, Weisenberg E, Zarins CK, Stankunavicius R, Kolettis GJ. Compensatory enlargement of human atherosclerotic coronary arteries. *New Engl J Med* 1987;316:1371–1375.
2. Pasterkamp G, Schoneveld AH, van der Wal AC, Haudenschild CC, Clarijs RJ, Becker AE, Hillen B, Borst C. Relation of arterial geometry to luminal narrowing and histologic markers for plaque vulnerability: the remodeling paradox. *J Am Coll Cardiol* 1998;32:655–662.
3. Varnava AM, Mills PG, Davies MJ. Relationship between coronary artery remodeling and plaque vulnerability. *Circulation* 2002;105:939–943.
4. Burke AP, Kolodgie FD, Farb A, Weber D, Virmani R. Morphological predictors of arterial remodeling in coronary atherosclerosis. *Circulation* 2002; 105:297–303.
5. Rodriguez-Granillo GA, Serruys PW, Garcia-Garcia HM, Aoki J, Valgimigli M, van Mieghem CA, Mc Fadden E, de Jaegere PP, de Feyter P. Coronary artery remodelling is related to plaque composition. *Heart* 2006;92:388–391.
6. Yusuf S, Sleight P, Pogue J, Bosch J, Davies R, Dagenais G. Effects of an angiotensin-converting-enzyme inhibitor, ramipril, on cardiovascular events in high-risk patients. The Heart Outcomes Prevention Evaluation Study Investigators. *New Engl J Med* 2000;342:145–153.
7. Fox KM. Efficacy of perindopril in reduction of cardiovascular events among patients with stable coronary artery disease: randomised, double-blind, placebo-controlled, multicentre trial (the EUROPA study). *Lancet* 2003;362:782–788.
8. The CONSENSUS Trial Study Group. Effects of enalapril on mortality in severe congestive heart failure. Results of the Cooperative North Scandinavian Enalapril Survival Study (CONSENSUS). *New Engl J Med* 1987; 316:1429–1435.
9. The SOLVD Investigators. Effect of enalapril on survival in patients with reduced left ventricular ejection fractions, congestive heart failure. *New Engl J Med* 1991;325:293–302.
10. De Ciuceis C, Amiri F, Brassard P, Endemann DH, Touyz RM, Schiffrin EL. Reduced vascular remodeling, endothelial dysfunction, and oxidative stress in resistance arteries of angiotensin II-infused macrophage colony-stimulating factor-deficient mice: evidence for a role in inflammation in angiotensin-induced vascular injury. *Arterioscler Thromb Vasc Biol* 2005;25:2106–2113.
11. Dupuis F, Atkinson J, Liminana P, Chillon JM. Comparative effects of the angiotensin II receptor blocker, telmisartan, and the angiotensin-converting enzyme inhibitor, ramipril, on cerebrovascular structure in spontaneously hypertensive rats. *J Hypertens* 2005;23:1061–1066.
12. Ward MR, Pasterkamp G, Yeung AC, Borst C. Arterial remodeling. Mechanisms and clinical implications. *Circulation* 2000;102:1186–1191.
13. Hibi K, Ward MR, Honda Y, Suzuki T, Jeremias A, Okura H, Hassan AH, Maehara A, Yeung AC, Pasterkamp G, Fitzgerald PJ, Yock PG. Impact of different definitions on the interpretation of coronary remodeling determined by intravascular ultrasound. *Catheter Cardiovasc Interv* 2005;65: 233–239.
14. Rodriguez-Granillo GA, Agostoni P, Garcia-Garcia H, Biondi-Zoccai GGL, Mc Fadden E, Amoroso G, de Jaegere P, Bruining N, de Feyter P, Serruys PW. Meta-analysis of the studies assessing temporal changes in coronary plaque volume using intravascular ultrasound. *Am J Cardiol* 2007;99:5–10.
15. Rodriguez-Granillo GA, Bruining N, de Winter S, Vos J, Ligthart JM, Deckers J, Simoons ML, Fox K, de Feyter PJ. Long-term effect of perindopril on coronary atherosclerosis progression: results from the multicenter, randomized PERindopril's Prospective Effect on Coronary aTherosclerosis by angiography and IntraVascular ultrasound Evaluation (PERSPECTIVE) study, an EUROPA substudy. *Am J Cardiol* 2007 (in press).
16. De Winter SA, Hamers R, Degertekin M, Tanabe K, Lemos PA, Serruys PW, Roelandt JR, Bruining N. Retrospective image-based gating of intracoronary ultrasound images for improved quantitative analysis: the intelligate method. *Catheter Cardiovasc Interv* 2004;61:84–94.
17. Hausmann D, Lundkvist AJ, Friedrich GJ, Mullen WL, Fitzgerald PJ, Yock PG. Intracoronary ultrasound imaging: intraobserver and interobserver variability of morphometric measurements. *Am Heart J* 1994;128: 674–680.
18. de Winter SA, Heller I, Hamers R, de Feyter PJ, Serruys PWC, Roelandt JRTC, Bruining N. Computer assisted three-dimensional plaque characterization in ultracoronary ultrasound studies. *Comput Cardiol* 2003;30:73–76.
19. von Birgelen C, Klinkhart W, Mintz GS, Papatheodorou A, Herrmann J, Baumgart D, Haude M, Wieneke H, Ge J, Erbel R. Plaque distribution and vascular remodeling of ruptured and nonruptured coronary plaques in the same vessel: an intravascular ultrasound study in vivo. *J Am Coll Cardiol* 2001;37:1864–1870.
20. Smits PC, Pasterkamp G, Quarles van Ufford MA, Eefting FD, Stella PR, de Jaegere PP, Borst C. Coronary artery disease: arterial remodelling and clinical presentation. *Heart* 1999;82:461–464.
21. Sipahi I, Tuzcu EM, Schoenhagen P, Nicholls SJ, Ozduran V, Kapadia S, Nissen SE. Compensatory enlargement of human coronary arteries during progression of atherosclerosis is unrelated to atheroma burden: serial intravascular ultrasound observations from the REVERSAL trial. *Eur Heart J* 2006;27:1664–1670.
22. Schieffer B, Bunte C, Witte J, Hoeper K, Boger RH, Schwedhelm E, Drexler H. Comparative effects of AT1-antagonism and angiotensin-converting enzyme inhibition on markers of inflammation and platelet aggregation in patients with coronary artery disease. *J Am Coll Cardiol* 2004;44:362–368.
23. Schoenhagen P, Tuzcu EM, Apperson-Hansen C, Wang C, Wolski K, Lin S, Sipahi I, Nicholls SJ, Magyar WA, Loyd A, Churchill T, Crowe T, Nissen SE. Determinants of arterial wall remodeling during lipid-lowering therapy: serial intravascular ultrasound observations from the Reversal of Atherosclerosis with Aggressive Lipid Lowering Therapy (REVERSAL) trial. *Circulation* 2006;113:2826–2834.
24. Valgimigli M, Rodriguez-Granillo GA, Garcia-Garcia HM, Vaina S, De Jaegere P, de Feyter P, Serruys PW. Plaque composition in the left main stem mimics the distal but not the proximal tract of the left coronary artery: influence of clinical presentation, length of the left main trunk, lipid profile and systemic levels of C-reactive protein. *J Am Coll Cardiol* 2007;49:23–31.
25. Bruining N, Hamers R, Teo TJ, de Feijter PJ, Serruys PW, Roelandt JR. Adjustment method for mechanical Boston scientific corporation 30 MHz intravascular ultrasound catheters connected to a Clearview console Mechanical 30 MHz IVUS catheter adjustment. *Int J Cardiovasc Imaging* 2004;20:83–91.

CHAPTER 10.1

Virtual Histology and Optical Coherence Tomography: from Research to a Broad Clinical Application.

Garcia-Garcia HM, Gonzalo N, Regar E, Serruys PW.

Heart. 2009. In press.

SUMMARY

Invasive coronary imaging techniques have improved our understanding of atherosclerosis and have helped us to evaluate the effectiveness of new drugs and new intravascular devices. Rapidly, we have adopted them and integrated into our clinical-decision-making process in the catheterisation laboratory. Greyscale IVUS has been so far the most useful invasive imaging technique. Using greyscale IVUS, some lipid-lowering drugs showed to decrease plaque size, thereby these drugs have been widely included as part of standard of care[1, 2]. Moreover, IVUS-guided stenting, following strict criteria of implantation, proved to decrease the restenosis rate[3] and more recently it has been published that this approach apparently decreases stent thrombosis[4]. The recent introduction of tissue characterization by means of radiofrequency data analysis (Virtual Histology™) offers a more detailed evaluation of the atherosclerotic plaque. This technique brings the possibility to go beyond plaque size evaluation to a more sophisticated approach which is to assess changes in tissue types. In IBIS 2 study[5], after 12 months and despite high adherence to standard-of-care treatment, the necrotic core continued to expand among patients receiving placebo, while Lp-PLA2 inhibition with darapladib prevented necrotic core expansion.

However, the lack of high resolution of IVUS has hampered its broad clinical application. Therefore, new light-based imaging techniques have been introduced. Optical Coherence Tomography (OCT) and the new swept source OCT (SS-OCT or frequency domain OCT) have gained sympathy among interventionalists due to the sharp and informative images especially at the luminal side of the vessel wall. During stenting, OCT offers the possibility to assess stent apposition in great detail and can identify the presence of vessel injury due to stent implantation. At follow-up, the tissue coverage of individual struts can be imaged with OCT. This is of increasing interest in drug-eluting stents in which the neointimal proliferation is inhibited to such extent that might not be visualized with conventional intracoronary imaging techniques such as IVUS. Regarding plaque type characterization by OCT, although less complete due to its lack of penetration, this technique holds promise due to its ability to provide very detailed information about plaque composition, presence of macrophages and thickness of the fibrous cap.

INTRODUCTION

So far, only significant lesions in the coronary angiogram have been treated either by percutaneous cornary intervention (PCI) or coronary bypass artery grafting (CABG); while normal-looking coronary segments in angiography have been regarded as "disease-free" and mild/moderate stenoses as "non-treatable" neither by PCI or CABG; from these non-significantly diseased areas may potentially rise acute coronary events. In response to this, many imaging coronary techniques have been developed to study these areas to better understand the pathophysiology of atherosclerotic disease and to assess the performance of medical interventions that may ultimately have an important impact on the prevention of acute myocardial infarction and death. This review aims at describing the usefulness of virtual histology (VH) to study intact plaques as well as the performance of coronary interventions. Likewise, a review on the applicability of optical coherence tomography (OCT) in coronary plaques and interventional procedures is here reported.

INTRAVASCULAR ULTRASOUND RADIOFREQUENCY ANALYSIS: VIRTUAL HISTOLOGY

1. Description of the technique

Technologically speaking, the main difference between greyscale IVUS and Virtual Histology is that greyscale IVUS imaging is only formed by the envelope (amplitude) of the radiofrequency (RF) signal. The frequency and power of the signal commonly differ between tissues, regardless of similarities in the amplitude. **Figure 1.** IVUS-Virtual Histology (IVUS-VH, Volcano Corp., Rancho Cordoba, USA) involves spectral analysis of this data to construct tissue maps that classify plaque into four major components (fibrous - green, fibro-fatty – light green, necrotic core - red and dense calcium - white). [6] These tissue-maps have been validated ex-vivo by comparison with histology, the overall predictive accuracies were 93.5% for fibrous, 94.1% for fibro-fatty, 95.8% for necrotic core and 96.7% for dense calcium with sensitivities and specificities ranging from 72 to 99%. [7]

In the past, Virtual Histology was acquired using exclusively the In-Vision Gold console and a 20 MHz Eagle Eye™ Gold catheter (Volcano Corporation, Rancho Cordova, USA). Currently, the Volcano s5 Imaging System is used, one of his components, the Virtual Histology System, is intended to perform spectral analysis of RF ultrasound signals of vascular features. Two types of catheters can

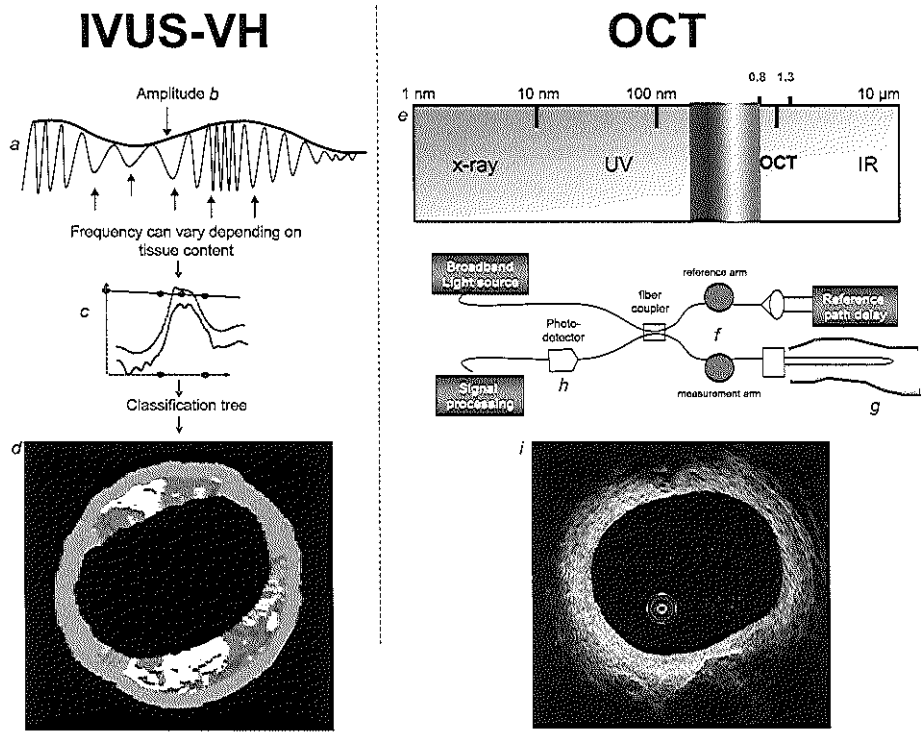

Figure 1: Schematic diagram of virtual histology (IVUS-VH) and optical coherence tomography (OCT). *Left:* The ultrasound signal is generated in a piezoelectric crystal that transmits and receives sound waves. Ultrasound reflected by the tissue deforms crystal generating radiofrequency (RF) signal (*a*). Greyscale IVUS is derived from the amplitude (*b*) of RF signal, discarding information beneath the peaks of the signal. IVUS-VH analysis uses several additional spectral parameters to identify four plaque components (*c*). Plaque components that are identified are dense calcium (white), fibrous (green), fibro-fatty (greenish-yellow) and necrotic core (red) (*d*).
Right: the electromagnetic spectrum encompasses the following regions: x-rays, microwaves and light (*e*). The visible part of the spectrum ranges from 0.4 to 0.77 µm. The wavelengths used for OCT are indicated. Since the speed of light is much faster than that of sound, it is needed to use correlation or an interferometer to measure the backscattered light. The interferometer splits the light source into two arms – a reference arm and a measurement arm- (*f*). The measurement arm is directed into the tissue through the image wire and collects the backscattered light (*g*). The light coming back from both arms is recombined at a detector (*h*) in which the interferogram – the sum of the two signals - is generated. The optical properties of the tissue can be deduced by comparing the back-reflected optical intensity of the two arms (*i*). Panel *d* and *i* correspond to the same anatomical region. Please note that the shape of the calcified regions is similar.

be used with this system, the 20 MHz electronic catheter or a 45 MHz mechanic catheter. The VH classification tree for the 45 MHz is under development. An automated pullback device is used, usually the pullback speed is set at 0.5 mm/s. IVUS-VH acquisition is ECG-gated at the R-wave peaks. **Table 1.**

Table 1. Technical specifications for virtual histology and optical coherence tomography

	Virtual Histology	M3	M4
Frame Rate, fps	Heart rate	20	100
# Lines/frame, n	256	240	450
Pullback speed, mm/s	0.5-1.0	3.0	20
Scan diameter, mm	10	6.8*	8.3*
Lateral resolution, µm	346µm at 2.3mm	25-30	25-30
Axial resolution, µm	138µm at 2.3mm	15-20	15-20
Catheter profile, F	3.1	1.4	2.6
Technology	IVUS	Time-domain OCT	Swept-source OCT

* In saline

2. Study of intact plaques

i. Virtual histology and necrotic core distribution

Identification of subclinical high-risk plaques is potentially important because they may have greater likelihood of rupture and subsequent thrombosis. In 55 patients, the mean necrotic core percentage – in nonculprit vessels - was significantly larger in patients with acute coronary syndrome (ACS) when compared with stable patients (12.2±7.0% vs. 7.4±5.5%, p=0.006). In addition, stable patients showed more fibrotic vessels (70.9±9.3% vs. 63.9±9.1%, p=0.007)[8]. However, not only the amount of necrotic core content is larger in patients with ACS, but it appears that NC is also unevenly distributed. In 51 patients, the overall length of the studied vessels (i.e. non-culprit), subsequently divided into 10 mm segments, was 41.5±13 mm. The percentage of necrotic core resulted to be increased in the first (median: 8.8%; IQR: 5.7-18) vs. the third (median: 6.1%; IQR: 3.2-12) (p=0.036) and fourth (median: 4.5%; IQR: 2.4-7.9) (p=0.006) segment. At multivariable regression analysis, distance from the ostium resulted to be an independent predictor of relative necrotic content [beta=-0.28 (95%CI: -0.15, -0.41)], together with older age, unstable presentation, no use of statin, and presence of diabetes mellitus[9].

ii. Plaque characterization

There is a continuous debate regarding how coronary atherosclerosis lesion progresses. Some believe that atherosclerotic lesion progression starts with pathologic intimal thickening (PIT) in which lipid accumulates in areas rich in proteoglycans (lipid pools), but no trace of necrotic core is seen. Others believe that the earliest change of atherosclerosis is the fatty streak, also called as intimal xanthoma. The earliest lesion with a necrotic core is the fibroatheroma (FA), and this is the precursor lesion that may give rise to symptomatic heart disease. Thin-capped fibroatheroma (TCFA) is a lesion characterized by a large necrotic core containing numerous cholesterol clefts. The overlying fibrous cap is thin and rich in inflam-

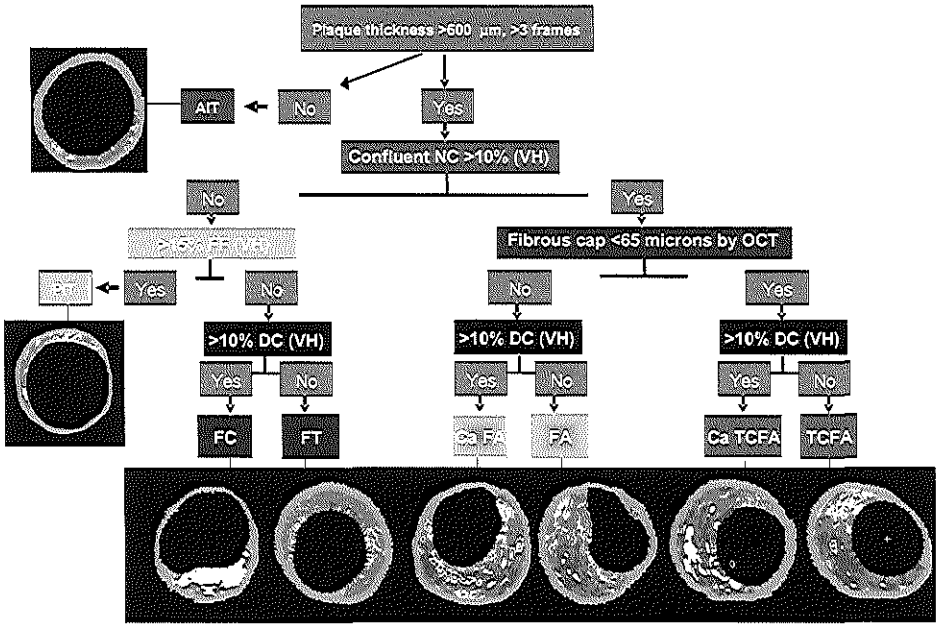

Figure 2: Plaque classification using OCT and IVUS-VH. OCT: optical coherence tomography; VH: virtual histology; NC: necrotic core; AIT: adaptive intimal thickening; PIT: pathological intimal thickening; FC: fibrocalcic; FT: fibrotic; CaFA: calcified fibroatheroma; FA: fibroatheroma; CaTCFA: calcified thin cap fibroatheroma; TCFA: thin cap fibroatheroma.

matory cells, macrophages and T lymphocytes with few smooth muscle cells. A study done by Burke et al[10]. identified a cut-off value for cap thickness of <65 microns for vulnerable coronary plaque definition.

Virtual Histology can potentially identify all above-mentioned plaque types including thin-capped fibroatheromas. The progression of the disease can also be followed-up. **Figure 2** outlines the virtual histology plaque and lesion types that are proposed based on the above pathologic data.

Our group evaluated the incidence of IVUS-derived thin-cap fibroatheroma (IDTCFA) using IVUS-VH [11]. IDTCFA was defined as a lesion fulfilling the following criteria in at least 3 consecutive frames: 1) necrotic core ≥10% without evident overlying fibrous tissue, 2) plaque burden ≥40%. In this study, 62% of patients had at least one IDTCFA in the interrogated vessels. ACS patients had a significantly higher incidence of IDTCFA than stable patients (p= 0.018). Finally, a clear clustering pattern was seen along the coronaries, with 66.7% of all IDTCFAs located in the first 20 mm. This distribution of IDTCFAs is consistent with previous clinical studies, with a clear clustering pattern from the ostium demonstrating a non-uniform distribution of vulnerable plaques along the coronary tree [12]. Rioufol et al., reported that patients presenting with ACS had

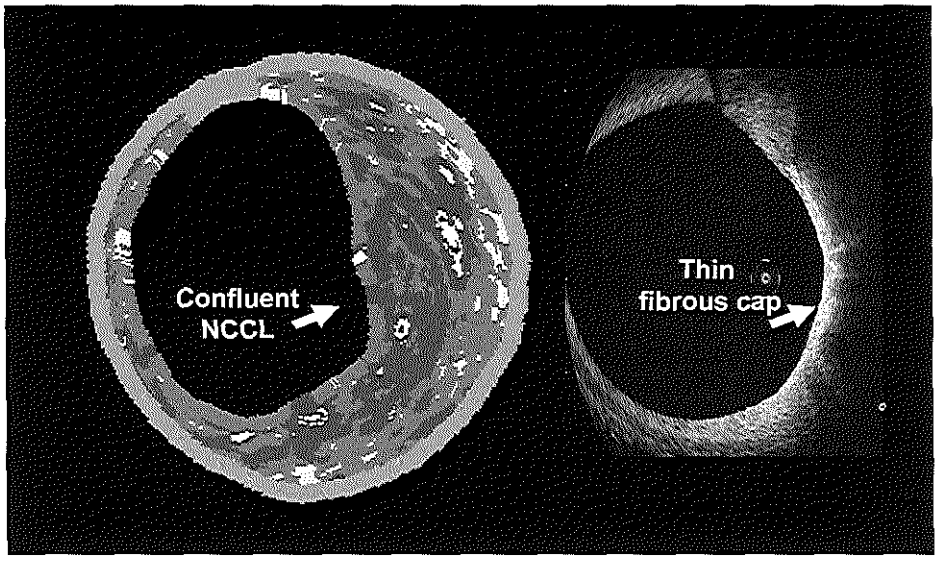

Figure 3. IVUS-derived thin cap fibroatheroma by and virtual histology and its corresponding optical coherence tomography image (OCT). *Right:* Virtual histology image is color coded: red – necrotic core, white – dense calcium, green – fibrous and greenish – fibro-fatty. There is an area of confluent necrotic core (NC) that is in direct contact with the lumen (CL). *Left:* OCT image shows an area with low reflectivity behind a thin cap. These characteristics have been correlated with a fibrous cap overlying a necrotic core rich area (arrow).

a significantly higher prevalence of plaque ruptures even in non-culprit vessels, supporting the concept of a multi-focal process [13]. Of note, the plaque burden and the mean necrotic core areas of the IDTCFAs detected by IVUS-VH were also similar to previously reported histopathological data (55.9% vs. 59.6% and 19% vs. 23% respectively) [14].

We have developed a software to quantify the amount of necrotic core in contact with the lumen, enabling refinement of our analysis. Our current definition of an IVUS-derived TCFA is a lesion fulfilling the following criteria in at least 3 frames: 1) plaque burden ≥ 40%; 2) *confluent* necrotic core ≥ 10% in direct contact with the lumen (i.e. no visible overlying tissue) [15]. Using this refined definition of IVUS-derived TCFA, in patients with ACS who underwent IVUS of all three epicardial coronaries, on average, there were 2 IVUS-derived thin cap fibroatheroma per patient with half of them showing outward remodeling [15]. **Figure 3.**

The frequency and distribution of TCFA identified by virtual histology intravascular ultrasound in acute coronary syndrome (ACS = 105 pts) and stable angina pectoris (SAP =107 pts) in a 3-vessel IVUS-VH study have been recently published by Hong et al.[16] There were 2.5 ± 1.5 in ACS and 1.7 ± 1.1 in SAP

TCFAs per patient, p <0.001). 76 patients with ACS and 58 with SAP had multiple ID-TCFA (p = 0.009). Presentation of ACS was the only independent predictor for multiple ID-TCFA (p = 0.011). Eighty-three percent of ID-TCFA were located within 40 mm of the coronary.

The potential value of these VH IVUS-derived plaque types in the prediction of adverse coronary events is currently under evaluation in an international multicentre prospective study (PROSPECT study).

Important technical considerations about Virtual Histology

- Provides information of four tissue types: fibrous, fibro-fatty, necrotic core and dense calcium.
- Evaluation of the layout of these four different tissue types gives information of different plaque types.
- As Virtual Histology is an IVUS derived technique, its axial resolution is limited. This precludes assessment of "thin" fibrous cap.
- Virtual Histology does not provide information on thrombus and inflammation.

iii. Virtual Histology and plaque rupture

Our group described the ruptured plaque profile in 40 patients referred for cardiac catheterization [17]. There were 13 with stable angina, 12 with unstable angina, and 15 with acute myocardial infarction. Ruptured plaque was identified in 26 patients and, as expected, was more frequent in patients with acute myocardial infarction and unstable angina. Patients with ruptured plaques have larger body mass index when compared with those without plaque rupture and were more likely smokers and patients with ruptures had more diffuse calcification and necrotic core area. Of note, the location of plaque ruptures in this study mirrors the pathological findings [18]. In our study, the proximal left anterior descending coronary artery was the most common site of plaque rupture. In a pathological series of 79 ruptures, Burke et al.[18] have found 74% in the proximal left anterior descending.

Similarly, in the report by Hong et al., the frequency and distribution of ruptured plaques identified by IVUS-VH in acute coronary syndrome (ACS = 105 pts) and stable angina pectoris (SAP =107 pts) in a 3-vessel IVUS-VH study were reported[16]. There were 76 ruptured plaques (55 in ACS and 21 in SAP). Twelve patients with ACS and 1 with SAP had multiple ruptured plaques (p <0.001). Presentation of ACS was also the only independent predictor for multiple ruptured plaques (p = 0.013).

iv. Coronary embolization

Two studies have evaluated the usefulness of IVUS-VH plaque composition to predict the risk of embolization during stenting [19, 20]. In one of them, 71 patients with STEMI that underwent primary PCI within 12 hours of the beginning of the symptoms were included. After performing thrombectomy with an aspiration catheter, IVUS-VH of the infarct-related vessel was performed. The stent was then deployed without embolic protection. ST segment re-elevation was used as a marker of distal embolization during stenting. Eleven patients presented with ST segment re-elevation after stenting. Total plaque volume was similar in both groups, but the NC volume was significantly higher in the group of patients with ST segment re-elevation (32.9 ± 14.1 mm^3 vs. 20.4 ± 19.1 mm^3, $p < 0.05$). On receiver-operating characteristic curves, NC volume was the best predictor of ST re-elevation after stent deployment. The cut-off point for NC volume that was best predictive for ST re-elevation was 33.4 mm^3, with a sensitivity of 81.7% and a specificity of 63.6%. The second study included 44 patients who underwent elective coronary stenting. Small embolic particles liberated during stenting were detected as high-intensity transient signals (HITS) with a Doppler guidewire. Patients were divided into the tertiles according to the HITS counts. Dense calcium and NC area were significantly larger in the highest tertile. In the multivariate logistic regression analysis, only necrotic core area was an independent predictor of high HITS counts (odds ratio 4.41, $p = 0.045$).

v. Virtual histology as imaging tool to assess temporal changes in coronary atherosclerotic plaques beyond plaque size

Lipoprotein-associated phospholipase A_2 (Lp-PLA_2) is expressed abundantly in the necrotic core of coronary lesions and products of its enzymatic activity may contribute to inflammation and cell death, rendering plaque vulnerable to rupture.

IBIS 2 study compared the effects of 12 months of treatment with darapladib (oral Lp-PLA_2 inhibitor, 160 mg daily) or placebo on coronary atheroma deformability (IVUS-palpography) and plasma hs-CRP in 330 patients with angiographically documented coronary disease. Secondary end points included changes in necrotic core size (IVUS-VH), atheroma size (IVUS-greyscale), and blood biomarkers. Background therapy was comparable between groups, with no difference in LDL-cholesterol at 12 months (placebo: 88±34 and darapladib: 84±31 mg/dL, p=0.37). In contrast, Lp-PLA_2 activity was inhibited by 59% with darapladib (p<0.001 versus placebo). After 12 months, there were no significant differences between groups in plaque deformability (p=0.22) or plasma hsCRP (p=0.35). In the placebo-treated group, however, necrotic core volume increased

significantly, whereas darapladib halted this increase, resulting in a significant treatment difference of -5.2 mm^3 (p=0.012). These intra-plaque compositional changes occurred without a significant treatment difference in total atheroma volume (p=0.95).

Despite adherence to a high level of standard of care treatment, the necrotic core continued to expand among patients receiving placebo. In contrast, Lp-PLA_2 inhibition with darapladib prevented necrotic core expansion.

3. Clinical findings in the stent studies

Stent thrombosis is one of the major concerns after drug-eluting stent implantation. Multiple mechanical causes (i.e. stent underexpansion, edge dissection, geographic miss, residual stenosis, incomplete stent apposition and aneurism) have been postulated. These features are easily identifiable by greyscale intravascular ultrasound. However, it is uncertain which of them are inextricably related to stent thrombosis, primarily due to the low number of such patients studied by IVUS in case control studies.

Our knowledge of the pathophysiology of late DES thrombosis is derived from pathologic samples[21-24]. It has been demonstrated that DES cause substantial delayed healing (the most common cause of late DES thrombosis at autopsy) characterized by the lack of complete reendothelialization and persistence of fibrin when compared with BMS[25]. This cannot be assessed by any IVUS modality due to its limited axial resolution.

Other proposed pathological mechanisms of coronary stent thrombosis are stenting of necrotic core-rich plaques with extensive tissue prolapse and plaque disruption in the proximity of the stented arterial segment[21, 25]

Complementary to greyscale IVUS, tissue characterization by IVUS-VH analysis has the potential to add valuable information on the pathogenesis of stent thrombosis by providing information on plaque composition, specifically on the amount of necrotic core and its location (superficial or deep)[26]. However, the clinical utility of IVUS-VH analysis in this context has yet to be demonstrated.

i. Characterization of Edge Effects

Virtual histology technique provides both geometrical and compositional analysis of each frame, allowing us to have the combined assessment of necrotic core and plaque size; we studied 24 patients in whom 26 stented segments (by angiography stenting was performed from "normal to normal" coronary segments) using IVUS-VH were assessed. [27] The objective of this study was to investigate in vivo the temporal changes occurring at the edges of paclitaxel-eluting stents using

IVUS-VH. Serial expansive vascular remodeling was observed at proximal and distal stent edges. Remodeling occurred in response to tissue growth, which was mainly due to increased fibrofatty tissue.

We also observed that necrotic core rich areas were left unstented (5mm-proximal edge mean necrotic core 17.0±13.5% and 5mm-distal edge 18.5±16.5%); however, no stent thrombosis has been observed in this small cohort of patients at 6 months follow-up. It has yet to be determined in a larger population whether incomplete coverage of necrotic core-rich coronary plaques or disruption of adjacent necrotic core areas by DES impact on long-term clinical events[27].

ii. Serial changes in patients stented with a fully absorbable stent

We assessed the feasibility and safety of a bioasorbable everolimus-eluting stent (BVS). In a prospective, open-label study we enrolled 30 patients with a single de-novo lesion that was suitable for treatment with a single BVS. The serial assessments of intravascular ultrasound assessments with virtual histology showed a significant decrease at 180 days in the dense calcium area, whereas we measured significant increases in fibro-fatty and fibrous areas. These two observations suggest on the one hand the first signs of the expected bioabsorption of struts, and on the other hand that the tissue growth documented at follow-up inside and outside the stent struts consists of fibrous and fibro-fatty tissues.

Clinical usefulness of Virtual Histology

- In the IBIS 2 study, the inhibition of Lp PLA_2 halted necrotic core progression.
- The potential value of VH IVUS-derived plaque types in the prediction of adverse coronary events is currently under evaluation in an international multicentre prospective study (PROSPECT study).
- Necrotic core rich plaques have been related to distal embolization during percutaneous coronary interventions.

OPTICAL COHERENCE TOMOGRAPHY

1. Introduction

Greyscale intravascular ultrasound allows evaluation of coronary atherosclerosis but its limited resolution (axial 150–200 μm, radial 200–400 μm) precludes the visualization of certain microstructures (such as the thin fibrous cap or the fine strut coverage)[28, 29]. Optical Coherence Tomography (OCT) is a light-based imag-

ing modality can be used to study tissues in vivo with near-histologic, ultrahigh resolution[30]. This has provided new insights into the interaction between the stent and the vessel wall and has allowed a more precise characterization of atherosclerotic plaques.

2. Technical principles of OCT

Current clinically available OCT systems use time-domain (TD) technology (M2 and M3 OCT Imaging Systems - LightLab Imaging, Inc., Westford, MA, USA) while newer systems that are currently under development for clinical application, are based on frequency domain technology also called swept-source – SS; i.e. M4 OCT LightLab Imaging). Time-domain OCT uses low-coherent near-infrared light. **Figure 1.** A wavelength around 1300 nm is selected because it minimizes the energy absorption in the light beam caused by protein, water, hemoglobin and lipids.

While IVUS uses backscattered ultrasound, OCT uses reflected light to create high-resolution cross sectional images of the vessel. Since the speed of light is much faster than that of sound, an interferometer is required to measure the backscattered light. The interferometer splits the light source into two "arms" – a reference arm and a measurement arm, which is directed into the tissue. When the back-reflected optical intensity of the two arms (interference signal) is measured and compared, the optical properties of the tissue can be deduced. **Figure 1.** The intensity of the back-reflected light can be measured and quantified digitally in grayscale, enabling the creation of a digital image. The imaging depth of TD-OCT is approximately 1.5-2.0mm with an axial and lateral resolution of 15μm and 25μm, respectively. **Table 1.**

The M2 and M3 OCT Imaging Systems use identical console and PC-based operating system, however M3 permits imaging at a higher frame rate (20/sec vs. 15.6/sec for the M2) with a faster maximum pullback speed (3.0mm/sec vs. 2.0mm/sec). **Table 1.**

The new generation of OCT (SS-OCT or frequency domain OCT) uses a swept frequency laser as light source rather than using a broadband light source as in conventional TD-OCT. The echo-time delay and amplitude of light reflected from the tissue microstructure at different depths are determined by processing the interference between the tissue sample and a fixed reference mirror to create the OCT images[31, 32]. These new technology allow a dramatically faster image acquisition (up to 40 mm/s), and an increased scan diameter. The latter permits imaging of larger arteries.

3. Techniques for image acquisition

Red blood cells represent a non-transparent tissue causing multiple light scattering and substantial signal attenuation. **Figure 4a**. Therefore, for an adequate OCT image acquisition blood must be removed from the vessel. In the past with the M2 system, this was achieved with proximal occlusion of the vessel with a low-pressure balloon and distal flush delivery (occlusive technique)[33]. However, recently the increase in the pullback speed (i.e. with the use of M3) has made possible the OCT acquisition while the blood is removed by continuous contrast flush trough the guiding catheter without the need of occluding the vessel (non-occlusive technique)[34, 35]. The M2 and M3 systems use an imaging wire that has a maximum outer diameter of 0.019" (with a standard 0.014" radiopaque coiled tip) and contains an optical fiber core covered by a protective sheath (ImageWire™ LightLab Imaging Inc., Westford, MA, USA). In the new swept-source systems (i.e. M4 LightLab Imaging) the optical probe is integrated in a rapid-exchange

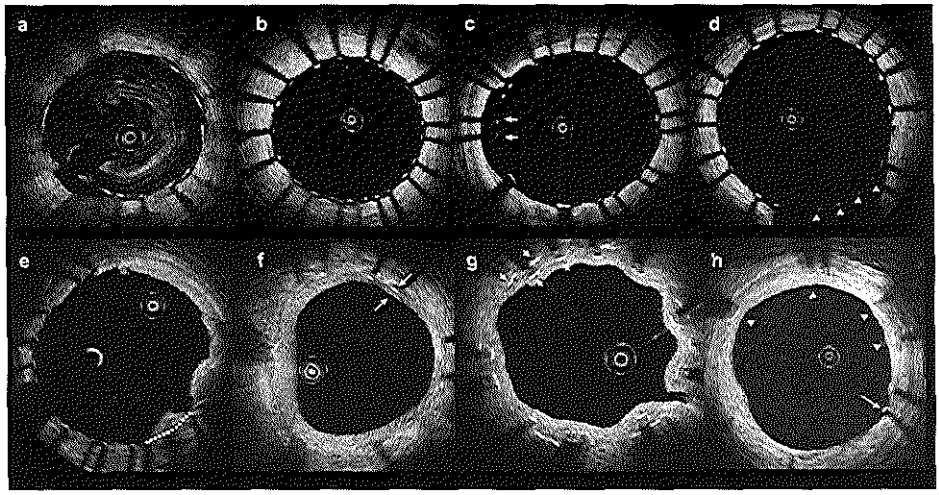

Figure 4. Optical coherence tomography images of common stent findings. *Panel a* depicts a frame with insufficient blood clearance. *Panel b* shows a newly placed stent. Stent struts are recognized as bright structures that span 360 degrees with shadowing. *Panel c* illustrates an incomplete stent apposition site. Of note, stent struts are not apposed to the vessel wall (arrows). *Panel d* shows the relationship of a stent and the ostium of a sidebranch (arrowhead). *Panel e* depicts a frame with tissue prolapse. Dotted line denotes the space between two struts. A mass of tissue is protruding into the lumen (asterisk). *Panel f* illustrates a stent with neointimal hyperplasia which is the signal-rich area between the stent struts and the lumen (arrows). *Panel g* shows an overlapped segment. Two layers of stent can be seen along the circumference (arrowheads). *Panel h* illustrates an uncovered strut (no tissue is at the endoluminal side of the strut - arrow). In contrast, some other struts are covered by neointimal tissue (arrowheads).

catheter (crossing profile 2.6 F) that can be delivered in the coronary artery over any conventional 0.014"guidewire.

Our current settings for OCT acquisition using M3 Light Lab system are: 1. continuous contrast injection (usually Visipaque ™ at 37 degree Celsius) at a flush flow rate of 3 mL/sec; 2. use of automatic injection (Medrad injection system); 3. pullback speed 3 mm/sec and 4. frame rate 20/sec.

4. Safety of intravascular OCT

The applied energies in intravascular OCT are relatively low (output power in the range of 5.0–8.0 mW) and are not considered to cause functional or structural damage to the tissue. Safety concerns thus seem mainly dependent on the need of blood clearance for image acquisition. One study evaluated the safety and feasibility of OCT in 76 patients using the occlusive technique. Vessel occlusion time was 48.3 ±13.5 seconds. The most frequent complication was the presence of transient events, such as chest discomfort, brady- or tachycardia, and ST-T changes on electrocardiogram, all of which resolved immediately after the procedure. There were no major complications, including myocardial infarction, emergency revascularization, or death. Furthermore, acute vessel occlusion, dissection, thrombus formation, embolism, or vasospasm along the procedure-related artery, were also not observed[36]. In our experience, the introduction in the clinical practice of the non-occlusive technique has led to an important reduction in the procedural time and in the rate of chest pain and ECG changes during image acquisition. This rate is expected to be even lower with the arrival of the new systems with high speed pullbacks that allow coronary imaging in few seconds.

Optical coherence tomography allows examination of the vessel wall in a microscopic manner.

- Its excellent axial resolution (15-20 μm) permits precise measurement of the thickness of the fibrous cap.
- Some investigators have reported macrophage detection in the fibrous cap.
- Although very detailed information can be obtained, its shallow penetration prevents from fully assessment of the coronary plaques.

5. Clinical application

i. Stent evaluation

Mostly, stent struts can be identified in OCT as highly reflective surfaces with shadowing behind. **Figure 4b**. Due to its high resolution OCT can be a very valu-

able tool for the evaluation of the acute and long-term impact of catheter-based intervention on plaque structure and vessel architecture. This is of increasing interest in drug-eluting and new-generation coronary stents such as bioabsorbable stents. Drug-eluting stents (DES) have been shown to significantly limit neointimal growth to such extent that the neointima tissue might consist of only a few cell layers that cannot be accurately visualised with IVUS[37]. The high resolution of OCT might offer the possibility to assess stent apposition and neointima growth patterns[38, 39].

A. Stent apposition

Classically in IVUS studies, incomplete stent apposition is defined as separation of at least one stent strut from the vessel wall with evidence of blood flow behind the strut (**Figure 4c**) and not related with a bifurcation (**Figure 4d**). In the DES era, the assessment of stent apposition has become critical due to reported observations suggesting an association between incomplete stent apposition and thrombosis[40]. OCT has demonstrated to be more accurate than IVUS for the detection of incomplete strut apposition to the vessel wall. In a study in porcine coronary arteries in vivo, microanatomic relationships between stents and the vessel walls could be clearly identified only by OCT[41]. Bouma et al., imaged 39 patients (42 stents) showing that incomplete stent apposition was more often observed with OCT than with IVUS[42] However, to avoid misclassification of struts as malapposed some considerations should be taken into account. Most DES are constituted by a metal body covered by a polymer. Since OCT can image only the endo-luminal surface of the strut due to limited penetration through the metal, strut and polymer thickness must be considered in assessing apposition for each type of DES design. Only if the distance from the endo-luminal surface of the strut to the vessel wall is longer than the sum of the metal and polymer thickness, it can be considered that the strut is malapposed. The thickness of the metal and polymer differs for each stent type. Therefore the cut-off point to establish malapposition must take into account the type of stent. The strut thickness for the most commonly used DES has been reported previously[43]. OCT has demonstrated its value to assess malapposition in the clinical practice. Tanigawa et al., reported that in overlapping segments in DES 40% of struts were malappposed despite high pressure dilatation with appropriate size balloons[44] The authors hypothesized that this could be related with the delayed reported endothelization and increased risk of stent thrombosis in those segments. The same group evaluated the usefulness of OCT to assess the struts apposition in heavily calcified lesions showing malapposition even after high pressure ballon dilatation and rotational atherectomy[45].

B. Stent expansion

OCT can be useful for the in vivo assessment of acute stent recoil one of the features identified as a contributor to inadequate stent expansion. Our group reported OCT findings during stepwise post-dilatation of a Cypher stent showing a change in stent diameter from 3.5 at 22 atm to 2.94 at 5 atm[46]. This could be clinically relevant as final stent area is known to be an important predictor for restenosis and subsequent clinical events. Stent asymmetry, another of the features related with stent thrombosis, can be assessed with high precision with OCT.

C. Identification of vessel injury after stenting

Due to its higher resolution OCT can also identify more often than IVUS acute complications after stent implantation such as edge dissection and tissue prolapse[42]. Edge dissection appears in OCT as a disruption in the vessel continuity with a visible flap **(Figure 5).** High-pressure stenting techniques have proved to be useful for stent deployment optimization but this strategy can often create certain degree of vessel damage in the stent edges[47]. Although animal and post-mortem information correlated vessel injury and in-stent restenosis[48, 49], some IVUS studies have shown that non-flow-limiting edge dissections may not be associated with an increase in acute or long-term events or the development of restenosis[50, 51]. However some data suggested that intracoronary imaging may be helpful to assess which of these residual dissections could be more prone to acute vessel occlusion. Nishida et al., reported that the area stenosis by IVUS at the site of the dissection was predictor for the incidence of in-hospital major cardiac adverse events[52].

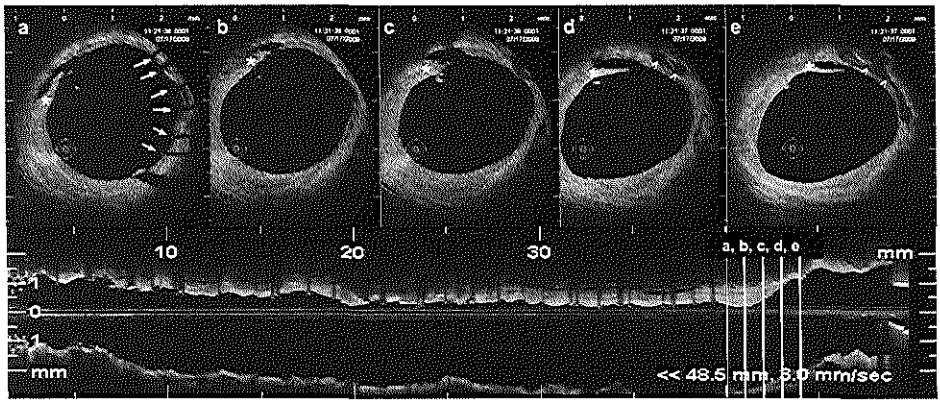

Figure 5. Edge dissection. In this patient a drug eluting stent was placed proximally in the left anterior descending. At the proximal edge of the stent a 4-mm dissection was noted in the optical coherence tomography images (a through e). In *panel a*, stent struts can still be seen (arrows) from 1 to 5 O'clock, while at 9 O'clock a dissection flap is noted (asterisk). At the proximal end of the dissection a calcified plaque can be seen (head arrows in *panels d and e*).

Tissue prolapse can be identified in OCT as protrusion of tissue between the struts (**Figure 4e**). The clinical relevance of the detection of this feature after stenting remains controversial. Pathological examinations have associated stent thrombosis with the prolapse of necrotic core between stent struts and is not able to provide tissue characterization[21]. However, greyscale IVUS study in diabetic patients undergoing PCI did not show higher incidence of stent thrombosis in patients with plaque prolapse[53]. This might be related with the resolution of grey-scale IVUS that is not able to detect small amount of tissue protruding between the stent struts. In this scenario a high resolution technique as OCT could provide very valuable information for a better understanding of the clinical implications of this phenomenon.

OCT has also demonstrated to be able to visualize the cuts in the atherosclerotic plaque made by the blades of a cutting balloon[54]. This can help to identify if the amount of cutting in the plaque has been enough and may help in the selection of the better technique to use this device.

D. Stent apposition at follow-up

Stent apposition at follow up can be assessed with OCT using the same criteria previously exposed for incomplete stent apposition at baseline. IVUS studies in patients with late stent thrombosis after DES implantation have shown a high prevalence of incomplete stent apposition[55, 56]. The incomplete stent apposition at follow-up can be persistent or acquired (not present after stent implantation). Several mechanisms have been proposed as cause of late acquired incomplete stent apposition: i) Expansive vessel remodelling ii) Chronic stent recoil. iii) Dissolution of thrombus jailed between the stent and the vessel wall in patients undergoing primary PCI for acute myocardial infarction, and iv) the resolution of an intramural haematoma created by vessel dissection during PCI has been also postulated as the origin of late incomplete stent apposition[57]. It has been reported that the prevalence of malapposed struts by OCT is higher in sirolimus-eluting stent (SES) than in bare metal stents (BMS)[58, 59]. In another study that evaluated 57 SES at 6 months follow up, 79 out of the 6840 struts visualized by OCT showed malapposition and were more often located in areas of SES overlap[60].

E. Struts coverage following DES implantation

Endothelial struts coverage has been identified in pathology as the most powerful histological predictor of stent thrombosis[61, 62]. Finn et al., reported that a stent with a ratio of uncovered to total stent struts per section >30% has an odds ratio for stent thrombosis of 9 (95% CI, 3.5 to 22) [40]. Angioscopic studies have shown a correlation between the neointimal grade and the presence of thrombi[63, 64]. DES inhibits

neointimal proliferation to such extent that it may not be detectable by IVUS[65-67]. The higher resolution of OCT allows the visualization and measurement of tiny layers of tissue covering the stent struts[68, 69] **(Figure 4f).** A study in carotid rabbit model evaluated the usefulness of OCT to identify struts coverage after stenting. No differences in the mean neointimal thickness measured by histology and OCT were found (the intra and interobserver reproducibility of neointimal thickness measurements by OCT was excellent, R^2 =0.90 and 0.88 respectively)[70]. Recently several OCT studies evaluating the struts coverage in DES in humans at different time intervals have been published. Xie et al., compared the neointimal coverage at 3 months follow-up in 16 patients treated with BMS and 24 patients that underwent SES implantation. The neointimal thickness per strut and the percentage of neontimal thickness area per cross section were higher in the BMS group than in the SES group (351± 248 vs 31± 39 μm; $p < 0.0001$; 45.0±14% vs 10.0 ±4%; $p < 0.0001$, respectively). The frequency of uncovered struts **(figure 4h)** and malapposed struts was higher in the SES group than the BMS group (15% vs 0.1%; $p < 0.0001$ and 15% vs 1.1% $p < 0.0001$ respectively). There was no significant difference in the incidence of stent thrombus between the 2 groups (14% vs 0%; p= 0.23)[58]. These results were confirmed in another similar study that compared BMS with SES. The percentage of uncovered struts in SES was significantly higher than in BMS while the neointimal thickness was lower in SES than in BMS[59]. Matsumoto et al., studied 34 patients (57 SES) with IVUS and OCT at 6 months follow-up. The authors reported that 64% of the struts were covered by thin neointima undetectable by IVUS (median neointima thickness 52.5 μm, 25th and 75th percentiles 28 and 147.6 μm respectively). Overall 89% of the struts were covered by tissue but only in 16% of the stents all the struts were covered[60]. A study evaluated the strut coverage in SES at 6 and 12 months follow-up. Forty-six SES (6561 struts) were studied in 36 patients. The authors reported that only 4 SES at 6 months (18.2%) and 10 SES at 12 months (41.7%) were fully covered by tissue. The analysis showed a significant increase in the average thickness of the tissue covering the struts from 42±28 μm at 6 months to 88±32 μm at 12 months[71]. Yamamoto et al., evaluated the long-term follow up of SES in 21 patients. Overall the frequency of uncovered struts was 5% and 81% of the patients presented uncovered struts at 2 years follow-up. The presence of uncovered struts was more frequent at side branches and at overlapping segments. They found 3 patients with thrombi by OCT examination but no clinical stent thrombosis was observed[72].

Some data suggest that OCT might be able to provide details on the characteristics of the neointimal tissue such as the presence of neovessels[73]. Neovascularization adjacent to stent struts is a common finding in experimental animal models but the incidence and significance in human is unknown.

Some considerations must be taken into account when studying struts coverage by OCT. Until now OCT can not distinguish if the tissue covering the struts is neointimal tissue or fibrin. Furthermore, different types of neointimal tissue can be present and may have different functionality[74]. Thus, the presence of tissue covering the strut does not warrant that the normal endothelial function in the area is restored. Pathological and functional studies are needed to understand the real meaning of the OCT findings in strut coverage.

F. Assessment of restenosis

OCT can be very useful in the evaluation of the causes that contribute to restenosis after DES implantation such as incomplete coverage lesion or gaps between stents[75].

Stent fracture (with subsequent defect of local drug delivery) has also been related to restenosis in DES and could be visualized with OCT[76]. Non-uniform distribution of stent struts could affect the drug delivery and therefore have an influence in restenosis in DES. This has been confirmed in pre-clinical[77] and IVUS studies. The maximum interstrut angle has been identified in IVUS as predictor of intimal hyperplasia cross-sectional area[78]. OCT allows the assessment of strut distribution in vivo with high accuracy. A study with phantom models showed how the strut distribution of SES and paclitaxel eluting stents (PES) assessed by OCT were significantly different, suggesting that SES maintained a more regular strut distribution despite expansion[79].

Another field of clinical use for OCT might be the assessment of the performance of DES in complex coronary interventions such as bifurcations. Buellesfeld et al., reported the 9-month OCT follow-up in a case of crush-stenting with PES. Crush stenting results in three layers of metal in the segment of the main vessel proximal to the stented side branch. There has been concern that this could release a higher dose of drug locally with the potential adverse effect of delayed endothelization. In this report, OCT imaging showed the overlapping struts layers in the crushed segment completely covered by tissue. Furthermore, OCT allowed clear visualization of the struts located in the ostium demonstrating a non-uniform distribution and different patterns of tissue coverage[80]. The effect of overlapping stents eluting different drugs in the development of endothelial coverage might also be studied with OCT.

G. Evaluation of future DES

Fully biodegradable stents has emerged as one of the most promising future stents because they may avoid the potential long-term complications of metallic drug-eluting stents such as late and very late stent thrombosis and the need

for prolonged dual anti platelet therapy. The ABSORB trial recently published, showed the feasibility of implantation of the bioabsorbable everolimus-eluting coronary stent (BVS: Abbott Laboratories, IL, USA), composed of a poly-L-lactic acid backbone, coated with a degradable polymer /everolimus matrix. In a subset of 13 patients, OCT was performed after stent implantation and at 6 months follow up. In that scenario OCT allowed not only a very precise characterization of the stent apposition and coverage but also demonstrated structural changes in the bioabsorbable DES along time. At baseline 738 struts were visualized while at follow up only 671 could be identified. The difference in number of struts can be explained presumably due to complete stent bioabsorption. Furthermore, the optical properties of the remaining struts changed from baseline to follow up probably related with the partial absorption process[81]. At present OCT appears as the best available tool for the assessment of the absorption of the stent struts.

Assessment of the relationship between coronary devices and vessel wall by optical coherence tomography

- OCT offers the possibility to study in great detail incomplete stent apposition. This has been related in IVUS studies with stent thrombosis
- Coverage of each of the struts can also be examined.
- Dissection, thrombus and tissue prolapse are clearly visible.
- OCT-guided stent implantation is still not in practice, due to lack of information that supports it use.

ii. Plaque characterization

Acute coronary syndromes caused by the rupture of a coronary plaque are common initial manifestations of coronary atherosclerosis. The detection of the lesions with high risk of rupture (the so called "vulnerable plaques") would be of main importance for the prevention of future ACS. In the last years there has been a growing interest in this field and a lot of different techniques have been developed to evaluate diverse aspects involved in plaque vulnerability. Among them, OCT has emerged as one of the most promising due to its ability to provide unique information about the plaque composition, the presence of macrophages and the thickness of the fibrous cap.

A. Plaque composition

The propensity of atherosclerotic lesions to destabilize and rupture is highly dependent on their composition. In comparison with histology OCT, has demonstrated to be highly sensitive and specific for characterizing different types of atherosclerotic plaques. Yabushita et al., analyzed 357 diseased carotid and coro-

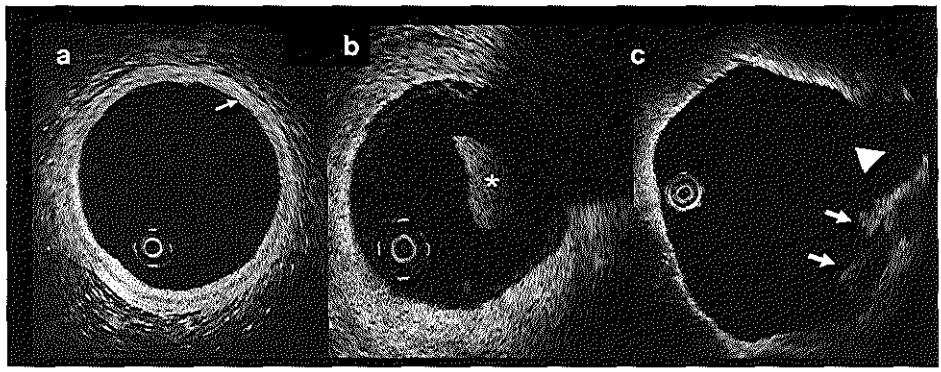

Figure 6. Optical coherence tomography images of intact atherosclerotic coronary plaques. *Panel a* shows a normal-looking vessel wall. *Panel b* depicts a red thrombus inside the lumen. Its OCT signature is the shadowing behind the mass (asterisk). *Panel c* illustrates a ruptured plaque. The cavity is at 2 O'Clock (arrowhead). Some disrupted tissue is adjacent to it (arrows). From 7 to 9 O'clock a poor-signal region with low reflectivity is seen, suggesting a thin fibrous cap fibroatheroma.

nary segments ex vivo and classified them as fibrous, fibrocalcific and lipid-rich plaques. Fibrous plaques were characterized as homogeneous, signal-rich regions; fibrocalcific plaques as signal-poor regions with sharp borders; and lipid-rich plaques as signal-poor regions with diffuse borders. The comparison with histology showed a sensitivity and specificity ranging from 71-79% and 97-98% for fibrous plaques, 95-96% and 97% for fibrocalcific plaques, and 90-94% and 90-92% for lipid-rich plaques[82]. Ex-vivo validations have also shown that OCT is superior to conventional and integrated backscatter IVUS for the characterization of coronary atherosclerotic plaque composition[83-86]. In vivo, OCT is able to identify most of the architectural features identified by IVUS and may be superior for the identification of lipid pools[87]. Several authors have evaluated the OCT appearance of coronary plaques in different groups of patients reporting higher prevalence of lipid-rich plaques in ACS than in patients with stable angina[88] and no differences in the culprit plaque imaged by OCT between diabetics and non-diabetics patients[89] and men or women with ACS[90]. According to histological and IVUS examinations, the percentage of lipid-rich plaque by OCT has been found to be higher in plaques with expansive remodelling[91].

However, a study comparing OCT to histopathology reported a lower sensitivity for plaque components. Misclassification occurred in 41% of lesions predominantly due to a combination of incomplete penetration depth into the vessel wall and the inability to distinguish calcium deposits from lipid pools[92].

B. Plaque rupture and intracoronary thrombus identification

Plaque rupture with subsequent thrombosis is the most frequent cause of ACS.

OCT can identify intracoronary thrombus (**figure 6b**) and plaque rupture (**figure 6c**) with high accuracy[93]. Recently, Kubo et al evaluated the ability of OCT for the assessment of the culprit lesion morphology in acute myocardial infarction in comparison with IVUS and angioscopy. They found an incidence of plaque rupture by OCT of 73%, significantly higher than that detected by both angioscopy (47%, p= 0.035) and IVUS (40%, p =0.009). Intracoronary thrombus was observed in all cases by OCT and angioscopy but was identified only in 33% of patients by IVUS[94]. Furthermore, Kume et al., demonstrated that OCT might be able to distinguish between white and red thrombus. Red thrombus appears in OCT as high-backscattering structure with signal-free shadowing (**figure 6b**) while white thrombus appears as a low-backscattering structure[95]. OCT could be helpful to identify the culprit lesion in ACS and might provide additional information about the underlying cause that lead to the plaque rupture.

C. Measurement of the fibrous cap

Autopsy studies of sudden cardiac death victims have shown that the most frequent cause of the coronary occlusion is rupture of a thin-cap fibroatheroma (TCFA) plaque. Such lesions are characterized by a large necrotic core with a thin fibrous cap usually < 65 microns in thickness. While conventional intracoronary imaging techniques such as IVUS-VH do not have enough resolution to evaluate in detail the fibrous cap, OCT has demonstrated in correlation with histological examinations that it is able to provide accurate measurements of the thickness of the fibrous cap[96, 97]. Therefore, it could be useful for the in vivo detection of TCFA (**Figure 3**). In the study with IVUS, OCT and angioscopy in acute myocardial infarction patients by Kubo et al., the incidence of TCFA was 83% and only OCT was able to estimate the fibrous cap thickness (mean 49±21μm). Two studies have reported that the plaque colour by angioscopy is related to the thickness of the fibrous cap as measured by OCT with yellow plaques often presenting thin caps[98, 99]. It has been suggested that the ability of OCT to measure changes in the fibrous cap thickness could be useful to assess the effect of statins in plaque stabilization [100, 101]. Furthermore, recent data suggest that new OCT technology (such as polarization-sensitive OCT) could be able to assess the collagen content and smooth muscle cell density in the fibrous cap[102]. This could provide very valuable information about the mechanical stability of the fibrous cap enabling the identification of lesions at high risk of rupture.

C. Macrophages detection

Intense infiltration by macrophages of the fibrous cap is another of the features of the vulnerable plaques. An ex-vivo study by Tearney et al., demonstrated OCT

could be able to quantify macrophage within the fibrous cap[103]. In vivo, it has been demonstrated that unstable patients present a significantly higher macrophage density detected by OCT in the culprit lesion than stable patients. Furthermore, in the same population, the sites of plaque rupture demonstrated a greater macrophage density than non-ruptured sites[104].

Raffel et al., reported that macrophage density in the fibrous cap detected by OCT correlated with the white blood cell count, and both parameters could be useful to predict the presence of TCFA[105].

COMBINED ASSESSMENT USING VIRTUAL HISTOLOGY AND OPTICAL COHERENCE TOMOGRAPHY

i. study of intact plaques

OCT can provide very valuable information for the detection of high-risk plaques in vivo especially measuring the thickness of the fibrous cap. However due to its limited penetration OCT can not provide a full analysis of large plaques. Further, histological examinations have demonstrated that OCT may not be sufficient to discriminate lipid pools from calcium deposits[92]. On the contrary, other techniques such as IVUS and IVUS-VH analysis can image the complete plaque thickness and can identify the presence of necrotic core but its limited axial resolution does not allow the evaluation of the fibrous cap. Thus, the combination of the IVUS-VH and OCT appears promising to better characterize such plaques. Indeed, Sawada et al., reported how the combined use of IVUS-VH analysis and OCT improved the accuracy for TCFA detection. 56 patients with angina (126 plaques) were included. Of the sixty-one plaques diagnosed initially as TCFA by IVUS-VH analysis criteria only 28 had a thin fibrous cap as measured by OCT, so they were considered as definite TCFAs. In addition, eight OCT-derived TCFA did not have necrotic in the IVUS-VH analysis mainly due to the misreading in OCT caused by dense calcium[106]. This data suggests that the combination of the information provided by different methods could be essential for better identification of high-risk coronary lesions. **(figure 3).**

We have evaluated the in-vivo frequency and distribution of high-risk plaques (i.e necrotic core rich) at bifurcations using a combined plaque assessment with IVUS virtual histology and optical coherence tomography **(figure 2)**. A total of 30 patients (103 bifurcations) were imaged. 27 fibroatheromas (26.2%) and 18 thin-cap fibroatheromas (17.4%) were found. Overall the % of necrotic core decreases from proximal to distal rim (16.8% vs. 13.5% respectively p=0.01)

First study reporting the definition of IVUS-derived thin capped fibroatheromas.

12. Wang JC, Normand SL, Mauri L, Kuntz RE. Coronary artery spatial distribution of acute myocardial infarction occlusions. Circulation 2004;110(3):278-84.
13. Rioufol G, Finet G, Ginon I, Andre-Fouet X, Rossi R, Vialle E, et al. Multiple Atherosclerotic Plaque Rupture in Acute Coronary Syndrome: A Three-Vessel Intravascular Ultrasound Study. Circulation 2002;106(7):804-808.
14. Virmani R, Burke AP, Kolodgie FD, Farb A. Vulnerable plaque: the pathology of unstable coronary lesions. J Interv Cardiol 2002;15(6):439-46.
15. Garcia-Garcia HM, Goedhart D, Schuurbiers JC, Kukreja N, Tanimoto S, Daemen J, et al. Virtual histology and remodeling index allow in vivo identification of allegedly high risk coronary plaques in patients with acute coronary syndromes: a three vessel intravascular ultrasound radiofrequency data analysis. Eurointervention 2006;2:338-344.

Three-vessel IVUS study looking at the frequency of IVUS derived thin capped fibroatheromas and its relation with expansive remodelling in patients with acute coronary syndrome.

16. Hong MK, Mintz GS, Lee CW, Lee JW, Park JH, Park DW, et al. A three-vessel virtual histology intravascular ultrasound analysis of frequency and distribution of thin-cap fibroatheromas in patients with acute coronary syndrome or stable angina pectoris. Am J Cardiol 2008;101(5):568-72.
17. Rodriguez-Granillo GA, Garcia-Garcia HM, Valgimigli M, Vaina S, van Mieghem C, van Geuns RJ, et al. Global characterization of coronary plaque rupture phenotype using three-vessel intravascular ultrasound radiofrequency data analysis. Eur Heart J 2006.

Patients with at least one PR in their coronary tree presented larger BMI and worse IVUS derived characteristics compared with patients without PR.

18. Burke AP, Joner M, Virmani R. IVUS-VH: a predictor of plaque morphology? Eur Heart J 2006;27(16):1889-90.
19. Kawaguchi R, Oshima S, Jingu M, Tsurugaya H, Toyama T, Hoshizaki H, et al. Usefulness of virtual histology intravascular ultrasound to predict distal embolization for ST-segment elevation myocardial infarction. J Am Coll Cardiol 2007;50(17):1641-6.
20. Kawamoto T, Okura H, Koyama Y, Toda I, Taguchi H, Tamita K, et al. The relationship between coronary plaque characteristics and small embolic particles during coronary stent implantation. J Am Coll Cardiol 2007;50(17):1635-40.
21. Farb A, Burke AP, Kolodgie FD, Virmani R. Pathological mechanisms of fatal late coronary stent thrombosis in humans. Circulation 2003;108(14):1701-6.
22. Virmani R, Farb A, Guagliumi G, Kolodgie FD. Drug-eluting stents: caution and concerns for long-term outcome. Coron Artery Dis 2004;15(6):313-8.
23. Virmani R, Guagliumi G, Farb A, Musumeci G, Grieco N, Motta T, et al. Localized hypersensitivity and late coronary thrombosis secondary to a sirolimus-eluting stent: should we be cautious? Circulation 2004;109(6):701-5.
24. Virmani R, Kolodgie FD, Farb A. Drug-eluting stents: are they really safe? Am Heart Hosp J 2004;2(2):85-8.

25. Finn AV, Nakazawa G, Joner M, Kolodgie FD, Mont EK, Gold HK, et al. Vascular responses to drug eluting stents: importance of delayed healing. Arterioscler Thromb Vasc Biol 2007;27(7):1500-10.
26. Garcia-Garcia HM, Gonzalo N, Kukreja N, Alfonso F. Greyscale intravascular ultrasound and IVUS-radiofrequency tissue characterization to improve understanding of the mechanisms of coronary stent thrombosis in drug-eluting stents. Eurointervention 2008;4(Supplement C):C33-C38.
27. Garcia-Garcia HM, Gonzalo N, Tanimoto S, Meliga E, de Jaegere P, Serruys PW. Characterization of Edge Effects With Paclitaxel-Eluting Stents Using Serial Intravascular Ultrasound Radiofrequency Data Analysis: The BETAX (BEside TAXus) Study. Rev Esp Cardiol 2008;61(10):1013-1019.
Study looking at the serial compositional changes at the reference segments of patients treated with paclitaxel eluting stent. Serial expansive vascular remodeling was observed at proximal and distal stent edges. Remodeling occurred in response to tissue growth, which was mainly due to increased fibrofatty tissue
28. Di Mario C, Gorge G, Peters R, Kearney P, Pinto F, Hausmann D, et al. Clinical application and image interpretation in intracoronary ultrasound. Study Group on Intracoronary Imaging of the Working Group of Coronary Circulation and of the Subgroup on Intravascular Ultrasound of the Working Group of Echocardiography of the European Society of Cardiology. Eur Heart J 1998;19(2):207-29.
29. Mintz GS, Nissen, S. E, Anderson, W. D, Bailey, S. R, Erbel, R, Fitzgerald, P. J, Pinto, F. J, Rosenfield, K, Siegel, R. J, Tuzcu, E. M, Yock, P. G. American College of Cardiology Clinical Expert Consensus Document on Standards for Acquisition, Measurement and Reporting of Intravascular Ultrasound Studies (IVUS). A report of the American College of Cardiology Task Force on Clinical Expert Consensus Documents. J Am Coll Cardiol 2001;37(5):1478-92.
30. Boppart SA, Bouma BE, Pitris C, Southern JF, Brezinski ME, Fujimoto JG. In vivo cellular optical coherence tomography imaging. Nat Med 1998;4(7):861-5.
31. Yun SH, Tearney GJ, Vakoc BJ, Shishkov M, Oh WY, Desjardins AE, et al. Comprehensive volumetric optical microscopy in vivo. Nat Med 2006;12(12):1429-33.
32. Liu B, Brezinski ME. Theoretical and practical considerations on detection performance of time domain, Fourier domain, and swept source optical coherence tomography. J Biomed Opt 2007;12(4):044007.
33. Asawa K, Kataoka T, Kobayashi Y, Hasegawa T, Nishioka H, Yamashita H, et al. Method analysis for optimal continuous imaging using intravascular optical coherence tomography. J Cardiol 2006;47(3):133-41.
34. Prati F, Cera M, Ramazzotti V, Imola F, Giudice R, Giudice M, et al. From bench to bedside. Circ J 2008;72(5):839-43.
35. Prati F CM, Ramazzotti V, Imola F, Giudice R, Albertucci M. Safety and feasibility of a new non-occlusive technique for facilitated intracoronary optical coherence tomography(OCT) acquisition in various clinical and anatomical scenarios. Eurointervention 2007;3:365-370.
36. Yamaguchi T, Terashima M, Akasaka T, Hayashi T, Mizuno K, Muramatsu T, et al. Safety and feasibility of an intravascular optical coherence tomography image wire system in the clinical setting. Am J Cardiol 2008;101(5):562-7.

37. Aoki J, Colombo A, Dudek D, Banning AP, Drzewiecki J, Zmudka K, et al. Peristent remodeling and neointimal suppression 2 years after polymer-based, paclitaxel-eluting stent implantation: insights from serial intravascular ultrasound analysis in the TAXUS II study. Circulation 2005;112(25):3876-83.
38. Jang IK, Tearney G, Bouma B. Visualization of tissue prolapse between coronary stent struts by optical coherence tomography: comparison with intravascular ultrasound. Circulation 2001;104(22):2754.
39. Grube E, Gerckens U, Buellesfeld L, Fitzgerald PJ. Images in cardiovascular medicine. Intracoronary imaging with optical coherence tomography: a new high-resolution technology providing striking visualization in the coronary artery. Circulation 2002;106(18):2409-10.
40. Alfonso F, Suarez A, Perez-Vizcayno MJ, Moreno R, Escaned J, Banuelos C, Jimenez P, Bernardo E, Angiolillo DJ, Hernandez R, Macaya C. Intravascular ultrasound findings during episodes of drug-eluting stent thrombosis. J Am Coll Cardiol 2007; 50:2095-2097.
41. Tearney GJ, Jang IK, Kang DH, Aretz HT, Houser SL, Brady TJ, et al. Porcine coronary imaging in vivo by optical coherence tomography. Acta Cardiol 2000; 55(4):233-7.
42. Bouma BE, Tearney GJ, Yabushita H, Shishkov M, Kauffman CR, DeJoseph Gauthier D, et al. Evaluation of intracoronary stenting by intravascular optical coherence tomography. Heart 2003;89(3):317-20.
43. Gonzalo N, Serruys PW, Regar E. Optical coherence tomography: clinical applications and the evaluation of DES. Minerva Cardioangiol 2008;56(5):511-25.
44. Tanigawa J BP, Dimopoulos K, Di Mario C. Optical coherence tomography to assess malapposition in overlapping drug-eluting stents. Eurointervention 2008;3: 580-583.
45. Tanigawa J, Barlis P, Di Mario C. Heavily calcified coronary lesions preclude strut apposition despite high pressure balloon dilatation and rotational atherectomy: in-vivo demonstration with optical coherence tomography. Circ J 2008;72(1):157-60.
46. Regar E, Schaar J, Serruys PW. Images in cardiology. Acute recoil in sirolimus eluting stent: real time, in vivo assessment with optical coherence tomography. Heart 2006; 92(1):123.
47. Schwarzacher SP, Metz JA, Yock PG, Fitzgerald PJ. Vessel tearing at the edge of intracoronary stents detected with intravascular ultrasound imaging. Cathet Cardiovasc Diagn 1997;40(2):152-5.
48. Schwartz RS, Huber KC, Murphy JG, Edwards WD, Camrud AR, Vlietstra RE, et al. Restenosis and the proportional neointimal response to coronary artery injury: results in a porcine model. J Am Coll Cardiol 1992;19(2):267-74.
49. Farb A, Sangiorgi G, Carter AJ, Walley VM, Edwards WD, Schwartz RS, et al. Pathology of acute and chronic coronary stenting in humans. Circulation 1999;99(1): 44-52.
50. Schroeder S, Baumbach A, Mahrholdt H, Haase KK, Oberhoff M, Herdeg C, et al. The impact of untreated coronary dissections on acute and long-term outcome after intravascular ultrasound guided PTCA. Eur Heart J 2000;21(2):137-45.

51. Hong MK, Park SW, Lee NH, Nah DY, Lee CW, Kang DH, et al. Long-term outcomes of minor dissection at the edge of stents detected with intravascular ultrasound. Am J Cardiol 2000;86(7):791-5, A9.
52. Nishida T, Colombo A, Briguori C, Stankovic G, Albiero R, Corvaja N, et al. Outcome of nonobstructive residual dissections detected by intravascular ultrasound following percutaneous coronary intervention. Am J Cardiol 2002;89(11):1257-62.
53. Futamatsu H, Sabate M, Angiolillo DJ, Jimenez-Quevedo P, Corros C, Morikawa-Futamatsu K, et al. Characterization of plaque prolapse after drug-eluting stent implantation in diabetic patients: a three-dimensional volumetric intravascular ultrasound outcome study. J Am Coll Cardiol 2006;48(6):1139-45.
54. Diaz-Sandoval LJ, Bouma BE, Tearney GJ, Jang IK. Optical coherence tomography as a tool for percutaneous coronary interventions. Catheter Cardiovasc Interv 2005; 65(4):492-6.
55. Cook S, Wenaweser P, Togni M, Billinger M, Morger C, Seiler C, et al. Incomplete stent apposition and very late stent thrombosis after drug-eluting stent implantation. Circulation 2007;115(18):2426-34.
56. Feres F, Costa JR, Jr., Abizaid A. Very late thrombosis after drug-eluting stents. Catheter Cardiovasc Interv 2006;68(1):83-8.
57. Sawada T, Shite J, Shinke T, Watanabe S, Otake H, Matsumoto D, et al. Persistent malapposition after implantation of sirolimus-eluting stent into intramural coronary hematoma: optical coherence tomography observations. Circ J 2006;70(11): 1515-9.
58. Xie Y, Takano M, Murakami D, Yamamoto M, Okamatsu K, Inami S, et al. Comparison of neointimal coverage by optical coherence tomography of a sirolimus-eluting stent versus a bare-metal stent three months after implantation. Am J Cardiol 2008; 102(1):27-31.
59. Chen BX, Ma FY, Luo W, Ruan JH, Xie WL, Zhao XZ, et al. Neointimal coverage of bare-metal and sirolimus-eluting stents evaluated with optical coherence tomography. Heart 2008;94(5):566-70.
60. Matsumoto D, Shite J, Shinke T, Otake H, Tanino Y, Ogasawara D, et al. Neointimal coverage of sirolimus-eluting stents at 6-month follow-up: evaluated by optical coherence tomography. Eur Heart J 2007;28(8):961-7.
61. Finn AV, Joner M, Nakazawa G, Kolodgie F, Newell J, John MC, et al. Pathological correlates of late drug-eluting stent thrombosis: strut coverage as a marker of endothelialization. Circulation 2007;115(18):2435-41.
62. Joner M, Finn AV, Farb A, Mont EK, Kolodgie FD, Ladich E, et al. Pathology of drug-eluting stents in humans: delayed healing and late thrombotic risk. J Am Coll Cardiol 2006;48(1):193-202.
63. Awata M, Kotani J, Uematsu M, Morozumi T, Watanabe T, Onishi T, et al. Serial angioscopic evidence of incomplete neointimal coverage after sirolimus-eluting stent implantation: comparison with bare-metal stents. Circulation 2007;116(8): 910-6.
64. Kotani J, Awata M, Nanto S, Uematsu M, Oshima F, Minamiguchi H, et al. Incomplete neointimal coverage of sirolimus-eluting stents: angioscopic findings. J Am Coll Cardiol 2006;47(10):2108-11.

65. Serruys PW, Degertekin M, Tanabe K, Abizaid A, Sousa JE, Colombo A, et al. Intravascular ultrasound findings in the multicenter, randomized, double-blind RAVEL (RAndomized study with the sirolimus-eluting VElocity balloon-expandable stent in the treatment of patients with de novo native coronary artery Lesions) trial. Circulation 2002;106(7):798-803.
66. Stone GW, Ellis SG, Cox DA, Hermiller J, O'Shaughnessy C, Mann JT, et al. A polymer-based, paclitaxel-eluting stent in patients with coronary artery disease. N Engl J Med 2004;350(3):221-31.
67. Morice MC, Serruys PW, Sousa JE, Fajadet J, Ban Hayashi E, Perin M, et al. A randomized comparison of a sirolimus-eluting stent with a standard stent for coronary revascularization. N Engl J Med 2002;346(23):1773-80.
68. Gerckens U LVY, Grube E. Optical Coherence Tomography Imaging in Coronary Drug-Eluting Stenting. Rev Esp Cardiol 2005;58(12):1469.
69. Takano M, Jang IK, Mizuno K. Neointimal proliferation around malapposed struts of a sirolimus-eluting stent: optical coherence tomography findings. Eur Heart J 2006;27(15):1763.
70. Prati F, Zimarino M, Stabile E, Pizzicannella G, Fouad T, Rabozzi R, et al. Does optical coherence tomography identify arterial healing after stenting? An in vivo comparison with histology, in a rabbit carotid model. Heart 2008;94(2):217-21.
71. Yao ZH, Matsubara T, Inada T, Suzuki Y, Suzuki T. Neointimal coverage of sirolimus-eluting stents 6 months and 12 months after implantation: evaluation by optical coherence tomography. Chin Med J (Engl) 2008;121(6):503-7.
72. Takano M, Yamamoto M, Inami S, Murakami D, Seimiya K, Ohba T, et al. Long-term follow-up evaluation after sirolimus-eluting stent implantation by optical coherence tomography: do uncovered struts persist? J Am Coll Cardiol 2008;51(9): 968-9.
73. Regar E, van der Giessen W.J, Serruys P.W. Optical Coherence Tomography Findings at 5-YearvFollow-Up After Coronary Stent Implantation. Circulation 2005;112: 345-346.
74. Takano M, Xie Y, Murakami D, Inami S, Yamamoto M, Ohba T, et al. Various optical coherence tomographic findings in restenotic lesions after sirolimus-eluting stent implantation. Int J Cardiol 2008.
75. Grube E, Lim V, Buellesfeld L. OCT findings in drug-eluting stents. London Informa Healthcare; 2007.
76. Shite J, Matsumoto D, Yokoyama M. Sirolimus-eluting stent fracture with thrombus, visualization by optical coherence tomography. Eur Heart J 2006;27(12):1389.
77. Schulz C, Herrmann RA, Beilharz C, Pasquantonio J, Alt E. Coronary stent symmetry and vascular injury determine experimental restenosis. Heart 2000;83(4):462-7.
78. Takebayashi H, Mintz GS, Carlier SG, Kobayashi Y, Fujii K, Yasuda T, et al. Nonuniform strut distribution correlates with more neointimal hyperplasia after sirolimus-eluting stent implantation. Circulation 2004;110(22):3430-4.
79. Suzuki Y, Ikeno F, Yeung AC. Drug-eluting stent strut distribution: a comparison between Cypher and Taxus by optical coherence tomography. J Invasive Cardiol 2006;18(3):111-4.

80. Buellesfeld L, Lim V, Gerckens U, Mueller R, Grube E. Comparative endoluminal visualization of TAXUS crush-stenting at 9 months follow-up by intravascular ultrasound and optical coherence tomography. Z Kardiol 2005;94(10):690-4.
81. Ormiston JA, Serruys PW, Regar E, Dudek D, Thuesen L, Webster MW, et al. A bioabsorbable everolimus-eluting coronary stent system for patients with single de-novo coronary artery lesions (ABSORB): a prospective open-label trial. Lancet 2008;371(9616):899-907.
Optical coherence tomography detects subtle structural changes of the polimeric struts.
82. Yabushita H, Bouma BE, Houser SL, Aretz HT, Jang IK, Schlendorf KH, et al. Characterization of human atherosclerosis by optical coherence tomography. Circulation 2002;106(13):1640-5.
Validation of OCT against pathology for coronary plaque characterization.
83. Rieber J, Meissner O, Babaryka G, Reim S, Oswald M, Koenig A, et al. Diagnostic accuracy of optical coherence tomography and intravascular ultrasound for the detection and characterization of atherosclerotic plaque composition in ex-vivo coronary specimens: a comparison with histology. Coron Artery Dis 2006;17(5): 425-30.
84. Patwari P, Weissman NJ, Boppart SA, Jesser C, Stamper D, Fujimoto JG, et al. Assessment of coronary plaque with optical coherence tomography and high-frequency ultrasound. Am J Cardiol 2000;85(5):641-4.
85. Kawasaki M, Bouma BE, Bressner J, Houser SL, Nadkarni SK, MacNeill BD, et al. Diagnostic accuracy of optical coherence tomography and integrated backscatter intravascular ultrasound images for tissue characterization of human coronary plaques. J Am Coll Cardiol 2006;48(1):81-8.
86. Kume T, Akasaka T, Kawamoto T, Watanabe N, Toyota E, Neishi Y, et al. Assessment of coronary arterial plaque by optical coherence tomography. Am J Cardiol 2006; 97(8):1172-5.
87. Jang IK, Bouma BE, Kang DH, Park SJ, Park SW, Seung KB, et al. Visualization of coronary atherosclerotic plaques in patients using optical coherence tomography: comparison with intravascular ultrasound. J Am Coll Cardiol 2002;39(4):604-9.
Optical coherence tomography identified most architectural features detected by IVUS and may provide additional detailed structural information.
88. Jang IK, Tearney GJ, MacNeill B, Takano M, Moselewski F, Iftima N, et al. In vivo characterization of coronary atherosclerotic plaque by use of optical coherence tomography. Circulation 2005;111(12):1551-5.
This is the first study to compare detailed in vivo plaque morphology in patients with different clinical presentations. Thin-cap fibroatheroma was more frequently observed in patients with AMI or ACS than SAP.
89. Chia S, Raffel OC, Takano M, Tearney GJ, Bouma BE, Jang IK. Comparison of coronary plaque characteristics between diabetic and non-diabetic subjects: An in vivo optical coherence tomography study. Diabetes Res Clin Pract 2008.
90. Chia S, Christopher Raffel O, Takano M, Tearney GJ, Bouma BE, Jang IK. In-vivo comparison of coronary plaque characteristics using optical coherence tomography in women vs. men with acute coronary syndrome. Coron Artery Dis 2007;18(6): 423-7.

91. Kume T, Okura H, Kawamoto T, Akasaka T, Toyota E, Watanabe N, et al. Relationship between coronary remodeling and plaque characterization in patients without clinical evidence of coronary artery disease. Atherosclerosis 2008;197(2):799-805.
92. Manfrini O, Mont E, Leone O, Arbustini E, Eusebi V, Virmani R, et al. Sources of error and interpretation of plaque morphology by optical coherence tomography. Am J Cardiol 2006;98(2):156-9.
In some cases, optical coherence tomography is not able to distinguish calcium deposits from lipid pools or the opposite, due to its low signal penetration.
93. Meng L, Lv B, Zhang S, Yv B. In vivo optical coherence tomography of experimental thrombosis in a rabbit carotid model. Heart 2008;94(6):777-80.
94. Kubo T, Imanishi T, Takarada S, Kuroi A, Ueno S, Yamano T, et al. Assessment of culprit lesion morphology in acute myocardial infarction: ability of optical coherence tomography compared with intravascular ultrasound and coronary angioscopy. J Am Coll Cardiol 2007;50(10):933-9.
Optical coherence tomography is a feasible in patients with AMI and allows identification of plaque rupture, fibrous cap erosion, intracoronary thrombus, and thin capped fibroatheromas in vivo more frequently compared with IVUS and angioscopy.
95. Kume T, Akasaka T, Kawamoto T, Ogasawara Y, Watanabe N, Toyota E, et al. Assessment of coronary arterial thrombus by optical coherence tomography. Am J Cardiol 2006;97(12):1713-7.
96. Kume T, Akasaka T, Kawamoto T, Okura H, Watanabe N, Toyota E, et al. Measurement of the thickness of the fibrous cap by optical coherence tomography. Am Heart J 2006;152(4):755 e1-4.
97. Cilingiroglu M, Oh JH, Sugunan B, Kemp NJ, Kim J, Lee S, et al. Detection of vulnerable plaque in a murine model of atherosclerosis with optical coherence tomography. Catheter Cardiovasc Interv 2006;67(6):915-23.
98. Takano M, Jang IK, Inami S, Yamamoto M, Murakami D, Okamatsu K, et al. In vivo comparison of optical coherence tomography and angioscopy for the evaluation of coronary plaque characteristics. Am J Cardiol 2008;101(4):471-6.
99. Kubo T, Imanishi T, Takarada S, Kuroi A, Ueno S, Yamano T, Tanimoto T, Matsuo Y, Masho T, Kitabata H, Tanaka A, Nakamura N, Mizukoshi M, Tomobuchi Y, Akasaka T. Implication of Plaque Color Classification for Assessing Plaque Vulnerability. J Am Coll Cardiol Intv 2008;1:74-80.
100. Chia S, Raffel OC, Takano M, Tearney GJ, Bouma BE, Jang IK. Association of statin therapy with reduced coronary plaque rupture: an optical coherence tomography study. Coron Artery Dis 2008;19(4):237-42.
101. Takarada S, Imanishi T, Kubo T, Tanimoto T, Kitabata H, Nakamura N, et al. Effect of statin therapy on coronary fibrous-cap thickness in patients with acute coronary syndrome: Assessment by optical coherence tomography study. Atherosclerosis 2008.
102. Nadkarni SK, Pierce MC, Park BH, de Boer JF, Whittaker P, Bouma BE, et al. Measurement of collagen and smooth muscle cell content in atherosclerotic plaques using polarization-sensitive optical coherence tomography. J Am Coll Cardiol 2007; 49(13):1474-81.

103. Tearney GJ, Yabushita H, Houser SL, Aretz HT, Jang IK, Schlendorf KH, et al. Quantification of macrophage content in atherosclerotic plaques by optical coherence tomography. Circulation 2003;107(1):113-9.
There was a high degree of positive correlation between OCT and histological measurements of fibrous cap macrophage density.

104. MacNeill BD, Jang IK, Bouma BE, Iftimia N, Takano M, Yabushita H, et al. Focal and multi-focal plaque macrophage distributions in patients with acute and stable presentations of coronary artery disease. J Am Coll Cardiol 2004;44(5):972-9.

105. Raffel OC, Tearney GJ, Gauthier DD, Halpern EF, Bouma BE, Jang IK. Relationship between a systemic inflammatory marker, plaque inflammation, and plaque characteristics determined by intravascular optical coherence tomography. Arterioscler Thromb Vasc Biol 2007;27(8):1820-7.

106. Sawada T, Shite J, Garcia-Garcia HM, Shinke T, Watanabe S, Otake H, et al. Feasibility of combined use of intravascular ultrasound radiofrequency data analysis and optical coherence tomography for detecting thin-cap fibroatheroma. Eur Heart J 2008;29(9):1136-46.
The combined use of OCT and VH-IVUS allows better characterization of TCFA

107. Gonzalo N, Garcia-Garcia HM, Regar E, Barlis P, Wentzel J, Onuma Y, Ligthart J, Serruys PW. In Vivo Assessment of High-risk Coronary Plaques at Bifurcations with Combined Intravascular Ultrasound Virtual Histology and Optical Coherence Tomography. JIMG 2009:In press.
The proximal rim of the ostium of the side-branch has been identified as a region more likely to contain thin fibrous cap and a greater proportion of necrotic core.

CHAPTER 10.2

Reproducibility of quantitative optical coherence tomography for stent analysis.

Gonzalo N, **Garcia-Garcia HM**, Serruys PW, Commissaris KH, Bezerra H, Barlis P, Gobbens P, Costa M, Regar E.

Submitted

ABSTRACT

Aims: to assess the inter and intra observer reproducibility for strut count, strut apposition and strut tissue coverage measurements with optical coherence tomography (OCT).

Methods and results: Ten drug-eluting stents (244 frames, 1712 struts) imaged with OCT 9 months after implantation were analyzed by 2 independent analysts. One of the analysts repeated the analysis of 5 stents (120 frames, 795 struts) one week later. Offline analysis was performed with the proprietary LightLab Imaging software. The number of struts was counted and lumen and stent area contours were traced. Tissue coverage thickness was measured at 360 degrees of vessel circumference and in front of every individual strut. The number of malapposed struts was determined. There was good agreement for strut number count (Kendall's Tau-b 0.90 for inter and 0.94 for intraobserver variability). The relative difference for lumen area, stent area and tissue coverage measurements was around 1%. There was complete inter and intraobserver agreement for malapposed struts classification (4 out of 1708 struts, Kappa=1).

Conclusions: In a corelab setting, the inter and intra observer reproducibility for strut count, strut apposition and strut tissue coverage measurements with OCT is excellent. This emphasizes the value of OCT as a tool for the clinical long-term assessment of stents.

CONDENSED ABSTRACT

The present study sought to evaluate the reproducibility of quantitative OCT for stent assessment in a detailed analysis on per strut level. Ten drug-eluting stents (244 frames, 1712 struts) imaged with OCT 9 months after implantation were analyzed by 2 independent analysts using the LightLab Imaging proprietary software. One of the analysts repeated the analysis of 5 stents (120 frames, 795 struts) one week later. There was very good agreement for strut number count and malapposition classification and a higher reproducibility of OCT measurements emphasizing the value of this technique as a tool for the clinical long-term assessment of stents.

Key words: optical coherence tomography, stent analysis, reproducibility

ABBREVIATIONS

OCT: optical coherence tomography
DES: drug-eluting stent
ROI: region of interest

INTRODUCTION

Optical Coherence Tomography (OCT) is a light-based imaging modality that can provide in vivo high-resolution images of the coronary artery(1). This technique offers the possibility to identify coronary stents and individual stent struts(2). Further, it is able to provide detailed information about struts apposition and tissue coverage. This is of special interest in drug-eluting stents (DES) in which the neointimal proliferation is inhibited to such extent that might not be visualized with conventional intracoronary IVUS(3). Animal studies demonstrated good correlation between intracoronary OCT and pathology for neointimal thickness measurements (4,5). However, no criteria have been established for the quantitative analysis of stents on a per strut level with OCT. The objective of the present study was to assess the inter and intra observer reproducibility for strut count, strut apposition and strut tissue coverage measurements with OCT.

METHODS

Study population

Ten stents (244 frames, 1712 struts) were analyzed in 8 asymptomatic patients undergoing an intracoronary OCT study 9 months after sirolimus (Cypher Select, Cordis, Johnson & Johnson, Miami, FL; 40%) or biolimus-eluting (Biomatrix III, Biosensors, Morges, Switzerland; 60%) stent implantation. The target vessel was the LAD in 50%, the LCX in 20% and the RCA in the 30% of the cases.

OCT acquisition

The OCT acquisition was performed using a commercially available system for intracoronary imaging (LightLab Imaging Inc, Westford, Massachusetts, US). The ImageWire (LightLab Imaging Inc, Westford, Massachusetts, US) consists of an optical fiber core (125 μm) covered by a protective sheath with a maximum

outer diameter of 0.019". It was positioned distal to the region of interest using a double lumen catheter (Twin Pass catheter, Vascular Solutions Inc) that had been previously placed in the artery over a conventional guide wire. The automated pullback was performed at 3 mm/s while the blood was removed by the continuous injection of iso-osmolar contrast (Iodixanol 370, Visipaque™, GE Health Care, Ireland) at 37° Celsius through the guiding catheter. The data was stored on CD for offline analysis.

OCT quantitative analysis

The analysis was performed with the proprietary LightLab software for off-line analysis (LightLab Imaging, Westford, Massachusetts, US). The data was imported in the workstation using the LightLab database format.

Z-Offset correction

The Z-Offset was adjusted in the catheterization laboratory before image acquisition while holding the ImageWire between two fingers. The Z-Offset is set properly when the ImageWire sheath is aligned with the yellow fiducials in the OCT image. During image acquisition, the optical fibers can stretch, especially at the beginning of the pullback. This may produce changes in the size of the Z-Offset along the pullback that can affect the accuracy of the measurements. Therefore, the Z-Offset was checked and modified if necessary in all the pullbacks before performing any measurement. To correct the Z-offset in saved pullbacks a frame in which the ImageWire sheath was in direct contact with the vessel wall was selected. In this frame the Z-Offset was corrected aligning the ImageWire sheath and the vessel wall with the yellow fiducials. This value of the Z-Offset was applied at the beginning of the pullback. If needed, the Z-Offset was recalibrated again along the pullback. The corrected Z-Offset was the same for both analysists.

Definition of the region of interest and frame selection

The region of interest (ROI) comprised the stented region and the reference segments. The ROI was systematically analysed in longitudinal intervals throughout the pullback. The stented region was defined as the region comprised between the first and the last frame with circumferentially visible struts. The reference segments were defined as the 5 mm proximal and distal to the stent. Frames were excluded when they presented severe artefacts such as incomplete blood clearance or non-uniform rotation distortion. When a frame was not analyzable an alternative frame located within the 2 proximal or distal frames was selected for analysis. No overlapping stent segments were included in the analysis.

Lumen analysis

The lumen contour was obtained with an automated detection algorithm available in the LightLab proprietary software and additional manual corrections were performed if necessary.

Stent analysis

Strut definitions: stent struts can show different appearances in OCT. In the present study structures were considered struts according to the following definitions.

a) Highly reflective surfaces (metal) with cast dorsal, radial shadows.
b) Highly reflective surfaces without dorsal shadowing.
c) Sector shaped shadows with sharp defined borders radial to the lumen.

Stent area

The stent contour was traced using a multiple point detection function. A support point for the contour was set in the middle of the endoluminal border of each stent strut. A semi-automated contour was then applied linking the points.

Struts coverage definitions and measurements

The tissue coverage area was calculated as stent area minus lumen area. Assessment of tissue coverage thickness was performed using a new function of the software which provides 360 degrees measurements, at 1 degree incremental, around the circumference of a given cross sectional image, developed in collaboration by Cardialysis-Cleveland, Cardialysis-Rotterdam and Lightlab (Figure 1). This also permits the measurement of the tissue located in front of every strut that was defined as strut coverage. The mean, maximum and minimum tissue coverage per strut were calculated.

Malapposition definitions and measurements

Malapossition was defined as separation of at least one stent strut from the vessel wall. To evaluate apposition by OCT, especially with DES, some considerations must be taken into account. Most DES are constituted by a metal body covered by a polymer. Since OCT can show only the endoluminal surface of the strut due to limited penetration through the metal, strut and polymer thickness must be considered in assessing apposition for each type of stent design. For the present study a strut was considered malapposed if the distance from its endo-luminal surface to the vessel wall was higher than the sum of the metal and polymer thickness (Figure 2).

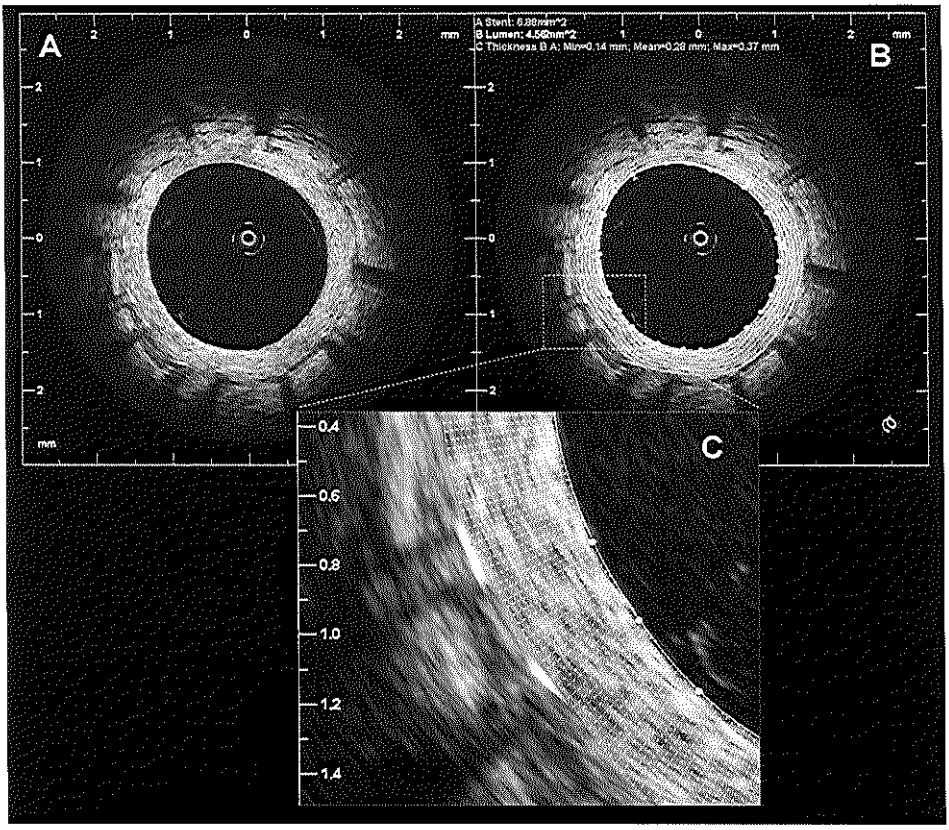

Figure 1: Tissue coverage measurement. A. Sirolimus eluting stent 9 months after stent implantation. B. The figure shows the lumen contour (white) and the stent contour (green). The tissue coverage area was calculated as stent area minus lumen area. The tissue coverage thickness was measured in 360 points (represented by the white chords). C. Magnification of 2 struts showing all the measurements (white chords) of the tissue coverage in front of every strut. For every strut the minimum, maximum and mean strut coverage was calculated.

Reproducibility design

The reproducibility for the struts count and the malapposition and tissue coverage thickness measurements were tested independently.

Strut count reproducibility

In order to assess the interobserver variability for the struts count, two experienced observers analyzed independently 100 cross sections and counted the number of struts in each one. To test the intraobserver variability one of the two observers repeated the analysis of 50 randomly selected cross sections one week later.

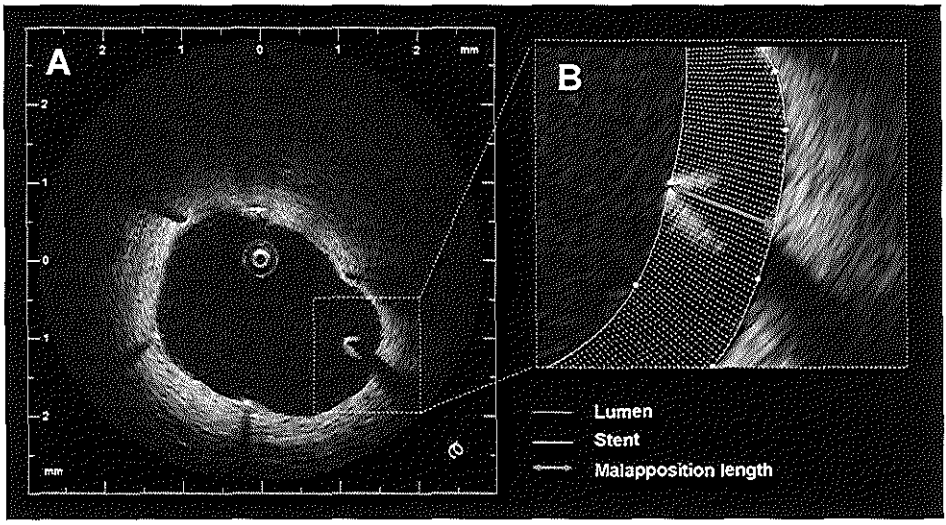

Figure 2: Malapposition. A. Example of a malapposed strut in a sirolimus eluting stent at 9 months follow up. **B.** Magnification of the malapposed strut. The yellow line represents the lumen contour and the white line corresponds to the stent contour. The distance from the endoluminal surface of the strut to the vessel wall (red arrow) was 440 μm (higher than the sum of the metal and polymer thickness for this type of stent).

Strut apposition and tissue coverage reproducibility

Two experienced observers analyzed independently 10 stents in order assess the interobserver variability for the struts apposition and tissue coverage measurements. One of the observers repeated the analysis in 5 of the cases one week later to evaluate the intraobserver variability.

Statistical analysis

The agreement of the number of struts counted in the same frame was estimated by calculating the Kendall's Tau-b rank correlation coefficient with its 95% confidence interval.

The inter and intraobserver reproducibility for lumen, stent and tissue coverage measurements were tested at 3 levels: per stent, per frame and per strut.

On a per stent level the mean and minimum lumen and stent area and the mean lumen and stent diameters were compared. The mean tissue coverage area and the mean, minimum and maximum tissue coverage thickness and strut coverage were also compared. The lumen, stent and tissue coverage volume were calculated by Trapezoidal rule. In the proximal and distal reference, the mean luminal area, diameter and volume were compared.

On a per frame level the luminal and stent areas and diameters were compared as well as the tissue coverage area and the mean, minimum and maximum tissue coverage thickness and strut coverage. In the frames corresponding to the proximal and distal edge, the mean luminal area and diameter were compared.

On a per strut level the mean, minimum and maximum tissue coverage in front of every strut were compared.

The reproducibility was calculated by estimating the residual standard deviation in an ANOVA model. The true value is expected to be within 1.96 times the calculated reproducibility of the single measurement for 95% of the observations. In addition the agreement between both observations has been expressed in Bland-Altman plots. The Bland-Altman plot depicts the differences of each pair of observations versus their mean values with reference lines for the mean difference of all paired observations and its 95% confidence limits, the so-called limits of agreement.

The Kappa coefficient for the agreement between observers for struts classification as incompletely apposed was tested for being not equal to zero.

RESULTS

A total of 244 frames and 1712 struts were evaluated for the interobserver reproducibility and 120 frames, 795 struts were evaluated for the intraobserver variability.

Strut count reproducibility

Interobserver variability

There was complete agreement in the number of struts between the two observers in 55% of the cross sections, difference of 1 strut in 31%, difference of 2 struts in 9% and difference of more than 2 struts in only 5% of the cross sections. The correlation between both observers was high, i.e. Kendall's Tau-b was 0.90 (95% confidence interval 0.85 – 0.94).

Intraobserver variability

There was complete agreement in the number of struts in 72% of the cross sections, difference of one strut in 24% and difference of 2 struts in 4% of the cross sections. The correlation between both observations was very high, i.e. Kendall's Tau-b was 0.94 (95% confidence interval 0.91 – 0.97).

Lumen, stent and tissue coverage measurements reproducibility

Stent level

The results for the inter and intraobserver reproducibility at the stent level are summarized in Tables 1 and 2 respectively.

Table 1. Interobserver reproducibility at stent level. N=10 stents. Min: minimum. Max: maximum. Obs1: observer 1 Obs2: observer 2. [aa] Reproducibility defined as residual standard deviation. [aaa] Bland-Altman limits of agreement defined as mean ± 1.96 SD of absolute difference.

Table 1				Difference			Limits of Agreement[aaa]	
		Observation 1	Observation 2	Absolute	Relative (Obs1/ Obs2)	Reproducibility[aa]	Lower	Upper
Stent	Mean Stent Area (mm^2)	5.44 ± 1.6	5.47 ± 1.5	-0.02 ± 0.2	1.0	0.1043	-0.32	0.28
	Mean Luminal Area (mm^2)	4.71 ± 1.5	4.70 ± 1.5	0.00 ± 0.0	1.0	0.0173	-0.05	0.05
	Mean Tissue Coverage Area (mm^2)	0.60 ± 0.5	0.63 ± 0.5	-0.03 ± 0.1	0.9	0.0780	-0.25	0.20
	Min Stent Area (mm^2)	3.89 ± 1.2	3.84 ± 1.1	0.05 ± 0.2	1.0	0.1549	-0.39	0.49
	Min Luminal Area (mm^2)	3.24 ± 1.1	3.26 ± 1.1	-0.01 ± 0.0	1.0	0.0158	-0.05	0.02
	Mean Tissue Coverage Thickness (mm)	0.08 ± 0.1	0.08 ± 0.1	0.00 ± 0.0	0.9	0.0100	-0.03	0.02
	Min Tissue Coverage Thickness (mm)	0.00 ± 0.0	0.00 ± 0.0	0.00 ± 0.0		0.0000	0.00	0.00
	Max Tissue Coverage Thickness (mm)	0.33 ± 0.1	0.33 ± 0.1	0.01 ± 0.0	1.1	0.0179	-0.04	0.06
	Mean Strut Coverage (mm)	0.08 ± 0.1	0.09 ± 0.1	-0.01 ± 0.0	0.9	0.0066	-0.02	0.01
	Min Strut Coverage (mm)	0.00 ± 0.0	0.00 ± 0.0	0.00 ± 0.0	0.0	0.0067	-0.02	0.02
	Max Strut Coverage (mm)	0.31 ± 0.1	0.32 ± 0.1	0.00 ± 0.0	1.0	0.0158	-0.05	0.04
	Mean Stent Diameter (mm)	2.60 ± 0.4	2.61 ± 0.4	-0.01 ± 0.0	1.0	0.0253	-0.08	0.07
	Mean Luminal Diameter (mm)	2.41 ± 0.4	2.41 ± 0.4	0.00 ± 0.0	1.0	0.0038	-0.01	0.01
	Stent Volume (mm^3)	101.58 ± 48.2	102.15 ± 48.3	-0.58 ± 2.7	1.0	1.8894	-5.97	4.81
	Luminal Volume (mm^3)	91.76 ± 48.0	91.67 ± 47.9	0.09 ± 0.5	1.0	0.3347	-0.87	1.05
	Tissue Coverage Volume (mm^3)	13.49 ± 11.6	14.13 ± 10.3	-0.65 ± 2.5	0.9	1.7454	-5.57	4.27
	In-stent Obstruction Volume (%)	13.73 ± 10.3	14.46 ± 9.0	-0.73 ± 2.2	0.9	1.5341	-4.95	3.49
Distal reference	Mean Luminal Area (mm^2)	4.13 ± 1.5	4.14 ± 1.4	0.00 ± 0.0	1.0	0.0085	-0.03	0.02
	Mean Luminal Diameter (mm)	2.20 ± 0.3	2.20 ± 0.3	0.00 ± 0.0	1.0	0.0067	-0.02	0.02
	Luminal Volume (mm^3)	18.39 ± 11.1	18.40 ± 11.1	-0.02 ± 0.1	1.0	0.0492	-0.16	0.12
Proximal reference	Mean Luminal Area (mm^2)	5.33 ± 2.4	5.27 ± 2.3	0.06 ± 0.1	1.0	0.1051	-0.23	0.35
	Mean Luminal Diameter (mm)	2.55 ± 0.6	2.54 ± 0.6	0.01 ± 0.0	1.0	0.0198	-0.04	0.07
	Luminal Volume (mm^3)	23.05 ± 8.6	22.87 ± 8.5	0.17 ± 0.4	1.0	0.3030	-0.67	1.01

Table 2. Intraobserver reproducibility at stent level. N=5 stents. Min: minimum. Max: maximum. Obs1: observation 1. Obs2: observation 2. [aa] Reproducibility defined as residual standard deviation. [aaa] Bland-Altman limits of agreement defined as mean ± 1.96 SD of absolute difference.

Table 2				Difference			Limits of Agreement[aaa]	
		Observation 1	Observation 2	Absolute	Relative (Obs1/Obs2)	Reproducibility[aa]	Lower	Upper
Stent	Mean Stent Area (mm^2)	5.95 ± 1.7	5.90 ± 1.6	0.05 ± 0.1	1.0	0.0621	-0.11	0.21
	Mean Luminal Area (mm^2)	4.97 ± 1.6	4.98 ± 1.6	-0.01 ± 0.0	1.0	0.0186	-0.06	0.05
	Mean Tissue Coverage Area (mm^2)	0.80 ± 0.7	0.76 ± 0.8	0.04 ± 0.1	1.1	0.0518	-0.09	0.17
	Min Stent Area (mm^2)	4.01 ± 1.0	3.88 ± 0.9	0.13 ± 0.2	1.0	0.1487	-0.24	0.49
	Min Luminal Area (mm^2)	3.14 ± 0.6	3.14 ± 0.6	0.00 ± 0.0	1.0	0.0077	-0.02	0.02
	Mean Tissue Coverage Thickness (mm)	0.10 ± 0.1	0.09 ± 0.1	0.00 ± 0.0	1.1	0.0060	-0.01	0.02
	Min Tissue Coverage Thickness (mm)	0.00 ± 0.0	0.00 ± 0.0	0.00 ± 0.0		0.0000	0.00	0.00
	Max Tissue Coverage Thickness (mm)	0.37 ± 0.1	0.35 ± 0.2	0.02 ± 0.0	1.1	0.0161	-0.02	0.05
	Mean Strut Coverage (mm)	0.11 ± 0.1	0.11 ± 0.1	0.00 ± 0.0	1.1	0.0029	-0.01	0.01
	Min Strut Coverage (mm)	0.00 ± 0.0	0.00 ± 0.0	0.00 ± 0.0		0.0000	0.00	0.00
	Max Strut Coverage (mm)	0.35 ± 0.2	0.34 ± 0.2	0.01 ± 0.0	1.1	0.0122	-0.01	0.04
	Mean Stent Diameter (mm)	2.72 ± 0.4	2.71 ± 0.4	0.01 ± 0.0	1.0	0.0138	-0.02	0.05
	Mean Luminal Diameter (mm)	2.48 ± 0.4	2.48 ± 0.4	0.00 ± 0.0	1.0	0.0043	-0.01	0.01
	Stent Volume (mm^3)	112.26 ± 58.0	111.37 ± 57.3	0.89 ± 1.5	1.0	1.1265	-2.00	3.78
	Luminal Volume (mm^3)	98.63 ± 58.2	98.74 ± 58.3	-0.11 ± 0.5	1.0	0.3502	-1.17	0.94
	Tissue Coverage Volume (mm^3)	18.05 ± 15.2	17.03 ± 16.0	1.02 ± 1.6	1.1	1.2617	-2.18	4.23
	In-stent Obstruction Volume (%)	16.81 ± 13.8	16.07 ± 13.9	0.74 ± 1.1	1.1	0.8790	-1.44	2.93
Distal reference	Mean Luminal Area (mm^2)	3.93 ± 1.4	3.93 ± 1.4	0.00 ± 0.0	1.0	0.0039	-0.01	0.01
	Mean Luminal Diameter (mm)	2.19 ± 0.3	2.19 ± 0.3	0.00 ± 0.0	1.0	0.0023	-0.01	0.01
	Luminal Volume (mm^3)	17.14 ± 8.6	17.14 ± 8.6	-0.01 ± 0.0	1.0	0.0239	-0.08	0.07
	Luminal Volume[a] (mm^3)	17.68 ± 9.2	17.69 ± 9.2	-0.01 ± 0.0	1.0	0.0196	-0.07	0.04
Proximal reference	Mean Luminal Area (mm^2)	5.86 ± 4.9	5.79 ± 4.8	0.07 ± 0.1	1.0	0.0628	-0.07	0.21
	Mean Luminal Diameter (mm)	2.60 ± 1.2	2.58 ± 1.2	0.02 ± 0.0	1.0	0.0121	-0.01	0.04
	Luminal Volume (mm^3)	18.61 ± 14.4	18.38 ± 14.2	0.23 ± 0.3	1.0	0.2035	-0.27	0.72
	Luminal Volume[a] (mm^3)	18.46 ± 15.3	18.23 ± 15.1	0.23 ± 0.2	1.0	0.1977	-0.21	0.67

Frame level

The results for the inter and intraobserver reproducibility at the frame level are summarized in Tables 3 and 4 respectively. Figures 3 and 4 show the results for the lumen, stent and tissue coverage area and mean neointimal thickness for inter and intraobserver reproducibility respectively.

Table 3. Interobserver reproducibility at frame level. N=244 frames. Min: minimum. Max: maximum. Obs1: observer 1 Obs2: observer 2. [a] Reproducibility defined as residual standard deviation. [aa] Bland-Altman limits of agreement defined as mean ± 1.96 SD of absolute difference.

Table 3		Difference					Limits of Agreement[aa]	
		Observer 1	Observer 2	Absolute	Relative (Obs1/ Obs2)	Reproducibility[a]	Lower	Upper
Stent	Stent Area (mm^2)	5.67 ± 1.7	5.71 ± 1.7	-0.03 ± 0.2	1.0	0.1694	-0.50	0.44
	Luminal Area (mm^2)	4.95 ± 1.7	4.95 ± 1.7	0.00 ± 0.1	1.0	0.0380	-0.10	0.11
	Tissue Coverage Area (mm^2)	0.56 ± 0.7	0.59 ± 0.6	-0.03 ± 0.2	0.9	0.1400	-0.41	0.36
	Mean Tissue Coverage Thickness (mm)	0.07 ± 0.1	0.07 ± 0.1	0.00 ± 0.0	0.9	0.0177	-0.05	0.05
	Min Tissue Coverage Thickness (mm)	0.02 ± 0.0	0.02 ± 0.0	0.00 ± 0.0	0.4	0.0132	-0.04	0.03
	Max Tissue Coverage Thickness (mm)	0.15 ± 0.1	0.15 ± 0.1	0.00 ± 0.0	1.0	0.0207	-0.06	0.06
	Mean Strut Coverage (mm)	0.08 ± 0.1	0.08 ± 0.1	-0.01 ± 0.0	0.9	0.0099	-0.03	0.02
	Min Strut Coverage (mm)	0.03 ± 0.1	0.04 ± 0.1	-0.01 ± 0.0	0.6	0.0125	-0.04	0.03
	Max Strut Coverage (mm)	0.14 ± 0.1	0.14 ± 0.1	0.00 ± 0.0	1.0	0.0141	-0.04	0.04
	Stent Diameter (mm)	2.66 ± 0.4	2.66 ± 0.4	-0.01 ± 0.1	1.0	0.0409	-0.12	0.10
	Luminal Diameter (mm)	2.47 ± 0.4	2.47 ± 0.4	0.00 ± 0.0	1.0	0.0090	-0.02	0.03
Distal reference	Luminal Area (mm^2)	4.34 ± 1.6	4.35 ± 1.6	-0.01 ± 0.0	1.0	0.0148	-0.05	0.03
	Luminal Diameter (mm)	2.28 ± 0.4	2.28 ± 0.4	0.00 ± 0.0	1.0	0.0077	-0.02	0.02
Proximal reference	Luminal Area (mm^2)	5.25 ± 2.1	5.20 ± 2.0	0.05 ± 0.1	1.0	0.0944	-0.21	0.30
	Luminal Diameter (mm)	2.54 ± 0.5	2.53 ± 0.5	0.01 ± 0.0	1.0	0.0180	-0.04	0.06

Strut level

Tables 5 and 6 show the inter (A) and intraobserver (B) reproducibility for the measurements at the strut level. Figure 5 shows the variability for the mean strut coverage.

Table 4. Intraobserver reproducibility at frame level. N=120 frames. Min: minimum. Max: maximum. Obs1: observation 1. Obs2: observation 2. [a] Reproducibility defined as residual standard deviation. [aa] Bland-Altman limits of agreement defined as mean ± 1.96 SD of absolute difference.

Table 4		Difference					Limits of Agreement[aa]	
		Observer 1	Observer 2	Absolute	Relative (Obs1/ Obs2)	Reproducibility[a]	Lower	Upper
Stent	Stent Area (mm^2)	6.28 ± 1.7	6.23 ± 1.7	0.05 ± 0.2	1.0	0.1224	-0.27	0.38
	Luminal Area (mm^2)	5.33 ± 1.8	5.34 ± 1.8	-0.01 ± 0.1	1.0	0.0596	-0.17	0.16
	Tissue Coverage Area (mm^2)	0.75 ± 0.9	0.70 ± 0.9	0.05 ± 0.1	1.6	0.1021	-0.22	0.32
	Mean Tissue Coverage Thickness (mm)	0.09 ± 0.1	0.08 ± 0.1	0.00 ± 0.0	1.2	0.0117	-0.03	0.04
	Min Tissue Coverage Thickness (mm)	0.03 ± 0.1	0.03 ± 0.1	0.00 ± 0.0	1.1	0.0197	-0.06	0.05
	Max Tissue Coverage Thickness (mm)	0.17 ± 0.2	0.17 ± 0.2	0.00 ± 0.0	1.1	0.0168	-0.04	0.05
	Mean Strut Coverage (mm)	0.10 ± 0.1	0.10 ± 0.1	0.00 ± 0.0	1.1	0.0083	-0.02	0.02
	Min Strut Coverage (mm)	0.05 ± 0.1	0.05 ± 0.1	0.00 ± 0.0	1.1	0.0181	-0.05	0.05
	Max Strut Coverage (mm)	0.17 ± 0.2	0.16 ± 0.2	0.00 ± 0.0	1.1	0.0125	-0.03	0.04
	Stent Diameter (mm)	2.80 ± 0.4	2.79 ± 0.4	0.01 ± 0.0	1.0	0.0272	-0.06	0.08
	Luminal Diameter (mm)	2.57 ± 0.4	2.57 ± 0.4	0.00 ± 0.0	1.0	0.0131	-0.04	0.04
Distal reference	Luminal Area (mm^2)	3.98 ± 1.6	3.98 ± 1.6	0.00 ± 0.0	1.0	0.0109	-0.03	0.03
	Luminal Diameter (mm)	2.20 ± 0.4	2.20 ± 0.4	0.00 ± 0.0	1.0	0.0041	-0.01	0.01
Proximal reference	Luminal Area (mm^2)	5.86 ± 3.8	5.79 ± 3.7	0.07 ± 0.1	1.0	0.0826	-0.12	0.27
	Luminal Diameter (mm)	2.60 ± 0.9	2.58 ± 0.9	0.02 ± 0.0	1.0	0.0164	-0.02	0.05

Malapposition classification reproducibility

The observers had complete agreement for the classification of malapposed struts (4 out of 1712 struts malapposed, Kappa coefficient 1). The intraobserver analysis show the same result (4 out of 795 struts malapposed, Kappa coefficient 1)

DISCUSSION

Due to its high resolution OCT can be a very valuable tool for the evaluation of the acute and long-term impact of stent implantation. OCT offers the possibility to assess stent apposition in great detail and allows the visualization and measurement of the tissue covering the struts even if this consists on tiny layers as it is frequently observed in DES(3). As the use of OCT is increasing rapidly,

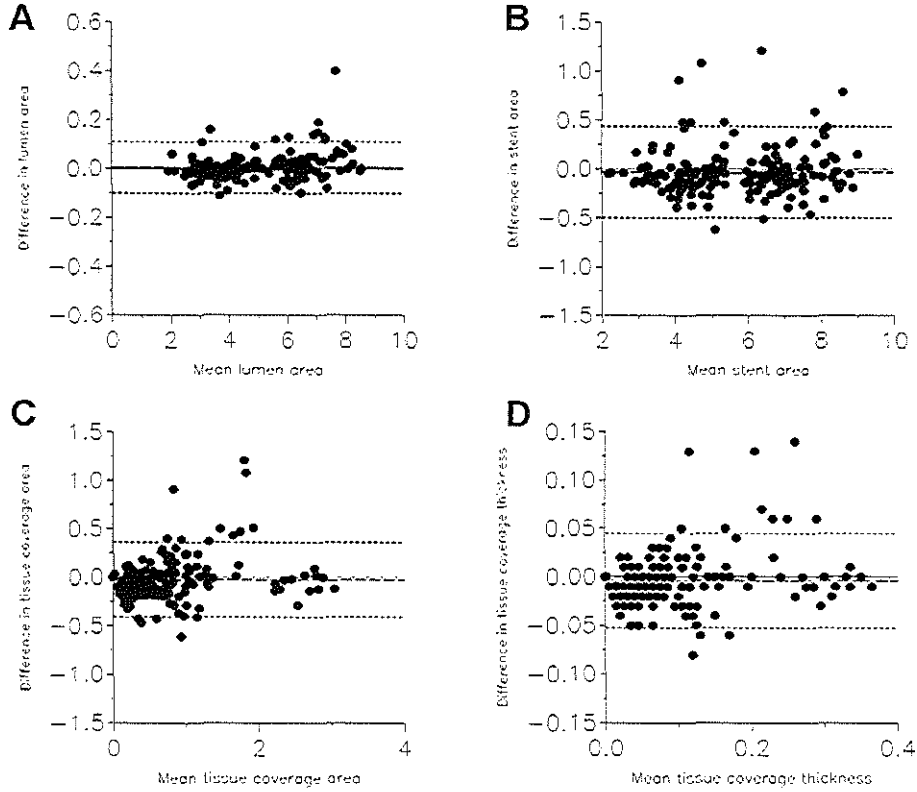

Figure 3: Interobserver reproducibility. Bland-Altman plots for the interobserver variability for mean lumen (A), stent (B) and tissue coverage area (C) and mean tissue coverage thickness (D).

Table 5. Interobserver reproducibility at strut level. N=1712 struts. Min: minimum. Max: maximum. [a] Reproducibility defined as residual standard deviation.
[aa] Bland-Altman limits of agreement defined as mean ± 1.96 SD of absolute difference.

Table 5			Difference			Limits of Agreement[aa]	
	Observer 1	Observer 2	Absolute	Relative (Obs1/Obs2)	Reproducibility[a]	Lower	Upper
Min Coverage Strut (mm)	0.09 ± 0.1	0.10 ± 0.1	-0.01 ± 0.0	0.9	0.0179	-0.05	0.04
Mean Coverage Strut (mm)	0.10 ± 0.1	0.11 ± 0.1	-0.01 ± 0.0	0.9	0.0174	-0.05	0.04
Max Coverage Strut (mm)	0.11 ± 0.1	0.11 ± 0.1	-0.01 ± 0.0	0.9	0.0175	-0.05	0.04

standardization of the methodology to measure and report stent apposition and tissue coverage is needed as well as data about the reproducibility of these measurements. Our results show that the methodology described in the present study allows analysis of stents by experienced analysts in a highly reproducible way.

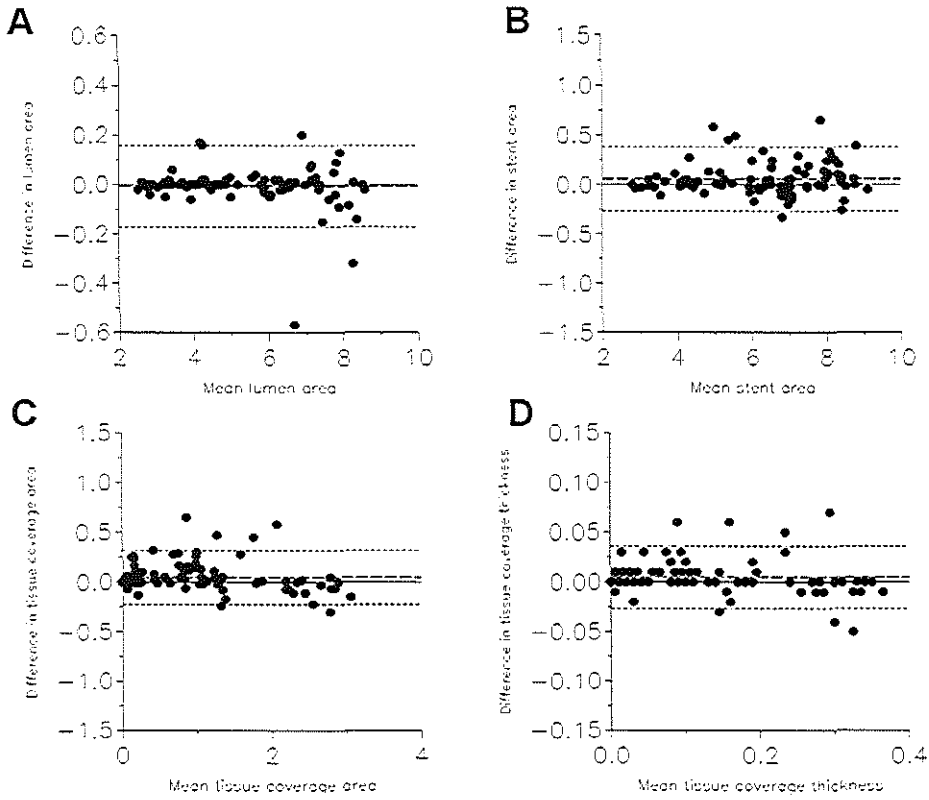

Figure 4: Intraobserver reproducibility. Bland-Altman plots for intraobserver variability for mean lumen (A), stent (B) and tissue coverage area (C) and mean tissue coverage thickness (D).

Table 6. Intraobserver reproducibility at strut level. N=795 struts. Min: minimum. Max: maximum. [a] Reproducibility defined as residual standard deviation.
[aa] Bland-Altman limits of agreement defined as mean ± 1.96 SD of absolute difference.

Table 6			Difference			Limits of Agreement[aa]	
	Observer 1	Observer 2	Absolute	Relative (Obs1/Obs2)	Reproducibility[a]	Lower	Upper
Min Coverage Strut (mm)	0.13 ± 0.1	0.13 ± 0.1	0.00 ± 0.0	1.1	0.0161	-0.04	0.05
Mean Coverage Strut (mm)	0.14 ± 0.1	0.13 ± 0.1	0.00 ± 0.0	1.1	0.0153	-0.04	0.04
Max Coverage Strut (mm)	0.14 ± 0.1	0.14 ± 0.1	0.00 ± 0.0	1.0	0.0154	-0.04	0.04

Stent struts can have different appearances by OCT. The reproducibility of struts count has not been previously reported. Our data suggests that the inter and intraobserver variability for strut count is low when applying strict strut definitions. For the intraobserver variability, only in 4% of the cases the difference between

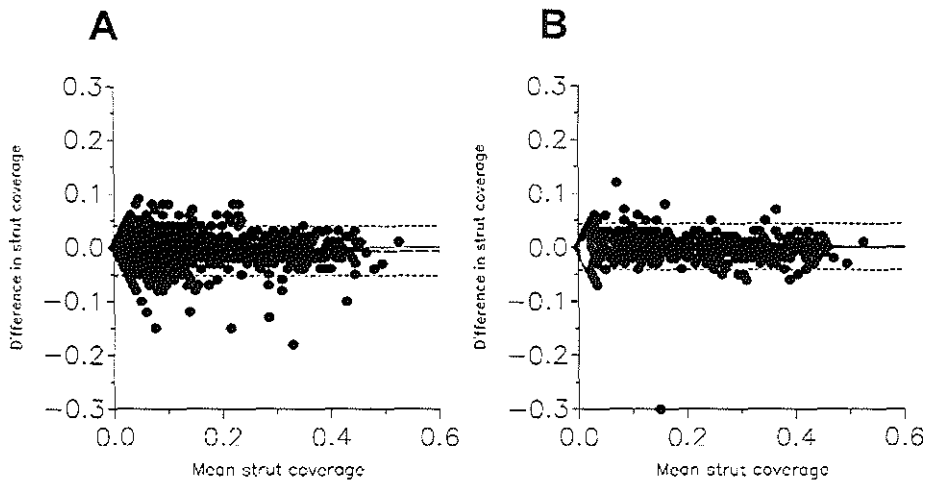

Figure 5: Strut coverage measurement reproducibility. Bland-Altman plots for the inter (A) and intraobserver (B) reproducibility for mean strut coverage measurements.

the 2 observations was more than one single strut while for the interobserver in only 5% of the cases the difference was higher than 2 struts.

High accuracy and precision for diameters measurement in vitro using proprietary software from LightLab has been reported(6). Tanimoto et al reported a low interobserver variability for lumen and stent area measurements with OCT using dedicated computer-assisted contour analysis(7). However, no specific study to assess the reproducibility of strut apposition and strut tissue coverage measurements by OCT has been reported.

Recently several OCT studies evaluating the struts apposition and tissue coverage in DES in humans at different time intervals using proprietary off-line software provided by LightLab Imaging have been published(8-11).

In most of these studies, the operator manually traced the stent and lumen area, to derive the tissue coverage area. Stent struts apposition and tissue coverage are usually individually measured at 1-mm intervals. However the way of reporting the tissue coverage varies between studies. Some authors report just tissue coverage thickness without detailed methodology (8,12). Other studies report the minimum, maximum or average tissue coverage but the selection method, the number of measurements and calculations method was not specified (9,10). The methodology used in the present study provides 360 data points for tissue coverage thickness for each cross section. Further the mean, the minimum and the maximum tissue coverage is reported for each individual strut. The mean tissue coverage per strut is derived from all the measurements at equidistal intervals along the strut.

Prati et al reported high inter and intraobserver reproducibility for neointima thickness measurements with OCT in carotid rabbit model (r^2 0.88 and 0.90 respectively)(4). Another study in humans comparing tissue coverage between SES and BMS reported 6 ± 8 μm and 8 ± 8 μm intra and interobserver variability for the measurement of tissue coverage(8). However the authors did not specify if the measurements correspond to mean, minimum or maximum tissue coverage, how many measurements were performed per strut or in which part of the strut measurements were taken. In the present study we observed absolute differences around 10 μm for the maximum and minimum strut coverage in repeated measurements. Those differences are in the limit of resolution of the technique. The absolute differences for tissue coverage area were 0.06 ± 0.02 mm^2 and 0.04 ± 0.02 mm^2 for the intra and interobserver variability respectively. Similar results were found when comparing stent and lumen area. A very good reproducibility for lumen measurement was expected as the automatic contour detection was used and not modified by the analyst in the majority of cases. The differences found in the present study are smaller than the ones reported previously by Xie et al for area measurements with OCT (0.3 ± 0.5 mm^2 and 0.2 ± 0.4 mm^2 for the intra and interobserver variability respectively). There are no reports on the reproducibility of lumen, stent and tissue coverage volumes derived from OCT. We found absolute differences around 1 mm^3 for the intra and 0.65 mm^3 for the interobserver variability for tissue coverage volume. Similar values (0.99 and 0.55 mm^3 for the intra and interobserver respectively) were obtained for the stent volume. As expected, the lumen volume variability was even lower (around 0.10 mm^3) as it was derived from automatic contour detection.

The higher resolution of OCT makes this technique superior to IVUS for the detection and measurement of tissue covering the stent struts. An IVUS study reported 62% of inter-observer agreement for the presence of neointimal tissue with discrepancy between observers in very thin neointimal layers and when the neointimal area was <2 mm^2 (13). In the present study evaluating DES, a very good agreement was found between observers for the measurement of tissue coverage even when the mean tissue coverage area was less than 1 mm^2. An increased variability in the classification of individual struts was observed when the tissue coverage was below 50 μm. This may be related to the image resolution but also to software limitations. Automatic algorithms for detecting stent coverage from OCT datasets are under development(14). This could help eliminating the remaining small observer-related variability found in our study.

Kubo et al reported a good intra and interobserver agreement (Kappa=0.90 and 0.75 respectively) for malapposed struts classification in sirolimus eluting stents(15). Those results are in line with our study in which the agreement between

observers for malapposed struts was excellent (kappa=1) even when applying customized cut-off points for each stent. However our results are limited by the small number of malapposed struts found in our population.

Clinical implications

The evaluation of strut apposition is essential in the evaluation of new stents designs as IVUS data have suggested a possible relation between apposition and the risk of stent thrombosis in DES(16,17). However interpretation of malapposition as assessed by OCT requires caution. Due to the high image resolution, malapposition of stent struts is a relatively common finding by OCT(8) but its clinical implications remain poorly understood. Incomplete endothelial struts coverage has been identified in pathology as the most powerful histological predictor of stent thrombosis(18,19). Pathological data in human suggests that neointimal coverage of stent struts could be used as a surrogate marker of endothelialization due to the good correlation between strut coverage and endothelialization. Animal data suggest good correlation between mean neointimal thickness measured by histology and OCT (4). The present study confirms that the tissue covering the strut can be measured with high reproducibility. However, the clinical relevance of uncovered struts as detected by OCT is not clear as some studies have reported presence of uncovered struts at follow-up not associated to clinical events(15). Further investigation and studies with longer follow up are needed in this field.

Although OCT has proved to be a highly informative imaging technique in assessing stents, standardization of the analysis of such images is not yet in place. In addition, OCT is a rapidly evolving imaging technology, and there is lack of large stent trials with long-term clinical follow-up linking OCT findings and clinical events. Thereby this methodology of analysis is prone to changes in the future in order to adjust to the new clinical needs.

CONCLUSIONS

In a corelab setting, the inter and intra observer reproducibility for strut count, strut apposition and strut tissue coverage measurements with OCT is excellent. This finding emphasizes the value of OCT as a tool for the clinical long-term assessment of stents.

REFERENCES

1. Regar E, van Leeuwen A, Serruys PW. 2007. Optical coherence tomography in cardiovascular research.London: Informa Healthcare. 338 p.
2. Gonzalo N, Serruys PW, Regar E. Optical coherence tomography: clinical applications and the evaluation of DES. Minerva Cardioangiol 2008;56(5):511-25.
3. Aoki J, Colombo A, Dudek D, Banning AP, Drzewiecki J, Zmudka K, Schiele F, Russell ME, Koglin J, Serruys PW. Peristent remodeling and neointimal suppression 2 years after polymer-based, paclitaxel-eluting stent implantation: insights from serial intravascular ultrasound analysis in the TAXUS II study. Circulation 2005;112(25):3876-83.
4. Prati F, Zimarino M, Stabile E, Pizzicannella G, Fouad T, Rabozzi R, Filippini A, Pizzicannella J, Cera M, De Caterina R. Does optical coherence tomography identify arterial healing after stenting? An in vivo comparison with histology, in a rabbit carotid model. Heart 2008;94(2):217-21.
5. Suzuki Y, Ikeno F, Koizumi T, Tio F, Yeung AC, Yock PG, Fitzgerald PJ, Fearon WF. In Vivo Comparison Between Optical Coherence Tomography and Intravascular Ultrasound for Detecting Small Degrees of In-Stent Neointima after Stent Implantation. J Am Coll Cardiol Intv 2008;1:168-73.
6. Tsuchida K, vd Giessen W, Patterson M, Tanimoto S,Garcia-Garcia H, Regar E, Ligthart J, Maugenest AM, Maatrijk G, Wentzel JJ, Serruys P.W. In-vivo validation of a novel three-dimensional quantitative coronary angiography system (CardioOp-B TM): Comparison with a conventional two-dimensional system (CASS II TM) and with special reference to optical cohence tomography. Eurointervention 2007;3:100-108.
7. Tanimoto S, Rodriguez-Granillo G, Barlis P, de Winter S, Bruining N, Hamers R, Knappen M, Verheye S, Serruys PW, Regar E. A novel approach for quantitative analysis of intracoronary optical coherence tomography: high inter-observer agreement with computer-assisted contour detection. Catheter Cardiovasc Interv 2008;72(2):228-35.
8. Xie Y, Takano M, Murakami D, Yamamoto M, Okamatsu K, Inami S, Seimiya K, Ohba T, Seino Y, Mizuno K. Comparison of neointimal coverage by optical coherence tomography of a sirolimus-eluting stent versus a bare-metal stent three months after implantation. Am J Cardiol 2008;102(1):27-31.
9. Chen BX, Ma FY, Luo W, Ruan JH, Xie WL, Zhao XZ, Sun SH, Guo XM, Wang F, Tian T and others. Neointimal coverage of bare-metal and sirolimus-eluting stents evaluated with optical coherence tomography. Heart 2008;94(5):566-70.
10. Matsumoto D, Shite J, Shinke T, Otake H, Tanino Y, Ogasawara D, Sawada T, Paredes OL, Hirata K, Yokoyama M. Neointimal coverage of sirolimus-eluting stents at 6-month follow-up: evaluated by optical coherence tomography. Eur Heart J 2007;28(8):961-7.
11. Takano M, Yamamoto M, Inami S, Murakami D, Seimiya K, Ohba T, Seino Y, Mizuno K. Long-term follow-up evaluation after sirolimus-eluting stent implantation by optical coherence tomography: do uncovered struts persist? J Am Coll Cardiol 2008;51(9):968-9.

12. Yao ZH, Matsubara T, Inada T, Suzuki Y, Suzuki T. Neointimal coverage of sirolimus-eluting stents 6 months and 12 months after implantation: evaluation by optical coherence tomography. Chin Med J (Engl) 2008;121(6):503-7.
13. Regar E, Werner F, Siebert U, Rieber J, Theisen K, Mudra H, Klauss V. Reproducibility of neointima quantification with motorized intravascular ultrasound pullback in stented coronary arteries. Am Heart J 2000;139(4):632-7.
14. Bonnema GT, Cardinal KO, Williams SK, Barton JK. An automatic algorithm for detecting stent endothelialization from volumetric optical coherence tomography datasets. Phys Med Biol 2008;53(12):3083-98.
15. Kubo T IT, Kitabata H, Kuroi A, Ueno S, Yamano T, Tanimoto T, Matsuo Y, Masho T, Takarada S, Tanaka A, Nakamura N, Mizukoshi M, Tomobuchi Y, Akasaka T. Comparison of vascular response after sirolimus eluting stent implantation between patients with unstable and stable angina pectoris. J Am Coll Cardiol Img 2008;1:475-84.
16. Alfonso F, Suarez A, Perez-Vizcayno MJ, Moreno R, Escaned J, Banuelos C, Jimenez P, Bernardo E, Angiolillo DJ, Hernandez R, Macaya C. Intravascular ultrasound findings during episodes of drug-eluting stent thrombosis. J Am Coll Cardiol 2007;50:2095-2097.
17. Cook S, Wenaweser P, Togni M, Billinger M, Morger C, Seiler C, Vogel R, Hess O, Meier B, Windecker S. Incomplete stent apposition and very late stent thrombosis after drug-eluting stent implantation. Circulation 2007;115(18):2426-34.
18. Finn AV, Joner M, Nakazawa G, Kolodgie F, Newell J, John MC, Gold HK, Virmani R. Pathological correlates of late drug-eluting stent thrombosis: strut coverage as a marker of endothelialization. Circulation 2007;115(18):2435-41.
19. Joner M, Finn AV, Farb A, Mont EK, Kolodgie FD, Ladich E, Kutys R, Skorija K, Gold HK, Virmani R. Pathology of drug-eluting stents in humans: delayed healing and late thrombotic risk. J Am Coll Cardiol 2006;48(1):193-202.

CHAPTER 10.3

In Vivo Assessment of High-risk Coronary Plaques at Bifurcations with Combined Intravascular Ultrasound Virtual Histology and Optical Coherence Tomography.

Gonzalo N, **García-García HM**, Regar E, Barlis P, Wentzel J, Onuma Y, Ligthart J, Serruys PW.

J Am Coll Cardiol Img. 2009;2:473– 82.

In Vivo Assessment of High-Risk Coronary Plaques at Bifurcations With Combined Intravascular Ultrasound and Optical Coherence Tomography

Nieves Gonzalo, MD, Hector M. Garcia-Garcia, MD, MSc, Evelyn Regar, MD, PhD, Peter Barlis, MBBS, MPH, Jolanda Wentzel, PhD, Yoshinobu Onuma, MD, Jurgen Ligthart, BsC, Patrick W. Serruys, MD, PhD

Rotterdam, the Netherlands

OBJECTIVES This study sought to evaluate the in vivo frequency and distribution of high-risk plaques (i.e., necrotic core rich) at bifurcations using a combined plaque assessment with intravascular ultrasound–virtual histology (IVUS-VH) and optical coherence tomography (OCT).

BACKGROUND Pathological examinations have shown that atherosclerotic plaque rich in necrotic core is prone to develop at bifurcations. High-risk plaque detection could be improved by the combined use of a technique able to detect necrotic core (IVUS-VH) and a high-resolution technique that allows the measurement of the fibrous cap thickness (OCT).

METHODS From 30 patients imaged with IVUS-VH and OCT, 103 bifurcations were selected. The main branch was analyzed at the proximal rim of the ostium of the side branch, at the in-bifurcation segment and at the distal rim of the ostium of the side branch. Plaques with more than 10% confluent necrotic core by IVUS-VH were selected and classified as fibroatheroma (FA) or thin-cap fibroatheroma (TCFA) depending on the thickness of the fibrous cap by OCT (>65 or ≤65 μm for FA and TCFA, respectively).

RESULTS Twenty-seven FA (26.2%) and 18 TCFA (17.4%) were found out of the 103 lesions studied. Overall the percentage of necrotic core decreases from proximal to distal rim (16.8% vs. 13.5% respectively, $p = 0.01$), whereas the cap thickness showed an inverse tendency (130 ± 105 μm vs. 151 ± 68 μm for proximal and distal rim, respectively, $p = 0.05$). The thin caps were more often located in the proximal rim (15 of 34, 44.1%), followed by the in-bifurcation segment (14 of 34, 41.2%), and were less frequent in the distal rim (5 of 34, 14.7%).

CONCLUSIONS The proximal rim of the ostium of the side branch has been identified as a region more likely to contain thin fibrous cap and a greater proportion of necrotic core. (J Am Coll Cardiol Img 2009;2:473–82) © 2009 by the American College of Cardiology Foundation

From the Thoraxcenter, Erasmus Medical Center, Rotterdam, the Netherlands.

Manuscript received September 30, 2008; revised manuscript received November 10, 2008, accepted November 16, 2008.

High-risk atherosclerotic plaques (i.e., rich in necrotic core) are prone to develop at bifurcations because of the specific shear stress conditions present in these regions (1,2). Stented bifurcations lesions represent a complex lesion subset at high risk of restenosis and thrombosis (3,4). These phenomena may reflect certain procedural aspects such as incomplete stent apposition, underexpansion, or gap regions (5,6), but may also be associated with specific compositional and morphological plaque features in these regions. Thin-cap fibroatheroma (TCFA) has been described as the plaque with an increased risk of rupture (7). Such lesions are characterized by a large necrotic core with a thin fibrous cap, usually <65 μm in thickness (8). Recently, it has been reported that TCFA detection could be improved by the combined use of intravascular ultrasound–virtual histology (IVUS-VH) and optical coherence tomography (OCT) (9).

See page 483

ABBREVIATIONS AND ACRONYMS

ACS = acute coronary syndrome
AIT = adaptative intimal thickening
CaFA = calcified fibroatheroma
CaTCFA = calcified thin-cap fibroatheroma
FA = fibroatheroma
IVUS-VH = intravascular ultrasound–virtual histology
LAD = left anterior descending artery
LCX = left circumflex artery
MMP = matrix metalloproteinase
NC = necrotic core
OCT = optical coherence tomography
PIT = pathological intimal thickening
RCA = right coronary artery
TCFA = thin-cap fibroatheroma

IVUS-VH uses spectral analysis of IVUS radiofrequency data to identify 4 tissue types in the atherosclerotic plaque, among them necrotic core (10). Optical coherence tomography is a high-resolution imaging modality that uses reflected near-infrared light, allowing a very precise visualization and measurement of vascular microstructures such as the fibrous cap (11). To our knowledge, in vivo characterization of necrotic core rich plaques at bifurcation regions has not been explored. The objective of the present study was therefore to evaluate in vivo the frequency and distribution of high-risk plaques at bifurcation lesions using a combined plaque assessment with IVUS-VH and OCT.

METHODS

Study population. All of the patients admitted to our hospital between January 2005 and March 2008 in whom IVUS-VH and OCT were performed in the same vessel were investigated for bifurcations adequately visualized by both imaging techniques. The indication for the IVUS-VH and OCT was the assessment of intermediate, nonflow-limiting lesions by angiography or post stent implantation assessment. Only regions located more than 5 mm beyond the stent were included. All patients gave written informed consent.

IVUS-VH acquisition. The IVUS was performed using the Eagle Eye 20 MHz catheter (Volcano Corp., Rancho Cordova, California) with an automatic continuous pullback at a rate of 0.5 mm/s. Grayscale images and radiofrequency data required for VH analysis were acquired during the same pullback. The VH processing was performed offline with pcVH 2.1 software (Volcano Corp.) that permits semiautomated contour detection and provides the compositional structure of the vessel. The IVUS-VH uses spectral analysis to classify the 4 different components of the atherosclerotic plaque and gives a color-coded map distinguishing between fibrous tissue (green), fibrofatty tissue (light green), necrotic core (red), and dense calcium (white).

OCT acquisition. The OCT acquisition was performed using a commercially available system for intracoronary imaging and a 0.019-inch ImageWire (LightLab Imaging, Westford, Massachusetts). Red blood cells represent a nontransparent tissue causing multiple light scattering and substantial signal attenuation. Therefore, for adequate OCT image acquisition blood must be temporarily removed from the vessel. In 77% of the cases this was achieved with the occlusion technique in which a proximal, low-pressure (0.4 atm) occlusion balloon (Helios, Goodman Inc., Nagoya, Japan) is inflated with simultaneous distal flush delivery (lactated Ringer solution; flow rate 0.8 ml/s) to remove blood from the vessel lumen. Images were acquired during a pullback rate of 1.0 mm/s. The possibility to increase the pullback speed up to 3 mm/s in the new OCT system permitted 23% of the cases to be acquired exclusively using a nonocclusive technique in which the blood was removed by the continuous injection of contrast (Iodixanol 370, Visipaque, GE Health Care, Cork, Ireland) through the guiding catheter. The nonocclusive technique reduces the procedural time and the incidence of chest pain and electrocardiographic changes during image acquisition without affecting the image quality (12).

Bifurcation selection and analysis. Simultaneous visual assessment of IVUS-VH and OCT pullbacks, in 2 contiguous screens, allowed the selection of all bifurcations that could be identified with both techniques (13). To ensure proper matching between 2 imaging modalities that have different lateral resolutions (20 μm for OCT and 300 μm for IVUS) and depth penetration, a strict selection of the frames was followed. Only the main branch was analyzed. The lesion analysis included: 1) proximal

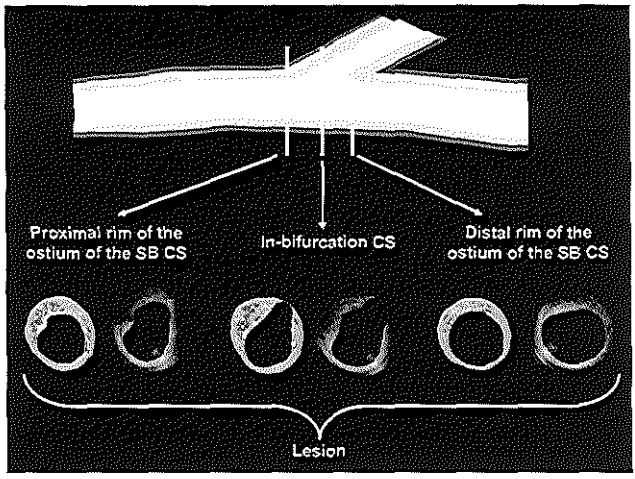

Figure 1. Bifurcation Selection and Analysis

Bifurcations that could be identified in both intravascular ultrasound-virtual histology (IVUS-VH) and optical coherence tomography (OCT) pullbacks were included. A strict selection of the analyzed cross-sections (CS) was followed to ensure correct matching between the 2 techniques. Plaques were analyzed only in the main branch. The lesion analysis included: 1) proximal rim of the ostium of the side branch (SB) CS (first frame proximal to the take-off of the SB); 2) in-bifurcation CS (frame with the larger ostial diameter of the SB); and 3) distal rim of the ostium of the SB CS (first frame distal to the take off of the SB).

rim of the ostium of the side branch cross-section (first frame proximal to the take-off of the side branch); 2) in-bifurcation cross-section (frame with the larger ostial diameter of the side branch); and 3) distal rim of the ostium of the side branch cross-section (first frame distal to the take off of the side branch) (Fig. 1). In each bifurcation the plaque location in relation to the flow divider was analyzed (Fig. 2).

Plaque type classification. Two experienced observers jointly analyzed the IVUS-VH data and the OCT measurements in the selected frames to characterize the plaque type according to the following hierarchical classification (7,14,15) (Figs. 3 to 5):

1. Adaptive intimal thickening (AIT): intimal thickening of <600 μm for <20% of the circumference.

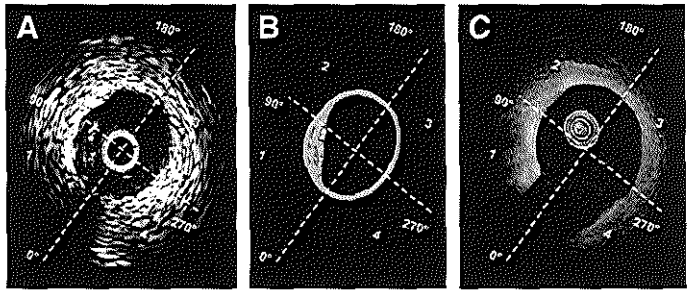

Figure 2. Location of the Plaque in Relation to the Flow Divider

To describe the plaque location in relation to the flow divider, the vessel cross-section was divided in 4 quadrants according to the position of the side branch. Quadrants 1 and 4 correspond to the ostium of the side branch, whereas quadrants 2 and 3 correspond to the part of the vessel wall located in front of the ostium of the side branch. (A) Grayscale IVUS. (B) Virtual histology. (C) OCT. Abbreviations as in Figure 1.

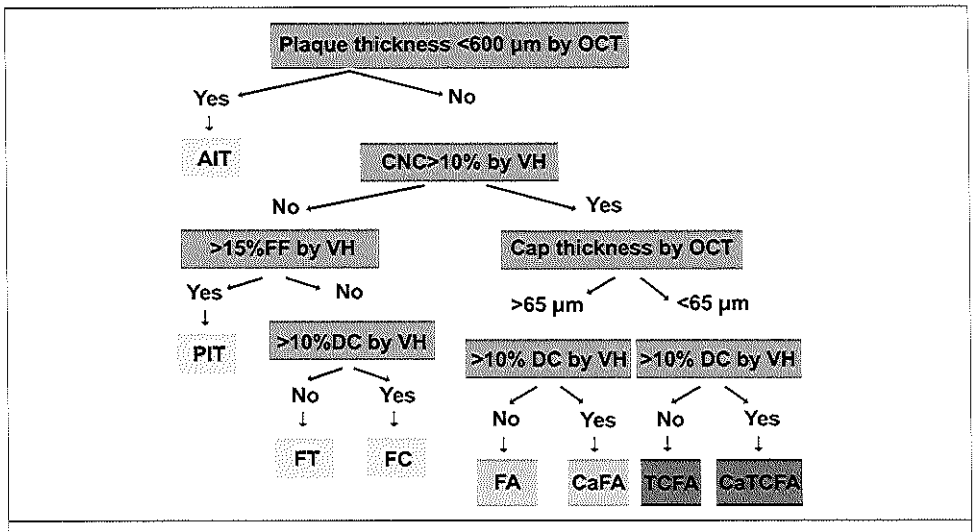

Figure 3. Plaque Classification Algorithm

AIT = adaptive intimal thickening; CaFA = calcified fibroatheroma; CaTCFA = calcified thin-cap fibroatheroma; CNC = confluent necrotic core; DC = dense calcium; FA = fibroatheroma; FC = fibrocalcic; FF = fibrofatty; FT = fibrotic; OCT = optical coherence tomography; PIT = pathological intimal thickening; TCFA = thin-cap fibroatheroma; VH = virtual histology.

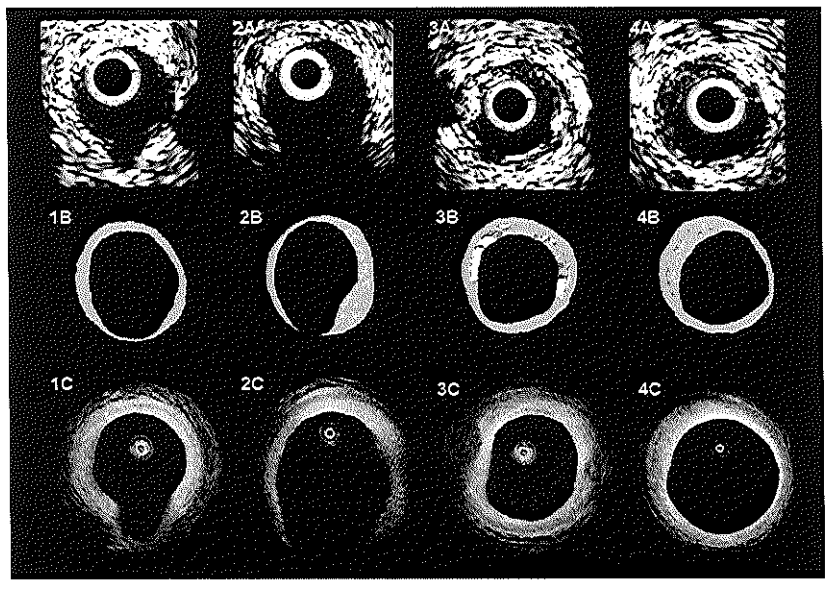

Figure 4. Low-Risk Plaques

Matched images of grayscale IVUS (A), virtual histology (B), and OCT (C) for the 4 types of plaques considered at low risk. 1: adaptive intimal thickening, 2: pathological intimal thickening, 3: fibrocalcific plaque, 4: fibrotic plaque. Abbreviations as in Figure 1.

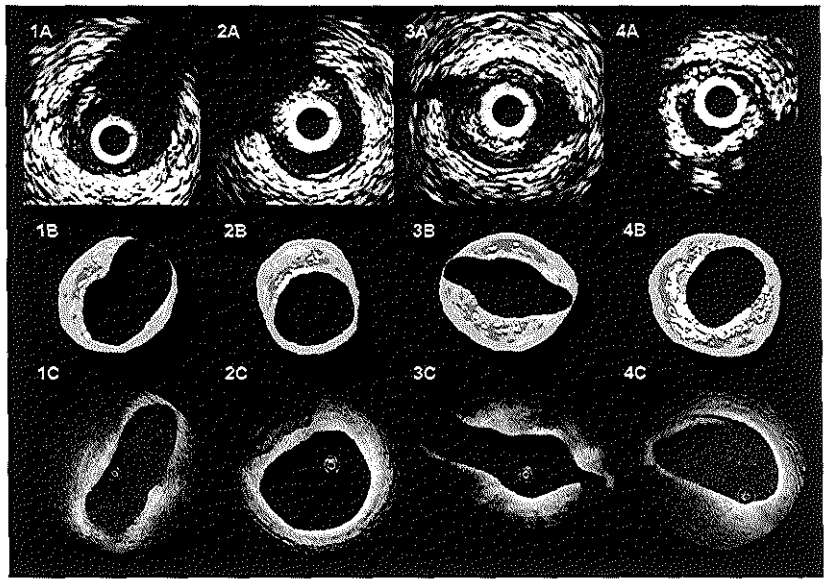

Figure 5. High-Risk Plaques

Matched images of grayscale IVUS (A), virtual histology (B), and OCT (C) for the 4 types of plaques considered at high risk of rupture. 1: fibroatheroma, 2: calcified fibroatheroma, 3: thin-cap fibroatheroma, 4: calcified thin-cap fibroatheroma. Abbreviations as in Figure 1.

2. Pathological intimal thickening (PIT): intimal thickening ≥600 μm for more than 20% of the circumference with more than 15% of fibrofatty tissue, and no confluent necrotic core or dense calcium.
3. Fibrotic plaque: plaque constituted predominantly by fibrous tissue without confluent necrotic core (NC) or dense calcium.
4. Fibrocalcific plaque: more than 10% of confluent dense calcium without confluent NC.
5. Fibroatheroma (FA): plaque characterized by the presence of more than 10% confluent NC covered by a fibrous cap thicker than 65 μm.
6. Calcified fibroatheroma (CaFA): fibroatheroma that contains more than 10% of confluent dense calcium.
7. IVUS/OCT-derived thin-capped fibroatheroma (TCFA): defined as the presence of more than 10% confluent NC at the lumen covered by a thin fibrous cap (<65 μm).
8. IVUS/OCT-derived calcified thin-capped fibroatheroma (CaTCFA): TCFA that contains more than 10% of confluent dense-calcium.

FAs and TCFAs are considered high-risk plaques in American Heart Association and Virmani classifications (7,16). The necrotic core was considered confluent when it was forming a major pool. This definition was used to avoid misclassification as high-risk plaques of lesions with isolated islets or individual pixels of necrotic core, which can be artifacts. The presence of confluent NC >10% at the lumen was measured using dedicated in house developed software (MATLAB MathWorks, Natick, Massachusetts) (9). A validation with pathology of a similar algorithm was reported in the CAPITAL (Carotid Artery Plaque Virtual Histology Evaluation) study (14). The diagnostic accuracy of IVUS-VH compared with histology in different carotid plaque types was 99.4% for TCFA, 96.1% for CaTCFA, 85.9% in FA, 85.5% for fibrocalcific, 83.4% in PIT, and 72.4% for CaFA. To overcome the limitations of IVUS-VH in the fibrous cap evaluation, the classification used in our study combines the information about plaque composition provided by IVUS-VH and the measurements of fibrous cap as assessed by OCT (9). The thinnest part of the fibrous cap was measured by OCT in all the plaques that contain more than 10% of confluent NC to distinguish between FA and TCFA. The fibrous cap measurement by OCT was guided by the IVUS-VH to avoid misclassification between lipid pools and calcium. The cap was measured in the area where the NC was closer to the lumen. The repro-

ducibility of fibrous cap measurements has previously been reported (12). If different morphologies were present along the lesion, the highest degree plaque was established as the definite plaque type.

Statistical analysis. Statistical analyses were performed using SPSS 12.0.1 for Windows (SPSS Inc., Chicago, Illinois). Continuous variables are expressed as mean ± SD. Categorical variables are expressed as percentages. The bifurcation (lesion) was the unit of analysis without corrections for correlated observations in the same subjects. To compare continuous variables between lesions, *t* test or analysis of variance was used. To compare continuous variables between different segments of the bifurcation, paired samples *t* test or Wilcoxon signed ranks test for 2 dependent samples was used. Comparison among groups for categorical variables was made with the chi-square method.

RESULTS

Clinical and procedural characteristics. One hundred and three bifurcations were selected in 32 pullbacks performed in 30 patients. The mean age was 60 ± 7 years, and 73% were male. Regarding cardiac risk factors, 48.3%, 6.9%, and 72.4% had hypertension, diabetes mellitus, and hyperlipidemia, respectively, and 27.6% were smokers. Seven percent had prior myocardial infarction, and 43.3% had undergone a prior percutaneous coronary intervention. The clinical presentation was stable angina in 86.7%, unstable angina in 10%, and acute myocardial infarction in 3.3%. The investigated vessel was the left anterior descending artery (LAD) in 34%, left circumflex artery (LCX) in 33% and right coronary artery (RCA) in 33% of the cases. The type of bifurcations studied were LAD/diagonal, LAD/septal branch, LCX/marginal, and RCA/right ventricular branch in 21.4%, 12.6%, 33%, and 33% of the cases, respectively. The indication for IVUS-VH and OCT was assessment of intermediate, non–flow limiting lesions by angiography in 40% of the cases and post-stent implantation assessment in the remaining 60% of cases. All studied lesions were considered nonsignificant by angiographic criteria and had a lumen area >4 mm^2 by IVUS. Overall the mean vessel and lumen area and plaque burden were 13.9 ± 3.7 mm^2, 7.7 ± 2.2 mm^2, and 43.2 ± 13%, respectively. Table 1 shows the number of quadrants containing plaque and the location of the thickest part of the plaque in relation to the side branch.

Table 1. Number of Quadrants Containing Plaque and Location of the Thickest Part of the Plaque in Relation to the Flow Divider

Number of quadrants containing plaque	
1	25/103 (24.3%)
2	33/103 (32.0%)
3	29/103 (28.2%)
4	16/103 (15.5%)
Location of the thickest part of the plaque	
Quadrant 1	28/103 (27.2%)
Quadrant 2	18/103 (17.5%)
Quadrant 3	26/103 (25.2%)
Quadrant 4	31/103 (30.1%)

Frequency of plaque type. The plaque type was analyzed in 103 lesions and 293 cross-sections. Eight distal and 8 proximal rims could not be analyzed because of artifacts. Overall, the frequency of each plaque type per lesion was: AIT 20 (19.4%), PIT 16 (15.5%), fibrocalcific 15 (14.6%), fibrotic 7 (6.8%), FA 8 (7.8%), CaFA 19 (18.4%), TCFA 10 (9.7%), and CaTCFA 8 (7.8%). In the analyzed cross-sections the distribution was as follows: AIT 76 (25.9%), PIT 53 (18.1%), fibrocalcific 42 (14.3%), fibrotic 28 (9.6%), FA 18 (6.1%), CaFA 42 (14.3%), TCFA 21 (7.2%), and CaTCFA 13 (4.4%).

NC and cap thickness distribution. The NC and cap thickness distribution in the proximal rim, in-bifurcation, and distal rim cross-sections are shown in Figure 6. Overall, the mean NC area and mean percentage of NC decreased from proximal to distal, whereas the mean cap thickness showed an inverse tendency.

High-risk plaque distribution and compositional and geometrical analysis. The distribution of the different plaque types in relation to the location is shown in Table 2. Figure 7 shows the number of cross-sections with high-risk plaque morphology in the proximal rim, in-bifurcation, and distal rim. The thin caps were more often located in the proximal rim (15 of 34, 44.1%), followed by the in-bifurcation (14 of 34, 41.2%), and were less frequent in the distal rim (5 of 34, 14.7%). The location of the thin cap in the 18 lesions classified as TCFAs was as follows: In 4 cases the thinning of the cap extended from the proximal rim into the distal rim, in 7 cases the thin cap was located in the proximal rim and in the in-bifurcation; in 3 TCFAs the thinning of the cap was located only in the in-bifurcation and, in 3 cases only in the proximal rim; there was 1 TCFA that presented the thin cap at both rims whereas the cap at the

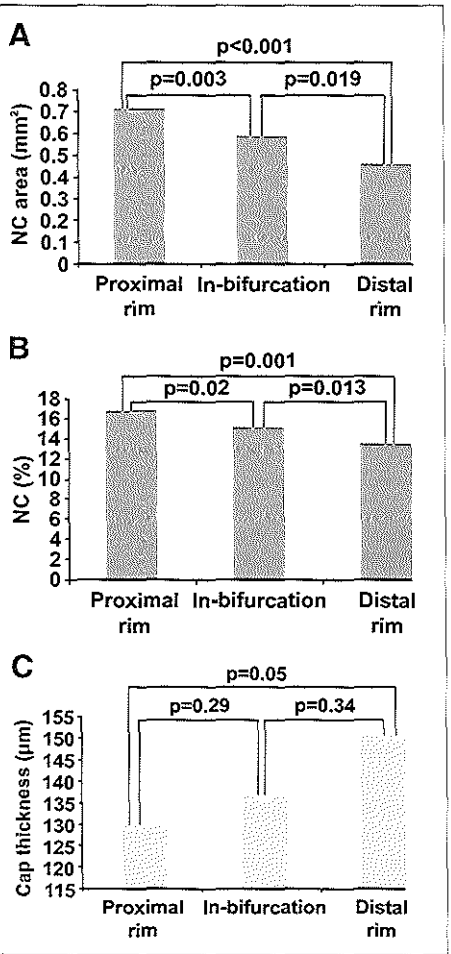

Figure 6. Necrotic Core and Cap Thickness Distribution

Necrotic core (NC) area (A), necrotic core percentage (B), and cap thickness (C) distribution in the proximal rim of the ostium of the side branch, in-bifurcation, and distal rim cross-sections.

in-bifurcation frame was thicker. There were no cases in which the thin cap was located only in the distal rim. The mean cap thickness in proximal rim, in-bifurcation, and distal rim in TCFAs is shown in Figure 8.

The vessel area and the plaque burden was significantly greater in the subgroup of lesions considered high risk (FA, CaFA, TCFA, and CaTCFA) than in the rest of lesions (16.5 ± 3 mm^2 vs. 14.1 ± 3 mm^2, p = 0.002 and 55 ± 9% vs. 42 ± 12%, p < 0.001 for vessel area and plaque burden, respectively), whereas the lumen area was not significantly different (6.8 ± 2 mm^2 vs. 7.1 ± 2 mm^2, p = 0.39). Table 3 shows the plaque burden, NC percentage, and cap thickness in FA, CaFA, TCFA, and CaTCFA.

Plaque type in relation to the clinical presentation. As exploratory analysis, patients with acute coronary syndromes (ACS) had a significant higher proportion of lesions with high-risk morphology plaques than stable patients (17 of 23 [73.9%] vs. 28 of 80 [35%], p = 0.002). Specifically the number of lesions with TCFA morphology was 6 of 23 (26.1%) vs. 12 of 80 (15%), p = 0.2, for ACS and stable patients respectively, and the number of lesions with FA morphology was 11 of 23 (47.8%) vs. 16 of 80 (20%), p = 0.01, for ACS and stable patients respectively.

DISCUSSION

To our knowledge this is the first in-vivo study evaluating the frequency and distribution of high-risk plaques at bifurcations in coronary arteries using a combined plaque assessment with IVUS-VH and OCT. The main finding is that the thinning of the fibrous cap occurs more often in the proximal rim of the ostium of the side branch. The NC shows also a differential distribution along the bifurcation being higher at the proximal rim.

Multi-modality plaque assessment. The detection of plaques at potentially high risk of rupture could prevent future occurrence of acute coronary syndromes. At present, multiple techniques are available that evaluate different aspects of the atherosclerotic plaque, such as its structure, composition, or mechanical properties (17). The combined infor-

Table 2. Distribution of the Different Plaque Types in the Proximal Rim of the Ostium of the Side Branch, In-Bifurcation, and Distal Rim Cross Sections

	AIT	PIT	FC	FT	FA	CaFA	TCFA	CaTCFA	Total
Proximal rim	21 (22.1%)	19 (20%)	13 (13.7%)	5 (5.3%)	8 (8.4%)	14 (14.7%)	10 (10.5%)	5 (5.3%)	95
In-bifurcation	24 (23.3%)	18 (17.5%)	15 (14.6%)	12 (11.7%)	5 (4.9%)	15 (14.6%)	8 (7.8%)	6 (5.8%)	103
Distal rim	31 (32.6%)	16 (16.8%)	14 (14.7%)	11 (11.6%)	5 (5.3%)	13 (13.7%)	3 (3.2%)	2 (2.1%)	95

N = 293 cross-sections.
AIT = adaptative intimal thickening; CaFA = calcified fibroatheroma; CaTCFA = calcified thin-cap fibroatheroma; FA = fibroatheroma; FC = fibrocalcic; FT = fibrotic; PIT = pathological intimal thickening; TCFA = thin-cap fibroatheroma.

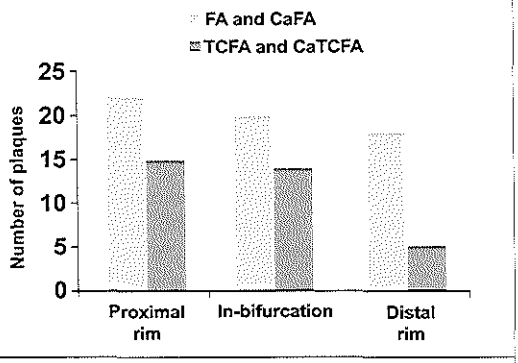

Figure 7. Distribution of the High-Risk Plaques in the Proximal Rim of the Ostium of the Side Branch, In-Bifurcation, and Distal Rim Cross-Sections

Number of cross-sections with high-risk plaque morphology in the proximal rim, in-bifurcation, and distal rim. Abbreviations as in Figure 3.

mation provided by the different methods is essential for better identification of high-risk coronary lesions. In this study, a combined approach with IVUS-VH and OCT was used. The IVUS-VH allows the detection and quantification of NC, one of the main components of high-risk plaques. However, the limited axial resolution of IVUS (approximately 200 μm) does not permit an accurate evaluation of the fibrous cap. On the contrary, OCT has a very high resolution (10 to 20 μm), allowing a very precise measurement of the fibrous cap. Sawada et al. (9) recently reported that the combined use of IVUS-VH and OCT improved the accuracy for TCFA detection. They studied 126 plaques in 56 patients with angina. Of the 61 plaques diagnosed as TCFA by IVUS-VH criteria, only 28 had a thin fibrous cap, as measured by OCT. In addition, 8 OCT-derived TCFA did not have NC in the VH analysis, mainly because of the misinterpretation in the OCT analysis caused by dense calcium. This source of error in plaque characterization by OCT has previously been described and indicates the difficulty in identifying TCFAs using only OCT (18). To avoid this misclassification in our study, the measurement of the fibrous cap in OCT was guided by IVUS-VH. At the present stage neither modality independently is sufficient for detecting the highest risk plaques; the combined approach seems to be mandatory for the accurate diagnosis of TCFA in vivo.

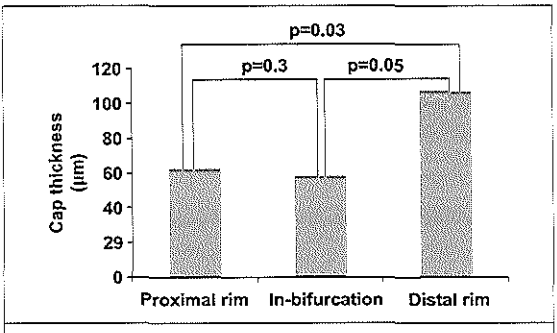

Figure 8. Cap Thickness Distribution in Thin-Cap Fibroatheromas

Mean cap thickness in the proximal rim of the ostium of the side branch, in-bifurcation, and distal rim cross-sections in thin-cap fibroatheromas.

High-risk plaque frequency, distribution, composition, and geometrical analysis. The in vivo frequency of TCFAs at bifurcations is not known. In our study, in which a highly selected population was included, 18 of 103 bifurcations presented TCFAs (17%). Considering that the number of bifurcations in the complete coronary tree is approximately 15 (19), the frequency of TCFAs per heart would be approximately 2.5. This is in agreement with reported pathological data (1). The bifurcation left main/LAD has been studied with IVUS-VH showing that the plaque burden and the amount of necrotic core are higher in the LAD than in the left main artery. However, plaque morphology in the different segments of other bifurcations has not been previously evaluated in vivo. The present study, which extended the assessment of bifurcation lesions beyond the left main artery, showed that the amount of necrotic core is higher at the proximal rim of the ostium of the side branch with a thin fibrous cap more often identified in the proximal rim. The fibrous cap thickness is determined by the balance between matrix synthesis by the smooth muscle cells and matrix degradation by metalloproteinases (MMP) produced by macrophages (20). It has been shown that the distribution of inflammatory cells in atherosclerotic plaques relates to the direction of the flow with higher concentration of macrophages and MMP activity in the upstream or proximal part (21). One of the mechanisms that have been proposed for the differential distribution of the high-risk plaques along the artery is the influence of endothelial shear stress. Bifurcations are geometrically irregular regions in which disturbed laminar flow occurs, generating abnormal endothelial shear stress patterns that may play a role in plaque destabilization. Previous studies showed that atherosclerosis develops preferentially at low shear stress locations such as the outer wall of bifurcations (2). However, in our data the thickest part of the plaque did not show a preferential location for this region.

Table 3. PB and NC Percent and Cap Thickness in FA, CaFA, TCFA, and CaTCFA

	FA (n = 8)	CaFA (n = 19)	TCFA (n = 10)	CaTCFA (n = 8)	p Value
PB (%)	51.7 ± 11	53.7 ± 10	54.2 ± 6	61.8 ± 5	0.13
NC (%)	20.1 ± 5.3	27.1 ± 6	33.0 ± 8	31.7 ± 8	0.002
Cap thickness (μm)	165 ± 59	174 ± 88	49 ± 15	51 ± 13	<0.001

NC = necrotic core; PB = plaque burden; other abbreviations as in Table 2.

Different pathological and IVUS studies have confirmed that plaque rupture occurs usually at sites of significant plaque accumulation associated with positive remodeling (2,22). This is in agreement with our data showing that the vessel area and the plaque burden were higher in high-risk plaques compared with stable lesions. In line with pathological series, TCFAs in our study were located in areas with nonsignificant lumen compromise, with a mean luminal area of 6.8 ± 2 mm^2 (8). Similarly, NC in TCFAs in this population is concordant with previously published pathological findings (8).

High-risk plaques in relation to clinical presentation. Although the comparison between ACS and stable patients in this study was exploratory, patients with unstable clinical presentation showed a high-risk profile of plaque types at bifurcations with a higher proportion of TCFAs and FA. This is in agreement with previous data regarding TCFA detection with IVUS-VH showing that ACS patients present a significantly higher prevalence of IVUS-derived TCFA than stable patients (10).

Study limitations. Currently VH-derived necrotic core rich plaques can only be considered as allegedly high-risk lesions because it has not been shown whether they are associated with a higher incidence of clinical events at follow-up. In the present study, OCT and VH were restricted to 1 or 2 vessels; therefore, and unlike pathological studies, this does not allow us to draw conclusions on the incidence of TCFA in bifurcations within the complete coronary tree. No comparison with nonbifurcation lesions was performed. Still the detailed plaque assessment combining 2 imaging modalities has given the first insight into the distribution of these allegedly high-risk lesions at bifurcations.

CONCLUSIONS

This study has given unique, in vivo data on the localization of plaque occurring at bifurcation lesions. Further, the proximal rim of the ostium of the side branch has been identified as a region more likely to contain thin fibrous cap and a greater proportion of necrotic core.

Reprint requests and correspondence: Prof. Patrick W. Serruys, Thoraxcenter, Ba583a, Gravendijkwal 230, 3015 CE Rotterdam, the Netherlands. *E-mail: p.w.j.c.serruys@erasmusmc.nl.*

REFERENCES

1. Virmani R, Burke A, Farb A, Kolodgie FD, Finn AV, Gold HK. Pathology of the vulnerable plaque. In: Waksman R, Serruys PW, Schaar J, editors. The Vulnerable Plaque. London, UK: Informa Healthcare, 2007: 13–27.
2. Slager CJ, Wentzel JJ, Gijsen FJ, et al. The role of shear stress in the generation of rupture-prone vulnerable plaques. Nat Clin Pract Cardiovasc Med 2005;2:401–7.
3. Al Suwaidi J, Berger PB, Rihal CS, et al. Immediate and long-term outcome of intracoronary stent implantation for true bifurcation lesions. J Am Coll Cardiol 2000;35:929–36.
4. Iakovou I, Schmidt T, Bonizzoni E, et al. Incidence, predictors, and outcome of thrombosis after successful implantation of drug-eluting stents. JAMA 2005;293:2126–30.
5. Costa RA, Mintz GS, Carlier SG, et al. Bifurcation coronary lesions treated with the "crush" technique: an intravascular ultrasound analysis. J Am Coll Cardiol 2005;46:599–605.
6. Alfonso F, Suarez A, Perez-Vizcayno MJ, et al. Intravascular ultrasound findings during episodes of drug-eluting stent thrombosis. J Am Coll Cardiol 2007;50:2095–7.
7. Virmani R, Kolodgie FD, Burke AP, Farb A, Schwartz SM. Lessons from sudden coronary death: a comprehensive morphological classification scheme for atherosclerotic lesions. Arterioscler Thromb Vasc Biol 2000;20:1262–75.
8. Virmani R, Burke AP, Farb A, Kolodgie FD. Pathology of the vulnerable plaque. J Am Coll Cardiol 2006;47:C13–8.
9. Sawada T, Shite J, Garcia-Garcia HM, et al. Feasibility of combined use of intravascular ultrasound radiofrequency data analysis and optical coherence tomography for detecting thin-cap fibroatheroma. Eur Heart J 2008;29:1136–46.
10. Rodriguez-Granillo GA, Garcia-Garcia HM, Mc Fadden EP, et al. In vivo intravascular ultrasound-derived thin-cap fibroatheroma detection using ultrasound radiofrequency data analysis. J Am Coll Cardiol 2005;46:2038–42.
11. Kume T, Akasaka T, Kawamoto T, et al. Measurement of the thickness of the fibrous cap by optical coherence tomography. Am Heart J 2006;152: 755e1–4.
12. Prati F, Cera M, Ramazzotti V, et al. From bench to bedside: a novel technique of acquiring OCT images. Circ J 2008;72:839–43.

13. Bruining N, Verheye S, Knaapen M, et al. Three-dimensional and quantitative analysis of atherosclerotic plaque composition by automated differential echogenicity. Catheter Cardiovasc Interv 2007;70:968–78.
14. Diethrich EB, Margolis P, Reid DB, et al. Virtual histology intravascular ultrasound assessment of carotid artery disease: The Carotid Artery Plaque Virtual Histology Evaluation (CAPITAL) study. J Endovasc Ther 2007;14:676–86.
15. Garcia-Garcia HM, Gonzalo N, Barlis P, Serruys PW. Novel intravascular imaging technologies. In: Nicholls S, Worthley S, editors. Imaging in Clinical Management. Sudbury, MA: Jones and Bartlett, 2009.
16. Stary HC, Chandler AB, Dinsmore RE, et al. A definition of advanced types of atherosclerotic lesions and a histological classification of atherosclerosis. Arterioscler Thromb Vasc Biol 1995;15:1512–31.
17. Garcia-Garcia HM, Gonzalo N, Granada JF, Regar E, Serruys PW. Diagnosis and treatment of coronary vulnerable plaques. Expert Rev Cardiovasc Ther 2008;6:209–22.
18. Manfrini O, Mont E, Leone O, et al. Sources of error and interpretation of plaque morphology by optical coherence tomography. Am J Cardiol 2006; 98:156–9.
19. Scanlon PJ, Faxon DP, Audet AM, et al. ACC/AHA guidelines for coronary angiography. A report of the American College of Cardiology/American Heart Association Task Force on practice guidelines (Committee on Coronary Angiography). J Am Coll Cardiol 1999; 33:1756–824.
20. Shah PK, Falk E, Badimon JJ, et al. Human monocyte-derived macrophages induce collagen breakdown in fibrous caps of atherosclerotic plaques. Potential role of matrix-degrading metalloproteinases and implications for plaque rupture. Circulation 1995; 92:1565–9.
21. Dirksen MT, van der Wal AC, van den Berg FM, van der Loos CM, Becker AE. Distribution of inflammatory cells in atherosclerotic plaques relates to the direction of flow. Circulation 1998;98:2000–3.
22. Cunningham KS, Gotlieb AI. The role of shear stress in the pathogenesis of atherosclerosis. Lab Invest 2005; 85:9–23.

Key Words: high-risk coronary plaques ▪ optical coherence tomography ▪ IVUS virtual histology ▪ bifurcation.

CHAPTER 10.4

Feasibility of Combined Use of Intravascular Ultrasound Radiofrequency Data Analysis and Optical Coherence Tomography for Detecting Thin-cap Fibroatheroma.

Sawada T, Shite J, **Garcia-Garcia HM**, Shinke T, Watanabe S, Otake H, Matsumoto D, Tanino Y, Ogasawara D, Kawamori H, Kato H, Miyoshi N, Yokoyama M, Serruys PW, Hirata K.

Eur Heart J. 2008 May;29(9):1136-46

Feasibility of combined use of intravascular ultrasound radiofrequency data analysis and optical coherence tomography for detecting thin-cap fibroatheroma

Takahiro Sawada[1], Junya Shite[1]*, Hector M. Garcia-Garcia[2], Toshiro Shinke[1], Satoshi Watanabe[1], Hiromasa Otake[1], Daisuke Matsumoto[1], Yusuke Tanino[1], Daisuke Ogasawara[1], Hiroyuki Kawamori[1], Hiroki Kato[1], Naoki Miyoshi[1], Mitsuhiro Yokoyama[1], Patrick W. Serruys[2], and Ken-ichi Hirata[1]

[1]Division of Cardiovascular Medicine, Department of Internal Medicine, Kobe University Graduate School of Medicine, 7-5-1 Kusunoki-cho, Chuo-ku, Kobe, Hyogo, 650-0017, Japan; and [2]Thoraxcenter, Erasmus MC, Rotterdam, The Netherlands

Received 5 October 2007; revised 25 February 2008; accepted 6 March 2008

Aims To evaluate the feasibility of the combined use of virtual histology (VH)-intravascular ultrasound (IVUS) and optical coherence tomography (OCT) for detecting *in vivo* thin-cap fibroatheroma (TCFA).

Methods and results In 56 patients with angina, 126 plaques identified by IVUS findings were analysed using both VH-IVUS and OCT. IVUS-derived TCFA was defined as an abundant necrotic core (>10% of the cross-sectional area) in contact with the lumen (NCCL) and %plaque-volume >40%. OCT-derived TCFA was defined as a fibrous cap thickness of <65 μm overlying a low-intensity area with an unclear border. Plaque meeting both TCFA criteria was defined as definite-TCFA. Sixty-one plaques were diagnosed as IVUS-derived TCFA and 36 plaques as OCT-derived TCFA. Twenty-eight plaques were diagnosed as definite-TCFA; the remaining 33 IVUS-derived TCFA had a non-thin-cap and eight OCT-derived TCFA had a non-NCCL (in discord with NCCL visualized by VH-IVUS, mainly due to misreading caused by dense calcium). Based on IVUS findings, definite-TCFA showed a larger plaque and vessel volume, %plaque-volume, higher vessel remodelling index, and greater angle occupied by the NCCL in the lumen circumference than non-thin-cap IVUS-derived TCFA.

Conclusion Neither modality alone is sufficient for detecting TCFA. The combined use of OCT and VH-IVUS might be a feasible approach for evaluating TCFA.

Keywords Thin-cap fibroatheroma • VH-IVUS • OCT • Necrotic core • Vessel positive remodelling

Introduction

Acute coronary syndrome (ACS) commonly results from plaque rupture,[1–3] and occasionally results from erosion or calcified nodules.[4,5] The pathologic features of plaque prone to rupture are a positively remodelled vessel, including a large necrotic core, a thin fibrous cap (<65 μm), and macrophage infiltration into the cap.[2,3] This entity is usually known as thin-cap fibroatheroma (TCFA).

The accurate detection of TCFA is vital for the diagnosis of vulnerable patients. New imaging modalities, such as virtual histology (VH)-intravascular ultrasound (IVUS) and optical coherence

* Corresponding author. Tel: +81 78 382 5846, Fax: +81 78 382 5859, Email: shite@med.kobe-u.ac.jp

tomography (OCT), were developed to precisely evaluate coronary plaques. Radiofrequency data analysis by VH-IVUS allows for atherosclerotic plaques to be classified as one of the four different types (fibrous, fibro-fatty, dense calcium, and necrotic core), and is especially useful for quantifying the necrotic core.[6,7] VH-IVUS cannot visualize the thin fibrous cap, however, because of its limited resolution (>100 μm). OCT, on the other hand, can provide a high resolution image (10–20 μm), but its penetration is limited (<2 mm).[8–11] OCT can visualize the thin fibrous cap, but is not able to detect a large and deep lipid core. Thus, it is difficult to diagnose TCFA using each modality alone. The combined use of these complementary imaging modalities, VH-IVUS and OCT, might result in more effective detection of TCFA.

The aim of this study was to elucidate the feasibility of the combined use of VH-IVUS and OCT to detect *in vivo* TCFA and to clarify the lesion characteristics of TCFA.

Methods

Patient and lesion population

Between August 2005 and March 2007, 402 patients with *de novo* ischaemic heart disease underwent coronary angiography in our hospital. Angina pectoris was identified as a significant coronary stenosis causing apparent myocardial ischaemia based on symptoms or electrocardiographic ST-T changes during an angina attack. To ensure safety during the OCT procedure, 121 patients were excluded because they had ST-segment elevation indicating an acute myocardial infarction or unstable angina pectoris warranting emergency percutaneous coronary intervention (PCI). Another 160 patients were excluded because 39 patients had chronic total occlusion, 20 patients had heavily calcified lesions that required rota-ablation, five patients had significant left main disease, and 96 patients had tortuous lesions expected to cause difficulty in advancing the IVUS and OCT catheters. Furthermore, we excluded six patients because they had vessels with a diameter >4.0 mm by angiography, which was too large to occlude blood flow. In the remaining 115 patients, 59 did not consent to the invasive intra-coronary examination, and the remaining 56 allowed us to perform the VH-IVUS and OCT examination. We identified plaques based on the IVUS findings and analysed each plaque using both VH-IVUS and OCT.

We assessed patient characteristics, including age, sex, body mass index, presence of coronary risk factors (hypertension, hyperlipidaemia, diabetes mellitus, smoking), and medication. Hypertension was defined as systolic blood pressure ≥140 mmHg, diastolic blood pressure ≥90 mmHg, or use of anti-hypertensive drugs. Hyperlipidaemia was defined as a present or past history of low-density lipoprotein–cholesterol level ≥140 mg/dl, or use of statin. Diabetes mellitus was defined as a fasting blood sugar >126 mg/dl and haemoglobin A1c ≥6.4%, or use of anti-diabetic medications (insulin or oral hypoglycaemics).

Binary examinations were performed if the patient experienced a severe angina attack or consented to a 6 month follow-up study (21 patients). This study was approved by the Ethics Committee of Kobe University.

Quantitative coronary arteriography measurement

Coronary angiogram was performed after intracoronary injection of nitroglycerin (250 μg), and the severity of stenosis was measured with a quantitative coronary arteriography cardiovascular measurement system (CMS-Medis Medical Imaging Systems, Leiden). We assessed traditional lesion types using the American Heart Association/American College of Cardiology's classification, and mapped the plaque location (proximal, mid, or distal vessel) angiographically. Because some plaques were completely undetectable by angiography, information from the IVUS was used to determine the plaque location.

Intravascular ultrasound procedure and quantitative coronary ultrasound measurement

A 2.9Fr 20 MHz IVUS catheter (Eagle-Eye™; Volcano Therapeutics, Inc., Rancho Cordova, CA, USA) was inserted into the coronary artery more than two-thirds distal, and subsequently pulled back with the aid of motorized pullback system (0.5 mm/s). The IVUS images obtained were digitized for quantitative and qualitative analysis according to the criteria of the American College of Cardiology's Clinical Expert Consensus Document on IVUS.[12] A 3D reconstruction of volumetric gray-scale IVUS data was performed using a semi-automated quantitative coronary ultrasound cardiovascular measurement system (CMS-Medis Medical Imaging Systems). If the patient required PCI, we obtained the IVUS data before the PCI procedure. Plaques in the same artery were considered to be separate lesions if the reference segment between them was >5 mm; otherwise, they were considered to be part of a single lesion.

IVUS data recorded on CD-ROM for off-line analysis were used to calculate the lesion length, lumen volume, vessel volume, and plaque volume (vessel volume−lumen volume) based on manual counter-detection of both the lumen and vessel interfaces in each cross-sectional frame. We then used these data to calculate %plaque-volume (plaque volume/vessel volume × 100) and remodelling index (vessel cross-sectional area of minimum lumen site/averaged reference vessel cross-sectional area).

Virtual histology analysis and definition of intravascular ultrasound-derived thin-cap fibroatheroma

Raw radiofrequency data of these lesions were stored on a DVD for off-line quantitative analysis, and plaques were classified by version 2.0 VH software into fibrotic, fibro-fatty, dense calcium, and necrotic core components. Plaque components were represented as a ratio of plaque volume (%fibrous, %fibro-fatty, %dense-calcium, %necrotic-core). Using a previously reported definition,[13] we defined IVUS-derived TCFA as a lesion meeting the following two criteria in at least three consecutive frames: (1) focal necrotic core-rich lesions (%necrotic-core >10%) without evident overlying fibrous tissue and (2) %plaque-volume ≥40%.

An independent investigator at the Erasmus Medical Center quantified the area of the necrotic core in contact with the lumen (NCCL) as well as the major confluent NCCL area and angle occupied by the NCCL in the lumen circumference using a program implemented in MATLAB™ (MathWorks, Natick, MA, USA). The angle formed by the connected necrotic core pixels on the border of the lumen was measured with respect to the lumen centre of gravity (*Figure 1*).[14]

Optical coherence tomography examination and definition of optical coherence tomography-derived thin-cap fibroatheroma

After the IVUS procedure, OCT examination was performed as previously described.[8] Briefly, an over-the-wire type occlusion balloon

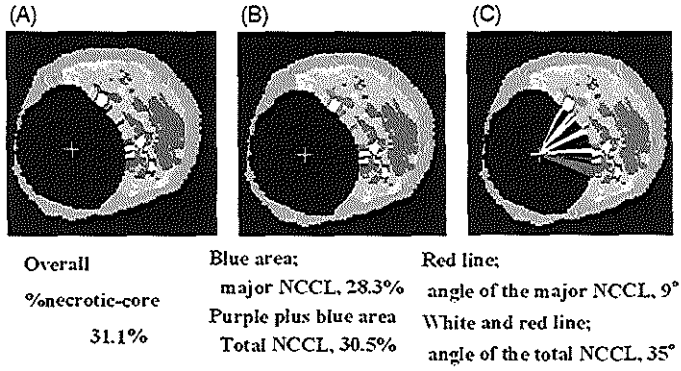

Figure 1 An example of selective quantification of the necrotic core in contact with the lumen (NCCL). (A) The original virtual histology-intravascular ultrasound cross-sectional area. (B) The blue area was selectively quantified as the major confluent NCCL areas and blue plus purple areas indicate total NCCL areas. (C) Measurement of the angle occupied by the total NCCL (white and red line) and the angle occupied by the major confluent NCCL (red line).

Table 1 Clinical characteristics

	Patients without definite-TCFA	Patients with definite-TCFA	*P*-value
Number (*n*)	32	24	
Age (year)	68.1 ± 8.7	70.1 ± 8.2	NS
Male (*n*)	18	17	NS
Body mass index (kg/m^2)	23.7 ± 2.8	24.6 ± 2.8	NS
Risk factor (*n*)			
Hypertension	25	19	NS
Hyperlipidemia	24	17	NS
Diabetes mellitus	18	11	NS
Smoke	10	9	NS
Acute coronary syndrome (*n*)	2	3	NS
Diseased vessel (1/2/3)	9/19/4	10/9/5	NS
Statin (*n*)	21	16	0.07
(Month)	15.0 (6.8, 34.5)	9.0 (6.3, 17.0)	0.09
ARB/ACEI (*n*)	21	19	NS
(Month)	22.0 (15.0, 96.0)	15.0 (12.0, 22.5)	NS
Total cholesterol (mg/dL)	177.1 ± 23.9	193.1 ± 40.2	0.07
LDL-cholesterol (mg/dL)	99.3 ± 17.4	112.8 ± 35.1	NS
HDL-cholesterol (mg/dL)	54.2 ± 21.6	52.1 ± 12.8	NS
Triglyceride (mg/dL)	132.6 ± 100.0	154.0 ± 93.0	NS
Fasting blood sugar (mg/dL)	115.1 ± 36.0	118.4 ± 40.2	NS
HemoglobinA1c (%)	6.2 ± 1.2	5.9 ± 0.9	NS
hs-CRP (mg/dl)	0.12 ± 0.11	0.15 ± 0.20	NS

Data are expressed mean value ± SD or median (25th, 75th percentile). $P < 0.05$ was considered statistically significant.
ARB, angiotensin receptor blocker; ACEI, angiotensin converting enzyme inhibitor; hs-CRP, high-sensitive C-reactive protein.

catheter (Helios™, LightLab Imaging Inc., Westford, MA USA) and an OCT imaging probe (ImageWire™, LightLab Imaging Inc.) were inserted into the coronary artery more than two-thirds distal. The entire vessel length was imaged with an automatic pullback device at 1 mm/s, and OCT data were recorded on a CD-ROM for off-line analysis.

An OCT image of a signal-poor lesion with an unclear border was diagnosed as a lipid core and a signal-rich homogenous lesion overlying lipid content was diagnosed as a fibrous cap.[9–11] The thinnest part of the fibrous cap was measured three times and the average value calculated. Because the previous histopathology report revealed that 95% of the fibrous cap thickness near a rupture site was <65 μm,[15] a lesion whose fibrous cap thickness at the thinnest part was <65 μm was diagnosed as OCT-derived TCFA.

Comparison of virtual histology-intravascular ultrasound and optical coherence tomography images and definition of definite-thin-cap fibroatheroma

We compared the VH-IVUS and OCT images of identical lesions using the locations of side branches, longitudinal plaque distribution, or calcification as landmarks. If the plaque met the criteria of both the IVUS-derived TCFA and OCT-derived TCFA, we diagnosed it as definite-TCFA. If IVUS-derived TCFA did not have a thin fibrous cap (<65 μm) by OCT measurement, we diagnosed it as non-thin-cap IVUS-derived TCFA. If VH-IVUS did not detect an NCCL that was detected by OCT-derived TCFA, the plaque was diagnosed as non-NCCL OCT-derived TCFA.

To assess intra- and inter-observer variability, all VH-IVUS and OCT data were read by two independent observers. The first observer repeated a blind analysis of all the data at two separate time points (with at least 1 month interval between the two analyses). If there was discordance of either the IVUS- or OCT-derived TCFA diagnosis between the two observers, a consensus diagnosis was obtained with repeated off-line readings.

Statistical analysis

This is a pilot study that compared the data between VH-IVUS and OCT. Because a previous study demonstrated that plaque volume, vessel remodelling, necrotic core volume, and circumference were associated with an unstable plaque type,[2,16] we hypothesized that the factors indicative of thin fibrous cap in IVUS-derived TCFA were %plaque-volume, remodelling index, and angle occupied by NCCL in the lumen circumference. Thus, the sample size was based on the preliminary data obtained in our laboratory and was determined on the basis of the following assumptions: A type-I error of 0.05 (two-sided); power of 80%; difference in the %plaque-volume, remodelling index, and the NCCL angle between definite TCFA and non-thin-cap IVUS-derived TCFA of 8.0%, 0.1, and 30°, respectively, and a standard deviation of 8.0, 0.12, and 35, respectively. Therefore, the minimum required sample size was 23 lesions in each group. We stopped recruitment at 20 months, because the power of these data was beyond 99.9%. Because of the limited sample size of non-NCCL OCT-derived TCFA (eight lesions), the data for this group were considered exploratory.

Statview version 5.0 (SAS, Cary, NC, USA) was used for the data analysis. Qualitative data are presented with frequencies and quantitative data are shown as medians (25th and 75th percentiles) or mean ± SD when indicated. Comparison of laboratory data between the two groups was performed using the unpaired *t*-test. If the data were not normally distributed, as determined by Kolmogorov–Smirnov analysis, the data were analysed using a Mann–Whitney test. A two-sided *P*-value of <0.05 was considered statistically significant.

Angiographical data, gray-scale IVUS and VH-IVUS data were analysed using random-effects generalized least-squares regression in order to account for repeated measurements on individual patients. Wald's test was used for assessing differences in means between plaque type categories. Fitted models were used in calculating predicted means and their 95% confidence intervals (CIs). For the values in *Table 2*, a model with two categories of plaque types (definite-TCFA and non-TCFA) was fit. For the values displayed in *Tables 3* and *4*, a separate model with four categories of plaque types (definite-TCFA and the three subcategories of non-TCFA plaque types) was fit. Predicted means and CIs for definite-TCFA in *Tables 3* and *4* occasionally differ slightly from those in *Table 2*, because separate models were used. An adjusted *P*-value of <0.0167 (0.05/3, Bonferroni's correction for multiple comparisons) was used as the threshold for significance to avoid an inflated type-I error because three pairwise planned comparisons were made.

To assess the inter- and intra-observer variability, the results were compared using the κ-test of concordance for the categorical data and Bland–Altman plot was fulfilled for continuous variables.

Results

Feasibility of virtual histology-intravascular ultrasound and optical coherence tomography examinations

In 56 patients, 82 diseased vessels were observed with VH-IVUS and OCT without any complications. We identified 126 plaques in the 82 diseased vessels. The average procedure time of VH-IVUS and OCT, including preparation of both devices, was 18.7 ± 4.4 min. The mean evaluation length by VH-IVUS was 48.6 ± 16.3 mm and that measured by OCT was 44.5 ± 12.8 mm. The average balloon occlusion time for one-time OCT imaging was 49.8 ± 11.4 s.

Identification of intravascular ultrasound-, optical coherence tomography-derived thin-cap fibroatheroma, and definite-thin-cap fibroatheroma

Of 126 plaques, VH-IVUS observations identified 61 plaques (48.4%) as IVUS-derived TCFA, and OCT examination diagnosed 36 plaques (28.6%) as OCT-derived TCFA. Twenty-eight (22.2%) of the plaques met both criteria for TCFA and were diagnosed as definite-TCFA. The remaining 33 IVUS-derived TCFA (26.2%) were diagnosed as non-thin-cap IVUS-derived TCFA (mean fibrous cap thickness by OCT was 99.0 ± 13.3 μm) and the remaining eight OCT-derived TCFA (6.3%) were diagnosed as non-NCCL OCT-derived TCFA. The positive ratio of VH-IVUS for detecting definite TCFA was 45.9% and that of OCT was 77.8%. A summary of the lesion diagnoses is shown in *Figure 2* and representative cases of non-thin-cap IVUS-derived TCFA,

Table 2 Comparison of angiographical data, gray-scale intravascular ultrasound, and virtual histology-intravascular ultrasound data between non-thin-cap fibroatheroma and definite-thin-cap fibroatheroma

	Non-TCFA (n = 98)	Definite-TCFA (n = 28)	P-value (vs. definite-TCFA)
Left anterior descending artery	40	12	
Left circumflex artery	16	4	
Right coronary artery	42	12	NS
Type of lesion			
A/B1	84	22	
B2/C	14	6	NS
Location of lesion			
Proximal	21	15	
Mid	56	12	
Distal	21	1	0.002
Quantitative coronary arteriography data			
Reference vessel diameter (mm)	2.42 (2.30, 2.55)	2.53 (2.30, 2.76)	NS
Minimum lumen diameter (mm)	1.84 (1.62, 2.05)	1.84 (1.62, 2.05)	NS
%Area-stenosis (%)	34.3 (30.6, 38.0)	45.1 (38.2, 52.1)	0.007
Gray-scale IVUS measurements			
Plaque volume (mm^3/cm)	71.2 (53.2, 89.3)	96.1 (73.7, 118.4)	0.0001
Vessel volume (mm^3/cm)	139.9 (109.0, 176.5)	162.1 (124.7, 200.0)	0.004
Plaque length (mm)	12.8 (11.1, 14.6)	17.5 (14.4, 20.6)	NS
%Plaque-volume (%)	48.6 (46.8, 50.4)	56.5 (53.3, 59.7)	<0.0001
Remodelling-index	1.06 (1.03, 1.08)	1.21 (1.17, 1.25)	<0.0001
VH measurements			
%Fibrous	62.1 (60.3, 65.1)	56.8 (52.6, 61.0)	0.01
%Fibro-fatty	13.4 (11.8, 14.9)	13.5 (10.7, 16.4)	NS
%Dense-calcium	8.8 (7.3, 10.4)	9.9 (7.0, 10.4)	NS
%Necrotic-core	15.3 (13.7, 16.9)	20.0 (17.0, 23.0)	0.006

Data are expressed predicted means and their 95% CIs. For the values in this table, a model with two categories of plaque types (definite-TCFA and non-TCFA) was fit. An adjusted P-value of < 0.0167 (Bonferroni's correction for multiple comparisons) was considered significant.

non-NCCL OCT-derived TCFA, and definite-TCFA are shown in *Figure 3A–C*, respectively.

Baseline characteristics and laboratory data

At least one definite-TCFA was identified in 24 patients (42.9%) but not in the other 32 patients (57.1%). The baseline characteristics and laboratory data for these two patient groups were summarized in *Table 1*. There were no differences in age, sex, body mass index, or cardiac risk factors between the two groups. In the present study, five (8.9%) patients had ACS that did not warrant emergency PCI and most of our study population (91.1%) had stable angina. Among the five ACS patients, three had at least one definite-TCFA.

Although patients without definite-TCFA tended to take statins for a longer duration and their total cholesterol level tended to be lower than that in patients with definite-TCFA ($P = 0.07$, both), there were no significant differences in the lipid profiles, blood sugar profiles, and high-sensitive C-reactive-protein between the two groups.

Comparison of non-thin-cap fibroatheroma and definite-thin-cap fibroatheroma

The summarized angiographical data, gray-scale IVUS, and VH-IVUS data for non-TCFA and definite-TCFA are shown in *Table 2*. There were no differences in lesion type, reference diameter, and minimum lumen diameter between the two groups, but definite-TCFA showed significantly higher %area-stenosis and tended to be located in the proximal part of the vessel ($P = 0.007$ and $P = 0.002$, respectively). Based on the gray-scale IVUS analysis, plaque volume and vessel volume of definite-TCFA were significantly higher than those of non-TCFA ($P = 0.0001$ and $P = 0.004$, respectively). Also, the values for %plaque-volume and the vessel remodelling index of definite-TCFA were significantly higher than those of non-TCFA ($P < 0.0001$, both). VH analysis showed that the %necrotic-core of definite-TCFA was significantly higher than that of non-TCFA and %fibrous of definite-TCFA was significantly lower than that of non-TCFA ($P = 0.006$ and $P = 0.01$, respectively).

Table 3 Comparison of angiographical data, gray-scale intravascular ultrasound, and virtual histology-intravascular ultrasound data between non-thin-cap intravascular ultrasound-derived thin-cap fibroatheroma and definite-thin-cap fibroatheroma

	Non-thin-cap IVUS-derived TCFA (n = 33)	Definite-TCFA (n = 28)	P-value (vs. definite-TCFA)
Quantitative coronary arteriography data			
Reference vessel diameter (mm)	2.40 (2.19, 2.61)	2.52 (2.31, 2.74)	NS
Minimum lumen diameter (mm)	1.92 (1.71, 2.12)	1.84 (1.62, 2.05)	NS
%Area-stenosis (%)	35.4 (28.6, 48.1)	45.1 (38.2, 52.1)	NS
Gray-scale IVUS measurements			
Plaque volume (mm^3/cm)	65.3 (39.3, 91.4)	96.3 (75.6, 117.0)	0.001
Vessel volume (mm^3/cm)	132.6 (89.1, 176.2)	162.0 (127.4, 196.4)	0.01
Plaque length (mm)	13.4 (10.5, 16.4)	17.4 (14.4, 20.5)	NS
%Plaque-volume (%)	48.1 (45.0, 51.1)	56.5 (53.4, 59.7)	0.0001
Remodelling index	1.10 (1.06, 1.13)	1.21 (1.17, 1.25)	0.0005
VH measurements			
%Fibrous	58.9 (55.1, 62.7)	57.0 (53.1, 60.9)	NS
%Fibro-fatty	12.3 (9.5, 15.1)	13.5 (10.7, 16.4)	NS
%Dense-calcium	10.5 (7.9, 13.1)	9.9 (7.3, 12.6)	NS
%Necrotic-core	18.6 (15.7, 21.4)	20.0 (17.0, 22.9)	NS
Major NCCL area (mm^2)	0.62 (0.46, 0.94)	1.15 (0.77, 1.39)	0.003
Total NCCL angle (degree)	54.6 (35.6, 73.5)	89.4 (63.6, 112.4)	0.0003
Major NCCL angle (degree)	19.0 (15.1, 21.2)	29.0 (20.2, 28.1)	0.005

Data are expressed predicted means and their 95% CIs. For the values in this table, a model with four categories of plaque types (definite-TCFA and three subcategories of non-TCFA plaque types) was fit. An adjusted P-value of <0.0167 (Bonferroni's correction for multiple comparisons) was considered significant.
NCCL, necrotic core contact with lumen.

Table 4 Comparison of angiographical data, gray-scale intravascular ultrasound, and virtual histology-intravascular ultrasound data between non-necrotic core in contact with the lumen optical coherence tomography-derived thin-cap fibroatheroma and definite-thin-cap fibroatheroma

	Non-NCCL OCT-derived TCFA (n = 8)	Definite-TCFA (n = 28)	P-value (vs. definite-TCFA)
Quantitative coronary arteriography data			
Reference vessel diameter (mm)	3.26 (2.85, 3.60)	2.52 (2.31, 2.74)	0.002
Minimum lumen diameter (mm)	2.50 (2.10, 2.90)	1.84 (1.62, 2.05)	0.004
%Area-stenosis (%)	38.8 (25.7, 47.8)	45.1 (38.2, 52.1)	NS
Gray-scale IVUS measurements			
Plaque volume (mm^3/cm)	122.5 (87.8, 157.2)	96.3 (75.6, 117.0)	NS
Vessel volume (mm^3/cm)	232.5 (171.9, 285.7)	162.0 (127.4, 196.4)	0.01
Plaque length (mm)	19.3 (13.6, 24.9.4)	17.4 (14.4, 20.5)	NS
%Plaque-volume (%)	52.9 (47.0, 58.8)	56.5 (53.4, 59.7)	NS
Remodelling index	1.04 (0.97, 1.12)	1.21 (1.17, 1.25)	0.003
VH measurements			
%Fibrous	49.8 (42.6, 56.9)	57.0 (53.1, 60.9)	NS
%Fibro-fatty	12.8 (7.4, 18.1)	13.5 (10.7, 16.4)	NS
%Dense-calcium	19.3 (14.3, 24.3)	9.9 (7.3, 12.6)	0.01
%Necrotic-core	17.3 (11.8, 22.7)	20.0 (17.0, 22.9)	NS

Data are expressed predicted means and their 95%CIs. For the values in this table, a model with four categories of plaque types (definite-TCFA and three subcategories of non-TCFA plaque types) was fit. An adjusted P-value of <0.0167 (Bonferroni's correction for multiple comparisons) was considered significant.

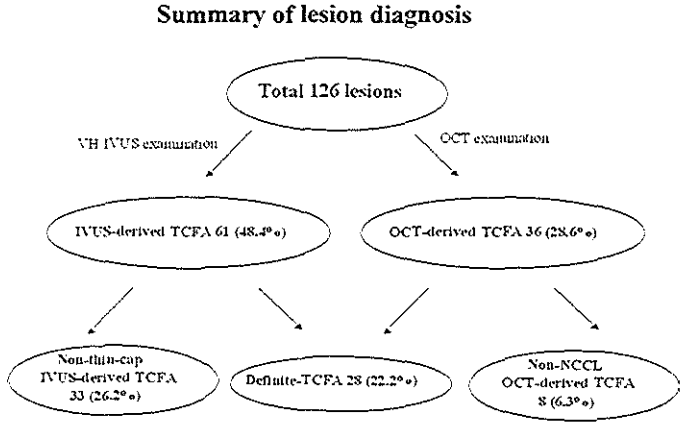

Figure 2 Among 126 lesions in 56 cases, virtual histology-intravascular ultrasound (VH-IVUS) diagnosed 61 lesions (48.4%) as IVUS-derived thin-cap-fiberatheroma (TCFA) and optical coherence tomography (OCT) revealed 36 lesions (28.6%) as OCT-derived TCFA. Twenty-eight lesions (22.2%) met the criteria of both IVUS-derived TCFA and OCT-derived TCFA and were diagnosed as definite-TCFA; 33 lesions were diagnosed as non-thin-cap IVUS-derived TCFA and eight lesions as non-NCCL OCT-derived TCFA.

Comparison of non-thin-cap intravascular ultrasound-derived thin-cap fibroatheroma and definite-thin-cap fibroatheroma

The summarized angiographical data, gray-scale IVUS, and VH-IVUS data for non-thin-cap IVUS-derived TCFA and definite TCFA are shown in *Table 3*. There were no differences in angiographical data between the two groups. Definite-TCFA, however, had a significantly larger plaque volume, vessel volume, %plaque-volume, and vessel remodelling index than non-thin-cap IVUS-derived TCFA ($P = 0.001$, $P = 0.01$, $P = 0.0001$ and $P = 0.0005$, respectively). Although there were no significant differences in the ratio of plaque components in the VH-IVUS analysis, definite-TCFA had a significantly larger major confluent NCCL area and a larger total angle occupied by NCCL in the lumen circumference compared with non-thin-cap IVUS-derived TCFA ($P = 0.003$ and $P = 0.0003$, respectively).

Comparison of non-necrotic core in contact with the lumen optical coherence tomography-derived thin-cap fibroatheroma and definite-thin-cap fibroatheroma

The summarized angiographical data, gray-scale IVUS, and VH-IVUS data for non-NCCL OCT-derived TCFA and definite TCFA are shown in *Table 4*. The sample size of non-NCCL OCT-derived TCFA was small, thus we considered these data exploratory, but non-NCCL OCT-derived TCFA had a significantly larger %dense-calcium and vessel volume, and smaller vessel remodelling index than definite-TCFA ($P = 0.01$, $P = 0.01$ and $P = 0.003$, respectively). Furthermore, non-NCCL OCT-derived TCFA had a larger reference diameter and minimum lumen diameter than definite-TCFA ($P = 0.002$ and $P = 0.004$, respectively).

Intra- and inter-observer variability

The estimated limit of agreement for the intra- and inter-observer variability in the VH-IVUS and OCT measurements was reasonable based on the Bland–Altman plot (%necrotic–core by VH-IVUS; intra-observer; mean difference: 0.03%, upper two-standard deviation (2SD): 1.63% and lower 2SD: −1.68%, inter-observer; mean difference: 0.10%, upper 2SD; 2.00% and lower 2SD: −1.90%, fibrous cap thickness by OCT; intra-observer; mean difference: 0.6 μm, upper 2SD: 12.2 μm and lower 2SD: −13.4 μm, inter-observer; mean difference: 1.9 μm, upper 2SD: 13.8 μm and lower 2SD: −17.7 μm).

There was little intra- or inter-observer disagreement in the diagnosis of IVUS-derived TCFA (intra-observer; $\kappa = 0.87$, 95% CI, 0.79–0.96, inter-observer; $\kappa = 0.81$, 95% CI 0.71–0.91) and in the diagnosis of OCT-derived TCFA (intra-observer; $\kappa = 0.87$ 0.77–0.96, inter-observer; $\kappa = 0.77$, 0.65–0.90).

Patient follow-up

In 21 patients with binary angiography (11 patients with definite-TCFA and 10 patients without definite-TCFA; 13 lesions were definite-TCFA and 32 lesions were non-TCFA; average span 205.0 ± 68.0 days), four lesions required PCI because of increasing plaque size and a constricting lumen, and three of these were definite-TCFA. A representative case of definite-TCFA progression is shown in *Figure 4*.

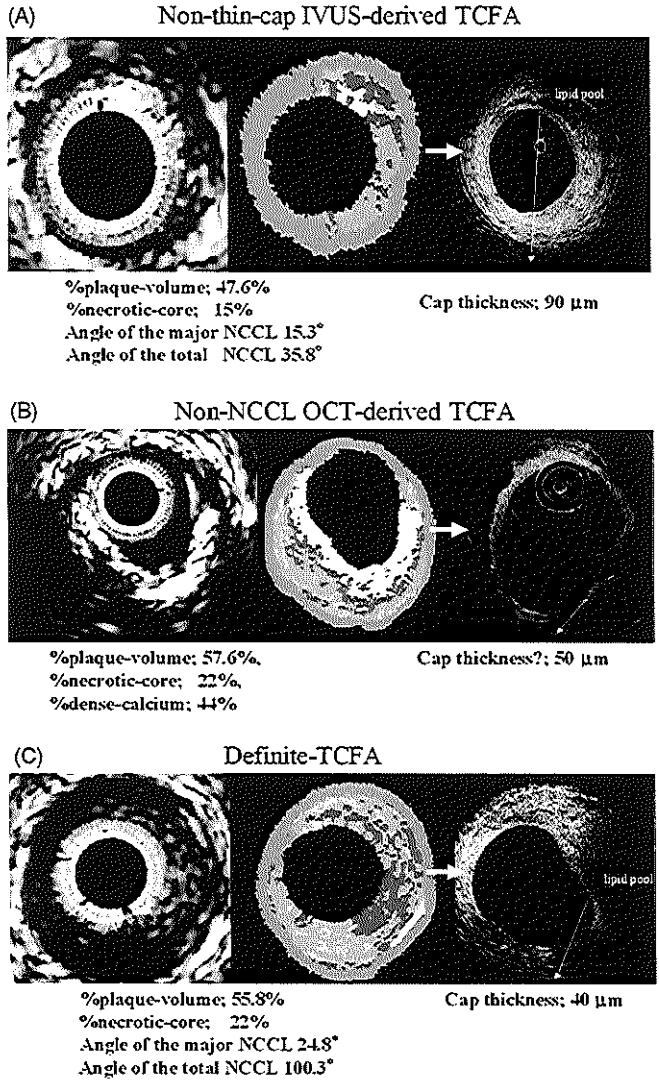

Figure 3 (A) A representative case of non-thin-cap IVUS-derived thin-cap fibroatheroma (TCFA). Virtual histology-IVUS shows 47.6% of %plaque-volume, 15% of %necrotic-core. The angle of the major NCCL was 15.3°, and that of the total NCCL was 35.8°. OCT shows signal-poor lesions with an overlying signal-rich band in the upper right quadrant. A signal-poor lesion indicates a lipid pool and signal-rich band indicates a fibrous cap. The fibrous cap thickness was 90 μm. (B) A representative case of non-NCCL OCT-derived TCFA. OCT identified a fibrous cap thickness of 50 μm which covers the low intensity area, but VH-IVUS did not identify the NCCL. (C) A representative case of definite-TCFA. Virtual histology-IVUS shows %plaque-volume of 55.8% and %necrotic-core of 22%. The angle of the major NCCL was 24.8°, and that of the total NCCL was 100.3°. Its minimum fibrous cap thickness was 40 μm.

Discussion

Pathology studies have demonstrated that acute coronary events most commonly arise from the disruption of TCFA. Several imaging modalities, including IVUS,[17] VH-IVUS,[13,14] angioscopy,[18] elastography,[19] and thermography,[20] have been used to detect TCFA. The sensitivity or specificity of these modalities for the detection of TCFA *in vivo*, however, has not been satisfactory.

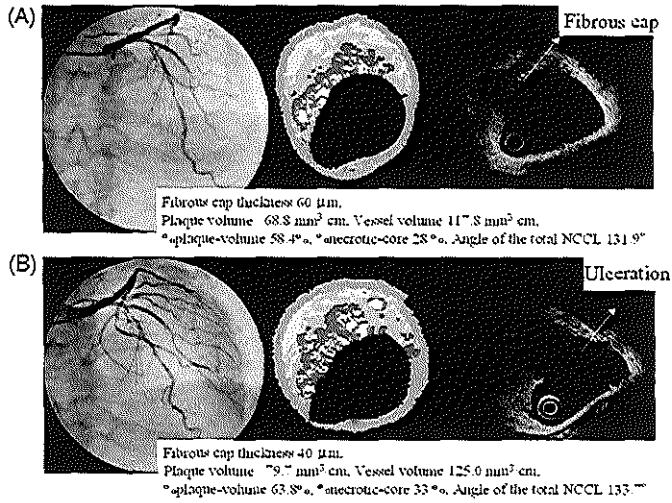

Figure 4 (*A*) Coronary angiography (CAG) revealed 50% stenosis in the mid-left anterior descending artery in July 2006. VH-IVUS revealed a 68.8 mm^3/cm plaque volume, 117.8 mm^3/cm vessel volume, 58.4% %plaque-volume, and 28% %necrotic-core. The fibrous cap thickness of this lesion was 60 μm by OCT measurement and this lesion was diagnosed as definite-TCFA. (*B*) After 6 months, because the patient experienced chest pain at rest with increased frequency, we performed CAG. The CAG revealed 90% stenosis at the site of the previous definite-TCFA lesion. VH-IVUS revealed an increase in plaque volume (68.8→79.7 mm^3/cm), vessel volume (117.8→125.0 mm^3/cm), %plaque-volume (58.4%→63.8%), and %necrotic-core (28%→33%). OCT revealed ulceration of the fibrous cap.

VH-IVUS for spectral analysis of radio-frequency data has the potential to detect TCFA. VH-IVUS is highly accurate for identifying plaque components both *in vitro* and *in vivo*.[6,7] Rodriguez-Granillo *et al.*[13] were the first to focus on the distribution of plaque components using VH-IVUS studies. They defined IVUS-derived TCFA based on pathologic data and demonstrated that the mean plaque volume and mean %necrotic-core of IVUS-derived TCFA were similar to previously reported histopathologic TCFA data. Thus, the ability of VH-IVUS to produce real-time assessment of plaque morphology has been established and might be useful for identifying TCFA. Because the maximum resolution of VH-IVUS is 100 μm, however, it is difficult to assess the thin fibrous cap (<65 μm).

Optical coherence tomography is a new imaging modality for detecting vulnerable plaque. OCT provides a high-resolution image and is able to evaluate detailed plaque morphology *in vivo*.[8-11] OCT, therefore, seems to have the potential to visualize the thin fibrous cap and detailed structures. The penetration of OCT is limited (<2 mm), so that it is frequently difficult to delineate large lipid plaques. Manfrini *et al.*[21] reported that OCT could be unreliable to differentiate areas with heterogenous composition because of its low signal penetration. In our study, eight OCT-derived TCFA lesions were not identified as an NCCL by VH-IVUS analysis. This discrepancy might be because of the penetration limitation of OCT. These lesions had a larger reference diameter, minimum lumen diameter, and minimum vessel volume than definite-TCFA ($P = 0.002$, $P = 0.004$, $P = 0.01$, respectively), and had severely calcified components compared with definite-TCFA ($P = 0.01$). When a target vessel or plaque is large, the optical signal might be attenuated by the plaque and failed to identify plaque morphology. It might also be sometimes difficult to discriminate between lipid and calcified lesions because both these appear as low-intensity images, usually differentiated in OCT by an unclear border (lipid) or a clear border (calcium). In this regard, large calcified lesions are likely to be misdiagnosed as TCFA by OCT examination. Therefore, it is difficult to detect TCFA using only one modality. Using a combination of complementary tools such as VH-IVUS and OCT might be a feasible approach for more accurate detection of TCFA.

Although the positive ratio of VH-IVUS for detecting definite-TCFA was 45.9% and that for OCT was higher than VH-IVUS (77.8%), OCT has several procedural limitations and is only used in selected hospitals. IVUS is now routinely used for PCI procedures. Thus, it is important to determine the criteria for TCFA by VH-IVUS. Previous IVUS and pathological studies showed that positive vessel remodelling is associated with an unstable clinical presentation and characteristic pathologic lesion types.[16,22,23] Kolodgie *et al.*[2] reported that whether the necrotic core is circumferential might be critical for determining the instability of a plaque, and they demonstrated that proximal coronary lesions with greater than 50% diameter stenosis with an necrotic core circumference >120° strongly suggests the presence of

plaque with a vulnerable morphology. In the present study, definite-TCFA identified by both modalities tended to locate in the proximal part of the vessels, areas with a higher %area-stenosis, %plaque-volume and more positively remodelled lesions in comparison to non-TCFA. These data are compatible with previously reported histopathologic data.[2,23] Furthermore, the major confluent NCCL area of definite-TCFA was larger and its NCCL occupied a larger circumference of the lumen than non-thin-cap IVUS-derived TCFA. Thus, %plaque-volume, vessel remodelling index, confluent major NCCL area, and degree of NCCL circumference were the identifying factors for definite-TCFA by VH-IVUS. One of the clinical implications of the present study was to identify the VH-IVUS indices useful for diagnosing definite-TCFA.

Limitations

Because patients excluded from the study were those with high risk-ACS, we could not reach any conclusions about the general prevalence of definite-TCFA. Further, we could observe only limited vessel areas, as the VH-IVUS and OCT procedures have several limitations for imaging certain lesions, such as severely calcified tortuous lesions or other complex lesions. Thus, our study results do not represent an unbiased sampling of all coronary arteries, and the detection rate of TCFA in our study patients might be underestimated.

There were three cases of definite-TCFA with progression requiring PCI; it is unclear whether the detected definite-TCFA will cause acute coronary events and was a true vulnerable plaque. Although the frequency of the progression was too low to reach any statistical significance, definite-TCFA tended to progress more compared with non-TCFA. Our findings, therefore, should be confirmed with a larger study population and the subsequent course of the lesions observed as well.

In the present study, 61 plaques were identified as IVUS-derived TCFA by VH-IVUS examination. This identification was based on the criteria of a previous published report.[13] This high prevalence of high-risk plaque, however, was at variance with previously published *in vivo* and *in vitro* studies,[5,13] which might be because of inaccurate VH determination by *in vitro* testing. Further, we selected cut-off values of IVUS-derived TCFA criteria as %plaque-volume $>40\%$ and %necrotic-core $>10\%$ because pathologic TCFA is very unlikely to be present in segments with $<40\%$ occlusive lesion, and nearly 90% of ruptured plaque comprised $>10\%$ necrotic core in the plaque area.[3] We did consider that the necrotic core size of 10% was too low, because the average %necrotic-core of definite-TCFA was $20.0 \pm 6.8\%$ and that of non-TCFA was $15.3 \pm 8.6\%$. This data is in line with the previous pathologic findings in this subset of lesions and also in previous VH-IVUS studies.[2,3,14] Thus, TCFA might be over-diagnosed if based on the current definition of IVUS-derived TCFA. Our study population was too small, however, to establish new criteria for defining IVUS-derived TCFA.

Although we could perform the VH-IVUS and OCT procedures within 20 min and without complications, the combined use of VH-IVUS and OCT is laborious and costly. A new device with both IVUS and OCT functions to enable the simultaneous use of both modalities should be developed.

Conclusions

This is the first study to evaluate TCFA using a combination of two new imaging modalities, VH-IVUS and OCT. Neither modality alone is sufficient for detecting TCFA. The combined use of these complementary imaging modalities, VH-IVUS and OCT, however, should be considered a feasible approach for more precise detection of TCFA.

Conflict of interest: none declared.

Funding

Funding to pay the Open Access publication charges for this article will be provided by Dr Junya Shite.

References

1. Falk E, Shah PK, Fuster V. Coronary plaque disruption. *Circulation* 1995;**92**:657–671.
2. Kolodgie FD, Virmani R, Burke AP, Farb A, Weber DK, Kutys R, Finn AV, Gold HK. Pathologic assessment of the vulnerable human coronary plaque. *Heart* 2004;**90**:1385–1391.
3. Virmani R, Burke AP, Farb A, Kolodgie FD. Pathology of the vulnerable plaque. *J Am Coll Cardiol* 2006;**47**:C13–C18.
4. Arbustini E, Dal Bello B, Morbini P, Burke AP, Bocciarelli M, Specchia G, Virmani R. Plaque erosion is a major substrate for coronary thrombosis in acute myocardial infarction. *Heart* 1999;**82**:269–272.
5. Virmani R, Kolodgie FD, Burke AP, Farb A, Schwartz SM. Lessons from sudden coronary death a comprehensive morphological classification scheme for atherosclerotic lesions. *Arterioscler Thromb Vasc Biol* 2000;**20**:1262–1275.
6. Nair A, Margolis MP, Kuban BD, Vince DG. Automated coronary plaque characterization with intravascular ultrasound backscatter: *ex vivo* validation. *EuroIntervention* 2007;**3**:113–120.
7. Nasu K, Tsuchikane E, Katoh O, Vince DG, Virmani R, Surmely JF, Murata A, Takeda Y, Ito T, Ehara M, Matsubara T, Terashima M, Suzuki T. Accuracy of in vivo coronary plaque morphology assessment: a validation study of in vivo virtual histology compared with in vitro histopathology. *J Am Coll Cardiol* 2006;**47**:2405–2412.
8. Matsumoto D, Shite J, Shinke T, Otake H, Tanino Y, Ogasawara D, Sawada T, Paredes OL, Hirata KI, Yokoyama M. Neointimal coverage of sirolimus-eluting stents at 6-month follow-up: evaluated by optical coherence tomography. *Eur Heart J* 2007;**28**:961–967.
9. Jang IK, Bouma BE, Kang DH, Park SJ, Park SW, Seung KB, Choi KB, Shishkov M, Schlendorf K, Pomerantsev E, Houser SL, Aretz HT, Tearney GJ. Visualization of coronary atherosclerotic plaques in patients using optical coherence tomography: comparison with intravascular ultrasound. *J Am Coll Cardiol* 2002;**39**:604–609.
10. Yabushita H, Bouma BE, Houser SL, Aretz T, Jang IK, Schlendorf KH, Kauffman CR, Shishkov M, Kang DH, Halpern EF, Tearney GJ. Characterization of human atherosclerosis by optical coherence tomography. *Circulation* 2002;**106**:1640–1645.
11. Jang IK, Tearney GJ, MacNeill B, Takano M, Moselewski F, Iftima N, Shishkov M, Houser S, Aretz HT, Halpern EF, Bouma BE. In vivo characterization of coronary atherosclerotic plaque by use of optical coherence tomography. *Circulation* 2005;**111**:1551–1555.
12. Mintz GS, Nissen SE, Anderson WD, Bailey SR, Erbel R, Fitzgerald PJ, Pinto FJ, Rosenfield K, Siegel RJ, Tuzuc EM, Yock PG. American College of Cardiology Clinical Expert Consensus Document on Standards for Acquisition, Measurement and

Reporting of Intravascular Ultrasound Studies (IVUS). A report of the American College of Cardiology Task Force on Clinical Expert Consensus Documents. *J Am Coll Cardiol* 2001;**37**:1478–1492.
13. Rodriguez-Granillo GA, Garcia-Garcia HM, Mc Fadden EP, Valgimigli M, Aoki J, de Feyter P, Serruys PW. In Vivo intravascular ultrasound-derived thin-cap fibroatheroma detection using radiofrequency data analysis. *J Am Coll Cardiol* 2005;**46**:2038–2042.
14. Garcia-Garcia HM, Goedhart D, Schuurbiers JC, Kukreja N, Tanimoto S, Daemen J, Morel MA, Bressers M, van Es GA, Wentzel JJ, Gijsen F, van der Steen AF, Serruys PW. Virtual histology and remodeling index allow in vivo identification of allegedly high-risk coronary plaques in patients with acute coronary syndromes: a three vessel intravascular ultrasound rediofrequency data analysis. *EuroIntervention* 2006;**2**:338–344.
15. Burke AP, Farb A, Malcom GT, Liang YH, Smialek J, Virmani R. Coronary risk factors and plaque morphology in men with coronary disease who died suddenly. *N Eng J Med* 1997;**336**: 1276–1282.
16. Burke AP, Kolodgie FD, Farb A, Weber D, Virmani R. Morphological predictors of arterial remodeling in coronary atherosclerosis. *Circulation* 2002;**105**:297–303.
17. Yamagishi M, Terashima M, Awano K, Kijima M, Nakatani S, Daikoku S, Ito K, Yasumura Y, Miyatake K. Morphology of vulnerable coronary plaque: insights from follow-up of patients examined by intravascular ultrasound before an acute coronary syndrome. *J Am Coll Cardiol* 2000;**35**:106–111.
18. Ohtani T, Ueda Y, Mizote I, Oyabu J, Okada K, Hirayama A, Kodama K. Number of yellow plaques detected in a coronary artery is associated with future risk of acute coronary syndrome: detection of vulnerable patients by angioscopy. *J Am Coll Cardiol* 2006;**47**:2194–2200.
19. de Korte CL, Scharr JA, Mastik F, Serruys PW, van der Steen AF. Intravascular elastography: from bench to bedside. *J Interv Cardiol* 2003;**16**:253–259.
20. Madjid M, Willerson JT, Casscells SW. Intracoronary thermography for detection of high-risk vulnerable plaques. *J Am Coll Cardiol* 2006;**47**:C80–C85.
21. Manfrini O, Mont E, Leone O, Arbustini E, Eusebi V, Virmani R, Bugiardini R. Sources of error and interpretation of plaque morphology by optical coherence tomography. *Am J Cardiol* 2006;**98**: 156–159.
22. Schoenhagen P, Ziada KM, Kapadia SR, Crowe TD, Nissen SE, Tuzcu EM. Extent and direction of arterial remodeling in stable versus unstable coronary syndromes: an intravascular ultrasound study. *Circulation* 2000;**101**:598–603.
23. Varnava AM, Mills PG, Davies MJ. Relationship between coronary artery remodeling and plaque vulnerability. *Circulation* 2002;**105**: 939–943.

Summary and Conclusions

Undoubtedly, intravascular ultrasound (IVUS) is a highly accurate tool for the serial assessment of the natural history of coronary atherosclerosis, and for the evaluation of the effect of established and emerging drug therapies on the progression of atherosclerosis.

The existing and future application of IVUS is connected to the study of the different applications of the analysis of radiofrequency data, both for the improvement of plaque characterization, and for the assessment of the mechanical properties of plaque.

This thesis provides important data regarding the internal and external validation of both the spectral analysis of radiofrequency data and optical coherence tomography for the assessment of the intact plaque composition and the performance of stents.

INTERNAL VALIDATION

We compared the ability of OCT and IVUS-RF to classify plaque and assessed the performance of a combination of the two modalities to identify different plaque types. In this work we present the first comparison between IVUS-RF and OCT, using histology as a benchmark (chapter 2.1).

The reproducibility study of IVUS-RF demonstrated that the geometrical and compositional output of IVUS-RF has acceptable reproducibility, and that non-uniform pullbacks, which can occur when using phased array catheters devoid of a covering sheath, remain an issue of concern, and this should be taken into account during the conductance of longitudinal studies (chapter 2.2).

DISTRIBUTION OF PLAQUE COMPOSITION ALONG CORONARY ARTERIES

In pathological studies and in clinical studies (using angiography and IVUS), it has been demonstrated that local factors play a role in determining the progression and stability of plaque throughout the coronary tree. This thesis extensively addressed the non-uniformity of plaque composition along the coronary tree (chapters 3.1-3.5). We established that plaque composition is unevenly distributed along the left coronary artery. There is a progressive increase in necrotic core starting from the proximal segment of the left anterior descending, followed by a steady decline towards those segments which are more distally located along the vessel.

In chapter 3.4, we found that atherosclerotic plaque located at the ostium of the left anterior descending artery had a larger plaque burden, eccentricity

and maximum plaque thickness than distal left main plaques. In addition, larger calcified necrotic core content was found distal to the circumflex take-off. Lesions were predominantly located in the outer wall of the carina, and such locations were associated with larger necrotic core content. Overall, these results confirm the key role of flow dynamics in the genesis and progression of atherosclerosis. In chapter 3.5, we replicated these observations and extended the analysis to other bifurcations. The bifurcation sites of LM-LAD had greater necrotic core at just and distal segments of the bifurcation, while non-LM bifurcations showed greater necrotic core in proximal segment of bifurcation.

RELATIONSHIP OF CARDIOVASCULAR RISK FACTORS AND CORONARY PLAQUE COMPOSITION

In chapter 4, we found after multivariate adjustment that in non-culprit vessels, patient demographics (age, male gender), anthropometric measurements (waist circumference), and clinical risk factors (systolic blood pressure) are all related to plaque composition (larger necrotic core area). Accordingly, necrotic core, as assessed by IVUS-RF, could be viewed as a novel in situ/in vivo biomarker, potentially reflecting the long-term impact of cardiovascular risk on plaque phenotype.

HIGH-RISK PLAQUES

The so-called IVUS-derived TCFA (IDTCFA) is common in non-culprit lesions of patients undergoing percutaneous intervention in another vessel; frequency is higher in patients with ACS compared to stable patients, and the distribution of IDTCFA lesions along the coronary vessels is clearly clustered. These findings were further confirmed in a 3-vessel population.

We explored *in vivo* the relationship between plaque composition and coronary remodelling. Necrotic core size was significantly larger in coronary lesions that demonstrated positive remodelling, than in those who experienced vessel shrinkage. In addition, the fibrotic burden of the plaque was significantly and inversely correlated to the remodelling index.

In a prospective 3-vessel IVUS study, patients with a least one plaque rupture in the coronary tree had a larger body mass index, and overall worse IVUS-derived characteristics, when compared to patients without evidence of plaque rupture. In addition, plaque ruptures sited had a worse phenotype than the most diseased sites of the same vessels.

FOCAL TREATMENT OF CORONARY HIGH-RISK ATHEROSCLEROTIC PLAQUES

Treatment of asymptomatic, non-obstructive coronary lesions may be a desirable pursuit, but the pre-emptive strike may be a risky, time-consuming and an expensive undertaking. Importantly, at present there is no evidence to support this focal treatment. We described in chapter 6 the current available options.

SYSTEMIC TREATMENT OF CORONARY HIGH-RISK ATHEROSCLEROTIC PLAQUES

In chapter 7, we described the results of IBIS 2, which to me is the most important piece of this thesis. This study demonstrated that necrotic core expansion occurs despite contemporary cardiovascular therapies, even in the absence of an increase in overall plaque size. This unabated necrotic core expansion could be responsible, in part, for the recurrent cardiovascular events in high-risk patients. Lp-PLA_2 inhibition with darapladib halted this process, and therefore may represent a new approach for the treatment of atherosclerosis. Firstly, however the benefit of this intervention needs to be confirmed by the results of future event-driven outcomes trials.

NOVEL INVASIVE IMAGING OF CORONARY STENTS

We investigated the IVUS-RF usefulness for the study of edge restenosis in metal stents. Serial expansive vascular remodelling was observed at proximal and distal stent edges. Remodeling occurred in response to tissue growth, which was mainly due to increased fibrofatty tissue. We used also IVUS-RF to assess the serial changes of lesions treated with bioabsorbable stents. IVUS-RF changes at 6 months suggest alteration of the BVS with reduction of RF backscattering by polymeric struts. Strained plaques on the palpograms were almost abolished following stent implantation. However, strain values reappeared within 6 months suggesting an increase in endoluminal deformability of the stented vessel. Chapter 8.

PLAQUE PROGRESSION/ REGRESSION

In chapter 9, we described the use of IVUS to assess in vivo, the effect of established and novel medical therapies on plaque size and composition. In a meta-analysis

of clinical studies that assessed IVUS-based progression/regression of coronary atherosclerosis to evaluate whether treatment with statins can promote coronary plaque regression over time, we found that statin therapy, in particular when achieving the target LDL-C <100mg/dl level, appears to promote a significant regression of plaque volume in coronary artery segments as measured by IVUS.

Additionally, we evaluated the effect of ACE-inhibitors on coronary atherosclerosis. Our results suggests that in patients with established CAD, and stable angina without overt heart failure, the clinical benefit obtained with perindopril treatment during a period of 3 years cannot be attributed to an effect on coronary plaque size.

Thiazolidinediones (TZDs) have effects on cardiovascular risk factors, including insulin sensitivity, inflammatory biomarkers, endothelial function, coagulability, plaque instability, and blood pressure, that may slow the progression of coronary atherosclerosis. Active-controlled trials of both thiazolidinediones (rosiglitazone and pioglitazone) in patients with type 2 diabetes have suggested a favourable effect of these agents on carotid atherosclerosis and in-stent restenosis, however, the applicability of these data to native vessel coronary disease is uncertain. The APPROACH study supports, but does not prove the hypothesis that rosiglitazone has a greater anti-atherosclerotic effect than glipizide in patients with type 2 diabetes.

COMBINING DIFFERENT IVUS-RF AND OPTICAL COHERENCE TOMOGRAPHY

In chapter 10, the combined use of IVUS-RF and optical coherence tomography is described. Greyscale intravascular ultrasound allows evaluation of coronary atherosclerosis but its limited resolution (axial 150–200 μm) precludes the visualization of certain microstructures (such as the thin fibrous cap or fine strut coverage). Optical coherence tomography (OCT) is a light-based imaging modality can be used to study tissues in vivo with near-histologic, ultrahigh resolution. This has also provided new insights into the interaction between the stent and the vessel wall, and has allowed a more precise characterization of atherosclerotic plaques.

OCT can provide very valuable information for the detection of high-risk plaques in vivo, especially by measuring the thickness of the fibrous cap. However due to its limited penetration OCT can not provide a full analysis of large plaques. Further, histological examinations have demonstrated that OCT may not be sufficient to discriminate lipid pools from calcium deposits. On the contrary, other techniques such as IVUS and IVUS-VH analysis can image the complete thickness of the plaque and can identify the presence of necrotic core, but their

limited axial resolution does not allow the evaluation of the fibrous cap. Thus, we showed that the combination of the IVUS-VH and OCT appears promising to better characterize such plaques.

CONCLUSION

I believe that this thesis is of value to better understand the extent, distribution, morphology and composition of coronary atherosclerosis in our patients.

We have provided important data regarding the accuracy of an in vivo tissue characterization technique (IVUS-RF and optical coherence tomography). The combination of the IVUS-RF and OCT appears promising to better characterize high-risk plaques. Nevertheless, these findings must be interpreted cautiously until conclusive data by prospective natural history studies is supplied.

Several systemic treatments have proved to be effective in reducing plaque size, however, perindopril and rosiglitazone, which were tested in this thesis, did not meet the primary endpoint.

Samenvatting en Conclusies

Ongetwijfeld is intravasculaire echografie (*intravascular ultrasound - IVUS*) een zeer nauwkeurig hulpmiddel voor de seriële beoordeling van het natuurlijke beloop van coronaire atherosclerose en voor de evaluatie van het effect van verschillende conventionele en moderne medicinale behandelingen op de progressie van atherosclerose.

De huidige en toekomstige toepassing van IVUS is gekoppeld aan het onderzoek naar de verschillende toepassingen van de analyse van radiofrequentiedata, zowel voor een betere plaque typering als voor de beoordeling van de mechanische eigenschappen van plaques. In het algemeen kan een dergelijke inzichtelijke analyse van de radiofrequentiedata potentieel zinnig zijn voor de opsporing van hoogrisico plaques en voor het vervolgen van de natuurlijke ontwikkeling van deze plaques in prospectieve natuurlijk beloop studies.

Dit proefschrift bevat belangrijke data over de interne en externe validatie van spectrumanalyse van radiofrequentiedata ter beoordeling van de plaquesamenstelling *in vivo*.

INTERNE VALIDATIE

Wij vergeleken OCT en VH-IVUS wat betreft classificatie van plaque en beoordeelden de prestatie van een combinatie van de twee modaliteiten ter identificatie van de verschillende plaquetypes. In dit werk presenteren wij de eerste vergelijking tussen VH-IVUS en OCT, met histologie als maatstaf (Hoofdstuk 2.1).

De reproduceerbaarheid van IVUS-VH toonde aan dat de geometrische en compositionele output van IVUS-VH acceptabel reproduceerbaar is, en dat non-uniforme uitzonderingen, in het bijzonder aanwezig bij het gebruik van gefaseerde array katheters zonder omhullende mantel, een punt van zorg blijven waarmee rekening gehouden moet worden bij longitudinale studies (Hoofdstuk 2.2).

DISTRIBUTIE VAN PLAQUESAMENSTELLING IN DE CORONAIRE ARTERIËN

Bij plaqueprogressie en -stabiliteit in de coronaire vaatboom lijken plaatselijke factoren een rol te spelen. Dit werd zowel in pathologische als in klinische studies aangetoond met behulp van angiografie en IVUS (het laatste ter detectie van plaqueruptuur). De non-uniformiteit van de plaquesamenstelling in de coronaire vaatboom wordt in dit proefschrift uitgebreid behandeld (Hoofdstuk 3.1 - 3.6).

Wij hebben met name vastgesteld dat de plaquesamenstelling niet gelijk is verdeeld over de linker coronaire arterie. Er is sprake van een progressieve toename

van necrotische kern die begint vanaf de proximale helft van de linker hoofd-coronaire arterie naar het meest proximale segment van de linker arteria anterior descendens of circumflexa, gevolgd door een gestage afname langs die segmenten die meer distaal in het vat zijn gelokaliseerd.

In Hoofdstuk 3.6 zagen wij dat atherosclerotische plaques die gelokaliseerd zijn in het ostium van de linker arteria anterior descendens presenteerden met een grotere plaquelast, excentriciteit en maximale plaquedikte dan plaques in de distale linker hoofdvaten. Bovendien werd distaal van de circumflexa oorsprong een grotere gecalcificeerde en necrotische kerninhoud gezien. De laesies waren voornamelijk in de buitenste wand van de carina gelokaliseerd. Een dergelijke locatie ging gepaard met een grotere necrotische kerninhoud. De sleutelrol van flow dynamica in de genese en progressie van atherosclerose wordt door deze resultaten nog eens bevestigd.

VERBAND TUSSEN CARDIOVASCULAIRE RISICOFACTOREN EN CORONAIRE PLAQUESAMENSTELLING

In hoofdstuk 4 zagen wij dat de demografische gegevens van de patiënt (leeftijd, mannelijk geslacht), antropometrische maten (tailleomvang), klinische risicofactoren (systolische bloeddruk) in niet-culpritvaten na multivariate correctie gerelateerd zijn aan de plaquesamenstelling (grotere necrotische kerninhoud). Hiermee in overeenstemming kan de necrotische kern, vastgesteld met IVUS-RF, gezien worden als een nieuwe *in situ/in vivo* biomarker, die mogelijk de lange-termijn gevolgen van het cardiovasculaire risico op het plaquefenotype weerspiegelt.

KWETSBAAR PLAQUE

In hoofdstuk 5 werd een prospectieve 3-taks IVUS- studie besproken waarin patiënten met ten minste één plaqueruptuur in de coronaire vaatboom een hogere body mass index en in het algemeen ernstiger IVUS-afgeleide kenmerken hadden, vergeleken met patiënten zonder bewezen plaqueruptuur. Bovendien hadden deze plaquerupturen een ongunstiger fenotype dan de meeste aangedane locaties in dezelfde vaten.

Aangetoond is dat de thin-cap fibroatheroom (TCFA) laesies met grote avasculaire, hypocellulaire, lipide kernen, het meest prevalente substraat van plaqueruptuur zijn. Onderzoek bij een groot aantal slachtoffers van plotse hartdood lijkt erop te wijzen dat geruptureerde TCFA de aanleiding was voor 60% van

acute coronaire trombi. Dezelfde studie toonde dat plaqueruptuur in TCFAs ook zonder klinische consequenties kan optreden. De mogelijkheid om TCFA te identificeren zou de natuurlijke ontwikkeling van deze laesies kunnen ophelderen en middelen aanreiken om de effecten van farmacologische of andere interventies te beoordelen.

Wij hebben tevens gevonden dat de IVUS-VH bevindingen, vergelijkbaar met IVUS-afgeleide TCFA (IDTCFA), vaak voorkwamen in niet-culpritlaesies van patiënten die in een ander vat percutane interventie ondergingen. Bovendien was de prevalentie van IDTFCA significant hoger bij patiënten die presenteerden met ACS vergeleken met stabiele patiënten. De distributie van IDTCFA laesies in de coronaire vaten was duidelijk geclusterd. Deze bevindingen werden verder bevestigd in een populatie met 3-taks lijden.

Wij verifieerden *in vivo* het verband tussen plaquesamenstelling en coronaire remodellering. De necrotische kerngrootte was significant groter in coronaire laesies met positieve remodellering dan in die met negatieve remodellering ('shrinkage').

Verder was de fibrotische last van de plaque significant en omgekeerd evenredig gecorreleerd aan de remodelleringsindex.

FOCALE BEHANDELING VAN CORONAIRE HOOGRISICO ATHEROSCLEROTISCHE PLAQUES

De behandeling van asymptomatische, niet-obstructieve coronaire laesies mag dan een wenselijk streven zijn, maar het aanpakken van deze laesies is een mogelijk riskante, langdurige en dure kwestie. Een focale behandeling wordt echter op dit moment niet door bewijs ondersteund. In hoofdstuk 6 worden de op dit moment beschikbare opties beschreven.

SYSTEMISCHE BEHANDELING VAN CORONAIRE HOOGRISICO ATHEROSCLEROTISCHE PLAQUES

In hoofdstuk 8 worden de resultaten van IBIS 2 beschreven, volgens mij het belangrijkste onderdeel van dit proefschrift. Deze studie toonde aan dat ondanks de moderne cardiovasculaire therapieën necrotische kernexpansie optreedt, zelfs als er in het algemeen geen toename van plaquegrootte is. Deze onverminderde necrotische kernexpansie kan, voor een deel, verantwoordelijk zijn voor de recidiverende cardiovasculaire events bij hoogrisico patiënten. Lp-PLA_2 remming met

Darapladib stopte dit proces en is daarmee mogelijk een nieuwe benadering voor de behandeling van atherosclerose, indien de gunstige effecten van deze interventie bevestigd worden door resultaten van toekomstige event-driven resultatentrials.

PLAQUE PROGRESSIE / REGRESSIE

In hoofdstuk 9 wordt het gebruik van IVUS beschreven om *in vivo* het effect van conventionele en nieuwe medische therapieën op plaquegrootte en samenstelling te beoordelen. In een meta-analyse van klinische studies die IVUS-gebaseerde progressie/regressie van coronaire atherosclerose bepaalden om te zien of een behandeling met statines de regressie van coronaire plaque in de tijd bevordert, vonden wij dat statinetherapie, met name bij het bereiken van het doelniveau LDL-C<100 mg/dl, een significante regressie van plaquevolume in coronaire arteriesegmenten (gemeten door IVUS) bevordert.

Daarnaast evalueerden wij het effect van ACE remmers op coronaire atherosclerose. De resultaten lijken erop te wijzen dat bij patiënten met vastgestelde CAD, stabiele angina zonder manifest hartfalen, het klinisch gunstige effect van Perindropril behandeling tijdens een periode van 3 jaar niet kan worden toegeschreven aan een effect op de coronaire plaquegrootte.

Thiazolidinediones (TZDs) hebben effect op cardiovasculaire risicofactoren, zoals insulinegevoeligheid, inflammatoire biomarkers, endotheliale functie, coagulabiliteit, plaque instabiliteit en bloeddruk, die de progressie van coronaire atherosclerose kunnen vertragen. Actief-gecontroleerde trials van zowel thiazolidinediones (rosiglitazone en pioglitazone) bij patiënten met T2DM suggereerden een gunstig effect van deze middelen op carotis atherosclerose en in-stent restenose. De toepasbaarheid van deze gegevens op natieve vat coronarialijden is niet zeker. De APPROACH studie ondersteunt de hypothese dat rosiglitazone een groter anti-atherosclerotisch effect heeft dan glipizide bij patiënten met type 2 diabetes, en suggereert dat rosiglitazone meer anti-atherosclerotisch is bij patiënten met gevorderde diabetes of met een hoger risico voor cardiovasculair lijden. In lopende analyses worden de factoren in verband met veranderingen in atherosclerose, gemeten door middel van IVUS, geëvalueerd en zullen de effecten van risoglitazone op atherosclerose en plaque nader worden onderzocht.

COMBINEREN VAN VERSCHILLENDE INVASIEVE BEELDVORMENDE TECHNIEKEN

In hoofdstuk 10 wordt het gecombineerde gebruik van meerdere beeldvormende technieken besproken. Met greyscale intravasculaire echografie is evaluatie van coronaire atherosclerose mogelijk, maar de beperkte resolutie (axiaal 150–200 µm) sluit visualisatie van bepaalde microstructuren (zoals de thin fibrous cap of de fine strut coverage) uit. Optical Coherence Tomography (OCT) is een beeldvormingsmethode op basis van licht, die gebruikt kan worden om weefsels *in vivo* te bestuderen met bijna-histologische, ultrahoge resolutie. Dit heeft tevens nieuwe inzichten opgeleverd over de wisselwerking tussen de stent en de vaatwand en heeft een nauwkeuriger typering van atherosclerotische plaques mogelijk gemaakt.

OCT kan zeer waardevolle informatie leveren voor *in vivo* detectie van hoogrisico plaques, met name bij het meten van de dikte van de fibreuze cap. Vanwege de beperkte penetratie van OCT kan geen volledige analyse verricht worden van grote plaques. Verder hebben histologische onderzoeken aangetoond dat OCT mogelijk niet voldoende kan differentiëren tussen lipide pools en kalkafzettingen. Daarentegen kunnen andere technieken zoals IVUS en IVUS-VH analyse de complete plaquedikte afbeelden en de aanwezigheid van necrotische kern identificeren. De beperkte axiale resolutie maakt een beoordeling van de fibreuze cap onmogelijk. Wij hebben hiermee aangetoond dat de combinatie van de IVUS-VH en ACT veelbelovend lijkt om dergelijke plaques te typeren.

CONCLUSIE

Wij zijn van mening dat het in dit proefschrift gepresenteerde werk van waarde is voor een beter begrip van de omvang, distributie, morfologie en samenstelling van atherosclerose in levende patiënten.

Wij hebben belangrijke gegevens gepresenteerd met betrekking tot de nauwkeurigheid van een *in vivo* weefseltyperingtechniek (IVUS-VH). Eén van onze bevindingen was dat wij een potentieel *in vivo* surrogaat van thin cap fibroatheroom hebben geïdentificeerd, de meest prevalente voorloper van plaqueruptuur. Desondanks moeten onze bevindingen voorzichtig worden geïnterpreteerd totdat definitieve data uit natuurlijk beloop studies vrij worden gegeven.

Verscheidene systemische behandelingen hebben bewezen effectief te zijn ter verkleining van de plaque. Perindopril en rosiglitazone, die in dit proefschrift werden getest, bereikten het primaire eindpunt echter niet.

De combinatie van IVUS-VH en OCT lijkt veelbelovend te zijn voor een betere typering van hoogrisico plaques.

Acknowledgements

ACKNOWLEDGEMENTS *TO THE PEOPLE FROM THE THORAXCENTER*

For me, the acknowledgement section of my thesis is one of the most important parts of it. Although it is difficult to convey in a few words all my gratitude to *the people* who work at the Thoraxcenter, please find here my most sincere thanks to all of you. Especially I would like to thank you, *the Thoraxcenter people,* for being part of my personal history and also for letting me be part of yours. What I appreciate the most is your way of greeting me every time we run into each other. I like to see you smiling and to see the change in your facial expressions generated by our encounter. This has been nourishing my heart with good feelings as well as being an important piece of the "motor" that keeps me going. I have no means to pay back what all of you have given to me and I can only say once again the words that best describe what I feel, Thank You.

The first day I arrived here, I promised myself that I would stay at the Thoraxcenter as long as I enjoy what I do and as long as what I do contributes to make me a better person, without harming anyone. So I can say that in this respect, I have been tremendously successful. To have all of you as colleagues, but more importantly as friends, is the yardstick I use to judge myself as a person. In other words, I measure my success by the number of friends I have.

As a testimony to my friendly relationship with all the fellows with whom I have had the privilege to work as colleagues, I am proud to say that I have collaborated on one or more manuscripts with everyone whose stay has overlapped with my own at the Thoraxcenter to date.

Dirck van Essen, you were such a great office mate. I spent my first 2 years in the Z120, at a desk next to you. You may think everything was easy then, but unfortunately that was not the case. You asked for coffee every 10 minutes. That meant that either Keiichi or I was supposed to get up and go to the coffee machine to get it for you! This was a sort of exchange for the favours you did for us by translating the letters we got in Dutch. Through you I learnt the Dutch sense of humour; you showed and told me many nice jokes. Some of you may find strange

my comment about Dutch humour; they do have a sense of humour, believe me! Dirck thanks for all your support.
Dennis, thanks for reminding me every time I see you of the "nicest" Mexican words, also for reminding me of things about my country such as food, people, places, etc. I was surprised to discover your broad knowledge of Mexico.

Elco, it has been always been a pleasure to talk with you. You have an adventurous spirit. Through your stories about all your adventures (i.e. paragliding and camping), I learnt that there are other ways of enjoying life.

Paul and Patrick, the newcomers to the Thoraxcenter. Paul and Patrick thanks for helping to improve my Nederlands while writing the reports in the cath Lab. You are pair of nice and fun guys.

John de Vries, thanks for all your support. You have facilitated my clinical research and clinical activities considerably, providing me with all the help I too frequently requested. But also thanks for many other things such as the copies of the latest movies and TV series and the good tips you gave me that have enabled me and my family to better enjoy this country.

Anne-marie, thanks for all your patience and help. Often I felt protected by you; you were always telling me what was not compatible with the Dutch/Thoraxcenter standards. That helped me to better survive without standing out as the newcomer. At the beginning, I, together with Keiichi spent hours and hours in the cath lab rooms collecting the crossing time, and there you were also crucial.

Gio, it is a pity you left the Thoraxcenter, although I understood, it was for a good reason. I had the opportunity to spend time with you outside the Thoraxcenter, during business dinners or at congresses. You were, both at the Thoraxcenter and outside, simply great. I really wish you all the best in your new position and thanks a million for being there all the time to support me.

Sander, I could not enjoy more working with a person like you. You have the intelligence and curiosity that complements very well what we (the fellows) do at the Thoraxcenter. I will never forget our close collaboration to devise the video where we show our theoretical approach to treating CTOs using magnetic navigation. You have shared your enormous collection of music, movies and TV series and you have also shared with me how your personal life outside the Thoraxcenter is. I learnt about your American girlfriend and your trip to Australia. You have been above all a good friend to me. Chap, thanks for all.

Jurgen, I could write a book describing my admiration and respect for you. Sometimes I see you as a father figure, sometimes as my best friend, sometimes as my brother, sometimes I simply think you are a PERSON in every sense of the word. Now I feel it a privilege to have the opportunity to write some words to you, words that have no other motivation than to thank you for being YOU all

this time. I really hope that soon you will have a similar moment in front of your computer writing the acknowledgements section of your own PhD thesis. Thanks for being part of the history of my life. Karen, you are such a hard worker and perfect partner for Jurgen. I hope that you find in this new facet of your career many more satisfactions.

Emile Onderwater, you were there at the beginning of my time at the Thoraxcenter. I never understood why you left us. You always had solutions for all our problems, and we went to you many times asking for help to speed up the acquisition of data from the Thoraxcenter database. Thanks for all your help.

The nurses of the Thoraxcenter, Marjo de Ronde, Caroline, Kim, Marianne, Tieneke, Sandy, Mercedes, Elsa, Bas, Evelyn and Nico. You have taught me a lot during the procedures and above of all helped me to better serve as a doctor to our patients by translating English to Dutch or making understandable my Nederlandspaans to the patients.

To the staff members of the Thoraxcenter, thanks for your help. Peter de Jaegere, I really like your efforts to greet me in Spanish. It is unfortunate that I have not yet had the opportunity to work with you on research projects or in the cath lab. Professor Pim de Feyter, the perfect example of a gentleman. I wish I could be able to handle all situations in the way you do, with such a calm but firm determination, without losing control of yourself. You have had always the right words to stimulate all of the fellows. It is going to be difficult to fill the big space you will leave at the Thoraxcenter. Martin van der Ent, I will always remember the very first days of my stay in Rotterdam, I spent many hours with you and Prof. Serruys in the cath lab collecting information during the CTO procedures. At Cardialysis, we have spent also many hours during lunch time talking about Dutch life. Robert and Eric, I was already at Thoraxcenter when you started with your training in interventional cardiology. Rapidly, you have become corner stones at the Thoraxcenter. I have had the opportunity to work with you during some procedures and can say that I have enjoyed them. Evelyn, I respect your work tremendously. Today, while writing these notes (26 March 2009), I though to myself that it has been interesting the way we have worked so far, as if we were working together but in parallel simultaneously.

Eugene McFadden, you were at the Thoraxcenter when I came. You were and you have been to me just like one more fellow. You were always extremely supportive to me and all my colleagues. After you left the Thoraxcenter, you continued working at Zuiderziekenhuis, so we had the opportunity to have some dinners

with you. We always enjoy your company and the way you make us remember the old good times when we were all together working at the Thoraxcenter.
My fellow colleagues, this is a long list. I arrived on the 4 Aug 2004, so I have seen several generations of fellows, who fortunately became also my friends. When I came, Gaston, Andrew, Marco, Carlos, Jiro, Angela and Keiichi were here as fellows with Prof. Serruys. At that moment, the group had a very good relationship with the fellows of Prof. Pim de Feyter, Francesca Pugliese, Patrizia Malaguti (Marco's wife), Bob, Nico, Alessandro, and Filipo.

To Gaston and Ines, when I arrived in Holland, you were very important pillars for me. You represented a natural connection with my roots, we spoke the same language and we had the same philosophy of life. I visited your house hundreds of times; I enjoyed very much Gaston's cooking. This is true. Ines did not cook much at that moment, although she was a wonderful host. How many hours I spent with Gaston, working hard, but mostly laughing a lot; Gaston (che!) you have such an enjoyable sense of humor. Of course, you were much younger then, but scientifically you have been always big. I still vividly remember the day we were discussing the criteria to define IDTCFA. We basically followed our common sense, we decided 3 consecutive frames to avoid scoring artefacts as IDTCFA, thereafter we realized that that was also the shorter length a real TFCA can have. At that moment, we never thought of confluency, but in the total amount of NC per cross-section, again following our instinct, we came up with the 10% NC, afterwards we also learnt that this value fit with previous pathological descriptions. Then, the definition of IDTCFA was born. After all the analyses, the overall numbers were in line with pathological descriptions, so together with Prof. Serruys, we thought that what first was only intuition, made a lot of sense. Gaston and Ines, we still miss you. Now you are back in Argentina, where you have formed a complete family with a beautiful daughter, Morita (Sunday, July 6th, 2008). Mil gracias por ser sobretodo unos grandes amigos.

Together with Marco and Patrizia, we also had several nice evenings. Marco and Patrizia were both good cooks. What I enjoyed the most was the aglio, olio, e peperoncino pasta. I will never forget the day when Patrizia was robbed in The Hague. First we thought that maybe she dropped the wallet on one of the streets, so we walked and walked, searching in every corner for her wallet. Around 3 AM, we went to the train station to take the train back to Rotterdam, but Patrizia convinced us to go back to The Hague's mains square to keep on looking for her wallet. By 5 AM, we gave up and came back to Rotterdam. Patrizia, you were not only a very good friend, but also a very good dancer. Marco Valgimigli: my friend,

my adviser, my "confidant". I admire you very much for your scientific skills, you are one of the most brilliant persons I have ever met. As a person, you are also a nice chap. I remember once, I do not remember anymore why, we were talking about the feeling of being a father, I told you that being a father was the best thing can happen to a person. Now, that you are also a father of a beautiful boy, Ricardo, you called me back to tell me that I was definitely right. I am happy that the roads of our life have crossed.

Jiro Aoki and Asato, you were always very kind to me. Asato, I have many nice memories of you. 1. the day you went by yourself biking to Amsterdam and all the nice stories you told us. 2. your farewell dinner at your house where we ate delicious traditional Japanese food prepared by you. 3. we shared with you all the excitement of the preparation of your trip back to Japan. You took the Tran Siberian train from where you sent us a beautiful picture that I still have. Thanks for being such a good friend. Jiro, you were one of my first Japanese colleagues. You are very intelligent and mentally strong; you bore lots of responsibilities while you were here and succeeded always to get the best of all of them. Thanks for being a good friend.

Keiichi, my best Japanese friend (this is nothing against all the others). I was your officemate during 2 years. I enjoyed every second. You were always supportive, attentive and overall a good person. You have a wonderful family, Junko, Yoshi and Kohei. Your children were classmates of my son at the Blijberg school. Further, they also spent together many nice days outside the school. We did together the first papers on magnetic navigation.

I have vivid memories of the day, you asked me about how to create the cumulative curve to illustrate the steady trend of stent thrombosis in the Rotterdam-Bern population. After a while, the famous curve was born. I especially remember the last days of your stay in Rotterdam, how many hours you spent on the Rotterdam-Bern study. I saw you and Sophia Vaina working a lot on this. This was the project that during 2 years, you were dreaming of doing, something that you liked, something that you were interested in, and the main reason you came to Rotterdam as you mentioned in the email where I was copied on October 7th, 2006; you initiated this, you devised it and you convinced also Stephan Windecker to get involved. Just before you left Thoraxcenter, the manuscript was sent to the Lancet. When the reviewer's comments came from the Journal, which by the way happened to be many and challenging to address, you were in Japan. What followed, needless to say, is the saddest thing I have ever lived through during my stay in Rotterdam. The details of this story will remain there for the future, as something that has

marked our lives. After a while, I visited Japan and then I had the opportunity to see you again. You and your family went to Hiroshima to meet me. You never told me, but I think you and your family went specifically to see me; you travelled ~ 6 hours on Nov 22, 2006, we had dinner in a typical Japanese restaurant; a restaurant where you have to be shoeless and seat on the floor. The next day, you were going back to your home town. I truly appreciated this.

Andrew Ong, unfortunately we did not have much time together. I still have the barbecue you gave us.

Joost Daemen, initially we worked quite a lot together and there are some manuscripts as a result of that. We spent also very much time together abroad. One time together with my family, we were in New York. We went together to the Central Park and also to get every day our meals. I still remember when at the cash desk the employee of the CVS pharmacy asked you where you bought your colourful scarf. It became clear to me that these colourful clothes can only be bought in Holland. Actually, this is the same sort of comment, Filippo Cademartiri wrote in his thesis about Nico Mollet's colourful trousers. Thanks for all.

Sophia Vaina, my neighbour during some years in Teilingerstraat. I really appreciated you a lot. I liked your determination to get a proper clinical training and the ways you used to achieve it.

Neville Kukreja, "big guy", I really enjoyed the time we worked together. I was a fan of your unique black sense of humour. The most unbelievable story we had together was at Harvard Square in Boston. There we took a cab in order to go back to our hotel. As expected, I let you speak to the taxi driver. So in your British accent, you gave him indications how to get our hotel. After a rather long drive, we asked the taxi driver where we were going to. He told us that he was heading to the place indicated by Neville. Then, we realized that he was taking us to a complete different place, in other words, there was a misunderstanding in the avenue name, and I dare to say today that that was due to the differences in pronunciation between Neville and the taxi driver. When we discovered that, you started discussing and arguing with him. At certain point, we were just going rounds, the taxi driver would not let us go out of the taxi, if we did not pay the quite expensive fee. You were determined not to pay, because he made the mistake of not making sure to get the correct address. Eventually, I suggested you to call 911, so you called them, we were getting instructions what to do from the 911 operator, because nothing worked out, the police was sent to chase the taxi that we were in. They came close to us and asked the taxi driver to pull over. Finally,

the deal was that the taxi would take us back to Harvard square and we did not pay anything. What an odd situation! Although what I just mentioned is not a good background to say thanks for helping me to improve my English in every way, you really did.

Anne-Louise was a Danish colleague. You have had always an excellent taste to pick your houses. The one in Denmark was extremely beautiful and the one now in Bergen is even more beautiful. I have been always envious about that. I was always puzzled as to why you did and said things in a contradictory manner. Let me clarify what I mean. On one hand, you saw life so simply, but on the other hand your emotional life was so complex. I would like to thank you for your friendship and I wish you all the best. Finally, if you ever decide to move to a Spanish speaking country, I could help you to improve your Spanish.

Steve Ramcharitar, the way I will always remember you is asking: "Hector, how are you?" and before letting me answer you say: "Good, eh, I am also good". In other words, you greeted and answered yourself without letting the other people talk. We have had a sort of bumpy relationship, sometimes we argued, sometimes we laughed. From my perspective, the end result is positive, our friendship prevails. I wish you all the best.

Shuzo-san, only after few days in Holland, your wife had to be admitted to the hospital due to some pregnancy complications. Eventually, everything was OK and your first daughter was born. You were above of all a fair man. Because of this, I saw you struggling many times when you saw injustice, either inside or outside the hospital. We have had the opportunity to work together in the BETAX study where you were very supportive.

Carlos van Mieghem, my current neighbour in the Ommord wijk. It does not seem like it, but I think you are one of the fellows with whom I have spent the most hours working shoulder to shoulder. I say: it doesn't seem like it, because we only produced one manuscript together. I was happy to learn that your dream came true; you were asked to go to work to Aalst! I wish you all the success you deserve.

Emanuele Meliga, the most snob Italian colleague I have ever had. I really got to like you very much, although I never understood why you wore long knee-high, striped colourful toe socks. Through you I learnt a lot about Italian cuisine, especially in the last months when you were always cooking for all of us (Nieves,

Koen, Yoshi and Nick). We were also roommates at the Z120, when I moved to Cardialysis, you moved your office to Cardialysis as well. You could not cope with boredom, so you needed to be teasing Nieves and myself. Most of the memories I have about you is laughing for usually simple things, making fun of everybody. Professor Serruys should ask you how you mimic him (of course you did that always in a positive manner, "you know…").

Scientifically, we did together the entire DELFT saga, which became the core of your PhD thesis. I have to say that we got a lot support from the Italian mafia, they agreed on pooling their patients.

Last but not least, I met your beautiful wife, Sylvia, and as I write, you are becoming the parents of a beautiful boy (April 15th, 2009).

Lele, I really would like to thank you for your friendship, for being a good partner in work, but mainly for being a good partner in crime. I wish you all the best in your personal life and scientific career.

Yoshi-sama, as a researcher, you are really a master, almost a genius. But I think that what makes you special is that above of all, you are a very good friend. You are patient and listen carefully to everybody. This may have to do with your Japanese culture. If I have to move again, I will not hesitate to ask for your help. You proved yourself to be a skilled builder of IKEA furniture. However, I will only do it in combination with your other half, I mean together with Nick. You are a box full of surprises. Nobody doubts of your dancing skills (all sort of music, even salsa), your cooking skills (Japanese curry with steam rice) and you even resulted to be a good "pusher" (do not get it wrong!), I mean when you needed to push aside your one-day acquired car from the Erasmus bridge, you did it successfully. Thus, having all these good qualities, I do not understand why you have not got a beautiful Dutch woman.

Yoshi-san, you know what, we really enjoy your presence, your talking, and your uninterested help. Thanks for being my friend.

Nieves Gonzalo (la tia!), since you came was clear to me that we could work together. You are not only such a hard worker, but also an intelligent woman. The language undoubtedly played a role in our close research relationship, but we have also the same scientific curiosity. Fortunately, our friendship went beyond the hospital environment and I was next to you in important moments of your life (e.g. when you met Koen), but also in sad occasions. This strengthens our friendship considerably. One example of this last, it is that your friends became my friends and my friends were also your friends (Ceci, Poncho, Vera – in two words…-, Paul Vazquez and his family) and got to know through you all the nice people of the

Clinic Hospital in Madrid (Javier, Fernando, Roxana, Pilar, Camino, Manel and Carlos Macaya). I am sure you will be a corner stone at your new hospital. Thanks for being always there. Before finishing, iI may give you some advice, just make sure you learn how to cook Spanish food other than tortilla de patata, in other words, take advantage of this time at your mother's house, so next time we visit you in Madrid, we can enjoy your cooking.

Nicolo, Nico, Nick, Guey, etc...Guy, you know you are a special friend. It has been precious your friendship. Thanks to you, I realized I was unintentionally acting like the Godfather towards the entire community of fellows. You have confronted me many times with myself, in other words, you made me conscious of my acts. This has helped me to become a better person, because sometimes you do unconsciously good or bad things. Thanks to your generous presents, my son is now playing guitar (now I wonder who is really the Godfather). A word about your beautiful woman, whose name is Lisa. Together guys, you form a wonderful couple. I will never forget the day I tried ice in your house (actually it was snow brought by Lisa from Montreal) and maple syrup.

The new Fellows at Thoraxcenter, Joanna W., Giovanna, Carl, Scot, Shin, Takayuki, Juan Luis. Joanna, I still have to learn how to reply to the vast number of emails you are able to send in a short period of time, all marked "in red". Giovanna, thanks for being such a good person. I hope you have a successful stay in Rotterdam. I cannot wait to see all of what we have started consolidated in many manuscripts. But, more urgently, I cannot wait much longer to try some of your delicious Italian dishes. Carl, I started enjoying playing squash with you. I also wish you a wonderful career here in Rotterdam. I hope in the near future we can collaborate on some research projects. Scot, it has been nice to work with you on the InfraReDx project. I am pretty sure this is only the beginning of a fruitful research relationship between us. I am already looking forward to working with you on more projects. Eun-Seok Shin, I could not like you more, you are not only a wonderful person, but also an extremely hard worker and intelligent woman. We share the same scientific curiosity; therefore I think we will be working for a lot time together. Takayuki-sama, (Taka-nieves) you are extremely kind to everybody. We worked closely on the Terumo trial and it has been always a pleasure. We have some other lines of connection. Your daughter is my son's classmate. Thanks for the nice pictures you gave me after the school performance where my son was disguised as a small dog. Shen, I have been learning how to treat you. You are in a positive way, different to all my other colleagues It may be the age difference, or your large clinical experience in the field of Interventional Cardiology. Your short

stay has been extremely successful in the sense that you came here to get some experience in research, and in a short period of time, you have learnt to use many different imaging softwares and I can even say that you have mastered them by now. You have got involved in many interesting projects with many fellows. This emphasizes your capability to work in a team. I really hope this experience gives you enough background to boost research in your hospital in Beijing. Juan Luis, it has been short time that I know you. I can see already that you are not the typical Spanish sort of person. You have not told me, but I discovered that you are able to speak English, Italian, German and I think you also speak some Portuguese, I have heard that in less than a month you started to speak you first Dutch words. Being polyglot is of course not the main quality of your Spanish countrymen. We (Apostolos, Carl and myself) will remember always the circumstance in which you got the corneal erosion. Chris, after Sophia Vaina you were the second Greek colleague that I had. I empathized quite a lot with you. I share the way you see life in general, but in particular the way you face working situations. We have provoked already many situations to create the opportunity to work in some research projects with you. I hope at some point we can do it. Here I have to mention that I also feel lot of sympathy for your Eline. Apostolos, after only this short period of time, I can see you are also determined to be successful here at Thoraxcenter. Hope you find your way to get your echocardiography projects done.

Professor Patrick W. Serruys always reads this section in order to get ideas to write the speech that he gives at the end of the PhD ceremony, or at least this is what he has been doing for the last 5 years. As I am aware of that, I have to pick the right words and describe only the things that I want him to mention. While reading this text, I think that he will feel a challenge and try to write something from scratch, which of course will be a surprise for me during the ceremony. But if I do not write some hints here, it can be also risky; he can consider mentioning things that will make me uncomfortable at that moment. However, I am going to be fair and sincere, and write here a message that conveys above of all my immeasurable gratitude to him.

I would like to thank you for your patience but also for your impatience, for your thoughtfulness, but also for your thoughtlessness, for your unconditional support, but also for your conditional support, for teaching me how to work hard, but also for teaching me how to enjoy life. This dualism is what ultimately has given to our relationship a great balance. I sincerely hope our working relationship last for many years.

I would like also to take the opportunity and write some words of gratitude to Danielle Serruys. You have always been extremely kind and sensitive towards

me and my family. Your encouragement has helped me overcome many difficult situations I have encountered during my stay in Rotterdam. You have graciously offered me dinner many times at your house. For all of this, I would like to thank you sincerely.

Paul Cummins, the most Irish of my coworkers and the most catholic as well (Marie-angele, do not take me wrong). You are such a great chap; I do really enjoy working next to you. You know that, since you loaded the video in YouTube from the Buddy Guy's Blues Bar, Chicago, I am more famous now than before. I think I have not told you that my son enjoyed the video as well.

Nico Bruining, I would like to thank you for all you have taught me, mostly indirectly, I mean through Gaston. The other opportunity was in the meetings we have had to discuss the guidelines for progression/regression studies. I have always enjoyed the time I have spent with you outside of work. One nice memory was when we went to see the red bulls in Chicago. Thanks for being a good friend to me.

ACKNOWLEDGEMENTS TO *THE PEOPLE* FROM CARDIALYSIS

Marie-angele, of all the people I have met in a professional capacity, I can say that you are the person who stands out because of your ever-present willingness to help. You have been, all this time, somebody I could always count on. You have listened many times when I have had problems. You know that listening helps already a lot; being listened to is the beginning of the cure, the beginning of the solution of a problem. I remember the day of my birthday, 27th January 2008, when we (Prof. Serruys, Gerrit-Anne, you and me) were at the revolving roof top restaurant in NY city, the View Restaurant at the New York Marriot Marquis Hotel at Times Square. From that day on, you keep a picture of all of us in your office. Thanks for being such a great colleague and team partner.

Gerrit-Anne, I got to know you a lot during 2-week trip to US in the months of Octuber and November 2008. We visited many cities together and had all our dinners together. Then we talked about everything but work. I could see the way you see life and how you got through all the same sort of situations I am currently going through. You told me that you were also working, while trying to sort out your PhD. In my case, I have currently 2 chiefs, I am finishing up a PhD, getting the BIG registration and working at Cardialysis. This may sound simple, when

you do not consider that one of my chiefs is Prof. Serruys at Thoraxcenter and he is also part of the board of Directors at Cardialysis. Gerrit-Anne, a great deal of the credit for my success in this multi-task sort of position is you. You have made this time smoother, I can say a bit less traumatic. Thanks for being always there.

Peter-Paul, since day one, you have been always supportive and kind to me. I like from you especially your optimism. Thanks for all your help.

Yvonne and Marjorie, thank you for making my stay in Cardialysis easier. Sometimes you even talk to me in Spanish, so I can feel like working at Home. Yvonne, you specially understand quite well my background, because you know Mexico and the Mexicans very well. I was surprised to see all you have visited in Mexico. I am pretty sure that you have been to many more places in Mexico that I have been to. Thanks both of you for your help and assistance.

The other 3 people that are very important for me at Cardialysis are the 3 senior IVUS analysts, Ali, Jamal and Ravindra. You have taught me so much, but more importantly you have been so patient in so doing. Today I know, figuurlijk gesproken, that I do not have one right hand, but four. I enjoy very much working with you. I hope we can continue to be such a good team.

Koen Commisaris, gracias Koen for being a good collaborator and friend. Thanks also for being so helpful during our last verhuizen. More importantly, I would like to thank you for teaching me some interesting concepts about brewing.

Dick Goedhart, thanks for all your patience and help. I do really admire your energy to finish up statistical analysis during late evenings and even on weekends.

I wish I could have the opportunity to thank many other colleagues from Cardialysis such as Bianca Backx, Monique Schuijer, Janette Symons, Marco Bressers, Jessica, Tessa, Anouk, Barbara, Frits, Richard, Angelien, Claudia, Eline, Ana, Witteke, Rene, and Ad.

Agradecimientos

Todo empezó en 2003, cuando siendo residente del 2° año de Cardiología Intervencionista, escribí a Rotterdam, preguntando por los requisitos que se necesitaban para venir al Thoraxcenter. Cuando recibí contestación de mi e-mail de Anja, me fijé como meta, venir a este centro. Me platicaban que era un sitio de excelencia, donde se trabajaba bastante, aunque no me lo podía ni imaginar en ese entonces. A través de Mauricio López, me enteré un poco de la experiencia de Manuel Sabate. Mauricio mismo me decía que me vendría a las grandes ligas de la investigación en Cardiología Intervencionista, otra vez no comprendía del todo lo que eso significaba. La decisión principal de venir, la tomé, basado en dos hechos fundamentales: primero, que yo quería estar en el mejor lugar para hacer investigación clínica en Cardiología Intervencionista; y segundo, quería estar en Europa (nunca antes había estado en este continente). El primer paso que dí, fue convencer al Intituto Nacional de Cardiología "Ignacio Chávez" (INC) que necesitaba exponerme a este ambiente, que si me quedaba en México, me quedaría incompleto, que era una necesidad personal. Afortunadamente, el Doctor Fause Attie aceptó.

Se llegó el día de la entrevista con el Profesor Patrick W. Serruys, durante el AHA en la Ciudad de Orlando Florida en 2003. Me citó en un hotel relativamente pequeño y modesto, me acompañaban mi esposa Lourdes, mi hijo Andrés, Ernesto Luna y Sylvia Siu; cuando llegamos al hotel IBIS (será que desde ese entonces me seguía el nombre? – este es el nombre de uno de los estudios en los que mas activamente he participado) a preguntar por lobby del mismo, nos dijeron que ese hotel no tenia lobby, de hecho no tenia ninguna otra area, mas que los cuartos del hotel. De cualquier forma, el Profesor no se encontraba en el hotel. Así es que el viaje que había hecho específicamente para eso, no estaba siendo exitoso, le envíe un mensaje a Anja, que afortunadamente contesto rapidamente, dando una cita para mas tarde. Finalmente me reuní con el, fue una conversación acerca de los planes que tenia de investigación. Luego el Profesor escribió en una hoja que tenía que hablar con Wil Warthelemy para enviar mis papeles. Empecé a enviar todos los documentos a Wil Warthelemy para que arreglara el permiso de estancia y el de trabajo. Y finalmente todo estaba listo para que me viniera al Thoraxcenter.

Esta decisión de venir a Rotterdam afectó primordialmente a mi esposa Lourdes (Lulú), que cursaba el segundo año de Cardiología Pediátrica y cuando yo me tuve que venir, 4 de agosto de 2004, ella se quedó a terminar su formación.

Lulú, algún día me dijiste: "este ha sido tu sueño desde hace mucho tiempo, ve por el, y haz que se haga realidad" - Esto te lo voy agradecer infinitamente toda mi vida -.

Así que, mi esposa e hijo se quedaron en México. En aquellos momentos, experimente sentimientos encontrados, por un lado me sentía feliz de venir a Europa, y por el otro, triste de dejar a mi esposa, hijo, padres, amigos y a mi México.

Sin duda alguna quien más ha contribuido a que todo este tiempo en Rotterdam haya sido un éxito en muchos sentidos, ha sido mi esposa Lulú. - Tú has sido un gran soporte en mi carrera, no sólo demostrándome tu amor todos los días también por escucharme, por haber abandonado un poco tus ideales y unirte a los míos. Por todo esto, eres tú a la persona a quien más tengo que agradecer, te doy las gracias otra vez infinitamente. Le doy también gracias a Dios porque nos ha permitido compartir juntos esta experiencia, que sin duda ya ha marcado nuestras vidas para siempre. Te amo inmensamente.

Quien ha estado todo este tiempo ahí, como testigo silencioso, es mi hijo Andrés Alejandro. Cuando recién llegaste a Rotterdam (10 mayo 2005), tú tenías 7 años de edad. Aún recuerdo la celebración de tu cumpleaños, fue en la casa de Teilingestraat 51L, estábamos solamente nosotros tres, partimos un pastel que habíamos preparado previamente con nutela. Fue un día muy especial, porque cuando las celebraciones son más grandes, se pierde ese acercamiento que puedes tener con el festejado.

Tus primeros días en la escuela fueron relativamente fáciles, conociste a tu amigo Josué y eso ayudo a que te acostumbraras más rápido. Todos los días te llevaba a la escuela en el asiento de atrás de mi bicicleta. En ese entonces, en la escuela, te pedían que escribieras un diario describiendo las actividades que hacias y también tenías que dibujar los hechos más relevantes. Aún conservamos esos dibujos, que para ti, era lo mas importante que ocurría a tu alrededor. En uno de ellos ilustras como te llevo en el asiento de atrás a la escuela.

Hijo Andrés, a ti también te quiero dar las gracias por tu inmensa paciencia y por la comprensión que muestras hacia las profesiones de tus padres. Ahora que ya eres casi un adolescente y te enfrentaras a esos cambios físicos y psicológicos, yo te tendré toda la paciencia y comprensión que tú me haz tenido. Te amo hijo.

Mis padres, Héctor y Enedina. A ustedes les tengo que agradecer la vida, esos años de lucha para enviarme a la escuela. Creo que siguiendo su ejemplo, me he

enfrentado yo también a muchas situaciones difíciles. Nunca me he dejado vencer, siempre he luchado hasta lo último; esto ha hecho que afronte los resultados serenamente, sabiendo que he dado lo mejor de mí. Gracias por estar siempre ahí cuando los necesito.

A mis hermanos, Sandra, Juan, Adrián y Eduardo, también les quiero agradecer por compartir conmigo los buenos y malos momentos; y sobre todo por simpatizar, y a veces también por estar en desacuerdo con lo que hago. Les deseo con todo mi corazón que ustedes también sean muy felices con lo que decidan hacer con sus vidas.

Gracias a mis suegros, Manuel y Consuelo, por ser un gran apoyo para Lulú y Andrés cuando se quedaron en México. No tengo con que agadecer su amor y paciencia a mi hijo. A mis cuñados, Bárbara, Manuel y Margarita, igualmente mi agradecimiento por estar ahí cerca de ellos, alentándolos y haciéndoles sentir su apoyo. Especialmente quiero agradecer a Susana por su incondicional ayuda y sobre todo por dejarme ver su gran corazón y valentia.

A mis amigos, Arturo y Mónica, que además son mis compadres, gracias por todo este tiempo de amistad. Especialmente por que han sido un gran apoyo moral. Gracias por ser parte de mi historia y por dejarme ser parte de la suya. Paul y Karla, gracias también por su amistad incondicional.

A mi paisa Samuel Varela, gracias por tu amistad, tu paciencia y sobretodo por compartir conmigo ese gran ser humano que llevas por dentro.

A Tere Resendiz, durante mis años en el INC, no sólo demostraste ser la mas eficiente, leal y servicial de mis compañeros de trabajo, sino que además me dejaste conocer tu lado humano. Muchas veces me escuchaste, me diste consejos, pero sobre todo siempre me ayudaste en todo, aún estando en Rotterdam, siempre fuiste tú la persona a la que recurrí cuando algo necesitabamos. Gracias también por que nos dejaste conocer a tu familia. Tere, sigue siempre igual, eres una gran persona, gracias otra vez por tu inmensa ayuda.

Al Dr. José F. Guadalajara Boo también le quiero dar las gracias por su valioso ejemplo. Le tengo una gran admiración y respeto. No he conocido mejor Cardiólogo, en toda la extensión de la palabra, que Usted. Los tres años que trabajé junto a Usted fueron de gran aprendizaje y en general una gran experiencia. Gracias por

haber alimentado mis aspiraciones, cuando platicábamos de la posibilidad de venir a Holanda.

Al Dr. Martín Rosas también tengo mucho que agradecerle. La semilla que había en mí, de hacer investigación, fue sin duda promovida por su enseñanza y ejemplo. En los momentos en que más dudé acerca de mi futuro profesional, su consejo fue muy importante, sino es que casi determinante. Espero que pronto encontremos la forma de trabajar juntos, en la investigación, que es algo que nos satisface a los dos.

En general, quiero agradecer a los Cardiólogos del INC, sobre todo a aquéllos que me enseñaron Cardiología.

Agradezco también a la Sociedad Mexicana de Cardiología, por su apoyo económico durante los primeros años de mi estancia en Rotterdam.

Podría seguir agradeciendo a miles de personas más, que quiero y que admiro, pero creo que a las que aquí agradezco son las que forman parte de alguna manera de este capítulo en mi vida.

Curriculum vitae

Family name:	Garcia Garcia
First name:	Hector Manuel
Birth date:	January 27th, 1973.
Nationality:	Mexico
Professional address:	Department of Interventional Cardiology, Z120 Thoraxcenter, Erasmus MC, Dr. Molewaterplein 40, 3015 GD Rotterdam, the Netherlands.
Email	hect2701@yahoo.es hgarcia@cardialysis.nl, h.garciagarcia@erasmusmc.nl,
Professional qualifications:	Medicine
Awarded by:	Universidad Autonoma de Guadalajara, Guadalajara, Jalisco, Mexico
Date:	1994
Postgraduate qualifications:	Internal Medicine
Awarded by University of:	Universidad Nacional Autonoma de Mexico (UNAM) From 1997 to 1999.
Postgrade qualifications:	Cardiology
Awarded by:	Instituto Nacional de Cardiologia (INC) "Ignacio Chavez" and UNAM From 1999 to 2002
Postgrade qualifications:	Interventional Cardiology in INC
Awardes by:	UNAM and INC From March, 2002 to Feb, 2004
Master degree:	Master in Science
Awarded:	Erasmus University 2006.

RECENT CLINICAL RESEARCH EXPERIENCE

1. **Garcia-Garcia HM**, Goedhart D, Schuurbiers JC, Kukreja N, Tanimoto S, Daemen J, Morel MA, Bressers M, van Es GA, Wentzel J, Gijsen F, van der Steen AF, Serruys PW. Virtual histology and remodeling index allow in vivo identification of allegedly high risk coronary plaques in patients with acute coronary syndromes: a three vessel intravascular ultrasound radiofrequency data analysis. *Eurointervention.* 2006;2:338-344.
2. **Garcia-Garcia HM**, Goedhart D, Serruys PW. Relation of plaque size to necrotic core in the three major coronary arteries in patients with acute coronary syndrome as determined by intravascular ultrasonic imaging radiofrequency. *Am J Cardiol.* 2007;99(6):790-792.
3. **Garcia-Garcia HM**, Gonzalo N, Granada JF, Regar E, Serruys PW. Diagnosis and treatment of coronary vulnerable plaques. *Expert Rev Cardiovasc Ther.* 2008;6(2):209-222.
4. **Garcia-Garcia HM**, Gonzalo N, Kukreja N, Alfonso F. Greyscale intravascular ultrasound and IVUS-radiofrequency tissue characterisation to improve understanding of the mechanisms of coronary stent thrombosis in drug-eluting stents. *EuroIntervention.* 2008;4 Suppl C:C33-38.
5. **Garcia-Garcia HM**, Gonzalo N, Tanimoto S, Meliga E, de Jaegere P, Serruys PW. Characterization of edge effects with paclitaxel-eluting stents using serial intravascular ultrasound radiofrequency data analysis: the BETAX (BEside TAXus) Study. *Rev Esp Cardiol.* 2008;61(10):1013-1019.
6. **Garcia-Garcia HM**, Gonzalo N, Pawar R, Kukreja N, Dudek D, Thuesen L, Ormiston JA, Regar E, Serruys PW. Assessment of the absorption process following bioabsorbable everolimus-eluting stent implantation: temporal changes in strain values and tissue composition using intravascular ultrasound radiofrequency data analysis. A substudy of the ABSORB clinical trial. *EuroIntervention.* 2009;4(4):443-448.
7. **García-García HM**, Mintz G, Lerman A, Vince GD, Margolis P, van ES GA, Morel MA, Nair A, Virmani R, Burke AP, Stone S, Serruys PW. Tissue Characterization Using Intravascular Radiofrequency Data Analysis: Recommendations for Acquisition, Analysis, Interpretation and Reporting. *Eurointervention.* 2009.
8. **Garcia-Garcia HM**, Vaina S, Tsuchida K, Serruys PW. Drug-eluting stents. *Arch Cardiol Mex.* 2006;76(3):297-319.
9. **Garcia-Garcia HM**, Daemen J, Kukreja N, Tanimoto S, van Mieghem CA, van der Ent M, van Domburg RT, Serruys PW. Three-year clinical outcomes after coronary stenting of chronic total occlusion using sirolimus-eluting stents: insights from the rapamycin-eluting stent evaluated at Rotterdam cardiology hospital-(RESEARCH) registry. *Catheter Cardiovasc Interv.* 2007;70(5):635-639.
10. van der Waal EC, Mintz GS, **Garcia-Garcia HM**, Bui AB, Pehlivanova M, Girasis C, Serruys PW, van der Giessen WJ, Weissman NJ. Intravascular ultrasound and 3D angle measurements of coronary bifurcations. *Catheter Cardiovasc Interv.* 2008.
11. Valgimigli M, Rodriguez-Granillo GA, **Garcia-Garcia HM**, Vaina S, De Jaegere P, De Feyter P, Serruys PW. Plaque composition in the left main stem mimics the distal but not the proximal tract of the left coronary artery: influence of clinical

presentation, length of the left main trunk, lipid profile, and systemic levels of C-reactive protein. *J Am Coll Cardiol.* 2007;49(1):23-31.

12. Valgimigli M, Rodriguez-Granillo GA, **Garcia-Garcia HM**, Malagutti P, Regar E, de Jaegere P, de Feyter P, Serruys PW. Distance from the ostium as an independent determinant of coronary plaque composition in vivo: an intravascular ultrasound study based radiofrequency data analysis in humans. *Eur Heart J.* 2006;27(6):655-663.
13. Tsuchida K, **Garcia-Garcia HM**, Ong AT, Valgimigli M, Aoki J, Rademaker TA, Morel MA, van Es GA, Bruining N, Serruys PW. Revisiting late loss and neointimal volumetric measurements in a drug-eluting stent trial: analysis from the SPIRIT FIRST trial. *Catheter Cardiovasc Interv.* 2006;67(2):188-197.
14. Valgimigli M, Malagutti P, Rodriguez Granillo GA, Tsuchida K, **Garcia-Garcia HM**, van Mieghem CA, Van der Giessen WJ, De Feyter P, de Jaegere P, Van Domburg RT, Serruys PW. Single-vessel versus bifurcation stenting for the treatment of distal left main coronary artery disease in the drug-eluting stenting era. Clinical and angiographic insights into the Rapamycin-Eluting Stent Evaluated at Rotterdam Cardiology Hospital (RESEARCH) and Taxus-Stent Evaluated at Rotterdam Cardiology Hospital (T-SEARCH) registries. *Am Heart J.* 2006;152(5):896-902.
15. Valgimigli M, Malagutti P, Aoki J, **Garcia-Garcia HM**, Rodriguez Granillo GA, van Mieghem CA, Ligthart JM, Ong AT, Sianos G, Regar E, Van Domburg RT, De Feyter P, de Jaegere P, Serruys PW. Sirolimus-eluting versus paclitaxel-eluting stent implantation for the percutaneous treatment of left main coronary artery disease: a combined RESEARCH and T-SEARCH long-term analysis. *J Am Coll Cardiol.* 2006;47(3):507-514.
16. Tsuchida K, Daemen J, Tanimoto S, **Garcia-Garcia HM**, Kukreja N, Vaina S, Ong AT, Sianos G, de Jaegere PP, van Domburg RT, Serruys PW. Two-year outcome of the use of paclitaxel-eluting stents in aorto-ostial lesions. *Int J Cardiol.* 2007.
17. Tanimoto S, Daemen J, Tsuchida K, **Garcia-Garcia HM**, de Jaegere P, van Domburg RT, Serruys PW. Two-year clinical outcome after coronary stenting of small vessels using 2.25-mm sirolimus- and paclitaxel-eluting stents: insight into the RESEARCH and T-SEARCH registries. *Catheter Cardiovasc Interv.* 2007;69(1):94-103.
18. Serruys PW, Ormiston JA, Onuma Y, Regar E, Gonzalo N, **Garcia-Garcia HM**, Nieman K, Bruining N, Dorange C, Miquel-Hebert K, Veldhof S, Webster M, Thuesen L, Dudek D. A bioabsorbable everolimus-eluting coronary stent system (ABSORB): 2-year outcomes and results from multiple imaging methods. *Lancet.* 2009;373(9667):897-910.
19. Serruys PW, **Garcia-Garcia HM**, Regar E. From postmortem characterization to the in vivo detection of thin-capped fibroatheromas: the missing link toward percutaneous treatment: what if Diogenes would have found what he was looking for? *J Am Coll Cardiol.* 2007;50(10):950-952.
20. Serruys PW, **Garcia-Garcia HM**, Buszman P, Erne P, Verheye S, Aschermann M, Duckers H, Bleie O, Dudek D, Botker HE, von Birgelen C, D'Amico D, Hutchinson T, Zambanini A, Mastik F, van Es GA, van der Steen AF, Vince DG, Ganz P, Hamm CW, Wijns W, Zalewski A. Effects of the direct lipoprotein-associated

phospholipase A(2) inhibitor darapladib on human coronary atherosclerotic plaque. *Circulation.* 2008;118(11):1172-1182.

21. Segers D, **Garcia-Garcia HM**, Cheng C, de Crom R, Krams R, Wentzel JJ, van der Steen AF, Serruys PW, Leenen PJ, Laman JD. A primer on the immune system in the pathogenesis and treatment of atherosclerosis. *EuroIntervention.* 2008;4(3):378-390.
22. Sawada T, Shite J, **Garcia-Garcia HM**, Shinke T, Watanabe S, Otake H, Matsumoto D, Tanino Y, Ogasawara D, Kawamori H, Kato H, Miyoshi N, Yokoyama M, Serruys PW, Hirata K. Feasibility of combined use of intravascular ultrasound radiofrequency data analysis and optical coherence tomography for detecting thin-cap fibroatheroma. *Eur Heart J.* 2008;29(9):1136-1146.
23. Rodriguez-Granillo GA, Vos J, Bruining N, **Garcia-Garcia HM**, de Winter S, Ligthart JM, Deckers JW, Bertrand M, Simoons ML, Ferrari R, Fox KM, Remme W, De Feyter PJ. Long-term effect of perindopril on coronary atherosclerosis progression (from the perindopril's prospective effect on coronary atherosclerosis by angiography and intravascular ultrasound evaluation [PERSPECTIVE] study). *Am J Cardiol.* 2007;100(2):159-163.
24. Rodriguez-Granillo GA, Valgimigli M, **Garcia-Garcia HM**, Ong AT, Aoki J, van Mieghem CA, Tsuchida K, Sianos G, McFadden E, van der Giessen WJ, van Domburg R, de Feyter P, Serruys PW. One-year clinical outcome after coronary stenting of very small vessels using 2.25 mm sirolimus- and paclitaxel-eluting stents: a comparison between the RESEARCH and T-SEARCH registries. *J Invasive Cardiol.* 2005;17(8):409-412.
25. Rodriguez-Granillo GA, Vaina S, **Garcia-Garcia HM**, Valgimigli M, Duckers E, van Geuns RJ, Regar E, van der Giessen WJ, Bressers M, Goedhart D, Morel MA, de Feyter PJ, Serruys PW. Reproducibility of intravascular ultrasound radiofrequency data analysis: implications for the design of longitudinal studies. *Int J Cardiovasc Imaging.* 2006;22(5):621-631.
26. Rodriguez-Granillo GA, Serruys PW, **Garcia-Garcia HM**, Aoki J, Valgimigli M, van Mieghem CA, McFadden E, de Jaegere PP, de Feyter P. Coronary artery remodelling is related to plaque composition. *Heart.* 2006;92(3):388-391.
27. Valgimigli M, Malagutti P, Rodriguez-Granillo GA, **Garcia-Garcia HM**, Polad J, Tsuchida K, Regar E, Van der Giessen WJ, de Jaegere P, De Feyter P, Serruys PW. Distal left main coronary disease is a major predictor of outcome in patients undergoing percutaneous intervention in the drug-eluting stent era: an integrated clinical and angiographic analysis based on the Rapamycin-Eluting Stent Evaluated At Rotterdam Cardiology Hospital (RESEARCH) and Taxus-Stent Evaluated At Rotterdam Cardiology Hospital (T-SEARCH) registries. *J Am Coll Cardiol.* 2006;47(8):1530-1537.
28. Rodriguez-Granillo GA, **Garcia-Garcia HM**, Valgimigli M, Vaina S, van Mieghem C, van Geuns RJ, van der Ent M, Regar E, de Jaegere P, van der Giessen W, de Feyter P, Serruys PW. Global characterization of coronary plaque rupture phenotype using three-vessel intravascular ultrasound radiofrequency data analysis. *Eur Heart J.* 2006;27(16):1921-1927.
29. Rodriguez-Granillo GA, **Garcia-Garcia HM**, Valgimigli M, Schaar JA, Pawar R, van der Giessen WJ, Regar E, van der Steen AF, de Feyter PJ, Serruys PW. In vivo

relationship between compositional and mechanical imaging of coronary arteries. Insights from intravascular ultrasound radiofrequency data analysis. *Am Heart J.* 2006;151(5):1025 e1021-1026.

30. Rodriguez-Granillo GA, **Garcia-Garcia HM**, Mc Fadden EP, Valgimigli M, Aoki J, de Feyter P, Serruys PW. In vivo intravascular ultrasound-derived thin-cap fibroatheroma detection using ultrasound radiofrequency data analysis. *J Am Coll Cardiol.* 2005;46(11):2038-2042.
31. Rodriguez-Granillo GA, de Winter S, Bruining N, Ligthart JM, **Garcia-Garcia HM**, Valgimigli M, de Feyter PJ. Effect of perindopril on coronary remodelling: insights from a multicentre, randomized study. *Eur Heart J.* 2007;28(19):2326-2331.
32. Rodriguez-Granillo GA, Agostoni P, **Garcia-Garcia HM**, de Feyter P, Serruys PW. In-vivo, cardiac-cycle related intimal displacement of coronary plaques assessed by 3-D ECG-gated intravascular ultrasound: exploring its correlate with tissue deformability identified by palpography. *Int J Cardiovasc Imaging.* 2006;22(2):147-152.
33. Rodriguez-Granillo GA, Agostoni P, **Garcia-Garcia HM**, Biondi-Zoccai GG, McFadden E, Amoroso G, de Jaegere P, Bruining N, de Feyter P, Serruys PW. Meta-analysis of the studies assessing temporal changes in coronary plaque volume using intravascular ultrasound. *Am J Cardiol.* 2007;99(1):5-10.
34. Rivero-Ayerza M, Theuns DA, **Garcia-Garcia HM**, Boersma E, Simoons M, Jordaens LJ. Effects of cardiac resynchronization therapy on overall mortality and mode of death: a meta-analysis of randomized controlled trials. *Eur Heart J.* 2006;27(22):2682-2688.
35. Ormiston JA, Serruys PW, Regar E, Dudek D, Thuesen L, Webster MW, Onuma Y, **Garcia-Garcia HM**, McGreevy R, Veldhof S. A bioabsorbable everolimus-eluting coronary stent system for patients with single de-novo coronary artery lesions (ABSORB): a prospective open-label trial. *Lancet.* 2008;371(9616):899-907.
36. Meliga E, **Garcia-Garcia HM**, Valgimigli M, Chieffo A, Biondi-Zoccai G, Maree AO, Gonzalo N, Cook S, Marra S, Moretti C, De Servi S, Palacios IF, Windecker S, van Domburg R, Colombo A, Sheiban I, Serruys PW. Impact of drug-eluting stent selection on long-term clinical outcomes in patients treated for unprotected left main coronary artery disease: The sirolimus vs paclitaxel drug-eluting stent for left main registry (SP-DELFT). *Int J Cardiol.* 2008.
37. Meliga E, **Garcia-Garcia HM**, Valgimigli M, Chieffo A, Biondi-Zoccai G, Maree AO, Gonzalo N, Cook S, Cruz-Gonzalez I, Marra S, De Servi S, Palacios IF, Windecker S, van Domburg R, Colombo A, Sheiban I, Serruys PW. Diabetic patients treated for unprotected left main coronary artery disease with drug eluting stents: a 3-year clinical outcome study. The diabetes and drug eluting stent for LeFT main registry (D-DELFT). *EuroIntervention.* 2008;4(1):77-83.
38. Meliga E, **Garcia-Garcia HM**, Valgimigli M, Chieffo A, Biondi-Zoccai G, Maree AO, Cook S, Reardon L, Moretti C, De Servi S, Palacios IF, Windecker S, Colombo A, van Domburg R, Sheiban I, Serruys PW. Longest available clinical outcomes after drug-eluting stent implantation for unprotected left main coronary artery disease: the DELFT (Drug Eluting stent for LeFT main) Registry. *J Am Coll Cardiol.* 2008;51(23):2212-2219.
39. Meliga E, **Garcia-Garcia HM**, Kukreja N, Daemen J, Tanimoto S, Ramcharitar S, van Mieghem CA, Sianos G, van der Ent M, van der Giessen WJ, de Feyter P,

van Domburg R, Serruys PW. Chronic total occlusion treatment in post-CABG patients: saphenous vein graft versus native vessel recanalization-long-term follow-up in the drug-eluting stent era. *Catheter Cardiovasc Interv.* 2007;70(1):21-25.

40. Kukreja N, Onuma Y, **Garcia-Garcia HM**, Daemen J, van Domburg R, Serruys PW. Three-year survival following multivessel percutaneous coronary intervention with bare-metal or drug-eluting stents in unselected patients. *Am J Cardiol.* 2009;103(2):203-211.
41. Kukreja N, **Garcia-Garcia HM**, Serruys PW. Invasive imaging techniques for the assessment of vulnerable plaque. *Minerva Cardioangiol.* 2006;54(5):603-617.
42. Gonzalo N, Serruys PW, Barlis P, Ligthart J, **Garcia-Garcia HM**, Regar E. Multimodality intra-coronary plaque characterization: A pilot study. *Int J Cardiol.* 2008.
43. Gonzalo N, **Garcia-Garcia HM**, Ligthart J, Rodriguez-Granillo G, Meliga E, Onuma Y, Schuurbiers JC, Bruining N, Serruys PW. Coronary plaque composition as assessed by greyscale intravascular ultrasound and radiofrequency spectral data analysis. *Int J Cardiovasc Imaging.* 2008;24(8):811-818.
44. Daemen J, Tanimoto S, **Garcia-Garcia HM**, Kukreja N, van de Sande M, Sianos G, de Jaegere PP, van Domburg RT, Serruys PW. Comparison of three-year clinical outcome of sirolimus- and paclitaxel-eluting stents versus bare metal stents in patients with ST-segment elevation myocardial infarction (from the RESEARCH and T-SEARCH Registries). *Am J Cardiol.* 2007;99(8):1027-1032.
45. Daemen J, **Garcia-Garcia HM**, Kukreja N, Imani F, de Jaegere PP, Sianos G, van Domburg RT, Serruys PW. The long-term value of sirolimus- and paclitaxel-eluting stents over bare metal stents in patients with diabetes mellitus. *Eur Heart J.* 2007;28(1):26-32.
46. Agostoni P, Valgimigli M, Biondi-Zoccai GG, Abbate A, **Garcia Garcia HM**, Anselmi M, Turri M, McFadden EP, Vassanelli C, Serruys PW, Colombo A. Clinical effectiveness of bare-metal stenting compared with balloon angioplasty in total coronary occlusions: insights from a systematic overview of randomized trials in light of the drug-eluting stent era. *Am Heart J.* 2006;151(3):682-689.
47. De Jaegere PP, Piazza N, Galema TW, Otten A, Soliman OI, Van Dalen BM, Geleijnse ML, Kappetein AP, **Garcia-Garcia HM**, Van Es GA, Serruys PW. Early echocardiographic evaluation following percutaneous implantation with the self-expanding CoreValve Revalving System aortic valve bioprosthesis. *EuroIntervention.* 2008;4(3):351-357.
48. Martinez-Rios MA, Rosas M, Gonzalez H, Pena-Duque MA, Martinez-Sanchez C, Gaspar J, **Garcia-Garcia HM**, Gaxiola E, Delgado L, Carrillo J, Leyva JL, Lupi E. Comparison of reperfusion regimens with or without tirofiban in ST-elevation acute myocardial infarction. *Am J Cardiol.* 2004;93(3):280-287.

Color section

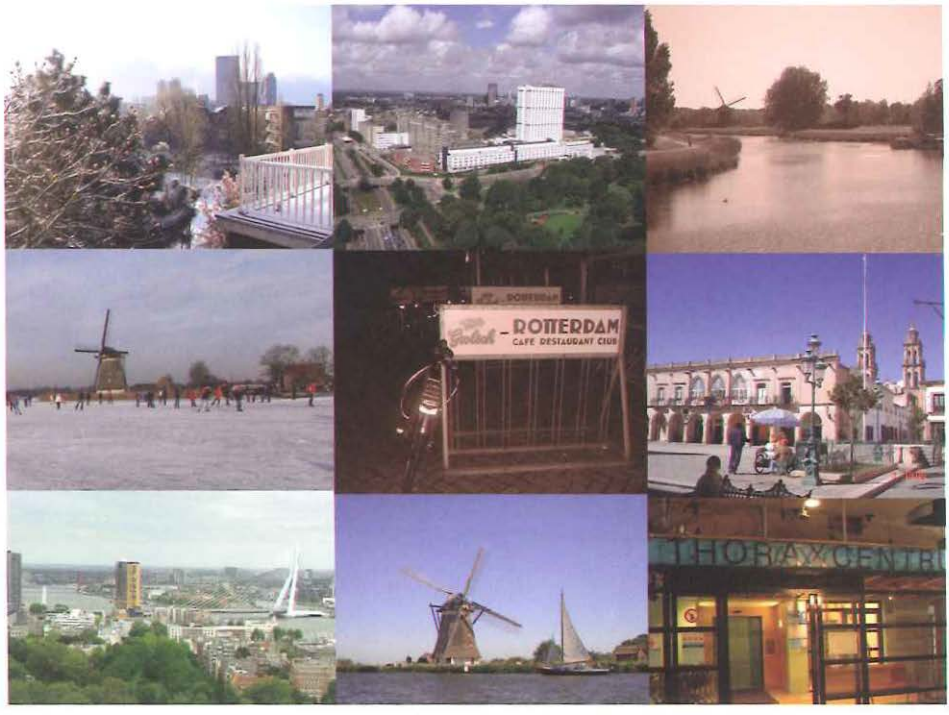
ROTTERDAM
CAFE RESTAURANT CLUB

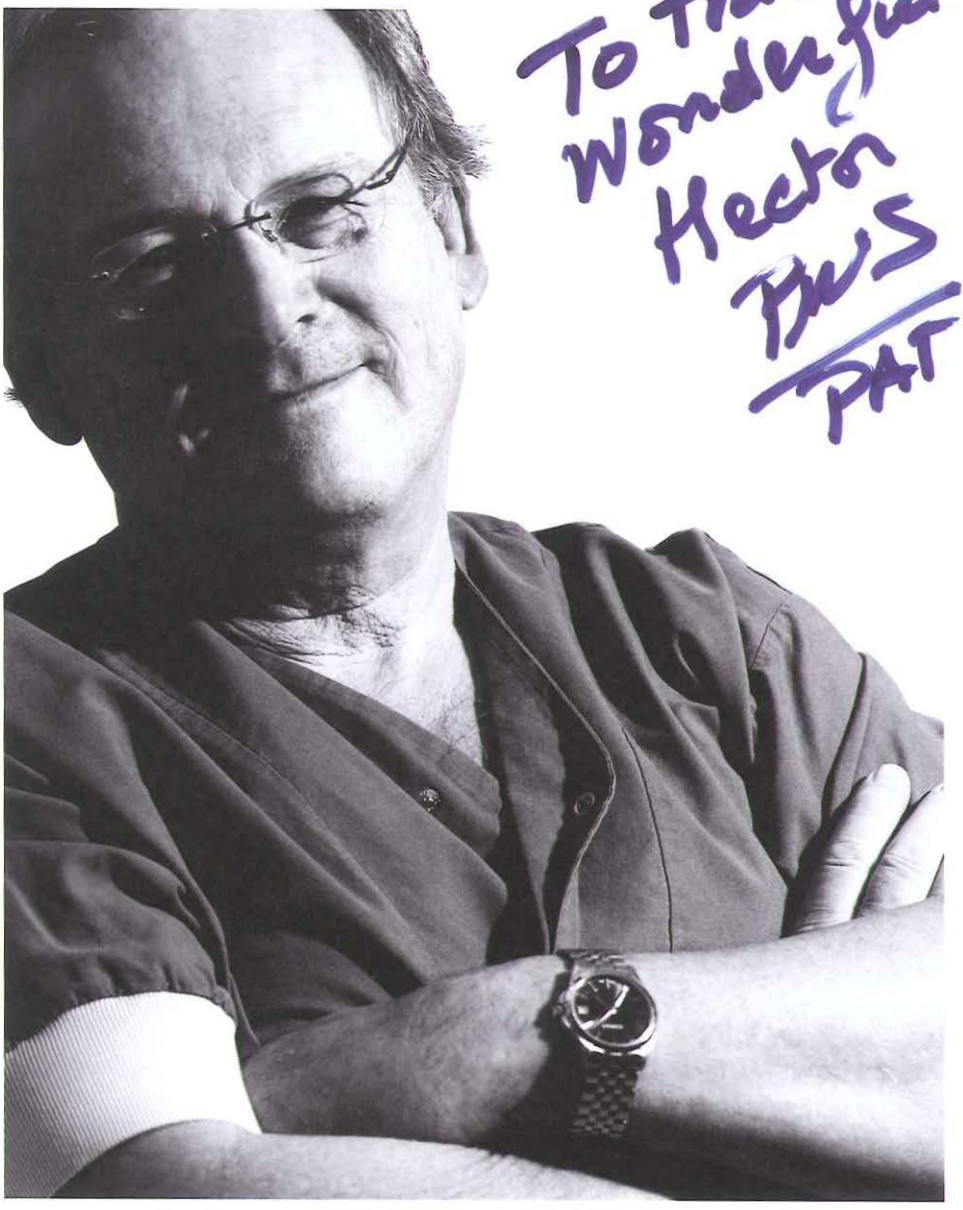
To this
wonderful
Hector
PAT

CHAPTER 1.1

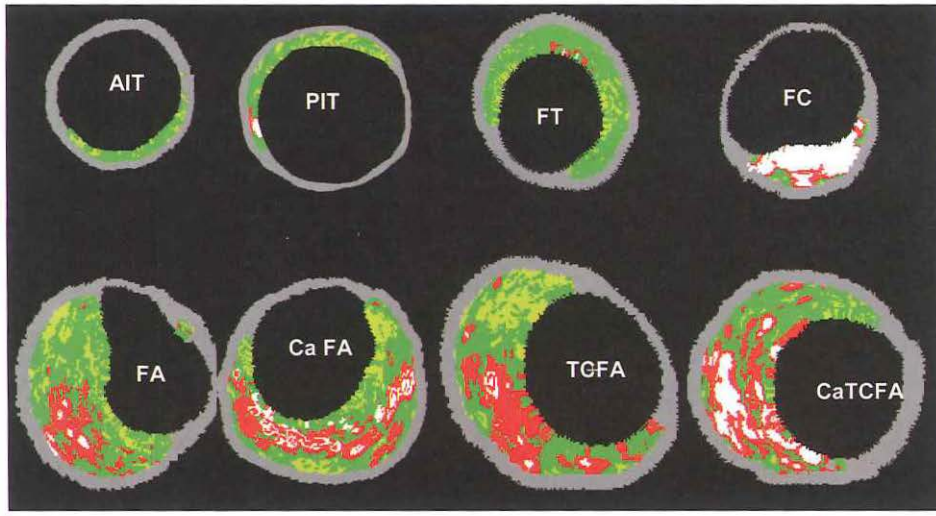

Figure 1. IVUS-Virtual histology proposed lesion types. AIT, adaptative intimal thickening; PIT, pathological intimal thickening; FT, fibrotic plaque; FC, fibrocalcific; FA, fibroatheroma;CaFA, calcified fibroatheroma; TCFA, thin-capped fibroatheroma.

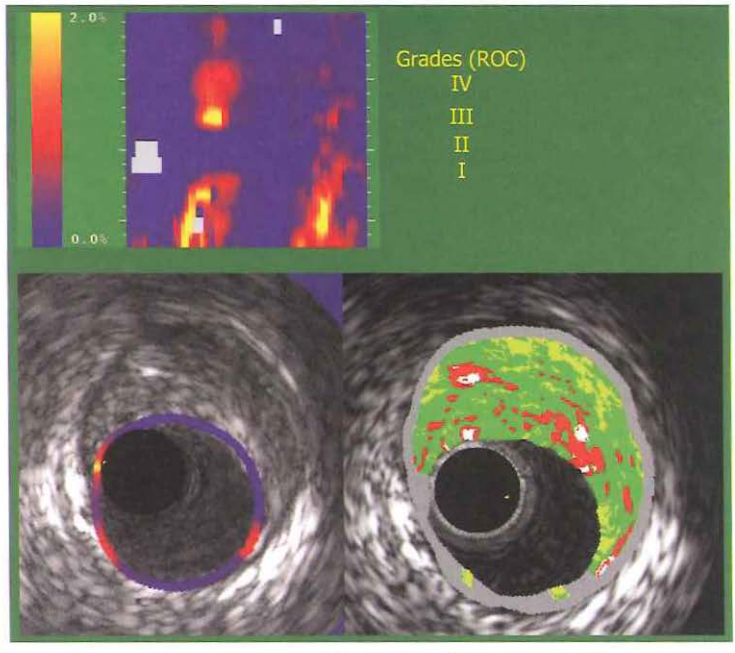

Figure 2. IVUS-palpography. In the upper left side the palpography strain map is opened up. The local strain is calculated from the gated radiofrequency traces using cross-correlation analysis and

displayed, color-coded, from blue (for 0% strain) to red to yellow (for 2% strain). Plaque strain values are assigned a Rotterdam Classification (ROC) score ranging from 1 to 4 (ROC I= 0-<0.6 %; ROC II= 0.6- <0.9 %; ROC III= 0.9-<1.2 %; ROC IV= >1.2 %). At the bottom, in the same cross-sectional area a high-strain spot (ROC III) is shown (left); in the virtual histology (VH) image (right) a confluent necrotic core area in contact with the lumen is seen, suggesting an IVUS-derived thin capped fibroatheroma. The IVUS-VH color-code is fibrous tissue (green), fibro-fatty tissue (light green), necrotic core (red) and dense calcium (white).

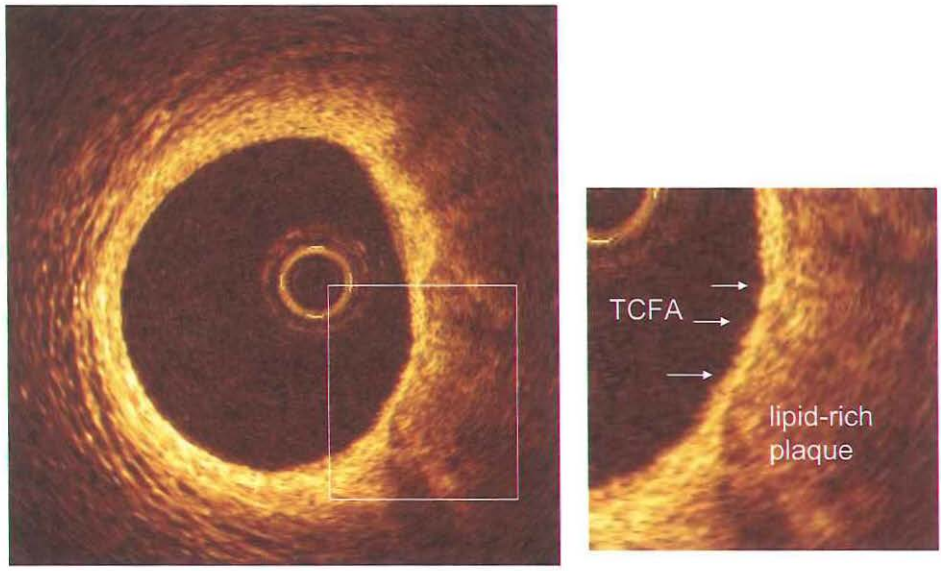

Figure 3. The optical coherence tomography image shows thin cap fibrous atheroma (TCFA). The cross-section demonstrates a region of low reflectivity with diffuse borders between the 3 and 5 o'clock position consistent with a lipid-rich plaque. This is covered by a thin, highly reflective fibrous cap (TCFA) which measured between 10-30 microns in thickness

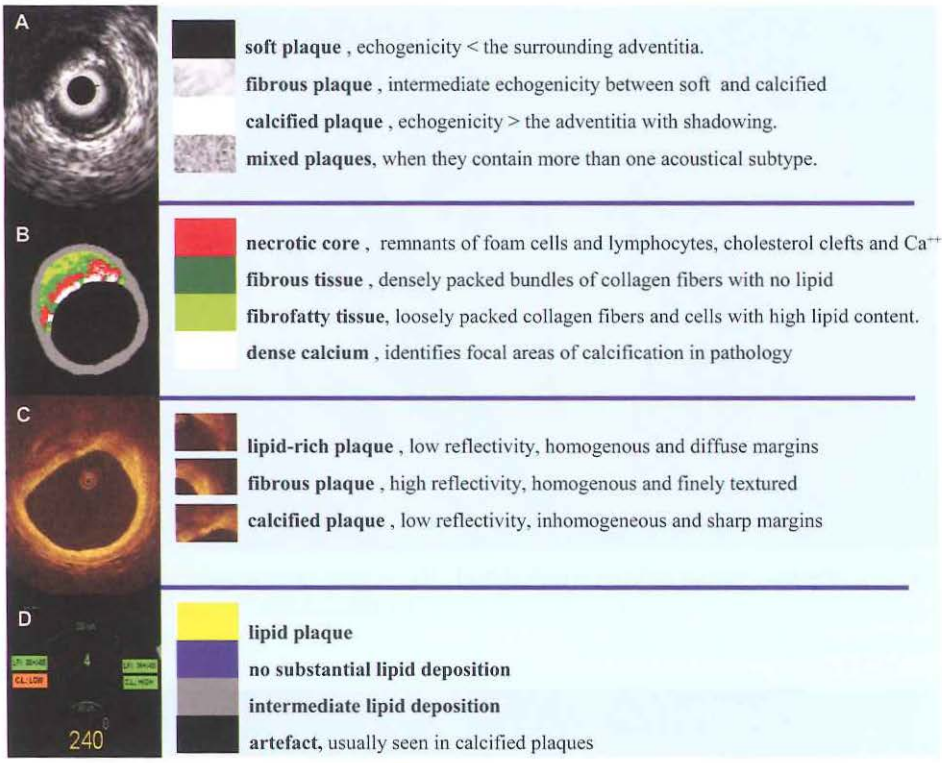

Figure 4. Multi-imaging in the coronary arteries. The same coronary segment (represented by one frame) has been imaged by 4 different imaging techniques. In the greyscale IVUS (panel A), IVUS-virtual histology (panel B), optical coherence tomography (panel C) and intravascular magnetic resonance spectroscopy (IVMR) the results of the same frame across different techniques are shown. Of note, in the upper left quadrant of the plaque a calcified area is seen in three imaging modalities, but in IVMR where an artifact is observed. On the right hand side, the different plaque and tissues types across the coronary imaging techniques is shown.

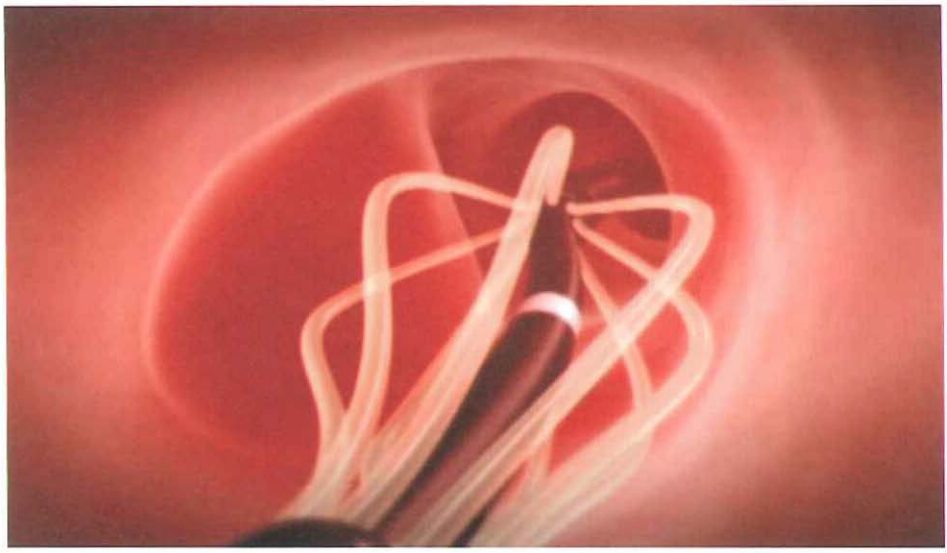

Figure 5. vPredict™ optical catheter system (OCS). This catheter has 8 optical fibers that deliver infrared light to the vessel wall and captures a portion of the reflected light for spectral analysis. Image courtesy of Prescient Medical, Inc

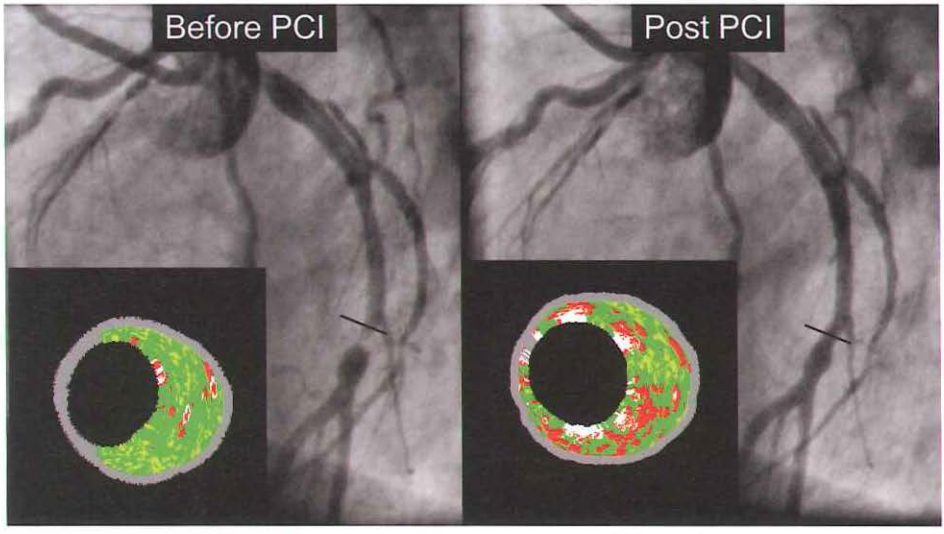

Figure 6. IVUS-virtual histology in stented segments. In the left hand side, a coronary angiogram of the left coronary system shows on the distal segment of the left circumflex artery an eccentric lesion. A pre-stenting virtual histology (VH) frame showed a fibrotic type of plaque (location of VH frame is indicated by a black line). On the right hand side, the post-stenting VH frame is depicted. Of note, at the lumen and surrounding areas an increase in the amount of "dense calcium" and "necrotic core" is observed. This is due to the presence of stent struts that are misclassified by VH. PCI, percutaneous coronary intervention.

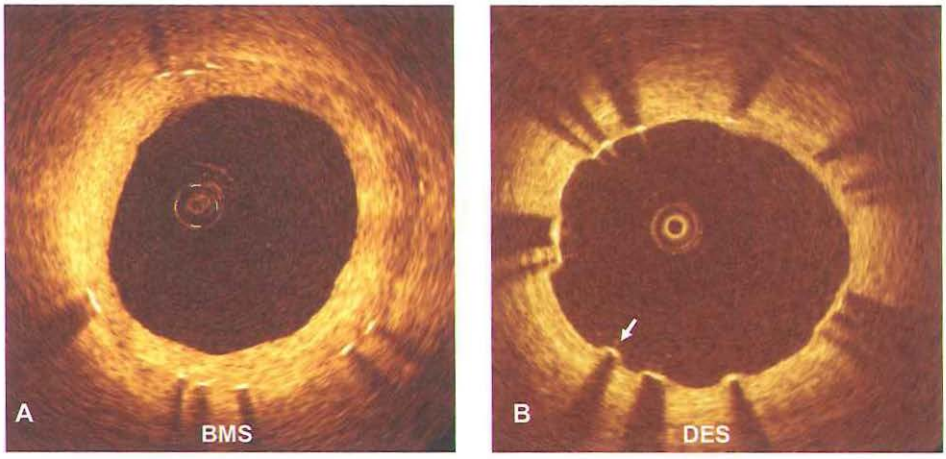

Figure 7. OCT and stent. Panel A: Demonstrates the optical coherence tomography (OCT) imaging of a bare metal stent 4 months following implantation. The circumferential tissue struts are visible with shadowing induced by the metal. The neointimal tissue measured between 140 and 220 microns in thickness. Panel B: OCT imaging of a drug-eluting stent (DES) at 4 months follow-up showing the circumferential struts with a very thin neointimal layer (10-40 microns thick). The arrow indicates a strut with no visible tissue coverage

CHAPTER 1.2

Catheter 1

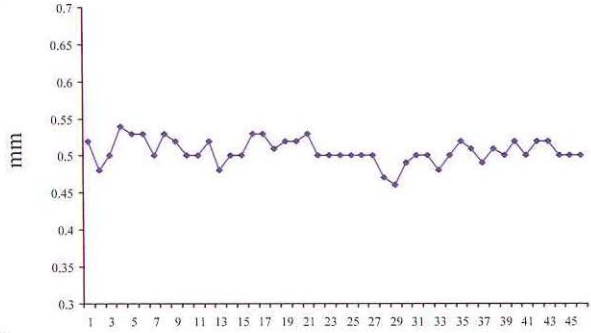

Mean distance = 0.51±0.02

Catheter 2

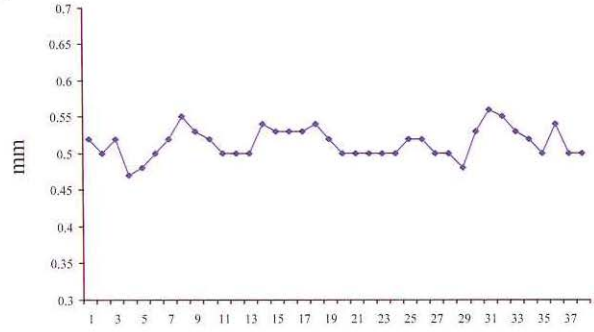

Mean distance = 0.52±0.02

Figure 1. This patient was imaged in the same region with two different catheters during the same procedure. The graphs show all the frames acquired (x axis) and in the y axis the distance between them is given. Small variations in the intervals were observed.

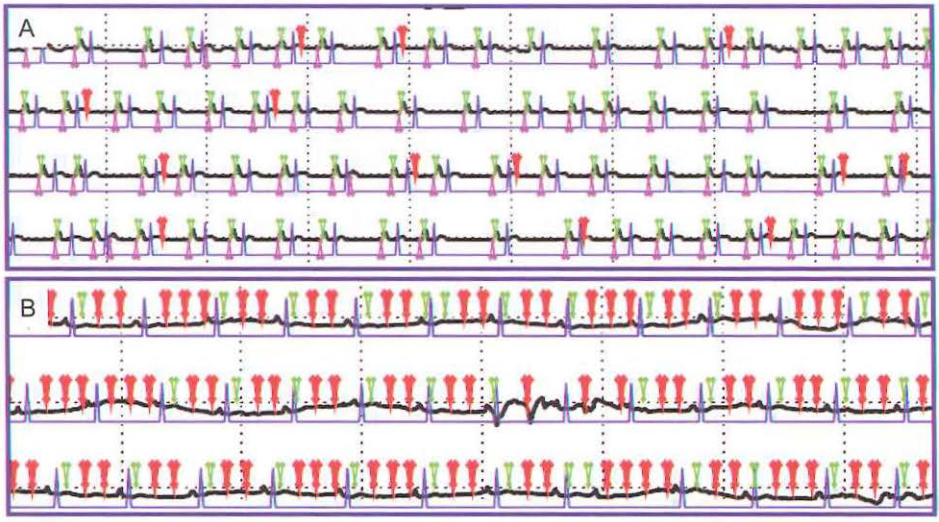

Figure 2. This figure shows the heart beats recorded during VH-IVUS acquisition (in this case palpography was also recorded simultaneously). In black, the ECG signal; in purple the "R" top marker; in green and red the acquired VH-IVUS frames. The blue line indicates the segmentation per heart beats based on the blood pressure signal (blood pressure curve not shown). In panel A, a quasi-normal ECG-gating acquisition is seen, the VH-IVUS frames (green markers) were constantly acquired throughout the pullback. Only few extra VH-IVUS non-"R"-top related were acquired (red markers). In panel B, due to a bad ECG signal the ECG gating was poor. This graph has been created by Frits Mastik at Erasmus Medical Center.

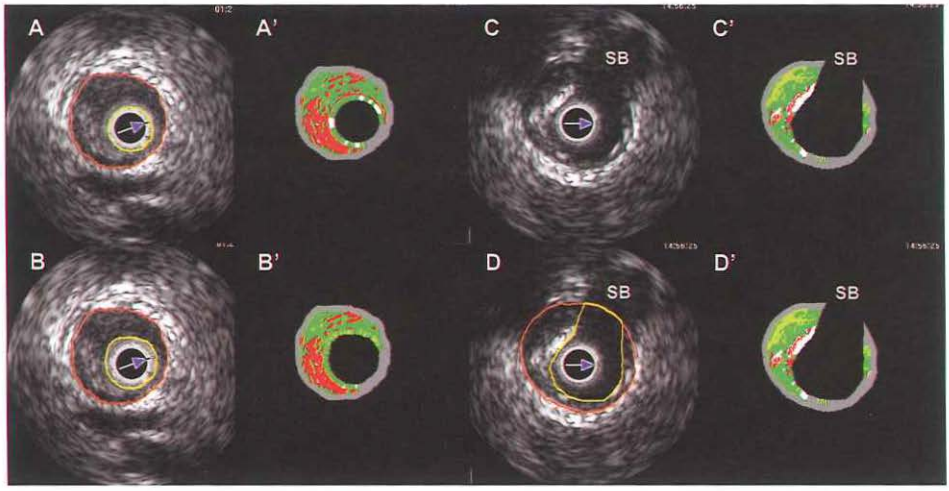

Figure 3. Panels A and A' show that the lumen border was drawn halfway into the flare (ring down artefact) of the catheter (yellow circle), in the VH frame this was misclassified as dense calcium. Panels B and B' show the recommended approach to draw the lumen border, away from the flare of the catheter. Panels C and D show the proposed method to draw the contours at side-branches. Luminal contour (yellow line) should be drawn just beyond the vessel contour, so that in the VH-IVUS this appears as an empty space. SB, side-branch.

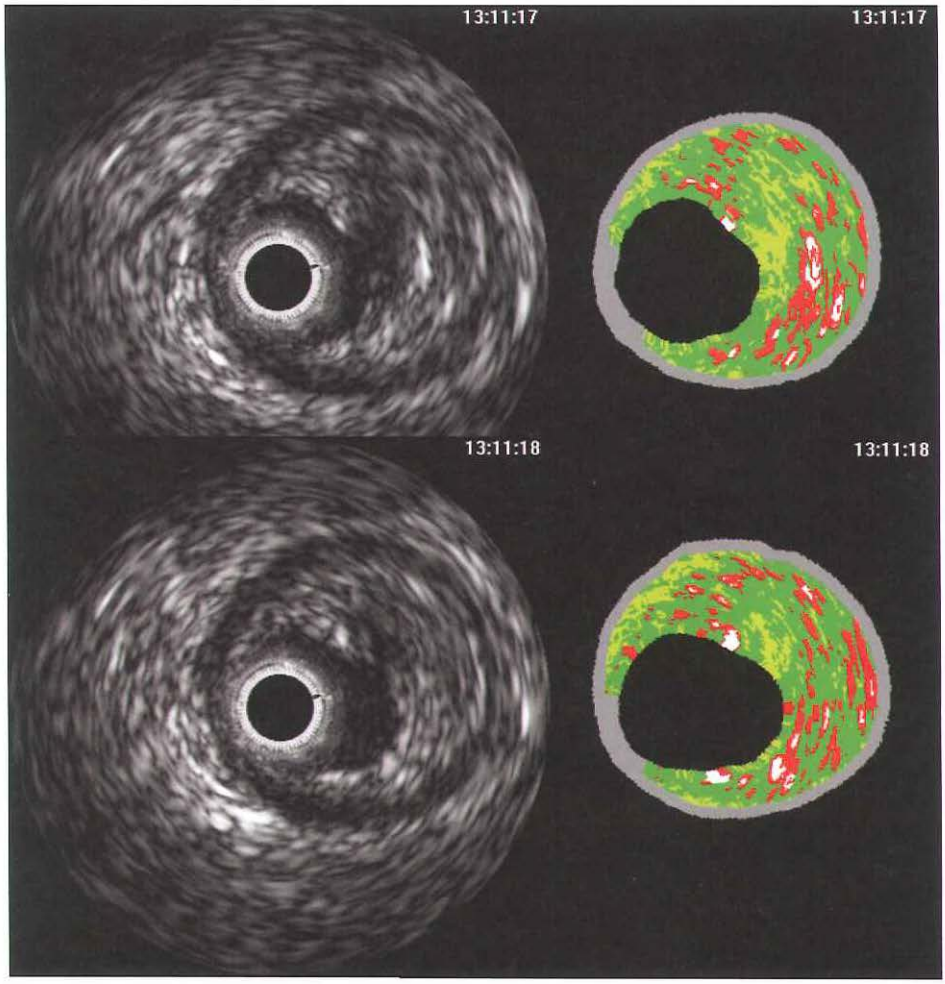

Figure 4. Two consecutive frames showing a ruptured plaque in a patient with an acute coronary syndrome. The luminal contour (not shown to allow visualisation of the discontinuity area of plaque surface) should be drawn including the cavity (white arrow) in the analysis.

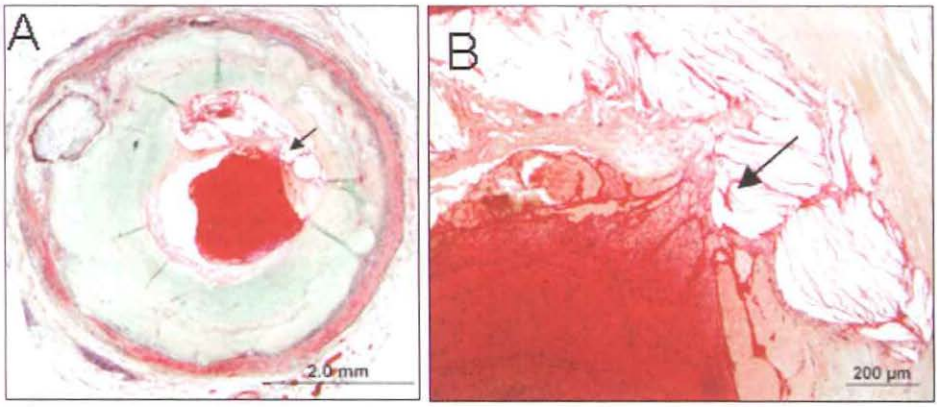

Figure 5. Coronary plaque rupture with overlying luminal thrombus. A shows the area of the thrombus and rupture site (arrow) and B shows the site of rupture (arrow) with the overlying thrombus at higher magnification.

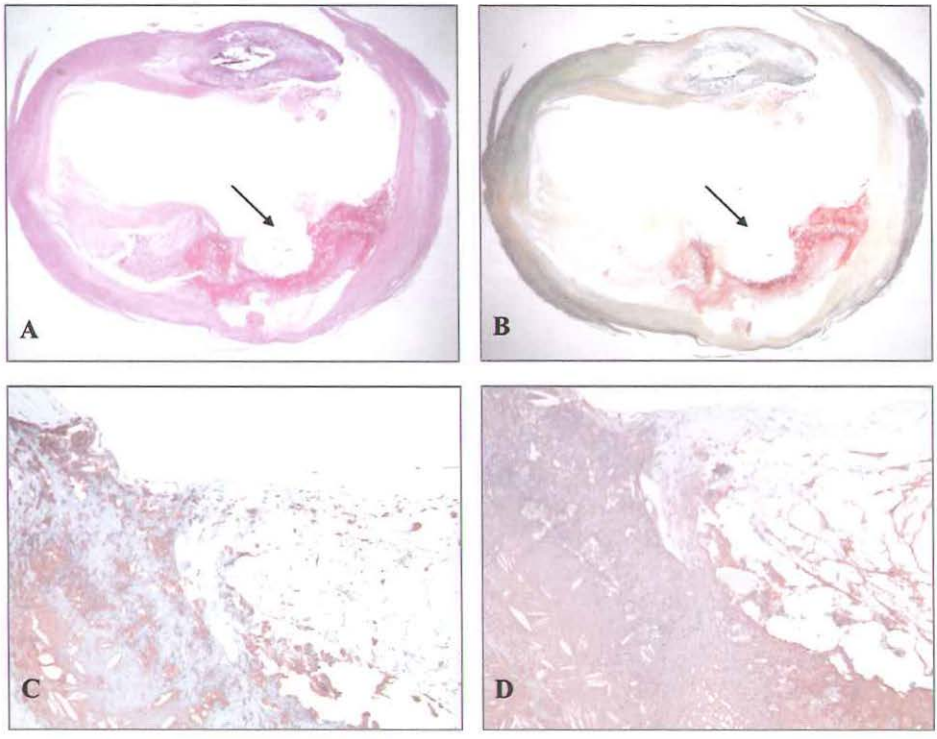

Figure 6. Ulcerated plaque, carotid artery. A. Haematoxylin eosin stain. B. Movat pentachrome stain showing the ulcerated plaque (arrow) and the various plaque components. C. Macrophage staining (CD68) showing macrophages (brown) close to the area of the ulceration and the underlying core. D. There is abundant fibrin within the ulcerated necrotic core.

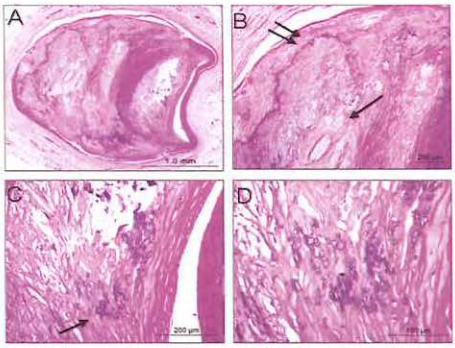

Figure 7. Stable plaque, coronary artery. A shows focal calcification (dark purple areas). B shows an area of sheet calcification (double arrow) of a collagen rich plaque where as the single arrow points to an area of necrotic core calcification. C illustrates as area of speckled calcification along a necrotic core. D is the area from C underneath the arrow at higher magnification showing single cell calcification.

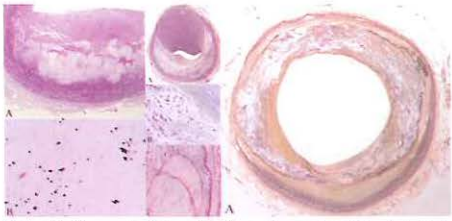

Figure 8. Coronary arteries showing patterns of calcification. Left: A. Pathologic intimal thickening. B. Calcium stain demonstrating microscopic calcifications (von Kossa). Middle: A. Fibrocalcific plaque, non-occlusive. B. Speckled calcification within an early necrotic core (Movat stain). C. Shows fibrous plaque calcification. Right: A. "Pipestem" calcification circumferentially around the vessel, with apparent stabilisation of the plaque.

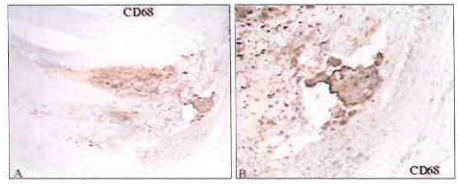

Figure 9. Unstable calcification. A. Macrophage marker (CD 68) demonstrating macrophage infiltration of an early necrotic core. B. Higher magnification of spicule of calcification (arrow) within an area of necrotic core.

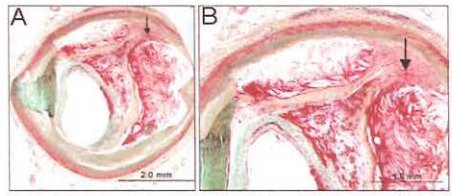

Figure 10. Coronary plaque showing healing plaque rupture. A and B at higher magnification show the site of previous plaque rupture where the fibrous cap is disturbed (arrow) and overlying healing thrombus. The rupture is almost fully healed towards the lumen.

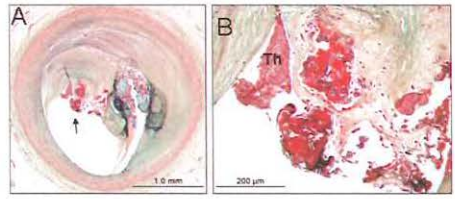

Figure 11. Nodular calcification in a coronary plaque. Note the calcification (A) some of which is nodular in nature in the area close to lumen. B is area underneath arrow in A at higher power showing nodular calcification with fibrin (dull red) in between nodules (bright red).

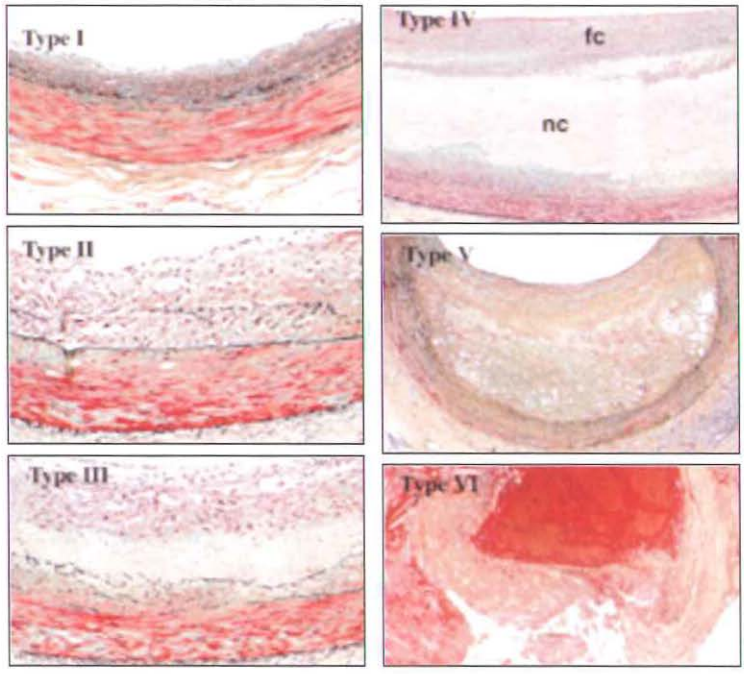

Figure 12. AHA plaque classification. (Stary HC. The histological classification of atherosclerotic lesions in human coronary arteries. In: Fuster V, Ross R, Topol E, eds. Atherosclerosis and Coronary Artery Disease.). fc: fibrous cap; nc: necrotic core

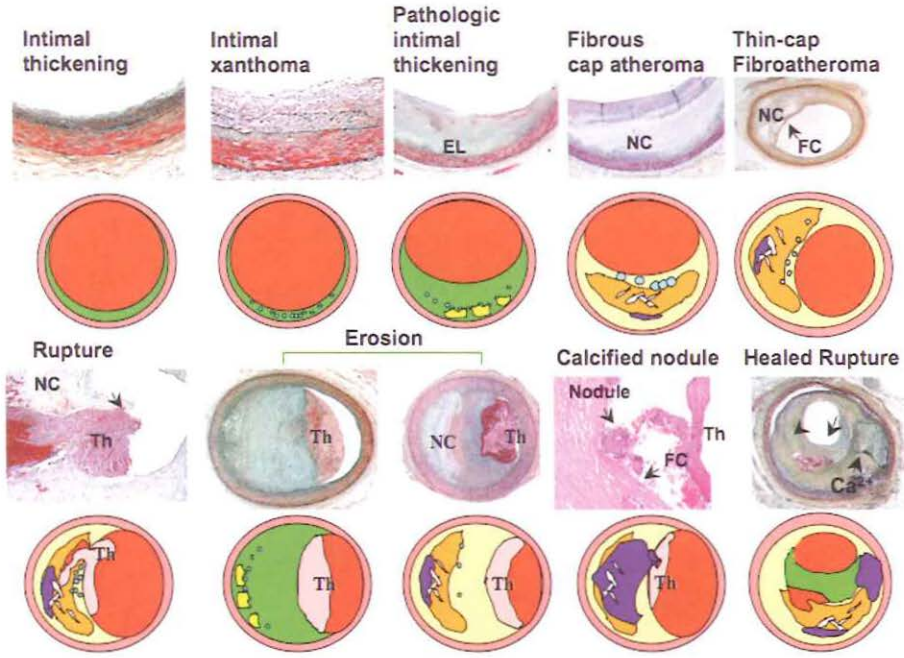

Figure 13. Modified AHA classification, Virmani et al, ATVB 2000; 20:1262-75. EL: extracellular lipid; nc: necrotic core; fc: fibrous cap; th: thrombus

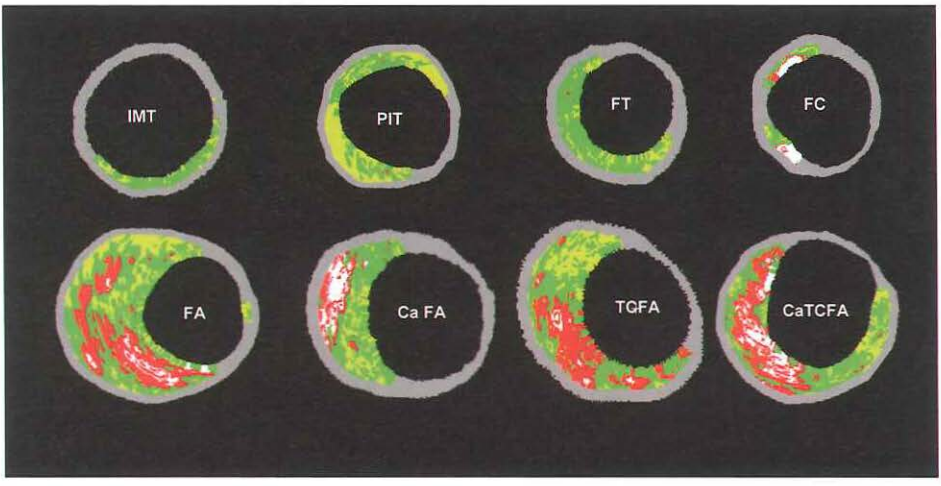

Figure 14. Examples of VH-IVUS images classified by a two-dimensional lesion analysis. (IMT) intimal medial thickening; (PIT) pathological intimal thickening; (FT) fibrotic plaque; (FC) fibrocalcific plaque; (FA) fibroatheroma and (caFA) calcified fibroatheroma; (VH-TCFA) Virtual Histology-thin cap fibroatheroma and (VH-caTCFA) Virtual Histology-calcified thin cap fibroatheroma.

CHAPTER 2.1

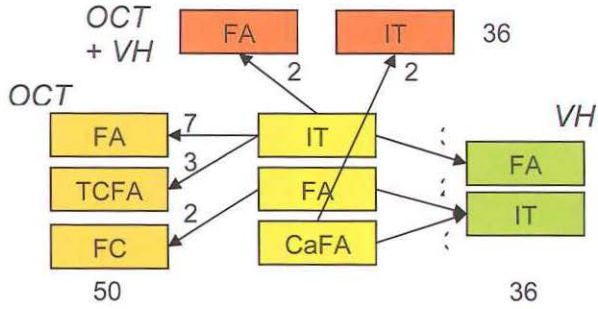

Figure 1. Chart of misclassifications. Only misclassifications occurring ≥2 are included in the figure. Misclassifications are derived from 36 cross-sections in VH-IVUS and OCT and VH-IVUS combined, misclassifications in OCT are derived from 50 cross-sections. Yellow = histology, green = VH-IVUS, orange = OCT, OCT/VH-IVUS = red. IT = intimal thickening, FC = fibrocalcific, FA = fibro-atheroma, CaFA = calcified fibroatheroma, TCFA = thin-cap fibro-atheroma. For example: of the lesions that were identified as IT in histology, 7 were classified as FA in OCT, 3 as FA in VH-IVUS, and 2 as FA in OCT and VH-IVUS combined.

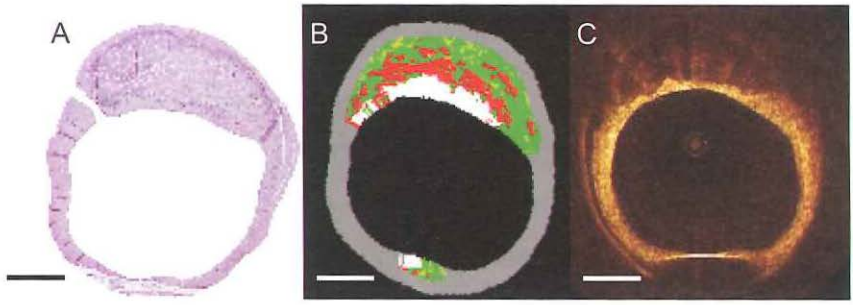

Figure 2. (A) Histology of a calcified fibroatheroma (hematoxylin-eosin stain). (B) Corresponding VH-IVUS classified as calcified fibroatheroma. (C) Corresponding OCT classified as calcified fibroatheroma. The needle used to mark the site can be seen in the bright feature at 6 o'clock in OCT, as well as in the appearance of dense calcium in that location in VH-IVUS.

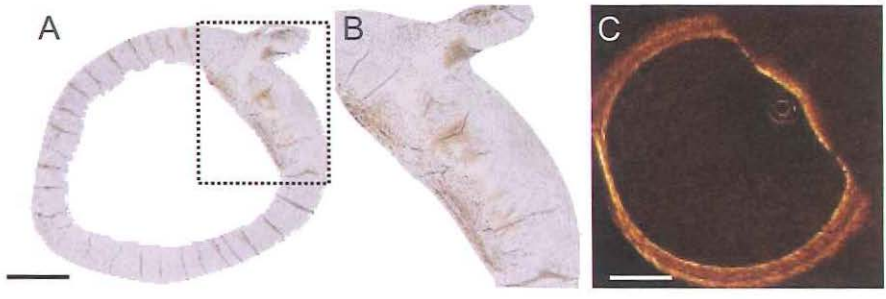

Figure 3 (A) CD68 stained cross-section. The intima consisting of a collagen/glycoprotein matrix is densely infiltrated by macrophages. (B) Magnification of selected region in A. (C) Corresponding OCT image. The region infiltrated by macrophages appears as a thin-cap fibro-atheroma. The bar indicates 1 mm.

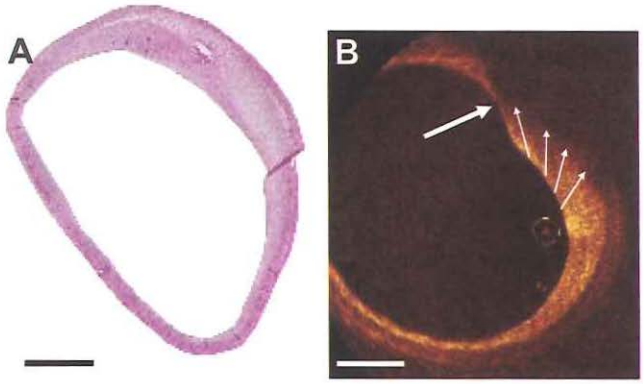

Figure 4. (A) H&E stained cross-section. (B) Intimal thickening is misinterpreted as thin-cap fibro-atheroma (TCFA) in optical coherence tomtography (OCT). The large arrow points at the spot interpreted as a thin-cap. The four small arrows indicate the OCT beams and are all of the same length. The loss of signal due to tissue penetration is similar for each arrow. Because of eccentric catheter position this cross-section, classified as intimal thickening in histology, appears as a thin-cap fibro-atheroma (TCFA) in OCT. The bar indicates 1 mm.

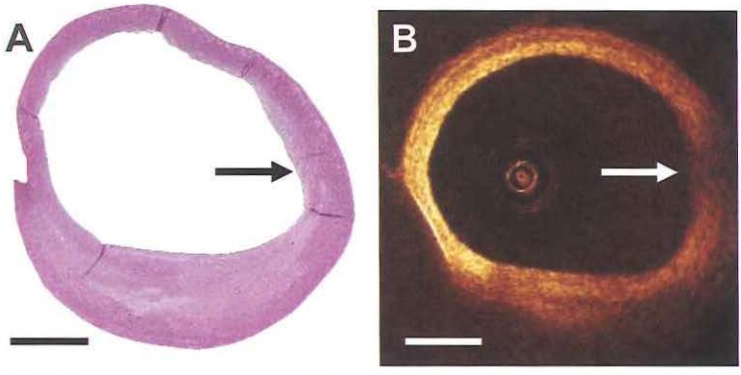

Figure 5. (A) H&E stained cross-section with (B) the corresponding optical coherence tomography (OCT). The arrow indicates a collagenous region in histology mistaken for a lipid region in OCT. Reduced optical efficiency of the catheter in this image section creates a dark sector, making mild intimal thickening appear as a fibro-atheroma. The bar indicates 1 mm.

CHAPTER 2.2

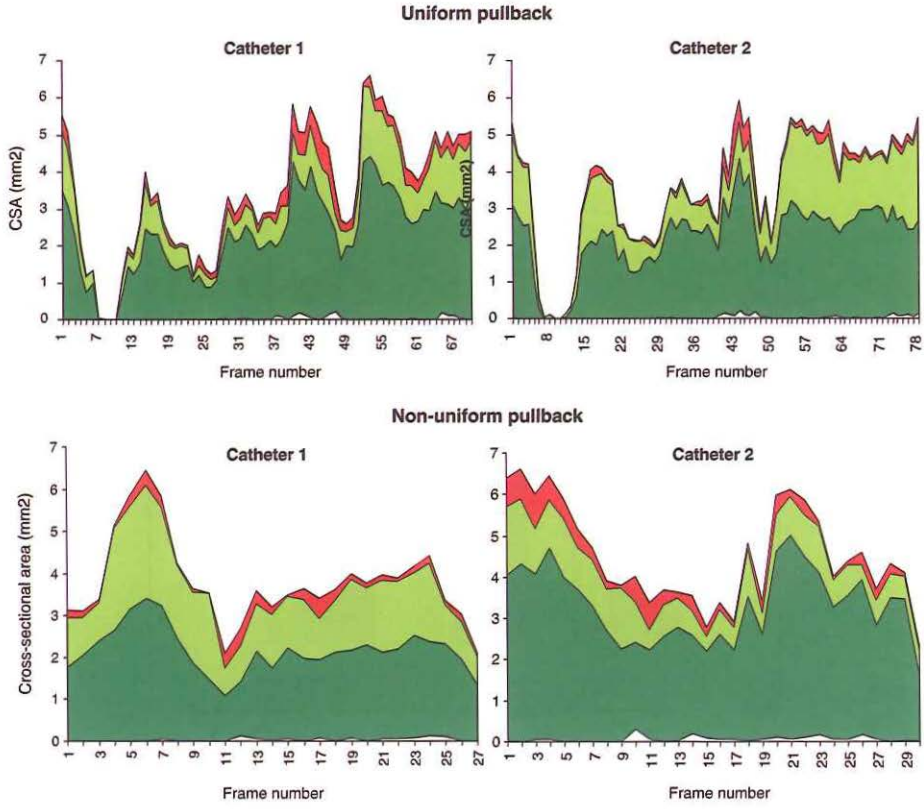

Figure 5. Sequential plotting of a matched ROI interrogated with two catheters. The mean CSA (*y* axis) of each plaque component is colour-coded (calcium: white, fibrous: green, fibrolipidic: greenish-yellow and necrotic core: red). This figure shows an example of the impact of non-uniform pullbacks on geometrical and compositional measurements.

CHAPTER 3.1

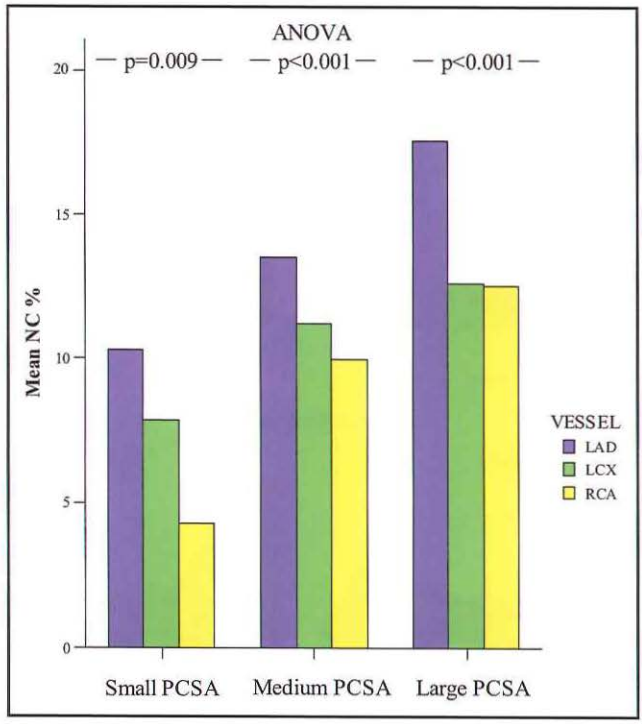

Figure 1. Bar graph shows plaque CSA (PCSA) categorized into 3 groups according to plaque size (x axis) and relative amount of the NC (y axis) in the left anterior descending coronary artery *(blue bars)*, left circumflex coronary artery *(green bars)*, and right coronary artery *(yellow bars)*. ANOVA = analysis of variance.

CHAPTER 3.3

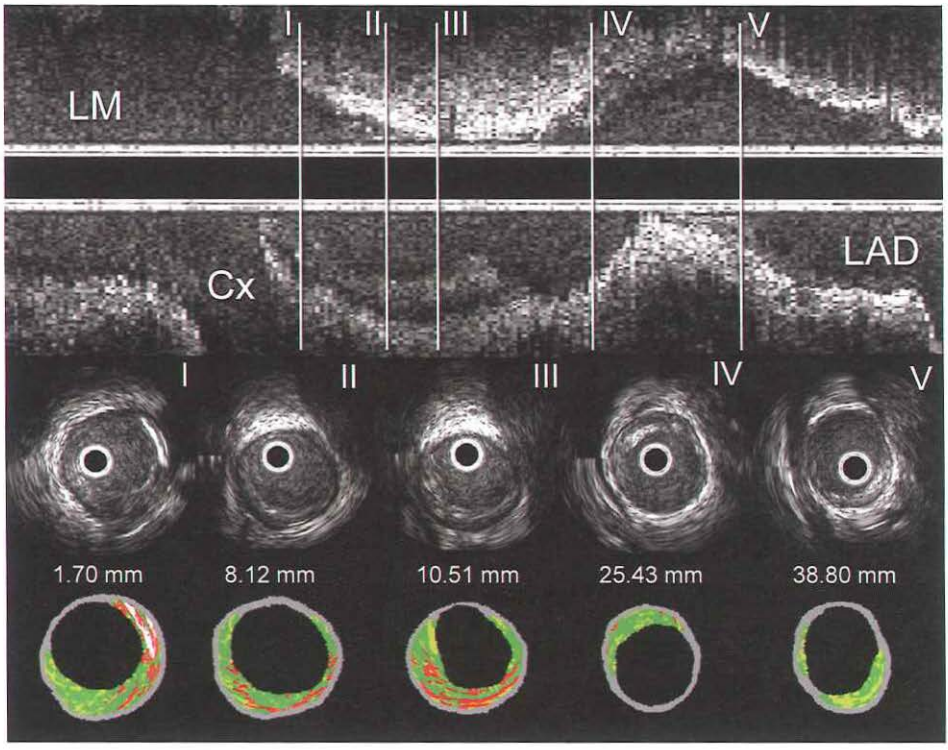

Figure 3 IVUS-VH CSA along a coronary vessel. IVUS-VH cross-sectional areas in a representative patient showing the change in plaque composition (calcium: white; fibrous: green; fibrolipidic: greenish-yellow; and lipid core: red) along the longitudinal axis of the vessel. LM, left main coronary artery; CFX, circumflex artery; LAD, left anterior descending artery. The distance between the cross-sectional area and the ostium of the vessel is reported in millimetres (mm).

CHAPTER 3.4

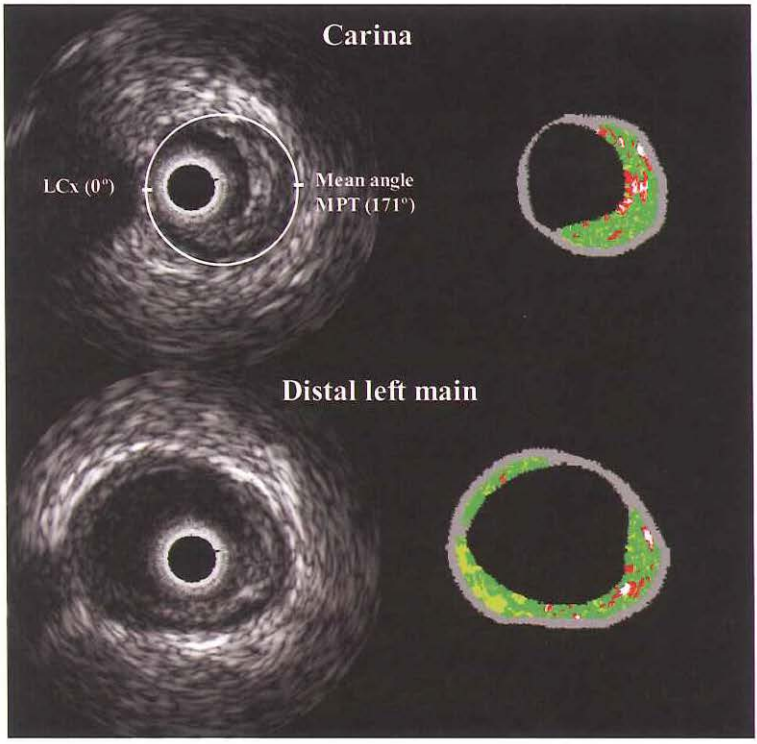

Figure 1. Intravascular ultrasound cross-section images from the carina of the left anterior descending coronary artery and of the left main coronary artery. The **left side** shows the reconstructed grayscale, and the **right side** shows the color-coded data (**green** = fibrous; **yellow-green** = fibrolipidic; **red** = necrotic core; **white** = calcium) provided by the IVUS-VH unit (Volcano Therapeutics, Rancho Cordova, California). LCx = left circumflex artery; MPT = maximal plaque thickness.

CHAPTER 3.5

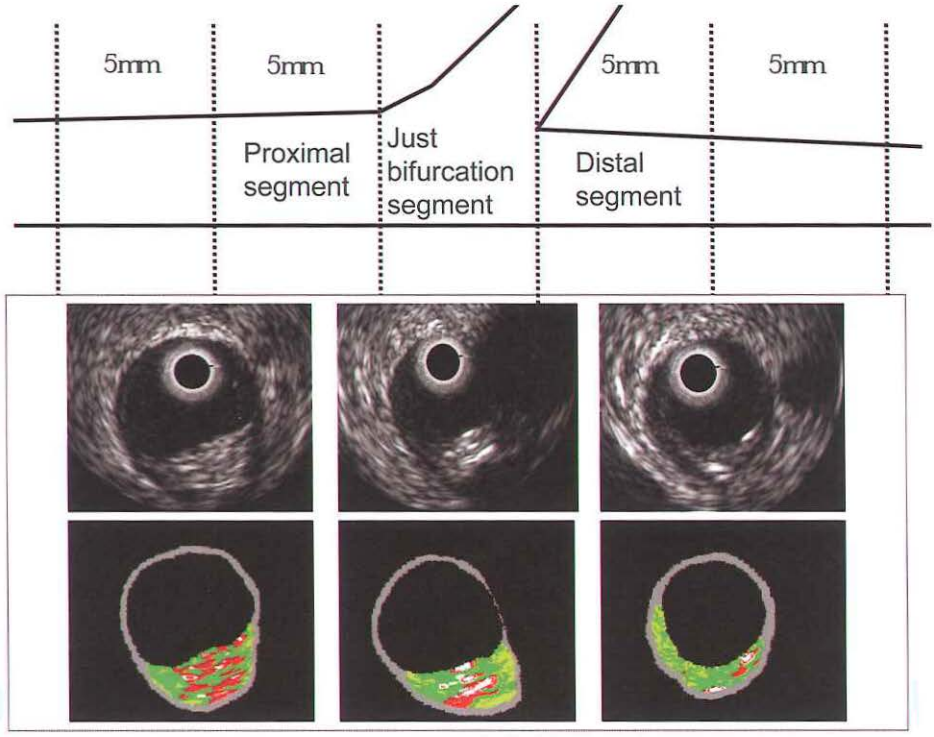

Fig. 1. The schematic definition of proximal, just bifurcation and distal segments of bifurcations (upper panel). Gray IVUS (middle panel) and VH-IVUS (lower panel) of each frame were analyzed. The proximal segment and distal segment of the bifurcation sites were analyzed in the 5 mm proximal and distal to bifurcation sites. The just bifurcation segment were analyzed in each segment length. The proximal and distal reference sites were analyzed in the frame which showed the least P+M % within 10 mm of the bifurcation site.

CHAPTER 4.1

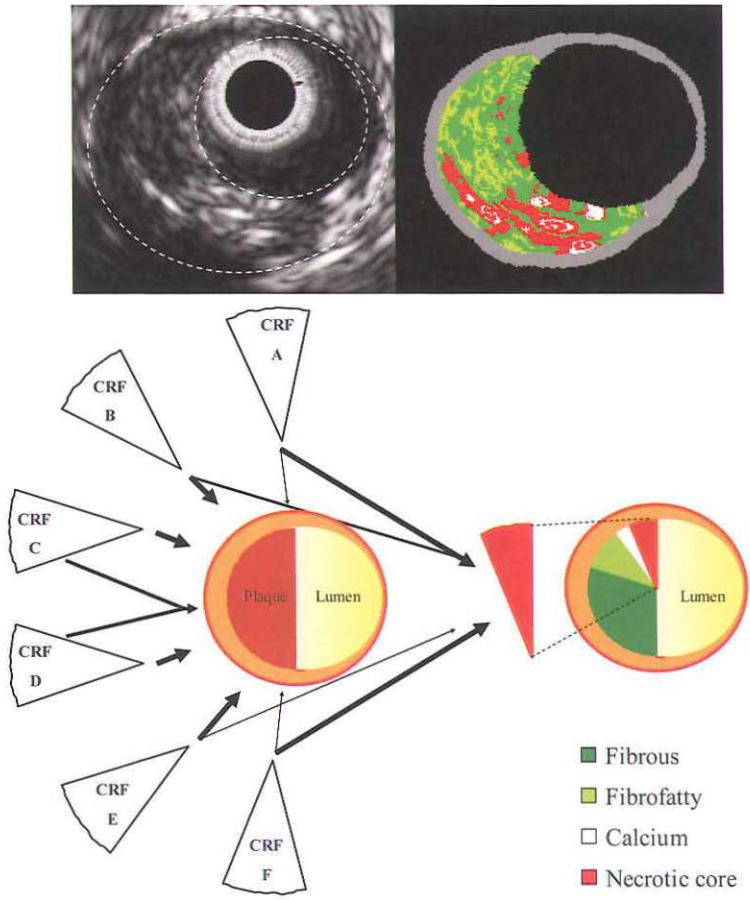

Figure 1. Top: Cross-sectional areas of the same coronary atherosclerotic plaque, on the left hand side a greyscale image and on the right hand side the corresponding IVUS radiofrequency data image. **Bottom:** Cardiovascular risk factors (CRF) act alone or in combination (biological interaction) to assert their effect on overall plaque composition. Note that the impact of these CRFs varies (thickness of the arrow). Their effect could exclusively be on overall plaque composition or simultaneously affect necrotic core, once again, individually or collectively.

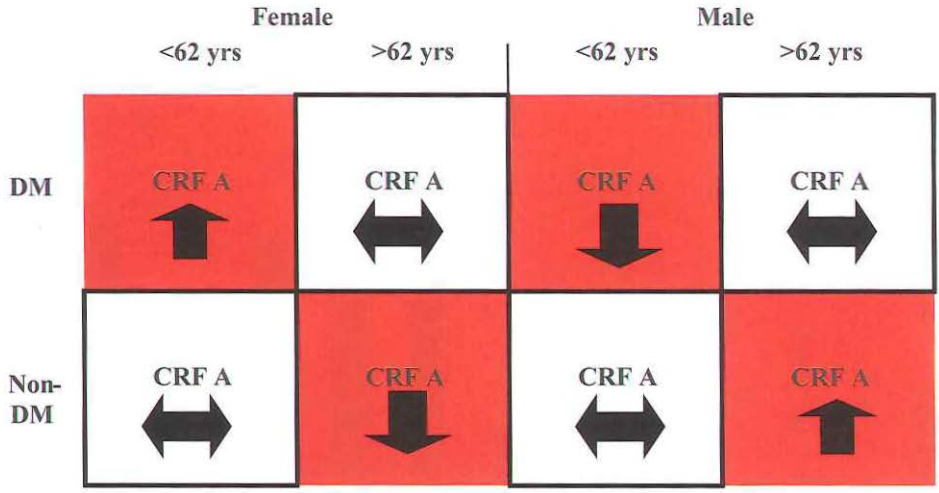

Figure 2. The population has been divided by age, gender and diabetes, resulting in eight categories. The same cardiovascular risk factor (CRF) "A" is assessed in each of them in terms of change in necrotic core. This CRF "A" can have not effect (horizontal arrow), increase (upward arrow) or decrease (downward arrow) the amount of necrotic core. When a population based analysis is conducted, either by age, gender or clinical presentation no effect can be found, although there is a significant change in some of the categories.

CHAPTER 4.2

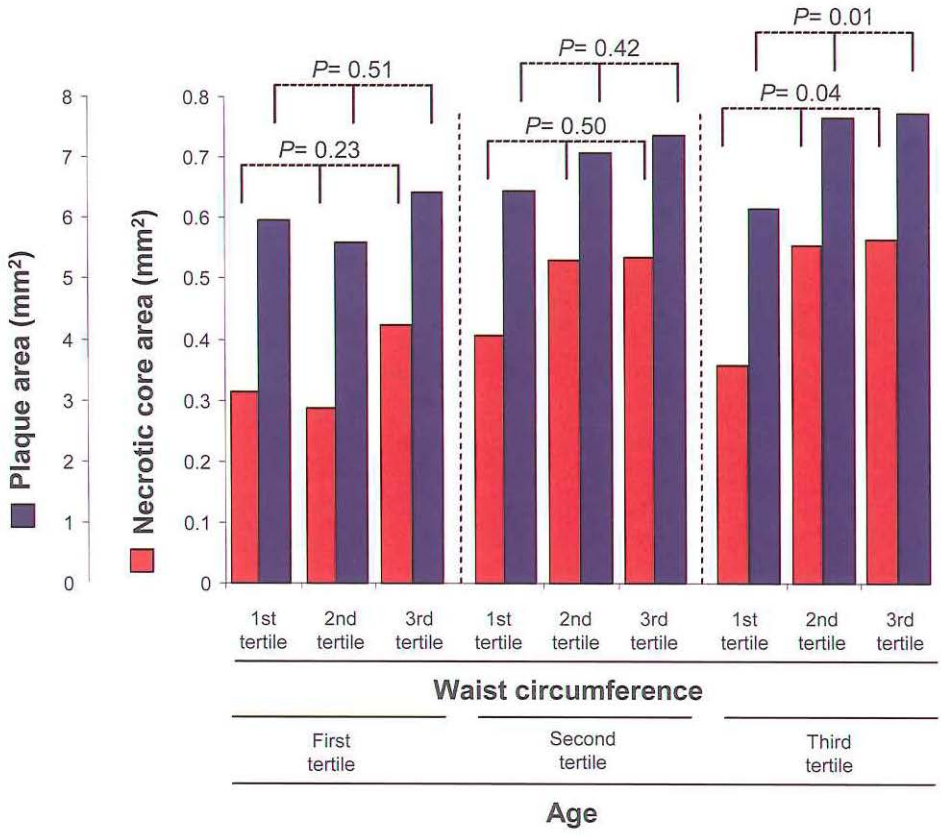

Figure 1. Stratification of mean plaque area and necrotic core area according to both age and waist circumference tertiles.

CHAPTER 5.1

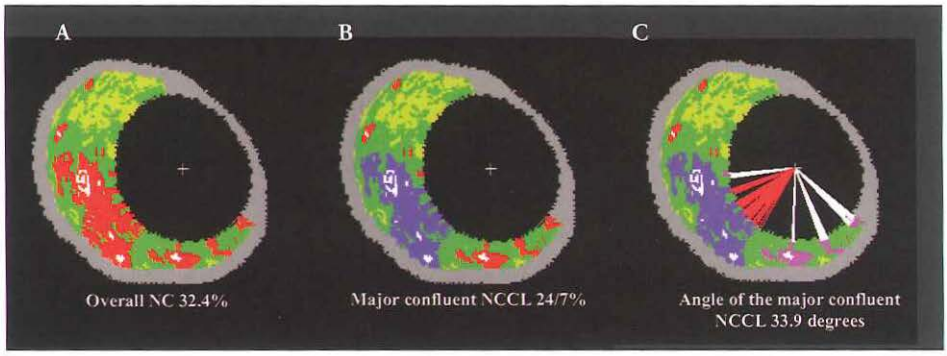

Figure 1. An example of selective quantification of the necrotic core in contact with the lumen. (a) The original IVUS-VH cross-sectional area; (b) Modification using the VH tool to selectively quantify the major confluent necrotic core that is in direct contact with the lumen. (c) Measurement of the angle occupied by the entire necrotic core in contact with the lumen (white and red lines) and specifically the angle occupied by the major confluent necrotic core in contact with the lumen (red lines).

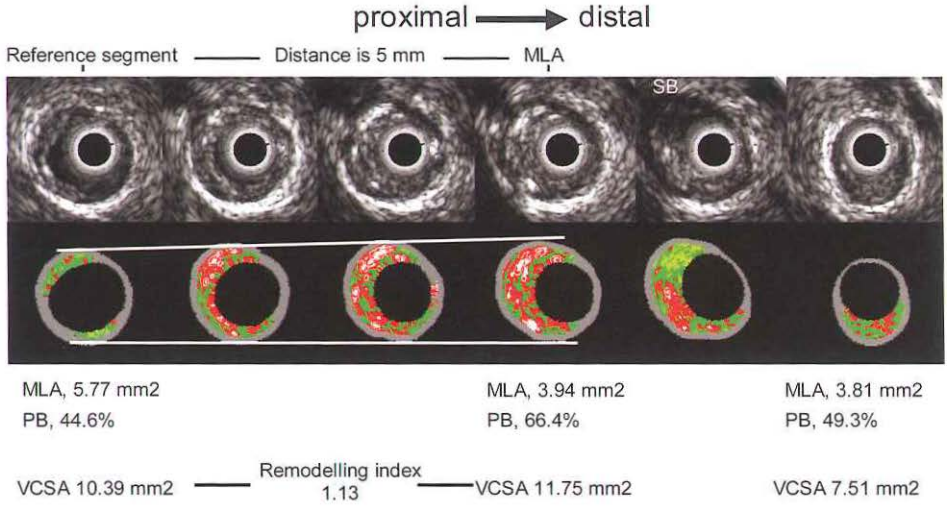

Figure 2. The figure shows the IVUS grey scale and the corresponding IVUS-VH frames of an IVUS derived thin cap fibro-atheroma (four central frames) and the proximal and distal reference segment in which the remodelling index was calculated. MLA, minimum luminal area; PB, plaque burden; VCSA, vessel cross sectional area.

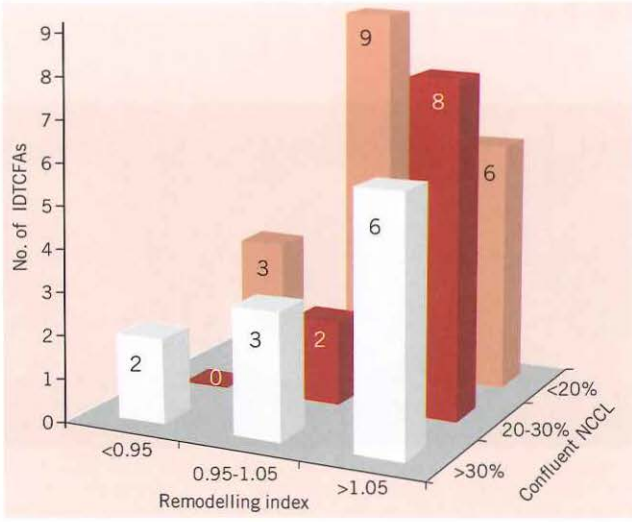

Figure 3. Bar graph shows the number of IVUS-derived thin cap fibroatheroma according to the largest confluent necrotic core in contact with the lumen (NCCL) and the remodelling index. It seems that among the IDTCFAs there are different degrees of disease, possibly with different likelihoods of rupture.

CHAPTER 5.2

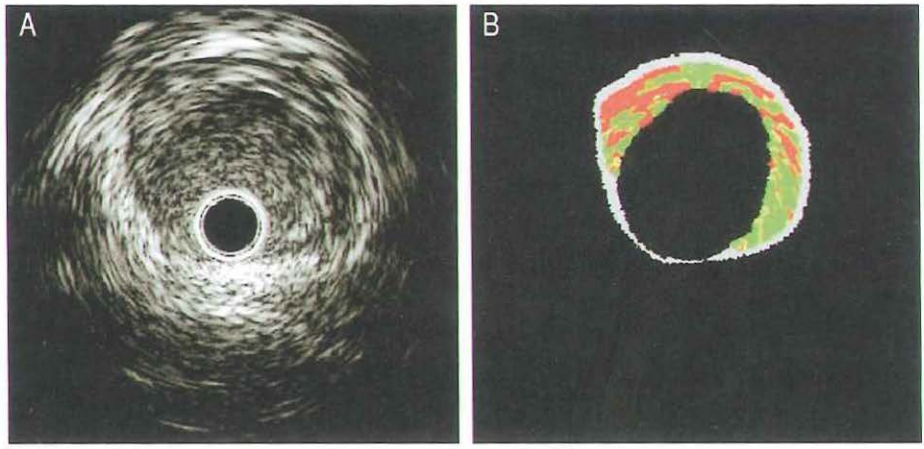

Figure 1. Left anterior descending artery depicted by Intravascular Ultrasound-Virtual Histology, where calcified, fibrous, fibrolipidic, and necrotic core regions are labeled **white, green, greenish-yellow**, and **red**, respectively. **Panel A** shows an intravascular ultrasound cross-sectional area reconstructed from backscattered signals. **Panel B** shows the corresponding tissue map depicting a necrotic core-rich plaque with necrotic core tissue in contact with the lumen.

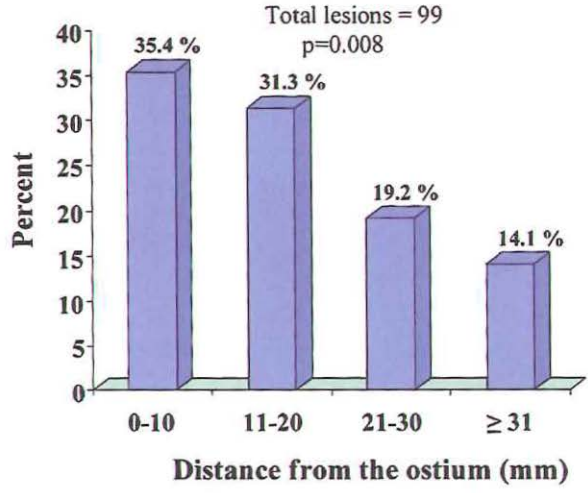

Figure 2. Bar graphs illustrating the frequency of intravascular ultrasound-derived thin-cap fibroatheroma (IDTFCA) starting from the ostium.

CHAPTER 5.3

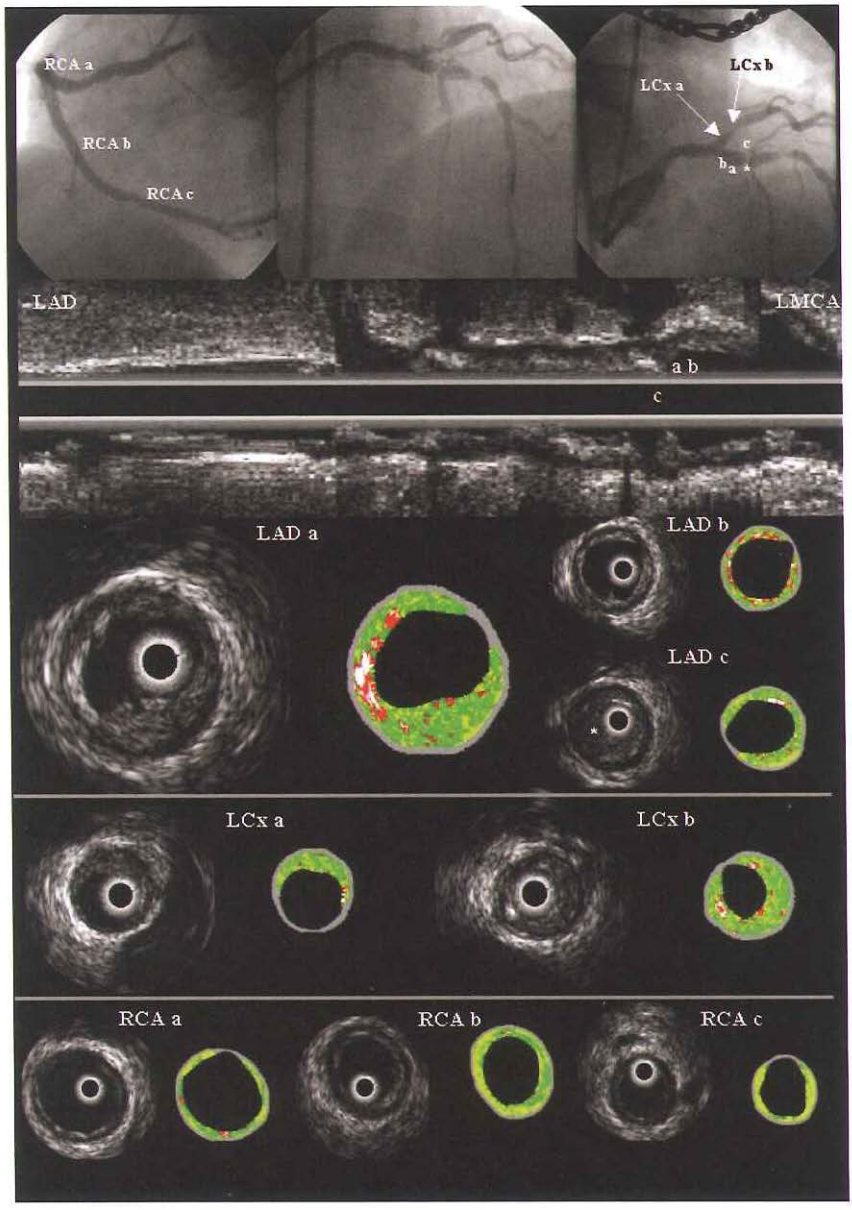

Figure 1 Three-vessel imaging using IVUS-VH (where calcified tissue is labelled as white, fibrous as green, fibrolipidic tissue as greenish-yellow, and necrotic core as red) in a 57-year-old male presenting with unstable angina. PR in the ostial LAD (LAD a). The underlying substrate of the cavity is rich in necrotic-core (red) and calcium (white), whereas the thrombus has migrated distally (LAD c, asterisk).

CHAPTER 5.4

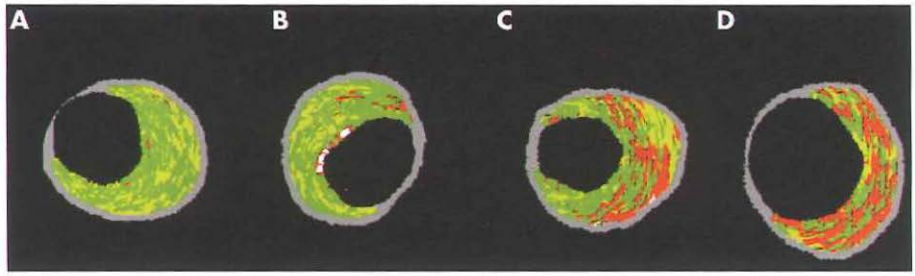

Figure 1 Minimum lumen area (MLA) sites depicting the progression of atherosclerotic disease. The plaque components were assigned colour codes. Calcified, fibrous, fibrolipidic, and lipid core regions were labelled white, green, greenish yellow, and red, respectively. MLA sites feature (A) pathological intimal thickening and (B) fibrocalcific, (C) fibroatheromatous, and (D) thin cap fibroatheromatous lesions.

CHAPTER 6.1

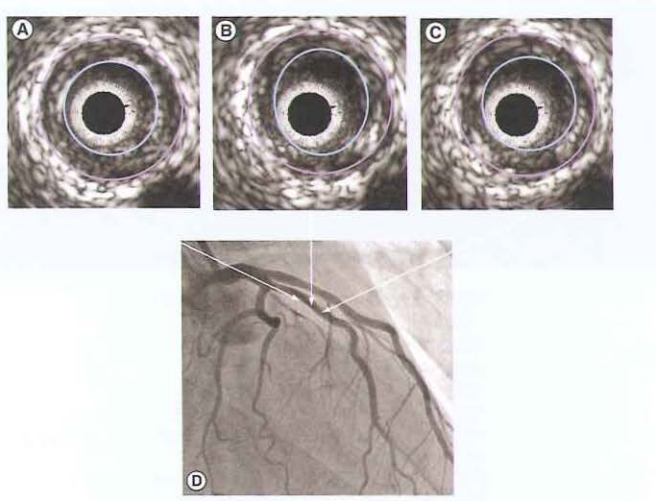

Figure 1. (A, B & C) show three consecutive intravascular ultrasound images of the proximal left anterior descending **(D)**, which is disease-free angiographically. Note that the intravascular ultrasound images show a plaque burden of 50%.

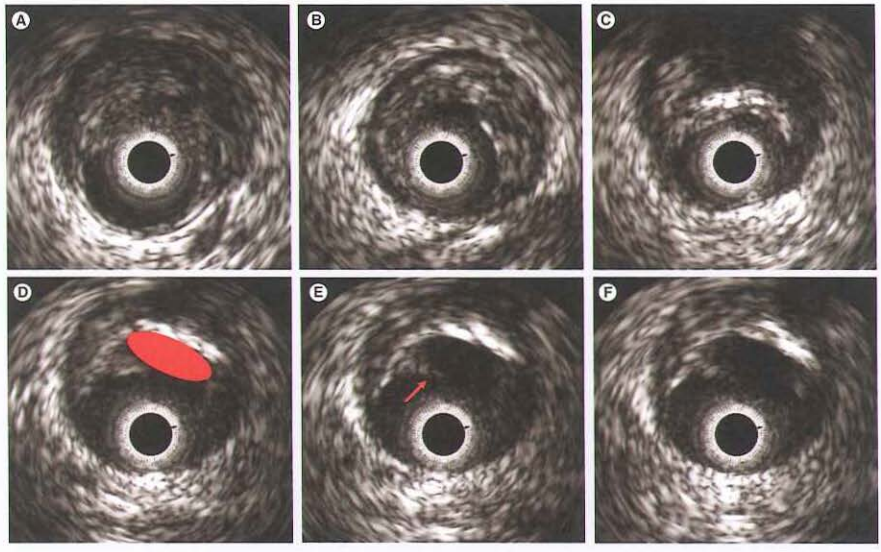

Figure 2. IVUS plaque types. These IVUS images, taken from distal to proximal in the same vessel **(A–F)**, represent different IVUS gray scale plaque types. **(A)** shows a soft plaque, large plaque burden and positive remodeling. On the contrary, **(B)** shows a fibrotic plaque (similar echogenicity to adventitia). **(C)** Depicts a superficial calcified plaque (see shadowing). **(D–F)**, a plaque rupture is illustrated; a large empty cavity (red oval, **[D]**) with the remnant of fibrous cap is overhanging the lumen (arrow, **[E]**).

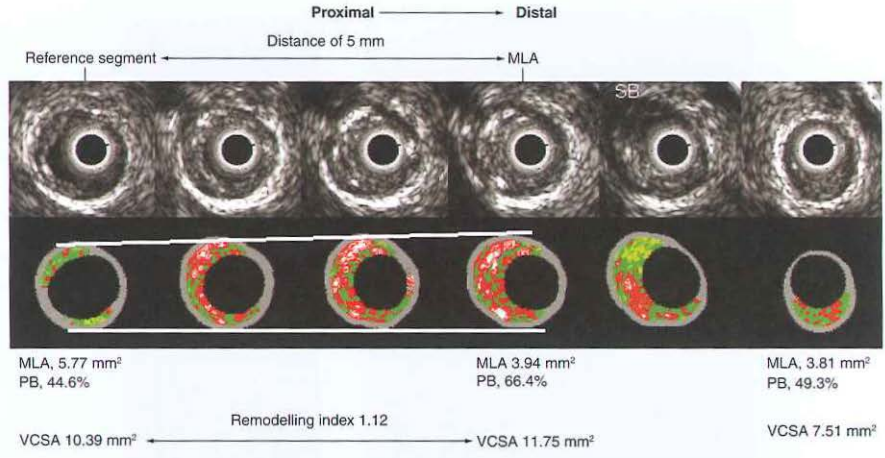

Figure 3. Intravascular ultrasound (IVUS) gray-scale frames and their corresponding virtual histology frames of an IVUS-derived thin-cap fibroatheroma (four central frames) and the proximal and distal reference segment in which the remodeling index was calculated.
MLA: Minimum luminal area; PB: Plaque burden; VCSA: Vessel cross-sectional area.
Virtual histology color code: green is fibrous, greenish is fibrofatty, red is necrotic core and white is dense calcium.

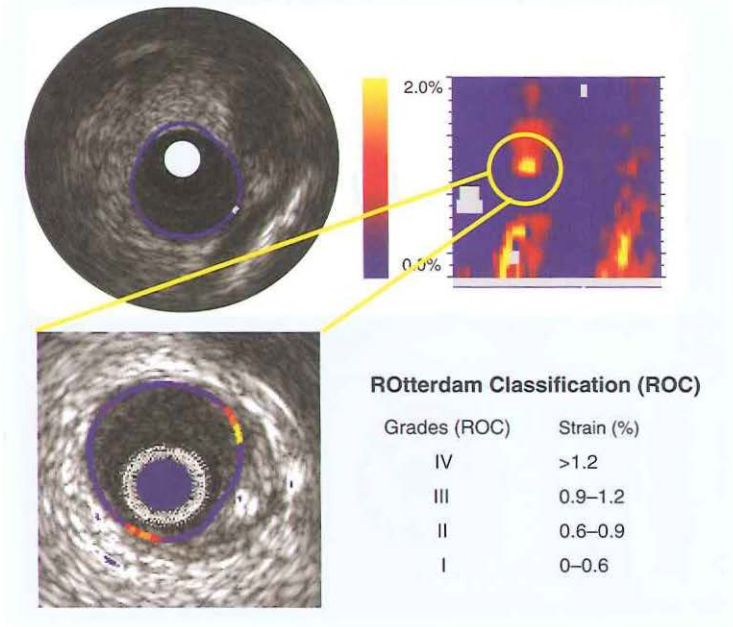

Figure 4. IVUS palpography. The local strain is calculated from the gated radiofrequency traces using cross-correlation analysis and displayed, color-coded, from blue (for 0% strain) to red to yellow (for 2% strain).
Plaque strain values are assigned a Rotterdam Classification (ROC) score ranging from 1 to 4 (ROC I= 0 to <0.6%; ROC II= 0.6 to <0.9%; ROC III= 0.9 to <1.2%; ROC IV >1.2%).

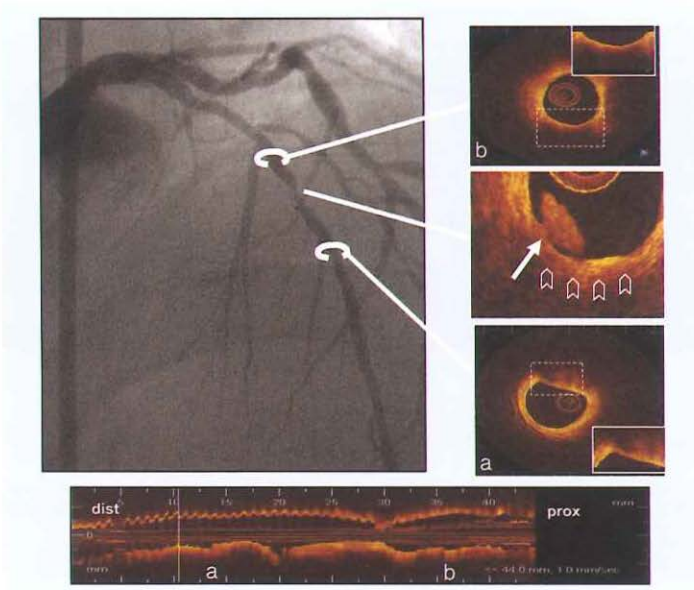

Figure 5. OCT and standard coronary angiography correlation. Angiography shows a complex lesion in the mid left anterior descending. The optical coherence tomography image shows a ruptured plaque with thrombus at that site (white arrow). Proximally and distally to the culprit lesion, thin-capped fibroatheroma lesions are present (**[B]** and **[A]** respectively).

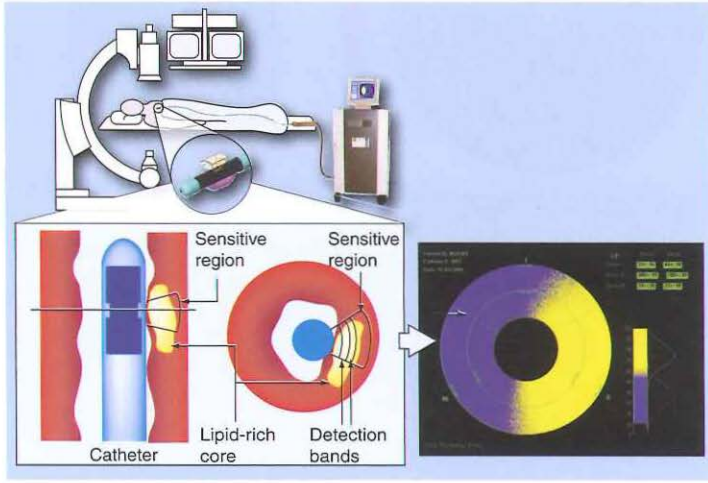

Figure 6. Intravascular magnetic resonance. The magnetic fields generated by the probe located at the tip of the catheter, create a FOV with a sector shape, looking sideways into the artery wall. The FOV has a lateral resolution of 60°, a longitudinal length of 2 mm and a depth of 200 µm. It makes the analysis for the area comprised between 50 and 200 µm from the lumen.
Acquired data is displayed as color-code sectors based of the lipid fraction index for each zone of the FOV. Blue indicates no lipid, gray correspond to intermediate lipid content and yellow indicates high lipid content.
FOV: Field of view.

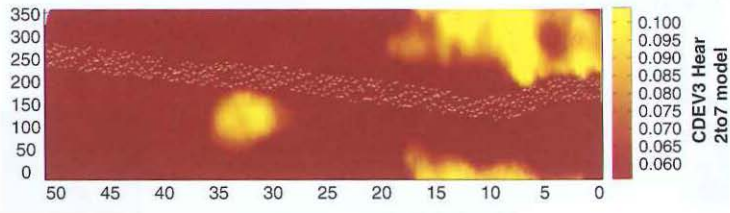

Figure 7. Near infra-red spectroscopy. Demonstration of spectral findings in the left anterior descending coronary artery of an autopsy specimen (unpublished data, on file InfraReDx, Inc., Burlington, Massachusetts). The panel shows the results of the scan, with distance along the lumen on the x-axis and arc of rotation on the y-axis. As indicated by the yellow signal, the scan successfully detected lipid necrotic core rich areas. Image courtesy of James E Muller.

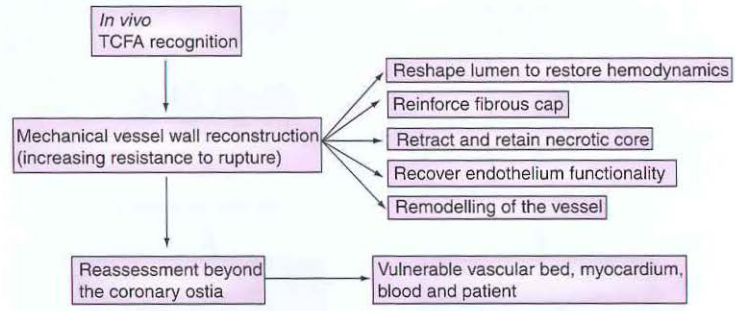

Figure 8. Treatment of coronary vulnerable plaques.

CHAPTER 7.1

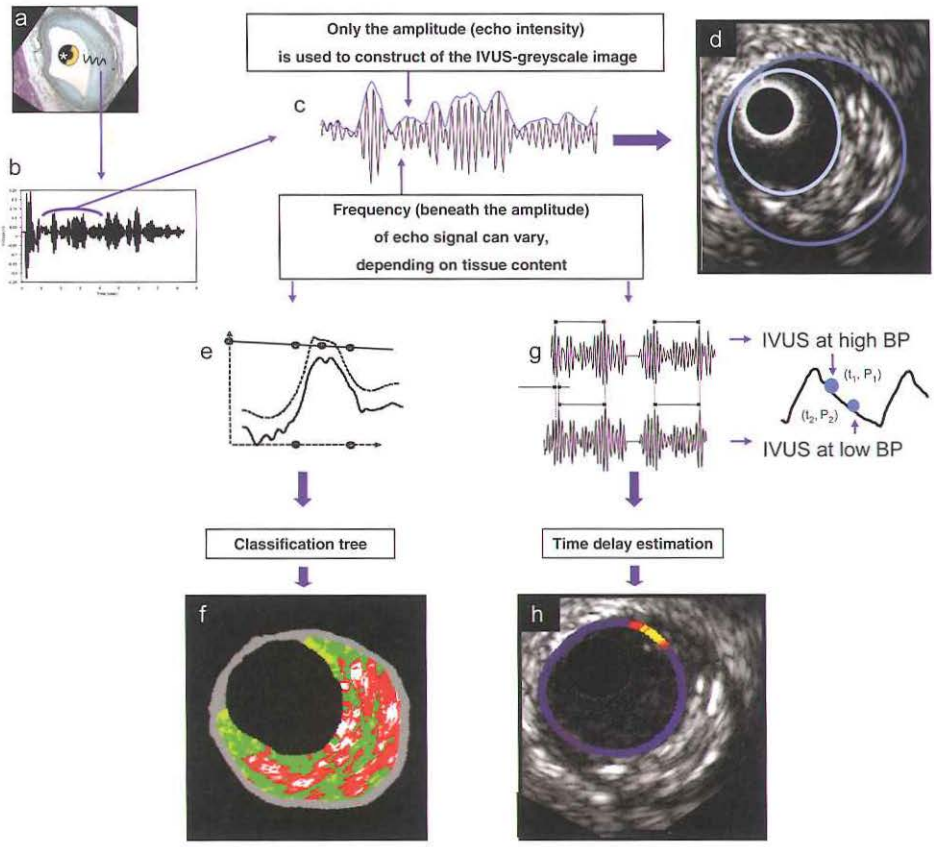

Figure 1. A, The ultrasound signal is generated in a piezoelectric crystal (*) that transmits and receives sound waves. B, Ultrasound reflected by the tissue deforms crystal, generating RF signal. C, Gray-scale IVUS is derived from the amplitude of RF signal, discarding information beneath the peaks of the signal. D, Changes in the electric field of the piezoelectric crystal caused by ultrasound reflection are used to generate a gray-tone image. E, IVUS RF analysis uses several additional spectral parameters to identify 4 plaque components. F, Plaque components that are identified are dense calcium (white), fibrous (green), fibrofatty (greenish-yellow), and necrotic core (red). G, IVUS palpography takes advantage of RF signals generated by the artery being deformed by blood pressure (BP). Using analysis of RF signals at "low" and "high" BP, the strain (deformation) in the inner layer of atheroma is determined. H, This strain is quantified and superimposed on the IVUS image at the lumen/vessel wall boundary. Note that high strain (yellow) is found at the shoulders of the eccentric plaque.

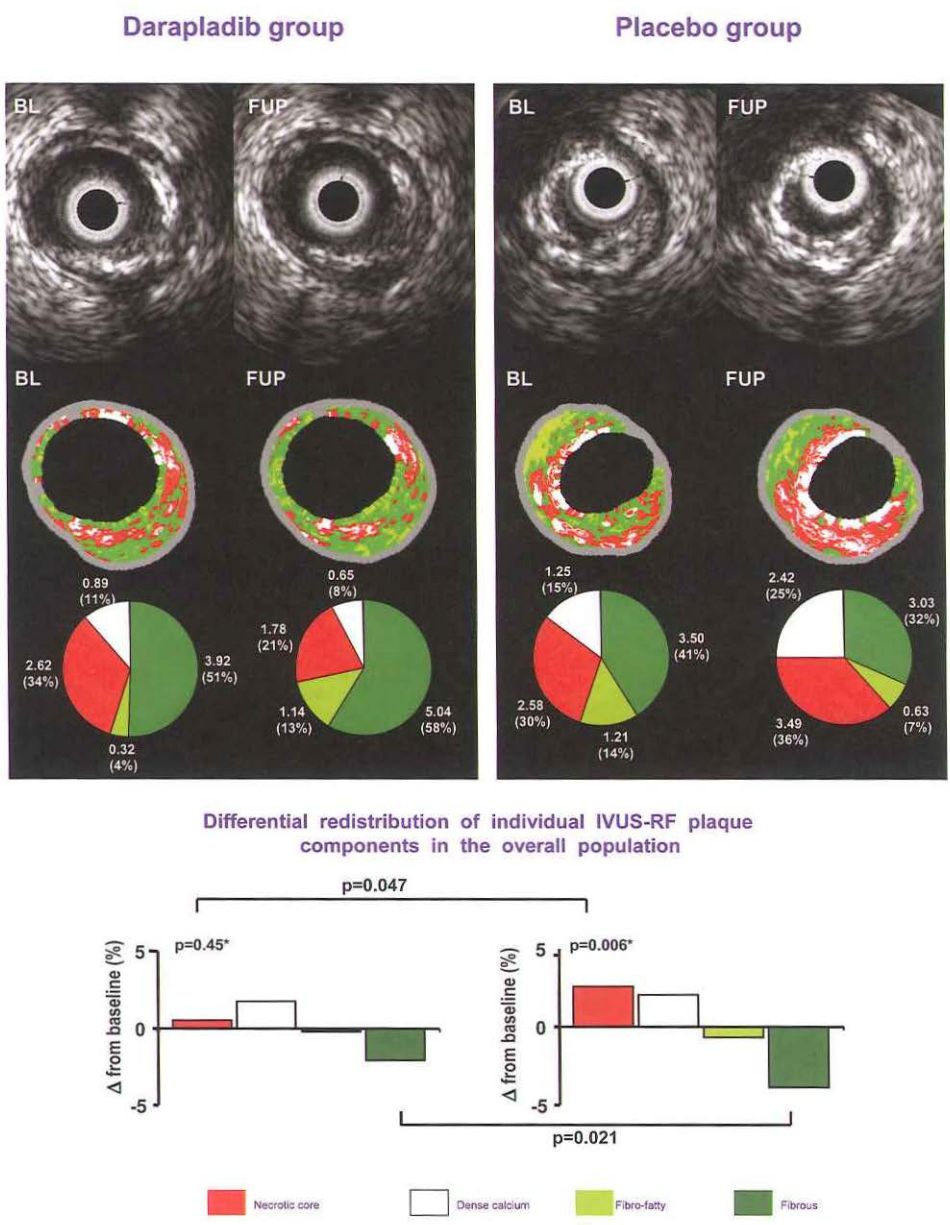

Figure 4. Top, Representative examples of plaque composition in the darapladib- and placebo-treated groups. The gray-scale frames and corresponding IVUS RF frames are shown. The pie charts provide quantitative display of individual plaque components in the cross sections. Values are in millimeters squared (and percent of RF-derived atheroma area). In the darapladib-treated patient, a decrease in necrotic core is seen. In the placebo-treated patient, an increase in necrotic core is demonstrated. Bottom, Differential changes in plaque components from IVUS RF analysis in the overall placebo and darapladib groups. Results are expressed as mean change from baseline (BL), with individual components expressed as percent of RF-derived atheroma volume. FUP indicates follow-up. *Within-group change from baseline.

CHAPTER 7.2

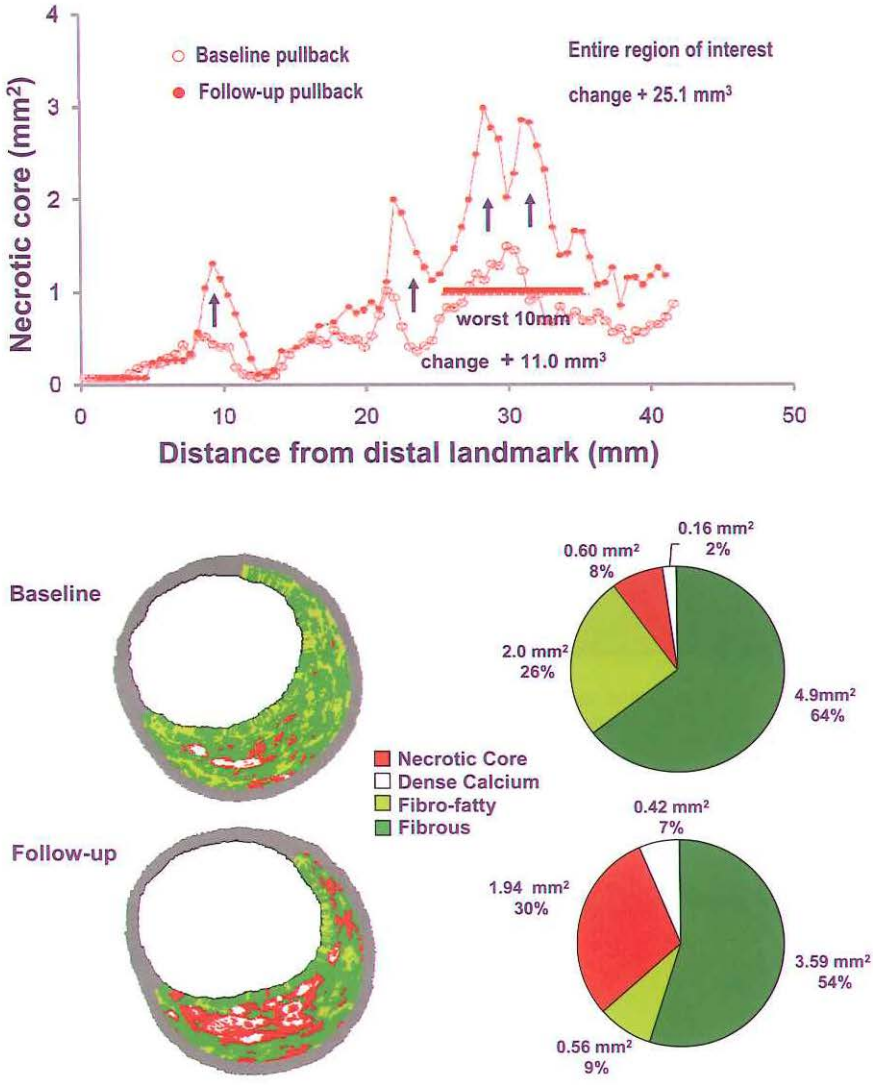

Figure 1. Temporal changes in necrotic core in a patient treated with placebo in the IBIS 2 study
Top: graph displayed the necrotic core (NC) areas in all consecutive cross-sections in this patient, the increase of necrotic core in placebo treated patient is apparent at several locations of the pullback, as highlighted by the arrows. In the entire analyzed region, there was increase in necrotic core volume of 25.1 mm^3 after one year, while in the worst 10 mm segment, an increase of 11 mm^3 in NC was observed.
Bottom: In these two sequential cross-sections from the same anatomical location, there is evidence of progression of necrotic core area (depicted in red) at the expense of fibrous tissue (depicted in green).

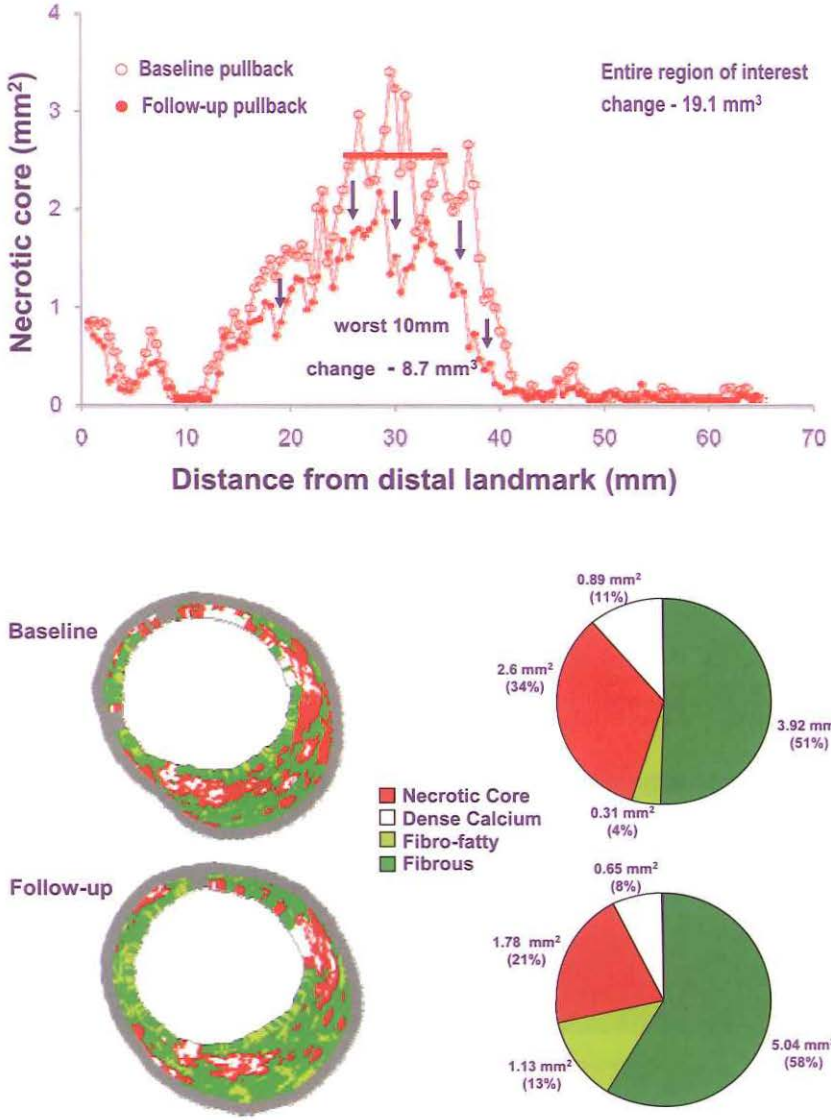

Figure 2. Temporal changes in necrotic core in a patient treated with an Lp-PLA2 inhibitor (darapladib) in the IBIS 2 study

Top: graph displayed the necrotic core (NC) areas in all consecutive cross-sections in this patient, a decrease of necrotic core in darapladib treated patient is apparent at several locations of the pullback, as highlighted by the arrows. In the entire analyzed region, there was increase in necrotic core volume of 19.1 mm^3 after one year, while in the worst 10 mm segment, a decrease of 8.7 mm^3 in NC was observed.

Bottom: In contrast to placebo, two cross-sections from the darapladib-treated patient demonstrate reduction in necrotic core area depicted in red. Of note, concomitant increase in fibrous tissue (in green) is consistent with plaque stabilization effect.

CHAPTER 7.3

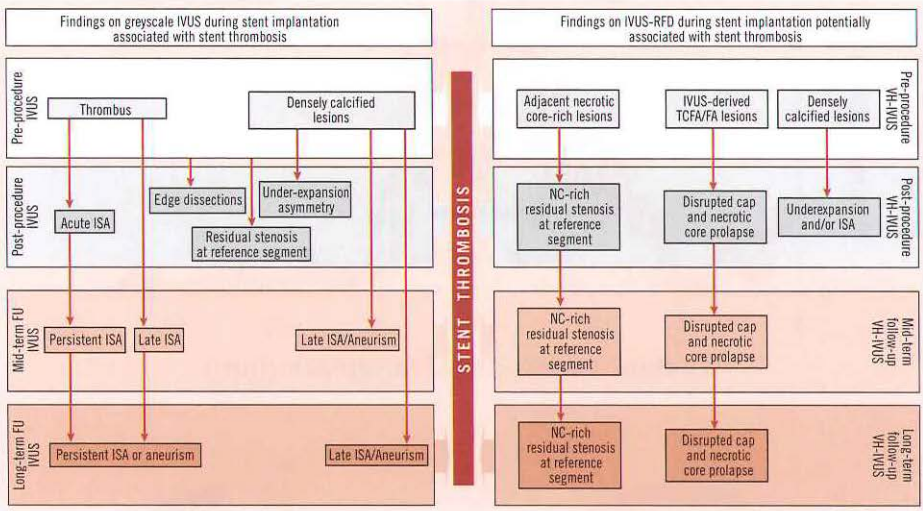

Figure 1. This illustration displays the potential use of greyscale IVUS and IVUS-radiofrequency data (RFD) analysis across the different stages of the interventional procedure and imaging follow-up of the patients. Greyscale IVUS can categorise plaque types and the acute result of the intervention, as well as provide useful information on some characteristics that have been related to stent thrombosis such as incomplete stent apposition (ISA), edge dissection, residual stenosis, under-expansion and thrombus. IVUS-RFD could provide valuable information on the intact plaque, especially on necrotic core (NC) amount and location.

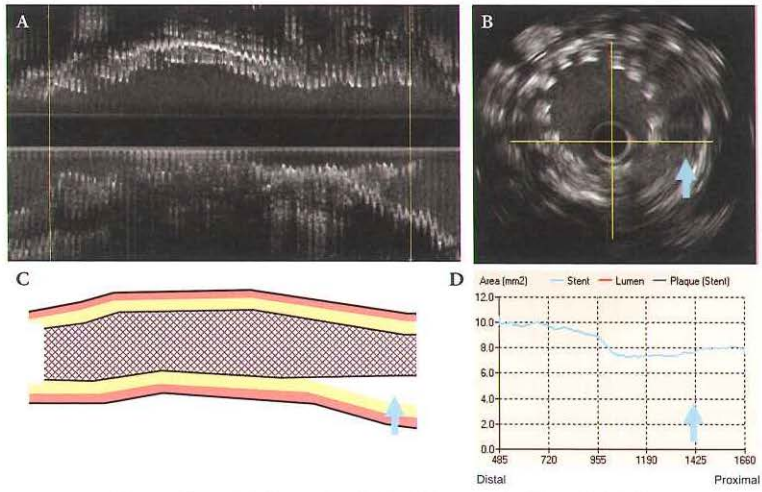

Figure 2. Panel A shows a longitudinal view of an IVUS pullback. The arrow points to a proximal segment that is not apposed to the vessel wall. Panel B is the corresponding cross-sectional area (CSA). The arrow shows multiple stent struts that are not apposed. Panel C is a diagrammatic representation of the longitudinal view. Notice the lack of stent apposition signalled by the arrow. Panel D indicates the stent CSA throughout the segment. An important decrease in stent area is seen at the proximal part.

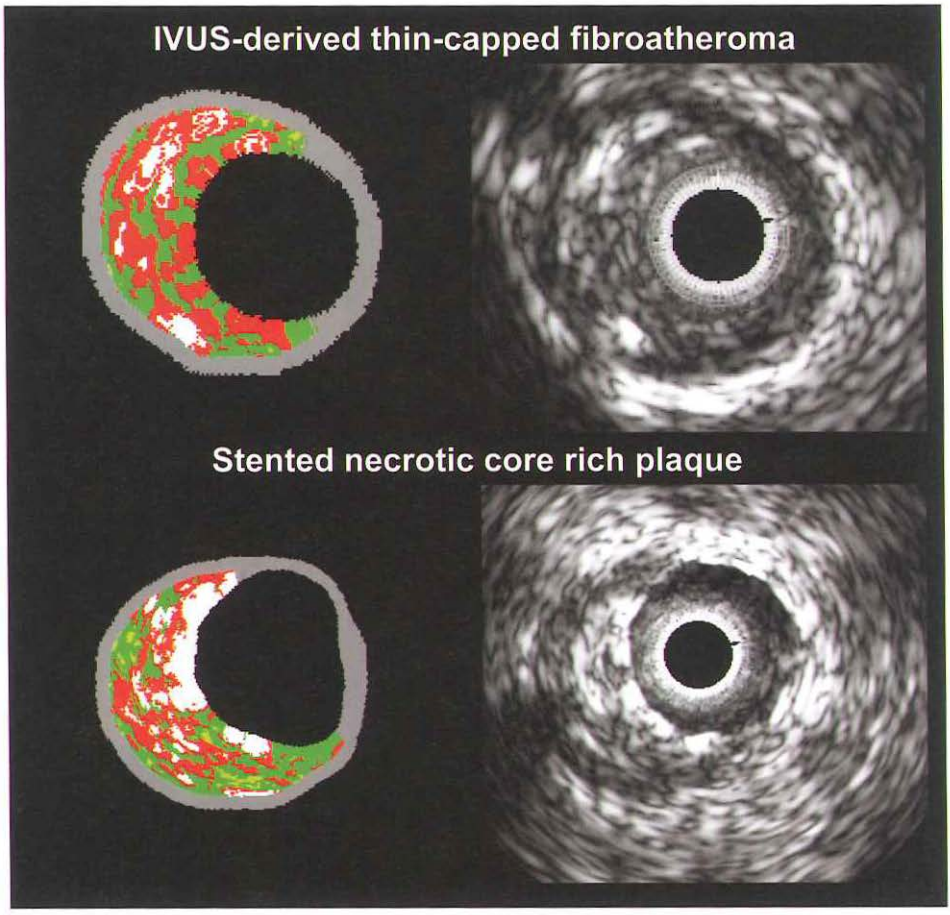

Figure 3. Greyscale IVUS frame and its corresponding IVUS-radiofrequency data frames of an IVUS derived thin cap fibro-atheroma (two upper frames). At the bottom, a stented necrotic core-rich plaque is shown. Notice the presence of stent struts at the lumen in the color picture as "dense calcium" on top of a confluent area of necrotic core. Virtual histology color code: green is fibrous, greenish is fibro-fatty, red is necrotic core and white is dense calcium.

CHAPTER 8.3

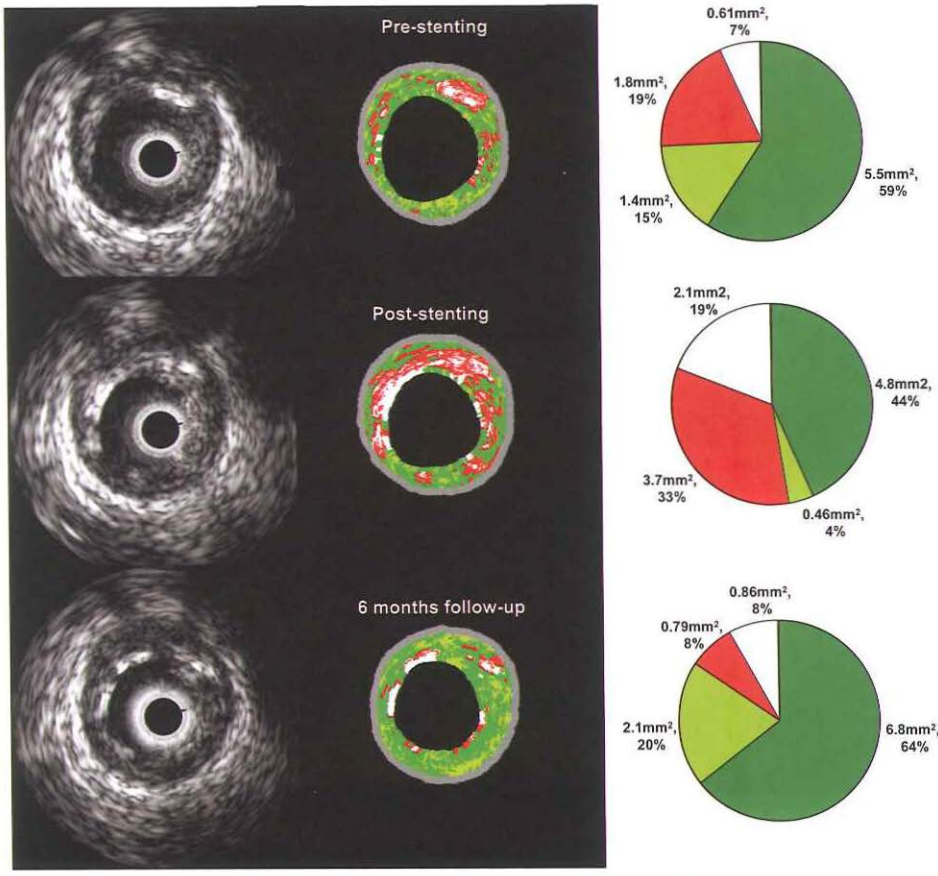

Figure 1. Serial changes in the stent struts as assessed by IVUS Virtual Histology™ (VH). On the left hand side, greyscale IVUS images are shown at pre-, post-stenting and follow-up. In the central part, their corresponding colour code VH images are depicted. On the right hand side, per-cross section quantification in absolute and relative terms is shown. Of note, increases in "dense calcium" (white) and "necrotic core" (red) are noted after stenting. At follow-up, a change in the stent strut appearance in greyscale IVUS is noted and decreases in the "dense calcium" and "necrotic core" contents in IVUS- VH are detected. Fibrous - green; and fibro-fatty - light green.

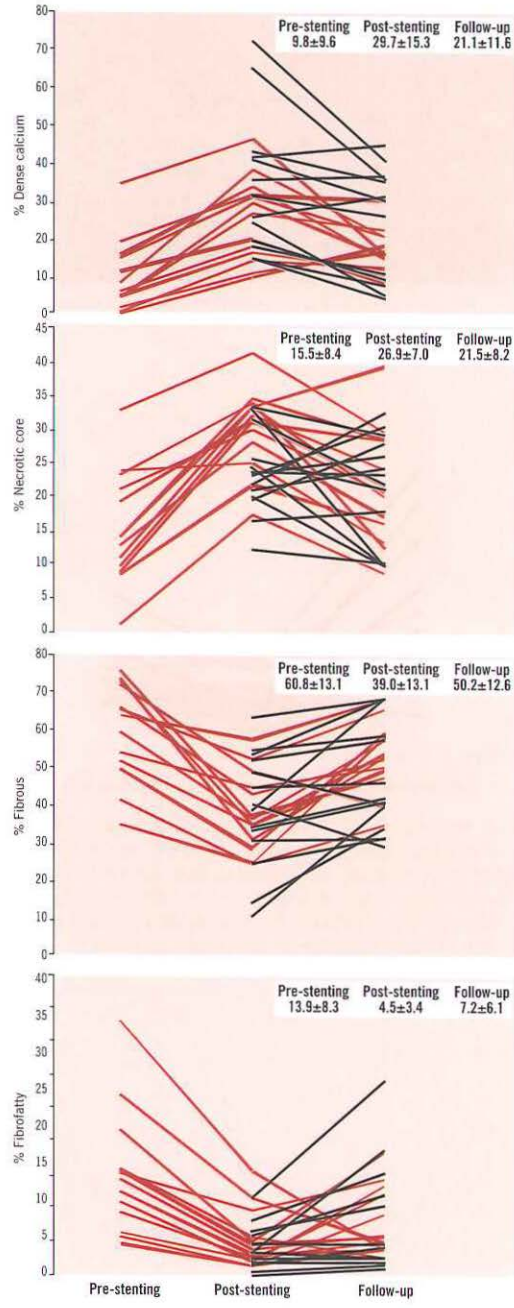

Figure 2. Temporal changes in virtual histology tissue types. From top to bottom, the mean percentage of "dense calcium", "necrotic core", fibrous tissue and fibro-fatty tissue is reported. Thirteen patients were imaged at pre-, post-stenting and follow-up (red solid lines). A further 14 patients were only imaged at post-stenting and follow-up (black dotted lines).

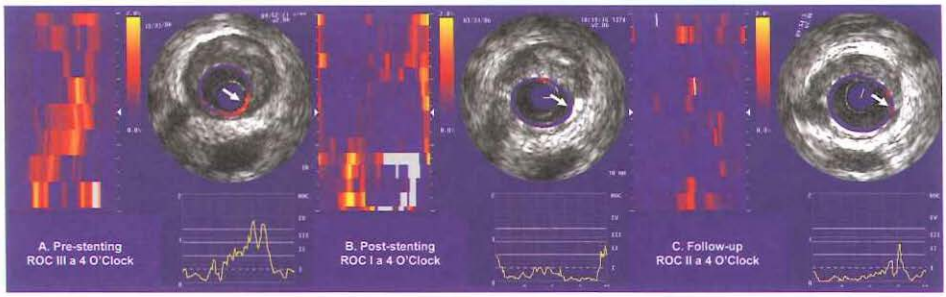

Figure 3. Sequential changes in high-strain values as assessed by IVUS-palpography. Panel A shows an intact plaque with a ROC III spot at 4 o'clock (white arrow). Panel B depicts abolition of this high strain spot following stenting (ROC I). In panel C a slight increase in plaque deformability was documented (ROC II).

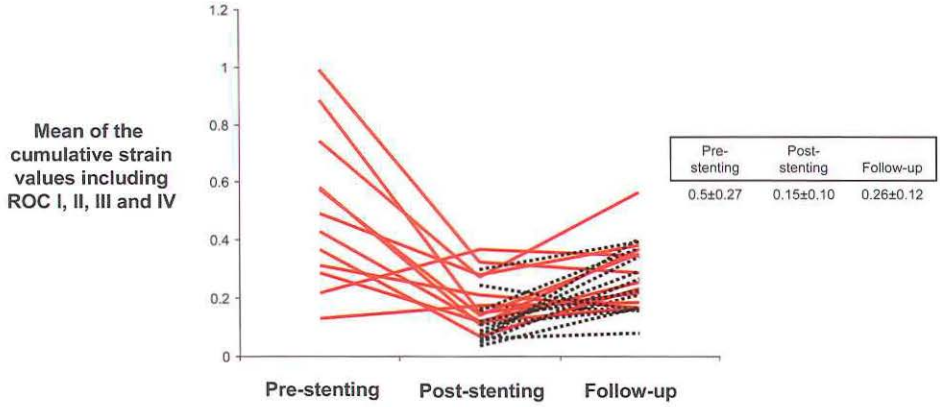

Figure 4. Temporal changes in strain values. The mean cumulative strain values in all frames with ROC I-IV scores are shown. Twelve patients were imaged at pre-, post-stenting and follow-up (red solid lines). Another 13 patients were only imaged at post-stenting and follow-up (black dotted lines). After stenting, abolition of the strain values was noted; however a higher level of plaque deformability was present at follow-up.

CHAPTER 8.4

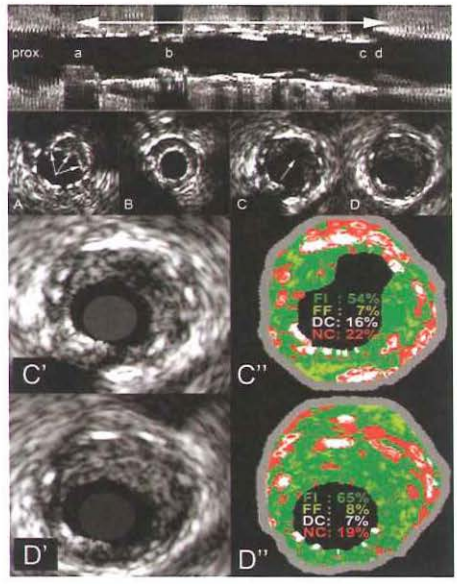

Figure 1. IVUS pullback. The top panel shows the longitudinal reconstruction. The double-headed arrow indicates the location of the stent. The characters "a" through "d" indicate the position of the cross sectional panels "A" through "D". Panel A: proximal part of the stent, arrows indicatestent malapposition. Panel B : minimal luminal area within the stent (MLA 4.6 mm²). Panel C: eccentric plaque rupture (arrowed). Panel D: directly distal, intact eccentric neo-intimal plaque. Panel C" (magnified frame): IVUS VH of ruptured plaque within the neo-intima. Panel D" (magnified frame): immediately after the rupture. Panels C" and D" show a majority of fibrous tissue. Of note IVUS-VH analysis included the stents' struts that were seen as spots of calcium and necrotic core. FI, fibrotic tissue; FF, fibrofatty; DC, dense calcium; NC, necrotic core.

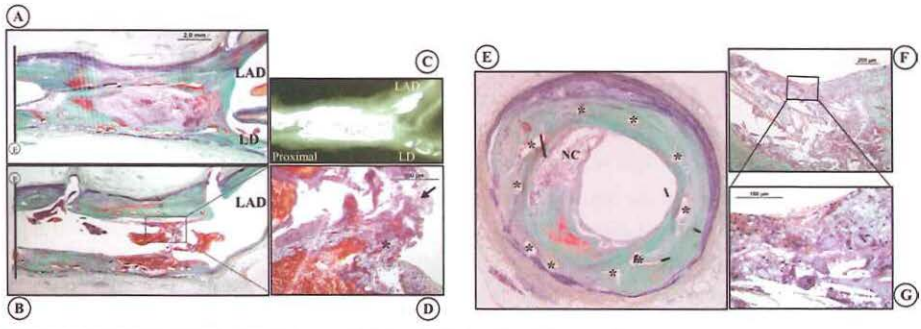

Figure 2. Histology of the case (Movat Pentachrome). A, B: Longitudinal section of the stent. The distal part of the stent shows site of plaque rupture and a superimposed platelet-rich adherent thrombus. C: X-ray of stented artery just above the bifurcation of LAD and left diagonal branch. D: High magnification image of the rupture site (*) and overlying platelet-rich thrombus is identified by the black arrow. E: The cross section of the proximal portion of the LAD stent. (corresponds to the black lines in panel A and B). Note the presence of a thin-cap fibroatheroma (vulnerable plaque) within the stent site (*). F, G: The fibrous cap is extremely thin and infiltrated by foamy macrophages with an underlying necrotic core (NC).

CHAPTER 10.1

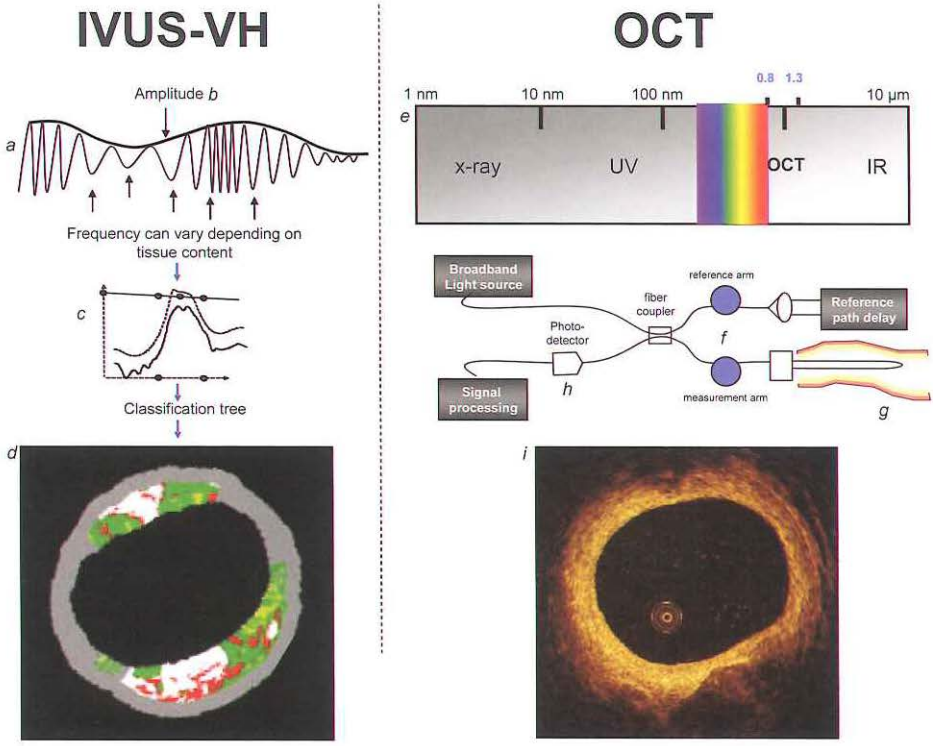

Figure 1: Schematic diagram of virtual histology (IVUS-VH) and optical coherence tomography (OCT). *Left:* The ultrasound signal is generated in a piezoelectric crystal that transmits and receives sound waves. Ultrasound reflected by the tissue deforms crystal generating radiofrequency (RF) signal (*a*). Greyscale IVUS is derived from the amplitude (*b*) of RF signal, discarding information beneath the peaks of the signal. IVUS-VH analysis uses several additional spectral parameters to identify four plaque components (*c*). Plaque components that are identified are dense calcium (white), fibrous (green), fibro-fatty (greenish-yellow) and necrotic core (red) (*d*).
Right: the electromagnetic spectrum encompasses the following regions: x-rays, microwaves and light (*e*). The visible part of the spectrum ranges from 0.4 to 0.77 µm. The wavelengths used for OCT are indicated. Since the speed of light is much faster than that of sound, it is needed to use correlation or an interferometer to measure the backscattered light. The interferometer splits the light source into two arms – a reference arm and a measurement arm- (*f*). The measurement arm is directed into the tissue through the image wire and collects the backscattered light (*g*). The light coming back from both arms is recombined at a detector (*h*) in which the interferogram – the sum of the two signals - is generated. The optical properties of the tissue can be deduced by comparing the back-reflected optical intensity of the two arms (*i*). Panel *d* and *i* correspond to the same anatomical region. Please note that the shape of the calcified regions is similar.

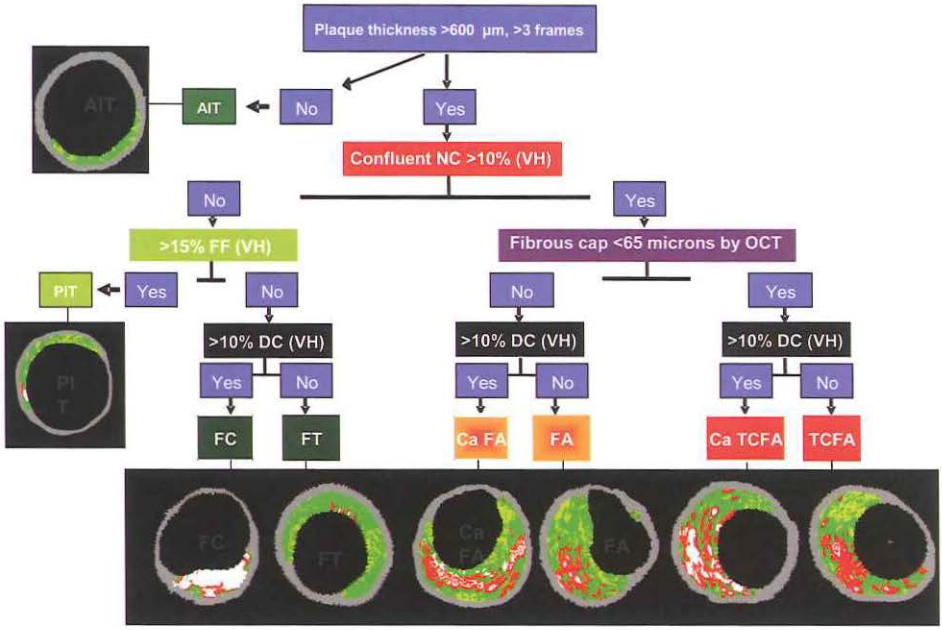

Figure 2: Plaque classification using OCT and IVUS-VH. OCT: optical coherence tomography; VH: virtual histology; NC: necrotic core; AIT: adaptive intimal thickening; PIT: pathological intimal thickening; FC: fibrocalcic; FT: fibrotic; CaFA: calcified fibroatheroma; FA: fibroatheroma; CaTCFA: calcified thin cap fibroatheroma; TCFA: thin cap fibroatheroma.

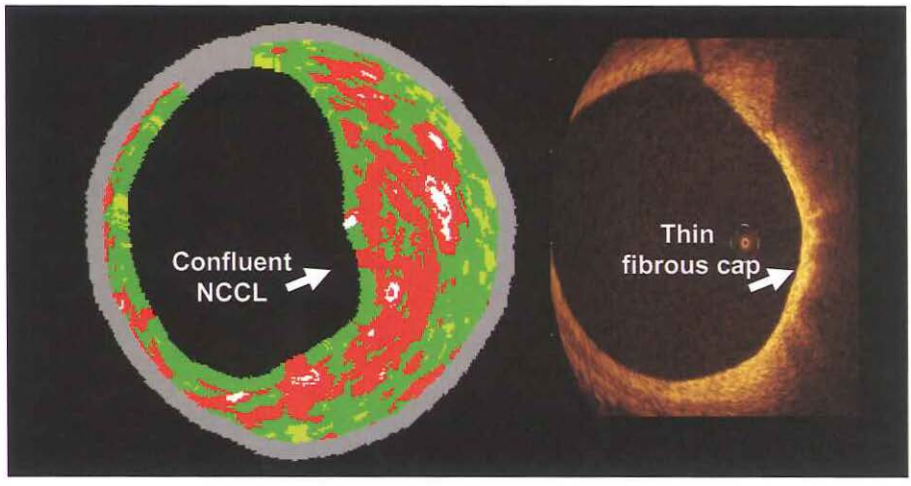

Figure 3. IVUS-derived thin cap fibroatheroma by and virtual histology and its corresponding optical coherence tomography image (OCT). *Right:* Virtual histology image is color coded: red – necrotic core, white – dense calcium, green – fibrous and greenish – fibro-fatty. There is an area of confluent necrotic core (NC) that is in direct contact with the lumen (CL). *Left:* OCT image shows an area with low reflectivity behind a thin cap. These characteristics have been correlated with a fibrous cap overlying a necrotic core rich area (arrow).

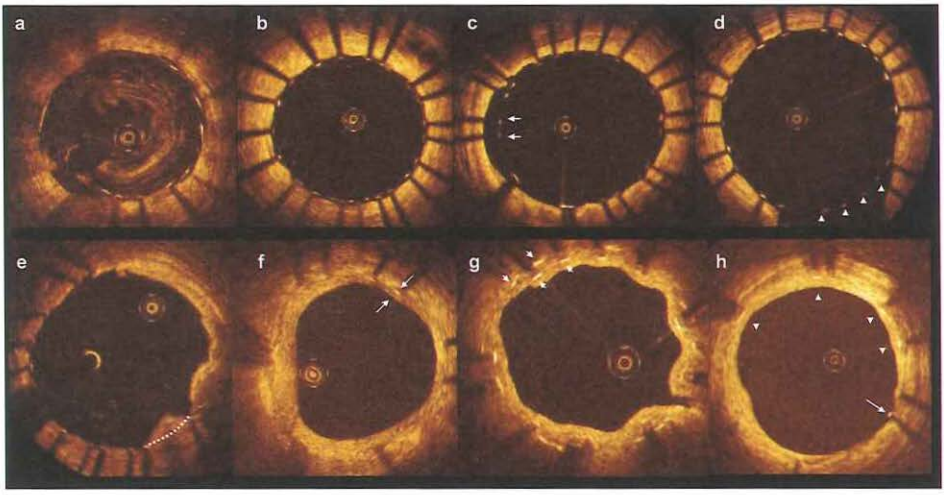

Figure 4. Optical coherence tomography images of common stent findings. *Panel a* shows a newly placed stent. Stent struts are recognized as bright structures that span 360 degrees with shadowing. *Panel b* depicts a frame with insufficient blood clearance. *Panel c* illustrates an incomplete stent apposition site. Of note, stent struts are not apposed to the vessel wall (arrows). *Panel d* shows the relationship of a stent and the ostium of a sidebranch (arrowhead). *Panel e* depicts a frame with tissue prolapse. Dotted line denotes the space between two struts. A mass of tissue is protruding into the lumen (asterisk). *Panel f* illustrates a stent with neointimal hyperplasia which is the signal-rich area between the stent struts and the lumen (arrows). *Panel g* shows an overlapped segment. Two layers of stent can be seen along the circumference (arrowheads). *Panel h* illustrates an uncovered strut (no tissue is at the endoluminal side of the strut - arrow). In contrast, some other struts are covered by neointimal tissue (arrowheads).

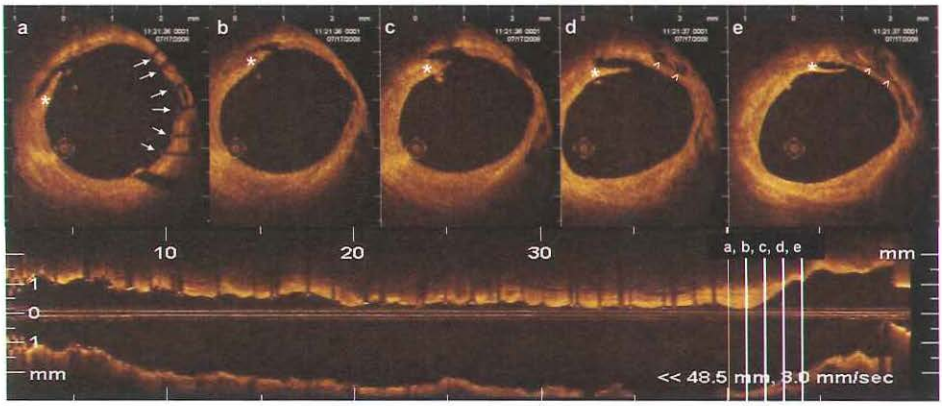

Figure 5. Edge dissection. In this patient a drug eluting stent was placed proximally in the left anterior descending. At the proximal edge of the stent a 4-mm dissection was noted in the optical coherence tomography images (a through e). In *panel a*, stent struts can still be seen (arrows) from 1 to 5 O'clock, while at 9 O'clock a dissection flap is noted (asterisk). At the proximal end of the dissection a calcified plaque can be seen (head arrows in *panels d and e*).

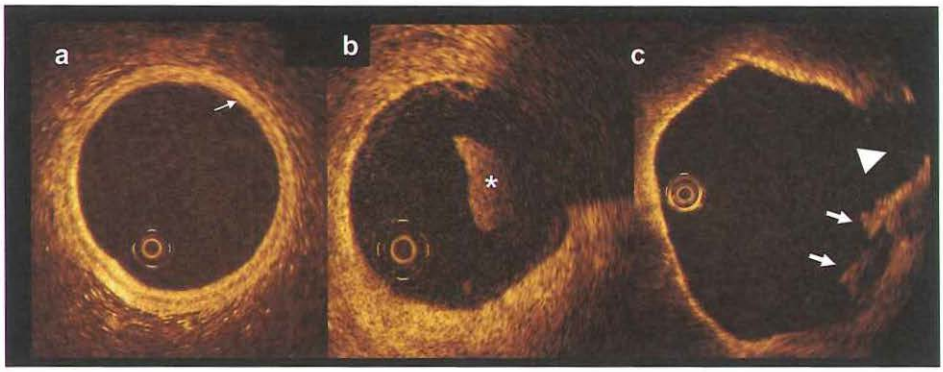

Figure 6. Optical coherence tomography images of intact atherosclerotic coronary plaques. *Panel a* shows a normal-looking vessel wall. *Panel b* depicts a red thrombus inside the lumen. Its OCT signature is the shadowing behind the mass (asterisk). *Panel c* illustrates a ruptured plaque. The cavity is at 2 O'Clock (arrowhead). Some disrupted tissue is adjacent to it (arrows). From 7 to 9 O'clock a poor-signal region with low reflectivity is seen, suggesting a thin fibrous cap fibroatheroma.

CHAPTER 10.2

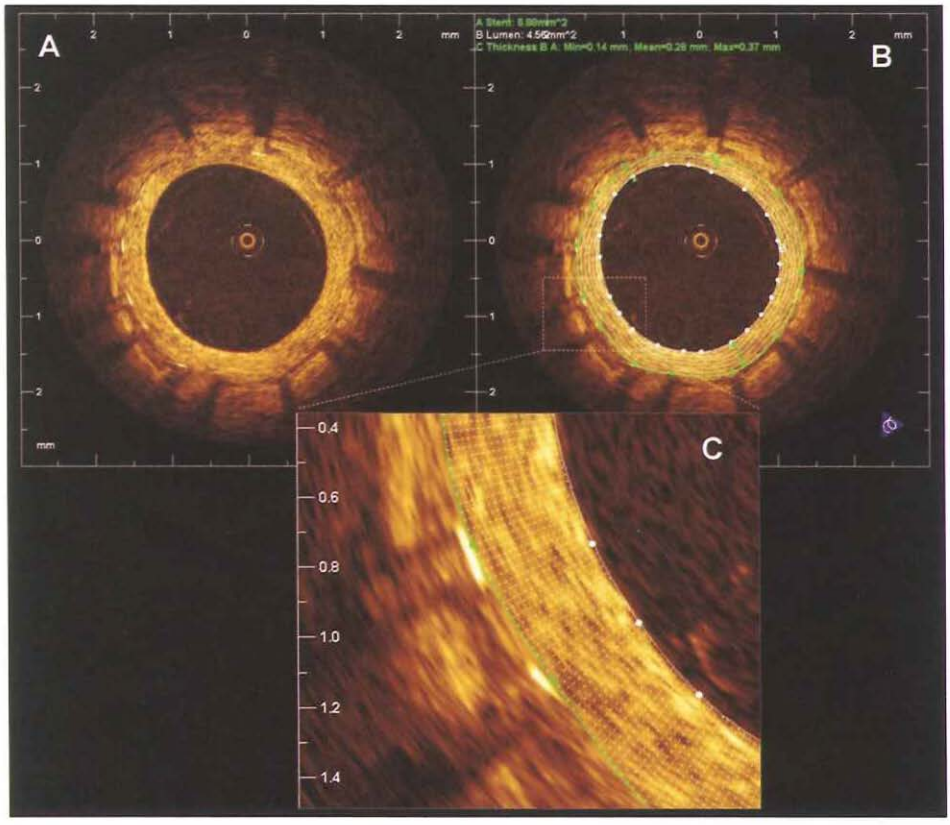

Figure 1: Tissue coverage measurement. A. Sirolimus eluting stent 9 months after stent implantation. B. The figure shows the lumen contour (white) and the stent contour (green). The tissue coverage area was calculated as stent area minus lumen area. The tissue coverage thickness was measured in 360 points (represented by the white chords). C. Magnification of 2 struts showing all the measurements (white chords) of the tissue coverage in front of every strut. For every strut the minimum, maximum and mean strut coverage was calculated.

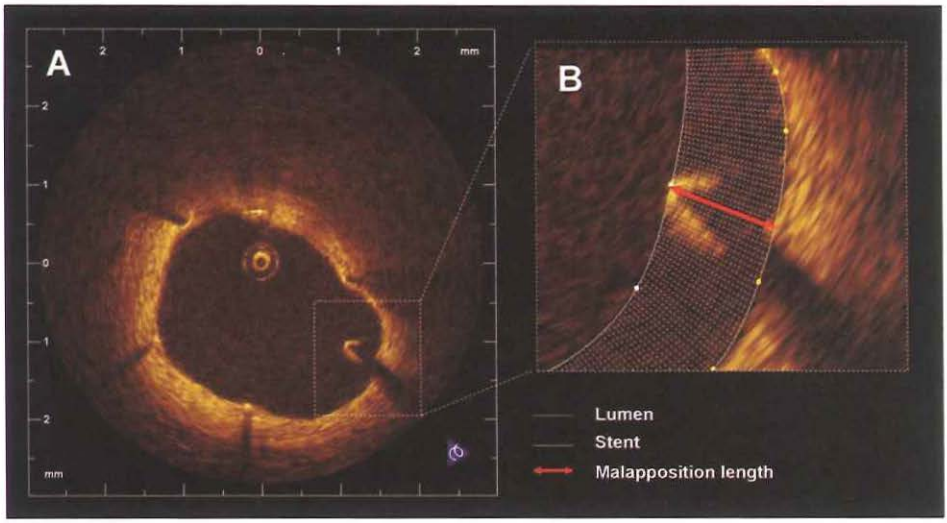

Figure 2: Malapposition. A. Example of a malapposed strut in a sirolimus eluting stent at 9 months follow up. **B**. Magnification of the malapposed strut. The yellow line represents the lumen contour and the white line corresponds to the stent contour. The distance from the endoluminal surface of the strut to the vessel wall (red arrow) was 440 μm (higher than the sum of the metal and polymer thickness for this type of stent).

CHAPTER 10.3

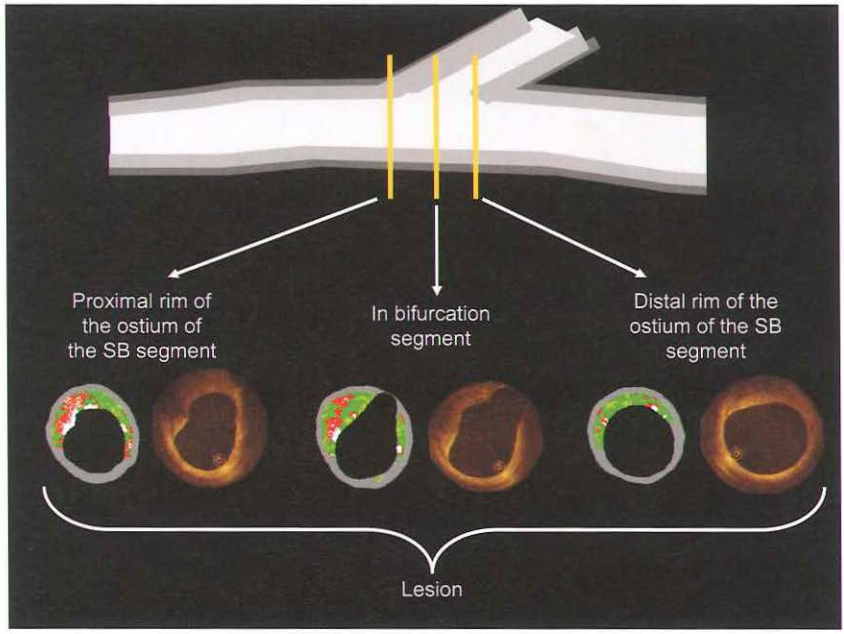

Figure 1. Bifurcation Selection and Analysis

Bifurcations that could be identified in both intravascular ultrasound-virtual histology (IVUS-VH) and optical coherence tomography (OCT) pullbacks were included. A strict selection of the analyzed cross-sections (CS) was followed to ensure correct matching between the 2 techniques. Plaques were analyzed only in the main branch. The lesion analysis included: 1) proximal rim of the ostium of the side branch (SB) CS (first frame proximal to the take-off of the SB); 2) in-bifurcation CS (frame with the larger ostial diameter of the SB); and 3) distal rim of the ostium of the SB CS (first frame distal to the take off of the SB).

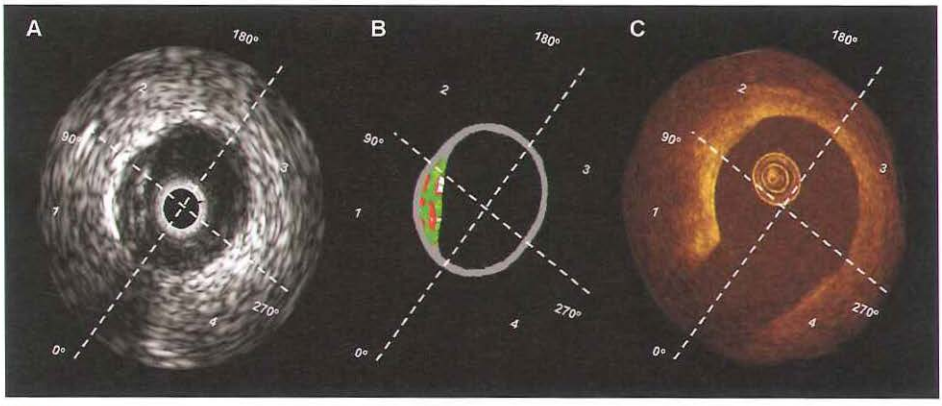

Figure 2. Location of the Plaque in Relation to the Flow Divider

To describe the plaque location in relation to the flow divider, the vessel cross-section was divided in 4 quadrants according to the position of the side branch. Quadrants 1 and 4 correspond to the ostium of the side branch, whereas quadrants 2 and 3 correspond to the part of the vessel wall located in front of the ostium of the side branch. **(A)** Grayscale IVUS. **(B)** Virtual histology. **(C)** OCT. Abbreviations as in Figure 1.

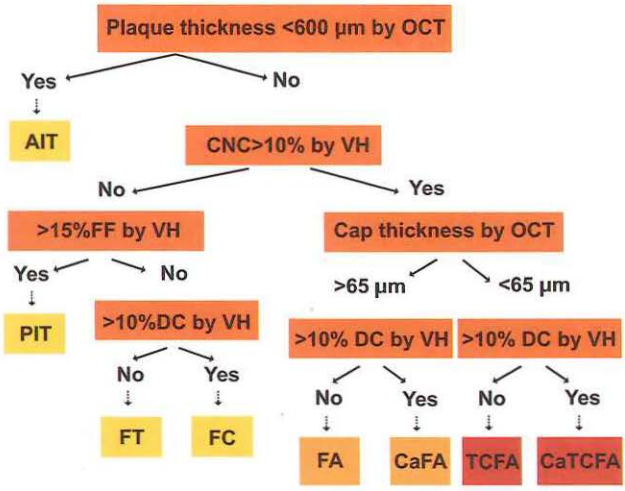

Figure 3. Plaque Classification Algorithm

AIT = adaptive intimal thickening; CaFA = calcified fibroatheroma; CaTCFA = calcified thin-cap fibroatheroma; CNC = confluent necrotic core; DC = dense calcium; FA = fibroatheroma; FC = fibrocalcic; FF = fibrofatty; FT = fibrotic; OCT = optical coherence tomography; PIT = pathological intimal thickening; TCFA = thin-cap fibroatheroma; VH = virtual histology.

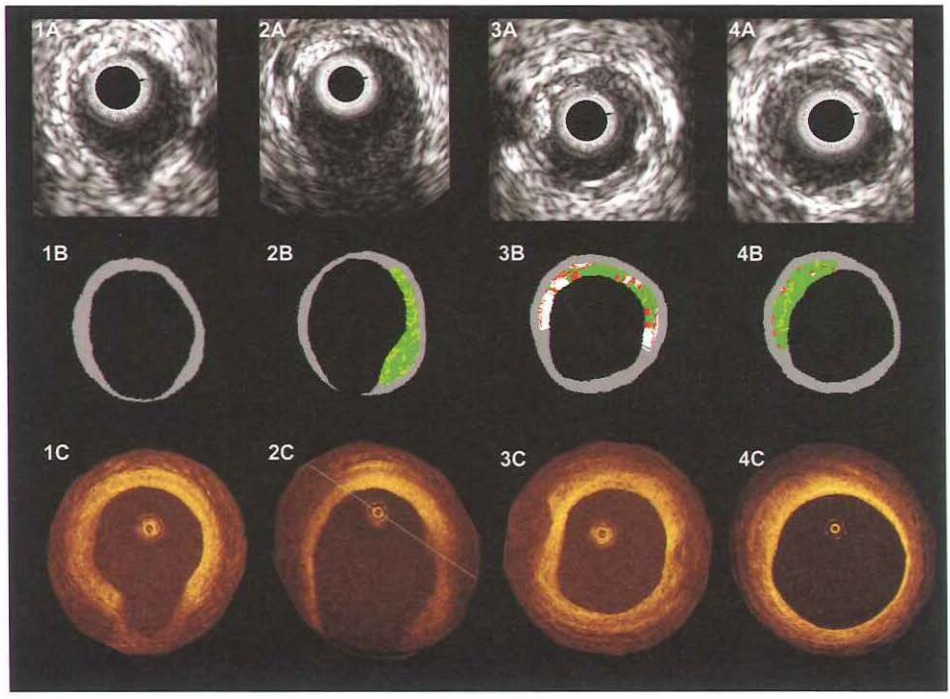

Figure 4. Low-Risk Plaques

Matched images of grayscale IVUS (**A**), virtual histology (**B**), and OCT (**C**) for the 4 types of plaques considered at low risk. 1: adaptive intimal thickening, 2: pathological intimal thickening, 3: fibrocalcific plaque, 4: fibrotic plaque. Abbreviations as in Figure 1.

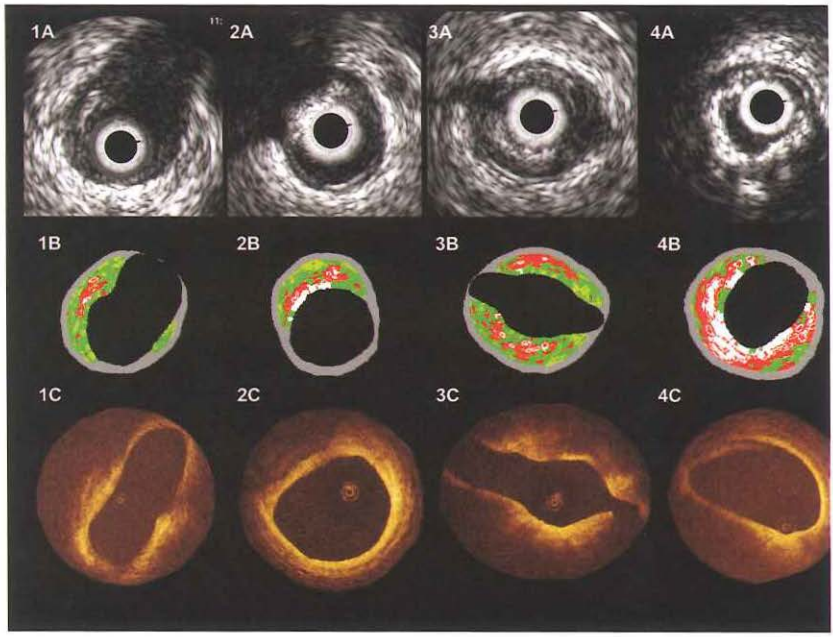

Figure 5. High-Risk Plaques

Matched images of grayscale IVUS (**A**), virtual histology (**B**), and OCT (**C**) for the 4 types of plaques considered at high risk of rupture. 1: fibroatheroma, 2: calcified fibroatheroma, 3: thin-cap fibroatheroma, 4: calcified thin-cap fibroatheroma. Abbreviations as in Figure 1.

CHAPTER 10.4

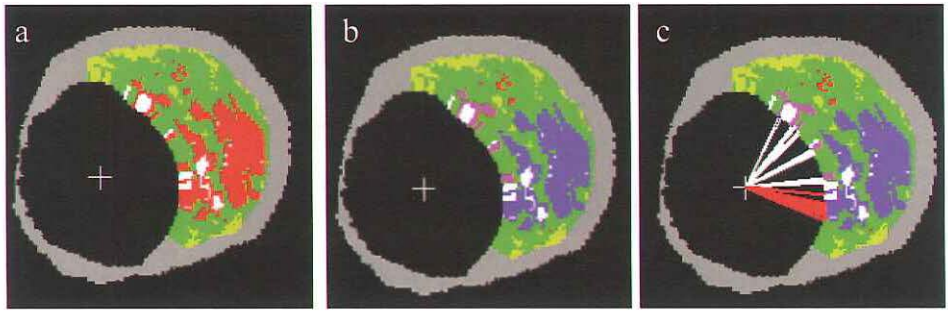

Figure 1 An example of selective quantification of the necrotic core in contact with the lumen (NCCL). (*A*) The original virtual histology-intravascular ultrasound cross-sectional area. (*B*) The blue area was selectively quantified as the major confluent NCCL areas and blue plus purple areas indicate total NCCL areas. (*C*) Measurement of the angle occupied by the total NCCL (white and red line) and the angle occupied by the major confluent NCCL (red line).

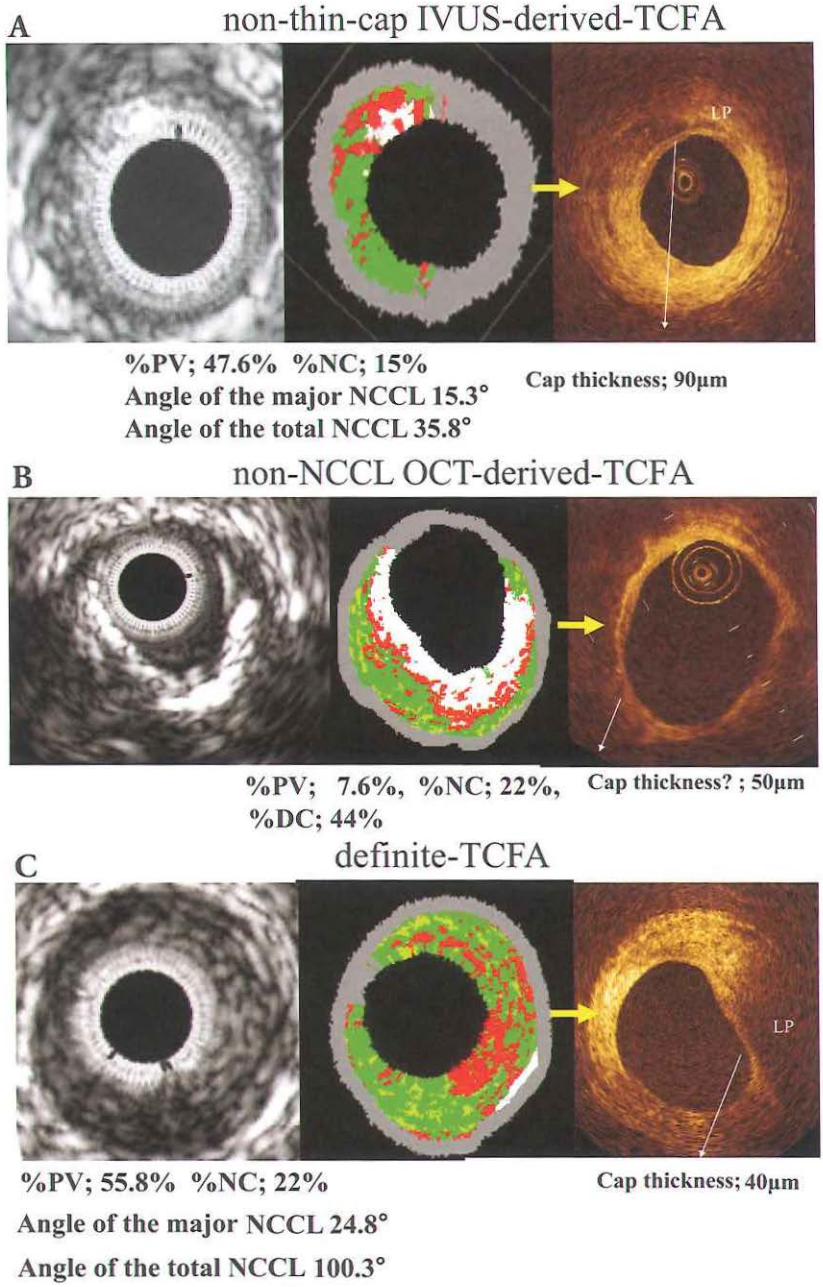

Figure 3 (*A*) A representative case of non-thin-cap IVUS-derived thin-cap fibroatheroma (TCFA). Virtual histology-IVUS shows 47.6% of %plaque-volume, 15% of %necrotic-core. The angle of the major NCCL was 15.3°, and that of the total NCCL was 35.8°. OCT shows signal-poor lesions with an overlying signal-rich band in the upper right quadrant. A signal-poor lesion indicates a lipid pool and signal-rich band indicates a fibrous cap. The fibrous cap thickness was 90 μm. (*B*) A representative case of non-NCCL OCT-derived TCFA. OCT identified a fibrous cap thickness of 50 μm which covers the low intensity area, but VH-IVUS did not identify the NCCL. (*C*) A representative case of definite-TCFA. Virtual histology-IVUS shows %plaque-volume of 55.8% and %necrotic-core of 22%. The angle of the major NCCL was 24.8°, and that of the total NCCL was 100.3°. Its minimum fibrous cap thickness was 40 μm.

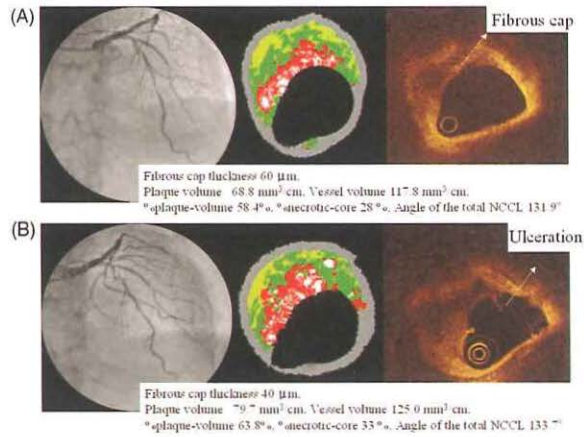

Figure 4 (A) Coronary angiography (CAG) revealed 50% stenosis in the mid-left anterior descending artery in July 2006. VH-IVUS revealed a 68.8 mm^3/cm plaque volume, 117.8 mm^3/cm vessel volume, 58.4% %plaque-volume, and 28% %necrotic-core. The fibrous cap thickness of this lesion was 60 μm by OCT measurement and this lesion was diagnosed as definite-TCFA. (B) After 6 months, because the patient experienced chest pain at rest with increased frequency, we performed CAG. The CAG revealed 90% stenosis at the site of the previous definite-TCFA lesion. VH-IVUS revealed an increase in plaque volume (68.8→79.7 mm^3/cm), vessel volume (117.8→125.0 mm^3/cm), %plaque-volume (58.4%→63.8%), and %necrotic-core (28%→33%). OCT revealed ulceration of the fibrous cap.

Financial support for the publication of this thesis was generously provided by:

Volcano Corporation

Terumo

GlaxoSmithKline

InfraReDx

Cardiałysis

Abbott

Medis